



The University of Strathclyde

Strathclyde Institute of Pharmacy and Biomedical Sciences

Novel Repurposed Drug Combinations for the treatment
of Glioblastoma

Roshine Akram

A thesis submitted in fulfilment of the requirements for the degree
of Doctor of Philosophy

January 2025

Declaration

This thesis is the result of the author's original research. It has been composed by the author and has not been previously submitted for examination which has led to the award of a degree.

The copyright of this thesis belongs to the author under the terms of the United Kingdom Copyright Acts as qualified by University of Strathclyde Regulation 3.50. Due acknowledgement must always be made of the use of any material contained in, or derived from, this thesis.

Signed: 

Date: 27/01/2025

"Only thing really worth chasing is a dream"

Aubrey Drake Graham

Acknowledgements

Firstly, I would also like to thank my supervisors Dr Marie Boyd and Prof Alex Mullen for all their help, guidance and support over the last 5 years. Thank you to Dr Annette Sorensen, who always lent support and advice. You have all been invaluable.

I'd like to thank all members of the Boyd group, past and present – Olena, Sara, Manal, Yasir, Amy, Wedad, Zainab and Reem, you have all made these years enjoyable. A special thanks to Calum, Hannah and Samantha for all their support, encouragement and friendship. A special thanks to Dr Scott who continued to support and guide me throughout the PhD. I'd like to thank the HW5 groups, Cunningham, Gould, McConnell, Gomez and also Graeme Mckenzie. All provided much support in various different areas of this thesis.

I would like to thank all my besties (H.P, R.W, K.M, S.O, L.M, E.K, Z.T, A.K) you have all provided continuous support and I value you all so much. I'd like to thank Pops, P, Pooja, Raj, Cruzy and Remy, who have given so much understanding, patience, and love. I would also like to thank Nano, who told me from the age of 3/4 that I was going to be a Dr, I know she's blessing me from somewhere up above. Thanks to all my Sattar, Sahin, Clawson clan, I love you all.

A major support system for the completion of this PhD were my parents, Akram and Neilam, who always encouraged me to pursue my higher education and who provided unlimited financial support over the years as well as unlimited love.

I'd like to thank my auntie-moms Kameil and Nyla, who together with my mum have raised me into the woman I am. They have provided me with encouragement, reassurance and unlimited advice, you three are my inspirational wonder woman dream team and I'd be nowhere without you.

Finally, I'd like to thank my husband and best friend Tazy, who learnt every assay in this thesis so he could understand my stress and help. Who unwillingly went out late to work so I could study in peace, provided solutions for all my problems when he could and who still told me daily that he was proud of me and loved me. You continue to be my forever hype man.

On a final note, I dedicate this thesis to the children of the Ummah, who's brilliance and future contributions to science and research will never be seen. You have been in my heart encouraging me to fulfil this privilege that you had taken away.

Table Of Contents

Contents

Declaration	I
Acknowledgements.....	II
Table Of Contents.....	III
List of Figures	XI
List of Tables	XVII
List of Abbreviations	XIX
Abstract	XXIII
Covid Impact Statement.....	XXIV
Chapter 1.....	1
Introduction	1
1.1 Cancer	1
1.1.1 Brain and central nervous System Cancers.....	2
1.1.2 Glioma Grading	3
1.2 Glioblastoma	5
1.2.1 Aetiology	6
1.2.2 Diagnosis and Prognosis.....	7
1.2.3 Glioblastoma IDH-Wildtype and Astrocytoma IDH-mutant.....	9
1.2.4 GBM cancer stem cells.....	13
1.2.4.1 Tumour Microenvironment and niche	15
1.3 Pathology, genetic mutations and molecular biology of GBM.....	16
1.3.1 Isocitrate Dehydrogenase 1 and 2.....	18
1.3.2 Methylguanine Methyltransferase (MGMT).....	19
1.3.3 EGFR.....	20
1.3.4 PTEN and P13K Signalling.....	21
1.3.5 p53.....	22
1.3.6 Hypoxia and Hypoxia inducible factor-1 (HIF-1).....	23
1.4. Current Treatments of GBM.....	24
1.4.1 Surgical Resection	25
1.4.2 Radiotherapy and Tumour treating Fields	27

1.4.2.1 Radiotherapy	27
1.4.2.2 Tumour treating Fields	29
1.4.3 Chemotherapies for GBM.....	30
1.4.3.1 Temozolomide.....	30
1.4.3.2 Temozolomide therapeutic resistance	32
1.5 Repurposing Drugs.....	34
1.5.1 The Fumarates	36
1.5.2 Dimethyl Fumarate	36
1.5.2.1 Glutathione	39
1.5.2.2 Ferroptosis and Glutathione Peroxidase 4	41
1.5.2.3 NrF2	42
1.5.3 Monomethyl Fumarate.....	43
1.6 Aims	45
Chapter 2.....	46
Materials and Methods	46
2.1 Cell Lines and Maintenance.....	46
2.2 Freezing and thawing cells.....	46
2.3 Cell Doubling Time	47
2.4 Drug Preparation	48
2.5 Cell Treatments with Drugs.....	48
2.6 Cell X-ray Irradiation treatment	48
2.7 Combination Therapy Treatments.....	49
2.7.1 Scheduled treatments	49
2.8 Clonogenic Assay	50
2.9 Combination Index Analysis.....	51
2.10 Glutathione Assay.....	52
2.11 Cell cycle	53
2.12 Apoptosis Detection	54
2.13 Comet Assay – Single cell gel electrophoresis.....	55
2.14 Western Blot Analysis	56
2.15 RNA extraction and quantification	57
2.16 RT-qPCR.....	57
2.17 Ferroptosis Assay	58
2.18 Spheroid Formation	58
2.19 Spheroid Treatment	59
2.20 Spheroid Analysis	59

2.21 Statistical Analysis	60
Chapter 3.....	61
Characterising single and combination treatments of Temozolomide and Monomethyl Fumarate on 2D Human Glioblastoma cell lines.....	61
3.1 Introduction.....	61
3.2 Aims	62
3.3 Materials and Methods.....	63
3.3.1 Combination and Scheduled treatments.....	63
3.4 Results	64
3.4.1 Determination of the MGMT status of UVW, U87 and T98g Human GBM cell lines	64
3.4.2 Assessing the cytotoxic effect of single therapies on human glioblastoma cell lines.	65
3.4.2.1 Assessment of the toxicity of Temozolomide, Dimethyl Fumarate and Monomethyl Fumarate on the UVW cell line.	66
3.4.2.2 Assessment of the toxicity of Temozolomide, Dimethyl Fumarate, Monomethyl Fumarate and Diroximel Fumarate on the U87 cell line.	67
3.4.2.3 Assessment of the toxicity of Temozolomide, Dimethyl Fumarate, Monomethyl Fumarate and Diroximel Fumarate on the T98g cell line.....	69
3.4.3 Developing the Temozolomide Monomethyl Fumarate combination in UVW, U87 and T98g cell lines.....	71
3.4.3.1 Cytotoxic effects of Temozolomide and Monomethyl Fumarate as single agents and in combination in the UVW human glioblastoma cell line.	73
3.4.3.2 Cytotoxic effects of Temozolomide and Monomethyl Fumarate as single agents and in combination in the U87 human glioblastoma cell line.	76
3.4.3.3 Cytotoxic effects of Temozolomide and Monomethyl Fumarate as single agents and in combination in the T98g human glioblastoma cell line	79
3.4.4 Determination of a scheduled administration for Monomethyl Fumarate	82
3.4.4.1 The effect of Monomethyl Fumarate on Glutathione levels over time in the UVW, U87 and T98g cell line.	83
3.4.5 Development of scheduled combination treatments in the UVW, U87 and T98g human glioblastoma cell lines.....	85
3.4.5.1 Cytotoxic effects of Temozolomide and Monomethyl Fumarate, when given as single therapies, as a combination and as a schedule in the UVW cell line.	85

3.4.5.2 Cytotoxic effects of Temozolomide and Monomethyl Fumarate, when given as single therapies, as a combination and as a schedule in the U87 cell line.	88
3.4.5.3 Cytotoxic effects of Temozolomide and Monomethyl Fumarate, when given as single therapies, as a combination and as a schedule in the T98g cell line.	91
3.4.6 Effects of Temozolomide and Monomethyl Fumarate on cell cycle progression in the UVW, U87 and T98g human glioblastoma cell lines.	94
3.4.6.1 Cell cycle analysis of UVW human glioblastoma cells lines after combination treatment exposure to Temozolomide and Monomethyl Fumarate.	95
3.4.6.2 Cell cycle analysis of U87 human glioblastoma cells lines after combination treatment exposure to Temozolomide and Monomethyl Fumarate.	98
3.4.6.3 Cell cycle analysis of T98g human glioblastoma cells lines after combination treatment exposure to Temozolomide and Monomethyl Fumarate.	101
3.4.7 Apoptotic/Necrotic induction in UVW human glioblastoma cells after treatment with Temozolomide and Monomethyl Fumarate.	104
3.4.7.1 Induction of Apoptosis after treatment with Temozolomide and Monomethyl Fumarate in the UVW human glioblastoma cell line.	105
3.4.7.2 Induction of Apoptosis after treatment with Temozolomide and Monomethyl Fumarate in the U87 human glioblastoma cell line.	108
3.4.7.3 Induction of Apoptosis after treatment with Temozolomide and Monomethyl Fumarate in the T98g human glioblastoma cell line.	111
3.4.8 Quantification of DNA damage and repair in UVW, U87 and T98g human glioblastoma cell lines after exposure to Temozolomide and Monomethyl Fumarate.	114
3.4.8.1 DNA damage response in the UVW human glioblastoma cell line after Temozolomide and Monomethyl Fumarate exposure.	116
3.4.8.2 DNA damage response in the U87 human glioblastoma cell line after Temozolomide and Monomethyl Fumarate exposure.	118
3.4.8.3 DNA damage response in the T98g human glioblastoma cell line after Temozolomide and Monomethyl Fumarate exposure.	120
3.4.9 Statistical analysis of Clonogenic Variability.	122
3.4.9.1 Statistical Comparison of UVW Temozolomide and Monomethyl Fumarate Data.	123
3.4.10.2 Statistical Comparison of U87 Temozolomide and Monomethyl Fumarate Data.	125
3.4.10.3 Statistical Comparison of T98g Temozolomide and Monomethyl Fumarate Data.	128
3.5 Discussion.	130

3.5.1 Cytotoxic effects of single therapies	131
3.5.2 Combination Development and Combination synergy	132
3.5.3 Schedule Development by glutathione depletion	134
3.5.4 Scheduled Combination development and synergy	135
3.5.5 Mechanistic Assay Cascade	137
3.5.5.1 Temozolomide.....	137
3.5.5.2 Monomethyl Fumarate	140
3.5.5.3 The simultaneous Combinations of Temozolomide and Monomethyl Fumarate	143
3.5.5.4 The scheduled combination of Temozolomide and Monomethyl Fumarate	145
3.6 Conclusion.....	149
Chapter 4.....	152
Evaluating the cytotoxicity of triple combination treatments on Human Glioblastoma cell lines in monolayer culture with Temozolomide Monomethyl fumarate and External beam X-irradiation.....	152
4.1 Introduction.....	152
4.2 Aims and Objectives	153
4.3 Materials and Methods.....	153
4.3.1 Combination and Scheduled treatments.....	153
4.4 Results	154
4.4.1 Assessing the Cytotoxicity of External beam X-irradiation on Human Glioblastoma cell lines.....	154
4.4.1.1 Cytotoxicity of External beam X-irradiation on the UVW, U87 and T98g cell line.	155
4.4.2 Assessing double combination cytotoxicity of external beam X-irradiation with Temozolomide and Monomethyl Fumarate on Human Glioblastoma cell lines.	157
4.4.2.1 Cytotoxicity of External beam X-irradiation and Temozolomide on the UVW cell line.	158
4.4.2.2 Cytotoxicity of External beam X-irradiation and Monomethyl Fumarate on the UVW cell line.	162
4.4.2.3 Cytotoxicity of External beam X-irradiation and Temozolomide on the U87 cell line.....	165
4.4.2.4 Cytotoxicity of External beam X-irradiation and Monomethyl Fumarate on the U87 cell line.....	168
4.4.2.5 Cytotoxicity of External beam X-irradiation and Temozolomide on the T98g cell line.	171

4.4.2.6 Cytotoxicity of External beam X-irradiation and Monomethyl Fumarate on the T98g cell line.....	174
4.4.3 Developing a double combination schedule of Monomethyl Fumarate with External beam X-irradiation on human glioblastoma cell lines.....	178
4.4.3.1 Cytotoxicity of External Beam X-irradiation when combined with Monomethyl Fumarate after a 4- hour pretreatment schedule on the UVW cell line.	178
4.4.3.2 Cytotoxicity of External Beam X-irradiation when combined with Monomethyl Fumarate after a 4- hour pretreatment schedule on the U87 cell line.....	181
4.4.3.3 Cytotoxicity of External Beam X-irradiation when combined with Monomethyl Fumarate after a 4- hour pretreatment schedule on the T98g cell line.	185
4.4.4 Cytotoxic response of External beam X-irradiation with Temozolomide and Monomethyl Fumarate given as a triple combination either simultaneously or as a schedule in human Glioblastoma cell lines	188
4.4.4.1 Cytotoxic effects of Temozolomide-Monomethyl Fumarate and External beam X-irradiation in the UVW cell line.....	189
4.4.4.2 Cytotoxic effects of Temozolomide-Monomethyl Fumarate and External beam X-irradiation in the U87cell line.....	192
4.4.4.3 Cytotoxic effects of Temozolomide-Monomethyl Fumarate and External beam X-irradiation in the T98g cell line	197
4.4.5 Combination Index Analysis of the simultaneous and scheduled administration of Temozolomide-Monomethyl fumarate and External beam X-irradiation in human Glioblastoma cell lines.....	202
4.4.5.1 Combination Index Analysis of the Temozolomide-Monomethyl Fumarate combinations with External beam X-irradiation in the UVW human glioblastoma cell line.....	203
4.4.5.2 Combination Index Analysis of the Temozolomide-Monomethyl Fumarate combinations with External beam X-irradiation in the U87 human glioblastoma cell line.....	205
4.4.5.3 Combination Index Analysis of the Temozolomide-Monomethyl Fumarate combinations with External beam X-irradiation in the T98g human glioblastoma cell line.....	207
4.5 Discussion	209
4.5.1 Cytotoxic effect of External beam X-irradiation on the human Glioblastoma cell lines.....	209
4.5.2 X-irradiation double combination cytotoxicity and synergy.....	210
4.5.3 Scheduled treatments of Monomethyl Fumarate with X-irradiation	213
4.5.4 Triple combination evaluation and synergy	215
4.6 Conclusions	218
Chapter 5.....	220

Assessing the effects of combination therapies using Temozolomide and Monomethyl Fumarate on three-dimensional spheroid models of Human Glioblastoma	220
5.1 Introduction.....	220
5.2 Aims	222
5.3 Results	223
5.3.1 Effects of Temozolomide on UVW and U87 3D Multicellular spheroid growth	223
5.3.1.1 The Effect of Temozolomide on UVW Multicellular Spheroid Growth over time.....	223
5.3.1.2 The Effect of Temozolomide on U87 Multicellular Spheroid Growth over time.....	225
5.3.2 Effects of Monomethyl Fumarate on UVW and U87 3D Multicellular Spheroid growth.....	228
5.3.2.1 Effects of Monomethyl Fumarate on UVW spheroid growth	228
5.3.2.2 Effects of Monomethyl Fumarate on U87 spheroid growth	231
5.3.3 Effects of External X- Beam Irradiation on UVW and U87 3D Multicellular Spheroid growth.....	233
5.3.3.1 Effects of External X- Beam Irradiation UVW spheroid growth	234
5.3.3.2 Effects of External X- Beam Irradiation U87 spheroid growth.....	236
5.3.4 Effects of combining Temozolomide and Monomethyl Fumarate on UVW and U87 3D Multicellular spheroid growth	239
5.3.4.1 The effect of combining Temozolomide and Monomethyl Fumarate on UVW spheroid growth.....	240
5.3.4.2 The effect of combining Temozolomide and Monomethyl Fumarate on U87 spheroid growth.....	243
5.5 Discussion	246
5.5.1 Effects of Temozolomide on 3D Multicellular tumour spheroid models.	247
5.5.2 Effects of Monomethyl Fumarate on 3D Multicellular tumour spheroid models.	248
5.5.3 Effects of External beam X-irradiation on 3D Multicellular tumour spheroid models.	250
5.5.4 Effects of combining Temozolomide and Monomethyl Fumarate on 3D Multicellular tumour spheroid models.	251
5.6 Conclusions	253
Chapter 6.....	254
Preliminary Study - Interrogating the varied response of Dimethyl Fumarate and Monomethyl Fumarate on 2D human Glioblastoma cell lines.	254
6.1 Introduction.....	254

6.2 Aims	257
6.3 Materials and Methods.....	257
6.3.2 Cell treatment.....	257
6.4 Results	258
6.4.1 Comparison of the effect of Dimethyl Fumarate and Monomethyl Fumarate on Glutathione depletion in the UVW, U87 and T98g human glioblastoma cell lines	258
6.4.1.1 Comparison of the effect of Dimethyl Fumarate and Monomethyl Fumarate on Glutathione levels in the U87 and T98g cell line.	258
6.4.2 Modulation of NrF2, P65, GPX4 and DJ1 after exposure to Monomethyl Fumarate and Dimethyl Fumarate on human glioblastoma cell lines via RT-qPCR.	260
6.4.2.1 The effect of Dimethyl Fumarate and Monomethyl Fumarate on NrF2, P65, GPX4 and DJ1 expression in the U87 and T98g cell line.....	261
6.4.3 Ferroptosis induction in human glioblastoma cells after treatment with Monomethyl Fumarate and Dimethyl Fumarate.....	267
6.4.3.1 Induction of Ferroptosis after exposure to Dimethyl Fumarate and Monomethyl Fumarate in the U87 cell line.....	268
6.4.3.2 Induction of Ferroptosis after exposure to Dimethyl Fumarate and Monomethyl Fumarate in the T98g cell line.....	271
6.5 Discussion	275
6.3.1 Glutathione Assay	275
6.3.2 RT-qPCR.....	278
6.3.2.1 NrF2	278
6.3.2.2 P65.....	279
6.3.2.3 GPX4.....	280
6.3.2.4 DJ1	281
6.3.2.5 RT-qPCR summary.....	282
6.3.3 Ferroptosis	283
6.6 Conclusions	285
Chapter 7.....	287
Conclusions and Future work.....	287
Chapter 8.....	290
References.....	290
Appendix	321
Appendix 1 – Cell Cycle Flow Cytometry Plots	321
Appendix 2 – Annexin V Flow Cytometry Plots	324

Appendix 3 – Comet Assay Images	326
Appendix 4 – Spheroid Images	327
Appendix 5 – RT-qPCR	332

List of Figures

Chapter 1

Figure 1.1: Glioblastoma management pathway.....	8
Figure 1.2: Glioma WHO grading, showing the development of primary and secondary GBM from a cell of origin.....	11
Figure 1.3: Origin of GSC.....	14
Figure 1.4: Patient treatment planning in Glioblastoma.....	25
Figure 1.5: Mechanism of Ionising radiation in radiotherapy, showing both the direct and indirect effect of ROS.....	28
Figure 1.6: TMZ schematic mechanism of action.....	31
Figure 1.7: Function of MGMT in GBM in relation to treatment resistance.....	33
Figure 1.8: The differences over time between development of de novo drug discovery and drug repurposing processing.....	35
Figure 1.9: Hypothesised mechanism of DMF-induced cell death in cancer cells.....	38
Figure 1.10: Mechanism of Michael addition (protein succination), the nucleophilic addition of the cysteine thiol group of GSH to DMF.....	40
Figure 1.11: The applications of glutathione depletion for treating cancer.....	42

Chapter 3

Figure 3.1: Human glioblastoma cell lines, UVW, U87 and T98g cell lysate western blot analysis for expression of MGMT.....	64
Figure 3.2: The effect on UVW glioblastoma cell clonogenic survival with increasing doses of treatment, Temozolomide, Dimethyl Fumarate, Monomethyl fumarate and.....	66

Figure 3.3: The effect on U87 glioblastoma cell clonogenic survival with increasing doses of treatment, Temozolomide, Dimethyl Fumarate, Monomethyl fumarate and.....	68
Figure 3.4: The effect on T98g glioblastoma cell clonogenic survival with increasing doses of treatment, Temozolomide, Dimethyl Fumarate, Monomethyl fumarate and.....	70
Figure 3.5: The dose response curves for the UVW human glioblastoma cell line to increasing doses of Temozolomide Monomethyl Fumarate and the combination of Temozolomide and Monomethyl fumarate.....	74
Figure 3.6: The dose response curves for the U87 human glioblastoma cell line to increasing doses of Temozolomide Monomethyl Fumarate and the combination of Temozolomide and Monomethyl fumarate.....	77
Figure 3.7: The dose response curves for the T98g human glioblastoma cell line to increasing doses of Temozolomide Monomethyl Fumarate and the combination of Temozolomide and Monomethyl fumarate.....	80
Figure 3.8: Relative glutathione levels of the UVW, U87 and T98g cell line after timed exposures Monomethyl Fumarate.....	83
Figure 3.9: Dose response curves for the UVW human glioblastoma cell line to increasing doses of Temozolomide, Monomethyl Fumarate, the simultaneously administered combination of Temozolomide and Monomethyl fumarate and the scheduled administered combination of Monomethyl fumarate followed by Temozolomide after 4 hours.....	86
Figure 3.10: Dose response curves for the U87 human glioblastoma cell line to increasing doses of Temozolomide, Monomethyl Fumarate, the simultaneously administered combination of Temozolomide and Monomethyl fumarate and the scheduled administered combination of Monomethyl fumarate followed by Temozolomide after 4 hours.....	89
Figure 3.11: Dose response curves for the T98g human glioblastoma cell line to increasing doses of Temozolomide, Monomethyl Fumarate, the simultaneously administered combination of Temozolomide and Monomethyl fumarate and the scheduled administered combination of Monomethyl fumarate followed by Temozolomide after 4 hours.....	92

Figure 3.12: Cell cycle progression in UVW cells treated with Temozolomide, Monomethyl fumarate, the Temozolomide-Monomethyl fumarate combination (T+M) and the scheduled administration of (T+M PT4) over 5 post treatment time points.....	96
Figure 3.13: Cell cycle progression in U87 cells treated with Temozolomide, Monomethyl fumarate, the Temozolomide-Monomethyl fumarate combination (T+M) and the scheduled administration of (T+M PT4) over 5 post treatment time points.....	99
Figure 3.14: Cell cycle progression in T98g cells treated with Temozolomide, Monomethyl fumarate, the Temozolomide-Monomethyl fumarate combination (T+M) and the scheduled administration of (T+M PT4) over 5 post treatment time points.....	102
Figure 3.15: Induction of apoptosis in UVW cells by Temozolomide, Monomethyl fumarate and the combination of Temozolomide and Monomethyl Fumarate combination given simultaneously (T+M) or in a schedule (T+M PT4) across 5 post treatment time points.....	106
Figure 3.16: Induction of apoptosis in U87 cells by Temozolomide, Monomethyl fumarate and the combination of Temozolomide and Monomethyl Fumarate combination given simultaneously (T+M) or in a schedule (T+M PT4) across 5 post treatment time points.....	109
Figure 3.17: Induction of apoptosis in T98g cells by Temozolomide, Monomethyl fumarate and the combination of Temozolomide and Monomethyl Fumarate combination given simultaneously (T+M) or in a schedule (T+M PT4) across 5 post treatment time points.....	112
Figure 3.18: Images of single cell gel electrophoresis after no treatment and little DNA damage or treatment which has caused DNA damage.....	115
Figure 3.19: DNA damage quantified as Tail Moment (AU) in the UVW cell line displayed as a percentage of the control mean after treatment with Temozolomide, Monomethyl Fumarate, the Temozolomide-Monomethyl fumarate combination (T+M) and the scheduled administration of (T+M PT4) across 4 post treatment time points.....	116

Figure 3.20: DNA damage quantified as Tail Moment (AU) in the U87 cell line displayed as a percentage of the control mean after treatment with Temozolomide, Monomethyl Fumarate, the Temozolomide-Monomethyl fumarate combination (T+M) and the scheduled administration of (T+M PT4) across 4 post treatment time points.....	118
Figure 3.21: DNA damage quantified as Tail Moment (AU) in the T98g cell line displayed as a percentage of the control mean after treatment with Temozolomide, Monomethyl Fumarate, the Temozolomide-Monomethyl fumarate combination (T+M) and the scheduled administration of (T+M PT4) across 4 post treatment time points.....	120
Figure 3.22: Comparison of the effect on UVW glioblastoma cell clonogenic survival after incubation with increasing doses of Temozolomide and Monomethyl-Fumarate after 24-hour exposure versus the untreated control.....	123
Figure 3.23: Comparison of the effect on U87 glioblastoma cell clonogenic survival after incubation with increasing doses of Temozolomide and Monomethyl-Fumarate after 24-hour exposure versus the untreated control.....	126
Figure 3.24: Comparison of the effect on T98g glioblastoma cell clonogenic survival after incubation with increasing doses of Temozolomide and Monomethyl-Fumarate after 24-hour exposure versus the untreated control.....	128
 Chapter 4	
Figure 4.1: The effect of increasing doses of X-irradiation on the clonogenic survival of UVW, U87 and T98g human glioblastoma cell lines.....	155
Figure 4.2: The effect of combining External beam X-irradiation with Temozolomide in the UVW cell line.....	159
Figure 4.3: The effect of combining External beam X-irradiation with Monomethyl Fumarate in the UVW cell line.....	163
Figure 4.4: The effect of combining External beam X-irradiation with Temozolomide in the U87 cell line.....	166
Figure 4.5: The effect of combining External beam X-irradiation with Monomethyl Fumarate in the U87 cell line.....	169

Figure 4.6: The effect of combining External beam X-irradiation with Temozolomide in the T98g cell line.....	172
Figure 4.7: The effect of combining External beam X-irradiation with Monomethyl Fumarate in the T98g cell line.....	175
Figure 4.8: The effect of combining external beam X-irradiation with Monomethyl Fumarate as simultaneous administration or as a 4- hour pretreatment of Monomethyl Fumarate (PT4) on the UVW cell line.....	179
Figure 4.9: The effect of combining external beam X-irradiation with Monomethyl Fumarate as simultaneous administration or as a 4- hour pretreatment of Monomethyl Fumarate (PT4) on the U87 cell line.....	182
Figure 4.10: The effect of combining external beam X-irradiation with Monomethyl Fumarate as simultaneous administration or as a 4- hour pretreatment of Monomethyl Fumarate (PT4) on the T98g cell line.....	185
Figure 4.11: The effect of combining External beam X-irradiation with Monomethyl Fumarate and Temozolomide as simultaneous administration or as a 4- hour pretreatment of Monomethyl Fumarate (PT4) followed by Temozolomide and X-irradiation on the UVW cell line.....	189
Figure 4.12: The effect of combining External beam X-irradiation with Monomethyl Fumarate and Temozolomide as simultaneous administration or as a 4- hour pretreatment of Monomethyl Fumarate (PT4) followed by Temozolomide and X-irradiation on the U87 cell line.....	193
Figure 4.13: The effect of combining External beam X-irradiation with Monomethyl Fumarate and Temozolomide as simultaneous administration or as a 4- hour pretreatment of Monomethyl Fumarate (PT4) followed by Temozolomide and X-irradiation on the T98g cell line.....	197
Figure 4.14: Combination index analysis of the Temozolomide-Monomethyl Fumarate combination with either 1Gy or 2Gy of X-irradiation, administered simultaneously or as a 4- hour pretreatment schedule of Monomethyl Fumarate in UVW human glioblastoma cells.....	203
Figure 4.15: Combination index analysis of the Temozolomide-Monomethyl Fumarate combination with either 1Gy or 2Gy of X-irradiation, administered simultaneously or	

as a 4- hour pretreatment schedule of Monomethyl Fumarate in U87 human glioblastoma cells.....**205**

Figure 4.16: Combination index analysis of the Temozolomide-Monomethyl Fumarate combination with either 1Gy or 2Gy of X-irradiation, administered simultaneously or as a 4- hour pretreatment schedule of Monomethyl Fumarate in T98g human glioblastoma cells.....**207**

Chapter 5

Figure 5.1: Combined representation of the different gradients in a spheroid section.....**221**

Figure 5.2: The UVW human glioblastoma multicellular spheroid growth curves (V/V₀) after treatment with increasing doses of Temozolomide over 24 days.....**224**

Figure 5.3: The U87 human glioblastoma multicellular spheroid growth curves (V/V₀) after treatment with increasing doses of Temozolomide over 24 days.....**226**

Figure 5.4: The UVW human glioblastoma multicellular spheroid growth curves (V/V₀) after treatment with increasing doses of Monomethyl Fumarate over 24 days.....**229**

Figure 5.5: The U87 human glioblastoma multicellular spheroid growth curves (V/V₀) after treatment with increasing doses of Monomethyl Fumarate over 24 days.....**231**

Figure 5.6: The UVW human glioblastoma multicellular spheroid growth curves (V/V₀) after treatment with increasing doses of External beam X-irradiation over 24 days.....**234**

Figure 5.7: The U87 human glioblastoma multicellular spheroid growth curves (V/V₀) after treatment with increasing doses of External beam X-irradiation over 24 days.....**237**

Figure 5.8: The UVW human glioblastoma multicellular spheroid growth curves (V/V₀) after treatment with Temozolomide, Monomethyl Fumarate and the combination of both given either simultaneously (T+M) or as a 4- hour MMF pretreatment (T+M PT4), over 24 days.....**241**

Figure 5.9: The U87 human glioblastoma multicellular spheroid growth curves (V/V₀) after treatment with Temozolomide, Monomethyl Fumarate and the combination of

both given either simultaneously (T+M) or as a 4- hour MMF pretreatment (T+M PT4), over 24 days.....**244**

Chapter 6

Figure 6.1: Proposed collective potential target pathways of DMF or MMF in GBM. DMF hydrolysis to MMF and modulation of the Nrf2, DJ1, GSH, GPX4, NF- κ B, IL-6 and TNF- α pathways.....**256**

Figure 6.2: Comparison of the effect of Dimethyl Fumarate and Monomethyl Fumarate on Glutathione levels in the U87 and T98g cell line.**259**

Figure 6.3: Modulation in U87 and T98g cells on Nrf2 (A) P65 (B) GPX4 (C) and DJ1 (D) gene expression after timed exposures of 4h and 24h to Monomethyl Fumarate and Dimethyl Fumarate quantified by RT-qPCR**263**

Figure 6.4: The effect on cell viability of the U87 cell line after exposure to Dimethyl Fumarate, Monomethyl Fumarate, RSL3, erastin, ferrostatin and the combination of Dimethyl Fumarate and Monomethyl Fumarate with ferrostatin.....**269**

Figure 6.5: The effect on cell viability of the T98g cell line after exposure to Dimethyl Fumarate, Monomethyl Fumarate, RSL3, erastin, ferrostatin and the combination of Dimethyl Fumarate and Monomethyl Fumarate with ferrostatin.....**272**

List of Tables

Chapter 1

Table 1.1: Glioma Grading by Who, incorporating the IDH mutation.....**4**

Table 1.2: The markers of GSCs.....**15**

Chapter 2

Table 2.1: Primer sequences used for each gene interrogated using RT-qPCR.....**58**

Chapter 3

Table 3.1: The combinations of Temozolomide and Monomethyl Fumarate used for the combination treatments and for the schedule treatments throughout Chapter 3.....	63
Table 3.2: UVW cell line Two-way ANOVA results to compare IC ₅₀ values between the repeated single curves for Temozolomide and Monomethyl Fumarate.....	124
Table 3.3: Summarised Bland Altman results from Graph-Pad Prism software, comparing the full data set for each clonogenic replicate for the UVW cell line.....	124
Table 3.4: U87 cell line Two-way ANOVA results to compare IC ₅₀ values between the repeated single curves for Temozolomide and Monomethyl Fumarate.....	126
Table 3.5: Summarised Bland Altman results from Graph-Pad Prism software, comparing the full data set for each clonogenic replicate for the U87 cell line.....	127
Table 3.6: T98g cell line Two-way ANOVA results to compare IC ₅₀ values between the repeated single curves for Temozolomide and Monomethyl Fumarate.....	129
Table 3.7: Summarised Bland Altman results from Graph-Pad Prism software, comparing the full data set for each clonogenic replicate for the T98g cell line.....	129

Chapter 4

Table 4.1: The combinations of Temozolomide and Monomethyl fumarate used for the combination treatments and for the schedule treatments throughout Chapter 4.....	154
---	------------

Chapter 5

Table 5.1: The concentrations of Temozolomide and Monomethyl Fumarate applied on the UVW and U87 cell line for combination studies on spheroid volume changes.....	236
--	------------

Chapter 6

Table 6.1: The concentrations of DMF and MMF used throughout chapter 6 studies.....	257
Table 6.2: The statistically significant findings only of the RT-qPCR data for the U87 and T98g cell line.....	264
Table 6.3: The concentrations of each treatment used in the ferroptosis assay throughout.....	267

List of Abbreviations

2HG – 2-hydroxyglutarate
AKT – Protein Kinase B
ARE – Antioxidant response elements
ARF – ADP ribosylation factors
AST-IDHMT – Astrocytoma-IDH Mutant
ATM – Ataxia telangiectasia mutated
ATR – Ataxia telangiectasia and Rad3-related protein
ATTC - American Type Culture Collection
AUC – Area under the curve
BBB – Blood Brain Barrier
BER – Base excision repair
BSA – Bovine serum albumin
CDK – Cyclin dependent kinase
CDKN2A – Cyclin-dependent kinase inhibitor 2A,
CHK – Checkpoint kinase
CI – Combination Index
CNS – Central nervous system
CNSCs - Central nervous system cancers
CSC – Cancer stem cells
CT – Computed tomography
Cys – Cysteine
Dj-1 – Parkinsonism-associated deglycase 1
DMF - Dimethyl Fumarate

DMSO – Dimethyl Sulfoxide
DNA – Deoxyribose nucleic acid
DSB – Double stranded breaks
DSB – Double stranded breaks
DT – Doubling time
EGFR – Epidermal growth factor receptor
ERK1/2 - Extracellular signal-regulated kinase
EMF – Diroxy methyl Fumarate
Fa/Fu – Fraction affected/fraction unaffected
FACs – Fluorescence-activated cell sorting
FAE – Fumaric acid esters
FDA – Food and drug administration
Fer-1 – Ferrostatin 1
FITC – Fluorescein isothiocyanate
GBM - Glioblastoma
GBM-IDHWT – Glioblastoma-IDH Wildtype
GI – Gastrointestinal
GLUT1 – Glucose transporter 1
GR – Glutathione reductase
GPX4 – Glutathione peroxidase 4
GSC – Glioma stem cells
GSH - Glutathione
GSSG - Glutathione disulphide
GST – Glutathione-s-transferase
GTR – Gross Total resection
Gy – Gray (radiation unit)
H2a.X – H2A histone family member
HER – Human EGFR related 1
HIF – Hypoxia inducing factor
HO-1 – Hemeoxygenase-1
IDH – Isocitrate dehydrogenase
IL – Interleukin

KEAP1 - Kelch-like ECH-associated protein 1
KPS – Karnofsky performance scale
Maf – Small Maf Proteins
MAPK – Mitogen associated protein kinase
MCTS – Multicellular tumour spheroid
MDM2 – Mouse double minute 2 homolog
MGMT – Methylguanine methyltransferase
MHRA – Medicines and healthcare products regulatory agency
MMF – Monomethyl Fumarate
MMR – Mismatch repair
MRI – Magnetic resonance imaging
Ms – Multiple Sclerosis
MTIC – 5-(3-methyltriazene-1-yl) imidazole-4-carboxamide
MTOR – Mammalian target of rapamycin
NADPH – Nicotinamide adenine dinucleotide phosphate,
NF1 – Nuclear factor I
NF- κ B - Nuclear factor kappa-light-chain-enhancer of activated B cells
Notch1 – Neurogenic locus notch homolog protein 1
NQO1 - NAD(P)H quinone oxidoreductase 1
NrF2 - Nuclear factor erythroid 2-related factor 2
NSC – Neural stem cells
OS – Overall survival
PBS – Phosphate buffered saline
PCR – Polymerase chain reaction
PDGF – Platelet-derived growth factor
PDK1 – Protein 3-phosphoinositide-dependent protein kinase-1,
PET – Positron emission tomography
PFS – Progression free survival
PHD – Prolyl hydroxylase
PI – Propidium iodide
PI3K – Phosphatidylinositol-3-kinase
PIP3 – Phosphatidylinositol (3,4,5)-trisphosphate

PT - Proton therapy
RT – Radiation therapy
PTEN – Phosphatase and tensin homolog
ROS – Reactive oxygen species
RSL3 – Ras selective Lethal 3
RT-qPCR – Reverse transcription quantitative polymerase chain reaction
RTK – Receptor tyrosine kinases
SD – Standard Deviation
SEM – Standard error mean
SSB – Single stranded breaks
STAT3 – Signal transducer and activator of transcription 3
TME – Tumour Microenvironment
TMZ – Temozolomide
TNF- α – Tumour necrosis factor
TP53 – Tumour protein P53
TRX – Thioredoxin
TTF – Tumour targeting fields
VEGF – Vascular endothelial growth factor
VPA – Vaporic acid
WHO – World health organisation

Abstract

Glioblastoma is the most aggressive and malignant subtype of brain and central nervous system cancers, accounting for >50% of all gliomas in adults. The glial tissue tumours cause over 1% of all cancer related deaths with the 5-year relative survival being 5% and 10-year survival rates being as low as 2%. Current treatments for the disease include, surgery, radiotherapy and the chemotherapy Temozolomide (TMZ), however in many cases the treatments fail due to a build-up of resistance to treatment causing aggressive recurrences. With increasing resistance in patients, the need for new novel treatment approaches is needed which minimise the burden of the disease on patients as well as the side effects. Monomethyl Fumarate (MMF) is a direct metabolite of Dimethyl Fumarate (DMF), a fumaric acid, currently used for the treatment of MS and psoriasis. Similarly to DMF, MMF has an inhibitory effect on the Nrf2 pathway regulating the antioxidant glutathione. We hypothesised that the inhibitory effects on glutathione are time-dependent and after 24 hours of treatment, MMF becomes an Nrf2 stabiliser, restoring its neuroprotective role against reactive oxygen species. Therefore, scheduling combinations of MMF with TMZ and radiotherapy would increase the treatment combinations efficacy by utilising the time window where glutathione levels have dropped to get the maximum response from the treatment combination. We have shown in three glioblastoma cell lines, U87, U87 and T98g that the combination of MMF with TMZ is synergistic in all cell lines, regardless of the cell DNA repair protein, MGMT status, when the combinations are scheduled. We also found the simultaneous combination to be synergistic when given simultaneously in the MGMT positive cell line T98g. Scheduling was assessed through glutathione detection over a range of time points. From our studies we have found the combination and MMF alone to initiate initial DNA damage, via comet assay. Triple combination studies of MMF, TMZ and RT also showed synergistic activity at both 1Gy and 2Gy doses. Glutathione assays, RT-qPCR and Ferroptosis assays were performed to distinguish differences between the fumarates and elucidated to a time and dose responsive effect of MMF and DMF on the cell lines. Differences in the GBM response to DMF and MMF were suggestive of an iron dependent, ferroptosis cell death pathway. However, future work is needed before development of MMF as a clinically relevant GBM therapeutic.

Covid Impact Statement

The laboratory work performed throughout this thesis began in August 2019 to September 2024 as a part time degree. Due to the impact of Covid-19, parts of this study were affected due to lockdown limitations, supply issues and time constraints. Between March 2020 and May 2021, access to the laboratory was limited to 2-3 days per week for social distancing purposes. This prevented the completion of some experiments such as murine models, radiation triple combination mechanistic experiments and the completion of triplicates in Chapter 6. I was able to obtain my personal animal handling licence from the home office and am completing *in vivo* work as part of my post-doctoral research. Additionally, it was planned for a more extensive analysis of the triple combinations, however the breakdown of our X-irradiator prevented the full chapter from being completed. Finally, it was hoped that further analysis by western blot assay would be performed to corroborate chapter 6 RT-qPCR data. However, due to time constraints these investigations will be completed as part of my post-doctoral position within the Boyd lab.

Additionally, there was many delays in the delivery of in certain essential plastics and reagents in some cases 6 months post covid which was a very limiting factor when carrying our experimental work. Therefore, the clonogenic assay method had to be altered and completed in 6 well plates from 60mm petri dishes.

Chapter 1

Introduction

1.1 Cancer

Cancer refers to a group of over 200 malignancies which ranks as the leading cause of death worldwide with it being the first or second cause of death in 112 of 183 countries (Sung *et al.*, 2021). The burden of cancer is growing rapidly worldwide due to the aging population with 19.3 million new cases of cancer in 2020 and 10 million deaths worldwide in 2020 (WHO, 2024). In the UK alone, between 2016-2018 there were 375,400 new cancer cases with someone being diagnosed with cancer every 2 minutes (CRUK, 2024). The most common cancers are breast, colorectal, prostate and lung cancer, with the male population having a higher incidence of disease than female (Santucci *et al.*, 2020; Zugazagoitia *et al.*, 2016). Over years of research, many cancers have better survival rates with survival doubling in cancer in general over the last 30 years (Santucci *et al.*, 2020). However, for aggressive cancers such as pancreatic, stomach and brain cancer, the survival rates remain as low as <20% in England and Scotland as of 2024 (CRUK, 2019).

Cancer arises from defects or mutations in the mechanisms that regulate cellular growth and division, leading to abnormal proliferation and the potential for metastasis (Stratton *et al.*, 2009). The “hallmarks of cancer,” first proposed in 2000, identified six key processes underpinning cancer development. These have since been expanded to include phenotypic plasticity, disrupted differentiation, a tumour-promoting microenvironment, and epigenetic reprogramming (Hanahan, 2022; Morgan *et al.*, 2022; Ravi *et al.*, 2022). These hallmarks function as an interconnected network, with variations across and within tumours highlighting the complexity and uniqueness of each cancer in its mutations, progression, and therapeutic needs (Floor *et al.*, 2012; Ravi *et al.*, 2022).

1.1.1 Brain and central nervous System Cancers

Brain and central nervous system (CNS) cancers are among the most fatal and rare forms of cancer, occurring in the brain and spinal cord. These cancers account for approximately 3% of total cancer cases worldwide and are the 8th most common cancer in individuals over 40 years old. With a low 5-year survival rate of ~15% and a poor prognosis, brain cancers are particularly challenging due to their location (Cancer Research, 2023; Miranda-Filho *et al.*, 2016; Ostrom *et al.*, 2021). The tumour's location can significantly affect neurological function, rendering even benign tumours potentially lethal (Huang *et al.*, 2022).

In 2020, 308,102 new cases of brain and CNS cancers were reported globally, along with 251,329 deaths attributed to these cancers. Data from 1990 to 2019 indicate a steady rise in the incidence of brain and CNS cancers, with predictions suggesting a further 0.14% annual increase in cases until 2035 (Hou *et al.*, 2024; Smittenaar *et al.*, 2016). The increasing number of cases in developed countries has been partly attributed to advancements in diagnostic imaging, such as MRI and CT scans, leading to the earlier and more frequent detection of brain and CNS tumours (Arnold *et al.*, 2019; Fan *et al.*, 2022). In contrast, lower incidence rates in developing countries are linked to delays in diagnosis and treatment, resulting in higher mortality rates (Fan *et al.*, 2022). Brain and CNS tumours account for 5.9% and 4.4% of cases in males and females, respectively, in developed countries compared to 3.3% and 2.7% in developing countries. These cancers are more prevalent in males (Khodamoradi *et al.*, 2017).

Despite decades of research, the global burden of brain and CNS cancers remains significant, and the identification of clear risk factors has proven elusive. The histological complexity of these tumours, comprising over 100 different subtypes, further complicates the search for causative factors (Ostrom *et al.*, 2021). These subtypes are defined by tissue based tests and molecular biomarkers (Louis *et al.*, 2021). As a result, the average survival for brain tumours remains at approximately 9 months, with a 5-year relative survival rate of <15%. While hypotheses have linked brain and CNS cancers to factors such as age, electromagnetic fields, ionising radiation, and pesticide exposure, the evidence for most of these factors is inconclusive, apart from ionising radiation, which will be discussed later (CRUK, 2023; Brown *et al.*, 2018; Pouchieu *et al.*, 2016).

1.1.2 Glioma Grading

Gliomas are a group of primary brain tumours and represent the most common form of cancer arising from the brain and central nervous system (CNS). Gliomas are primary tumours which are characterised by high morbidity and mortality and are responsible for 30% of all primary brain tumours and 80% of malignant tumours (Mesfin *et al.*, 2024; Śledzińska *et al.*, 2021; Weller *et al.*, 2015). Incidence of gliomas in adults varies depending on age, sex and location with between 1.9 to 9.6 cases per 100,000 (Śledzińska *et al.*, 2021). The primary brain tumours are grouped by their origin cells, which include astrocytic tumours (astrocyte cells), ependymomas (ependymal cells) and oligodendrogliomas (oligodendrocyte cells) (Hanif *et al.*, 2017).

To better understand the different categories of glioma the world health organisation (WHO) classified gliomas from stage I to IV with Glioblastoma (GBM) grouped as the most aggressive subtype IV (Bai *et al.*, 2020). The grading system is based on histological features and is important for prognosis and prediction of survival in patients. Additionally, in 2021 the WHO incorporated molecular changes within the cells most importantly the isocitrate dehydrogenase (IDH) mutation as part of the prognostic criteria (Mair *et al.*, 2021). This sub-group previously known as Glioblastoma multiforme was changed into Glioblastoma IDH-wildtype (WT) and Astrocytoma IDH- mutant (MT), both grade IV (Louis *et al.*, 2021). IDH-mutations are commonly found in lower grade gliomas and are associated with better prognosis (Bai *et al.*, 2020). Mutant IDH1 affects the cancer metabolism pathways by producing 2-hydroxyglutarate over α -ketoglutarate which IDH1 wildtype produces. α -ketoglutarate influences hypoxia-inducible factor subunit HIF-1 α , a transcription factor which promotes tumorigenesis. It's reported that GBM could arise from lower grade gliomas, making them what was previously known as "secondary GBM's", now known as astrocytoma IDH mutant. Patients with IDH-mutant phenotypes tended to be younger and with a better prognosis than the IDH-wildtype phenotype, as shown in Table 1.1 (Reuss, 2023; Wesseling and Capper, 2018;).

	WHO Grade	5-year survival	IDH Mutant	Anaplastic
Pilocytic Astrocytoma	I	90%	No	No
Oligodendroglioma Astrocytoma	II	78% 47.3%	Yes Yes	
Oligodendroglioma Astrocytoma	III	50.4 26.3%	Yes Yes	Yes
Glioblastoma	IV	5%	No	
Astrocytoma	IV	30%	Yes	

Table 1.1: Glioma Grading by WHO, incorporating the IDH mutation, 5-year survival and Anaplasia (Gareton *et al.*, 2020) (Agnihotri *et al.*, 2013) (Wesseling and Capper, 2018) (Antonelli and Poliani, 2022) (Okamoto *et al.*, 2004) (Ostrom *et al.*, 2014) (Louis *et al.*, 2021).

Grade I, Pilocytic astrocytoma's are common primary tumours making up 15.6% of all brain tumours and 5.4% of gliomas. Polycystic astros are commonly found in children with incidence decreasing with age and this grade of glioma has been described as having low proliferative potential and a better chance of survival after resection, with these tumours generally considered benign (Salles *et al.*, 2020).

Grade II-III gliomas, are rare malignant gliomas that account for approximately 30% of glial tumours and are made up of diffuse astrocytoma's and anaplastic astrocytoma's with grade II and III oligodendroglioma's (Mair *et al.*, 2021). Grade I and II are considered low grade gliomas, however wild-type IDH tumours have a significantly worse prognosis and are more likely to transform into higher grade tumours (Youssef and Miller, 2020).

1.2 Glioblastoma

Glioblastoma accounts for 57% of all gliomas and 48% of primary CNS malignant tumours and is the most malignant and lethal form of glioma, with an international incidence of 0.59-5 cases per 100,000 per year (Grech *et al.*, 2020; McKinnon *et al.*, 2021; Stark *et al.*, 2012; Yang *et al.*, 2022). GBM has a very poor prognosis, and tumours are hard to eradicate, even with advances in modern therapies due to its heterogeneity and increased resistance to treatments (Grochans *et al.*, 2022). GBM is highly diffuse and proliferating with genomic instability that causes invasion in patients (King and Benhabbour, 2021). GBM were originally thought to originate from glial cell lineage, however new research has shown GBM to arise from GBM stem cells derived from neural stem cells (NSC) and glial precursor cells (Ah-Pine *et al.*, 2023; Biserova *et al.*, 2021). These neural stem cells, reside in neurogenic niches and can proliferate in the adult brain, suggesting GBM may arise from these cells (Ah-Pine *et al.*, 2023; Biserova *et al.*, 2021). Development of GBM creates areas of hypoxia leading to angiogenesis in the trans-barrier space of the blood brain barrier (BBB) and changes the aquaporin protein family expression in the BBB, aiding the tumours progression (Silantyev *et al.*, 2019). The aquaporin protein family are intrinsic membrane proteins which transfer water and small solutes across the membrane (Varricchio and Yool, 2023). In GBM these aquaporins enhance glycolytic tumour cell metabolism in hypoxic areas supporting brain cancer growth by facilitating the uptake of substrates like glycerol that feed into glycolysis (Maugeri *et al.*, 2016).

GBM is difficult to define in terms of incidence as data is varied across the literature, it is however seen to increase in incidence with age, with the highest incidence seen in a population >75 years of age, which could be due to accumulations of genetic mutations over time (McKinnon *et al.*, 2021). Although GBM is commonly found more in an ageing population, the incidence in the paediatric population is 3-15% of all primary brain tumours (Grochans *et al.*, 2022). The age of diagnosis of GBM correlates to survival as the younger the patient the greater the chance of survival (McKinnon *et al.*, 2021; Ohgaki and Kleihues, 2005). GBM is also more prevalent in males than females with 5.6 male cases to 3.5 female per 100,000 population (Miller *et al.*, 2021). The median survival in adult patients is around 14.6 months with a 5-year survival of only 5% and after combination treatments, a 5-year survival of 27.2% (Batash *et al.*, 2017 Grech *et al.*, 2020; Schaff and Mellinghoff, 2023).

1.2.1 Aetiology

The aetiology of GBM is not well understood, with genetic and environmental factors being investigated such as age, sex, weight and demographic, all of which have been linked to incidence. However no single risk factor accounts for the majority of cases, making the disease sporadic. Some risk factors are associated with the disease such as alcohol consumption, exposure to magnetic fields, type 2 diabetes, BMI, radiation exposure, head injury and allergies, however the population where this is shown is small and does not equate to the population affected by the disease. Overall, the available data is inconclusive on any of these factors being causative (CRUK, 2023; Nelson *et al.*, 2012; Yoshikawa *et al.*, 2023).

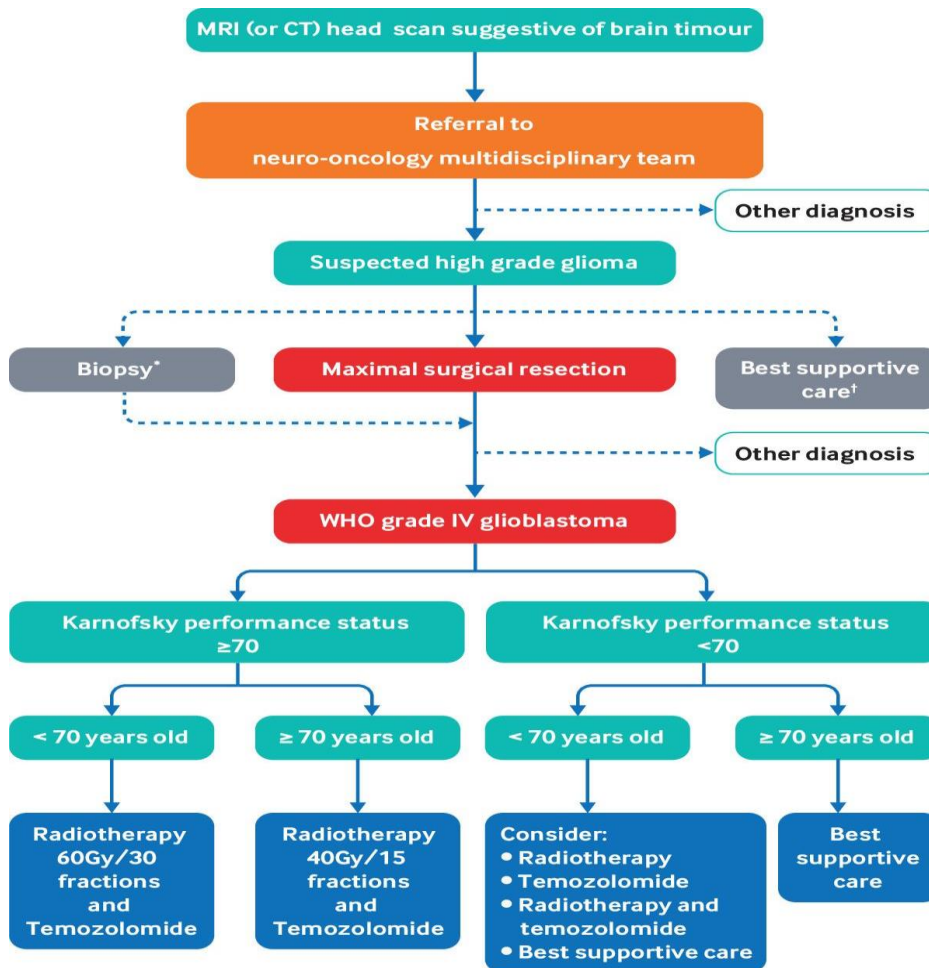
Exposure to ionizing radiation and certain inherited genetic disorders are the only proven risk factors for GBM. Ionizing radiation only accounts for 2.5% of cases and is linked to low doses of radiation used to treat children for cancers such as acute lymphocytic leukaemia, as well as low dose radiation for skin haemangioma leukaemia (Hanif *et al.*, 2017; Schaff and Mellinghoff, 2023). These children are at risk for GBM development later in life, due to their exposure at such a young age however it does not account for the bulk of the disease in the population, and further research is needed to find a potential causative factor, if there is one.

Familial cases of GBM have been observed although it is rare. GBM is not likely to appear in a family often and only occurs in 5% of all glioma cases (Backes *et al.*, 2015; Mukherjee *et al.*, 2020). The familial clusters of gliomas are connected to neoplastic syndromes such as Li-Fraumeni syndrome, nevoid basal cell carcinoma syndrome and neurofibromatosis type 1 and 2 (CRUK, 2023; Blumenthal and Cannon-Albright, 2008; Norris *et al.*, 2023). Again, this population is small and does not explain the major causative factor of the disease. However, in the remaining familial GBM cases some studies have shown mutations in tumour suppressor and promotor genes which can be linked to disease prognosis (Backes *et al.*, 2015; Fisher *et al.*, 2007). With few cases of familial GBM in the literature, it can be concluded that the disease occurs sporadically from build-up of genetic mutations over time. It is however useful for familial cases to be studied as it can highlight risk factors or overexpression of genes which could help in treating the disease.

1.2.2 Diagnosis and Prognosis

GBM as previously discussed, has low survival rates and poor prognosis, therefore early diagnosis is important to classify the tumour into a grade and for personal treatment plans to be put in place. The diagnostic tools are imaging techniques such as MRI, PET scans and neurological tests which are effective. However, too often patients are being diagnosed after the disease has progressed to advanced stages which is resulting in poor response to treatments and low survival rates (Silantyev *et al.*, 2019). GBM is not easy to identify in patients as it presents non-specifically and has similar signs and symptoms to other brain tumours and diseases, with approximately 50% of patients only diagnosed after emergency hospitalisation (McKinnon *et al.*, 2021). Headaches are the more common symptom, as well as visual disturbances and seizures, with the presentation of these varying due to the location, progression and size of the tumour (Dührsen *et al.*, 2019; Kirby and Purdy, 2014; Peeters *et al.*, 2020). Changes in sleep, concentration, depression and cognitive impairment are also symptoms, however collectively the symptoms tend to be widespread and therefore cannot be used for GBM diagnosis alone. As the disease is commonly seen at later stages of progression, after treatment, GBM almost always reoccurs with an increased invasiveness and aggressive behaviour which causes increased resistance to treatment which is also responsible for the poor long term survival rates (Stringer *et al.*, 2019).

As mentioned, diagnosis is performed with contrast enhanced CT scans, MRI scans, electroencephalogram and neurological tests, such as the Karnofsky performance scale test (KPS). The route of diagnosis to management is shown in Figure 1.1 taken from (McKinnon *et al.*, 2021).



*Consider biopsy if surgical resection not considered possible (for example, poor performance status).

†Consider if histopathological diagnosis cannot be made due to high risk of biopsy or very unfavourable prognosis.²⁹

Figure 1.1: Glioblastoma management pathway from diagnosis with MRI/CT followed by either biopsy, surgery or supportive care, confirmation of GBM. Following confirmation, patients are scored with Karnofsky performance score and age and treatment options are put in place (McKinnon *et al.*, 2021).

Once diagnosed as GBM grade IV, the Karnofsky performance scale/score (KPS) is carried out which is a measure of performance status and a method used to aid prognosis and treatment management (Chambless *et al.*, 2015). The system was originally used for systematic malignancies and determines disease impact and functional status by “scoring” patients on activity and medical care requirements from 0 to 100 (Yates *et al.*, 1980). In GBM patient functional independence is ranked by a score >70% and this determines a favourable prognosis. However, from Figure 1.1 we can see the age of the patient is important in prognosis also, as a favourable prognosis is seen in patients with an age of 70 years and younger and a KPS score

>70. Age is important in GBM, as previously discussed, as the disease presents later in life and the older the patient the poorer the prognosis, therefore both factors are considered when creating treatment plans (Elder and Chiocca, 2011; Grochans *et al.*, 2022). Older patients with low KPS scores may be offered aggressive treatment but these have shown to be less effective and can result in rapid neurological decline, therefore supportive care may be most appropriate (Elder and Chiocca, 2011). Treatment plans following a patient's KPS score and known age, can be modified to the patient as either more aggressive radiation and chemotherapy regimens, possible entry to clinical trial and further surgery. This tends to improve overall survival and progression free survival time in patients, although with treatment resistance, this improvement tends to be minimal (Hamisch *et al.*, 2017; Malakhov *et al.*, 2018; Socha *et al.*, 2016).

Prognosis in GBM is patient specific, due to each patient's age, KPS score, response to treatment, tumour location, tumour lesions, surgical resection status and molecular changes within the tumours (Delgado-Martín and Medina, 2020; Stark *et al.*, 2012). Molecular changes, which will be discussed later, such as IDH status, O6-methylguanine DNA methyltransferase (MGMT), tumour protein (p53), epidermal growth factor receptor (EGFR), phosphate and tensin homolog (PTEN) and the 1p, 19q chromosome codeletion, all play a role in patient outcome and response to treatment (Delgado-Martín and Medina, 2020; Karsy, 2015). These biomarkers of GBM provide information on the aggressiveness and pathophysiology of the disease which collectively if identified could assist disease prognosis and treatment. Effective targeted treatments and predictive markers are constantly under investigation to target tumours specifically in each patient, however with limited success over the years in patient survival, new ideas and approaches are required to improve the overall survival.

1.2.3 Glioblastoma IDH-Wildtype and Astrocytoma IDH-mutant

Glioblastoma's can be divided into two groups based on their IDH status, Glioblastoma IDH-Wildtype (GBM-IDHWT) and Astrocytoma IDH-Mutant (Ast-IDHMT), these subtypes are both WHO grade IV and receive similar treatments. GBM-IDHWT are most common, making up 90% of GBM tumours and appear in an

older population between 59 and 62 years of age (Delgado-López *et al.*, 2020; Li *et al.*, 2022). GBM-IDHWT is more aggressive, due to higher levels of anaplasia and therefore has a median survival of 4.7 months with most patients not surviving longer than 3 months after clinical diagnosis (Hanif *et al.*, 2017; Ohgaki and Kleihues, 2007). Ast-IDHMT presents in a younger population with a mean age of 45 and has a marginally better median survival rate of 7.8 months (Delgado-Martín and Medina, 2020; Ohgaki and Kleihues, 2007).

GBM-IDHWT develops *de novo*, in the first instance, and originates from either NSC or glial progenitor cells with a variety of common mutations that may be present including upregulated EGFR, TP53 mutations and PTEN mutations (Ah-Pine *et al.*, 2023). These GBM-IDHWT tumours proliferate rapidly, developing high grade lesions from onset (Kanderi *et al.*, 2024; Tso *et al.*, 2006). Ast-IDHMT is a secondary disease progressing from low grade glial tumours or anaplastic tumours (which are grade II or III respectively) (D'Alessio *et al.*, 2019; Ohgaki and Kleihues, 2013). Ast-IDHMT also tends to progress slower from its low-grade tumour and its earliest genetic change tends to be TP53 mutations (Ohgaki and Kleihues, 2007; Tso *et al.*, 2006). The difference in the development of both these grade IV tumours from a cell of origin and the approximate gene alterations at each stage in gene expression is illustrated in Figure 1.2.

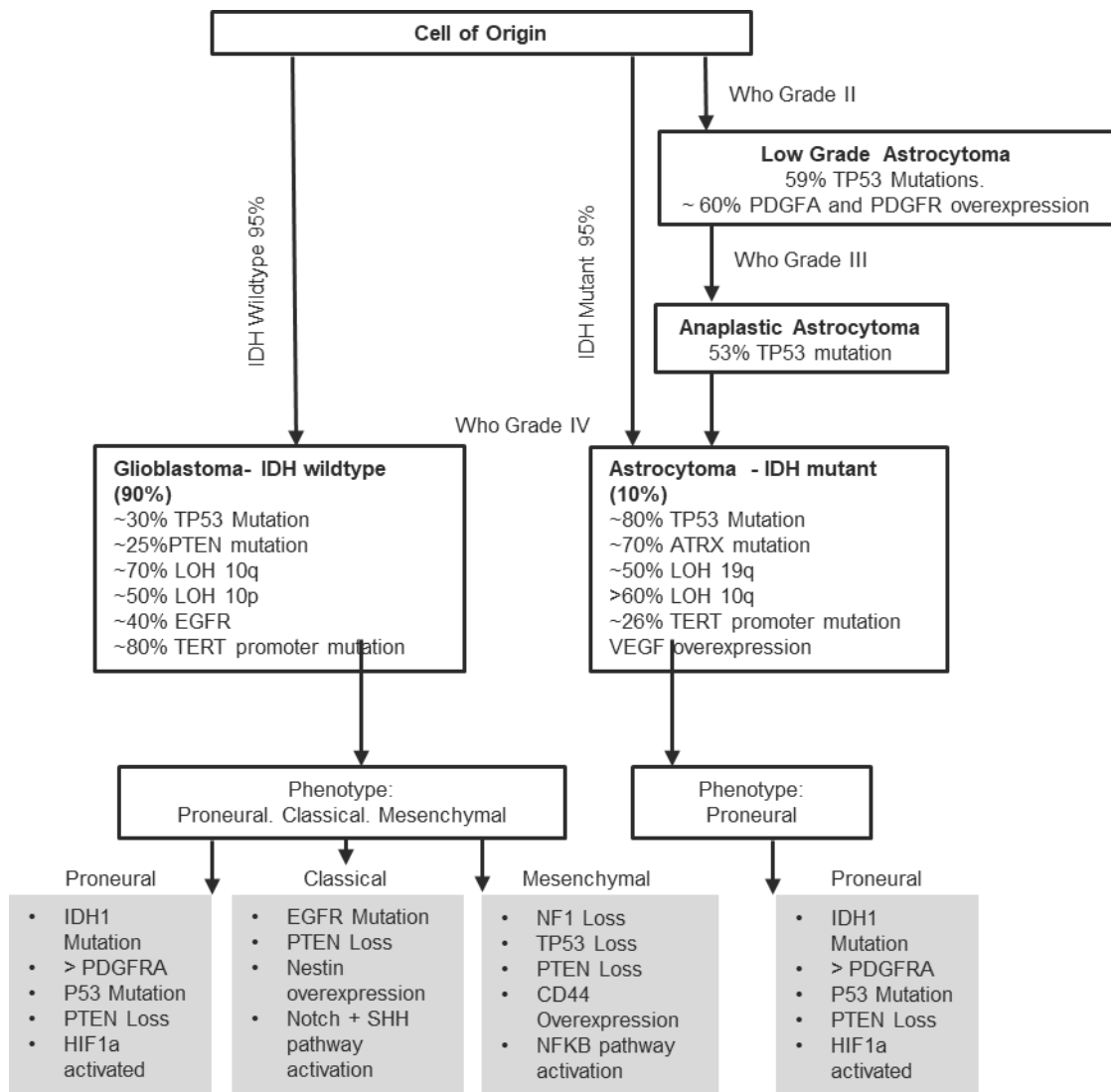


Figure 1.2: Glioma WHO grading, showing the development of Glioblastoma-IDHWT and Astrocytoma-IDHMT from a cell of origin and the approximate gene alterations at each stage simplified. The transcriptomic subclasses are also shown by phenotype with their alterations. Derived from (Agnihotri *et al.*, 2013; Delgado-López *et al.*, 2020; Hanif *et al.*, 2017; Ohgaki and Kleihues, 2007; Olar and Aldape, 2014; Silantyev *et al.*, 2019; Verhaak *et al.*, 2010).

GBM-IDHWT tumours predominantly have the IDH1 wildtype gene and only 5% have IDH1 mutations, giving them a lower overall survival. 95% of Ast-IDHMT GBM tumours have IDH1 mutations, making IDH1 status a definitive prognostic marker in GBM, with the IDH mutation being associated with an increase in overall survival (Delgado-López *et al.*, 2020; D'Alessio *et al.*, 2019; Ohgaki and Kleihues, 2007).

Mutated IDH1, as previously mentioned, can transform isocitrate into 2-hydroxyglutamate, an oncometabolite involved in impairing the function of epigenetic related enzymes. This leads to new DNA methylation profiles associated with tumorigenesis (Delgado-López *et al.*, 2020). With IDH being included in the WHO classification of glioma tumours, it has resulted in further research into the epigenetic alterations, and the mutated state of IDH has shown to affect the transcriptional profile of the tumours (Delgado-López *et al.*, 2020). Epigenetics describes the change in gene expression or cell phenotypes that do not alter the DNA sequence. Epigenetic modifications can be 'gained' during cell division and can also be reversed (Liu *et al.*, 2024).

The two subtypes of grade IV tumours are morphologically identical; however, both have distinct differences in genetic and epigenetic profiles which led to the development of further subtypes (Tso *et al.*, 2006; Wu *et al.*, 2021). As is demonstrated in the literature these subtypes of GBM, showed variations in transcriptomic profiles, somatic genomic alterations and DNA methylation within the disease which created a further four subclasses termed proneural, neural, mesenchymal and classical (Bv and Jolly, 2024; Lee *et al.*, 2018). These four subtypes were classified at transcriptomic level through the genes they highly express as illustrated in Figure 1.2 (Olar and Aldape, 2014; Verhaak *et al.*, 2010). As the literature progressed and new data analysis techniques were performed, this was simplified down to proneural, proliferative and mesenchymal, based on prognostic value and dominant gene features, with neural seen as contaminated healthy brain tissue and no longer regarded as a subtype (Lee *et al.*, 2018; Wang *et al.*, 2017; Wu *et al.*, 2021). Proneural subtypes have better prognosis and express genes linked to normal brain function, they are highly prevalent in IDH1/2 mutations and TP53 mutations, therefore making up most of the Ast-IDHMT cases (Phillips *et al.*, 2006). Mesenchymal GBM is highly proliferative, with poor prognostic outcome and overexpression of nuclear factor 1 (NF1), TP53 and PTEN, with CD44 and nuclear kappa-light chain enhancer of activated B cells (NF-κB) activation linked to the poor prognosis (Delgado-López *et al.*, 2020). The classical or proliferative subtype has overexpression of proliferative markers, such as EGFR and expression of neural stem cell markers such as nestin, with a common chromosome 7 amplification and chromosome 10 loss (Lee *et al.*, 2018; Verhaak *et al.*, 2010; Wu *et al.*, 2021).

The classifications described above were investigated to improve patient outcomes by integrating genomic and epigenomic profiling into tumour characterisation. This approach is based on the premise that a deeper understanding of the molecular drivers of gliomagenesis - such as IDH mutation status, transcriptional profiles, and epigenetic alterations - can support the development of more effective, tailored therapies (Lee *et al.*, 2018). While our knowledge of GBM biology has advanced considerably, translating these insights into successful treatments remains challenging. This is largely due to the complexity of the disease, which includes both inter- and intra-tumour heterogeneity. The literature attributes this variability to several factors, including the presence of cancer stem-like cells, the influence of the tumour microenvironment, and the diffuse infiltrative nature of glioblastoma (Li *et al.*, 2022).

1.2.4 GBM cancer stem cells

Cancer stem cells (CSC) or tumour initiating cells have been vastly researched recently due to the part they may play in tumour progression and resistance to treatment in malignant cancers (Biserova *et al.*, 2021). Stem cells are pluripotent, self-renewing cells which generate daughter cells, more stem cells and replace functional cells. Neural stem cells (NSC) were reported in the literature by de Almeida Sassi *et al.*, (2012), which reported the cells' ability to preserve its proliferative capacity in the brain. This demonstrated that these cells would differentiate into neurons, astrocytes and oligodendrocytes (Biserova *et al.*, 2021). The concept of CSCs is controversial as many of the stem cell properties such as self-renewal and proliferation are seen in many cancers, as previously described as a hallmark of cancer.

In GBM, glioma stem cells (GSC) are a small sub-population of tumour cells, which are like the NSCs in their functional similarities (D'Alessio *et al.*, 2019). GSC's are thought to arise from activation of oncogenic pathways within NSC (Ah-Pine *et al.*, 2023). Glioma stem cells were discovered in IDH wildtype GBM by their surface markers, CD133, CD44, PDGFRA and EGFR *in vivo* (Suvà and Tirosh, 2020). GSCs can differentiate into multiple cell lineages, self-renew, proliferate, invade and modulate the immune response. The presence of GSCs can explain the heterogeneity of GBM tumours, their ability to quickly renew tumours post treatment and the distinct differences in phenotype such as classical or proneural (Lee *et al.*, 2018; Vollmann-

Zwerenz *et al.*, 2020). The origin of the mesenchymal phenotype however has yet to be eluded as literature suggests a phenotypic shift from proneural to mesenchymal or that the cells originate from neural crest derived cells as they share surface markers (Ah-Pine *et al.*, 2023; Hamed *et al.*, 2025).

The GSCs represent a small subpopulation of GBM cells and can upregulate signalling pathways to ensure stemness and consequently tumorigenesis, making GSCs a relevant target for GBM eradication (Liebelt *et al.*, 2016). Similarly to the molecular subtypes of GBM from transcriptomics, GSCs can also be grouped by molecular subtype with both mesenchymal and proneural GSCs reported in the literature which mimic characteristics of the GBM groups (Guardia *et al.*, 2020). These GSC could explain GBM tumours switching subtype between proneural and mesenchymal subtypes, as either the GSCs can make the switch or a small number of both cell types are present within the tumours and the mesenchymal survive better and reform the tumours (Biserova *et al.*, 2021). The hypothesised transition of NSC to GSC is shown in Figure 1.3. This potential explanation for the recurrence of GBM, could improve patient outcome as treatments could be targeted to the GSCs and prevent the tumours from reforming post treatment.

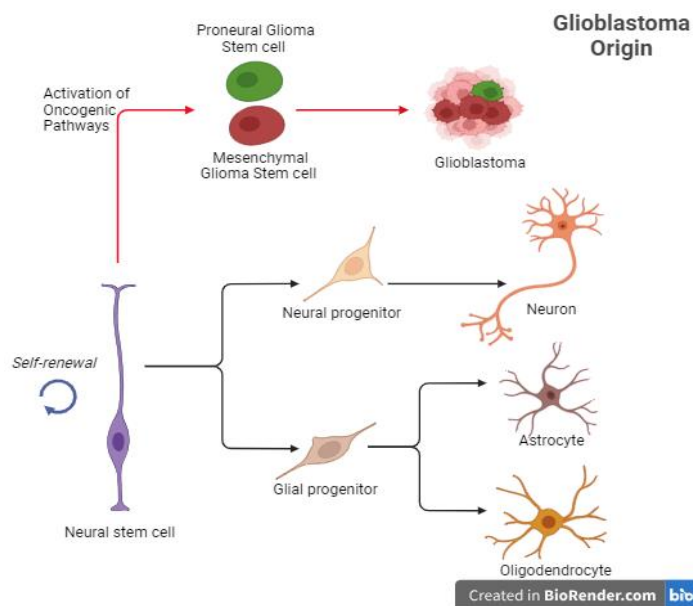


Figure 1.3: The hypothesised transition from neural stem cell to glioma stem cell subtypes proneural or mesenchymal. Adapted from (Biserova *et al.*, 2021; Tang *et al.*, 2017; Wang *et al.*, 2021), Created using Biorender.com

A problem with targeting the GSCs described in the literature by (Sattiraju *et al.*, 2017), was the hypoxic or necrotic environments in which they reside often making it hard to penetrate through or access with current treatments. Additionally, cells would be quiescent i.e., lying dormant, with slow or halted cell cycle progress making them further resistant to treatments which target proliferating cells (Wang *et al.*, 2021). Many markers of GSCs have been found with many signalling pathways implicated in the promotion of these cells, these have been highlighted in Table 1.2

GSC Marker	Significance
CD133	Used to identify CSC
Nestin	Cells with Nestin markers have increased tumour forming capacity
SSEA-1	Co-expression with CD133
Integrin- α 6	Overexpressed in GSCs. Promotes self-renewal
A2B5	Linked to tumour initiation

Table 1.2: Highlights the markers of GSCs which promote the “stem like” quality of the cells. Derived from (Biserova *et al.*, 2021)

1.2.4.1 Tumour Microenvironment and niche

The tumour microenvironment (TME) in GBM is a complex heterogenous system containing not only cancer cells, but immune cells and various non-cancerous brain cells. The TME is highly influenced by cell interactions, metabolic products and chemical factors (Sharma *et al.*, 2023). The TME niche in GBM is where GSCs are found, and is composed of endothelial cells, NSCs, brain cells, immune cells, signalling molecules, and extracellular matrix components (ECM), making it a dynamic ecosystem (Sharma *et al.*, 2023). Niches are areas of maximum expression of the TME to maintain stemness, and in GBM we see perivascular and hypoxic niches with many forms of neovascularization, aiding the tumour cells with access to oxygen and nutrients to survive (Sattiraju *et al.*, 2017). The high vascularisation of GBM is associated with the GSCs present in the perivascular niche that interact with endothelial cells to promote invasion and growth, as they cross talk with other GSCs in other niches (Ho and Shim, 2017). Hypoxia is a critical factor in GBM, with it

influencing the response to treatment. Hypoxic niches contain GSCs, again directly influencing the self-renewal, invasive and survival signalling pathways involved in GBM.

Therefore, from the literature, the lack of progress in effective treatments is hampered due to these different factors; grade, age, subtype, subclass, GSC, TME, niches, crosstalk, shifts in subtype and all the obscured signalling which occurs at each stage, creating an almost impossible maze to overcome.

1.3 Pathology, genetic mutations and molecular biology of GBM

Cancers are developed through a build-up of mutations in the cells which over time leads to the development of one or more of the hallmarks of cancer as previously discussed. With these mutations in the genes and corresponding aberration of signalling pathways, the loss of cell regulatory mechanisms leads to tumorigenesis.

GBM is a complex cancer with cellular, metabolic, immune and genomic disruption that causes the significant tumour heterogeneity. The process of gliomagenesis is not singular, with many cells undergoing genetic alterations and epigenetic changes causing activation of proto-oncogenes and inhibition of tumour suppressor genes (Esemen *et al.*, 2022).

The DNA damage response (DDR) is a critical mechanism in maintaining genomic integrity by coordinating DNA repair, cell cycle checkpoints, and cell death pathways (Rominiyi and Collis, 2022). Under normal conditions, the cell cycle is regulated by checkpoints controlled by cyclin-dependent kinases (CDKs) and TP53. These factors phosphorylate downstream proteins to facilitate DNA synthesis and repair (Esemen *et al.*, 2022). In response to DNA damage, TP53 activation halts the cell cycle, inducing apoptosis or allowing for repair.

Cell cycle and apoptosis are important biological processes in a cell, allowing growth and homeostasis (Gousias *et al.*, 2022). Changes to the processes of cell cycle can lead to tumorigenesis. The cycle itself is divided into four phases, the G1 phase where cell growth occurs, S phase where DNA is synthesised, G2 phase where the cell is prepped for mitosis and M phases where mitosis occurs. Alternatively, these can be divided into 2 phases, interphase (G1, G2 and S) and mitosis. Within the cell cycle,

several metabolic states are seen, quiescence, most commonly during the G₀ phase where cells can reverse growth arrest and have lower metabolisms (Zarneshan *et al.*, 2023). Cells may be in a metabolic state of senescence, where they are in permanent cell cycle arrest. Cells are able to come out of quiescence via stimulation from the cyclins, such as cyclin dependent kinase-2 (Gousias *et al.*, 2022). Both states of arrest are triggered by external and internal stimulation such as DNA damage, ROS and ionising radiation (Zarneshan *et al.*, 2023).

Cells can also be in apoptosis or necrotic states, with apoptosis being an energy dependent mode of programmed cell death and necrosis an energy independent process after cell death (Gousias *et al.*, 2022). Severely damaged cells can induce death without the need for apoptosis, as apoptosis functions to maintain homeostasis. Caspases are a group of cysteine proteases with initiators and effectors which regulate apoptosis (Dong *et al.*, 2018).

In GBM, the cell cycle process is dysregulated due to various mutations and overexpression of factors related to the cellular pathways controlling cell cycle. P53 as previously discussed is mutated in both GBM-IDHwt and Ast-IDHMT, as well as upregulation of the P13/AKT pathway and NF- κ B pathway. The upregulation of these pathways in GBM causes evasion of apoptosis, unregulated replication, apoptosis and neuroinflammation (Gousias *et al.*, 2022).

In glioblastoma, DDR pathways are frequently compromised due to dysregulated signalling, resulting in failure to arrest the cell cycle or initiate apoptosis. This leads to uncontrolled proliferation and tumour growth (Dietlein *et al.*, 2014; Majd *et al.*, 2021). Paradoxically, the DDR is often upregulated in GBM, due to increased hypoxia and therefore ROS (Begg and Tavassoli, 2020). It is also upregulated due to high genomic instability caused by mutations in tumour suppressor genes (Mazzoleni *et al.*, 2024). The upregulation of the DDR enables tumour cells to repair DNA damage caused by therapeutic agents, contributing to treatment resistance (Majd *et al.*, 2021). TP53 mutations, common in GBM, further impair DDR function, promoting genetic instability and gliomagenesis (Leung *et al.*, 2000; Rominiyi and Collis, 2022).

Deficiencies in DNA repair mechanisms create mutational signatures within the tumour genome, driving the heterogeneity characteristic of GBM. Each subgroup of GBM, GBM-IDHWT and AST-IDHMT, and subtypes such as proneural, classical, and mesenchymal exhibit distinct genetic aberrations identified through omics studies (Figure 1.2). Key mutations frequently observed include IDH1/2, MGMT, EGFR,

PTEN-PI3K, TP53, and HIF-1 α , all of which contribute to glioblastoma's aggressive phenotype and will be explored in detail below (Wrensch *et al.*, 2005).

1.3.1 Isocitrate Dehydrogenase 1 and 2

Isocitrate dehydrogenase (IDH) plays a pivotal role in glioblastoma (GBM) and is recognized by the WHO as an important histopathological marker (Grochans *et al.*, 2022). IDH1 and IDH2 encode enzymes critical to the Krebs cycle, facilitating the oxidative decarboxylation of isocitrate to produce CO₂ and α -ketoglutarate, alongside nicotinamide adenine dinucleotide phosphate (NADPH) generation (El Khayari *et al.*, 2022; Karsy, 2015). IDH1, a cytosolic protein, and IDH2, a mitochondrial protein, function as homodimers. Mutations in IDH1 are far more prevalent than those in IDH2, constituting 95% of IDH mutations observed in gliomas (Molenaar *et al.*, 2014).

NADPH is essential for maintaining cellular antioxidants such as glutathione, which protect GBM cells from DNA damage caused by ionizing radiation (Wahl *et al.*, 2017). Additionally, α -ketoglutarate serves vital roles in nitrogen scavenging and as a source of glutamate for protein synthesis within the Krebs cycle (Wu *et al.*, 2016). Wildtype IDH1 promotes tumour progression by supporting fatty acid synthesis and scavenging reactive oxygen species (ROS). It further aids hypoxic tumour cells by enabling glutamine-dependent carboxylation for lipid synthesis. Inhibiting wildtype IDH1 under hypoxic conditions has been shown to impair GBM cell proliferation (Alzial *et al.*, 2022).

Mutant IDH1, a heterodimer of wildtype IDH, acquires a neomorphic function, reducing α -ketoglutarate to produce the oncometabolite 2-hydroxyglutarate (2HG) (Aldape *et al.*, 2015). This mutation often arises early during gliomagenesis. 2HG inhibits prolyl-hydroxylase (PHD) enzymes, which in turn disrupts hypoxia-inducible factor-1 α (HIF-1 α) activity (El Khayari *et al.*, 2022; Agnihotri *et al.*, 2014). The relationship between mutant IDH1 and HIF-1 α remains complex: while HIF-1 α and its targets (e.g., GLUT1, VEGF, and PDK1) are typically associated with poor prognosis, some studies suggest that mutant IDH1 destabilizes and degrades HIF-1 α , leading to better outcomes (Liu *et al.*, 2016; Molenaar *et al.*, 2014).

Mutant IDH1 also impacts epigenetic regulation. Accumulation of 2HG or depletion of α -ketoglutarate inhibits enzymes involved in DNA and histone demethylation,

contributing to CpG island methylation and MGMT promoter methylation phenotypes. These epigenetic changes are associated with better prognosis in IDH-mutant gliomas (Aldape *et al.*, 2015; Wang *et al.*, 2022). Clinically, IDH mutations provide a significant prognostic advantage. Reduced NADPH production sensitizes tumour cells to treatment and starves cancer cells in hypoxic niches. Median survival in patients with IDH-mutant GBM is improved by approximately 16 months compared to those with wildtype IDH (Han *et al.*, 2020).

1.3.2 Methylguanine Methyltransferase (MGMT)

Non-cancerous cells have several repair processes for resolution of DNA damage such as the mismatch repair system (MMR), base excision repair (BER), single stranded break (SSB) repair, double stranded break (DSB) repair and direct repair systems (Erasimus *et al.*, 2016; Rominiyi and Collis, 2022). MGMT is a suicide DNA repair enzyme, meaning it can only repair one DNA lesion as it uses a cysteine residue in its active site to transfer the methyl group from the DNA, onto itself resulting in irreversible inactivation (Nguyen *et al.*, 2021). The MGMT enzyme functions by repairing guanine nucleotides on DNA, damaged by alkylating agents. MGMT transfers the methyl group at the O⁶ site of guanine to its cysteine residue on the DNA, preventing cell death (Yu *et al.*, 2020). Epigenetics is the change in gene expression by either DNA methylation, histone modification, non-coding RNA regulation and chromatin remodelling, which does not affect the DNA sequence (Liu *et al.*, 2024). Epigenetic modifications regulate the expression of MGMT and in GBM loss of MGMT expression is due to the methylation of CpG island in the MGMT promoter, preventing the synthesis of MGMT, (Butler *et al.*, 2020; Sharma *et al.*, 2009).

Tumour cells can reverse damage caused by treatments which induce DNA damage by initiating the repair mechanisms. In GBM the current standard of care chemotherapy is temozolomide (TMZ) an alkylating agent, which acts by methylating DNA (Nguyen *et al.*, 2021). In GBM, MGMT status in patients is a biomarker in evaluating how the patient will respond to TMZ treatment. Unmethylated MGMT is a cause of treatment resistance, as it repairs the alkylating DNA damage caused by TMZ (Erasimus *et al.*, 2016). GBM patients with a methylated MGMT have shown an improvement in overall survival by ~50% compared to unmethylated MGMT promoter patients, with median survival improved from 12.7 months in MGMT unmethylated

patients to 21.7 months in MGMT methylated patients (Chen *et al.*, 2017; Wen *et al.*, 2020). MGMT status is therefore used by oncologists to determine patient treatment options, with various studies showing an estimated 50% of patients to have MGMT methylation (Butler *et al.*, 2020; Chen *et al.*, 2017; Szyberg *et al.*, 2022). However, with few alternatives TMZ is still given to MGMT positive patients as both age and KPS score are factors in determining how a patient will respond (Fisher and Adamson, 2021). Additionally, studies have shown a small population of MGMT positive patients to still be responsive to TMZ (Maher and Bachoo, 2025; Wick *et al.*, 2012). However, MGMT methylation is found more commonly in lower grade tumours, Ast-IDHMT patients compared to GBM-IDHWT patients and therefore remains an important prognostic factor (Maher and Bachoo, 2025; Nakamura, 2001)

MGMT status therefore plays an important prognostic role in the outcome of GBM patients, however the status of promoter methylation is not as black and white as first assumed with research showing evidence as to why MGMT negative patients would still acquire resistance or not benefit from TMZ treatment as expected which will be discussed later.

1.3.3 EGFR

The Epidermal growth factor receptors (EGFR) are a family of single chain transmembrane proteins, and subclass of receptor tyrosine kinase (RTK) proteins (Murphrey *et al.*, 2024). Human EGFR related 1 (HER) or ErbB1 is the transmembrane receptor of tyrosine kinase EGFR which is located on chromosome 7p11.2 (Oprita *et al.*, 2021). EGFR is activated by epidermal growth factor, transforming growth factor α (TGF α) or other ligands. EGFR activation causes a cascade of downstream signalling activation including the MAPK/PI3K pathway, MTOR complex 1/ 2 activation, STAT 3 and various other targets ultimately leading to DNA synthesis and cell proliferation (Saadeh *et al.*, 2018). EGFR variant III (vIII), is a common mutation of EGFR caused by deletion of exons 2 through 7, causing constitutive EGFR activation and unregulated cell growth (Pan and Magge, 2020). The mutated EGFR activates similar downstream pathways to unmutated EGFR, which control cell cycle regulation and additionally neural stem cell regeneration. EGFRvIII upregulates vascular endothelial growth factor (VEGF), interleukin 8 (IL-8)

and NF- κ B. This upregulation ultimately leads to angiogenesis and tumour progression (Wu *et al.*, 2004).

In cancer, molecular alterations to EGFR include overexpression, partial gene deletion or amplification and it is therefore known as a potent oncogene (Saadeh *et al.*, 2018). EGFR amplification is commonly seen in GBM-IDHWT (Figure 1.2) with 57.4% of patients showing the amplification, 60% showing overexpression and 24-67% with an EGFR mutation caused by partial gene deletion (Brennan *et al.*, 2013; Saadeh *et al.*, 2018). In GBM, EGFR is upregulated or amplified to cause invasion, proliferation and resistance to treatment (Oprita *et al.*, 2021). Studies on EGFR expression suggested its role as a prognostic factor in GBM, however in long term studies the alteration of EGFR has no impact on patient survival or prognostics (Karsy, 2015).

Due to EGFR's dysregulation in GBM being so prevalent, it was targeted as a therapeutic approach for the disease. Much research was carried out to test small molecule receptor tyrosine kinase inhibitors, such as Gefitinib and Erlotinib, however these did not show efficacy in trial (Oprita *et al.*, 2021). Many other approaches such as the use of various nanoparticles, targeting gene expression and EGFR targeted Car-T cells, have either seen therapy resistance, targeting failure due to the BBB or are still in early trials (Westphal *et al.*, 2017). The complexity of EGFR and its signalling pathways has caused a loss of attraction for treatment development, mainly due to issues with penetrating the BBB.

1.3.4 PTEN and P13K Signalling

Phosphate and tensin homolog (PTEN) is a key tumour suppressor gene that inhibits cell growth and proliferation while promoting apoptosis (Fusco *et al.*, 2020). PTEN exerts its effects both dependently and independently of the phosphatidylinositol-3-kinase (PI3K)/protein kinase-B (AKT) pathway, including inhibition of the PI3K/AKT/MTOR pathway (Hashemi *et al.*, 2023). PTEN mutations or depletion occur in approximately 30% of GBM cases, with low PTEN expression correlating to poorer prognosis.

The PI3K/AKT/MTOR pathway is dysregulated in 90% of GBM patients, driving tumour cell proliferation, invasion, and metastasis (Khabibov *et al.*, 2022). Activation

begins with receptor tyrosine kinases (RTKs) phosphorylating PI3K, producing phosphatidylinositol (3,4,5)-trisphosphate (PIP3), which in turn activates PDK1 and PDK2. These kinases phosphorylate AKT and MTOR, promoting protein synthesis, cell survival, and division (Daisy Precilla *et al.*, 2022). PTEN loss and EGFR upregulation further hyperactivate this pathway, fostering gliomagenesis and resistance to therapy (Hashemi *et al.*, 2023).

Therapeutic strategies targeting the PI3K/AKT/MTOR pathway show promise. Curcumin and demethoxycurcumin have been investigated for their ability to induce PTEN and inhibit PI3K/AKT signalling (Hashemi *et al.*, 2023). Additionally, pharmacological inhibitors such as paxalisib and idelalisib target this pathway, with idelalisib receiving FDA approval in the US and MHRA approval in the UK for chronic lymphocytic leukaemia (Liu *et al.*, 2022). Understanding and modulating PTEN and PI3K interactions remain critical for GBM treatment advancements.

1.3.5 p53

Tumour suppressor genes, like TP53, typically exist as two copies; in many cancers, one copy is deleted, and mutations in the remaining copy led to loss of function. TP53 encodes the P53 protein, which plays a central role in tumour prevention by maintaining genomic stability, inhibiting angiogenesis, regulating the cell cycle, and initiating apoptosis. P53 halts the cell cycle at the G1 and G2/M checkpoints, allowing time for DNA repair or driving apoptosis if damage is irreparable (Kastenhuber and Lowe, 2017; Zhang *et al.*, 2018).

Functionally, P53 is a homotetramer with distinct domains responsible for transcription, DNA binding, and interactions with MDM2 and other regulatory proteins (Koo *et al.*, 2022). In healthy cells, P53 expression is kept low by MDM2 and MDM4, which promote its degradation via E3 ubiquitin ligases. Stress signals, such as DNA damage or oncogene activation, stabilise and activate P53, allowing it to fulfil its tumour-suppressing functions. Dysregulation of the MDM2-P53 feedback loop, often due to MDM2 or MDM4 overexpression, can result in loss of tumour suppression (England *et al.*, 2013; Zhang *et al.*, 2018).

P53 mutations are a hallmark of glioblastoma (GBM), present in ~30% of GBM-IDHWT and 60–80% of Ast-IDHMT (Ohgaki and Kleihues, 2011; Verhaak *et al.*, 2010).

These mutations impair P53's tumour-suppressing abilities, leading to unchecked proliferation. The prevalence of P53 mutations varies among GBM subtypes: proneural (54%), neural (21%), mesenchymal (32%), and classical (0%) (Koo *et al.*, 2022; Zhang *et al.*, 2018).

The ARF-MDM2-P53 pathway is deregulated in 84% of GBM cases, highlighting its importance in gliomagenesis (The Cancer Genome Atlas Research Network, 2008). In GBM, mutations in TP53 often occur alongside alterations in PTEN and CDKN2A/ARF. Loss of ARF function diminishes its ability to inhibit MDM2, further impairing P53 activity. Similarly, PTEN mutations promote tumorigenesis by disrupting the P13K/AKT pathway, which also affects MDM2 regulation (England *et al.*, 2013; Shen *et al.*, 2023). ATM and ATR proteins, activated by stress signals such as DNA damage, can upregulate P53 via the CHK1/CHK2 pathway, creating a complex interplay between DNA repair, P53 regulation, and tumour progression (Shen *et al.*, 2023).

Hypoxia, reactive oxygen species (ROS), and DNA damage exacerbate this disruption, creating a feedback loop that promotes glioblastoma heterogeneity and resistance to treatment. Strategies targeting the P53 pathway, such as MDM2 inhibitors (e.g., AMG-223, currently in clinical trials), show potential but face challenges due to acquired resistance and toxicity (Canon *et al.*, 2015; Pellot Ortiz *et al.*, 2023).

1.3.6 Hypoxia and Hypoxia inducible factor-1 (HIF-1)

Tumour cells exhibit distinct metabolic adaptations, such as the Warburg effect, where glycolysis predominates even in the presence of oxygen, leading to lactic acid build-up and a low tumour pH (Park and Lee, 2022). Hypoxia, a hallmark of GBM, is linked to tumour progression and poor outcomes, as it promotes angiogenesis and metabolic reprogramming. GBM tumours are characteristically hypoxic and demonstrate high vascularization in an unsuccessful attempt to meet the oxygen demands of proliferating cancer cells. The brain's reliance on oxygen, consuming 20% of the body's supply under normal conditions, exacerbates the impact of hypoxia in GBM (Park and Lee, 2022).

Hypoxia-inducible factor-1 α (HIF-1 α) is a key transcription factor stabilized under hypoxic conditions. In normoxia, HIF-1 α is hydroxylated by prolyl hydroxylase (PHD), tagged by von Hippel–Lindau (VHL) protein, and degraded via the ubiquitin-proteasome pathway (He *et al.*, 2021; Womeldorff *et al.*, 2014). In hypoxia, PHD is inactive, allowing HIF-1 α to dimerize with HIF-1 β and drive the transcription of genes involved in angiogenesis, autophagy, and cell invasion (Yang *et al.*, 2012). This includes upregulation of VEGF, GLUT1, and PDGF, which contribute to tumour vascularization and metabolic adaptations essential for growth and proliferation (Tang *et al.*, 2016; Colwell *et al.*, 2017).

In GBM, HIF-1 α promotes glioblastoma stem cell (GSC) survival within hypoxic niches, furthering tumour heterogeneity and resistance to treatment (Begagić *et al.*, 2024; Yang *et al.*, 2012). Hypoxia-induced angiogenesis, mediated by VEGF and other markers, correlates with poor patient survival (Monteiro *et al.*, 2017). Dysregulation of HIF-1 α is influenced by EGFR amplification, P53 mutations, and PTEN loss, with downstream effects on the PI3K/AKT pathway, reinforcing the tumour's resistance mechanisms (Monteiro *et al.*, 2017). Notch1, a regulator of stemness and tumorigenesis, is also upregulated by HIF-1 α , further contributing HIF-1 α 's role in tumour progression (Yi *et al.*, 2019).

Hypoxia and HIF-1 α present significant challenges to GBM therapy. Hypoxic regions often harbour quiescent cells, less sensitive to chemotherapy and radiotherapy, which rely on oxygen-induced free radicals to damage DNA (Begagić *et al.*, 2024). The tumour microenvironment and its hypoxic niches protect GSCs, driving recurrence and resistance. Addressing HIF-1 α and its downstream effects is critical for improving GBM treatment, yet advancements have been limited, with the gold standard therapy remaining unchanged for nearly 20 years.

1.4. Current Treatments of GBM

Much of the challenge in treating GBM is the location and heterogenous nature of the disease, with patients requiring not only therapeutic aid but also support in managing the many symptoms such as a seizure, cognitive impairment, cerebral oedema and visual disturbances (Hanif *et al.*, 2017; Shikalov *et al.*, 2024).

The standardised treatment for GBM since 2005 has been surgery, radiotherapy (RT) and concomitant and adjuvant alkylating chemotherapy using TMZ (Cantidio *et al.*, 2022). GBM treatment is tailored to individual patients and costly, with treatment options based on tumour size and location which is determined by MRI and PET scans as shown in Figure 1.4. Treatment is also tailored to biomarkers expressed such as IDH and MGMT, as well as KPS score and age as previously discussed (Janjua *et al.*, 2021). Patients younger than 70 with a good KPS score receive maximal safe resection of the tumour followed by fractionated radiotherapy, - 60Gy in 2Gy fractions – over 30 fractions or 6 weeks with 75mg/m²/d daily TMZ and 6 to 12 cycles of adjuvant TMZ at a maximum dose of 200mg/m²/d (Nam and De Groot, 2017). Clinical trial data has shown the combination of TMZ and RT significantly improves the 2-year survival rate by 16.1% (Jezierzański *et al.*, 2024; Stupp *et al.*, 2005). Therefore, improvement upon the combination of TMZ and RT without removal of either component serves as a logical place to begin advancement in treatment options.

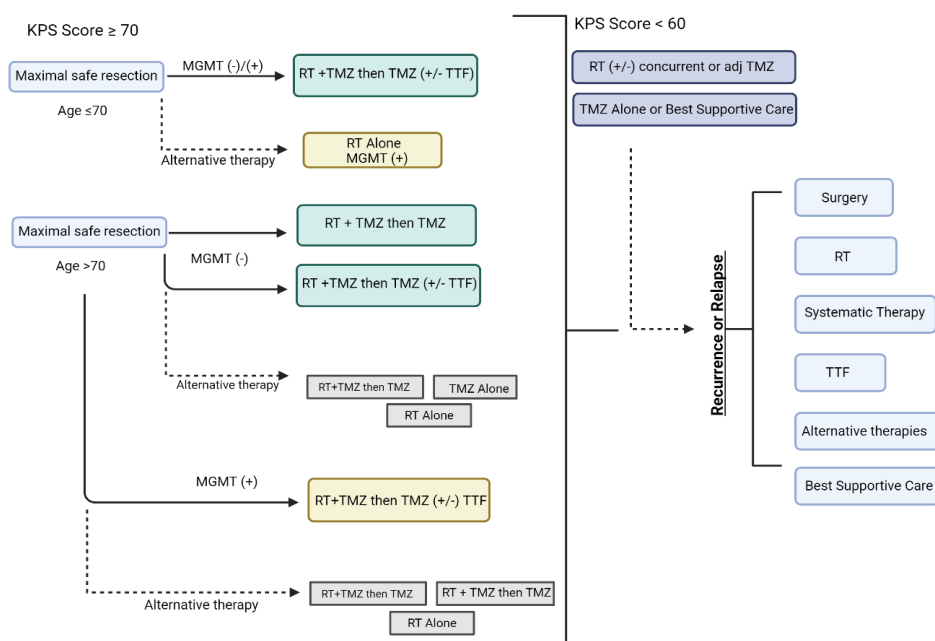


Figure 1.4: Patient treatment planning in Glioblastoma. (+/-) indicates with or without adjuvant therapy. The differences in treatment between MGMT status as well as Age, KPS score and treatment regimens available upon recurrence/relapse. Adapted from (Tan *et al.*, 2020) created with Biorender.com.

1.4.1 Surgical Resection

Surgery is the first treatment option for many GBM patients, however it is only performed if deemed safe for the patient, as the aim is to reduce morbidity and increase the patient's quality of life. Before, or in replacement of surgical resection a stereotactic needle biopsy or open biopsy may be performed for pathological diagnosis. This approach may be used when a tumours location or patients' status is not suitable for resection (Young *et al.*, 2015). If suitable, gross total resection (GTR) of the tumour is performed, reducing tumour volume and obtaining tissue for molecular diagnosis (Sales *et al.*, 2022; Wirsching and Weller, 2017).

GTR is recommended compared to supramaximal resection as GTR increases 1 year survival by ~60% and PFS by ~50%, with maximal volume resection >80% having a better prognosis for patients (Kanderi *et al.*, 2024). Review and meta-analysis have shown a correlating improvement in overall survival in relation to the extent of tumour resection, and with the advancement of intraoperative imaging such as 5-aminolevulinic acid fluorescence guiding, GTR is now possible in ~80% of patients (Kanderi *et al.*, 2024). Other advancements in medicine have suggested that preoperative and intraoperative procedures improve GTR, such as awake craniotomy's using motor and speech mapping to help preserve long term functionality of the patient and specialised MRI-compatible surgical equipment for imaging guidance (Tan *et al.*, 2020).

After tumour resection carmustine polymer wafers have also been utilised to improve patient survival. These wafers are placed in the tumour cavity at the time of surgery and slowly release the chemotherapy agent for up to 5 days (Qi *et al.*, 2015; Ricciardi *et al.*, 2022). Carmustine, known as Gliadel is an alkylating chemotherapy preventing DNA replication and transcription. It has been used in GBM treatment to bridge the gap between surgery and radiotherapy (Xiao *et al.*, 2020). The implantation was seen to improve overall survival by 2-4 months however the side effects and its efficacy have been questioned (Xiao *et al.*, 2020).

Due to the invasive nature of GBM and lack of tumour boundaries, relapse and recurrence occurs after 7-8 months in ~90% of patients, normally within 2 cm from the original lesion margin (Janjua *et al.*, 2021). Therefore, although surgery is beneficial in alleviating the tumour burden on patients, it is not able to eradicate the cancer and multiple combined therapeutic regimes are needed to improve overall survival and PFS.

1.4.2 Radiotherapy and Tumour treating Fields

1.4.2.1 Radiotherapy

Radiation therapy (RT) remains a primary and integral treatment for GBM in patients with both resectable and unresectable tumours and it is the most effective treatment for GBM (Li *et al.*, 2022). Ionising radiation induces cell death through either direct or indirect mechanisms as shown in Figure 1.5. Radiation causes DNA damage to cancer cells through ionising radiation from gamma rays, X-rays or radioactive particles, which form reactive oxygen species (ROS) and hydroxyl radicals. Damage to the DNA can be single, double, base lesions or clustered and initiates the DNA repair pathways (Wang *et al.*, 2018). Single stranded breaks normally do not induce enough damage to the DNA and can be repaired, however the repair can lead to mutated DNA. If enough insult is caused to induce DSBs (which cannot easily be repaired) or repair mechanisms are not functioning, the cells halt the cell cycle at the G2/M phase and cell death occurs via mitotic catastrophe, apoptosis, necroptosis senescence or immunogenic cell death (Evans and Staffurth, 2018). Indirect damage from ROS has also been shown to initiate an anti-tumour immune response, reducing the tumour in areas surrounding the targeted field (Li *et al.*, 2022). The extent of DNA damage is reliant on the presence of oxygen, as oxygen oxidises the radical DNA lesions in DNA, therefore much of the resistance seen with RT is the hypoxic areas in the GBM TME (Wang *et al.*, 2018).

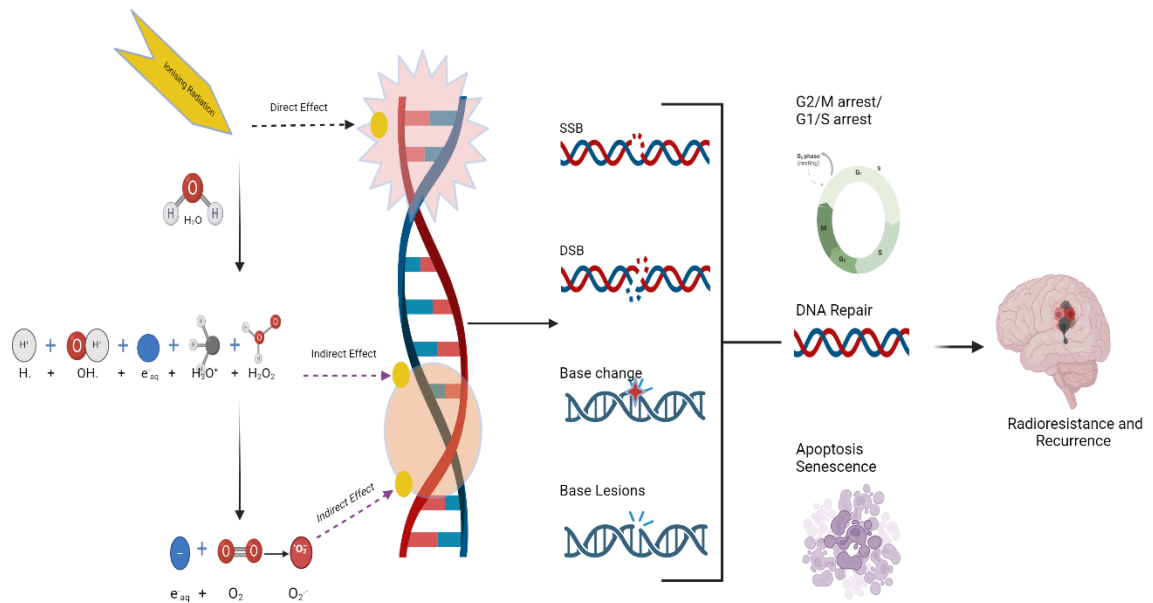


Figure 1.5: Mechanism of Ionising radiation in radiotherapy, showing both the direct and indirect effect of ROS and IR after cleaving water molecules to elicit DNA damage as SSB, DSB, Base Change and Base Lesions. The response from the cells is shown as cell cycle arrest, apoptosis, senescence and DNA repair ultimately leading to radioresistance. Adapted from (Wang *et al.*, 2018), created using Biorender.com.

Radiotherapy in GBM as previously mentioned, is given after surgery and in fractions of 2Gy for a total of 60Gy. Due to the non-invasiveness of the therapy radiotherapy is suitable for most patients and with imaging advances can be localised to the site of disease (Li *et al.*, 2022). RT can be given with TMZ, can begin 4-6 weeks after surgery or can be accelerated for patients in poor health (Li *et al.*, 2022). RT for GBM patients in most cases uses 3D conformal X-ray photons or intensity modulated RT, which causes both direct and indirect biological damage (Wu *et al.*, 2021).

Recent advances in RT have provided more options that potentially could minimise adverse effects and be more targeted to the site of disease (Goff *et al.*, 2022). Some of these advances include whole brain radiation therapy (WBRT) for non-surgical patients which has been successful in controlling disease, however it has been linked to loss of neurocognitive ability. Stereotactic radiosurgery has also been used and has shown significant improvement in OS (Angom *et al.*, 2023). The Gamma Knife (GK) a form of SRS, enables highly localised treatment with the advantage of a single-session procedure and minimal side effects (Angom *et al.*, 2023). Brachytherapy is

also used to target small cancers by implanting radio particles such as iodine and iridium into the brain, however in GBM, brachytherapy has shown no significant improvement in OS or PFS compared to external beam RT (Barbarite *et al.*, 2017).

Proton beam therapy (PT) for GBM is an emerging new treatment, which utilises proton particles for more precise tumour targeting at larger doses of radiation (LaRiviere *et al.*, 2019). The advantage of PT over photon-based RT is the entry/exit of the beam and energy deposition. X-ray beam RT has an exit dose as the energy is deposited along the X-ray beam and peak energy deposition is on entry. Proton therapy deposits the majority of its energy at the tumour site due to deceleration of proton energy. This means the tumour receives the maximum dose of RT and limits exposure to other sites. Localised precision PT could potentially reduce the side effects of RT in GBM patients by reducing radiation exposure to healthy brain tissue (Goff *et al.*, 2022). Clinical trials are still ongoing in the UK with some completed but not yet published. Worldwide however, proton therapy is becoming increasingly accessible with 118 proton radiation therapy centres in use in the USA in 2022 (Chen *et al.*, 2023). In the UK however only two proton beam therapy centres are available, however head and neck cancer treatment in adults have not yet begun (NHS England, 2024) (As of 09/2021).

Radiation remains central to the treatment of GBM and when used in combination with surgical resection and chemotherapies, provides an improved outcome for patients. The development around proton therapy opens many doors for future research including in our own lab and combination therapy work which could significantly enhance patient outcome.

1.4.2.2 Tumour treating Fields

A new device known as the tumour treating field (TTF) was authorised by the FDA for newly diagnosed GBM therapy in 2015 (Angom *et al.*, 2023). The device works by being fixed to the patient scalp and delivering intermediate low frequency alternating electrical fields. This inhibits the proliferation of GBM by preventing mitosis, causing chromosome missegregation, disrupting DNA repair and inducing apoptosis (Obrador *et al.*, 2024). Use of the device has been linked to improved OS and therapeutic response; however, patient adherence is poor, with the device being placed on the

scalp for 18h/day for 4-week cycles. The use of TTF has shown similar outcomes to chemotherapy and improved median free survival when used in combination with TMZ compared to TMZ alone, with 6.5 months of median free survival compared to 4 months (Obrador *et al.*, 2024). Due to less toxicity than chemotherapy and less invasive therapeutic regime than surgery, TTF has shown to be an advantageous treatment option for patients in terms of quality of life, however the time required to use the device (18h/day) has shown to be a corresponding disadvantage (Obrador *et al.*, 2024).

1.4.3 Chemotherapies for GBM

Chemotherapeutic agents for GBM which have been approved by the FDA and MHRA are limited. Alkylating agents such as Carmustine and Lomustine are used, as well as TMZ, and bevacizumab. Carmustine, a DNA alkylating agent as previously mentioned, has been used in wafer implantation after surgical resection. Its use however, leads to liver and kidney toxicity which has halted its use in many patients as an IV medication (Li *et al.*, 2022). Bevacizumab is an anti- VEGF antibody that reduces tumour growth and promotes regression of the tumour (Janjua *et al.*, 2021). Bevacizumab is given orally once fortnightly as either a monotherapy or combination therapy but has shown many side effects such as GI perforation (Angom *et al.*, 2023). The benefit of Bevacizumab has been varied with some 2021 studies showing improvements in OS. Contradictory studies have ultimately shown no significant improvement in OS; however, the drug is still administered due to symptom management and improvement of quality of life (Singh *et al.*, 2020).

1.4.3.1 Temozolomide

Temozolomide or brand name Temodal/Temodar, is a DNA alkylating agent, discovered in 1940 for its anti-tumorigenic effect, with its licence for administration beginning in the 2000's (Singh *et al.*, 2020). The drug belongs to a group of triazene compounds and is commonly used in concomitant or adjuvant therapy with RT for GBM (Strobel *et al.*, 2019). TMZ is a lipophilic prodrug, able to cross the BBB and be administered orally, making it a suitable chemotherapy for GBM, where much of the

initial problem with chemotherapies is their inability to bypass the blood brain barrier (BBB) (Singh *et al.*, 2020). TMZ does not require metabolic activation and is converted to 5-(3-methyl-1-triazeno)imidazole-4-carboxamide (MTIC). The active compound of TMZ is electrophilic methyldiazonium ions that cause DNA damage. TMZ disrupts single strands of DNA at specific sites via methylation of the DNA, commonly at guanine residues on the O⁶ and N⁷ sites, and N³ position of adenine (Denny *et al.*, 1994; Lee, 2016). Guanine site alkylation at the O⁶ position, leads to mispairing of the bases as thymine residues are inserted which cause single and double stranded DNA breaks ultimately resulting in cell death and apoptosis via cell cycle arrest at G2/M (Said *et al.*, 2023; Stupp *et al.*, 2005). The methylated DNA is repairable via base excision or the MMR pathway or MGMT as shown in Figure 1.6.

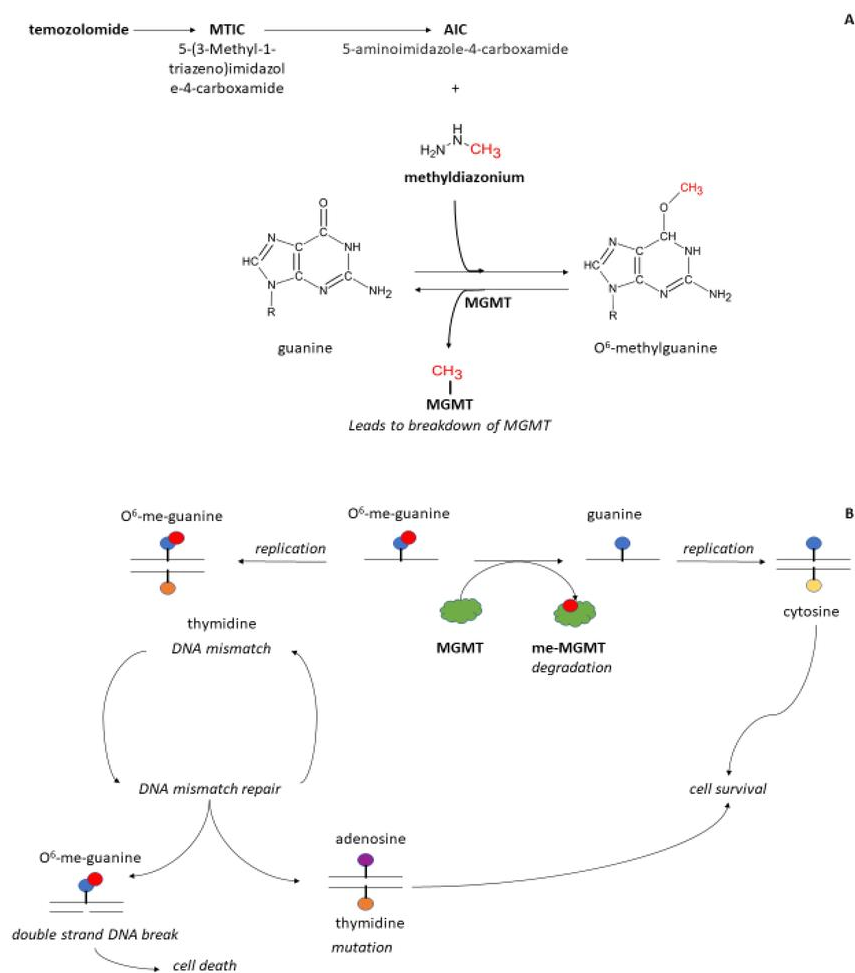


Figure 1.6: TMZ schematic mechanism of action (A) and MGMT mechanism of action on DNA (B). TMZ in Figure 1.6 (A) shows the breakdown of TMZ into MTIC and methyldiazonium, which methylates O⁶ guanine. MGMT in (B), either removes the methylation and degrades, allowing correct DNA matching with guanine to cytosine

and cell survival. Without MGMT action incorrect replication occurs as a thymidine is matched to the methylated guanine. This causes MMR activation which can either remove the methylation and substitute it with adenosine leading to mutations in the DNA and cell survival or cause double stranded breaks as the thymidine is removed leading to cell death (Said *et al.*, 2023).

1.4.3.2 Temozolomide therapeutic resistance

TMZ resistance has become a major problem in GBM patients, with >50% of patients unresponsive to treatment, with many having MGMT resistance and others acquiring drug resistance (Singh *et al.*, 2020). MGMT works against TMZ by removing the methylation in a suicidal manner as previously discussed in 1.3.2 (Lee, 2016). Many studies are now finding differences in not only MGMT methylation but its gene expression levels in GBM, as well as the functionality of the MMR which is crucial to TMZ induced cell death (Butler *et al.*, 2020). In GBM only ~50% of MGMT negative cells show methylation of the CpG promoter, with the remaining 50% thought to have hypomethylation in the gene body of the protein which would result in decreased MGMT expression similar to that of CpG methylation. Hypermethylation of the gene body increases MGMT expression and therefore studies have shown dividing groups into methylation status and gene expression levels could stratify patients and provide the best prognostic outcome (Moen *et al.*, 2014; Shah *et al.*, 2011).

Additionally, tumours initially with MGMT methylation, after treatment, have shown reduced methylation ratios when the tumours recur, insinuating reduced MGMT promoter methylation is a path of acquired resistance to TMZ (Park *et al.*, 2012). Studies have shown MGMT activity could be induced by TMZ, with many studies being undertaken into GBM cell lines showing this acquired MGMT expression and TMZ resistance (Mansouri *et al.*, 2019; Rominiyi and Collis, 2022; Wang *et al.*, 2015).

Additionally, MMR deficiency is caused by the absence of any of the four MMR proteins and is seen commonly in recurring tumours after TMZ treatment, potentially explaining resistance to treatment regardless of MGMT status (Szyberg *et al.*, 2022). The mechanism of MGMT and MMR in causing cell death is shown in Figure 1.7 and provides another potential path of TMZ resistance.

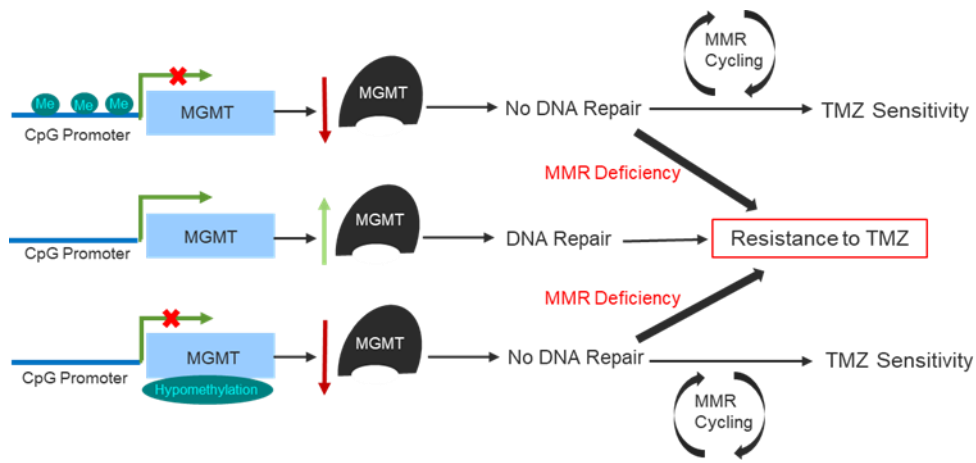


Figure 1.7: Function of MGMT in GBM in relation to treatment resistance. The hypothesised role of MGMT and the MMR in TMZ sensitivity in GBM. When the MGMT CpG promoter is methylated (top line), the reduced expression of MGMT leads to TMZ sensitivity unless there is a deficiency in one of the MMR proteins causing MMR deficiency. When CpG is unmethylated, an increased MGMT expression results in TMZ resistance (middle line). When CpG is unmethylated, there is a proposed hypomethylation of the MGMT gene body, decreasing MGMT expression and leading to TMZ sensitivity unless there is MMR deficiency. Adapted from (Butler *et al.*, 2020).

As much of the therapy resistance observed with TMZ is not primarily due to the MGMT status, much research has been employed to find the pathways of resistance. GSC are thought to be a source of TMZ resistance, as the stem like cells are enriched post treatment with upregulated DNA repair mechanisms allowing them to repopulate with acquired resistance (Singh *et al.*, 2020). Genome sequencing of recurrent tumours has shown mutations in the genomic profiles which are shared with primary tumours and can be linked to resistant GSCs (Garnier *et al.*, 2018). Aiming future research at the GSCs seems a promising path as the GSCs show resistance to TMZ and RT, and with their ability to repopulate through stemness, are highlighted as the main route of tumour recurrence.

Furthermore, oncogenic pathways and DNA repair mechanisms have shown regulatory relationships, with the PI3k/Akt pathway, commonly unregulated in GBM. The upregulated pathway has shown connections to increased TMZ resistance via upregulation of MGMT. This occurs with the inhibition of NF- κ B subunit epsilon, which

in turn inhibits the Akt/NF- κ B pathway and increases resistance, with correlation seen between MGMT status and PI3K/Akt activity (Guo *et al.*, 2020; Harder *et al.*, 2019).

In spite of all the resistance mechanisms observed following TMZ administration to glioma patients, TMZ remains an important therapy for GBM patients as it improves OS from 7.7 months when RT is given alone to 13.4 months when given in combination with RT (Fernandes *et al.*, 2017; Stupp *et al.*, 2005). TMZ has also shown to improve patient survival time after recurrence when combined with TTF therapy vs TMZ alone, with OS being 12 months vs 10.8 months respectively (Kesari *et al.*, 2017). With no other chemotherapies able to match the impact of TMZ on GBM, it remains the standard of care, and future therapeutic research building upon TMZ's efficacy with combination treatments seems a promising route. Additionally, research into preventing the resistance development could be equally beneficial.

1.5 Repurposing Drugs

Repurposing drugs has been gaining popularity as a way to find effective treatments for difficult to treat diseases. The demonstrated success of drug repurposing in cancer is highlighted with the use of metformin which was classically utilised for treatment of diabetes and is now in clinical trials as a cancer therapy for breast, endometrial, pancreatic, prostate, colorectal and GBM cancers (Fuentes-Fayos *et al.*, 2023; Kasznicki *et al.*, 2014). Repurposing of drugs is an attractive route to take when researching novel therapies as they have already undergone clinical trials to obtain full toxicity and pharmacokinetic profiles, have known drug targets and known blood plasma levels, making it easier for regulatory approval (Hernandez *et al.*, 2017; Zhang *et al.*, 2020). Their usage also reduces cost, as less developmental research is needed as well as fewer and quicker clinical trials (Hernandez *et al.*, 2017). It has been demonstrated that repurposed drugs are approved sooner, normally within 3-12 years vs the 11-16 years for new drugs, they cost 50-60% less than a new drug and 20% more repurposed drugs applications are approved over new drug applications, as shown in Figure 1.8 (Chong and Sullivan, 2007; Hernandez *et al.*, 2017; Ashburn and Thor, 2004).

Although drug repurposing seems a favourable approach to GBM treatment, some challenges present which should be considered such as safety concerns, drug

patenting, epidemiological factors and potential negative interference with patient health (Siegelin *et al.*, 2021). Repurposed drugs could prevent patentability which would prevent pharmaceutical companies from pursuing repurposed approaches as it limits profitability (Pinzi, Bisi and Rastelli, 2024). Additionally, if the dose required for repurposing is higher than the clinically delivered dose, phase 1 trials may need to be completed, such as with DMF which was put through a phase 1 trial for dosage safety (Shafer *et al.*, 2020). If a repurposed drug has been tested on one age group or sex, further investigation and clinical trials would be needed to test the safety against different sex/age (Siegelin *et al.*, 2021). Repurposing for GBM would also need to factor in the BBB and which dose of treatment would be needed to enter across into the brain (Siegelin *et al.*, 2021).

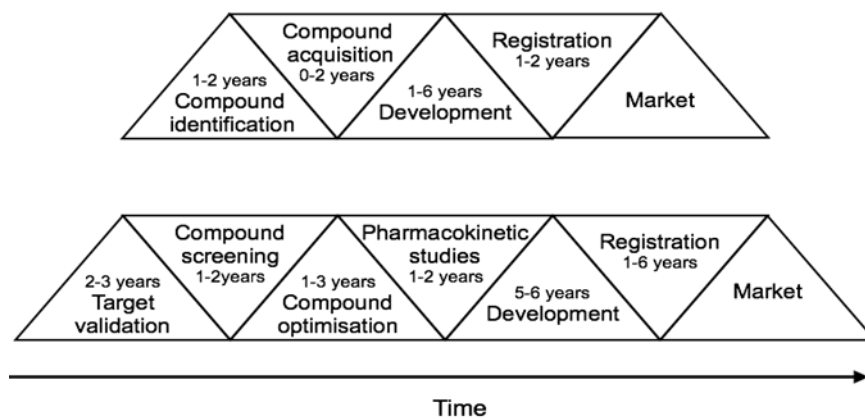


Figure 1.8: The differences over time between development of de novo drug discovery (bottom) and drug repurposing processing (Top) (adapted from Ashburn and Thor, 2004; Scott, 2020)

The use of repurposed drugs in GBM has been successful, with metformin diabetes drug in an ongoing clinical trial (NCT0143035) with TMZ after RT in newly diagnosed patients (Hernandez *et al.*, 2017). Repurposing also eliminates the obstacle of the BBB, as drugs can be trialled for GBM with a known ability to cross the BBB. Also, with the vast number of mutations and signalling pathways associated with GBM, repurposing can identify drugs for different targets in these pathways, which could potentially aid in understanding the pathways to GBM development and recurrence (Alomari *et al.*, 2021). With the identification of GSCs, combination-based therapies targeting these stem-like cells after the standard of care to prevent recurrence is a strategy being considered in the literature (Alomari *et al.*, 2021). Many drugs are under

clinical investigation for GBM repurposing as reviewed in the literature by Alomari *et al.* (2021).

1.5.1 The Fumarates

Fumaric acid esters (FAE) salts were first used for treating disease in Medieval Europe. The FAEs are a group of simple structured compounds that were shown to have therapeutic effect on psoriasis in 1950. Dimethyl fumarate (DMF) was the first fumarate to be approved for use on psoriasis, under the name Fumaderm ~30 years later (Hoogendoorn *et al.*, 2021). Since then, four fumarates have been approved for human use, Monomethyl Fumarate (MMF), DMF, diroximel fumarate (DRF) and zinc, magnesium and calcium salts of Monoethyl fumarate (MEF). All four drugs are used either for MS or psoriasis (Hoogendoorn *et al.*, 2021). As the fumarates all show neuroprotective and anti-inflammatory action, they have become increasingly interesting for repurposing, with much research into their use for chronic pain, Parkinson's, Alzheimer's, heart disease and of course cancer (Hoogendoorn *et al.*, 2021; Yao *et al.*, 2016).

1.5.2 Dimethyl Fumarate

Dimethyl Fumarate (DMF) formulated as Tecfidera, is used in the treatment of multiple sclerosis and psoriasis by reducing inflammation and reducing immune T cell function. A member of the FAE family, DMF grew increasingly popular for its use as a repurposed drug due to antioxidant, anti-inflammatory, neuroprotective and anti-proliferative effects (Bresciani *et al.*, 2023). DMF has a half-life of 12 minutes and is able to hydrolyse into MMF bypassing the BBB. DMF is also undetectable in blood plasma due to the rapid conversion to MMF, with much of the literature referring to MMF and DMF as the same compound affecting the same pathways (Ahmadi-Beni *et al.*, 2019). Although MMF is an active metabolite of DMF, various papers looking at DMF and other fumarates suggest they have in fact different mechanisms of action (Brennan *et al.*, 2015; Yazdi and Mrowietz, 2008; Yao *et al.*, 2016). The mechanism of action of DMF is not yet fully understood as DMF affects many different pathways, primarily the cellular redox systems, where it modulates glutathione (GSH), NrF2 and

the thiols (Gold *et al.*, 2012). DMF is thought to operate primarily on hormesis, where the Nrf2 pathway is activated by subtoxic levels of harmful oxidants (Matteo *et al.*, 2022). DMF interacts with GSH and protein thiols by the addition of a cysteine to fumarate, a process known as protein succination (Saidu *et al.*, 2019).

In GBM cells, DMF has been shown to reduce GSH levels, GSH is an antioxidant which increases in response to cellular stress such as ROS. ROS is generated by chemotherapy and radiotherapy, to cause DNA damage and kill tumour cells. Therefore, by the antioxidant response and decrease in ROS by GSH, treatments are not as effective (Gola *et al.*, 2023; Scott, 2020). A phase 1 clinical trial, NCT02337426, investigated DMF combination therapy with TMZ and RT for newly diagnosed GBM patients and concluded the safe use of combining DMF, with TMZ and radiotherapy (Shafer *et al.*, 2020). The study established an OS of 13.8 months in the triple combination, compared to 13.4 months for the standard of care, a 0.4-month survival advantage (Alomari *et al.*, 2021; Shafer *et al.*, 2020; Stupp *et al.*, 2005). Although the study by Shafer *et al.*, (2020), observed a small improvement in patient survival, only 11 patients were studied, with 1 withdrawal and all had a KPS of ~50. Therefore, in larger patient groups with better KPS scores, the benefit of DMF on OS, in theory, would be hypothesised to increase. Shafer *et al.*, (2020) also demonstrated that DMF reduced proinflammatory cytokine IL-6, TNF- α and the radiation induced P65 phosphorylation. These pathways all promote GBM and its survival, so by repurposing of DMF, we will see off target effects which are beneficial to treating GBM.

DMF's function in GBM is thought to be through depletion of interleukin-6 (IL-6) and tumour necrosis factor- α (TNF- α) both of which in GBM have a role in angiogenesis (Shafer *et al.*, 2020). DMF also inhibits nuclear factor kappa-light-chain-enhancer of activated B cells (NF- κ B), reduces P65 phosphorylation after exposure to radiation therapy (RT) and reduces extracellular signal-regulated kinase (ERK1/2) and Protein Kinase B (AKT) signalling (Shafer *et al.*, 2020). NF- κ B -P65 and ErK1/2-AKT have all been shown to be upregulated in GBM and promote chemoresistance. Inhibition of NF- κ B in GBM cells promotes apoptosis and improves the effects of Temozolomide (TMZ) (Avci *et al.*, 2020). NF- κ B is a group of transcription factors with five subunits which control gene expression for processes including inflammation and stress response (Saidu *et al.*, 2019). The fumarate suppresses signals translocating NF- κ B into the nucleus and stops gene expression. This in turn decreases anti-inflammatory

pathways and leads to apoptosis or inhibits tumorigenesis (Ahmadi-Beni *et al.*, 2019). Thus, inhibition of NF- κ B is desirable because it will promote tumour cell apoptosis.

In non-cancerous cells DMF induces NrF2, however in cancers DMF has been shown to have a dose-dependent anticancer mechanism (Saidu *et al.*, 2019). The mechanism behind this is thought to be inhibition of the NrF2/Dj-1 axis of the antioxidant pathway. High concentrations of DMF were shown to reduce nuclear NrF2 and its downstream targets (Saidu *et al.*, 2019). Low DMF concentrations studied by Saidu *et al.*, (2019), showed decreased oxidative stress and an upregulated NrF2 system as well as upregulated intracellular GSH levels (0.25-5 μ m). Higher concentrations showed inhibition of the detox system and increased cell death (Figure 1.9).

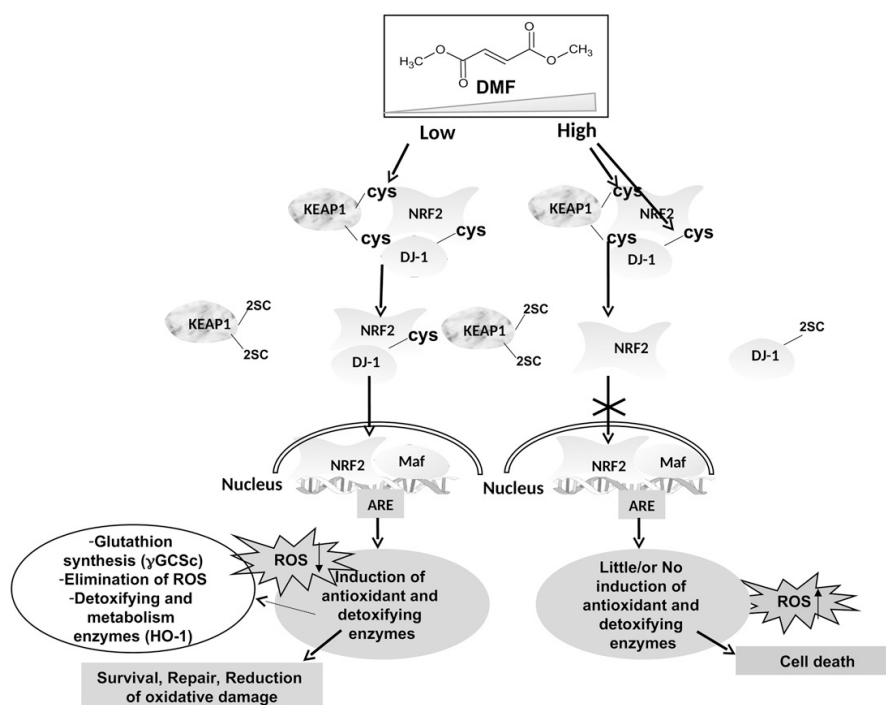


Figure 1.9: Hypothesised mechanism of DMF-induced cell death in cancer cells. Low concentrations of DMF on the left, induce NrF2 and its antioxidant pathway, translocating into the nucleus and activating the detoxification system, including GSH, promoting cell survival and repair due to lower levels of oxidative stress. High concentrations of DMF shown on the right, disrupt the NrF2 pathway via DJ-1, prevent dissociation of NrF2 from Keap 1 and its translocation. In turn cells are vulnerable to oxidative stress, the detoxification enzymes have not been activated and cell death occurs (Saidu *et al.*, 2019).

As highlighted in Figure 1.9, DMF has significant modulatory effects on how cells react to oxidative stress, with higher doses of DMF acting against tumorigenesis and lower doses promoting cell survival (Saidu *et al.*, 2019). Additionally, much of the *in vitro* work with DMF does not translate across *in vivo*, specifically this dose effect response, as *in vivo* DMF is quickly metabolised to MMF, highlighting a difference between the two fumarates *in vivo* (Saidu *et al.*, 2019).

Previous research by the Boyd lab into the mechanism of action of DMF in GBM, with TMZ and RT showed synergistic increases in cell kill on both MGMT positive and negative cell lines (Scott, 2020). DMF was shown to deplete GSH levels, however the mechanism of cell kill by DMF-TMZ-RT combination was not identified. The depletion of antioxidant GSH that was seen by DMF initiated further work into GSH's role across various cancers in the Boyd lab and continuation of the research in this project (Scott, 2020).

1.5.2.1 Glutathione

Glutathione and its related enzymes are an important mechanism of self-defence for cells against oxidative stress (Kennedy *et al.*, 2020; Zhu *et al.*, 2018). GSH maintains homeostasis in the cells acting as a detoxifier against ROS and maintaining the intracellular antioxidant systems. GSH also has a role in cell signalling, gene expression, and cell differentiation/proliferation (Kennedy *et al.*, 2020; Zhu *et al.*, 2018). GSH is the most important redox system in the cells as its expressed 500-1000-fold higher than other antioxidants (Filomeni *et al.*, 2002). GSH is found in two forms, its reduced form as GSH or its oxidised form, GSSG (Averill-Bates, 2023; Vašková *et al.*, 2023).

Two important systems related to GSH are the NADPH and Thioredoxin (TRX) systems. NADPH works with GSH by acting as a hydrogen donor in the reduction of GSSG to GSH. TRX proteins have oxidoreductase activity and have protein disulphide targets on transcription factors such as P53 and NF- κ B. As well as being ROS scavengers and reducing oxidised GSH (GSSG) back to its reduced form (Averill-Bates, 2023; Filomeni *et al.*, 2002). GSH can be present either reduced as GSH or oxidised into glutathione disulphide (GSSG) and glutathione mixed with protein thiols (GS-R) (Filomeni *et al.*, 2002). The enzymes Glutathione S-transferase (GST) and

glutathione reductase (GR) are integral in the GSH antioxidant defence system (Korkmaz, 2024).

Reduced GSH is 10-100-fold higher in non-cancer cells than the oxidised form and with oxidative stress, the GSH/GSSG ratio remains stable using different cellular mechanisms to maintain homeostasis, upregulating GSSG production. Under extensive periods of oxidative stress, free GSH levels drop and cause cell death through a mitochondrial related apoptotic pathway (Filomeni *et al.*, 2002).

In GBM cells, GSH has increased expression levels in relation to treatment, with both TMZ and RT creating elevated oxidative stress levels in the cell (Zhu *et al.*, 2018). The increased glutathione levels, prevent the ROS created by therapeutic regimens to elicit their full effect, and therefore GSH may contribute to therapy resistance in GBM (Backos *et al.*, 2012). Under oxidative stress conditions, GSH is regulated by the Nrf2/Keap1 pathway. Nrf2 has been reported to have a significant role in GBM pathogenesis as well as therapy resistance (Awuah *et al.*, 2022). DMF decreases GSH levels by stably conjugating with GSH (Figure 1.10) and depleting free circulating GSH in a time-dependent manner. GSH levels decrease in the first 10 hours of exposure to DMF, returning to normal by 12 hours and increasing GSH levels after 24hours (Brennan *et al.*, 2015).

Glutathione's upregulated protective mechanism in GBM and its ability to prevent DNA damage to the cancer cells, has been highlighted in the literature as a pathway to therapeutic resistance.

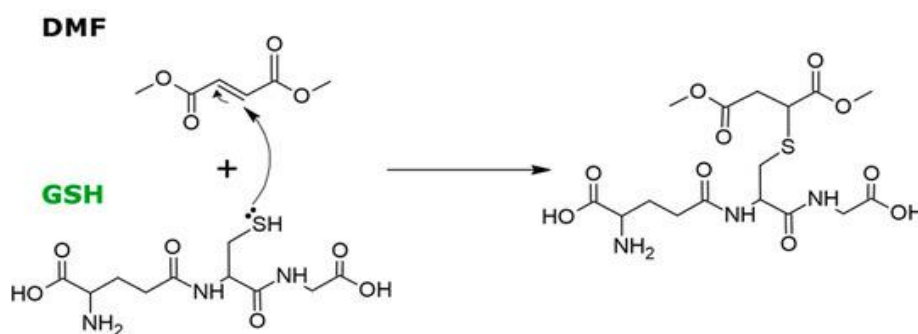


Figure 1.10: Mechanism of Michael addition (protein succination), the nucleophilic addition of the cysteine thiol group of GSH to DMF forming a conjugate (Rosito *et al.*, 2020).

1.5.2.2 Ferroptosis and Glutathione Peroxidase 4

Glutathione (GSH) plays a critical role in cellular processes, including differentiation, proliferation, apoptosis, and ferroptosis (Kennedy *et al.*, 2020). Ferroptosis, a distinct form of iron- and ROS-dependent cell death, arises from the loss of control over membrane lipid peroxidation (Ursini and Maiorino, 2020). During ferroptosis, reactive oxygen species (ROS) generated through iron metabolism accumulate, leading to lipid peroxidation, membrane rupture, and ultimately cell death (Niu *et al.*, 2021). This process is morphologically, genetically, and biochemically distinct from apoptosis and necrosis (Xie *et al.*, 2016).

The depletion of GSH, as facilitated by fumarates such as dimethyl fumarate (DMF), is a key mechanism in enhancing the therapeutic response to GBM treatments. Lower GSH levels reduce ROS scavenging capacity, deplete intracellular antioxidants, and sensitise cells to ferroptosis. Glutathione peroxidase 4 (GPX4), a mitochondrial enzyme within the glutathione peroxidase family, is critical for detoxifying lipid hydroperoxides (PL-OOH) and limiting reactive radical species. By preventing the interaction of PL-OOH with ferrous iron, GPX4 suppresses lipid peroxidation and ferroptosis (Galaris *et al.*, 2019).

In cancers, the deregulation of ferroptosis provides an opportunity to exploit this pathway as a therapeutic target. Depletion of GPX4 or its cofactor GSH results in ferroptosis cell death, underscoring the potential of GSH-targeted therapies (Niu *et al.*, 2021). In GBM, targeting GSH through fumarates offers a dual benefit: enhancing oxidative stress-mediated cell death and inducing ferroptosis independent of conventional radio-chemotherapy responses. This dual mechanism could improve tumour cell eradication and overcome resistance.

However, the complex interplay between GSH, GPX4, and ferroptosis in cancer requires further research. Figure 1.11 highlights the three primary strategies for leveraging GSH depletion in cancer therapy. Overall, the role of GSH and its downstream targets in ferroptosis underscores its critical importance in advancing GBM treatment approaches.

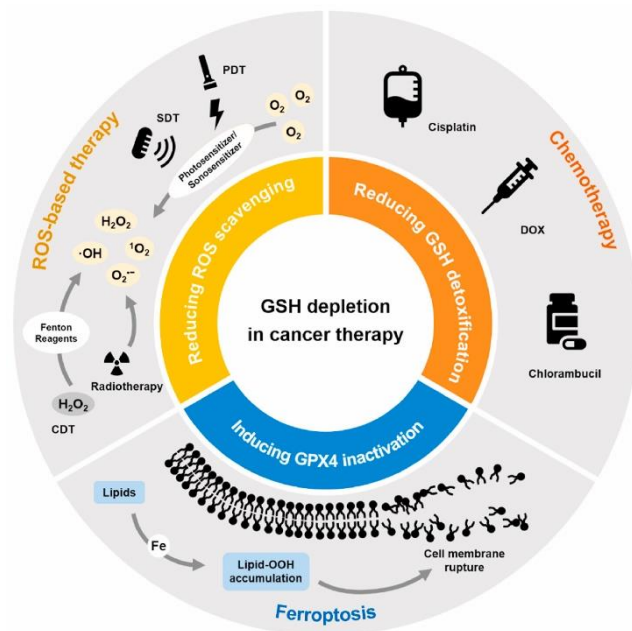


Figure 1.11: The applications of glutathione depletion for treating cancer. Application 1, reducing ROS scavenging by depletion of the antioxidant mechanisms, Reducing GSH detoxification and the induction of ferroptosis via GPX4 depletion. Figure taken from (Niu *et al.*, 2021).

1.5.2.3 Nrf2

Oxidative stress, driven by the accumulation of ROS, impacts cell survival and growth. In normal cells, ROS can initiate diseases such as cancer, but cellular mechanisms such as the detoxification system, involving GSH and Nrf2, prevent ROS buildup (Kaspar *et al.*, 2009; Yoo *et al.*, 2019). Nrf2, a transcription factor with a cap'n'collar DNA-binding domain, collaborates with the KEAP1-ARE pathway to regulate antioxidant responses (Liu *et al.*, 2022). Under oxidative stress, Nrf2 dissociates from its repressor protein KEAP1, translocates to the nucleus, and forms a complex with Maf proteins as shown in Figure 1.9. This Nrf2-Maf complex binds to antioxidant response elements (AREs), upregulating detoxification genes such as GSH (Awuah *et al.*, 2022; Shahcheraghi *et al.*, 2022).

In GBM, NrF2 is highly expressed, particularly in GSCs, promoting malignant proliferation and differentiation (Zhu *et al.*, 2014). Increased NrF2 levels are also linked to high-grade gliomas with IDH mutations and contribute to apoptosis resistance in GBM cell lines (Pan *et al.*, 2013). Moreover, NrF2 regulates heme-oxygenase-1 (HO-1), a downstream target that stabilizes HIF-1 α , enabling cancer cell survival under oxidative stress (Awuah *et al.*, 2022; Bae *et al.*, 2024).

Epigenetic modifications, such as hypermethylation of KEAP1 promoter CpG sites, further increase NrF2 expression, correlating with poor prognosis in GBM (Almeida Lima *et al.*, 2023). Elevated NrF2 and GSH levels support antioxidant defences, aiding tumour progression and limiting the efficacy of chemotherapy and radiotherapy. Although these pathways may initially protect normal cells from ROS-induced damage, their upregulation in advanced GBM promotes tumorigenesis and treatment resistance (Almeida Lima *et al.*, 2023).

NrF2-mediated GSH homeostasis plays a central role in GBM resistance to TMZ. Overexpressed NrF2 enhances GSH synthesis, transport, and recycling, correlating with increased intracellular GSH levels and TMZ resistance (Harvey *et al.*, 2009; Jaganjac *et al.*, 2020). Targeting the NrF2-GSH axis offers a promising approach to overcoming resistance and improving therapeutic outcomes. DMF has been explored for its ability to target GSH levels and NrF2, potentially enhancing the effects of TMZ and RT. Further research into these combinations could provide effective strategies for improving GBM patient outcomes.

1.5.3 Monomethyl Fumarate

Monomethyl fumarate (MMF), marketed as Bafiertam, is the pharmacologically active metabolite of Dimethyl Fumarate (DMF). Approved by the FDA in 2020, MMF is used to treat relapsing-remitting multiple sclerosis (MS) and psoriasis, offering reduced gastrointestinal side effects compared to DMF (Wynn *et al.*, 2020). It is administered orally at an initial dose of 95 mg for seven days, followed by 190 mg daily.

Although both MMF and DMF belong to the fumarate family, they are structurally distinct, with differing administered concentrations required to elicit similar cellular responses (Gillard *et al.*, 2015; Saidu *et al.*, 2019). Like DMF, MMF's precise mechanism is not fully understood but includes activation of the NrF2 and NF- κ B

pathways, contributing to reduced oxidative stress and decreased monocyte migration across the blood-brain barrier (Berger *et al.*, 2021).

Notably, MMF exhibits distinct biological effects compared to DMF, particularly in its modulation of NrF2 and NF- κ B. In lymphocytes, MMF alters downstream targets differently from DMF (Gillard *et al.*, 2015). Moreover, at a concentration of 5 μ M, MMF has no impact on NrF2 activation in GBM cells, contrasting with DMF (Dent *et al.*, 2020). However, *in vivo* studies suggest that both MMF and DMF mediate the NrF2 pathway and reduce glutathione (GSH) levels in a similar manner (Yao *et al.*, 2016).

Brennan *et al.* (2015) further highlighted the biochemical differences between DMF and its derivative, Monoethyl fumarate, suggesting that distinct fumarate formulations may function differently at the cellular level. This variability raises questions about MMF's potential role in GBM. While DMF has shown promising effects in glioblastoma studies, MMF's direct application in GBM remains unexplored. Given the scattered literature on MMF's mechanisms and effects, it is hypothesized that MMF may exert unique biological actions in GBM compared to DMF.

1.6 Aims

The main aims of this project were to investigate the use of novel combination therapies using repurposed MMF for use with TMZ and Radiation in Glioblastoma. The study also aimed to differentiate the pharma-biological effect of MMF vs DMF in glioblastoma cells. As reviewed, GBM therapies mainly consist of surgery, radiotherapy and chemotherapy with TMZ. Due to the aggressive diffuse nature of the disease, patient survival is still as low as ~ 14 months, with very low quality of life. Combining therapies to enhance the current standard of care has been increasingly popular, with much therapy resistance seen in GBM due to the MGMT status seen in patients which prevents TMZ eliciting its full potential. Repurposing drugs for GBM treatment allows for drugs that can bypass the blood brain barrier to be investigated and reduces cost and developmental delays. Through single, double and triple combinations of MMF, MMF + TMZ and MMF+ TMZ+ RT, we aim to investigate any synergistic potential of the combinations as to enhance the standard of care. Due to the variation in the literature on the effect of MMF and DMF, we aim to compare the effects of MMF against DMF through mechanistic assays, RT-qPCR and ferroptosis assays, we aimed to uncover more information on the pathways MMF directly targets. We hypothesise that the combination of MMF with TMZ + RT will be synergistic in both double and triple combinations.

Chapter 2

Materials and Methods

2.1 Cell Lines and Maintenance

For this study, three established human glioblastoma cell lines were used. UVW human glioblastoma cells (developed in house) (Boyd *et al.*, 1999; Mairs *et al.*, 2007), the U87 cell line (ATCC®, Virginia, USA) and T98g human glioblastoma cells (ATCC, UK). All three cell lines were cultured in MEM supplemented with 10% foetal bovine serum, 100µg/mL penicillin-streptomycin, 200mmol/L L-glutamine and 2µg/mL fungizone. T98g and U87 cells were maintained with additional 1% (v/v) sodium pyruvate and 1% (v/v) non-essential amino acids (all Gibco, UK). Cells were incubated at 37°C in a 5% CO₂ environment.

Cells were subcultured as required once they had reached ~80% confluency. Confluent cells were washed with PBS to remove any serum and 0.05% (v/v) trypsin-ethylenediaminetetracetic acid (Gibco, UK) was added to the flask for cell detachment. Cell suspension was added to complete media for neutralisation of trypsin and if required the cell suspension was passed through a 21-gauge needle to disaggregate cells and create a single cell suspension. Disaggregation was essential for the U87 cell line due to formation of small cell spheres. The cell suspension was then added to 15mL of media in 3 x 75cm³ flasks (ThermoFisher, UK) and incubated at 37°C in a 5% CO₂ environment. Cells were routinely tested for the presence of mycoplasma with a Microstrip test (InvivoGen, UK)

2.2 Freezing and thawing cells

To preserve the cell lines, they were frozen down at low passage number for future experiments. All cell lines were cryopreserved between passage 2-8. Once cell lines had reached passage 25, they were discarded, and frozen stocks were brought up.

All cell lines once confluent were washed with PBS and detached using 0.05% trypsin. The cell suspension was spun down at 1000 RPM for 5 minutes and media removed. The cell pellet was resuspended in 5mL of complete MEM and cells were counted using a haemocytometer (Jencons, UK). 1×10^6 cells were then aliquoted in cryovial tubes (StarLab UK) containing 10% FBS, 10% DMSO (Sigma Aldrich, UK) and 80% complete media, making up the freeze buffer. Cells were placed in a -80°C freezer for 2 weeks and then placed in liquid nitrogen.

Cryovials containing 1mL of frozen cells were removed from the -80°C freezer and defrosted before being spun at 1000 RPM for 5 minutes. Freeze buffer was then removed, and the cell pellet resuspended in 1mL of complete media and then transferred to a 25cm^3 flask (Fisher Scientific UK) containing 5mL of complete MEM. Flasks were checked daily and once confluent; cells were passaged into 75cm^3 flasks containing 15mL of complete MEM.

2.3 Cell Doubling Time

To determine the time required for each cell line to double in number a population doubling time assay was performed. Cell doubling times for each cell line determined the time cells would be incubated with drugs. This assay was performed with 3 technical and 3 biological replicates. 1×10^5 cells were plated out in 14 x $T25\text{cm}^3$ flasks. Each 24-hour period 3 flasks were washed with PBS and cells detached with 0.05% trypsin. Detached cells were neutralised in 5mL of complete MEM and a haemocytometer used to count the cells. This was repeated for 7 days and cell doubling time was determined using the following equation, where q_1 and q_2 are the number of cells measured at initial time t_1 and final time t_2 respectively.

$$\text{Doubling time} = (t_2 - t_1) \times \left[\frac{\log 2}{\log (q_2) - \log (q_1)} \right] \quad (\text{Equation 1})$$

This assay was carried out in triplicate and the results were analysed in GraphPad prism (version 10.3.1).

2.4 Drug Preparation

Temozolomide, Dimethyl fumarate and Monomethyl Fumarate (All Sigma-Aldrich, UK), were dissolved in 100% DMSO (Sigma-Aldrich, UK) to give a master stock. All solutions were then filtered using a 0.22µm sterile filter (Merck UK). Master stocks of each drug were aliquoted and stored at -20°C to avoid freeze thaw cycles. Workable stocks from each master stock were prepared using PBS and aliquoted for -20°C storage to avoid freeze thaw cycles.

2.5 Cell Treatments with Drugs

For the treatments of all cell lines, cells were seeded into T25cm³ flasks (ThermoFisher, UK) at 1 x10⁵ cells and incubated at 37°C in a 5% CO₂ environment and left until exponential growth phase was reached (2 days or ~70% confluency). Cells were then washed with PBS and 1.5mL of media containing the appropriate concentration of drugs was added. Incubation period of the cells with the drugs was dependent on the assay.

2.6 Cell X-ray Irradiation treatment

X-ray irradiation treatment for radiation studies were performed on all three lines. Cells were seeded into T25cm³ flasks at 1 x10⁵ cells and incubated at 37°C in a 5% CO₂ environment and left until exponential growth phase was reached. Cells were then washed with PBS and 1.5mL of fresh complete media was added to the flasks before X-ray exposure. X-ray exposure was performed with a X-RAD225KV X-ray cell irradiation cabinet (Precision X-ray, USA). Doses between 0-12Gy were delivered at a dose rate of 2.2Gy/min.

2.7 Combination Therapy Treatments

Combination treatments were carried out on all three lines. Due to supply issues during the covid-19 pandemic, cells were seeded into 6 well dishes at 1×10^5 cells/well and incubated at 37°C in a 5% CO₂ environment and left until exponential growth phase was reached. Media was then removed from the cells and 1.5mL of fresh media containing the appropriate single or combination treatment of TMZ or MMF was added to the wells. For double or triple combinations with either MMF+RT, TMZ+RT or MMF+TMZ+RT, media containing drug(s) was added to the well and subsequent X-ray exposure was performed for either 1Gy or 2Gy exposure.

2.7.1 Scheduled treatments

For treatment scheduling with MMF prior to TMZ, RT or TMZ+RT exposure, cells were seeded into 6 well dishes (ThermoFisher, UK) at 1×10^5 cells/well and incubated at 37°C in a 5% CO₂ environment and left until exponential growth phase was reached. Media was then removed from the cells and 1.5mL of fresh media containing MMF at the appropriate concentration were added. MMF treatment was left on the cells for 4 hours before media containing drug was removed. Cells were washed with PBS and 1.5mL of fresh media containing the combination drugs were added. For RT combinations, cells were subsequently exposed to X-ray radiation as described in section 2.7.

All combination treatments were given in two schedules, simultaneous administration or 4hr MMF pretreatment (PT4) followed by the combination. IC₅₀ values for each drug/cell line were calculated using non-linear regression analysis of single agent curves on GraphPad Prism 10 software (version 10.3.1). Combination doses were calculated by using drug IC₅₀ values in ratio to each other, with two combinations above and below the IC₅₀ combination being constructed. Drug combinations are not linear with the interaction between the drugs not known, hence a range higher and lower than the IC₅₀ was utilised. A fixed ratio method for designing drug combinations for combination index analysis is encouraged by the combination index analysis model used.

2.8 Clonogenic Assay

Clonogenic assays were performed on all three cell lines to measure the clonogenic capacity of individual cells and the relative cell survival following exposure to both drugs and RT. UVW, U87 and T98g GBM cells were seeded at 1×10^5 cells in T25cm³ flasks and incubated at 37°C in a 5% CO₂ environment and left until exponential growth phase was reached. Media was removed from the cells and flasks washed with PBS; the appropriate treatment added as described in section 2.5 to 2.7.1. Cells were exposed to the drugs for one doubling time of ~24 hours. Media containing drug was then removed and cells washed with PBS. Treated cells were detached from flasks with the addition of 2mL of 0.05% trypsin. Once detached, cells were neutralised in 5mL of media and disaggregated to a single cell suspension with a 21-gauge needle. A haemocytometer was then used to count cells. 250 UVW cells, 500 U87 cells and 300 T98g cells were then seeded in triplicate into 60mm petri dishes (ThermoFisher, UK), with 5mL of medium. Dishes were incubated for 10-12 days until colonies of more than 50 cells were visible to the eye.

Combination clonogenics due to supply issue during covid-19 were seeded and plated into 6 well dishes. UVW, U87 and T98g GBM cells were seeded into 6 well dishes at 1×10^5 cells/well and incubated at 37°C in a 5% CO₂ environment and left until exponential growth phase was reached. Media was removed from the cells and flasks washed with PBS; the appropriate treatment added as described in section 2.5 to 2.7.1. Cells were exposed to drug for one doubling time of ~24 hours. Media containing drug was then removed and cells washed with PBS. Treated cells were detached from plates with the addition of 2mL of 0.05% trypsin. Once detached, cells were neutralised in 5mL of media and disaggregated to a single cell suspension with a 21-gauge needle. A haemocytometer was then used to count cells. 250 UVW cells, 500 U87 cells and 300 T98g cells were then seeded in triplicate into 6 well plates (ThermoFisher, UK), with 5mL of medium. Plates were incubated for 7-12 days until colonies of more than 50 cells were visible to the eye.

Once colonies had formed, media was removed from UVW and T98g cells colonies and dishes washed with PBS before being fixed in 100% methanol (ThermoFisher,

UK). Cells were left to fix for ~15 minutes and methanol removed. Fixed colonies were stained with 10% Giemsa solution (ThermoFisher, UK) for 30 minutes. Dishes were washed with water and visible colonies counted by eye. U87 colonies were gently washed with PBS and fixed with 4% Paraformaldehyde (Thermo Fisher, UK) for 20 minutes. Fixed colonies were stained with 0.01% crystal violet in dH₂O for 30-60 minutes. Dishes were washed with water and visible colonies counted by eye.

Survival fraction was calculated as:

$$\text{Survival Fraction} = \frac{\text{(Number of colonies/number of colonies seeded)}}{\text{(Number of control colonies/number of colonies seeded)}}$$

(Equation 2)

2.9 Combination Index Analysis

Combination index analysis was performed on combinations described in section 2.7 and 2.7.1 using Compusyn software (Biosoft UK) (Chou, 2006; Chou, 2010). Combination index analysis determined if combinations had synergy, were antagonistic or additive when combined at the concentrations used.

The median effect equation was applied to each drug used in combination as a single treatment and on the combination itself. Median effect characterised the proportion of cells in the population affected by treatment and was calculated individually for each drug used in combination and the combination itself by the software:

$$F_a/F_u = (D/IC_{50})^m \quad \text{(Equation 3)}$$

Where F_a is fraction affected and F_u is fraction unaffected in the population by the drug dose D . m signifies the sigmoidicity of the curve and is a Hill-equation type coefficient. Median effect was linearised by transforming each side of the equation to be log to give median effect plot:

$$\log Fa/Fu = m \log (D) - m \log (IC_{50}) \quad (\text{Equation 4})$$

From this equation, the dose of drug and the combination required to produce a set amount of toxicity was determined using:

$$D = IC_{50}(Fa/Fu)^{1/m} \quad (\text{Equation 5})$$

From these equations it is assumed the mode of action of drugs are mutually exclusive and the effect of the combination is described using:

$$CI = (D)_1/(Dx)_1 + (D)_2/(Dx)_2 \quad (\text{Equation 6})$$

Where D is the dose of each drug used in combination required to inhibit x percentage of cells. Dx is the dose of each drug required to inhibit x percentage of cells as a single agent. CI is the combination index, which can be:

CI < 0.9 = synergistic

CI 0.9-1.1 = Additive

CI >1.1 = Antagonistic

2.10 Glutathione Assay

For assessment of relative glutathione levels, UVW, T98 and U87 cells were seeded into 6 well plates at 50,000 cells per well and incubated for 48 hours at 37°C in a 5% CO₂ environment with 3mL of complete media. Media was then removed, cells washed with PBS and treated with the relevant drug. Depending on the time point, treatment was either removed after 4 hours, 24 hours, 48 hours or cells were washed with PBS after 24 hours and fresh media was added for the appropriate length of time

corresponding to the time point. At the time point, treatment or media was removed and cells washed with PBS and detached with trypsin. Once detached cells were neutralised in media and spun down at 1000 RPM for 5 min. Cells were then treated following the Glutathione colorimetric detection Kit EIAGSHC (Thermo Fisher, UK). Cell pellets were resuspended in 5% SSA at 1×10^6 cells/mL. Cells were then centrifuged and underwent freeze thaw cycling to lyse the cells. Samples were incubated for 10 minutes at 4°C and respun at 14,000 RPM for 10 minutes. Supernatant was collected for analysis. The reaction mixture was prepared using NADPH, glutathione reductase with assay buffer. The Colorimetric detection was prepared by mixing colourimetric detection concentrate and assay buffer. 50µL of sample was added to a flat bottom 96 well plate with 25µL of reaction mixture and colorimetric detection reagent. The plate was gently mixed and left to incubate in the dark at room temperature. GSH absorbance was then determined by reading absorbance of the plate at 405nm using a Flexstation 3 Multimode microplate reader (Molecular Devised, California, USA). Each glutathione experiment was carried out in three biological replicates unless stated otherwise. Standard curves were generated for each replicate and used to calculate the total GSH levels from the absorbance reading.

2.11 Cell cycle

Cell cycle analysis was performed to assess the effect of treatments at the different stages of the cell cycle. UVW, T98 and U87 cells were seeded into 6 well plates at 50,000 cells per well and incubated for 48 hours at 37°C in a 5% CO₂ environment with 3mL of complete media. Media was then removed, cells washed with PBS and treated with the relevant single or double therapy combinations as described in sections 2.5-2.71 and incubated for a further 24 hours. Depending on the time point, treatment was either removed after 24 hours or cells were washed after 24 hours and fresh media was added for the appropriate length of time corresponding to the time point. At the time point treatment or media was removed and cells washed with PBS and detached with trypsin. Once detached cells were spun down at 1000 RPM for 5 minutes to pellet and fixed with 70% cold ethanol. After fixation, supernatant was removed and pellets were resuspended in PBS and centrifuged at 1000 RPM for 5 minutes. Fixed pellets were incubated with 50µg/mL bovine ribonuclease A (Sigma-

Aldrich, UK) and 10µg/mL propidium iodide (Sigma-Aldrich, UK). Stained cells were incubated at 4°C for 1 hour minimum and away from light before analysis. Samples were analysed with a flow cytometer on an Attune™ NxT (Thermo Fisher Scientific USA) with 10,000 events per sample. Propidium iodide binds to DNA and fluoresces with the fluorescence intensity related to the quantity of DNA within the cell, measured using a 488nm laser. Data was analysed using GraphPad software version 10.3.1 and data reported as an average of three independent experiments. Representative flow cytometer plots for cell cycle data is shown in Appendix 1.

2.12 Apoptosis Detection

Annexin V staining was used on UVW, U87 and T98 cells, to assess the population of cells undergoing apoptosis using an anti-annexin V FITC conjugate and propidium iodide. The use of an Annexin V assay enabled the percentage of cells undergoing apoptosis to be quantified, through PI stain and FITC stain. The use of both stains allowed for early and late phase apoptotic cells to be distinguished from necrotic cells. FITC binds to phospholipid phosphatidylserine (PS) which translocate to the outer parts of the cell membrane when cells are undergoing early apoptosis. PI staining, similarly, to cell cycle, binds to DNA and RNA. This occurs when membranes are disrupted, and cells are in late stages of apoptosis or in necrosis. By use of positive FITC and PI controls, identification of each fluorescent stain was done through flow cytometry. Cells which are FITC+ and PI- show early apoptosis, FITC+ and PI + shows late apoptosis, FITC- and PI positive distinguishes necrotic cells and FITC- and PI-negative distinguishes viable cells. Each stain identified different stages of the apoptotic pathway, with early, late and necrotic cells. Controls of cells treated with triton X and hydrogen peroxide were used to distinguish populations on the Flow cytometer plot. Representative Flow cytometer plots are shown in Appendix 2. 50,000 cells were plated into 6 well plates containing 3mL of complete media. Cells were incubated at 37°C in a 5% CO₂ environment for 48 hours. Media was then removed, cells washed with PBS and treated with the relevant single or double therapy combinations as described in sections 2.5-2.7.1 and incubated for a further 24 hours. Depending on the time point, treatment was either removed after 24 hours or cells were washed after 24 hours and fresh media was added for the appropriate length of

time corresponding to the time point. At the time point treatment or media was removed and cells washed with PBS and detached with trypsin. Cell suspension was pelleted at 1000 RPM for 5 minutes and supernatant removed. Pellets were resuspended in PBS and respun twice. PBS was removed and 1×10^6 cells were resuspended in 100 μ l of binding buffer (BD science). 5 μ l of propidium iodide and 5 μ l of FITC conjugated Annexin V stain (both BD science) were added to samples and left to incubate in the dark for 15 minutes at room temperature. After incubation a further 250 μ l of binding buffer was added to samples and Flow cytometry was performed using an Attune™ NxT Flow cytometer (Thermo Fisher Scientific USA). 10,000 events were measured per sample and the percentage of cells which were, necrotic, viable or in early or late apoptosis provided by the FACs analysis. Data was analysed on GraphPad Prism software version 10.3.1. Appendix 2 shows representative gating and flow cytometer plots.

2.13 Comet Assay – Single cell gel electrophoresis

A comet assay was performed to assess the DNA damage caused by treatments on the UVW, T98 and U87 cell lines following the Comet SCGE assay kit, (ADI-900-166, ENZO, UK). Cells were seeded into 6 well plates at 50,000 cells per well and incubated for 48 hours at 37°C in a 5% CO₂ environment with 3mL of complete media. Media was then removed, cells washed with PBS and treated with the relevant single or double therapy combinations as described in sections 2.5-2.71 and incubated for a further 24 hours. Depending on the time point, treatment was either removed after 24 hours or cells were washed after 24 hours and fresh media was added for the appropriate length of time corresponding to the time point. At the time point media was removed and cells washed with PBS and detached with trypsin. Once detached cells were passaged through a 23-gauge needle to create a single cell suspension. Cells were counted using a haemocytometer (Jenson, UK) and suspended at a density of 5×10^5 cells/mL combined with low melting point agarose (1%). 80 μ L of the cells suspended in low melting point agarose were placed on ENZO comet slides. Slides were lysed for 2 hours in lysis solution and then placed in sodium hydroxide for 1 hour. Slides were then placed in a gel tank and ran at 45V for 12 minutes. Slides were stained with 1X SYBR green and left overnight to dry in the dark. Slides were

analysed using an EVOS FL auto system (Life Technologies, UK). Comets were imaged and analysed as described by Geller *et al.*, (1999). Cells were analysed using ImageJ with plug in Open Comet v1.3. Open Comet provided an output after measuring both tail length and intensity of the SYBR green signal, known as tail moment. The mean number of comets analysed in each treatment group was 100 and the measurement of tail moment was taken. Representative comet assay images are shown in Appendix 3.

2.14 Western Blot Analysis

Expression of MGMT status of the cells was determined on untreated cells. Cells were seeded into 6 well plates at 50,000 cells per well and incubated for 48 hours at 37°C in a 5% CO₂ environment with 3mL of complete media. Media was then removed and the untreated cells harvested at this point for MGMT protein detection in the cell lines. Media was removed from the cells and lysed with Laemmli's sample buffer. SDS-polyacrylamide Gel Electrophoresis was performed using resolving gels containing 0.1% SDS, 0.375M Tris base (pH 8.8), 3% glycerol, distilled water and the appropriate amount of 30% acrylamide/bisacrylamide stock depending on the size of the protein of interest, 10% ammonium persulfate and 0.05% TEMED (all Sigma-Aldrich, UK).

Lysed cell samples were run in triplicate in a 12% tris-glycine gel at 135 volts for 80 minutes. Gels were transferred onto a nitrocellulose membrane (Thermo Fisher, UK) at 300 volts for 135 minutes. Following transfer, a picosin stain was added to the membranes to detect for protein. Membranes were then washed in dH₂O to remove stain and blocked for 2 hours in 3% BSA at room temperature. Membranes were then incubated overnight at 4°C with rabbit anti MGMT primary antibody (Abcam UK) diluted 1:1000 in 0.3% BSA in tween tris-buffered Saline (TBST). Following incubation, the membranes were washed 3x in TBST and incubated with anti-rabbit secondary HRP-conjugated antibody, diluted 1:7000 (Millipore, UK) for 2 hours at room temperature. The membranes were washed a further 3 times in TBST and developed using ECL 1 (1:1 mixture of solution (1M Tris pH 8.5, 250mM luminol, 250mM p-cymuric acid and water) and ECL 2 (1M Tris pH8.5, 0.19% H₂O₂ and water) system (all Sigma-Aldrich, UK). Membranes were stripped using beta-mercaptothion and left on a shaker at 60°C for 15 minutes. Membranes were washed in TBST and

blocked for 2 hours in 3% BSA. A GAPDH loading control antibody (Abcam, UK) was diluted 1:3000 in 0.3% BSA and left overnight on the membrane at 4°C. Steps were then repeated as previously stated.

2.15 RNA extraction and quantification

For direct determination of the differing effects of DMF and MMF on GBM cells, RT-qPCR was performed on RNA extracted cells treated with DMF and MMF as single treatments and at 2 concentrations and time points. Cells were seeded at 1×10^5 cells/well in a 6 well plate and incubated for 48 hours at 37°C and 5% CO₂ environment. Cells were then treated following a similar protocol to section 2.5 with DMF and MMF as single therapies. A 4 hour and 24 hour time point was assessed. Following incubation with drug, media was removed and cells detached with trypsin and spun down to pellet at 1000 RPM for 5 minutes. RNA extraction was performed using Monarch Total RNA miniprep kit (New England Biolabs; LOT 10210910).

Once RNA was extracted RNA was quantified using a nanodrop (Nanodrop 2000c, Thermo Scientific) prior to RT-qPCR.

2.16 RT-qPCR

To determine how MMF and DMF effect the gene expression of NrF2, P65, DJ2 and GPX4, RT-qPCR was performed following RNA extraction as described in section 2.15. RT-qPCR was performed using SensiFast SYBR Hi-ROX One-Step kit (Meridian Bioscience).

Extracted RNA was mixed with 2x SensiFast SYBR Green mix (10µL), forward primer (10µM), reverse primer (10µM), reverse transcription, Ribosafe RNase inhibitor and RNase free water for a total volume of 20µL per sample. Primers used are shown in Table 2.1. 20µL of reaction mix was added to each well and reactions were carried out in a Step-one plus (Applied biosystems, UK) with 40 cycles. Data was analysed using the $2^{-\Delta\Delta CT}$ method to reference gene GAPDH (Livak and Schmittgen, 2001). Representative amplification plots are shown in Appendix 5.

Gene	Primer Pair
NrF2	Forward 5'-AAACCAGTGGATCTGCCAAC-3' Reverse 5'-TCTACAAACGGGAATGTCTGC-3'
P65	Forward 5'-CCGCACCTCCACTCCATCC -3' Reverse 5'-ACATCAGCACCCAAGGACACC-3'
DJ1	Forward 5'-GAGCAGAGGAAATGGAGACGGTCAT3' Reverse 5'-CACGGCTACACTGTACTGGGTCTT-3'
GPX4	Forward 5'-AGCAAGATCTGCGTGAACGG-3' Reverse 5'-GACGGTGTGCAAACCTTGGTG-3'
GAPDH	Forward 5'-GAAATGTGCTTTGGGGAGGC-3' Reverse 5'-GGGGACAGGACCATATTGAGG-3'

Table 2.1: Primer sequences used for each gene interrogated using RT-qPCR

2.17 Ferroptosis Assay

A ferroptosis assay was performed to assess if DMF and MMF were able to induce ferroptosis in the UVW, U87 and T98g cell line. Cells were seeded at 3000 cells per well into a 96 well plate and left for 24 hours. Media was then removed and cells treated with DMF, MMF, RSL3, Erastin or Ferrostatin (all Sigma-Aldrich) following the same protocol as 2.5, DMF and MMF were combined with Ferrostatin following the same protocol as 2.7. Treatments were left for 24 hours and then removed and replaced with Resazurin stain (Scientific laboratory Supplied) at a concentration of 0.15mg/mL and incubated in the dark for 4 hours. Following the incubation, fluorescence was measured at 560nm excitation/590nm emission using the FlexStation3 plate reader.

2.18 Spheroid Formation

3D spheroid models were used to analyse the effect of single, combination and scheduled treatments, TMZ, MMF and Radiation on 3D cultured glioblastoma cell lines. The UVW and U87 cell lines were utilised as they could form and develop into 3D spheroid models whereas T98 cells were unable to thrive over time and develop hypoxic cores. 1.5×10^6 cells were seeded into spinner flasks (Corning, UK) with fresh medium and gassed with 5% CO₂. Spinner flasks were left in a 37°C environment on

a Techne stirrer flask. Media and gas were renewed every 2 days until spheroids reached a diameter of ~300nM. Spheroids were then individually picked and seeded into 3% agarose coated 24 well plates with 1mL of complete medium (Thermo Fisher UK).

2.19 Spheroid Treatment

Spheroids were treated once plated into 24 well plates. Media was removed from each well without disturbing the spheroid and 1mL of medium containing the appropriate concentration of drug was added similar to section 2.5 to 2.7.1. Each treatment per replicate was performed on 12 individual spheroids. Following a 24-hour incubation with treatment, treatment was removed and spheroids washed with PBS before fresh medium was added. Spheroids were imaged on the day treatment was removed and then every 3-4 days for 24 days using an EVOS FL auto system at 4x magnification (Life Technologies, UK). Media was replenished twice a week by removing 250µL and replacing it with fresh medium. Representative spheroid images are shown in Appendix 4.

2.20 Spheroid Analysis

Spheroid images taken every 3-4 days were analysed using SpheroidSizer software (Chen *et al.*, 2014) for MATLAB (version R2013a). Spheroid volumes were determined by the software using the following equation, with Dmax representing the maximum diameter and Dmin representing the minimum diameter of the spheroid:

$$V = \frac{1}{2} (d_{max} \times (d_{min})^2) \quad (\text{equation 7})$$

The change in spheroid volume (V/V_0) at each measurement was calculated by dividing the spheroid volume (V) at each time point by the initial spheroid volume (V_0). Data was reported as V/V_0 , to compare the change in volume between treatments. Each V/V_0 was taken as an average of three independent experiments \pm standard error of the mean, with a total of 12 individual spheroids per treatment group per replicate. Area under the curve (AUC) was calculated for each treatment using GraphPad prism software version 10.3.1.

2.21 Statistical Analysis

All data reported was an average of three independent experiments, unless stated otherwise. All data was analysed using GraphPad Prism software (version 10.3.1 GraphPad Software Inc, USA). Before statistical significance Shapiro-wilk tests were performed on the data to check for normality and stated if the data was non-parametric. Parametric data was analysed using either a one-way or two-way ANOVA

For single variables, the degree of significance was measured using a one-way ANOVA with Bonferroni post-tests. P-values of less than 0.05 were taken as statistically significant. For combination treatments or where multiple groups or variables were being assessed, the degree of significance was measured using a two-way ANOVA with Bonferroni's post-testing. Again P-values less than 0.05 were taken as significant.

Chapter 3

Characterising single and combination treatments of Temozolomide and Monomethyl Fumarate on 2D Human Glioblastoma cell lines.

3.1 Introduction

Management of Glioblastoma (GBM) is normally multimodal and includes surgery, radiotherapy and Temozolomide (TMZ) as the standard of care. However, as previously discussed, many patients either develop resistance to treatment or have an MGMT+ status making them resistant to the alkylating agent TMZ (Strobel *et al.*, 2019). Due to time and cost restraints in progressing novel treatments, repurposing drugs has become more common. Creating novel drugs for GBM has an added element of difficulty due to the presence of the blood brain barrier (BBB) which prevents penetration of many drugs into the brain and hence into tumours located in the brain.

Monomethyl Fumarate (MMF) the metabolite of DMF, has elicited contradicting views in the literature over its mechanism of action, with some papers stating it functions in the same way as DMF as it is the direct metabolite of DMF. Some papers more recently have shown the two compounds have alternative functions and have also shown their mechanisms to be dose-dependent (Brennan *et al.*, 2015; Saidu *et al.*, 2019; Yazdi and Mrowietz, 2008; Yao *et al.*, 2016). MMF is also used more commonly now than DMF as it has fewer side effects on the gastrointestinal tract than DMF (Wynn *et al.*, 2020).

Glutathione plays an important role in mammalian tissues as the most abundant non-protein thiol present. As previously discussed, GSH can regulate the cellular redox state of cells and protect them from damage (Kennedy *et al.*, 2020). In more recent studies GSH has been shown to play an important role in cell differentiation, apoptosis, proliferation and ferroptosis (Kennedy *et al.*, 2020). Different approaches have been taken to control GSH levels in cancerous cells, with some researchers

directly depleting GSH via pro-oxidant—benzoyloxy dibenzyl carbonate preventing its antioxidant properties (Yoo *et al.*, 2019).

As DMF has shown promise as a combination therapy for GBM in both clinical trials (Shafer *et al.*, 2020) and by our group (Scott, 2020) we sought to assess if MMF would have similar or alternating effects on GBM cell lines and if MMF synergised with the current GBM chemotherapy Temozolomide. Additionally, within our group MMF has shown promise when combined with current treatments in both breast and pancreatic cancer studies (Gardiner, 2023; Mullen, 2024). Mechanistic DMF combination studies were not taken forward and MMF was focused on due to this work being completed by (Scott 2020).

We hypothesise that MMF could be more cytotoxic than DMF due to MMF being the direct metabolite of DMF, and therefore already in active form and will be synergistic with TMZ. We also hypothesised that determining the correct scheduling of treatments used in combination will elicit a greater toxicity on the glioma cells over simultaneous administration due to the glutathione/Nrf2 homeostasis within the cells. Through a series of cell survival assays and mechanistic assays, the use of MMF in GBM was interrogated as a combination therapy with TMZ.

3.2 Aims

The aims of this chapter were:

- To characterise the 2D response of U118, U87 and T98g human glioblastoma cell lines to the combination treatment of Temozolomide and Monomethyl-Fumarate
- To determine the optimal schedule of treatment based on MMF's inhibition of glutathione levels
- To identify the potential mechanism of action of the combination and schedule underpinning MMF and TMZ cytotoxicity, using 2D cell culture.

3.3 Materials and Methods

3.3.1 Combination and Scheduled treatments

Combination treatments of Temozolomide and Monomethyl Fumarate were prepared as described in section 2.7 and 2.71. The combinations of Temozolomide and Monomethyl Fumarate were calculated using the IC₅₀ and using two concentrations above and 2 concentrations below following a fixed ratio method. Combinations are shown in table 3.1 for all three cell lines.

UVW		
Combination	Temozolomide (µM)	Monomethyl Fumarate (µM)
1	8.75	1.19
2	13.10	1.79
3	19.7	2.7
4	29.5	4.05
5	44.32	6.07
T98		
1	75	0.75
2	150	1.5
3	250	2.5
4	350	3.5
5	450	4.5
U87		
1	0.71	0.84
2	1.06	1.26
3	1.6	1.9
4	2.4	2.8
5	3.6	4.2

Table 3.1: The combinations of Temozolomide and Monomethyl Fumarate used for the combination treatments and for the schedule treatments throughout Chapter 3.

3.4 Results

3.4.1 Determination of the MGMT status of UVW, U87 and T98g Human GBM cell lines

The O6-methylguanine (O6-MeG)-DNA methyltransferase (MGMT) gene is an important molecular biomarker for how patients will respond to the alkylating agent TMZ. To fully decipher our combination treatments, both MGMT positive and negative human glioma cell lines were interrogated. MGMT+ human GBM cell line T98g was used, as well as MGMT negative UVW human GBM cells and MGMT negative cell line U87s (Scott, 2020; Wang *et al.*, 2017). To confirm the MGMT status of the cell lines, a western blot analysis was performed using the Anti-MGMT antibody (Abcam, UK) which detects the presence of the MGMT protein (22kDa).

Figure 3.1 shows the basal expression of MGMT in the T98g cell line, with three distinct bands at 22kDa in the three separate cell lysate samples. Three cell lysates for UVW and U87 show no positive gene expression for MGMT, confirming their MGMT negative status.

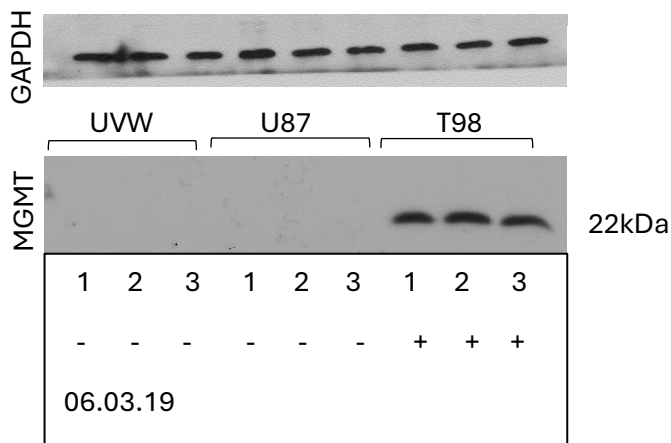


Figure 3.1: Human glioblastoma cell lines, UVW, U87 and T98g cell lysates western blot analysis for expression of MGMT. Data presented is one of three independent experiments. Numbers “1, 2 and 3” represent the 3 samples per cell line. 20µL of sample was loaded per well.

3.4.2 Assessing the cytotoxic effect of single therapies on human glioblastoma cell lines.

Single agent curves were used to determine each drug's individual cytotoxicity on UVW, U87 and T98g cell lines. Temozolomide (TMZ), Monomethyl Fumarate (MMF) and Dimethyl fumarate (DMF) were all used as single therapies in a clonogenic survival assay. This allowed the IC_{50} to be elucidated and informed on the potency of the drug on 2D cell culture. Clonogenic assays also allow observation of the long-term effects of a drug on the ability of the cell to form colonies. This is important as cells may not die immediately and will carry the damage caused by a drug through a few cell cycles before ultimately succumbing to the elevated levels of damage and entering mitotic catastrophe (Bai *et al.*, 2023).

Unlike DMF, which has been used in a clinical trial for GBM with TMZ and radiation (Shafer *et al.*, 2020), there is no known literature on the effect of MMF on these GBM cell lines.

3.4.2.1 Assessment of the toxicity of Temozolomide, Dimethyl Fumarate and Monomethyl Fumarate on the UVW cell line.

Initial assessment of the cytotoxic effect of TMZ, DMF and MMF, on the UVW cell survival after 24- hour incubation with each single agent treatment was assessed via clonogenic assay. Figure 3.2 shows the cytotoxic response of UVW cells to increasing doses of single agents compared to the untreated control.

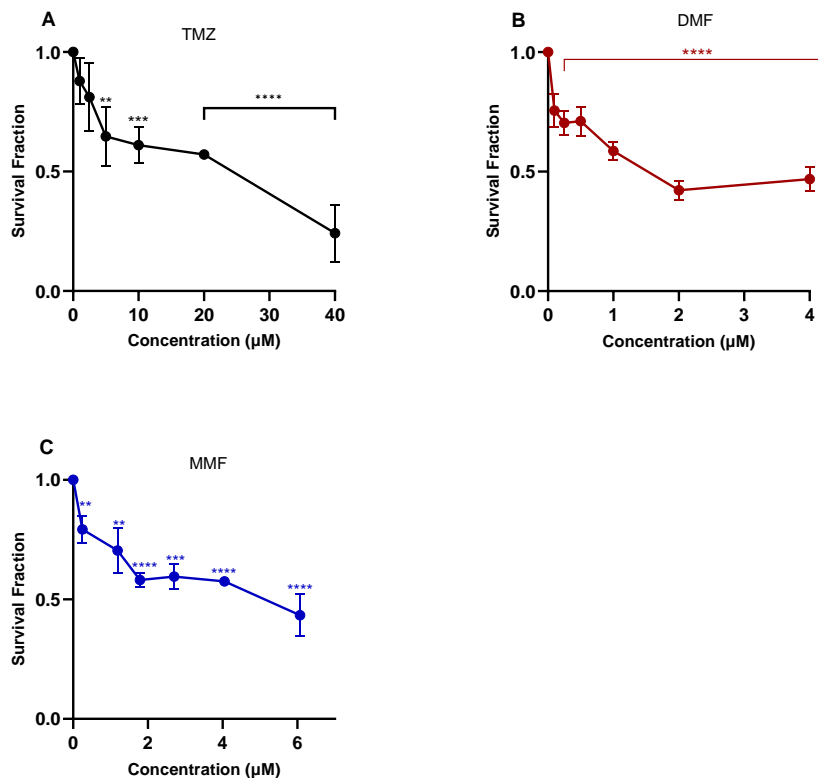


Figure 3.2: The effect on UVW glioblastoma cell clonogenic survival after incubation with increasing doses of (A) Temozolomide, (B) Dimethyl Fumarate and (C) Monomethyl Fumarate after 24-hour exposure versus the untreated control. The data presented is an average of 3 independent experiments \pm standard deviation. Statistical analysis of data was performed using a one-way ANOVA with Bon-Ferroni post-test. With P-values of $<0.05 = *$, $<0.01 = **$, $<0.001 = ***$ and $P<0.0001 = ****$ reported as significant.

As seen in Figure 3.2 (A), the UVW cell line (MGMT-) had a dose response to increasing concentrations of TMZ. A maximum reduction in clonogenic survival of 77% \pm 12% was seen after incubation of the cells with 40 μ M TMZ, a statistically significant

reduction in clonogenic survival compared to the untreated control ($P < 0.0001$). The IC_{50} was determined to be $19.7\mu\text{M}$ ($R^2 = 0.85$). using the non-linear regression model fit on GraphPad prism.

Figure 3.2 (B) shows the response of UVW cells to increased concentrations of DMF. We observed an initial dose dependent reduction in clonogenic survival after incubation of the cells with $0.1\mu\text{M}$ to $2\mu\text{M}$ DMF. There was a statistically significant reduction in clonogenic survival in treated cells compared to the untreated control ($P < 0.0001$). The reduction in clonogenic survival of cells increased from $25\% \pm 7\%$ at $0.1\mu\text{M}$ to $58\% \pm 3.9\%$ after exposure to $2\mu\text{M}$ DMF. After incubation of the cells with higher DMF concentrations there was a plateau of clonogenic survival. Incubation of UVW cells with $4\mu\text{M}$ of DMF gave a $46\% \pm 4.9\%$ reduction in clonogenic survival, which was statistically significant compared to the untreated control ($P < 0.0001$). The IC_{50} was calculated to be $12.4\mu\text{M}$ ($R^2 = 0.88$).

The effect of MMF on the UVW cell line is shown in Figure 3.2 (C). We can see a reduction of clonogenic survival, in a dose-dependent manner. A maximum of $57\% \pm 8\%$ reduction in clonogenic survival was observed after exposure to $6\mu\text{M}$ MMF. All concentrations used gave a statistically significant cell kill over the untreated control (all $P < 0.01$). The data show the UVW cell line to be more sensitive to MMF than DMF or TMZ, with an IC_{50} of $2.7\mu\text{M}$ ($R^2 = 0.96$).

Cumulatively data from Figure 3.2 suggests that MMF was more cytotoxic to UVW cells than TMZ and DMF which is surprising as no known mode of cell death is known for MMF on the UVW cell line. The data also suggests all fumarates are more cytotoxic to the UVW cell line than TMZ at the concentrations tested here, as TMZ has the highest IC_{50} .

3.4.2.2 Assessment of the toxicity of Temozolomide, Dimethyl Fumarate, Monomethyl Fumarate and Diroximel Fumarate on the U87 cell line.

Initial assessment of the cytotoxic effect of TMZ, DMF and MMF, on the U87 cell survival after 24- hour incubation with each single agent treatment was assessed via clonogenic assay. Figure 3.3 shows the cytotoxic response of U87 cells to increasing doses of single agents compared to the untreated control.

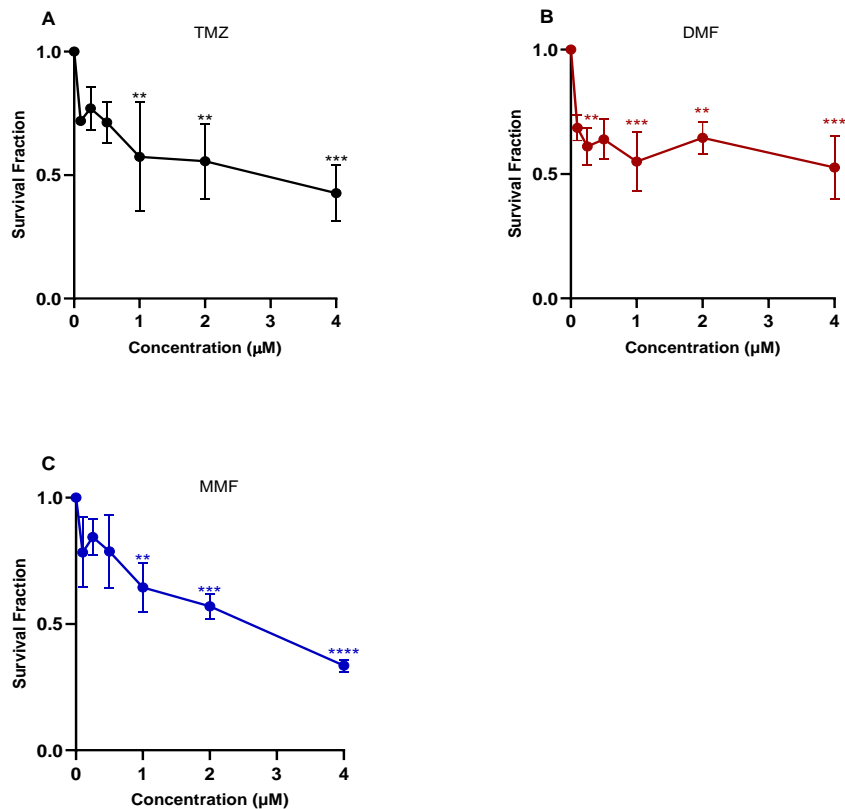


Figure 3.3: The effect on U87 glioblastoma cell clonogenic survival with increasing doses of treatment (A) Temozolomide, (B) Dimethyl-Fumarate and (C) Monomethyl-Fumarate after 24-hour exposure versus the untreated control. The data presented is an average of 3 independent experiments \pm standard deviation. Statistical analysis of data was performed using a one-way ANOVA with Bon-Ferroni post-test. With P-values of $<0.05 = *$, $<0.01 = **$, $<0.001 = ***$ and $P < 0.0001 = ****$ reported as significant.

The effect of increasing doses of TMZ on the U87 cell line (MGMT-) is shown in Figure 3.3 (A) where there is a statistically significant reduction in clonogenic survival after 1 μ M compared to the untreated control (all $P < 0.01$). Incubation of cells with 0.1 μ M to 0.25 μ M TMZ induced a $29\% \pm 1.2\%$ and $23\% \pm 8.6\%$ reduction in clonogenic survival respectively. A maximum reduction in clonogenic survival of $29\% \pm 8\%$ was reached after exposure to 0.5 μ M TMZ. A second phase of reduction in clonogenic survival was seen between 1 μ M and 4 μ M, as the maximum reduction in clonogenic survival reached $58\% \pm 11\%$ after 4 μ M TMZ exposure, a statistically significant reduction in clonogenic survival compared to the untreated control ($P < 0.001$). The response of TMZ on the U87 cell line is unusual, as the literature and previous work has shown a

steady dose response curve (Babaloui, 2022; Zou *et al.*, 2021). The data shown provided an IC₅₀ of 1.6µM (R²=0.94)..

From Figure 3.3 (B), the effect of increasing doses of DMF on the U87 cell demonstrated a statistically significant reduction in clonogenic survival across all concentrations against the untreated control (all P<0.01). No trend is seen with the reduction in clonogenic survival, as the reduction in clonogenic survival does not pass 50% at any concentration. At 0.1µM, 0.25µM and 0.5µM DMF we see 32% ± 5%, 39% ± 7% and 37% ± 8% reduction in clonogenic survival respectively. At 1µM, 2µM and 4µM of DMF we see 46% ± 11.8%, 36% ± 6% and 48% ± 12.8% reduction in clonogenic survival respectively. From the data, the IC₅₀ was undetermined.

The cytotoxicity of MMF is shown in Figure 3.3 (C). A steep dose response curve was observed after 0.25µM MMF exposure with statistically significant increases in the reduction of clonogenic survival compared to the untreated control after 1µM MMF (all, P<0.01). Incubation of cells with 0.1µM MMF induced a reduction in clonogenic survival of 22% ± 13%. Clonogenic survival increased after exposure to 0.25µM MMF, with a 16% reduction on clonogenic survival ± 7%. As the concentration of MMF increased a steep dose response was observed, with a maximum of 67% ± 2% reduction in clonogenic survival after 4µM MMF exposure. Based on the data U87 cells respond to treatment with MMF in a dose-dependent manner with a calculated IC₅₀ of 1.9µM (R²=0.98).

From Figure 3.3 the order of potency of the drugs was TMZ, MMF then DMF. The data also indicates an increased sensitivity of U87 cells to MMF over DMF.

3.4.2.3 Assessment of the toxicity of Temozolomide, Dimethyl Fumarate, Monomethyl Fumarate and Diroximel Fumarate on the T98g cell line.

Initial assessment of the cytotoxic effect of TMZ, DMF and MMF on T98g cell survival after 24- hour exposure to each single agent was again assessed with clonogenic assays. Figure 3.4 shows the cytotoxic response of T98g cells to increasing doses of single agents compared to the untreated control.

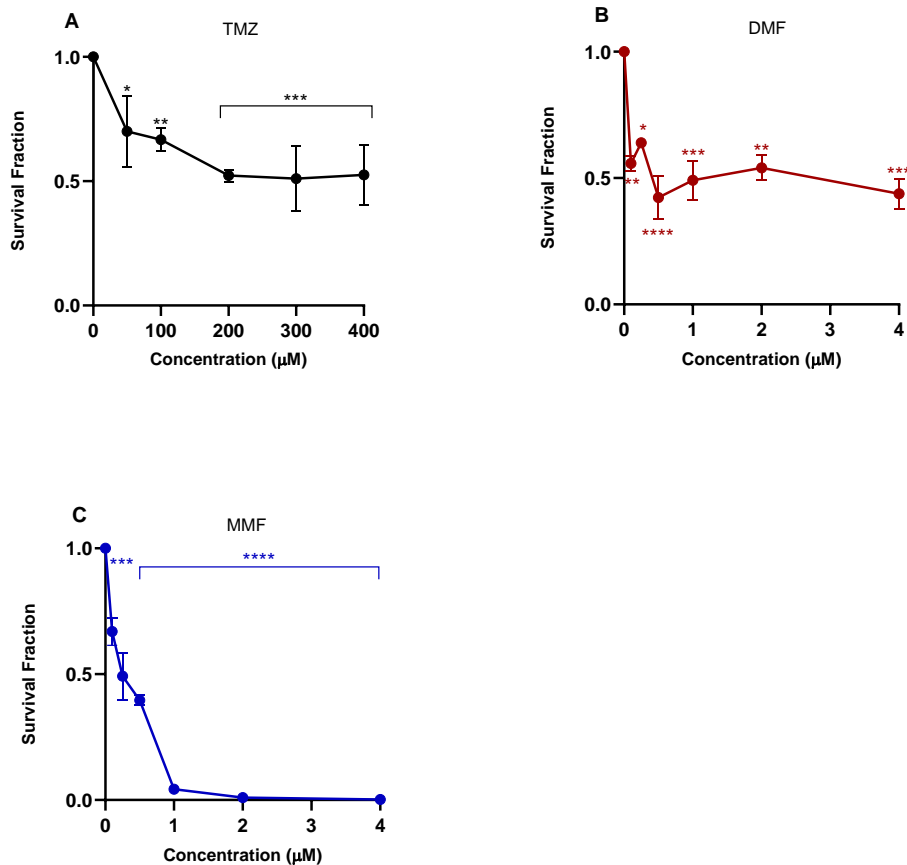


Figure 3.4: The effect on T98g glioblastoma cell clonogenic survival with increasing doses of treatment (A) Temozolomide, (B) Dimethyl-Fumarate and (C) Monomethyl-Fumarate after 24-hour exposure versus the untreated control. The data presented is an average of 3 independent experiments \pm standard deviation. Statistical analysis of data was performed using a one-way ANOVA with Bon-Ferroni post-test. P-values of $<0.05 = *$, $<0.01 = **$, $<0.001 = ***$ and $P < 0.0001 = ****$ reported as significant.

Incubation of cells with increasing doses of TMZ (Figure 3.4(A)) on the T98g cell line (MGMT+) reduced cell survival in a dose-dependent manner. Statistically significant reduction in clonogenic survival was observed at all administered doses of TMZ 50µM ($P < 0.5$), 100µM ($P < 0.01$), 200µM ($P < 0.0001$), 300µM ($P < 0.0001$) and 400µM ($P < 0.0001$) relative to the untreated control. Maximum reduction in clonogenic survival was reached after incubation of the cells with 400µM TMZ with $48\% \pm 11\%$ reduction in clonogenic survival. As the reduction in clonogenic survival did not hit 50% or more, the IC_{50} was undetermined.

The effect of increasing doses of DMF on the T98g cell survival is presented in Figure 3.4 (B). No trend in clonogenic survival was observed as the doses of DMF increased; however, we observed a statistically significant reduction in cell survival compared to the untreated control at all administered doses (all, $P < 0.05$). After treatment of the cells with 0.1 μ M and 0.25 μ M DMF there was a 45% \pm 4.9% and 37% \pm 0.06% reduction in clonogenic survival respectively. At 0.5 μ M, 1 μ M, 2 μ M, and 4 μ M DMF exposure we see a 58% \pm 14.9%, 51% \pm 13.5%, 46% \pm 8.5% and 57% \pm 10.4% reduction in clonogenic survival respectively. From the data, the IC_{50} was calculated to be 1.9 μ M ($R^2=0.73$).

Figure 3.4 (C) shows the effect of MMF on the T98g cell clonogenic survival after 24-hour exposure to increasing doses of MMF. We see T98g to be highly sensitive to MMF, with a steep dose response curve. A statistically significant reduction in clonogenic survival was observed at all concentrations versus the untreated control (all $P < 0.001$). A maximum reduction in clonogenic survival was achieved after exposure to 4 μ M MMF, with a 99.9% reduction in clonogenic survival \pm 0.18%. The IC_{50} was calculated as 0.29 μ M ($R^2=0.94$).

Data collectively shows the T98 cell line to be most sensitive to MMF. The high concentration range for TMZ was expected with the T98g cell line due to its MGMT positive status.

3.4.3 Developing the Temozolomide Monomethyl Fumarate combination in UVW, U87 and T98g cell lines.

For the development of our combination treatments, the IC_{50} values were taken from single therapy clonogenic assays shown in Figures 3.2, 3.3 and 3.4. Due to the consistent dose response of MMF in the reduction of clonogenic survival in all three cell lines a combination of MMF with TMZ was designed. DMF was not progressed for combination studies as this data was obtained by (Scott, 2020).

MMF was hypothesised to decrease the production of glutathione in the cells in order to sensitise the cells to the cytotoxicity of TMZ, causing a greater reduction in clonogenic survival compared to single drug administrations and the untreated controls. Each cell lines combinations used the determined IC_{50} values of each single

drug (taken from section 3.4.2) in the concentration range. As the UVW cell line had an IC_{50} of $19.7\mu\text{M}$ for TMZ and $2.7\mu\text{M}$ for MMF, this was taken and using a ratio calculator, two concentrations above and two concentrations below were calculated. The same method was applied to the U87 cell line, with the combination ranges shown in Table 3.1, with each set of IC_{50} 's shown as the third treatment combination. As the IC_{50} value for TMZ in the T98g cell line remained undetermined and MMF in the T98g cell line had a low IC_{50} of $0.29\mu\text{M}$, a direct ratio of TMZ to MMF was designed as shown in Table 3.1.

The combinations were designed in this way as theoretically the IC_{50} of a drug when combined with another IC_{50} will result in 100% cell death, however cell biology and the interaction between drugs is not linear. Hence, we utilise models such as the combination index analysis equations to determine the relationship between drugs. Further to this, literature analysis on CIA states the use of a ratio model to prevent emphasis on one drug over another (Chou, 2010). The paper by Ting-Chao also suggests the use of concentrations above and below the IC_{50} to be advantageous when using the Compusyn software (Chou, 2010).

Combination index analysis is a widely used mathematical model to characterise the relationship between drugs. Using the median effect principle, synergism (better than the single agents), summation (no difference over single agents) or antagonism (no better combined effect over single agents) between dose response curves can be assessed through their cytotoxicity and the fraction of the population unaffected (Chou and Talalay, 1984). The theoretical model quantifies the drug interaction through the "mass action law" and is widely used to interrogate combination interactions throughout the literature (Banerjee *et al.*, 2021).

Compusyn software utilises the cytotoxic response of each drug and the line of best fit (R^2 value) to create its own median effect plot and dose effect plot. The method relies on the median effect to determine synergy. As the equation uses the lines of fit to determine the relationship between drugs, a good R^2 value is representative of how well the dose response curves will fit the CIA model. Higher R^2 values indicate appropriate drug combinations, whereas low R^2 values suggests the refinement of the assays. The software uses the fraction of unaffected cells at each concentration to determine synergy. Due to the nature of combination index analysis, experimental data is shown as the line of fit calculated by Compusyn software. The software utilises the equations described in Section 2.9.

For the combination of TMZ and MMF, it was hypothesised that the combination will be synergistic and MMF will sensitise the cells to TMZ, enhancing the effect of cytotoxic stress caused by TMZ (Yao *et al.*, 2016).

3.4.3.1 Cytotoxic effects of Temozolomide and Monomethyl Fumarate as single agents and in combination in the UVW human glioblastoma cell line.

Figure 3.5 demonstrates the response of the UVW cell line to the administration of each single drug TMZ and MMF in the concentration range calculated by the IC_{50} 's, followed by the combination of both. All drugs were administered for 24- hours and the survival fraction relative to the untreated controls was calculated through the cell lines clonogenic survival. Statistical analysis is also shown in Figure 3.5 (G). Combination index analysis and line of fit for the UVW cell line with Temozolomide and Monomethyl Fumarate, calculated using Compusyn software with fraction unaffected is shown in Figure 3.5 (E and F).

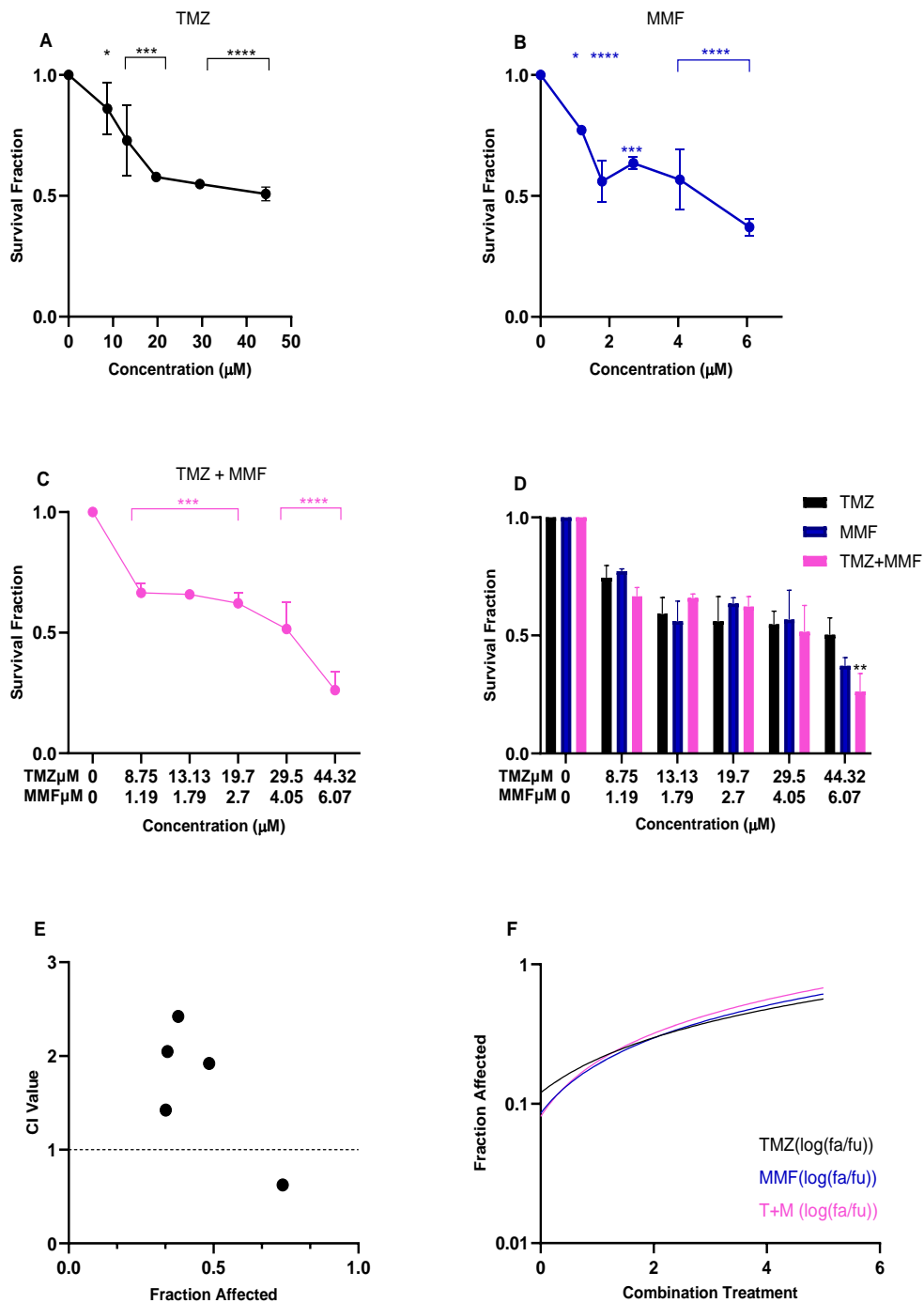


Figure 3.5: The dose response curves for the UVW human glioblastoma cell line following exposure to increasing doses of Temozolomide (A), Monomethyl Fumarate (B) and the combination of Temozolomide and Monomethyl Fumarate (C). Comparison between the single agent curves and the combination curve for both drugs (D). Combination index values and associated fraction affected for each dose in the Temozolomide-Monomethyl Fumarate combination, dotted line represents the

line of additivity with $CI < 0.9$ showing synergism (E). Line of best fit from single and combination dose response curves (F). Data shown is an average of three independent experiments \pm standard deviation. A one-way ANOVA with Bonferroni post-test was performed on single agent curves, and a two-way ANOVA with Bonferroni post-test was performed to compare single agents to the combination, with P-values of $< 0.05 = *$, $< 0.01 = **$, $< 0.001 = ***$ and $P < 0.0001 = ****$ reported as significant. $*$ = significant against the control $*$ = significant against TMZ, $*$ = significant against MMF and $*$ = significant against T+M.

The response of TMZ administration as a single agent is shown in Figure 3.5 (A) with a steady dose response curve. A statistically significant reduction in clonogenic survival was seen across the range of concentrations versus the untreated control (all $P < 0.05$). Single therapy MMF's cytotoxic effect on the UVW cell line is shown in Figure 3.5(B). A statistically significant reduction in clonogenic survival was seen across the concentration range compared to the untreated control (all $P > 0.05$). The clonogenic reduction in cell survival of the UVW cell line to a simultaneous administration of TMZ and MMF is shown in Figure 3.5 (C). Statistically significant reduction in clonogenic survival was observed after administration of each concentration combination versus the untreated control (all $P < 0.001$). The highest combination of $44.32\mu\text{M}$ TMZ with $6.07\mu\text{M}$ MMF gave a reduction in clonogenic survival of $74\% \pm 4.4\%$. Figure 3.5 (D) shows the response of each single agent and the combination over the dose range. From the Figure a statistically significant difference between the reduction in clonogenic survival of the combination versus the single therapy TMZ was only seen at the highest concentration of $44.32\mu\text{M}$ TMZ with $6.07\mu\text{M}$ MMF ($P < 0.01$). The combination of $44.32\mu\text{M}$ TMZ with $6.07\mu\text{M}$ MMF did not show a statistically significant reduction in clonogenic survival over single agent MMF. It can be seen from Figure 3.5 (E), that the combination of TMZ with MMF in the UVW cell line was synergistic only at the highest combination concentrations ($44.32\mu\text{M}$ TMZ + $6.07\mu\text{M}$ MMF), represented with a value < 0.9 , showing synergy of the combination. The log (Fa/Fu) line of fit shown in figure 3.5(F) shows the overlap between the single treatment curves and the combination curve, with R^2 values of 0.79, 0.84 and 0.86 for TMZ, MMF and the combination of TMZ + MMF respectively. Higher R^2 values are required for a greater reliability of the CIA, as the software cannot interpret generated data but

will use lines of fit. The R^2 values therefore confirm the reliability of synergy by combining TMZ and MMF at the concentrations of 44.32 μ M TMZ + 6.07 μ M MMF.

Data partially supports our hypothesis of a synergistic combination between TMZ and MMF, as synergy is only seen at the highest concentration.

3.4.3.2 Cytotoxic effects of Temozolomide and Monomethyl Fumarate as single agents and in combination in the U87 human glioblastoma cell line.

Figure 3.6 demonstrates the response of the U87 cell line to the administration of each single drug TMZ and MMF in the concentration range calculated by the IC_{50} 's, followed by the combination of both. All drugs were administered for 24- hours and the survival fraction relative to the untreated controls was calculated through the cell lines clonogenic survival. Statistical analysis is also shown in Figure 3.6 (G). Combination index analysis and line of fit for the U87 cell line with Temozolomide and Monomethyl Fumarate, calculated using Compusyn software with fraction unaffected is shown in Figure 3.6 (E and F).

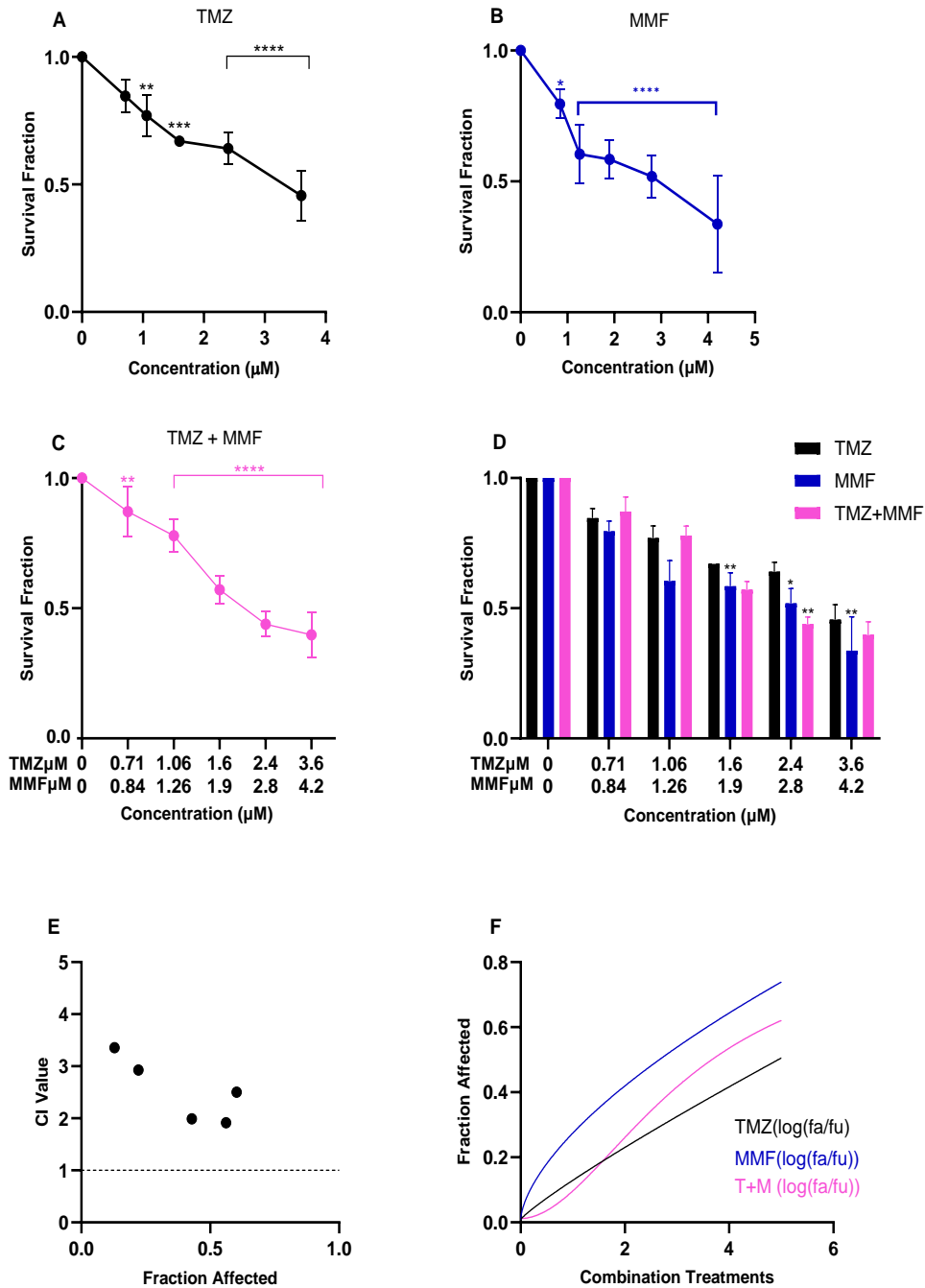


Figure 3.6: The dose response curves for the U87 human glioblastoma cell line following exposure to increasing doses of Temozolomide (A), Monomethyl Fumarate (B) and the combination of Temozolomide and Monomethyl Fumarate (C). Comparison between the single agent curves and the combination curve for both drugs (D). Combination index values and associated fraction affected for each dose in the Temozolomide-Monomethyl Fumarate combination, dotted line represents the line of additivity with $CI < 0.9$ showing synergism (E). Line of best fit from single and

combination dose response curves (F). Data shown is an average of three independent experiments \pm standard deviation. A one-way ANOVA with Bonferroni post-test was performed on single agent curves, and a two-way ANOVA with Bonferroni post-test was performed to compare single agents to the combination, with P-values of $<0.05 = *$, $<0.01 = **$, $<0.001 = ***$ and $P < 0.0001 = ****$ reported as significant. $*$ = significant against the control $*$ = significant against TMZ, $*$ = significant against MMF and $*$ = significant against T+M.

Figure 3.6 (A) shows the response of the U87 cell line to increasing concentrations of TMZ. A statistically significant reduction in clonogenic survival was seen with 1.06 μ M TMZ to 3.6 μ M TMZ compared to the untreated control (all $P < 0.01$). A maximum reduction in clonogenic survival was reached after incubation of the cells with 3.6 μ M TMZ with a 55% reduction in clonogenic survival \pm 5.7%. The response of U87 cells to increasing concentrations of MMF is shown in Figure 3.6 (B), with statistically significant reduction in clonogenic survival seen after exposure to all concentrations of MMF versus the untreated control (all $P < 0.01$). A maximum reduction in clonogenic survival of 86% \pm 1.4% was reached after exposure to 4.2 μ M MMF.

The combinations of TMZ + MMF versus the untreated control, induced a statistically significant reduction in clonogenic survival after exposure to combinations \geq 1.06 μ M TMZ + 1.26 μ M MMF compared to the untreated control shown in Figure 3.6 (C) (all $P < 0.05$). The combinations decreased cell survival in a dose-dependent manner with 3.6 μ M TMZ and 4.2 μ M MMF, showing a maximum reduction in clonogenic survival of 61% \pm 5%. From Figure 3.6 (D) the response of the U87's to each single treatment and the combination is shown. A greater reduction in clonogenic survival was reached with each single agent versus the corresponding combinations apart from combination 4. The combination of 2.4 μ M TMZ and 2.8 μ M MMF (combination 4) was the only combination to elicit greater reduction in clonogenic survival than the single treatments, however this was only statistically significant against 2.4 μ M TMZ given as a single treatment ($P < 0.05$). MMF from figure 3.6 (D) showed statistically significant greater reductions in clonogenic survival than TMZ after exposure to concentrations \geq 1.26 μ M (all $P < 0.05$). Additionally, after exposure to 1.26 μ M MMF, MMF instigated a statistically significant reduction in clonogenic survival compared to the combination at the corresponding concentration.

Combination index analysis on the U87 cell line shown in Figure 3.6 (E), observed the combination to be antagonistic ($CI > 1.1$) for the TMZ and MMF combinations. This is further represented in Figure 3.6 (F), with the log (Fa/Fu) line of fit observing MMF to have a greater fraction affected than either the combination or TMZ, with R^2 values of 0.96, 0.85 and 0.97 for TMZ, MMF and the combination of TMZ + MMF respectively. The R^2 values show a good fit of the line to the model and support the lack of synergy calculated by the software

Cumulatively data rejects our hypothesis of MMF synergising with TMZ in a double combination within the U87 cell line. MMF as a single treatment showed increased cytotoxicity, supporting previous data in Figure 3.3 (C) and suggesting MMF as a possible single treatment option for GBM.

3.4.3.3 Cytotoxic effects of Temozolomide and Monomethyl Fumarate as single agents and in combination in the T98g human glioblastoma cell line

Figure 3.7 demonstrates the response of the MGMT+ T98g cell line to the administration of each single drug TMZ and MMF in the concentration range calculated by the IC_{50} 's, followed by the combination of both. All drugs were administered for 24- hours and the survival fraction relative to the untreated controls was calculated through the cell lines clonogenic survival. Statistical analysis is also shown in Figure 3.7 (G). Combination index analysis and line of fit for the T98g cell line with Temozolomide and Monomethyl Fumarate, calculated using Compusyn software with fraction unaffected is shown in Figure 3.7 (E and F).

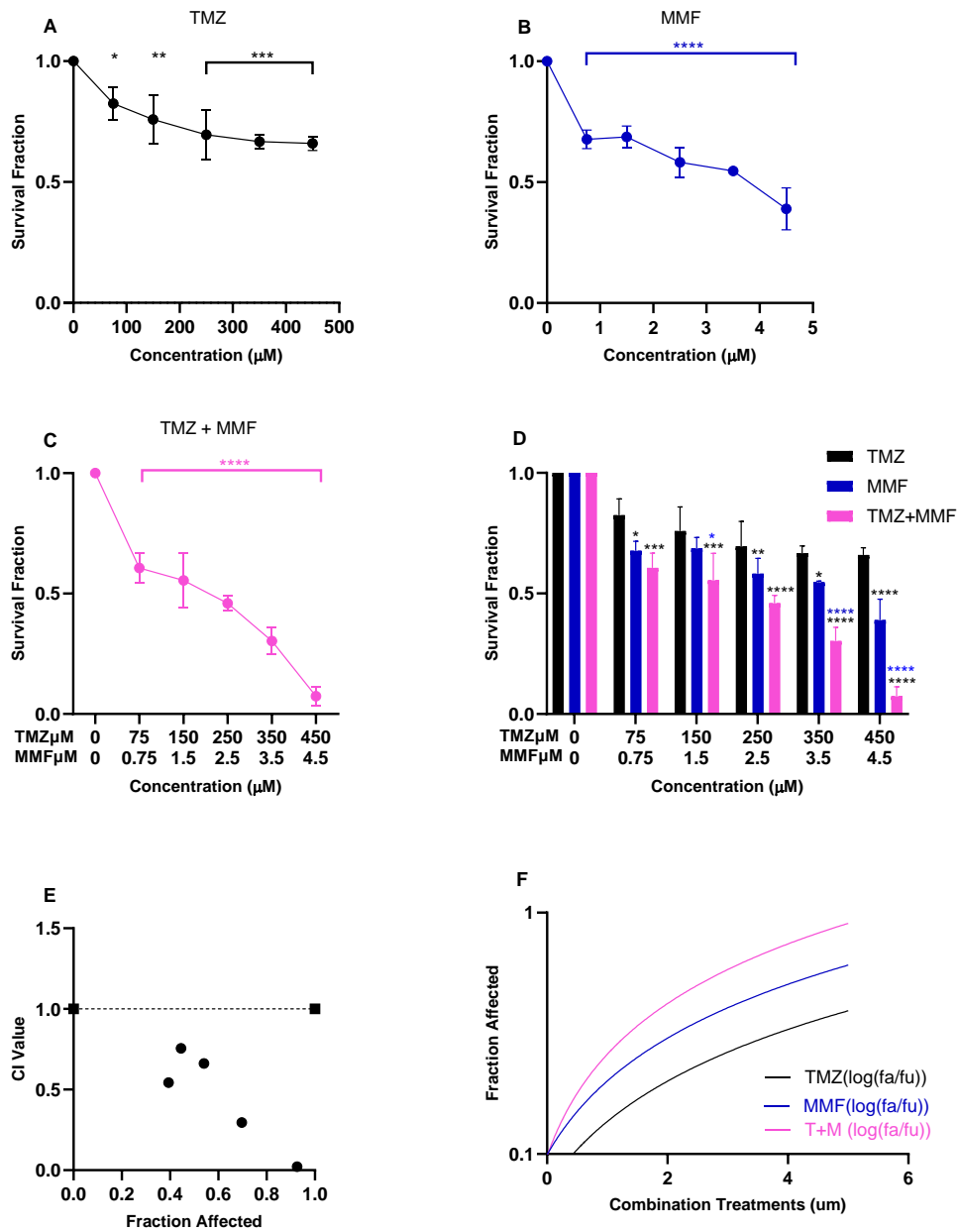


Figure 3.7: The dose response curves for the T98g human glioblastoma cell line following exposure to increasing doses of Temozolomide (A), Monomethyl Fumarate (B) and the combination of Temozolomide and Monomethyl Fumarate (C). Comparison between the single agent curves and the combination curve for both drugs (D). Combination index values and associated fraction affected for each dose in the Temozolomide-Monomethyl Fumarate combination, dotted line represents the line of additivity with $CI < 0.9$ showing synergism (E). Line of best fit from single and combination dose response curves (F). Statistical analysis summary of data showing only significant results, all other comparisons were not significant (G). Data shown is

an average of three independent experiments \pm standard deviation. A one-way ANOVA with Bonferroni post-test was performed on single agent curves, and a two-way ANOVA with Bonferroni post-test was performed to compare single agents to the combination, with P-values of $<0.05 = *$, $<0.01 = **$, $<0.001 = ***$ and $P < 0.0001 = ****$ reported as significant. $*$ = significant against the control $*$ = significant against TMZ, $*$ = significant against MMF and $*$ = significant against T+M.

Temozolomide administration as a single therapy is shown in Figure 3.7 (A) with a steep dose response curve. A statistically significant reduction in clonogenic survival was seen across the range of concentrations versus the untreated control (all, $P < 0.05$). Single therapy MMF's cytotoxic effect on the T98g cell line is shown in Figure 3.7(B). Statistically significant reductions in clonogenic survival were seen across the concentration range compared to the untreated control (all, $P < 0.0001$).

Simultaneous administration of TMZ and MMF is shown in Figure 3.7 (C). Statistically significant reduction in clonogenic survival was observed at each combination versus the untreated control (all, $P < 0.0001$). Reduction in clonogenic survival increased to a maximum of 99.93% at the final combination of $450\mu\text{M}$ TMZ and $4.5\mu\text{M}$ MMF $\pm 3.9\%$.

Figure 3.7 (D) compares the response of each single agent and the combination over the dose range. At each relative concentration of single treatment vs the combination, the combination showed an increased reduction in clonogenic survival over the single treatments. Each combination had a statistically significant reduction in clonogenic survival over the relative single TMZ concentrations (all, $P < 0.001$). A statistically significant reduction in clonogenic survival against both single treatments was seen after exposure to combinations 2, 4 and 5 against relative doses of $150\mu\text{M}$ TMZ and $1.5\mu\text{M}$ MMF, doses of $350\mu\text{M}$ TMZ and $3.5\mu\text{M}$ MMF, as well as $450\mu\text{M}$ TMZ and $4.5\mu\text{M}$ MMF (all, $P < 0.05$). After exposure to MMF concentrations of $0.75\mu\text{M}$, $2.5\mu\text{M}$, $3.5\mu\text{M}$ and $4.5\mu\text{M}$, MMF also had a statistically significant reduction in clonogenic survival over TMZ at the relative single concentration (Figure 3.7(G) ($P < 0.05$)).

From Figure 3.7 (E), each combination of TMZ and MMF shows synergy, with all combination points having a CI value < 0.9 . From the line of best fit $\log(F_a/F_u)$ (Figure 3.7 (F)), the combination line observes a distinguishable greater F_a than both MMF and TMZ. R^2 values were 0.84, 0.86 and 0.93 for TMZ, MMF and the combination of TMZ + MMF respectively showing a good line fit, validating the CIA data. The R^2

values support the synergy calculated by the software as it represents good experimental conditions

This suggests in the T98g cell line, MMF acts in synergy with TMZ to elicit greater reductions in clonogenic survival, supporting our hypothesis.

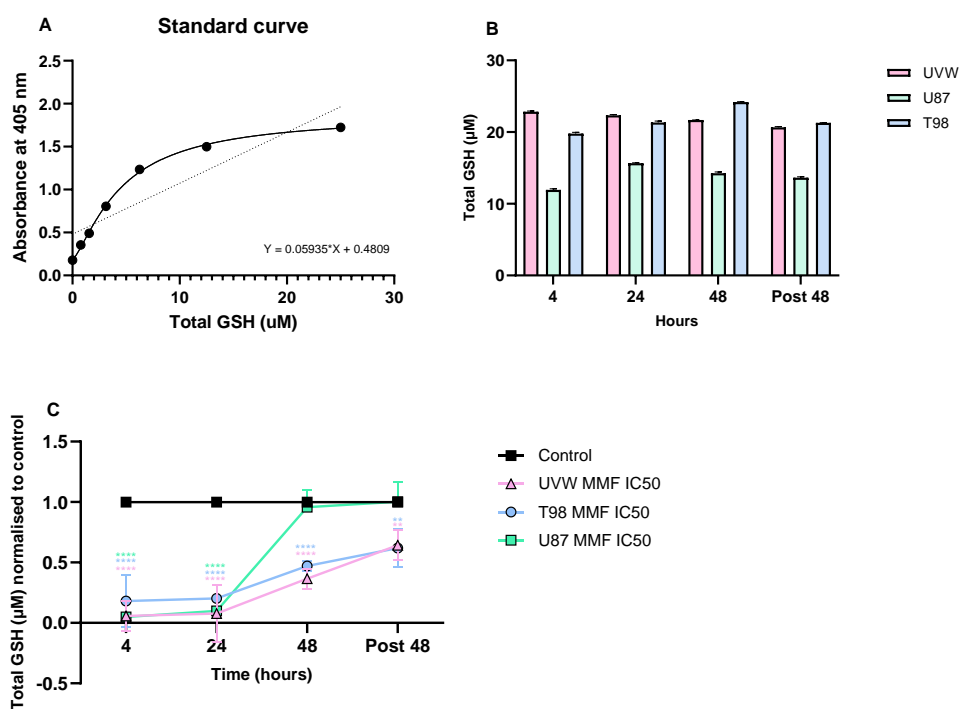
3.4.4 Determination of a scheduled administration for Monomethyl Fumarate

The fumaric acid family has shown in the literature to deplete glutathione levels in cells in a time-dependent manner and also concentration dependent manner (Brennan *et al.*, 2015; Saidu *et al.*, 2019). It has been suggested that upon administration of DMF, glutathione levels are depleted from 0-12 hours post administration before recovering and reaching basal levels if not higher after 24 hours in human spinal cord astrocytes (Brennan *et al.*, 2015). MMF is hypothesised to work similarly to DMF, in a tight equilibrium with NrF2 and Keap1 to create this depletion and recovery of glutathione. Recent studies however have shown MMF to have no effect on GSH and to reduce reactive oxygen species in a pathway independent to GSH and NrF2 (Gola *et al.*, 2023; Zhang *et al.*, 2022). However, with DMF metabolising to MMF, the conjugates formed with GSH are in theory MMF, with DMF in the literature which has metabolised to MMF showing some function on NrF2 (Campioni *et al.*, 2022).

To assess the expression of Glutathione in GBM cell lines, the IC₅₀ concentration of MMF was utilised over four time points, to determine if one specific time range was advantageous in lowering GSH levels (section 2.10). This also allowed comparison of our findings to the literature, where the response of MMF on GSH had varied opinions as previously discussed above. However, with both DMF and MMF being referred to as the same product in much of the literature, MMF's response on GSH needed to be established in GBM cells before designing a combination schedule around the GSH/NrF2 depletion and rebound (Brennan *et al.*, 2015)

3.4.4.1 The effect of Monomethyl Fumarate on Glutathione levels over time in the UVW, U87 and T98g cell line.

Figure 3.8 displays UVW, U87 and T98g cells treated with the IC₅₀ concentration of MMF for either 4- hours, 24- hours, 48- hours or for post 48- hours. Post 48- hour treatments were treated with MMF for 24 hours, followed by removal of the treatment, and the addition of media for 48- hours. Each time point was normalised to the total GSH levels of each control at each time point.



(D)

Bonferroni's multiple comparisons test	Summary	Adjusted P Value
UVW MMF IC₅₀		
Control vs. 4	****	<0.0001
Control vs. 24	****	<0.0001
Control vs. 48	****	<0.0001
Control vs. Post 48	**	0.0035
4 vs 48	*	0.0150
4 vs. Post 48	****	<0.0001
24 vs 48	*	0.0256
24 vs. Post 48	****	<0.0001
U87 MMF IC₅₀		
Control vs. 4	****	<0.0001
Control vs. 24	****	<0.0001
4 vs. 48	****	<0.0001
4 vs. Post 48	****	<0.0001
24 vs. 48	****	<0.0001

24 vs. Post 48	****	<0.0001
T98 MMF IC₅₀		
Control vs. 4	****	<0.0001
Control vs. 24	****	<0.0001
Control vs. 48	****	<0.0001
Control vs. Post 48	**	0.0018
4 vs. 48	*	0.0248
4 vs. Post 48	***	0.0003
24 vs. 48	*	0.0446
24 vs. Post 48	***	0.0006

Figure 3.8: Relative glutathione levels of the UVW, U87 and T98g cell line after timed exposures to the IC₅₀ concentration of Monomethyl Fumarate for each cell line. The standard curve used to determine total GSH for all samples before comparison to the control (A). Untreated control total GSH levels at each time point (B). Relative glutathione levels compared to the untreated control at each time point (C). Statistical analysis summary following a one-way ANOVA showing only statistically significant results, all non-reported data comparisons were insignificant (D). Data reported is an average of three independent experiments ± standard deviation. A one-way ANOVA with Bonferroni post testing was performed using GraphPad prism 10.3.1 comparing each treated and untreated group to each other, with P-values of <0.05 = *, <0.01=**, <0.001 = *** and P<0.0001=**** reported as significant.

Figure 3.8 (A) shows the standard curve generated from the GSH kit and used to calculate total GSH levels. Figure 3.8 (B) shows the slight variation in total GSH levels in the untreated control cells prompting total GSH levels for each untreated control time point to be used to normalise each treated time point to. From Figure 3.8 (C) relative glutathione levels indicated a statistically significant decrease in relative glutathione levels after a 4- hour and 24- hour MMF incubation time compared to the untreated control (P<0.0001) for all cell lines. For the UVW and T98g cell line at the 48h and post 48h time point, GSH levels remained statistically significantly lower than their untreated control (all P<0.05). The U87 cell line however showed an increase in GSH levels after 48h and post 48h exposure to MMF compared to the untreated control (P>0.05). Data suggests in the UVW and T98g cell line GSH levels take longer to recover to basal levels. For all three cell lines GSH levels were most reduced at the 4h exposure time point and with a statistically significant increase in GSH levels between 4h and post 48h exposure in all three cell lines (P<0.05) and a statistically significant difference in GSH levels between 24h and 48h exposure in all cell lines (P<0.05). Data supports our hypothesis of a time dependent reduction in glutathione levels and confirms that MMF does indeed deplete GSH.

3.4.5 Development of scheduled combination treatments in the UVW, U87 and T98g human glioblastoma cell lines.

From results in section 3.4.4, glioblastoma cell lines, UVW, U87 and T98g all showed a time dependent response of relative GSH levels when exposed to MMF. Across all three cell lines, 4- hour and 24- hour exposure with MMF showed significant reduction in GSH levels when compared to the untreated control. As MMF and TMZ combinations with 24h MMF exposure given simultaneously with TMZ have been shown, 4-hours was taken as a scheduled time point.

For schedule development across all three cell lines, a 4- hour pretreatment with MMF was given to the cells to lower GSH levels, before administration of Temozolomide. As previously described in sections 2.9 and section 3.4.3, combination index analysis was used to assess the potential for synergy.

Therefore, we hypothesis the 4- hour pretreatment with MMF would significantly increase reduction in clonogenic survival, analysed through combination clonogenics and combination index analysis. The same combination models were used for each cell line as previously discussed in section 3.4.3, following Table 3.1, with the addition of the scheduled 4-hour pre-treatment.

3.4.5.1 Cytotoxic effects of Temozolomide and Monomethyl Fumarate, when given as single therapies, as a combination and as a schedule in the UVW cell line.

Figure 3.9 illustrates the cytotoxic effect of TMZ, MMF, the combination of both TMZ and MMF and the scheduled administration of MMF for 4- hours followed by the addition of TMZ (T+M PT4). Each individual treatment response was assessed through clonogenic survival assays.

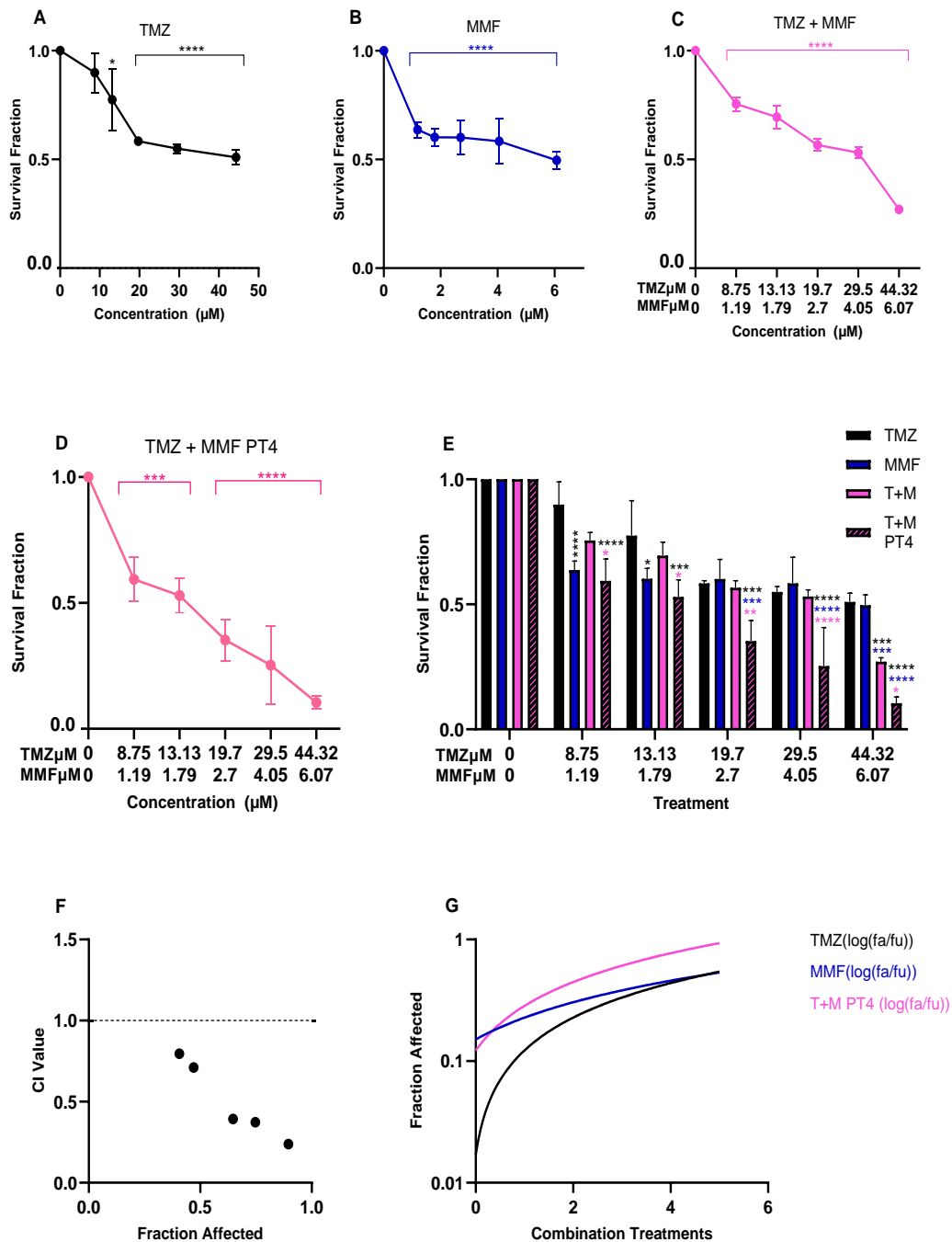


Figure 3.9: The dose response curves for the UVW human glioblastoma cell line following exposure to increasing doses of Temozolomide (A), Monomethyl Fumarate (B) simultaneous combinations of Temozolomide and Monomethyl Fumarate (C) and scheduled combinations of Monomethyl Fumarate for 4-hours followed by Temozolomide (PT4) (D). Comparison between the single agent curves and the combination curves for both drugs (E). Combination index analysis of the Temozolomide-Monomethyl Fumarate combination when given in a 4- hour

pretreatment schedule (T+M PT4), dotted line represents the line of additivity with $CI < 0.9$ showing synergism (F). Line of best fit from single and scheduled combination dose response curves (G). Data shown is an average of three independent experiments \pm standard deviation. A one-way ANOVA with Bonferroni post-test was performed on single dose response curves, and a two-way ANOVA with Bonferroni post-test was performed to compare single agents to the combination and the scheduled combination, with P-values of $< 0.05 = *$, $< 0.01 = **$, $< 0.001 = ***$ and $P < 0.0001 = ****$ reported as significant. $*$ = significant against the control $*$ = significant against TMZ, $*$ = significant against MMF and $*$ = significant against T+M.

Single agent dose response curves for TMZ and MMF are shown in Figure 3.9 (A) and 3.9 (B) respectively. Both show dose response curves similar to that in Figure 3.5 (A and B). A statistically significant reduction in clonogenic survival was observed after exposure to all concentrations of TMZ versus the untreated control (all, $P < 0.05$). Statistically significant reduction in clonogenic survival was also seen after exposure to all concentrations of MMF versus the untreated control (all, $P < 0.0001$). Figure 3.9 (C) displays the simultaneous combinations of TMZ and MMF across the combination range, with statistically significant reductions in clonogenic survival observed after exposure to all combinations compared to the untreated control (all, $P < 0.0001$). Data between Figure 3.5 and 3.9 is similar for the single agent curves and the combination data, showing replicable results between assays undertaken at different times.

Figure 3.9 (D) illustrates the cytotoxic response of the scheduled administration of MMF and TMZ on the UVW cell line. Statistically significant reductions in clonogenic survival were observed at all concentrations of the scheduled TMZ and MMF combinations vs the untreated control (all, $P < 0.001$). The IC_{50} combinations of TMZ and MMF of $19.7\mu\text{M}$ and $2.7\mu\text{M}$, gave a 44% reduction in clonogenic survival $\pm 2.8\%$ for simultaneous administration vs a 65% reduction in clonogenic survival $\pm 8.1\%$ for the scheduled administration. The highest combination of $44.32\mu\text{M}$ TMZ and $6.07\mu\text{M}$ MMF, in Figure 3.9 (C) showed a 73% reduction in clonogenic survival $\pm 1.6\%$ and after scheduled administration the same concentrations showed a 90% $\pm 2.5\%$ reduction in clonogenic survival (Figure 3.9(D)). Data suggest the scheduled combination reduces clonogenic survival greater than the simultaneous administration.

Comparison of the scheduled combinations vs the simultaneous combinations and each single agent's cytotoxic response is shown in Figure 3.9 (E). Through a two-way ANOVA, statistical significance was seen for the scheduled administration against the simultaneous administration for each combination (all $P < 0.05$). Statistically significant reductions in clonogenic survival of the schedule over both the single treatments was also seen after exposure to combination 3, 4 and 5 (all, $P < 0.001$).

From Figure 3.9 (F), each combination of TMZ and MMF when given as a schedule showed synergy, with all combination points having a CI value < 0.9 . From the line of best fit log (F_a/F_u), the combination line observed a distinguishable greater F_a than both MMF and TMZ. R^2 values were 0.94, 0.67 and 0.93 for TMZ, MMF and the combination of TMZ + MMF PT4 respectively. Higher R^2 values are required for a greater reliability of the CIA, as the software cannot interpret generated data but will use lines of fit. With the MMF R^2 value being lower, it shows the data used may need to be tested on additional concentrations to increase the reliability of the result.

The data shown agrees with the hypothesis of MMF sensitising cells to TMZ, as with simultaneous administration (Figure 3.5) only 1 combination was showing synergy. Data therefore supported the hypothesis that pretreatment of MMF, enhances cell response to treatment with TMZ, with the schedule showing greater reduction in clonogenic survival and statistical significance over both single treatments and the simultaneous combination.

3.4.5.2 Cytotoxic effects of Temozolomide and Monomethyl Fumarate, when given as single therapies, as a combination and as a schedule in the U87 cell line.

Figure 3.10 illustrates the cytotoxic effect of TMZ, MMF, the combination of both TMZ and MMF and the scheduled administration of MMF for 4- hours followed by the addition of TMZ (T+M PT4). Each individual treatment response was assessed through clonogenic survival.

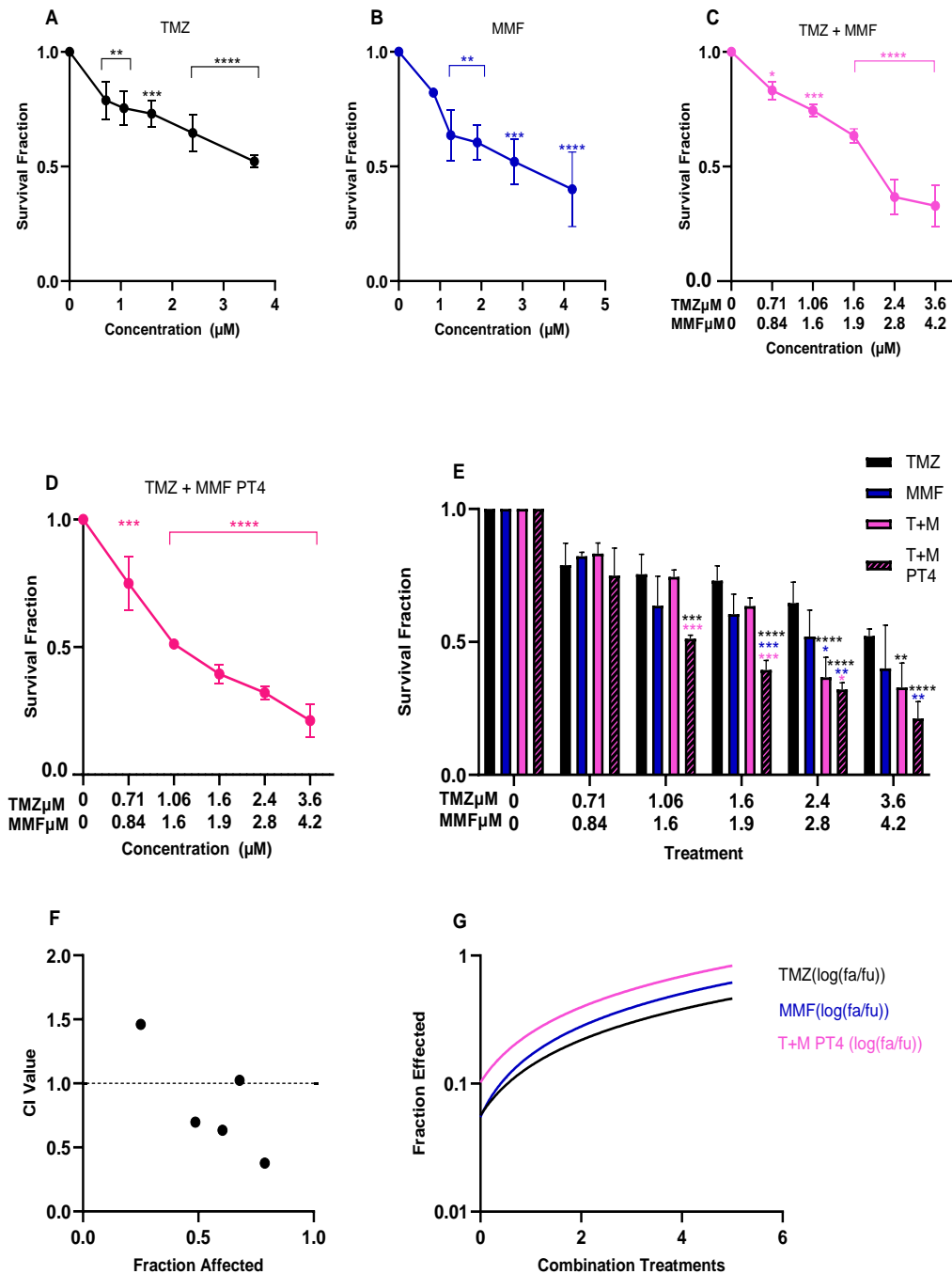


Figure 3.10: The dose response curves for the U737 human glioblastoma cell line following exposure to increasing doses of Temozolomide (A), Monomethyl Fumarate (B) simultaneous combinations of Temozolomide and Monomethyl Fumarate (C) and scheduled combinations of Monomethyl Fumarate for 4-hours followed by Temozolomide (PT4) (D). Comparison between the single agent curves and the combination curves for both drugs (E). Combination index analysis of the Temozolomide-Monomethyl Fumarate combination when given in a 4- hour

pretreatment schedule (T+M PT4), dotted line represents the line of additivity with $CI < 0.9$ showing synergism (F) Line of best fit from single and scheduled combination dose response curves (G). Data shown is an average of three independent experiments \pm standard deviation. A one-way ANOVA with Bonferroni post-test was performed on single dose response curves, and a two-way ANOVA with Bonferroni post-test was performed to compare single agents to the combination and the scheduled combination, with P-values of $< 0.05 = *$, $< 0.01 = **$, $< 0.001 = ***$ and $P < 0.0001 = ****$ reported as significant. $*$ = significant against the control $*$ = significant against TMZ, $*$ = significant against MMF and $*$ = significant against T+M

TMZ and MMF single agent curves are shown in Figure 3.10 (A) and (B). Cytotoxicity of both agents showed dose response curves with statistically significant reduction in clonogenic survival seen after exposure to all concentrations of TMZ and MMF apart from $0.84 \mu\text{M}$ MMF, versus the untreated control all ($P < 0.01$). Figure 3.10 (C) shows the cytotoxic response of simultaneous administration of the combinations against the untreated control. Similar dose response curves are seen for Figure 3.6 (C) and Figure 3.10 (C), again showing good replicability of the data. A statistically significant reduction in clonogenic survival was seen across all combination concentrations of TMZ and MMF versus the untreated control (all, $P < 0.05$)

Scheduled administration of MMF then TMZ after 4 hours is shown in Figure 3.10 (D). A dose response curve was displayed with statistically significant reduction in clonogenic survival after administration of all combinations versus the untreated control (all, $P < 0.001$).

Figure 3.10 (E) compares the dose response curves of each single agent, the simultaneous administration of the combination and the scheduled administration of the combination. Using a two-way ANOVA, statistically significant reduction in clonogenic survival was observed for the scheduled treatments against the simultaneous treatments for combinations 2 ($1.06 \mu\text{M}$ TMZ and $1.6 \mu\text{M}$ MMF, $P < 0.001$), combination 3 ($1.6 \mu\text{M}$ TMZ and $1.9 \mu\text{M}$ MMF $P < 0.001$) and combination 4 ($2.4 \mu\text{M}$ TMZ and $2.8 \mu\text{M}$ MMF $P < 0.05$). Scheduled combinations 3, 4 and 5 also showed a statistically significant reduction in clonogenic survival compared to both the relative single treatments of TMZ and MMF (all, $P < 0.01$).

From Figure 3.10 (F), the combinations of TMZ and MMF when given as a schedule showed synergy at combination 2, 3 and 4, with all combination points having a CI value <0.9 . The highest combination of $3.6\mu\text{M}$ TMZ and $4.2\mu\text{M}$ MMF provided an additive response with a CI value $=1$. The lowest combination of $0.71\mu\text{M}$ TMZ and $0.84\mu\text{M}$ MMF observed an antagonistic response ($\text{CI}>1.1$). From the line of best fit $\log(\text{Fa}/\text{Fu})$, the combination line observes a distinguishable greater Fa than both MMF and TMZ Figure 3.10 (G). R^2 values were 0.91, 0.95 and 0.86 for TMZ, MMF and the combination of TMZ + MMF PT4 respectively. Higher R^2 values show good line fits to the CIA model, as these are used for the median effect equation.

Again, the data agrees with the hypothesis that MMF would enhance the cytotoxicity of TMZ, as simultaneous administration (Figure 3.6) did not result in synergy. From Figure 3.10, it was indicated that pretreatment with MMF sensitises cells to TMZ, with a difference of 9%, 23%, 23%, 11% and 4% reduction in clonogenic survival between simultaneous administration and scheduled administration across combinations 1-5 respectively, supporting our hypothesis.

3.4.5.3 Cytotoxic effects of Temozolomide and Monomethyl Fumarate, when given as single therapies, as a combination and as a schedule in the T98g cell line.

Figure 3.11 shows the cytotoxic effect of TMZ, MMF, the combination of both TMZ and MMF and the scheduled administration of MMF for 4- hours followed by TMZ (T+M PT4) on the T98g cell line. Each individual treatment response was assessed through clonogenic survival.

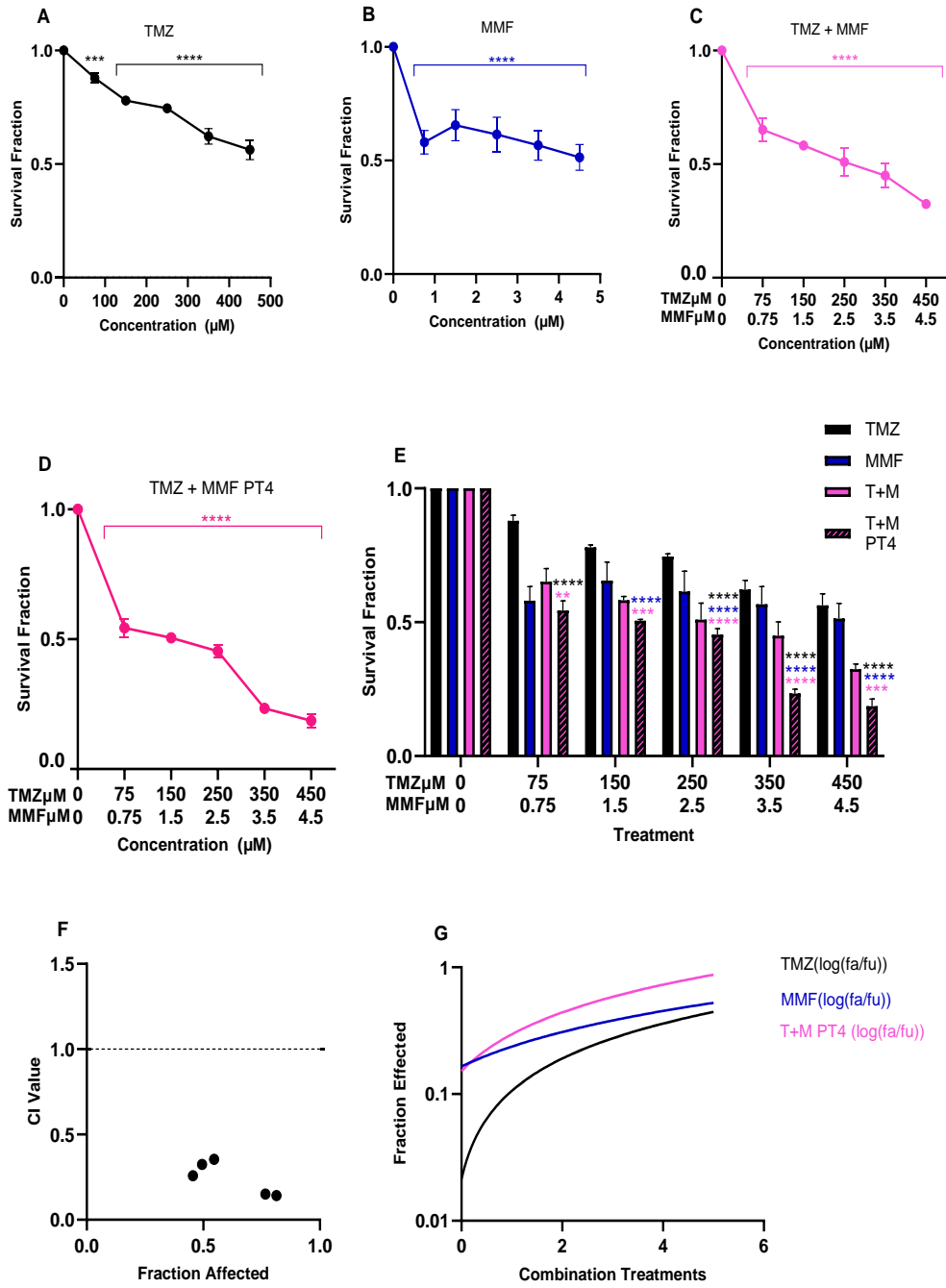


Figure 3.11: The dose response curves for the T98g human glioblastoma cell line following exposure to increasing doses of Temozolomide (A), Monomethyl Fumarate (B) simultaneous combinations of Temozolomide and Monomethyl Fumarate (C) and scheduled combinations of Monomethyl Fumarate for 4-hours followed by Temozolomide (PT4) (D). Comparison between the single agent curves and the combination curves for both drugs (E). Combination index analysis of the Temozolomide-Monomethyl Fumarate combination when given in a 4- hour

pretreatment schedule (T+M PT4), dotted line represents the line of additivity with $CI < 0.9$ showing synergism (F) Line of best fit from single and scheduled combination dose response curves (G). Data shown is an average of three independent experiments \pm standard deviation. A one-way ANOVA with Bonferroni post-test was performed on single dose response curves, and a two-way ANOVA with Bonferroni post-test was performed to compare single agents to the combination and the scheduled combination, with P-values of $< 0.05 = *$, $< 0.01 = **$, $< 0.001 = ***$ and $P < 0.0001 = ****$ reported as significant. * = significant against the control * = significant against TMZ, * = significant against MMF and * = significant against T+M

The dose response curves of TMZ (Figure 3.11(A)) and MMF (Figure 3.11(B)) observed statistically significant reduction in clonogenic survival after exposure to all concentrations versus the untreated control (all, $P < 0.001$). Figure 3.11 (C) displays the cytotoxicity of the simultaneous administration of TMZ and MMF versus the untreated control, with all combination exposure showing statistically significant reductions in clonogenic survival over the untreated control (all, $P < 0.0001$). Figure 3.11 (D) displays the cytotoxicity of the scheduled administration of MMF then TMZ 4-hours after versus the untreated control, with all combinations having a statistically significant reduction in clonogenic survival over the untreated control (all, $P < 0.0001$).

Comparison of each single treatment dose curve, the simultaneous dose curve and the scheduled dose curve is shown in Figure 3.11 (E). A statistically significant reduction in clonogenic survival for the scheduled combinations versus the simultaneous administration combinations were observed against all combinations (all, $P < 0.01$). Combination 1 of $75\mu\text{M}$ TMZ and $0.75\mu\text{M}$ MMF, showed the scheduled administration to give 11% greater reduction in clonogenic survival than the simultaneous administration ($P < 0.01$). At $350\mu\text{M}$ TMZ and $3.5\mu\text{M}$ MMF, a maximum difference of 21% in clonogenic reduction was seen when the combinations were given in the schedule versus the simultaneous administration. Combinations 3, 4 and 5 all observed significant reductions in clonogenic survival over each single corresponding single treatment dose for both TMZ and MMF (all, $P < 0.0001$ for each single treatment vs each scheduled combination respectively).

From Figure 3.11 (F), each combination of TMZ and MMF when given as a schedule showed synergy, with all combination points having a CI value < 0.9 . From the line of best fit log (Fa/Fu) (Figure 3.11(G)), the combination line observed a distinguishable

greater Fa than both MMF and TMZ. R² values were 0.98, 0.58 and 0.86 for TMZ, MMF and the combination of TMZ + MMF respectively. Again, the R² value of 0.58 for MMF shows the MMF line of fit to be less than ideal and may require an extended concentration range for better reliability of the CIA.

Although synergy cannot be quantified as more or less synergistic, the scheduled combinations observe lower CIA values than the simultaneous combinations, indicating a better response of the scheduled combinations and further supporting our hypothesis. The clonogenic data was again indicative of the pretreatment of MMF to sensitise cells to TMZ, with increased reduction in clonogenic survival against all combinations when compared to the simultaneous administration. With MMF showing lower toxicity, the reduction remains relative as both simultaneous and scheduled treatments were given the same batch of MMF. However, MMF as a single treatment as per Figure 3.4, also showed significant cytotoxicity as a single treatment, and therefore although the hypothesis is supported, MMF as a single treatment could also be a promising candidate alone against GBM.

3.4.6 Effects of Temozolomide and Monomethyl Fumarate on cell cycle progression in the UVW, U87 and T98g human glioblastoma cell lines.

For interrogation of our simultaneous and scheduled combination models, a series of mechanistic assays were performed using the best combination treatment characterised from the CIA models. Cell cycle, Annexin V, Glutathione and Comet assays were all performed using a range of time points to try distinguishing the mode of action of MMF and TMZ.

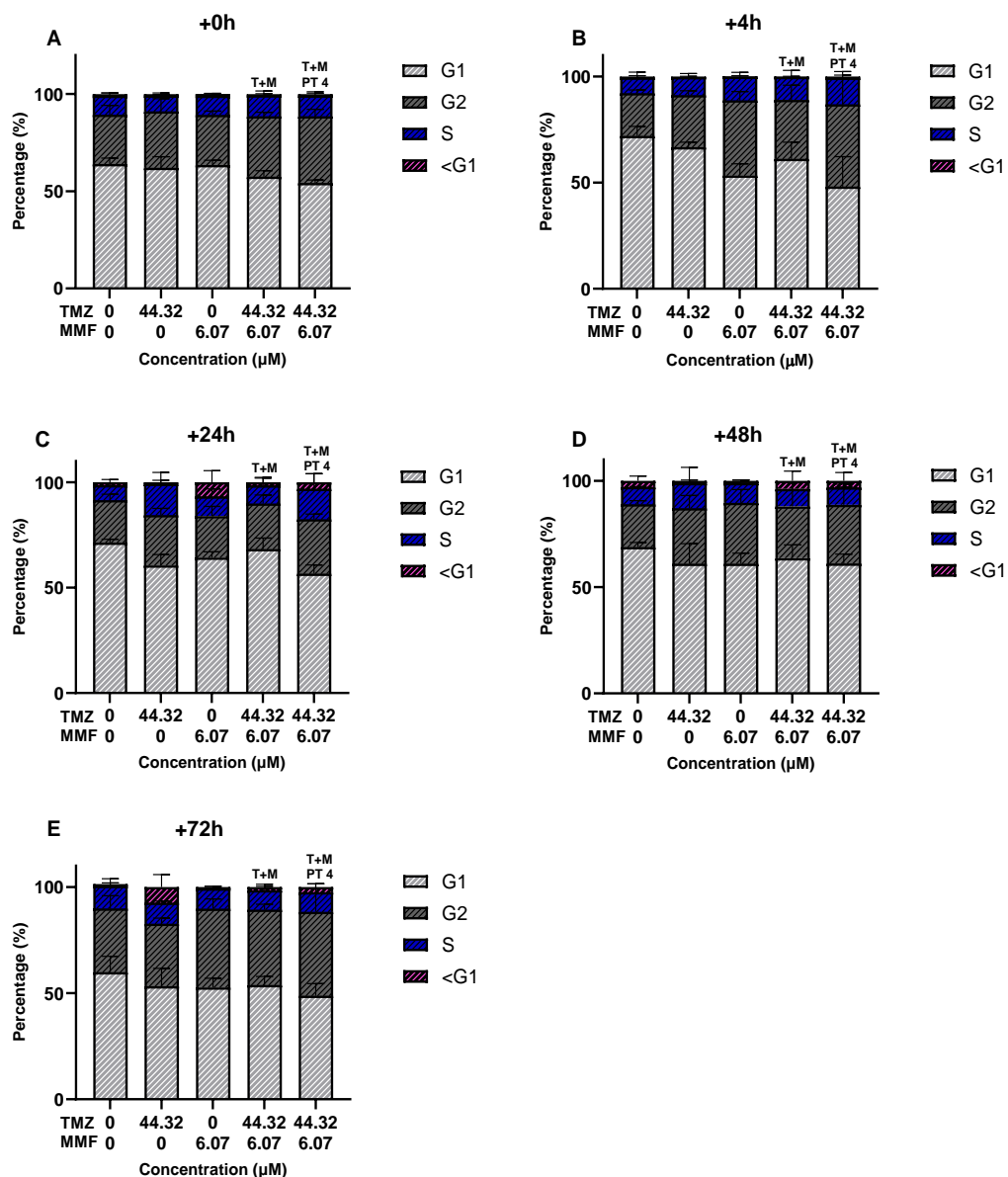
Cell cycle and apoptosis are important biological processes in a cell, allowing growth and homeostasis (Gousias *et al.*, 2022). Changes to the processes of cell cycle can lead to tumorigenesis. The cycle itself is divided into four phases, the G1 phase where cell growth occurs, S phase where DNA is synthesised, G2 phase where the cell is prepped for mitosis and M phases where mitosis occurs. Alternatively, these can be divided into 2 phases, interphase (G1, G2 and S) and mitosis. Cell cycle analysis is not conclusive of the cells metabolic state, as some cells may simply be in arrest and return to the cell cycle, therefore through Annexin V staining and DNA damage assessment, a whole picture can be brought together of the mode of cell death. Representative flow cytometry plots are shown in Appendix 2.

Through single treatments with TMZ and MMF, as well as combination treatments of TMZ and MMF in both simultaneous (T+M) and scheduled treatments (T+M PT4), we aim to decipher if MMF promotes cell cycle arrest with TMZ and if MMF can cause any cell cycle arrest as a single therapy. We hypothesise that the combination schedule will elicit a greater cell cycle arrest than the simultaneous combination, with MMF enhancing TMZ response.

3.4.6.1 Cell cycle analysis of UVW human glioblastoma cells lines after combination treatment exposure to Temozolomide and Monomethyl Fumarate.

UVW human glioblastoma cell lines were exposed to 44.32 μ M TMZ, 6.07 μ M MMF and the combination of both given either simultaneously or with a 4-hour pretreatment of MMF followed by TMZ for a total of 24- hours. The combination of concentrations were chosen for mechanistic interrogation as in both simultaneous and scheduled treatments, the CIA showed synergy. Figure 3.12 demonstrates the distribution of cells in each phase of the cell cycle for each single treatment and the combinations at simultaneous and scheduled administration. The Figure shows the change in cell distribution between the phases over five time points, +0h, +4h, +24h, +48h and +72h, with 0h representing treatment exposure for 24 hours and +4h representing 4h after treatment is removed after the 24h incubation period, the same applies for +24h +48h and +72h. Simultaneous combination administration is represented by T+M and the schedule by T+M PT4. A summary of the significant changes found following a two-way ANOVA on GraphPad prism version 10.3.1 are shown in Figure 3.12 (F).

Significance was assessed for each treatment versus the untreated control and for each treatment versus the other treatments in that time point.



(F)

Phase	Treatment	Significance Summary	Adjusted P value
+0h Time Point			
G1	Control vs (T+M PT4)	Yes*	0.0109
	MMF vs (T+M PT4)	Yes*	0.0176
G2	Control vs T+M PT4	Yes*	0.0226
	MMF vs (T+M PT4)	Yes*	0.0308
+4h Time point			
G1	Control vs MMF	Yes***	0.0009
	Control vs T+M PT4	Yes****	<0.0001

	TMZ vs MMF	Yes*	0.0360
	TMZ vs (T+M PT4)	Yes**	0.0010
	(T+M) vs (T+M PT4)	Yes*	0.0412
G2	Control vs MMF	Yes**	0.0099
	Control vs T+M PT4	Yes***	0.0009
	TMZ vs (T+M PT4)	Yes*	0.0195
+24h Time Point			
G1	Control vs TMZ	Yes*	0.0137
	Control vs T+M PT4	Yes***	0.0003
	(T+M) vs (T+M PT4)	Yes**	0.0069
+72h Time Point			
G1	Control vs T+M PT4	Yes*	0.0500

Figure 3.12: Cell cycle progression in UVW cells treated with (44.32 μ M) Temozolomide, (6.07 μ M) Monomethyl Fumarate, the simultaneous Temozolomide-Monomethyl Fumarate combination (T+M) and the scheduled administration of the Temozolomide-Monomethyl Fumarate combination (T+M PT4). The cell cycle distribution of UVW cells in response to 24- hour exposure at post time points +0h (A), +4h (B), +24h (C), +48h (D), and +72h (E). Statistical analysis of each time points statistically significant changes only, all other comparisons of the data were not significant (F). Data shown is an average of at least 3 independent experiments \pm standard deviation. A two-way ANOVA with Bonferroni post-test was performed with P-values of values of <0.05 = *, <0.01=**, <0.001 = *** and P<0.0001=**** reported as significant.

Figure 3.12 (A and F) shows cell cycle distribution after 24 hours of treatment. A significant increase in G2 phase cells and a corresponding decrease in G1 phase cells were observed between the untreated control and T+M PT4 group (P<0.05). Similarly, compared to MMF alone, the scheduled combination (T+M PT4) significantly increased G2 phase cells and decreased G1 phase cells (P<0.05), suggesting G2 phase arrest of the scheduled combination relative to untreated control and MMF-treated cells.

Four hours post-treatment (Figure 3.12 (B and F)), MMF and T+M PT4 groups showed significant reductions in G1 phase cells compared to the untreated control (P<0.001 and P<0.0001, respectively). A reduction in G1 was also seen between TMZ vs MMF (P<0.05) and TMZ vs T+M PT4 (P<0.01), as well as between the scheduled and simultaneous combinations (P<0.05). Correspondingly, G2 phase cells significantly increased in MMF and T+M PT4 treated groups versus the untreated control (P<0.01 and P<0.001), and between TMZ and the scheduled combination (P<0.05). These findings indicate G2 phase arrest induced by MMF and the scheduled combination.

TMZ data suggests the scheduled combination to instigate greater G2 phase arrest than TMZ. No other significant changes in cell cycle phase were observed

At 24 hours post-treatment (Figure 3.12 (C)), significant G1 phase reductions were seen for TMZ versus the untreated control ($P < 0.05$), scheduled combination versus the untreated control ($P < 0.001$), and between scheduled versus simultaneous combination ($P < 0.01$), with no other significant changes. At 48 and 72 hours post-treatment, no major changes were observed except for a significant G1 decrease between the untreated control and T+M PT4 at 48 hours ($P < 0.05$).

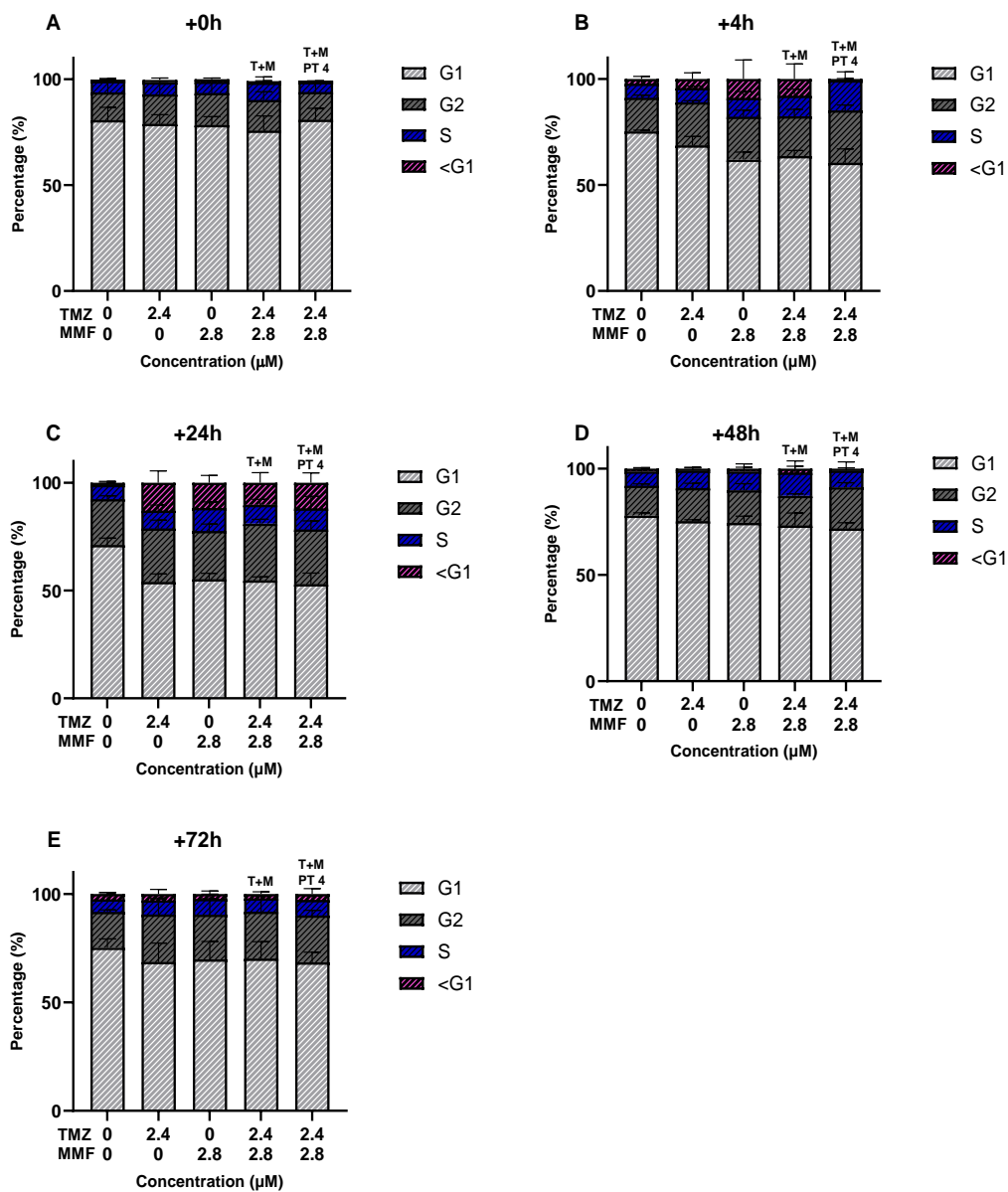
Overall, significant G2 phase increases at 0 and +4 hours post-treatment support the hypothesis that the scheduled combination enhances G2 phase arrest. MMF alone also induced G2 arrest at 4 hours. However, no consistent long-term trends in cell cycle arrest were observed. Data again highlights MMF's potential as a single treatment option for GBM.

3.4.6.2 Cell cycle analysis of U87 human glioblastoma cells lines after combination treatment exposure to Temozolomide and Monomethyl Fumarate.

U87 human glioblastoma cell lines were exposed to 2.4 μ M TMZ, 2.8 μ M MMF and the combination of both given either simultaneously or with a 4- hour pretreatment of MMF followed by TMZ for a total exposure of 24- hours. The combination of concentrations was chosen for mechanistic interrogation as in simultaneous administration, 2.4 μ M TMZ and 2.8 μ M MMF, was the only combination to show greater reductions in clonogenic survival than either single agent, with the increase in reduction in clonogenic survival statistically significant over TMZ. Combination 4 of 2.4 μ M TMZ, 2.8 μ M MMF also gave a higher reduction in clonogenic survival over the single agents when given simultaneously (Figure 3.6) and when given as a schedule (Figure 3.10).

Figure 3.13 demonstrates the distribution of cells in each phase of the cell cycle for each single treatment and the combinations at simultaneous and scheduled administration. The Figure shows the change in cell distribution between the phases over five time points, +0h, +4h, +24h, +48h and +72h. Simultaneous combination administration is represented by T+M and the schedule by T+M PT4. A summary of the significant changes found following a two-way ANOVA on GraphPad prism version 10.3.1 are shown in Figure 3.13 (F). Significance was assessed for each treatment

versus the untreated control and for each treatment versus the other treatments in that time point.



(F)

Phase	Treatment	Significance Summary	Adjusted P value
+4h Time Point			
G1	Control vs MMF	Yes***	0.0010
	Control vs (T+M)	Yes**	0.0049
	Control vs T+M PT4	Yes***	0.0002
+24h Time Point			
G1	Control vs TMZ	Yes****	<0.0001

	Control vs MMF	Yes****	<0.0001
	Control vs (T+M)	Yes****	<0.0001
	Control vs T+M PT4	Yes****	<0.0001
<G1	Control vs TMZ	Yes**	0.0016
	Control vs MMF	Yes**	0.0054
	Control vs (T+M)	Yes*	0.0230
	Control vs T+M PT4	Yes**	0.0045

Figure 3.13: Cell cycle progression in U87 cells treated with (2.4 μ M) Temozolomide, (2.8 μ M) Monomethyl Fumarate, the simultaneous Temozolomide-Monomethyl Fumarate combination (T+M) and the scheduled administration of the Temozolomide-Monomethyl Fumarate combination (T+M PT4). The cell cycle distribution of U87 cells in response to 24- hour exposure at post time points +0h (A), +4h (B), +24h (C), +48h (D), and +72h (E). Statistical analysis of each time points statistically significant changes only, all other comparisons of the data were not significant (F). Data shown is an average of at least 3 independent experiments \pm standard deviation. A two-way ANOVA with Bonferroni post-test was performed with P-values of values of <0.05 = *, <0.01=**, <0.001 = *** and P<0.0001=**** reported as significant.

No significant changes in cell cycle phase distribution were observed at the +0h time point across any treatments (Figure 3.13 (A)). At 4 hours post-treatment (Figure 3.13 (B)), a significant decrease in the G1 phase population was detected for MMF alone (P<0.001), the simultaneous combination (P<0.01), and the scheduled combination (P<0.001) compared to the untreated control, with no other significant changes observed.

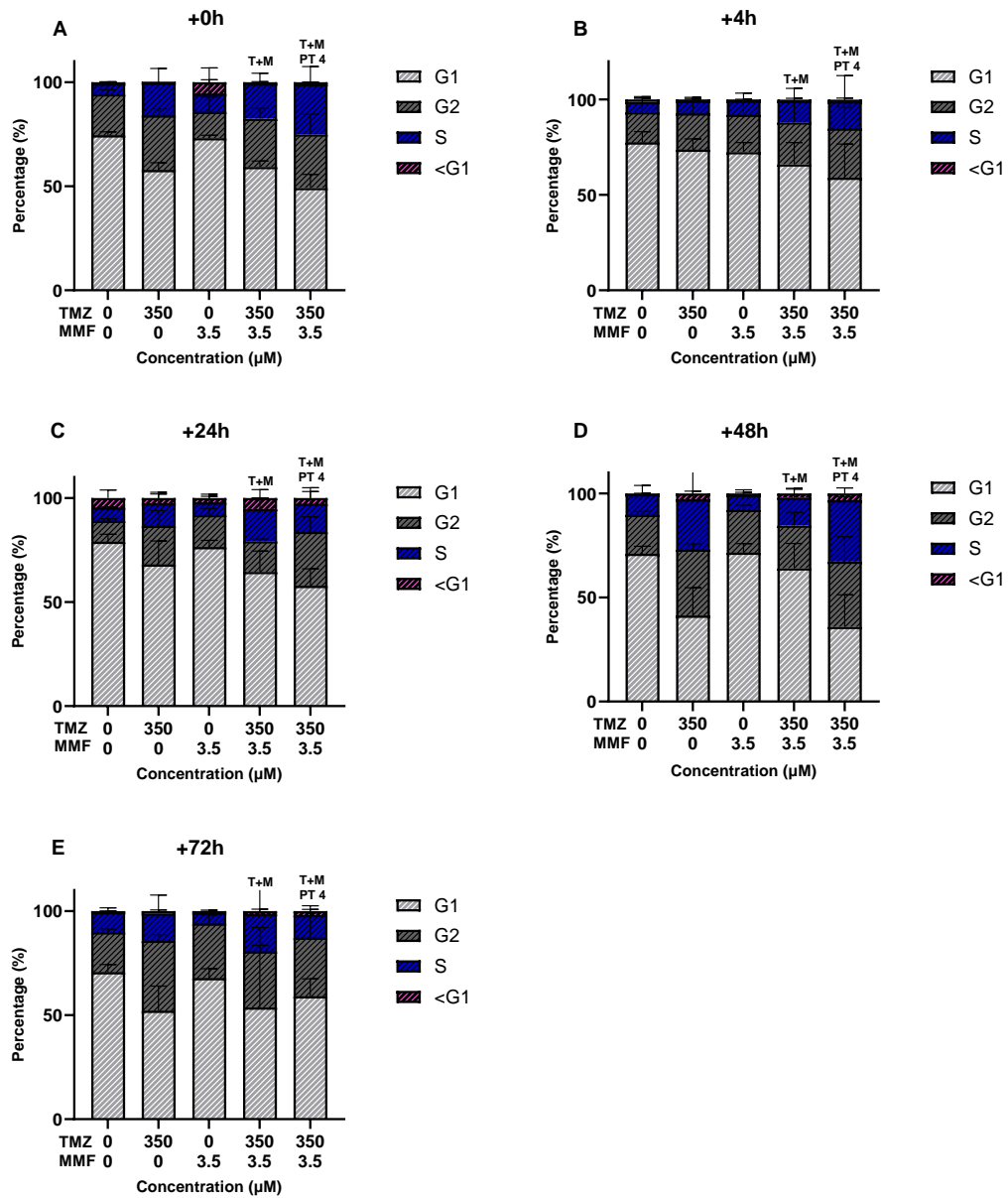
At 24 hours (Figure 3.13 (C)), all treatments, both single and combination, showed a significant decrease in G1 phase cells (P<0.0001) compared to the untreated control. A corresponding increase in <G1 phase cells was noted for TMZ (P<0.01), MMF (P<0.01), T+M (P<0.05), and T+M PT4 (P<0.01), suggesting progression through the cell cycle and accumulation in <G1.No significant changes were observed at +48h (Figure 3.13 (D)) or +72h (Figure 3.13 (E)).

Collectively, the U87 data did not support the original hypothesis, as no major G2 phase arrest was observed. Instead, cells appeared to accumulate in <G1, suggesting entry into a quiescent state or a possible mode of cell death.

3.4.6.3 Cell cycle analysis of T98g human glioblastoma cells lines after combination treatment exposure to Temozolomide and Monomethyl Fumarate.

T98 human glioblastoma cell lines were exposed to 350 μ M TMZ, 3.5 μ M MMF and the combination of both given either simultaneously or with a 4- hour pretreatment of MMF followed by TMZ for a total exposure of 24- hours. The combination of concentrations were chosen for mechanistic interrogation as for both combination index analysis models, all combinations were synergistic.

Figure 3.14 demonstrates the distribution of cells in each phase of the cell cycle in T98g cells, for each single treatment and the combinations of TMZ and MMF at simultaneous and scheduled administration. The Figure shows the change in cell distribution between the phases over five time points, +0h, +4h, +24h, +48h and +72h. A summary of the significant changes found following a two-way ANOVA on GraphPad prism version 10.3.1 are shown in Figure 3.14 (F). Significance was assessed for each treatment versus the untreated control and for each treatment versus the other treatments in that time point.



(F)

Phase	Treatment	Significance Summary	Adjusted P value
+0h Time Point			
G1	Control vs TMZ	Yes*	0.0126
	Control vs (T+M)	Yes*	0.0267
	Control vs (T+M PT4)	Yes****	<0.0001
	TMZ vs MMF	Yes*	0.0260
	MMF vs (T+M PT4)	Yes***	0.0002
S	Control vs (T+M PT4)	Yes**	0.0034
	MMF vs (T+M PT4)	Yes*	0.0238
+4h Time Point			
G1	Control vs (T+M PT4)	Yes*	0.0403
+24h Time Point			

G1	Control vs (T+M)	Yes*	0.0190
	Control vs T+M PT4	Yes***	0.0003
	MMF vs (T+M PT4)	Yes**	0.0015
G2	Control vs (T+M PT4)	Yes**	0.0088
+48h Time Point			
G1	Control vs TMZ	Yes***	0.0001
	Control vs T+M PT4	Yes****	<0.0001
	TMZ vs MMF	Yes****	<0.0001
	TMZ vs (T+M)	Yes**	0.0040
	MMF vs (T+M PT4)	Yes****	<0.0001
	(T+M) vs (T+M PT4)	Yes***	0.0003
S	Control vs (T+M PT4)	Yes*	0.0161
	TMZ vs MMF	Yes*	0.0498
	MMF vs (T+M PT4)	Yes**	0.0046

Figure 3.14: Cell cycle progression in T98g cells treated with (350 μ M) Temozolomide, (3.5 μ M) Monomethyl Fumarate the simultaneous Temozolomide-Monomethyl Fumarate combination (T+M) and the scheduled administration of the Temozolomide-Monomethyl Fumarate combination (T+M PT4). The cell cycle distribution of U87 cells in response to 24- hour exposure at post time points +0h (A), +4h (B), +24h (C), +48h (D), and +72h (E). Statistical analysis of each time points statistically significant changes only, all other comparisons of the data were not significant (F). Data shown is an average of at least 3 independent experiments \pm standard deviation. A two-way ANOVA with Bonferroni post-test was performed with P-values of values of <0.05 = *, <0.01=**, <0.001 = *** and P<0.0001=**** reported as significant.

Figure 3.14 shows changes in cell cycle distribution over time following 24-hour treatment. At +0h (Figure 3.14 (A)), TMZ alone, and both the simultaneous and scheduled combinations (T+M, T+M PT4), caused a significant decrease in G1 phase cells compared to the untreated control (all P<0.05). Additionally, G1 phase cells decreased significantly between MMF and TMZ (P<0.05) and between MMF and T+M PT4 (P<0.001). No significant changes were seen in G2 or <G1 phases. S phase cells significantly increased after exposure to T+M PT4 compared to the untreated control (P<0.01) and MMF (P<0.05) (Figure 3.14 (F)).

At +4h (Figure 3.14 (B and F)), only the scheduled combination (T+M PT4) showed a significant decrease in G1 phase cells versus the untreated control (P<0.05). No other significant changes were observed at this time point.

At +24 hours (Figure 3.14 (C)), T+M PT4 significantly increased G2 phase cells compared to the untreated control (P<0.01). In the G1 phase, significant decreases were observed for T+M and T+M PT4 versus the untreated control (P<0.05 and P<0.001, respectively) and between T+M PT4 and MMF (P<0.01).

Post 48-hour treatment (Figure 3.14 (D)), G1 phase cells significantly decreased for TMZ and T+M PT4 compared to the untreated control ($P<0.001$). Additional decreases were seen for MMF and T+M versus TMZ (both $P<0.01$) and for T+M PT4 versus MMF ($P<0.0001$) and versus T+M ($P<0.001$). In the S phase, T+M PT4 induced a significant increase compared to the untreated control ($P<0.05$) and MMF ($P<0.01$), while MMF showed a significant decrease compared to TMZ ($P<0.05$). No changes were seen in G2 or <G1 populations. No significant changes in any cell cycle phase populations were observed at 72 hours post-treatment (Figure 3.14 (E)).

Overall data suggests T+M PT4 to cause early disruption to the cell cycle with a G1 phase reduction and increase in G2 and S phases post 24h, however this was not consistent over time and the hypothesis was rejected.

3.4.7 Apoptotic/Necrotic induction in UVW human glioblastoma cells after treatment with Temozolomide and Monomethyl Fumarate

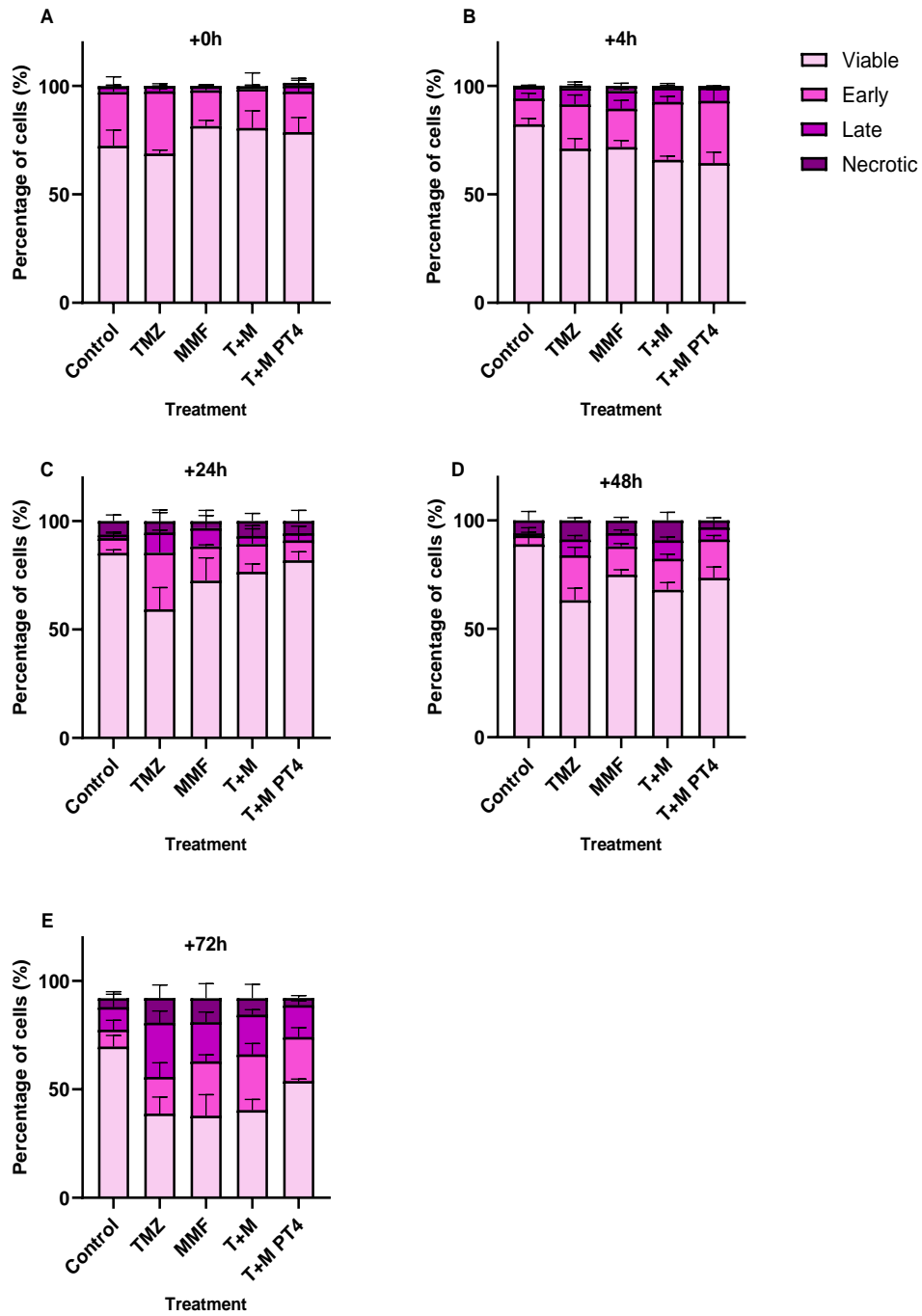
As discussed, apoptosis is a form of programmed cell death which can be induced from a cell with too much damage, or through cell cycle arrest. TMZ induces senescence, autophagy and apoptosis in a time dependent manner, with both senescence and autophagy responses preceding apoptosis (Pawlowska *et al.*, 2018).

Detection of apoptotic and necrotic cells after treatment with TMZ, MMF and the combination given simultaneously or scheduled was determined through an Annexin V apoptotic detection assay. The assay was performed with the same treatments as cell cycle in section 3.4.8, to decipher the mechanisms of action of the combinations (section 2.12). Representative flow cytometry plots are shown in Appendix 2.

Through Annexin V staining of treated cells, we hypothesise that MMF and TMZ as a combination will cause more cells to be in stages of apoptosis and necrosis than the single treatments, and the scheduled treatment of the combination to cause a greater level of apoptosis/necrosis than simultaneous administration.

3.4.7.1 Induction of Apoptosis after treatment with Temozolomide and Monomethyl Fumarate in the UVW human glioblastoma cell line.

UVW cells were treated similarly to section 3.4.6, with a total exposure time to drugs of 24h, followed by the post treatment time points where cells were taken for assessment. Figure 3.15 shows the change in the percentage of UVW cells which are viable or in early, late apoptosis or necrosis stages overtime. The percentage of cells in each phase is divided between the four stages and statistically significant changes summarised in Figure 3.15 (F). Significant changes were calculated following a two-way ANOVA on GraphPad prism version 10.3.1. Significance was assessed for each treatment versus the untreated control and for each treatment compared to each other treatment.



(F)

Phase	Treatment	Significance Summary	Adjusted P value
+4h Time Point			
Viable	Control vs (T+M)	Yes**	0.0014
	Control vs T+M PT4	Yes***	0.0004
Early Apoptosis	Control vs (T+M)	Yes**	0.0045
	Control vs T+M PT4	Yes***	0.0010
+24h Time Point			
Viable	Control vs TMZ	Yes*	0.0308

+48h Time Point			
Viable	Control vs TMZ	Yes****	<0.0001
	Control vs MMF	Yes*	0.0179
	Control vs (T+M)	Yes***	0.0001
	Control vs T+M PT4	Yes**	0.0065
Early Apoptosis	Control vs TMZ	Yes**	0.0028
	Control vs T+M PT4	Yes*	0.0221
+72h Time Point			
Viable	Control vs TMZ	Yes**	0.0015
	Control vs MMF	Yes***	0.0010
	Control vs (T+M)	Yes**	0.0029

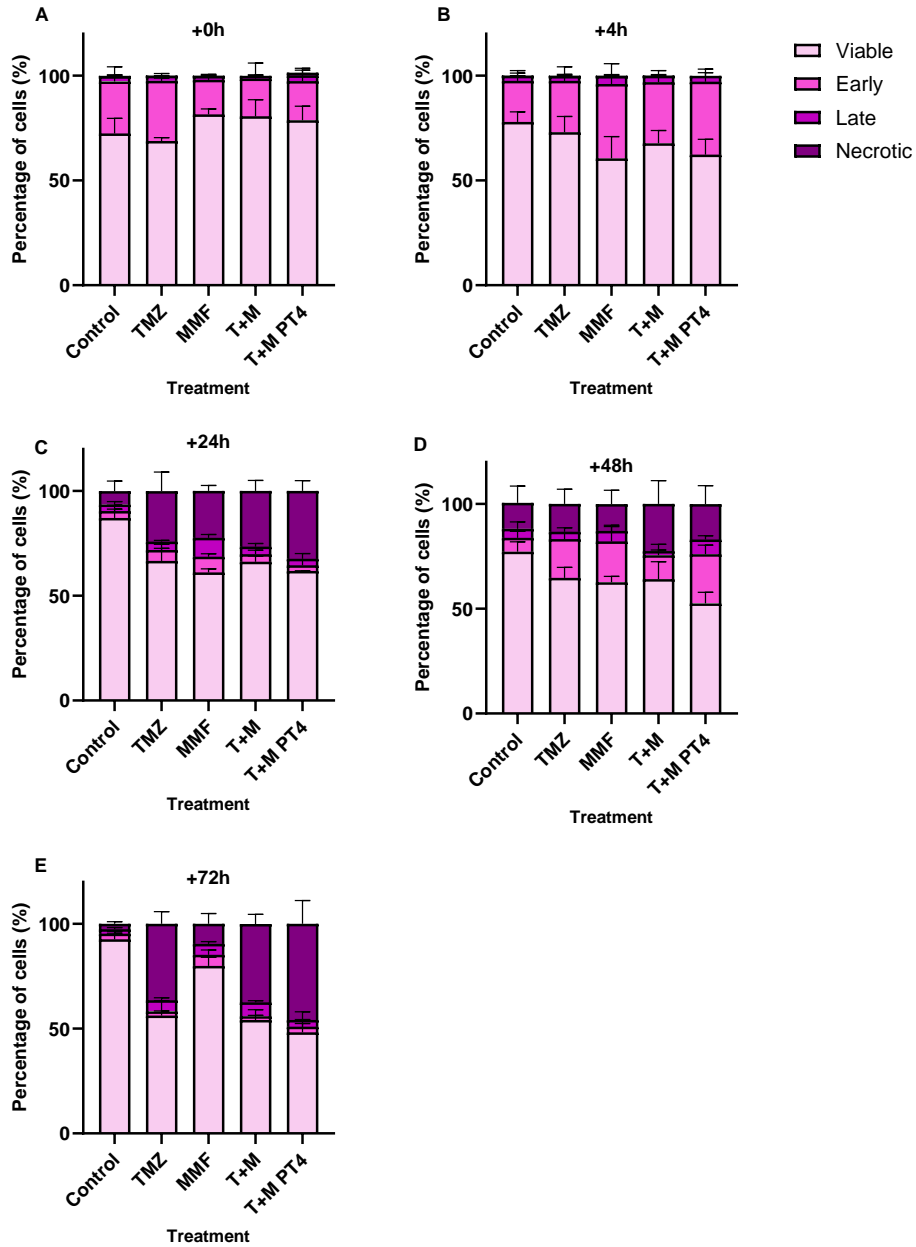
Figure 3.15: Induction of apoptosis in UVW cells by Temozolomide (44.32 μ M), Monomethyl Fumarate (6.07 μ M) and the combination of Temozolomide and Monomethyl Fumarate combination given simultaneously (T+M) or in a schedule (T+M PT4). Apoptotic induction in UVW cells after +0h (A), +4h (B) +24h (C) +48h (D) and + 72h (E). Statistical comparisons of cell phases over time after exposure to treatments, only showing statistically significant differences, all other comparisons were insignificant (F). Data shown is an average of at least 3 independent experiments \pm standard deviation. A two-way ANOVA with Bonferroni post-test was performed with P-values of values of <0.05 = *, <0.01=**, <0.001 = *** and P<0.0001=**** reported as significant.

Figure 3.15 shows the effects of treatments on UVW cell populations over time. At +0h (Figure 3.15 (A)), no statistically significant changes were observed across viable, apoptotic, or necrotic cell populations compared to the untreated control. At +4h (Figure 3.15 (B)), both T+M and T+M PT4 treatments led to a statistically significant decrease in viable cells ($P<0.01$ and $P<0.001$, respectively) and a statistically significant increase in early apoptotic cells compared to the untreated control ($P<0.01$ and $P<0.001$). No statistically significant changes were observed for TMZ, MMF, or between single treatments and combinations. At 24h, a statistically significant decrease in viable cells was observed for TMZ compared to the untreated control ($P<0.05$), with no other statistically significant changes. At 48h, statistically significant reductions in viable cells were observed for TMZ ($P<0.0001$), MMF ($P<0.05$), T+M ($P<0.001$), and T+M PT4 ($P<0.01$) versus the untreated control. Early apoptotic cell populations were statistically significantly increased for TMZ ($P<0.01$) and T+M PT4 ($P<0.05$). At 72h, viable cell populations remained statistically significantly reduced for TMZ ($P<0.01$), MMF ($P<0.001$), and T+M ($P<0.01$) compared to the untreated control, with no other statistically significant changes observed in apoptotic or necrotic cell populations.

Overall, although apoptotic and necrotic cell populations tended to increase over time, these changes were not consistently statistically significant. Therefore, the hypothesis was rejected, as the scheduled combination (T+M PT4) did not induce greater changes in apoptosis or necrosis compared to the simultaneous combination at any time point. Overall, From Figure 3.15 we found an increase in apoptotic and necrotic cell populations with time, although this was not consistently significant. Therefore, from the data our hypothesis is rejected, as both single and combination treatments had a significant decrease in viable cells after 24h, 48h and 72h. Additionally, the scheduled combination did not induce significant changes in the apoptotic and necrotic cell populations over the simultaneous combination at any time point.

3.4.7.2 Induction of Apoptosis after treatment with Temozolomide and Monomethyl Fumarate in the U87 human glioblastoma cell line.

U87 cells were treated similarly to section 3.4.6, with a total exposure time to drugs of 24h, followed by the post treatment time points where cells were taken for assessment. Figure 3.16 shows the change in the percentage of U87 cells which are viable or in early, late apoptotic or necrotic stages overtime. The percentage of cells in each phase was divided between the four stages and statistically significant changes summarised in Figure 3.16 (F). Significant changes were calculated following a two-way ANOVA on GraphPad prism version 10.3.1. Significance was assessed for each treatment versus the untreated control and for each treatment compared to each other treatment.



(F)

Phase	Treatment	Significance Summary	Adjusted P value
+24h Time Point			
Viable	Control vs TMZ	Yes**	0.0038
	Control vs MMF	Yes***	0.0001
	Control vs (T+M)	Yes**	0.0030
	Control vs T+M PT4	Yes***	0.0002
Necrotic	Control vs TMZ	Yes*	0.0167
	Control vs MMF	Yes*	0.0432
	Control vs (T+M)	Yes**	0.0046
	Control vs T+M PT4	Yes***	0.0002
+48h Time Point			
Viable	Control vs T+M PT4	Yes*	0.0402

+72h Time Point			
Viable	Control vs TMZ	Yes****	<0.0001
	Control vs (T+M)	Yes****	<0.0001
	Control vs T+M PT4	Yes****	<0.0001
	TMZ vs MMF	Yes**	0.0064
	MMF vs (T+M)	Yes**	0.0024
	MMF vs (T+M PT4)	Yes***	0.0001
Necrotic	Control vs TMZ	Yes****	<0.0001
	Control vs (T+M)	Yes****	<0.0001
	Control vs T+M PT4	Yes****	<0.0001
	TMZ vs MMF	Yes**	0.0014
	MMF vs (T+M)	Yes***	0.0009
	MMF vs (T+M PT4)	Yes****	<0.0001

Figure 3.16: Induction of apoptosis in U87 cells by Temozolomide (2.4 μ M) Monomethyl Fumarate (2.8 μ M) and the combination of Temozolomide and Monomethyl Fumarate combination given simultaneously (T+M) or in a schedule (T+M PT4). Apoptotic induction in U87 cells after +0h (A), +4h (B) +24h (C) +48h (D) and + 72h (E). Statistical comparisons of cell phases over time after exposure to treatments, only showing statistically significant differences (F). Data shown is an average of at least 3 independent experiments \pm standard deviation. A two-way ANOVA with Bonferroni post-test was performed with P-values of values of <0.05 = *, <0.01=**, <0.001 = *** and P<0.0001=**** reported as significant.

Figure 3.16 displays the changes in apoptotic, viable, and necrotic cell populations over time. At +0h (Figure 3.16 (A)) and +4h (Figure 3.16 (B)), no statistically significant changes were observed across any treatment groups compared to the untreated control ($P>0.05$). At 24h (Figure 3.16 (C)), statistically significant reductions in viable cells were observed for TMZ ($P<0.01$), MMF ($P<0.001$), T+M ($P<0.01$), and T+M PT4 ($P<0.001$) compared to the untreated control. MMF and T+M PT4 showed the greatest decrease in viable cell populations. Complementary increases in necrotic cell populations were also statistically significant for TMZ ($P<0.05$), MMF ($P<0.05$), T+M ($P<0.01$), and T+M PT4 ($P<0.001$) compared to the untreated control, with the combination treatments showing the greatest increases.

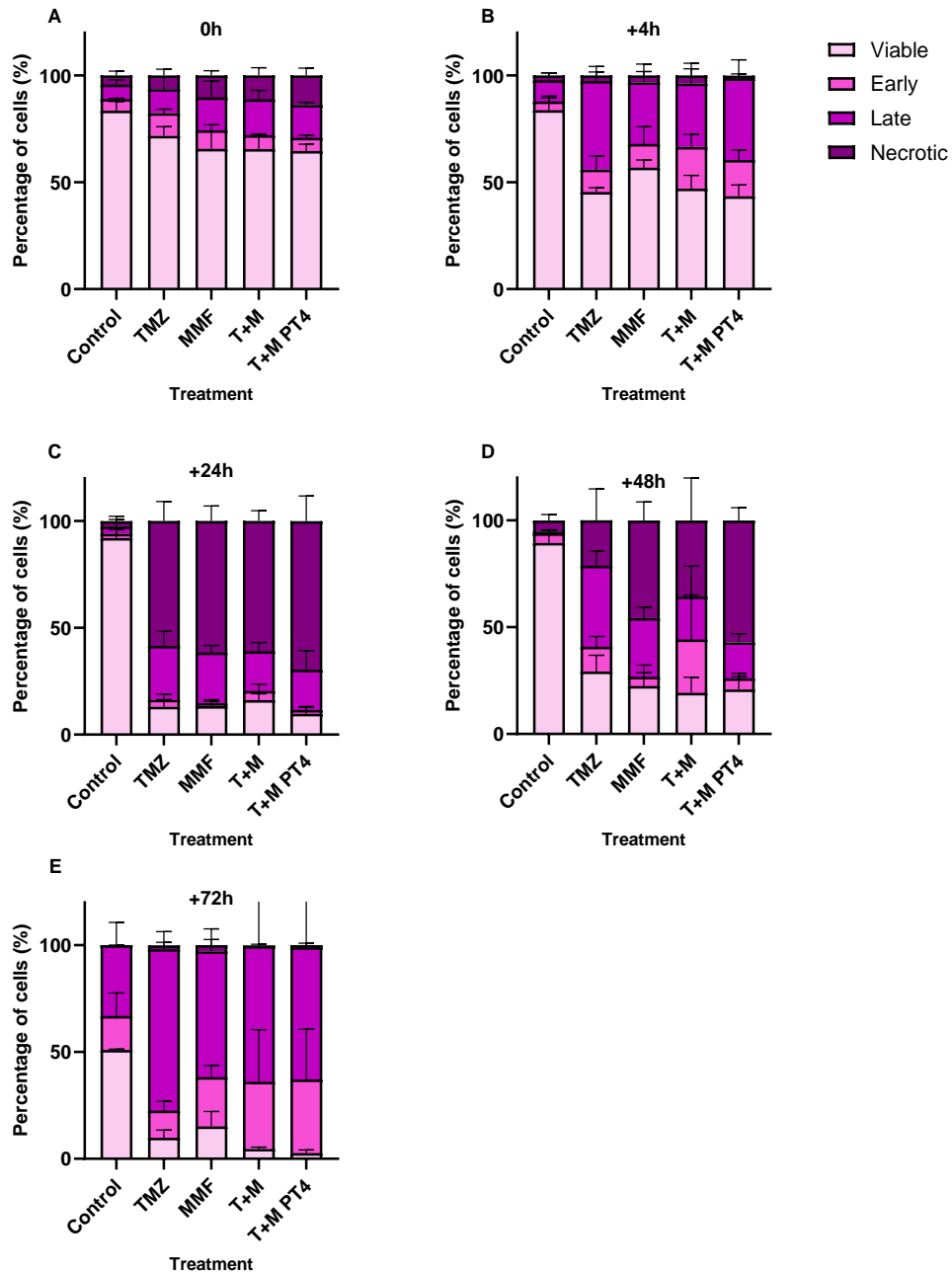
At 48h (Figure 3.16 (D)), necrotic cell populations decreased relative to 24h levels. A statistically significant reduction in viable cells was observed for T+M PT4 compared to the untreated control ($P<0.05$). No other statistically significant changes were detected in apoptotic or necrotic phases at this time point. By 72h (Figure 3.16 (E)), marked changes were evident. Statistically significant decreases in viable cell populations compared to the untreated control were observed for TMZ, T+M, and T+M PT4 (all $P<0.0001$). Viable cells were statistically significantly higher in MMF-treated

cells compared to TMZ ($P < 0.01$), while T+M and T+M PT4 showed statistically significant reductions in viable cells compared to MMF (both $P < 0.01$). Corresponding statistically significant increases in necrotic cell populations were observed for TMZ, T+M, and T+M PT4 (all $P < 0.0001$) compared to the untreated control. MMF-treated cells showed statistically significantly lower necrosis compared to TMZ ($P < 0.01$), while both combination treatments induced greater necrosis than MMF (both $P < 0.001$).

Over time an increase in the necrotic cell populations was observed, with T+M PT4 showing the largest necrotic cell population post 72h treatment supporting our hypothesis. Both T+M and T+M PT4 showed statistically significant changes with increasing necrotic cell populations, somewhat supporting our hypothesis.

3.4.7.3 Induction of Apoptosis after treatment with Temozolomide and Monomethyl Fumarate in the T98g human glioblastoma cell line.

T98g cells were similarly to section 3.4.6, with a total exposure time to drugs of 24h, followed by the post treatment time points where cells were taken for assessment. Figure 3.17 shows the change in the percentage of T98g cells which are viable or in early, late apoptotic or necrotic stages overtime. The percentage of cells in each phase was divided between the four stages and statistically significant changes summarised in Figure 3.17 (F). Significant changes were calculated following a two-way ANOVA on GraphPad prism version 10.3.1. Significance was assessed for each treatment versus the untreated control and for each treatment compared to each other treatment.



(F)

Phase	Treatment	Significance Summary	Adjusted P value
+0h Time Point			
Viable	Control vs MMF	Yes*	0.0365
	Control vs (T+M)	Yes*	0.0344
	Control vs T+M PT4	Yes*	0.0218
+4h Time Point			
Viable	Control vs TMZ	Yes***	0.0001
	Control vs MMF	Yes*	0.0124
	Control vs (T+M)	Yes***	0.0003

	Control vs T+M PT4	Yes****	<0.0001
Late Apoptosis	Control vs TMZ	Yes**	0.0021
	Control vs T+M PT4	Yes**	0.0073
+24h Time Point			
Viable	Control vs TMZ	Yes****	<0.0001
	Control vs MMF	Yes****	<0.0001
	Control vs (T+M)	Yes****	<0.0001
	Control vs T+M PT4	Yes****	<0.0001
Necrotic	Control vs TMZ	Yes****	<0.0001
	Control vs MMF	Yes****	<0.0001
	Control vs (T+M)	Yes****	<0.0001
	Control vs T+M PT4	Yes****	<0.0001
+48h Time Point			
Viable	Control vs TMZ	Yes***	0.0005
	Control vs MMF	Yes****	<0.0001
	Control vs (T+M)	Yes****	<0.0001
	Control vs T+M PT4	Yes****	<0.0001
Necrotic	Control vs MMF	Yes*	0.0392
	Control vs T+M PT4	Yes**	0.0035
+72h Time Point			
Viable	Control vs T+M PT4	Yes*	0.0446

Figure 3.17: Induction of apoptosis in T98g cells by Temozolomide (350 μ M), Monomethyl Fumarate (3.5 μ M) and the combination of Temozolomide and Monomethyl Fumarate combination given simultaneously (T+M) or in a schedule (T+M PT4). Apoptotic induction in U87 cells after +0h (A), +4h (B) +24h (C) +48h (D) and + 72h (E). Statistical comparisons of cell phases over time after exposure to treatments, only showing statistically significant differences (F). Data shown is an average of at least 3 independent experiments \pm standard deviation. A two-way ANOVA with Bonferroni post-test was performed with P-values of values of <0.05 = *, <0.01=**, <0.001 = *** and P<0.0001=**** reported as significant.

Figure 3.17 displays changes in T98G cell populations following 24-hour treatment exposure. At +0h (Figure 3.17 (A)), statistically significant decreases in viable cell populations compared to the untreated control were observed for MMF, T+M, and T+M PT4 (all P<0.05). Although TMZ-treated cells showed a decrease in viability, it was not statistically significant (P>0.05). No statistically significant changes were observed in apoptotic or necrotic populations at this time point (Figure 3.17 (F)). At +4h (Figure 3.17 (B)), statistically significant reductions in viable cell populations were observed for TMZ (P<0.001), MMF (P<0.05), T+M (P<0.001), and T+M PT4 (P<0.0001) compared to the untreated control. Late apoptotic cell populations also increased statistically significantly for TMZ (P<0.01) and T+M PT4 (P<0.01) compared to the untreated control (Figure 3.17 (F)). At 24h (Figure 3.17 (C)), statistically significant decreases in viable cell populations and corresponding increases in

necrotic cell populations were observed for all treatments compared to the untreated control (all $P < 0.0001$). No statistically significant differences between treatments were detected ($P > 0.05$). At 48h (Figure 3.17 (D)), necrotic cell populations decreased relative to 24h. Viable cells remained statistically significantly reduced for TMZ ($P < 0.001$), and for MMF, T+M, and T+M PT4 (all $P < 0.0001$) compared to the untreated control. Statistically significant increases in necrotic cells were observed for MMF ($P < 0.05$) and T+M PT4 ($P < 0.01$) compared to the untreated control. Although increases in early and late apoptotic populations were observed for T+M and T+M PT4, these were not statistically significant ($P > 0.05$).

At 72h (Figure 3.17 (E)), necrotic populations decreased markedly compared to 24h and 48h, suggesting clearance of dead cells. Despite visible reductions in viable, early apoptotic, and late apoptotic cells, only the decrease in viable cells for T+M PT4 compared to the untreated control reached statistical significance ($P < 0.05$). T+M PT4 treatment resulted in the lowest viable cell population at 72h, though not statistically significant compared to other treatments ($P > 0.05$).

Temozolomide resistant T98g cells gave no statistically significant differences between combination treatment groups compared to single treatment groups, therefore rejecting our hypothesis of the combination initiating more apoptosis and necrosis than TMZ and MMF as single agents. The scheduled treatment T+M PT4 when compared to T+M given simultaneously, observed no significant differences in changes between cell populations, also rejecting our hypothesis. T+M PT4 consistently reduced cell viability over time and had some of the strongest effects, although differences between treatments were often not statistically significant at later time points.

3.4.8 Quantification of DNA damage and repair in UVW, U87 and T98g human glioblastoma cell lines after exposure to Temozolomide and Monomethyl Fumarate

For further assessment of the mechanisms behind Temozolomide (TMZ), Monomethyl Fumarate (MMF) and the combination of both on GBM cells, DNA damage was quantified using a comet assay as described in section 2.13. By use of an alkaline comet assay small amounts of DNA damage could be detected through single and

double strand breaks initiated by treatments (Lu *et al.*, 2017). Single cell gel electrophoresis was performed on treated cells, with the fragmented DNA being pulled out across low melting point agarose, with the greater the damage in the cell, the longer the migration of the fragments as observed in Figure 3.18 and the stronger the fluorescent signal, quantified as tail moment.

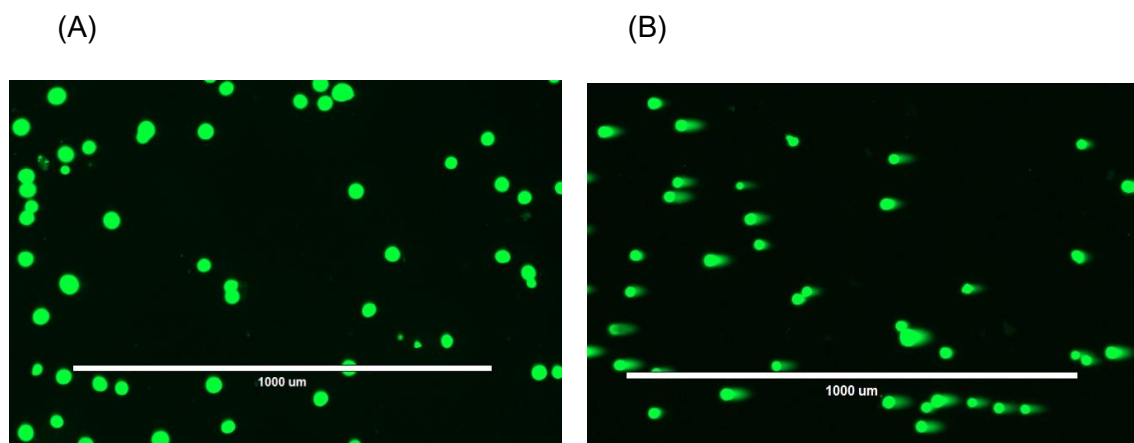


Figure 3.18: Representative images of single cell gel electrophoresis after (A) no treatment and little DNA damage or (B) treatment which has caused DNA damage, indicated by the distinct tails.

DNA damage is a common process in the lifecycle of a healthy cell. Both radiotherapy and chemotherapy work by instigating additional DNA damage on a scale that cannot be repaired leading to cell cycle arrest. Temozolomides mode of action is primarily to cause DNA damage by methylation of the DNA bases. Therefore, a comet assay was performed comparing the damage instigated by TMZ and comparing it to MMF as a single agent and both the simultaneous combination and scheduled combinations previously used, as well as the untreated control.

As we expect damage to repair over time, the +4h time point was removed from the mechanistic cascade as after the initial damage at +0h, a +4h time point would not show much DNA damage repair and we found from +24h data a significant increase in damage.

The combination of Temozolomide and Monomethyl Fumarate given both simultaneously and scheduled, was hypothesised to induce a greater level of DNA damage when compared to the single treatments. The scheduled combination was further hypothesised to instigate greater DNA damage than the simultaneously administered combination.

3.4.8.1 DNA damage response in the UVW human glioblastoma cell line after Temozolomide and Monomethyl Fumarate exposure.

Figure 3.19 represents the mean tail moment of UVW cells (AU%) normalised as a percentage to the untreated control, at +0h, +24h, +48h and +72h. Administered treatments were 44.32 μ M TMZ, 6.07 μ M MMF, the simultaneous administration of both (T+M) and the scheduled administration of MMF for 4h followed by TMZ (T+M PT4). Representative images are shown in Appendix 3 (A).

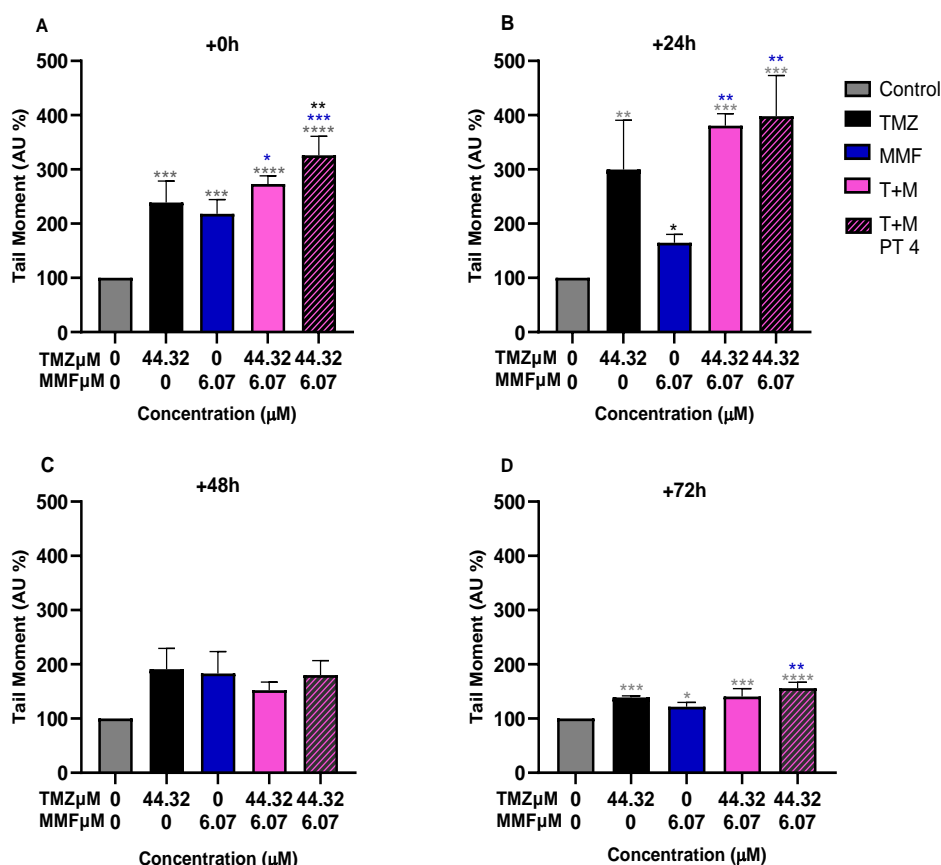


Figure 3.19: DNA damage quantified as Tail Moment (AU) is displayed as a percentage of the control mean after treatment with (44.32 μ M) Temozolomide, (6.07 μ M) Monomethyl Fumarate, the Temozolomide-Monomethyl Fumarate combination (T+M) and the scheduled administration of the combination (T+M PT4). The change in tail movement of UVW cells in response to 24- hour exposure at post time points +0h (A), +24h (B), +48h (C) and +72h (D). Data shown is an average of at least 3 independent experiments \pm standard deviation, with 100 comets per

treatment group. A two-way ANOVA with Bonferroni post-test was performed with P-values of values of $<0.05 = *$, $<0.01 = **$, $<0.001 = ***$ and $P < 0.0001 = ****$ reported as significant. $*$ = significant against the control $*$ = significant against TMZ, $*$ = significant against MMF and $*$ = significant against T+M.

Figure 3.19 quantifies DNA damage over time following 24-hour treatment with TMZ, MMF, T+M, and T+M PT4. At +0h (Figure 3.19 (A)), statistically significant increases in tail moment were observed for TMZ ($P < 0.001$), MMF ($P < 0.001$), T+M ($P < 0.0001$), and T+M PT4 ($P < 0.0001$) compared to the untreated control. Statistically significant increases were also detected between MMF and T+M ($P < 0.05$), MMF and T+M PT4 ($P < 0.001$), and between TMZ and T+M PT4 ($P < 0.01$), indicating that the scheduled combination induced greater DNA damage than either single agent. T+M PT4 produced the highest DNA damage, with a $326\% \pm 35\%$ increase in tail moment, although no statistically significant difference was observed between the simultaneous and scheduled combinations.

At 24h (Figure 3.19 (B)), statistically significant increases in DNA damage were observed for TMZ ($P < 0.01$), T+M ($P < 0.001$), and T+M PT4 ($P < 0.001$) compared to the untreated control. Both combination treatments showed significantly greater DNA damage than MMF alone ($P < 0.001$). TMZ also induced greater DNA damage than MMF ($P < 0.05$). At 48h (Figure 3.19 (C)), no statistically significant differences in tail moment were detected between any treatment groups or compared to the untreated control ($P > 0.05$).

By 72h (Figure 3.19 (D)), statistically significant increases in DNA damage were detected for TMZ ($P < 0.01$), MMF ($P < 0.05$), T+M ($P < 0.001$), and T+M PT4 ($P < 0.0001$) compared to the untreated control. T+M PT4-treated cells also showed a statistically significant increase compared to MMF ($P < 0.05$). However, overall DNA damage levels were lower at 72h compared to earlier time points.

Collectively, these data support the hypothesis that the combination treatments, particularly the scheduled combination (T+M PT4), induce greater DNA damage than either single agent. Notably, the scheduled combination maintained higher levels of DNA damage at 72h compared to the control and MMF, suggesting that the damage was substantial and not fully repaired by the cancer cells..

3.4.8.2 DNA damage response in the U87 human glioblastoma cell line after Temozolomide and Monomethyl Fumarate exposure.

Figure 3.20 represents the mean tail moment of UVW cells (AU) normalised as a percentage to the untreated control, at +0h, +24h, +48h and +72h. Administered treatments were 2.4µM TMZ, 2.8µM MMF, the simultaneous administration of both (T+M) and the scheduled administration of MMF for 4h followed by TMZ (T+M PT4). Representative images are shown in Appendix 3 (B).

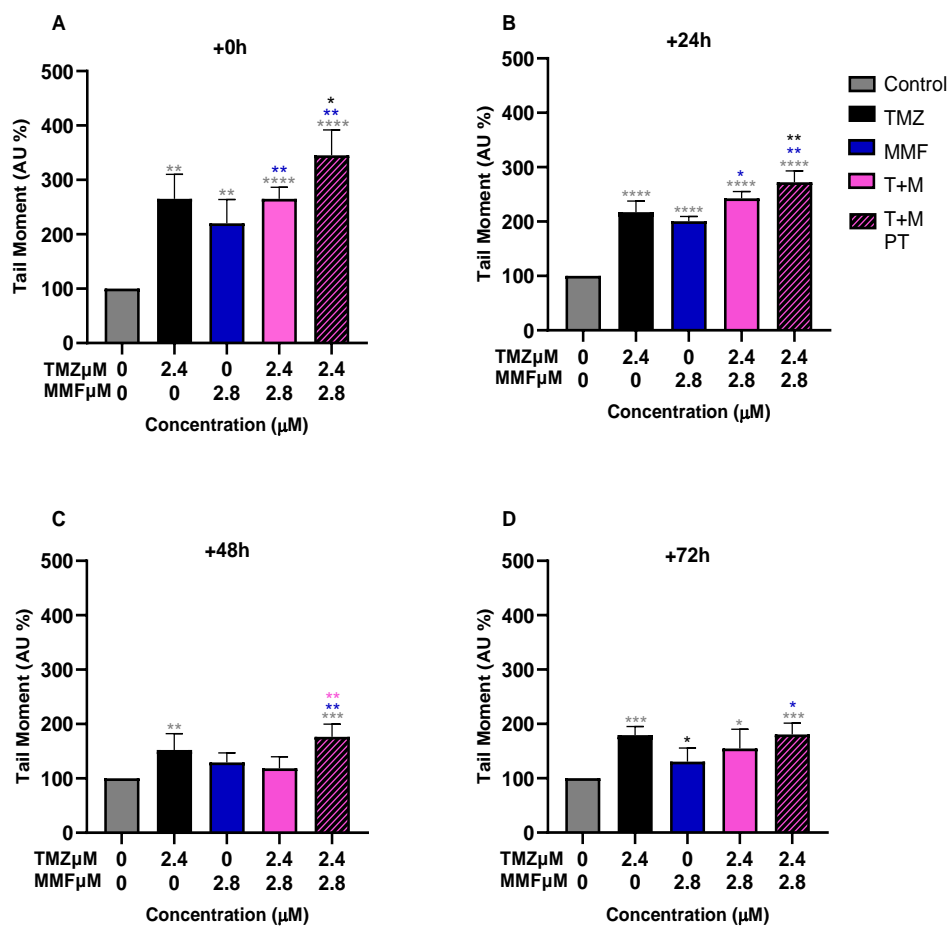


Figure 3.20: DNA damage quantified as Tail Moment (AU) in the U87 cell line, displayed as a percentage of the control mean after treatment with (2.4µM) Temozolomide, (2.8µM) Monomethyl Fumarate, the Temozolomide-Monomethyl Fumarate combination (T+M) and the scheduled administration of (T+M PT4). The change in tail movement of U87 cells in response to 24- hour exposure at post time points +0h (A), +24h (B), +48h (C) and +72h (D). Data shown is an average of at least

3 independent experiments \pm standard deviation, with 100 comets per treatment group. A two-way ANOVA with Bonferroni post-test was performed with P-values of values of $<0.05 = *$, $<0.01 = **$, $<0.001 = ***$ and $P < 0.0001 = ****$ reported as significant. * = significant against the control * = significant against TMZ, * = significant against MMF and * = significant against T+M.

Figure 3.20 shows the levels of DNA damage following treatment exposure. At +0h (Figure 3.20 (A)), statistically significant increases in DNA damage were observed for TMZ ($P < 0.01$), MMF ($P < 0.01$), T+M ($P < 0.0001$), and T+M PT4 ($P < 0.0001$) compared to the untreated control, following two-way ANOVA with Bonferroni's post-test. Both combination treatments (T+M and T+M PT4) induced greater DNA damage than MMF ($P < 0.01$) and TMZ ($P < 0.05$) as single treatments, with the scheduled combination (T+M PT4) eliciting the highest damage.

At +24h (Figure 3.20 (B)), similar trends were observed, although overall DNA damage levels were reduced compared to +0h. Statistically significant increases in DNA damage persisted for TMZ, MMF, T+M, and T+M PT4 versus the untreated control (all $P < 0.0001$). Again, T+M and T+M PT4 induced significantly greater DNA damage than MMF ($P < 0.05$ and $P < 0.01$, respectively) and the scheduled combination induced greater damage than TMZ ($P < 0.01$).

At 48h (Figure 3.20 (C)), DNA damage decreased across all treatments, indicating DNA repair in surviving cells. However, statistically significant increases in DNA damage were maintained in TMZ treated cells ($P < 0.01$) and T+M PT4 treated cells ($P < 0.001$) compared to the untreated control. T+M PT4 treated cells also showed statistically significant increases in DNA damage compared to MMF and T+M-treated cells (both $P < 0.01$).

At 72h (Figure 3.20 (D)), a slight increase in DNA damage was observed. Statistically significant increases were detected for TMZ ($P < 0.001$), T+M PT4 ($P < 0.001$) versus the untreated control, and T+M PT4 compared to MMF ($P < 0.05$). The simultaneous combination (T+M) also showed a statistically significant increase in DNA damage compared to the untreated control ($P < 0.05$). MMF as single treatment showed a statistically significant reduction in DNA damage compared to TMZ ($P < 0.05$).

The data suggests that the scheduled combination elicits not only higher levels of DNA damage than either single agent, but over time, as seen in Figure 3.20 (C), the schedule elicits more damage than the simultaneously administered combination

supporting our hypothesis that the scheduled combination will cause more DNA damage than the single treatments and the simultaneous combination. Additionally, we see a new mode of action for MMF as a single treatment with significant DNA damage shown at 0h and +24h.

3.4.8.3 DNA damage response in the T98g human glioblastoma cell line after Temozolomide and Monomethyl Fumarate exposure.

Figure 3.21 represents the mean tail moment of T98g cells (AU) normalised as a percentage to the untreated control, at +0h, +24h, +48h and +72h. Administered treatments were 350µM TMZ, 3.5µM MMF, the simultaneous administration of both (T+M) and the scheduled administration of MMF for 4h followed by TMZ (T+M PT4). Representative images are shown in Appendix 3 (C).

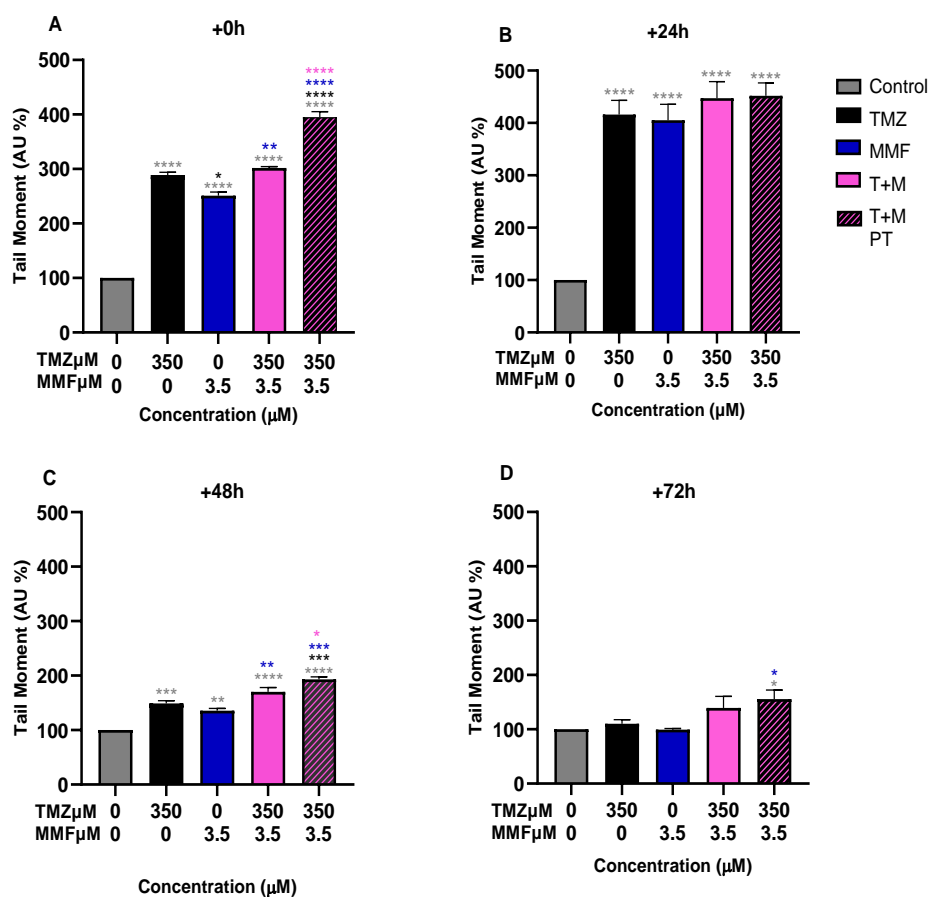


Figure 3.21: DNA damage quantified as Tail Moment (AU) in the T98g cell line, displayed as a percentage of the control mean after treatment with Temozolomide (350 μ M), Monomethyl fumarate (3.5 μ M), the Temozolomide-Monomethyl fumarate combination (T+M) and the scheduled administration of (T+M PT4). The change in tail movement of T98g cells in response to 24- hour exposure at post time points +0h (A), +24h (B), +48h (C) and +72h (D). Data shown is an average of at least 3 independent experiments \pm standard deviation, with 100 comets per treatment group. A two-way ANOVA with Bonferroni post-test was performed with P-values of values of $<0.05 = *$, $<0.01 = **$, $<0.001 = ***$ and $P < 0.0001 = ****$ reported as significant. $*$ = significant against the control $*$ = significant against TMZ, $*$ = significant against MMF and $*$ = significant against T+M.

Figure 3.21 displays the quantified DNA damage response across four time points following treatment exposure. At +0h (Figure 3.21 (A)), statistically significant increases in DNA damage were observed for TMZ, MMF, T+M, and T+M PT4 compared to the untreated control (all $P < 0.0001$). Statistically significant differences were also seen between TMZ and MMF ($P < 0.05$), and between TMZ and T+M PT4 ($P < 0.0001$), with the scheduled combination inducing greater DNA damage. Both combination treatments exhibited statistically significantly greater DNA damage compared to MMF ($P < 0.01$ for T+M and $P < 0.0001$ for T+M PT4), and T+M PT4 induced significantly more DNA damage than T+M ($P < 0.0001$).

At 24h (Figure 3.21 (B)), statistically significant increases in DNA damage were observed for all treatments compared to the untreated control ($P < 0.0001$). No statistically significant differences were detected between treatment groups at this time point, although DNA damage levels increased substantially from +0h.

At 48h (Figure 3.21 (C)), DNA damage levels decreased relative to 24h, but statistically significant increases remained for TMZ ($P < 0.001$), MMF ($P < 0.01$), T+M ($P < 0.0001$), and T+M PT4 ($P < 0.0001$) compared to the untreated control. Statistically significant differences were also observed between TMZ and T+M PT4 ($P < 0.001$), and between MMF and both T+M ($P < 0.01$) and T+M PT4 ($P < 0.001$). Additionally, T+M PT4 induced statistically significantly greater DNA damage than T+M ($P < 0.05$).

At 72h (Figure 3.21 (D)), overall DNA damage decreased further. T+M PT4 was the only treatment to induce statistically significant increases in DNA damage compared to both the untreated control and MMF ($P < 0.05$). Overall, data clearly represents DNA damage and repair across the time points. An increase in DNA damage for the

combinations compared to the single therapies was also deciphered, with significant increases in DNA damage for combination treated cells, compared to single treatments and the untreated control, supporting our hypothesis. Additionally, the scheduled combination observed a statistically significant DNA damage response when compared to the simultaneous combination at +0h and +48h, further supporting the hypothesis of the schedule instigating more DNA damage in the cells than the simultaneous combination. MMF as a single treatment also showed significant DNA damage as a single treatment, coinciding well with combination data and single clonogenic data. This suggests MMF to have a mode of action as a single treatment option in GBM cells.

3.4.9 Statistical analysis of Clonogenic Variability

To account for variability observed between replicates of the single clonogenic curves for each cell line, including single therapy (Section 3.4.2), combination therapy (Section 3.4.3), and scheduled therapy (Section 3.4.5), statistical analyses were performed to compare the effects of Temozolomide (TMZ) and Monomethyl Fumarate (MMF). These analyses aimed to identify significant differences and assess the reliability of the data.

Given the differences in concentration ranges between the initial single therapy curves (Section 3.4.2) and the combination and scheduled therapy data (Sections 3.4.3 and 3.4.5), non-linear regression models were employed to calculate IC_{50} values for each curve. These IC_{50} values were then analysed using a two-way ANOVA with Bonferroni post-tests to determine whether significant differences existed between the datasets. This approach ensured that any variability or trends across the datasets were systematically interrogated, highlighting areas where assay reproducibility might need improvement or additional validation. This analysis helped identify whether variability in IC_{50} values was influenced by treatment modality or other experimental factors.

Additionally, Bland-Altman analysis was performed to directly compare datasets. Bland-Altman is designed to evaluate agreement between two datasets. It assesses whether two methods or treatments produce comparable results across their entire range of values. This method provided insight into the degree of agreement between treatment modalities by identifying systematic biases and assessing limits of

agreement. The Bland-Altman analysis was particularly valuable in quantifying both the consistency and variability of the datasets, ensuring reproducibility.

Overall, these statistical methods enabled a comprehensive evaluation of variability, ensuring the data could be interpreted confidently and identifying areas for potential optimization in experimental design or data collection.

3.4.9.1 Statistical Comparison of UVW Temozolomide and Monomethyl Fumarate Data

The UVW cell line data for Temozolomide and Monomethyl Fumarate single clonogenic assay curves were compared using IC_{50} values and a two-way ANOVA. Figure 3.22 shows the non-linear regression curve lines and corresponding IC_{50} values. Table 3.2 summarises the statistical analysis results from the two-way ANOVA comparison. A Bland Altman was also applied between data set groups and results shown in Table 3.3.

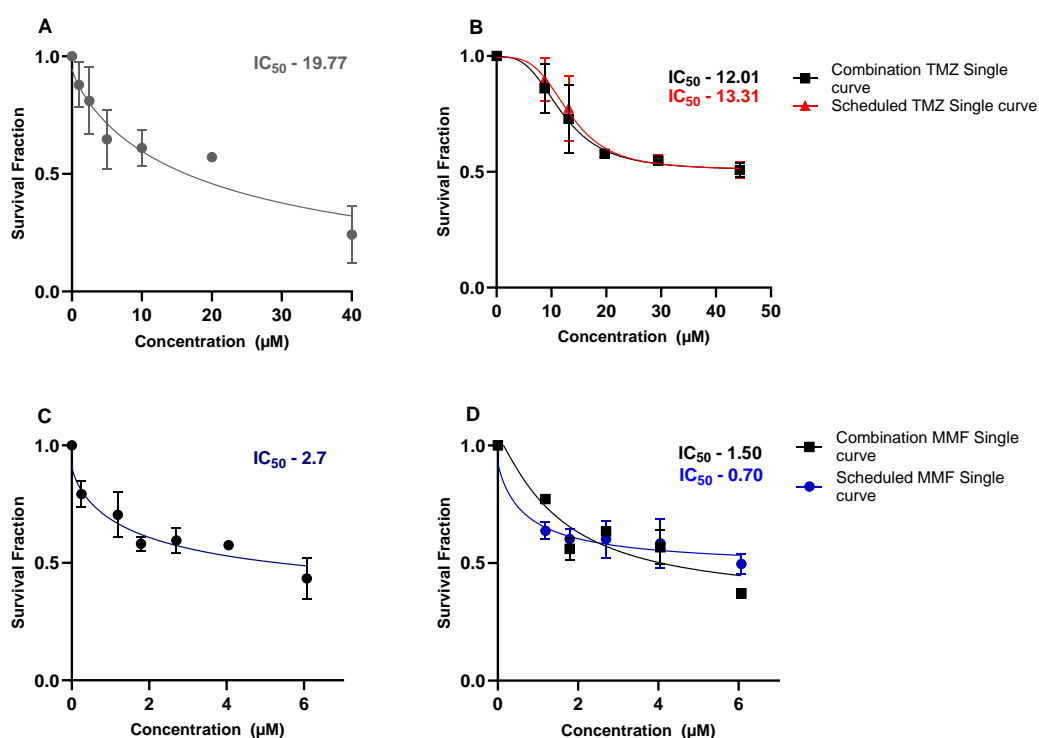


Figure 3.22: The effect on UVW glioblastoma cell clonogenic survival after incubation with increasing doses of Temozolomide and Monomethyl Fumarate after 24-hour

exposure versus the untreated control. Single clonogenic assay data for Temozolomide (A) and the single Temozolomide curves repeated for the combination data and scheduled combination data (B). Single clonogenic assay data for Monomethyl Fumarate (C) and the single Monomethyl Fumarate curves repeated for the combination data and scheduled combination data (D). The data presented is an average of 3 independent experiments \pm standard deviation. IC_{50} values shown were calculated using a fitted non-linear regression curve. Table 3.2 and 3.3 reference the statistical tests applied to the data to determine significant differences.

Bonferroni's Multiple comparisons test	Significant	Adjusted P value
MMF:Single 2.7 μ M vs. MMF:Combo 1.5 μ M	ns	>0.9999
MMF:Single 2.7 μ M vs. MMF:Sched 0.7 μ M	ns	>0.9999
MMF:Combo 1.5 μ M vs. MMF:Sched 0.7 μ M	ns	>0.9999
TMZ:Single 19.7 μ M vs. TMZ:Combo 12.01 μ M	ns	>0.9999
TMZ:Single 19.7 μ M vs. TMZ:Sched 13.23 μ M	ns	>0.9999
TMZ:Sched 13.23 μ M vs. TMZ:Combo 12.01 μ M	ns	>0.9999

Table 3.2: Two-way ANOVA results to compare IC_{50} values between the repeated single curves for Temozolomide and Monomethyl Fumarate performed throughout chapter 3, for single, combination and scheduled clonogenic assay. With P-values of $<0.05 = *$, $<0.01 = **$ $<0.001 = ***$ and $P < 0.0001 = ****$ reported as significant.

Bland Altman Comparison	Bias	SD of Bias
Single TMZ data vs Combination TMZ Data	-0.049	0.03
Single TMZ data vs Scheduled TMZ Data	0.033	0.035
Single MMF Data vs Combination MMF Data	-0.002	0.045
Single MMF Data vs Scheduled MMF Data	-0.0049	0.042

Table 3.3: Summarised Bland Altman results from Graph-Pad Prism software, comparing the full data set for each clonogenic replicate.

The IC_{50} values for Temozolomide (TMZ) showed variation between repeats of the single therapy clonogenic curves (Figure 3.22 A and B). For the UVW cell line, an IC_{50} of 19.7 μ M was calculated for the initial TMZ single curve (A). When repeated for

combination clonogenics and scheduled combination clonogenics, the IC_{50} values were 12.01 μ M and 13.23 μ M (B), respectively. To assess these differences, IC_{50} values were compared using a two-way ANOVA, which revealed no significant difference between the datasets (Table 3.2). Additionally, for TMZ the survival fraction obtained at 19.7 μ M and 20 μ M were compared across the three clonogenic data sets. This was also shown to be insignificant ($P>0.05$).

Similarly, Monomethyl Fumarate (MMF) IC_{50} values exhibited variation across repeats. The initial IC_{50} for MMF was 1.9 μ M (C), while repeated measures for combination clonogenics and scheduled clonogenics yielded IC_{50} values of 1.5 μ M and 0.7 μ M (D). A two-way ANOVA was performed to compare these IC_{50} values, with no significant differences observed (Table 3.2). Data for the 2.7 μ M concentration point for MMF was compared across the three data sets. A one-way ANOVA calculated no significant difference between MMF single curves at the concentration of 2.7 μ M ($P>0.05$).

To further interrogate the agreement between the datasets, a Bland-Altman analysis was conducted. This analysis compared the single therapy clonogenic data to both the combination and scheduled data for TMZ and MMF (Table 3.3). Results indicated low bias values for each comparison, suggesting that the mean differences between datasets are minimal. Moreover, the high agreement observed across datasets confirms the reliability of the clonogenic assay results despite minor variations in IC_{50} values.

3.4.10.2 Statistical Comparison of U87 Temozolomide and Monomethyl Fumarate Data

The U87 cell line data for Temozolomide and Monomethyl Fumarate single clonogenic assay curves were compared using IC_{50} values and a two-way ANOVA. Figure 3.23 shows the non-linear regression curve lines and corresponding IC_{50} values. Table 3.4 summarises the statistical analysis results from the two-way ANOVA comparison. A Bland Altman was also applied between data set groups and results shown in Table 3.5.

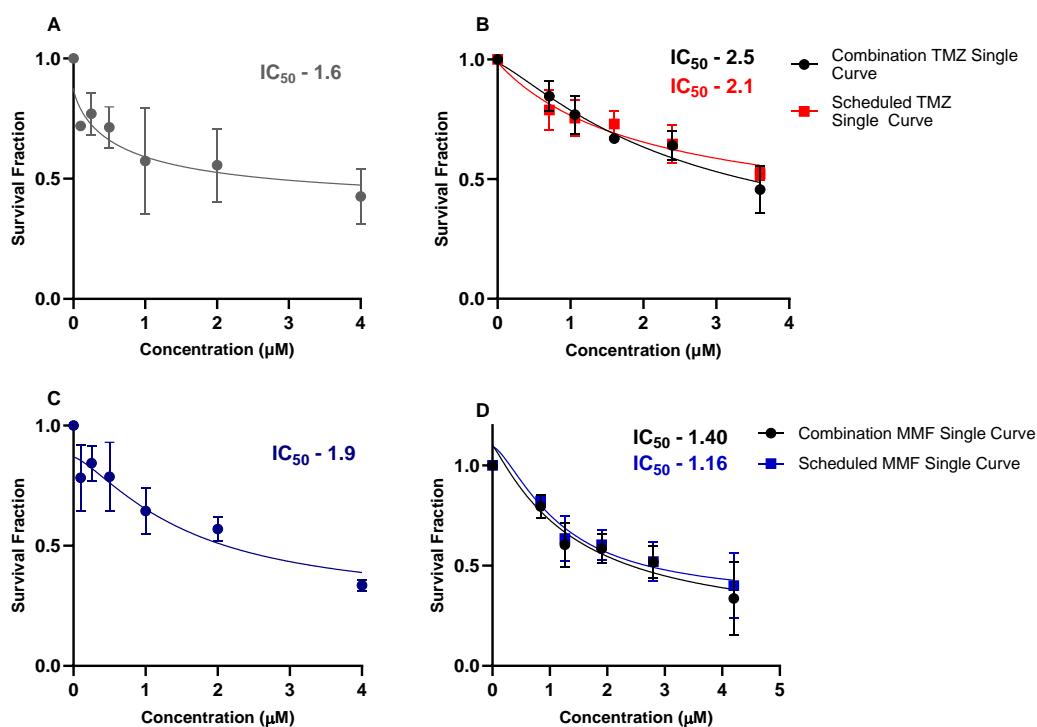


Figure 3.23: The effect on U87 glioblastoma cell clonogenic survival after incubation with increasing doses of Temozolomide and Monomethyl Fumarate after 24-hour exposure versus the untreated control. Single clonogenic assay data for Temozolomide (A) and the single Temozolomide curves repeated for the combination data and scheduled combination data (B). Single clonogenic assay data for Monomethyl Fumarate (C) and the single Monomethyl Fumarate curves repeated for the combination data and scheduled combination data (D). The data presented is an average of 3 independent experiments \pm standard deviation. IC_{50} values shown were calculated using a fitted non-linear regression curve. Table 3.4 and 3.5 reference the statistical tests applied to the data to determine significant differences.

Bonferroni's Multiple comparisons test	Significant	Adjusted P value
MMF:Single 1.9 μ M vs. MMF:Combo 1.4 μ M	ns	>0.9999
MMF:Single 1.9 μ M vs. MMF:Sched 1.16 μ M	ns	>0.9999
MMF:Combo 1.4 μ M vs. MMF:Sched 1.16 μ M	ns	>0.9999
TMZ:Single 1.6 μ M vs. TMZ:Combo 2.5 μ M	ns	>0.9999
TMZ:Single 1.6 μ M vs. TMZ:Sched 2.1 μ M	ns	>0.9999
TMZ:Sched 2.1 μ M vs. TMZ:Combo 2.5 μ M	ns	>0.9999

Table 3.4: Two-way ANOVA results to compare IC₅₀ values between the repeated single curves for Temozolomide and Monomethyl Fumarate performed throughout chapter 3, for single, combination and scheduled clonogenic assay. With P-values of <0.05 = *, <0.01=** <0.001 = *** and P<0.0001=**** reported as significant.

Bland Altman Comparison	Bias	SD of Bias
Single TMZ data vs Combination TMZ Data	0.008	0.08
Single TMZ data vs Scheduled TMZ Data	-0.01	0.04
Single MMF Data vs Combination MMF Data	-0.13	0.11
Single MMF Data vs Scheduled MMF Data	-0.10	0.10

Table 3.5: Summarised Bland Altman results from Graph-Pad Prism software, comparing the full data set for each clonogenic replicate.

The IC₅₀ values for Temozolomide (TMZ) showed small variations between repeats of the single therapy clonogenic curves (Figure 3.23 A and B). For the UVW cell line, an IC₅₀ of 1.6µM was calculated for the initial TMZ single curve (A). When repeated for combination clonogenics and scheduled combination clonogenics, the IC₅₀ values were 1.4µM and 1.16µM (B), respectively. To assess these differences, IC₅₀ values were compared using a two-way ANOVA, which revealed no significant difference between the datasets (Table 3.4). To further elucidate the data sets, the data from 2µM TMZ on the single curve was compared to both the 1.6µM and 2.4µM data from both the combination and the schedule data sets. Two concentrations from the combo were compared to the single curve concentration of 2µM as there was no direct comparison. A one-way ANOVA calculated no significant changes between any of the data (P>0.05).

Similarly, Monomethyl Fumarate (MMF) IC₅₀ values exhibited variation across repeats. The initial IC₅₀ for MMF was 1.9µM (C), while repeated measures for combination clonogenics and scheduled clonogenics gave IC₅₀ values of 2.5µM and 2.1µM (D). A two-way ANOVA was performed to compare these IC₅₀ values, with no significant differences observed (Table 3.4). Additionally, for MMF the survival fraction obtained at 2µM and 1.9µM were compared across the three clonogenic data sets. This was also shown to be insignificant.

To further interrogate the agreement between the datasets, a Bland-Altman analysis was conducted. Similarly to the UVW data, the analysis compared the single therapy clonogenic data to both the combination and scheduled data for TMZ and MMF (Table 3.5). Results indicated low bias values for each comparison, suggesting that the mean differences between datasets are minimal.

Statistical interrogation suggests no significant differences between data sets, and reproducibility of the data. It also suggests that the combination and schedule combination data is valid when applying the CIA model.

3.4.10.3 Statistical Comparison of T98g Temozolomide and Monomethyl Fumarate Data

The T98g cell line data for Temozolomide and Monomethyl Fumarate single clonogenic assay curves were compared using IC_{50} values and a two-way ANOVA. Figure 3.24 shows the non-linear regression curve lines and corresponding IC_{50} values. Table 3.6 summarises the statistical analysis results from the two-way ANOVA comparison. A Bland Altman was also applied between data set groups and results shown in Table 3.7.

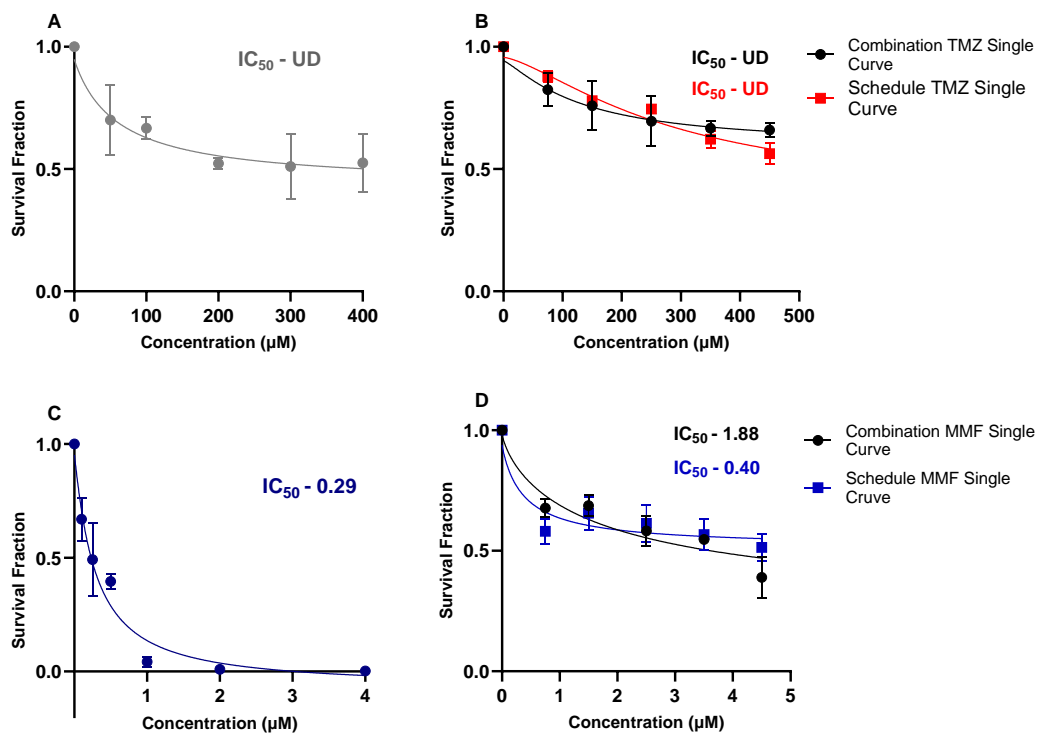


Figure 3.24: The effect on T98g glioblastoma cell clonogenic survival after incubation with increasing doses of Temozolomide and Monomethyl Fumarate after 24-hour exposure versus the untreated control. Single clonogenic assay data for Temozolomide (A) and the single Temozolomide curves repeated for the combination data and scheduled combination data (B). Single clonogenic assay data for Monomethyl Fumarate (C) and the single Monomethyl Fumarate curves repeated for the combination data and scheduled combination data (D). The data presented is an average of 3 independent experiments \pm standard deviation. IC₅₀ values shown were calculated using a fitted non-linear regression curve. Table 3.6 and 3.7 reference the statistical tests applied to the data to determine significant differences.

Bonferroni's Multiple comparisons test	Significant	Adjusted P value
MMF:Single 0.28 μ M vs. MMF:Combo 1.8 μ M	ns	>0.9999
MMF:Single 0.28 μ M vs. MMF:Sched 0.4 μ M	ns	>0.9999
MMF:Combo 1.8 μ M vs. MMF:Sched 0.4 μ M	ns	>0.9999

Table 3.6: Two-way ANOVA results to compare IC₅₀ values between the repeated single curves for Temozolomide and Monomethyl Fumarate performed throughout chapter 3, for single, combination and scheduled clonogenic assay. With P-values of <0.05 = *, <0.01=** <0.001 = *** and P<0.0001=**** reported as significant.

Bland Altman Comparison	Bias	SD of Bias
Single TMZ data vs Combination TMZ Data	-0.11	0.06
Single TMZ data vs Scheduled TMZ Data	-0.11	0.08
Single MMF Data vs Combination MMF Data	-0.21	0.20
Single MMF Data vs Scheduled MMF Data	2.00	0.01

Table 3.7: Summarised Bland Altman results from Graph-Pad Prism software, comparing the full data set for each clonogenic replicate.

The IC₅₀ values for Temozolomide (TMZ) showed small variations between repeats of the single therapy clonogenic curves (Figure 3.24 A and B). For the T98g cell line, the IC₅₀ was undetermined for the initial TMZ single curve (A). When repeated for combination clonogenics and scheduled combination clonogenics, the IC₅₀ values

remained undetermined (B). To assess these differences, as IC₅₀ values couldn't be compared the Bland-Altman test was applied (Table 3.7) and results indicated low bias between the data sets.

Similarly, Monomethyl Fumarate (MMF) IC₅₀ values exhibited variation across repeats. The initial IC₅₀ for MMF was 0.29µM (C), while repeated measures for combination clonogenics and scheduled clonogenics gave IC₅₀ values of 1.88µM and 0.7µM (D). A two-way ANOVA was performed to compare these IC₅₀ values, with no significant differences observed (Table 3.6). The Bland Altman test was applied, and a low bias was indicated between data sets, suggesting good reproducibility (Table 3.7).

The differences between each repetition of the single clonogenic assays for TMZ and MMF when interrogated suggest no significant differences.

3.5 Discussion

The aims of this chapter of research were to characterise the UVW, U87 and T98g human glioblastoma cell lines with the treatment of Temozolomide and Monomethyl Fumarate. Once this was determined, we aimed to find a suitable schedule for the combination based on literature where a rebound effect of GSH levels was discussed after exposure to DMF (Brennan *et al.*, 2015). The determination of a schedule once proven to be effective by combination index analysis and clonogenic assay, was then interrogated with a mechanistic assay cascade to identify the mechanisms of action behind the combination cytotoxicity. Through knowledge based on pilot data, previous group research and literature reviews, we hypothesised MMF to elicit a greater cytotoxic effect than DMF and synergise with TMZ when combined. We also hypothesised the benefit of a scheduled combination over a simultaneously administered combination to elicit a greater reduction in clonogenic survival.

3.5.1 Cytotoxic effects of single therapies.

Initial assessment of cytotoxicity of TMZ, DMF and MMF on GBM cells using clonogenic assays were performed. TMZ as the standard of care, was assessed as a single treatment in our cell lines to determine the IC₅₀ of the drug in 2D and between the UVW, U87 and T98g cell lines, with T98g cells being TMZ resistant. Low concentration ranges were used for MMF, as previous data collected from the Boyd group observed the MMF response to be too toxic for meaningful combinations to be designed (Gardiner 2023, Mullen 2024).

The clonogenic survival data was as hypothesised for TMZ in the T98g (MGMT +) and UVW cell line (MGMT -), however in the U87 cell line (MGMT -) an increased sensitivity to TMZ was seen with an IC₅₀ of 1.6µM. The literature reports on the U87 cell line provide a range of IC₅₀ values between 7-172µM (Lee, 2016; Soni *et al.*, 2021; Yoshino *et al.*, 2010). The vast range of IC₅₀ values for the cell line is primarily due to differences in exposure time, with some assays exposing the cell line for up to 72h. Additionally, the low IC₅₀ found with the clonogenic assay in our hands, could be due to difficulties culturing the cell line, with mini spheroid formations in 2D which began to lift during incubation and during staining. Again, due to this reason, a second MGMT negative cell line, UVW, was added to the research to validate findings.

Cytotoxic findings between the fumarates observed MMF to elicit an increasingly cytotoxic dose dependent reduction in clonogenic survival across all three cell lines. With no previous literature on the use of MMF in the UVW, U87 and T98g cell lines, rendering this investigation the first time this drug had been assessed in these cell lines as a potential combination therapy with TMZ, propelling MMF for combination studies. The findings also show MMF's potential as a single treatment option, with lower IC₅₀'s and increased cytotoxicity compared to TMZ.

Direct comparison of the cytotoxicity of DMF and MMF in the three cell lines saw striking differences in cytotoxicity levels across all three cell lines. For example, MMF induced an IC₅₀ lower than 3µM in all three cell lines compared to DMF where the IC₅₀ ranged from 1.9µM to undetermined with a maximum of 47-57% reduction in clonogenic survival across the cell lines. DMF was initially hypothesised to have a mechanism of action similar to MMF, with both fumarates thought to form conjugates with glutathione and in turn elicit an effect on Nrf2 succination, activate

hydroxycarboxylic acid receptor 2 and elicit an effect on NF- κ B. (Hoogendoorn *et al.*, 2021). However, our data clearly indicated distinct differences in cytotoxicity between the fumarates, with the IC₅₀ in the U87 cell line for DMF being undetermined and MMF having a low IC₅₀ of 1.9 μ M. The differences found supported our hypothesis that MMF has a different mechanism of action to DMF, however how this difference occurs requires further investigation.

3.5.2 Combination Development and Combination synergy

Monomethyl Fumarate as a combined therapy with Temozolomide was hypothesised to enhance reduction in clonogenic survival. Using the IC₅₀ values determined from the single therapy survival curves, combinations were developed using a ratio process suggested by the CIA model (Chou, 2006). Reasoning for the combinations used were previously discussed in 3.4.3. By use of a range of combinations, dose response curves were created and comparison between single therapies and the combinations explored.

In the UVW cell line, the combination of TMZ and MMF induced significant reductions in clonogenic survival over the untreated control ($P < 0.0001$), however the reduction in clonogenic survival of the combination was only significant over TMZ as a single therapy and not MMF. The data displayed a distinct dose response curve for the combination, however after combination index analysis only the highest combination of TMZ and MMF, was found to be synergistic in the UVW cell line. Contrastingly to this, in the U87 cell line, no combination gave synergy, and MMF was seen to induce a higher cytotoxicity than the combinations, suggesting that in this cell line the single administrations were better at reducing cell survival than the combinations. Collectively in both MGMT (-) cell lines a mode of action for MMF as a single treatment is shown, as MMF was able to reduce survival fraction over TMZ and the combination of the two over a range of concentrations.

In the MGMT positive T98g cell line, there was statistically significant reductions in clonogenic survival of the combinations against the untreated control ($P < 0.0001$) against TMZ as a single therapy ($P < 0.001$) and MMF as a single therapy ($P < 0.05$) at the highest concentration of 450 μ M TMZ and 4.5 μ M MMF administered respectively. Surprisingly, through the combination index analysis, all combinations were seen to

have synergy. As T98g cells have an increased TMZ resistance due to the active MGMT gene, with less than 50% reduction in clonogenic survival reached in our clonogenic assays with TMZ as a single agent in Figure 3.7 (A). The data seen when combining TMZ and MMF would suggest MMF is somehow enhancing TMZ's reduction in clonogenic survival in the MGMT positive and TMZ resistant cell line, more than the MGMT negative and TMZ sensitive cell lines.

Possible reasoning for this could be MMF's downregulation of GSH, in turn increasing the levels of ROS present in the cells after treatment with TMZ, and therefore DNA damage instigated by TMZ is above the repair capacity of MGMT, which is a suicide enzyme and must be resynthesized by the cell (Fang, 2024). MGMT, once it repairs the alkylation of the DNA strand becomes inactive and degrades. Resynthesis of MGMT takes on average in glioma cells 1-2 cell cycles (Kaina *et al.*, 2010). Therefore, the damage caused by TMZ and MMF, has had full effect on the DNA and has cycled through the cell cycle, leading to programmed cell death before MGMT has had a chance to resynthesize and repair the initial damaged DNA. Further to this, MMF has a half-life of 30 mins, and TMZ 1.8 hours in humans, showing both drugs to have taken full effect before MGMT can be resynthesized (Lategan *et al.*, 2021; Wesolowski *et al.*, 2010). Additionally, with both the UVW and U87 cell lines, the increased reduction in clonogenic survival with combining TMZ and MMF, may not be as profound as on the T98g cell line due to TMZ already initiating a substantial cytotoxic response as a single therapy in the MGMT negative cells. Therefore, the combination of the two drugs, TMZ and MMF in a MGMT negative cell line, although increasing cytotoxicity it is not better than the cell death TMZ can cause alone. Further to this MMF as a single treatment also instigates a dose responsive cytotoxicity which at some concentrations in the combination initiated more of a reduction in clonogenic survival than TMZ. This suggests MMF has its own mechanism of cell death, which is independent to TMZ, as its unaffected by the MGMT status of the cells, as all three cell lines have similar IC₅₀'s. This possible mode of action of TMZ has never before been clarified in the literature on GBM cells and therefore further investigations looking into MMF's mechanism on a panel of GBM cell lines would benefit the literature. Therefore, as both TMZ and MMF initiate a significant reduction in clonogenic survival as single therapies, their combined effect is not as profound as the TMZ resistant T98g cell line. A possible reason for MMF's response as a single treatment could be that MMF has previously been seen to activate CD95, a death receptor promoting an apoptotic pathway to cell death, which would also explain the

increased cell death of MMF in the UVW, T98g and U87 cell lines (Booth *et al.*, 2014). To investigate whether this is the mechanism behind MMF's cytotoxic response, the response of MMF on the population of apoptotic and necrotic cells was evaluated.

Further reasoning for the increased synergy seen with the T98g cell line could be T98g showing an increased NrF2 activation at basal levels in the literature (De Souza *et al.*, 2022). Increased NrF2 expression modulates the intracellular redox homeostasis and promotes drug resistance (De Souza *et al.*, 2022). The U251 and U87 cell lines in the literature have shown lower basal levels of NrF2, which makes them less resistant to treatments (De Souza *et al.*, 2022; Tang *et al.*, 2022). MMF is thought in the literature to modulate NrF2 expression, which due to NrF2 being elevated in T98g cells, is having a profound effect on sensitising cells when the TMZ and MMF combination is applied. Additionally low NrF2 levels have shown in the literature to succumb the cells to ferroptosis – an iron dependent cell death. With the T98g cell line having increased basal NrF2 levels compared to MGMT negative cell lines, the increased cell death and synergy seen with the combination may be a result of ferroptosis (De Souza *et al.*, 2022). Reduction of NrF2 expression by MMF, would promote ferroptosis in the cells. DMF has shown a concentration dependent inhibition or activation of NrF2 (Saidu *et al.*, 2019). Therefore, at the concentrations of MMF used in our study, whether MMF is inhibiting or activating NrF2, would need investigated. If MMF at the concentrations used, inhibits NrF2, it will be allowing ROS to cause substantial DNA damage when combined with TMZ. This hypothesis could be tested in future experiments by undertaking a ferroptosis assay as well as quantitative PCR, where NrF2 expression is monitored before and after MMF exposure across all cell lines. The presented data is suggestive of a promising use for MMF as a combination or as a single treatment in TMZ resistant patients, more so over TMZ sensitive patients. Data also supports our hypothesis of MMF synergising with TMZ to reduce clonogenic survival.

3.5.3 Schedule Development by glutathione depletion

From Figure 3.8 a trend in relative glutathione (GSH) can be observed, with levels steadily increasing over time after exposure to MMF. Post 24 hours after MMF treatment, relative GSH levels had not returned to basal control levels, in the UVW,

and T98g cell lines, suggesting that Monomethyl Fumarates (MMF) effect on GSH to have a slower rebound than that reported for Dimethyl Fumarate (DMF) (Brennan *et al.*, 2015). The data complimented the results of DMF on GSH levels found in the literature where over time the depletion of GSH is due to stably formed conjugates of DMF with GSH (Brennan *et al.*, 2015). This data also suggests MMF may also form stably formed conjugates with GSH similar to DMF, suggesting their differences is not due to the ability to deplete GSH. The U87 cell line did recover to basal levels of GSH post 24h, however the U87 untreated control cells had lower GSH levels overall compared to the UVW and T98g cell lines. The use of MMF on GBM has not been previously evaluated, the reasoning behind the slower rebound of MMF in the UVW and T98g cell line is not known. Further analysis using western blot or reactive oxygen species assays could look at the effect of MMF on the antioxidant system and elucidate to differences in the cell line. The data does further strengthen our hypothesis of MMF and DMF having different mechanisms that have not yet been elucidated and require further study. The GSH data therefore suggested a 4- hour pretreatment schedule with MMF to deplete GSH levels in order for TMZ to elicit an increased ROS response leading to further cell death.

3.5.4 Scheduled Combination development and synergy

Scheduled combinations in both UVW and T98g cells induced statistically significant reductions in clonogenic survival over the untreated control, TMZ as a single treatment, MMF as a single treatment and the simultaneous combination of (TMZ + MMF) at combinations 3, 4 and 5 (all $P < 0.05$) (Table 3.1). Both cell lines showed synergy at every combination when scheduled, with the schedule enhancing synergy in the UVW cell line as when given simultaneously only the highest combination, 5, of (44.32 μ M TMZ + 6.07 μ M MMF) was synergistic. The U87 cell line also provided synergy at combination 2, 3 and 4 (Table 3.1), with statistically significant reductions in clonogenic survival observed at these combinations when MMF administration was scheduled 4- hours before, compared to both single agents. Therefore, the scheduled clonogenics and combination index analysis, support our hypothesis of a 4 -hour pre-treatment lowering GSH levels, allowing for enhanced cytotoxicity of TMZ. The initial GSH depletion caused by MMF, suggests TMZ when administered to elicit greater damage with ROS, with literature studies showing lower GSH levels to upregulate

TMZ induced ROS (Guo *et al.*, 2021). Additionally, as previously discussed, pretreatment of the GBM cells to MMF at these concentrations used, could potentially decrease NrF2 levels and increase the cell susceptibility to ferroptosis. A counter argument to this is that the DMF response in cancer cells was seen as dose dependent, with higher doses of DMF inhibiting NrF2 rather than activating it, as found in the literature (Saidu *et al.*, 2019). This may potentially apply to MMF, with increasing concentrations of the combinations seen eliciting a greater reduction in clonogenic survival, due to cellular homeostasis taking longer to return to normal due to increased NrF2 inhibition (Saidu *et al.*, 2019). For confirmation of this hypothesis of cell death, GSH and NrF2 levels should both be measured in the cell lines after exposure to MMF and DMF. These assays were performed in Chapter 6.

A limitation of the combination studies is a varied clonogenic reduction on cell survival when single agents TMZ and MMF were repeated for the combination study (Section 3.4.3) and the scheduled combination study (3.4.5), compared to the single curves in Section 3.4.2. As the method of clonogenic assay changed due to plastic supplier issues from Covid-19, we expected some differences. Additionally biological responses of a cell line to a drug will most likely not be identical when repeated. This is due to cell passage, drug batches and human error. To minimise this, cells were discarded after passage ~25 and drugs were allocated and frozen to keep stability. Even with these processes in place, the switch from 60mm petri dish to 6 well plate, did open up room for variation. Therefore, to validate findings of the synergistic combinations, statistical interrogation methods were applied as shown in Section 3.4.10. This allowed identification of any significant changes in the cell line responses to the drugs, which may require repetition. As concentration ranges were different between the single curves and the combinations, IC₅₀ values were determined for each curve, and these were compared. The statistical analysis through ANOVAs and Bland-Altman identified no significant variation between TMZ curves and MMF curves across all three cell lines between 6 well plates and 60mm petri dishes. Where possible, when concentrations were similar, the direct reduction in clonogenic survival after treatment was also compared and through a one-way ANOVA, again no significant differences were observed.

The lack of significant differences in IC₅₀ values supports the validity of the synergism calculated for the scheduled and simultaneous combinations. To further ensure consistency, single-agent curves were repeated concurrently with the combination

studies, maintaining identical techniques, drug batches, passage numbers, and analytical methods. Consequently, any differences observed in the initial single agent clonogenic assays (Section 3.4.2) are not expected to correlate with the combination synergy. This is because the drug batches used for the combination studies were the same as those for the corresponding single-agent repeats, ensuring that the interactions between the two drugs in combination remain internally consistent.

3.5.5 Mechanistic Assay Cascade

To determine the mechanisms underpinning the observed reduction in clonogenic survival from both single and combination treatments given as a schedule or as simultaneous administration, a mechanistic assay cascade was performed, looking at Cell Cycle, Annexin V and Comet assay.

3.5.5.1 Temozolomide

Temozolomides mechanism in GBM is the alkylation of the DNA causing double and single strand breaks ultimately resulting in cell death and apoptosis via cell cycle arrest at the G2/M phase (Said *et al.*, 2023; Stupp *et al.*, 2005). As concentrations of TMZ used in the cell cycle analysis were higher than the IC₅₀ values calculated from the clonogenic assay, we hypothesised significant G2/M arrest after exposure of the cells to TMZ, in the MGMT negative cell lines UVW and U87. The T98g cell line is TMZ resistant due to the presence of the MGMT protein which repairs the damage in the DNA caused by TMZ, we therefore expected less G2/M arrest in this resistant cell line. Additionally, the concentration of TMZ used for cell cycle analysis did not result in a 50% reduction in clonogenic survival, so less significant changes in the cell cycle were expected in the T98g cell line.

Cell cycle analysis in the UVW cell line over 5 time points, showed small but statistically significant changes in the cell cycle populations after TMZ exposure at the concentration of 44.32µM (Figure 3.12). TMZ as a single treatment induced a significant decrease in the G1 population of cells against the untreated control 24 hours after TMZ exposure. The data is not as expected for TMZ as a single treatment,

as TMZ induces senescence, autophagy and apoptosis, all of which would indicate a <G1 or G2/M arrest (Pawlowska *et al.*, 2018). From the data at 72 hours post treatment exposure, an increase in the <G1 phase can be seen, however this was not significant and suggests that the TMZ cell cycle arrest may be occurring at later points.

TMZ as a single treatment in the U87 cell line instigated significant decreases in G1 and subsequent increases in the <G1 phase vs the untreated control, 24 hours after TMZ exposure (Figure 3.13). Data suggests TMZ in the U87 cell line elicited a <G1 arrest rather than a G2 phase arrest, a finding consistent with the literature, where a <G1 phase arrest would be indicative of apoptosis (Pawlowska *et al.*, 2018). Although we do see a <G1 arrest, in the MGMT negative cell lines a higher level of G2/M arrest would be expected also (Tai *et al.*, 2021). With TMZ in MGMT negative cells, the DNA damage induced may go through several cell cycles with the mismatch repair system (MMR) attempting to repair the damage, which would cause yet more damage which over time would result in the G2/M arrest. Previous studies have indicated an apoptosis response in GBM cells after TMZ administration to be prevalent 3-5days after treatment, which may indicate a later time point is required for cell cycle analysis to be able to observe the G2/M arrest (Jezierzański *et al.*, 2024).

In the T98g cells, surprisingly at +0h, immediately after treatment was removed, TMZ elicited a significant decrease in the G1 phase population compared to the control (Figure 3.14). The decrease in G1 correlated to an insignificant increase in G2 and S phase populations. By +48h a drastic decrease in G1 phase cells was seen against the untreated control. This would suggest in the T98g cell line that the chemotherapy is not eliciting enough damage for a G2/M arrest. Lack of G2/M arrest could possibly be due to the concentration used, as less than 50% reduction in clonogenic survival was achieved at the concentration of 350µM TMZ, therefore we would not expect large increases in cell cycle arrest. Overall, between the three cell lines, the lack of significant changes suggests later time points should be analysed to allow for the cell cycle arrest to occur after several progressions through the cell cycle. Additionally, to validate the lack of G2/M arrest, which is inconsistent with the literature, western blot assays probing for cell cycle proteins such as cyclin D1 and α -tubulin should be applied before publication (Tai *et al.*, 2021).

Following on from cell cycle, an Annexin V assay was undertaken to confirm TMZ's ability to initiate apoptosis and reduce viable cell populations. TMZ has been shown to induce apoptosis in a time dependent manner in both MGMT + and MGMT – cell

lines (Tai *et al.*, 2021; Tomicic *et al.*, 2015; Zhang, 2012). After TMZ exposure in UVW cells, viable cell populations significantly decreased by +48h and +72h. This correlated with significant increases in early apoptotic cells +48h and insignificant increases in the necrotic and late apoptotic phases +72h. Although not significant, the trends in the data overall correlate well with the literature (Figure 3.15). U87 cells exhibited predominant necrosis by +24h and +72h, consistent with literature findings of TMZ on the U87 cell line (Khazaei and Pazhouhi, 2017) (Figure 3.16). In T98g cells TMZ caused significant increases in necrotic and late apoptotic populations at +4h and +24h despite intrinsic resistance. Data is consistent with the literature where TMZ can instigate apoptosis (Jakubowicz-Gil *et al.*, 2013; Pawlowska *et al.*, 2018). However, between the cell lines we would expect more of an apoptotic response from the T98g cells at later time points due to MGMT repairing damage in the cells caused by TMZ. In Figure 3.17, the viable cell population were massively reduced +72h after TMZ exposure (although insignificant). This suggests the cells are following the trends of the literature, however significant findings are not being seen due to the large error bars. For further confirmation of our results and for significant data, the use of a viability assay or mitochondrial membrane potential detection assay may validate some of the trends seen. In retrospect TMZ has also been shown to induce autophagy and senescence in cells before apoptosis, by use of both an autophagy assay and senescence assay the trends in the apoptotic and necrotic changes may be further validated (Kaina, 2019).

With both cell cycle and apoptosis data after TMZ treatment, loosely agreeing with the literature due to a lack of significance, a DNA damage assay – comet assay – was used to further add to the mechanistic interrogation. Comet assays demonstrated significant DNA damage across all cell lines after TMZ exposure. In UVW cells, damage peaked at +24h and gradually decreased by +72h, reflecting repair or progression to cell death (Figure 3.19). In U87 cells, damage induced peaked immediately after TMZ exposure and slowly declined over time, consistent with TMZ's cytotoxic effects (Annovazzi *et al.*, 2017) (Figure 3.20). In T98g cells (Figure 3.21), damage was more pronounced than the UVW and U87 cell line 24 hours after exposure, but by +72h was fully recovered, whereas in the UVW and U87 cell lines, significant damage remained compared to the untreated control +72h hours, highlighting MGMT's DNA damage repair mechanism present in T98g cells (Tang *et al.*, 2022). As we found significant increases in DNA damage at the +0h, +24h, +48h and +72h between all three cell lines, we would expect this to correlate to a G2/M

arrest at later points in our cell cycle analysis, which when looking at the trends of the data can be seen, but again the changes were insignificant and as previously mentioned, further experimentation using assays such as western blot, autophagy or senescence may aid in validating the trends.

Overall TMZ's primary mechanism of causing DNA damage was clearly shown by the comet assay data and within the trends of the annexin V data. However, both Annexin V and cell cycle data showed insignificant trends and use of the assays discussed throughout would benefit in validating the TMZ response.

3.5.5.2 Monomethyl Fumarate

Monomethyl Fumarates effect as a single treatment on GBM cell lines U87, UVW and T98g have never been published previously. From single treatment clonogenic assays, MMF alone was able to instigate significant reductions in clonogenic survival and had a potent cell kill.

MMF's effect as a single treatment on UVW cell cycle changes (Figure 3.12), showed significant increases in the G2 population and decreases in the G1 population compared to the untreated control +4h after treatment exposure. At +24h we see a small but insignificant increase in the <G1 phase of cells, after which by +48 and +72h has decreased again. Similarly, in the U87 cell line (Figure 3.13), a significant decrease in G1 phase cells was seen at the +4h hours and +24h time points after treatment exposure. A significant increase in the <G1 phase of cells +24h, was suggestive of a <G1 arrest similar to the changes shown with TMZ. In the T98g cells (Figure 3.14), no significant changes after MMF exposure on cell cycle phases were seen. As no previous literature on MMF's effect on these cell lines cell cycle arrest have been reported, the data cannot be compared to previous data. Cell cycle changes across the cell lines are suggestive of both a G2 and <G1 arrest at earlier time points. A <G1 arrest would show fragmented DNA and is a strong indicator of apoptosis and a G2/M arrest is indicative of DNA damage. DMF has shown in colorectal cancer studies to instigate a <G1 phase arrest which correlated to an increased expression of P21 (Kaluzki *et al.*, 2019). P21 is a cell cycle regulatory protein and in response to stress or DNA damage pauses the cell cycle (Abbas and Dutta, 2009). As DMF metabolises to MMF in the body, this may be the same pathway

in which MMF is causing cell cycle arrest at <G1. Further to this DMF has shown to increase caspase-3 and PARP expression in a concentration dependent manner in cervical cancer (Han and Zhou, 2016). Caspase 3 is an executioner caspase in the apoptotic pathway and PARP is involved in DNA repair, with levels of the enzyme increasing after damage, indicative of DNA damage and a <G1, G2/M cell cycle arrest (Han and Zhou, 2016). Additionally, the cell cycle is sensitive to inflammatory markers such as IL-6 and TNF- α which in cancerous cells aid the promotion of the cell cycle (Detchou and Barrie, 2024). MMF as an anti-inflammatory may be inhibiting these factors, as seen with DMF in the literature, and is causing the cell cycle arrest (Saha *et al.*, 2024). With DMF showing an effect on cell cycle, it could be suggestive of MMF behaving in a similar manner. However, MMF has shown to work differently to DMF when comparing cytotoxicity in this study and when comparing GSH depletion over time in the literature with DMF to what we observed with MMF (Brennan *et al* 2015). As the changes in cell cycle occurred at earlier time points, the response of MMF on cell cycle changes may occur at earlier time points, such as those used for the GSH assay in 3.4.4. By looking at earlier time points where we know from our data GSH is depleted, we may see more significant changes. Additionally, a western blot to assess the change in expression of P21, caspase 3, P53 and PARP would help decipher whether MMF is working similarly or differently to DMF on cell cycle arrest. Data suggests a mode of action for MMF on the GBM cell lines which may be different to DMF.

As DMF has shown to upregulate caspase 3 and PARP, involved in cell death and DNA damage respectively, it would suggest MMF may also elicit a response on cells entering apoptosis. Via an Annexin V assay, MMF exposure on the UVW cell line over post treatment times, showed a significant reduction of viable cells +48h and +72h, however no significant increases in apoptotic cell populations were found (Figure 3.15). In the U87 cell line +24h, MMF significantly reduced viable cells and significantly increased necrotic cell populations (Figure 3.16). In the T98g cell line, MMF significantly reduced viable cells +0h, +4h, +24h and +48h, with a significant increase after MMF exposure on the necrotic cell population +24h and +48h (Figure 3.17). Data suggests the T98g cell line is more sensitive to MMF induced apoptosis, than the MGMT negative cell lines. As the significant changes in cell populations doesn't correlate well to the cell cycle data, and with the increase in necrotic cell populations, it is suggestive of MMF inducing cell death in a mechanism both dependent and independent to the programmed cell death of apoptosis which

requires ATP (Eguchi *et al.*, 1997). With DMF shown in the literature to reduce ATP levels leading to necrosis, its suggestive of MMF functioning in the same way (Mantione *et al.*, 2024). The increased necrosis is also suggestive of increased cellular damage overwhelming cells resulting in cell death. Another possible reason for MMF's response, is its ability to activate CD95, a death receptor promoting an apoptotic pathway to cell death in primary GBM isolates (Booth *et al.*, 2014). To investigate whether this is the mechanism behind MMF's cytotoxic response, the response of MMF on CD95 should be evaluated in future studies by either flow cytometry or RT-qPCR. The data further supports MMF to be a potential single treatment option with data suggesting MMF to induce necrosis in MGMT (+) cell lines.

To confirm MMF is causing DNA damage, a comet assay was performed. MMF in both the UVW and U87 cell line showed significant increases in DNA damage immediately after MMF exposure +0h, +24h after exposure and +72h after exposure compared to the untreated control, with damage ultimately decreasing over time (Figure 3.19 and 3.20). In the T98g cells, MMF exposure caused significant DNA damage immediately after treatment +0h, +24h and +48h, compared to the untreated control with damage returning to basal levels after 72h (Figure 3.21). This suggests MMF instigates an initial onslaught of damage that is most likely single stranded and is repaired over time (Chen *et al.*, 2020). Data clearly shows MMF to be able to initiate DNA damage, with the T98g cell line showing the greatest increase in DNA damage compared to the other cell lines and time points post 24h after exposure. As the T98g cell line seems the most responsive to MMF, with increased DNA damage and necrotic cell populations, the response of MMF seems independent to MGMT status as expected, as MGMT only repairs alkylated DNA. Data correlates well with our clonogenic assay responses to MMF, as well as annexin V data where MMF was instigating necrosis and apoptosis. As MMF's effect on these GBM cell lines has never been published, this novel data cannot be explained as to why MMF is causing DNA damage but suggests a new mode of action on GBM cells. However, DMF as we know is broken down to MMF, and in the literature DMF has shown to deplete GSH levels through succination as well as prevent Nrf2 from entering the nucleus, resulting in a corresponding increase in ROS, PARP, P21, Caspase 3 as well as increased oxidative stress, all of which would contribute to DNA damage (Saidu *et al.*, 2019). Depletion of GSH, Nrf2, NF- κ b and Keap1, have all shown to have a role in apoptosis as well as DNA damage through increased oxidative stress (Morito *et al.*, 2003). Another mechanism behind MMF induced DNA damage, is through the depletion of GSH seen

in our studies, causing disturbances of intracellular lipid-OOH scavenging systems which subsequently subject the cells to ferroptosis (Niu *et al.*, 2021). To investigate the DNA damage response of MMF, ROS levels after exposure to MMF, as well as corresponding GSH levels, and ferroptosis assays should all be applied. However, our data clearly shows MMF to be able to instigate DNA damage irrespective of MGMT expression. As the UVW and U87 response to MMF is slightly different, western blot assays to see MMR expression in the cells would be interesting as we have previously discussed how the MMR can be dysregulated in GBM cells. Therefore, cells which are MGMT negative may also have dysregulated MMR – leading to resistance to treatments.

3.5.5.3 The simultaneous Combinations of Temozolomide and Monomethyl Fumarate

As the mechanisms behind the combinations of TMZ and MMF have never been investigated, we aimed to decipher how the combination was synergising. We hypothesised that MMF was depleting GSH levels allowing TMZ to initiate an increased cytotoxic response.

Through cell cycle analysis, the simultaneous combination of T+M showed no significant changes in cell cycle populations against the control or the single treatments in the UVW cell line (Figure 3.12). From the data no conclusions can be drawn of the effect of the simultaneous combination, except for the combination possibly killing cells in a non-programmed cell death pathway, such as necrosis due to the lack of cell cycle arrest (Gousias *et al.*, 2022). In the U87 cell line, the combination of TMZ and MMF given simultaneously, significantly decreased G1 phase populations of the cells (+4h and +24h) and significantly increased the <G1 phase of the cells (+24h) (Figure 3.13). These findings were only significant against the untreated control, suggesting no difference over the single treatments for the simultaneous combination on cell cycle arrest. In the T98g cell line the combination of T+M instigated a significant decrease in the G1 phase population of cells, compared to TMZ ($P < 0.01$) 48h after exposure (Figure 3.14). This was the only significant change against a single treatment, suggesting the simultaneous combination to not elicit greater cell cycle arrest than the single treatments.

Apoptosis analysis of the simultaneous combination also showed no significant changes in the apoptotic phases of the cells compared to the single treatments over time in the UVW cell line (Figure 3.15). 72h after combination treatment exposure in the U87 cell line (Figure 3.16), the simultaneous combination instigated a reduction in the viable cell population and increase in the necrotic cell population compared to MMF as a single treatment. This suggests the combination of TMZ and MMF over time causes enough irreparable damage to the cells that they succumb to necrosis. This coincides with single data where both MMF and TMZ had significantly increased levels of necrosis (+72h). In the T98g cells the simultaneous combination instigated no significant increase in apoptotic cells over the single treatments at any time point (Figure 3.17). Although no significant change was calculated, trends in the data clearly show a reduction in viable cells compared to the single treatments over time. Additionally, as the T98g cell line showed increased necrotic populations +24h compared to the untreated control, it suggests necrotic and late apoptotic cells over time have lifted and been removed before analysis. Application of a viability assay using a dye such as acrylamide orange on the whole cell suspension may create a better understanding of the population of cells.

Comet assay investigation into the simultaneous combination of TMZ and MMF on DNA damage, showed in the UVW and U87 cell line, an increased DNA damage response over MMF immediately after treatment exposure (+0h) and +24h after treatment exposure (Figure 3.19 and 3.20). In T98g cells, the DNA damage response was increased when compared to MMF as a single treatment only, +0h and +48h. Data correlates with the Annexin V analysis, where significance over MMF's response as a single treatment was found. This suggests the combination of MMF and TMZ when given together instigates enough DNA damage in the cells when combined to result in apoptosis and necrosis, more than MMF alone. As the combination when given simultaneously did not instigate significant damage over TMZ given alone, it doesn't suggest MMF to be enhancing TMZ's effect on DNA damage initiation and instead the response is just a combination of both single drugs overwhelming the cells.

Cumulatively the data show the simultaneous combination to instigate no significant increase in cell cycle arrest, apoptosis or DNA damage when compared to TMZ alone. Data also showed small changes in apoptotic populations as well as DNA damage over MMF. As both TMZ and MMF as single treatment showed a pronounced effect

on DNA damage as well as reductions in viable cells, it suggests that MMF is not sensitising cells to TMZ but rather overwhelming cells with the amount of DNA damage caused when the treatments are given simultaneously. Theoretically when MMF and TMZ are administered simultaneously, TMZ will be inducing oxidative stress and DNA damage, increasing the antioxidant response, while MMF would potentially be inhibiting the response, ultimately causing only minor decreases in the antioxidant upregulation. Further to this, as single treatment data also showed a lack of significant findings with the cell cycle and annexin V data, the use of alternative assays as previously discussed throughout would be useful to apply to the combination also.

3.5.5.4 The scheduled combination of Temozolomide and Monomethyl Fumarate

The scheduled combination of (T+M PT4) was hypothesised to instigate greater cell cycle arrest than the simultaneous combination and single treatments, as well as a greater population of apoptotic cells and DNA damaged cells when compared to the single treatments of TMZ and MMF. This was hypothesised as the combination index analysis showed more combined synergistic combinations when the two drugs were scheduled.

The scheduled combination of T+M PT4, as hypothesised induced the greatest changes in distribution of cells across the various phases of the cell cycle. In the U251 cell line (Figure 3.12), the scheduled combination of MMF pretreatment for 4 hours followed by administration of TMZ, resulted in a significant increase in the G2 phase of cells and decrease in the G1 phase of cells compared to MMF immediately after treatment (+0h). 4 hours after treatment exposure, the scheduled combination instigated a significant decrease in the G1 phase compared to both TMZ and (TMZ+MMF) administrations as well as a significant increase in the G2 phase population of cells compared to TMZ only. 24 hours after exposure, the scheduled combination significantly reduced the G1 population of cells compared to the simultaneous combination. This suggests that the scheduled treatment induced initial cell cycle arrest at the G2/M phase, suggesting the scheduled combination to instigate substantial DNA damage within the cells after administration leading to apoptosis (Pucci *et al.*, 2000).

These changes did not translate into the U87 cell line (Figure 3.13), suggesting the combinations of TMZ and MMF to work differently in the MGMT negative cell lines. U87 is a known expressor of wild type P53 and the expression of P53 in UVW cells is unknown (Lee, 2016). P53 induces cell cycle arrest and cell death, however with DMF having an effect on P21, MMF may also have an effect on P53. P21 is downstream of P53 and with wild type P53 activating P21, it would suggest an increased cell cycle arrest (Pucci *et al.*, 2000). As we do not find this, through western blot analysis the expression of P53 and P21 in the cells should be investigated as well as the expression of P53 post MMF exposure to determine whether the lack of significant findings is due to the assay used.

In the T98g cell line T+M PT4, induced a reduction in G1 phase cells and corresponding increase in S phase cells compared to MMF (+0h) (Figure 3.14). 24 hours after treatment exposure T+M PT4, also instigated a decreased G1 phase population compared to MMF, and +48h a significant decrease in G1 phase cells compared to both MMF and the simultaneous combination (T+M). 48 hours after treatment exposure the scheduled combination also had a significantly increased S phase population compared to MMF. This suggests the two combinations to be working differently with T+M causing a G1 arrest and T+M PT4 a larger S phase population. A greater S phase arrest in the T98g cells, could be explained by significant activation of the DNA damage response due to the overwhelming damage, leaving cells in the S phase to repair. This could be due to cells accumulating as replication forks which would ultimately succumb to damage (Patro *et al.*, 2011; Xiao *et al.*, 2003). Additionally, as the cells may be excessively damaged, with both TMZ, MMF and the TMZ+MMF combinations all showing significant DNA damage responses, the scheduled combination when analysed via flow cytometry could be showing necrotic or apoptotic cells which have fragmented DNA leading to intermediate DNA content (Gong *et al.*, 1994). This could be checked with a TUNEL assay or Annexin V to see the presence of these apoptotic populations or if the S phase increase is genuine replication. With the T98g cell line synergy of TMZ and MMF at all concentrations of the combination, a greater cell cycle G2 phase arrest was expected. With no significant change in the later time points, the function of the combinations on the cell cycle is not clear. An alternative method for tracking cell cycle progression such as the use of Fucci reporters or western blotting for cell cycle specific proteins needs to be undertaken in future work.

With the data showing a lack of consistent findings throughout the cell cycle analysis, conclusions can't be made on the effect of the MMF, T+M and T+M PT4 on the cell cycle and different methods that are not as variable need to be used in tandem to help decipher the cell cycle analysis.

Annexin V assay results, in the UVW cell line after exposure of the scheduled combination showed no significant changes over each single treatment and the simultaneous combination (Figure 3.15). Contrastingly the MGMT negative U87 cell line, showed significant differences +72h after treatment exposure between the schedule and MMF with a reduction in viable cells and increase in necrotic cell populations (Figure 3.16). As this is shown at a later time point, it suggests over time the scheduled combination succumbs to apoptosis and necrosis further suggesting that cells are moving through several cell cycles before being overwhelmed by the cell damage. Also, the scheduled combination shows greater significant changes than the simultaneously administered combination against MMF, from Figure 3.16, the scheduled treatment T+M PT4, resulted in less viable cells than T+M at +4h, +24h, +48h and +72h time points. This would suggest the schedule induces more apoptosis than the combination given simultaneously, although lack of significance between the treatments prevents conclusions to be made. With the cytotoxicity of the scheduled administration of the combination showing significant cell death over all the other treatments in both the UVW and U87 cell line (Figure 3.9 and 3.10) we would expect a greater apoptotic population. The reason for the lack of apoptotic/necrotic cells could be that the schedule instigates such high levels of cytotoxicity in the cells that they die and lift before analysis, with the cells being washed away during cell processing. Another possible reason behind the lack of apoptotic cells is the schedule may be causing cell death via a different cell death process such as autophagy, senescence or mitotic catastrophe, all of which we know can be instigated by TMZ (Li *et al.*, 2021; Tai *et al.*, 2021). Further to this, the lack of correlation between the cell cycle and Annexin V assay, suggests further experimentation as discussed before final conclusions can be made.

As expected in the T98g cell line (Figure 3.17), significant changes are observed between viable, late apoptotic and necrotic cell populations. By +72h, very few viable cell populations are left after exposure to T+M PT4, with the lowest population of viable cells when compared to the untreated control. Due to the substantial error bars at +72h, although clear distinctions can be seen between the control and the

treatments, the changes are not detected as significant. Both combinations worked similarly across the time points with increased necrotic cell populations at +24h compared to the untreated control. By +48h, T+M PT4 showed a significant increase in necrotic cell populations compared to the control, which T+M does not show. With no significant change between T+M PT4 vs either single treatment, it doesn't necessarily show the combination to be eliciting a greater apoptotic response than the single treatments. This is not as expected, as through the CIA and clonogenic data, the synergy observed with the combination was expected to translate across in cell cycle and apoptosis assays which it hasn't. This either suggests again a different mode of cell death or experimental limitations, with the substantial error bars throughout. By use of different methods to determine viable cell populations such as acrylamide orange, the apoptotic changes between the treatments could be better shown.

Detection of DNA damage through single gel electrophoresis showed the scheduled combination overall to elicit greater levels of DNA damage than TMZ, MMF or the simultaneous combination of the two, TMZ+ MMF. In the UVW cell line shown in Figure 3.19, the scheduled combination elicited higher levels of DNA damage immediately after treatment (+0h) than either single treatment or the untreated control. By +48h and +72h, damage across all treatments recedes, as its repaired or has progressed onto programmed cell death. From the data it would suggest that the scheduled combination and not the simultaneous combination enhances the DNA damage response of TMZ with scheduling MMF pretreatment supporting our hypothesis. Similar trends are observed in the U87 cell line, with the scheduled combination eliciting greater levels of DNA damage than both single treatments at +0h, +24h and +48h (Figure 3.20). The schedule also induces significant DNA damage over the simultaneous combination at +48h showing the schedule to cause more damage than all other treatments. This aligns with our CIA data (Figure 3.10) where scheduling the MMF pretreatment showed synergy in the T+M combinations, where it was not seen when given simultaneously.

Again, in the T98g cell line a similar trend is observed, at +0h, the scheduled combination T+M PT4 elicits a higher percentage of DNA damage than TMZ, MMF and T+M (Figure 3.20). Between +0h and +24h we see an increase across all treatments in DNA damage which by +48h drastically decreases before further decreasing by +72h. At +48h the scheduled combination induces a higher percentage

of DNA damage than TMZ, MMF and T+M. The significant increase in DNA damage of the schedule over either single or the simultaneously administered combo aligns with our previous data in Figure 3.111 where the scheduled combination is synergistic as well as more cytotoxic than either single treatment or the T+M combination.

DNA damage analysis clearly shows the combinations to elicit greater damage than single treatments, with the schedule further enhancing the reduction in clonogenic survival through increased DNA damage. MMF as a single agent collectively across the three cell lines has also shown to be able to instigate DNA damage but as a lower percentage than TMZ or either combo. The ability of MMF to cause DNA damage in the GBM cell lines has never been evaluated in the literature, with DMF in the literature showing to initiate DNA damage through an upregulation of ROS (Saidu *et al.*, 2019). Additionally the pathway to enhanced DNA damage with MMF and TMZ, may be as previously suggested in the downregulation of glutathione which allows the ROS instigated by both TMZ and MMF to remain at a higher level, therefore with the scheduled treatment, MMF as a single agent is inducing DNA damage and lowering GSH levels with TMZ administered after 4h causing more DNA damage and an increase in ROS resulting in more cell death (Brennan *et al.*, 2015).

Overall, the scheduled combination data suggests an increased apoptotic response through increased DNA damage, thought to be through the GSH depletion of pre-treating cells with MMF. Although the findings somewhat show the mechanism of TMZ and MMF, further experimentation should be performed investigating specific pathways and proteins such as P53, P21 and the cyclins which control cell cycle progression and the caspases which would show apoptosis.

3.6 Conclusion

As MMF provided greater cytotoxicity than DMF across all three cell lines when evaluated through clonogenic assay, it supported our hypothesis and the literature findings that MMF works differently to DMF (Yazdi and Mrowietz, 2008; Yao *et al.*, 2016). Our hypothesis of MMF synergising with TMZ was also supported with clonogenic assay results, where the combination instigated higher levels of reduction in clonogenic survival than either single treatment in the UVW and T98g cell line. Our evaluation of the time dependent rebounding MMF/DMF effect discussed in the

literature was proven by quantification of relative GSH levels after MMF exposure. This supported our determination of a 4h pretreatment schedule, which from literature findings would decrease GSH levels allowing TMZ to instigate a greater ROS/DNA damage effect. By clonogenic assay and CIA, the scheduled combination administration showed the schedule to elicit greater reduction in clonogenic survival than either single treatment or the simultaneously administered combination in all cell lines, supporting our hypothesis that a scheduled administration would be beneficial over a simultaneous combination. To evaluate how the scheduled combination was enhancing reduction in clonogenic survival, the mechanistic assay cascade observed the scheduled combination to cause some G2 arrest as well as decreasing G1 phase populations, with significant but inconsistent changes in cell cycle across the three lines. The data was further supported by annexin V where over time the number of viable cells decreased, and apoptotic/necrotic cells increased. Data for annexin V between the three cell lines was drastically different, and due to the difference in sensitivity between MGMT+ and MGMT negative cell lines, it suggested an importance of MGMT status in the cells for increased sensitivity. With little conclusive findings from cell cycle and annexin V, the DNA damage assay clarified the mechanism behind the combination, with the scheduled combination eliciting greater DNA damage than either single agent or the simultaneous combination across all three cell lines. This supported our hypothesis that MMF would enhance the effect of TMZ, with TMZ known to cause cell death through DNA damage. The findings also elucidated the mechanism of MMF as a single therapy in the GBM cell lines, with MMF as a single treatment also able to instigate DNA damage, with literature suggesting MMF causes damage by initiation of ROS. A limitation to the study was detection of autophagy was not evaluated in the cell lines with the mechanistic combinations. DMF in more recent studies has shown to instigate autophagy in GBM cell isolates (Basso *et al.*, 2018). It would therefore be useful to determine whether MMF works in a similar manner to DMF on inducing autophagy before publication.

Overall, the data is promising that MMF can be combined with TMZ to elicit greater reduction in clonogenic survival in both MGMT negative and MGMT positive patients. For further evaluation of this, the combinations and schedule were evaluated in 3D culture as shown in Chapter 5. The translation from 2D to 3D is important to assess how the combination will work before any *In vivo* work is carried out. Further to this, as the combination and schedule has shown promise as a double combination, the addition of radiation to the combination is useful as radiotherapy and Temozolomide

is the standard of care. Therefore, determining how MMF will work as a triple combination is also required before advancing MMF as a repurposed treatment. This is shown in Chapter 4.

Additionally, the data clearly shows MMF to enhance the effect of TMZ while also suggesting a mechanism behind MMF that causes DNA damage as a single agent. For full evaluation of MMF it would be beneficial to interrogate the pathways MMF is thought to activate/inhibit, while also directly comparing it to DMF. As literature suggests ferroptosis is a mechanism behind the cytotoxicity seen with MMF, a ferroptosis assay would also be supportive of the data. Both RT-qPCR was performed, ferroptosis assays and further glutathione assays in chapter 6 for the full evaluation of the difference in mechanism behind MMF and DMF.

Chapter 4

Evaluating the cytotoxicity of triple combination treatments on Human Glioblastoma cell lines in monolayer culture with Temozolomide Monomethyl fumarate and External beam X-irradiation.

4.1 Introduction

Due to the lack of advances in the standard of care for GBM patients, the combination of TMZ and RT remains the gold standard irrespective of MGMT status (Arabzadeh *et al.*, 2021). By combining a third treatment with the standard of care it could potentially lower the doses of TMZ and RT required to cause cancerous cell death, improving a patient's quality of life by reduction of adverse effects, while also potentially decreasing the tumour burden. Additionally, GBM tumours are highly heterogenic and have many different genetic mutations. These mutations cause an increased resistance to treatments and prevent the progression of novel therapies due to a build-up of resistance to the treatments. By using a repurposed drug, it decreases the cost of progressing a third treatment, while also potentially lowering the chances of developing resistance, if the triple combination is able to utilise lower doses of treatment with increased cell death (Shafizadeh *et al.*, 2022).

Combining Monomethyl Fumarate (MMF) with TMZ and RT in GBM has not been previously investigated. A 2014 paper by Booth *et al.*, examined DMF and MMF combined with proteasome inhibitors in primary GBM cell lines and found both DMF and MMF to safely combine with the standard of care to enhance cell kill (Booth *et al.*, 2014). DMF as a combination therapy in GBM was successfully shown in studies to combine safely in GBM patients with TMZ and RT as well as improve patient wellbeing (Shafer *et al.*, 2020; Shafizadeh *et al.*, 2022). The radio-sensitising effect of the fumarates has also been researched as they deplete glutathione as well as activate the death receptor CD95 (Booth *et al.*, 2014). Additionally, the inactivation of NF- κ B as well as increased production of autophagosomes and autolysosomes makes the fumarates an interesting drug combination for GBM (Booth *et al.*, 2014). Inactivation

of NF- κ B is beneficial to patients as its activation in GBM promotes chemoresistance (Avci *et al.*, 2020).

Due to the successful clinical trial of DMF with TMZ and radiation, as well as the positive effect of MMF seen as a double combination with TMZ in Chapter 3, the double combinations of MMF with RT and TMZ with RT were studied. Triple combinations of RT, MMF and TMZ were also evaluated. We hypothesised that the triple combination of RT, TMZ and MMF would provide synergistic combinations. Due to the radiation machine becoming nonfunctional for the majority of 2024, the mechanistic assay behind the triple combinations could not be established. This work will be carried out for future publications once a new radiotherapy source is in place.

4.2 Aims and Objectives

The aims of this chapter were:

- To characterise the response of UVW, U87 and T98g human glioblastoma cells to external beam radiation alone and in combination with both Temozolomide and Monomethyl Fumarate.
- To optimise a scheduled treatment of external beam radiation in combination with both Temozolomide and Monomethyl Fumarate.

4.3 Materials and Methods

4.3.1 Combination and Scheduled treatments

Combination treatments of Temozolomide and Monomethyl Fumarate were prepared as described in section 2.7 and 2.7.1. The combinations of Temozolomide and Monomethyl fumarate used for the triple combination were the same as described in section 3.3.5 as shown in Table 4.1 with the addition of 1Gy or 2Gy of radiation exposure as described in section 2.6 and 2.7. For the double combinations the highest

three combinations (3,4 and 5) were taken into Chapter 4 for evaluation as a double treatment with external beam irradiation as shown in Table 4.1.

UVW		
Combination	Temozolomide (μM)	Monomethyl Fumarate (μM)
3	19.7	2.7
4	29.5	4.05
5	44.32	6.07
T98		
3	250	2.5
4	350	3.5
5	450	4.5
U87		
3	1.6	1.9
4	2.4	2.8
5	3.6	4.2

Table 4.1: The combinations of Temozolomide and Monomethyl fumarate used for the combination treatments and for the schedule treatments throughout Chapter 4. Development of these combinations was described in section 3.4.3 and 3.4.6.

4.4 Results

4.4.1 Assessing the Cytotoxicity of External beam X-irradiation on Human Glioblastoma cell lines.

To firstly assess how X-irradiation exposure affects the cell survival of the human glioblastoma cells lines UVW, U87 and T98g before combination treatments, cells were treated with increasing doses of radiation and the clonogenic capacity of the cells observed (section 2.6). A dose range of 0.5Gy, 1Gy, 2Gy, 4Gy, 6Gy and 8Gy was given to each cell line for 24- hours, the doubling time, after which the clonogenic

assay was performed. A one-way ANOVA with Bonferroni post-test was applied using GraphPad prism software version 10.3.1.

We hypothesis that radiation will induce a cell survival curve after exposure to increasing doses of radiation.

4.4.1.1 Cytotoxicity of External beam X-irradiation on the UVW, U87 and T98g cell line.

Glioblastoma cell line UVW (A), U87 (B) and T98g (C) were exposed to increasing doses of radiation to observe its clonogenic survival and radiosensitivity as shown in Figure 4.1.

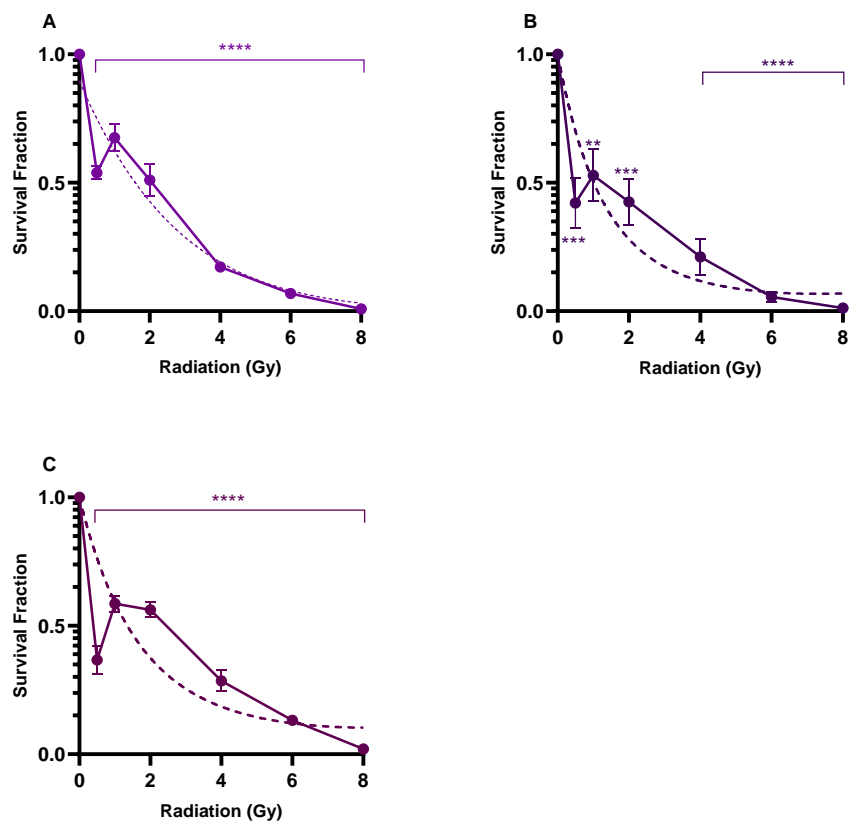


Figure 4.1: The effect of increasing doses of X-irradiation on the clonogenic survival of UVW (A), U87 (B) and T98g (C) human glioblastoma cell lines. The predicted linear quadratic is shown as a broken line and the fit of the dose induced reduction in survival as a solid line on each plot. Data shown is an average of three independent

experiments \pm standard deviation. A one-way ANOVA with Bonferroni post testing was performed using GraphPad Prism 10.3.1 software, with P-values of $<0.05 = *$, $<0.01 = **$, $<0.001 = ***$ and $P < 0.0001 = ****$ reported as significant.

Figure 4.1 (A) displays the response of the UVW cell line to increasing doses of external beam X-irradiation. A clear dose response with respect to clonogenic survival was shown with a statistically significant reduction in clonogenic survival observed at all doses compared to the untreated control (all, $P < 0.0001$). In the UVW cell line low dose hypersensitivity (HRS) is displayed after 0.5Gy exposure, a commonly seen phenomenon in the glioblastoma cell lines which indicates increased radiation sensitivity (C. Short *et al.*, 1999; Enns *et al.*, 2004). After exposure to 0.5Gy, a 47% reduction in clonogenic survival $\pm 4\%$ was shown which decreased to 33% $\pm 8\%$ reduction in clonogenic survival after 1Gy exposure, known as increased radioresistance, the phenomenon of increased resistance (IRR) to radiation at slightly higher doses after initial low dose exposure (C. Short, S. A. Mitchell, P. Boulton, 1999). UVW cells after 1Gy exposure followed a distinct dose response curve until 8Gy where 99% reduction in clonogenic survival $\pm 7\%$ was seen. A line of best fit was applied using GraphPad Prism software to determine the ED_{50} of the UVW cell lines to radiation ($R^2 = 0.87$ which indicated a good correlation between the data and line fit model used), with an ED_{50} of 2.4Gy determined.

The U87 cell lines response to increasing doses of radiation is shown in Figure 4.1 (B) and displayed similar trend to the UVW cells, with a clear dose response. All doses of X-irradiation induced a statistically significant reduction in clonogenic survival compared to the untreated control (all, $P < 0.05$). After 0.5Gy exposure, a 56% reduction in clonogenic survival was shown $\pm 16\%$ which observed HRT. After exposure to 1Gy of X-irradiation there was a 48% reduction in clonogenic survival $\pm 17\%$ (IRR). As the doses increased after 1Gy exposure, a distinct dose response can be observed with maximum reduction in clonogenic survival of 99% seen after 8Gy exposure $\pm 0.8\%$. A line of best fit was applied and an ED_{50} of 1.6Gy was determined with an R^2 value of 0.79 showing good correlation between the data and line fit model used.

From Figure 4.1 (C), a statistically significant reduction in clonogenic survival of the T98g cell line was observed compared to the untreated control after administration of all radiation doses (all, $P < 0.001$). After 0.5Gy exposure, 64% reduction in clonogenic survival was shown $\pm 9\%$, which followed the UVW and U87 cell line response of HRT.

After 1Gy exposure this decreased to a 42% reduction in clonogenic survival \pm 5%, showing IRR, and after 2Gy exposure 44% reduction in clonogenic survival \pm 5% was seen. Following the increasing doses of radiation, reduction in clonogenic survival increased until reaching a 98% reduction in clonogenic survival after 8Gy exposure \pm 1%. By applying a line of best fit the ED₅₀ value was determined as 3.2Gy.

From the clonogenic assay performed on the cell lines following increasing doses of external beam X-irradiation, the U87 cell was seen as the most sensitive to radiation with an ED₅₀ of 1.6. The UVW cell line gave an ED₅₀ of 2.4Gy and the T98g cell line was least radiosensitive with an ED₅₀ of 3.2Gy. All cell lines observed increased hypersensitivity at the lowest exposure of 0.5Gy, with increased radioresistance after exposure to 1Gy.

4.4.2 Assessing double combination cytotoxicity of external beam X-irradiation with Temozolomide and Monomethyl Fumarate on Human Glioblastoma cell lines.

To assess how exposure to external beam X-irradiation will affect the cell lines after combining X-irradiation with Temozolomide or Monomethyl Fumarate, clonogenic assays were performed on all three cell lines.

For comparison between double combinations and the single therapy, three concentrations of TMZ and MMF were taken from the combinations used previously in Chapter 3 and seen in Table 4.1. For the combinations with radiation, the single treatment doses used in the highest three combinations were utilised. The highest three doses of each single treatment from the combination of TMZ and MMF were taken, as in Chapter 3, at least 2 of these combinations provided synergy when combined in a scheduled treatment.

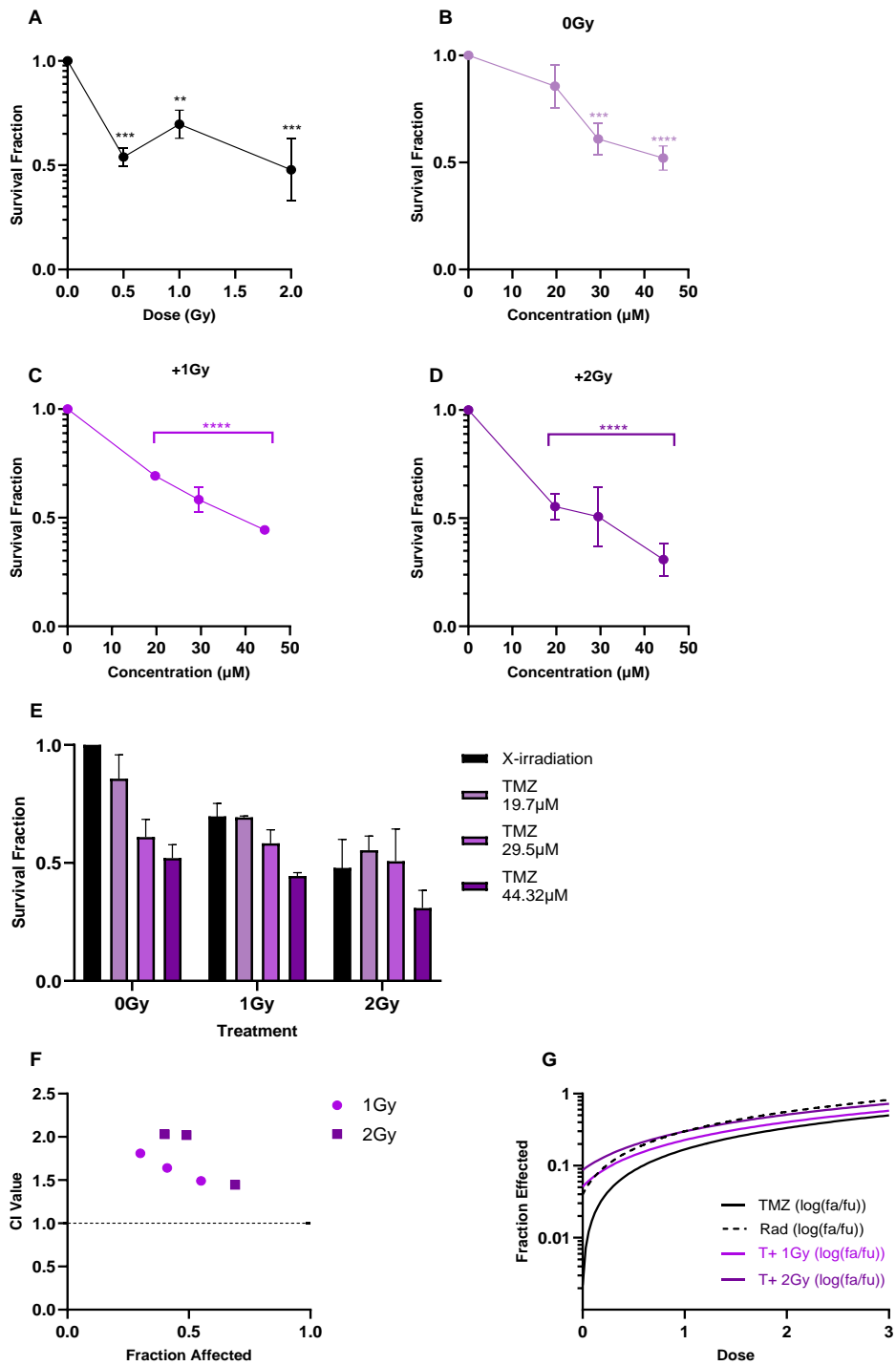
Cells treated with single doses of TMZ or MMF were also exposed to either 1Gy or 2Gy of external beam X-irradiation as 2Gy is the clinically accepted dose fraction given to patients and by combining treatments we would aim to decrease the dose given to patients, hence why 1Gy exposure was also used. All double doses of TMZ +RT or MMF + RT were given in simultaneous combinations.

Similarly to Chapter 3, combination index analysis was applied to distinguish whether the combinations administered would be synergistic, antagonistic or additive. The fraction affected for the concentrations of the double combination were directly compared to the fraction affected of the single treatments at the same concentrations. Due to the nature of combination index analysis, where the better the line fit, the more robust the CIA result, experimental data is shown as the line of fit calculated by Compusyn software (Elwakeel *et al.*, 2019). The software utilises the equations described in section 2.9 with a $CI > 1.1$ deemed antagonistic and $CI < 0.9$ deemed synergistic.

As TMZ is used in combination with RT as the current standard of care, we hypothesis in our data that the double combinations of TMZ + RT will provide synergy. We also hypothesis due to MMF's reduction of glutathione, reactive oxygen species induced from X-irradiation when combined will cause significant reduction in clonogenic survival and a synergistic combination.

4.4.2.1 Cytotoxicity of External beam X-irradiation and Temozolomide on the UVW cell line.

UVW human glioblastoma cells, were treated with three increasing doses of Temozolomide, X-irradiation and the combination of Temozolomide combined with either 1Gy or 2Gy of external beam X-irradiation as shown in Figure 4.2. Statistical analysis following a one-way and two-way Anova is shown in 4.2 (H). Combination index analysis and line of fit for the UVW data is shown in 4.2 (F and G) calculated using Compusyn software.



(H)

Bonferroni's multiple comparisons test	Significance Summary	Adjusted P Value
Two-way ANOVA (Figure 4.2 (E))		
Temozolomide vs Temozolomide + X-irradiation		
19.7 μM vs 19.7 μM +1Gy	Yes*	0.0147
19.7 μM vs 19.7 μM +2Gy	Yes****	<0.0001
19.7 μM + 1Gy vs 19.7 μM +2Gy	Yes*	0.0447
29.5 μM vs 29.5 μM + 1Gy	ns	>0.9999

29.5µM vs 29.5µM + 2Gy	ns	0.1940
29.5µM +1Gy vs 29.5µM +2Gy	ns	0.4955
44.32µM vs 44.32µM +1Gy	ns	0.4871
44.32µM vs 44.32µM +2Gy	Yes**	0.0015
44.32µM +1Gy vs 44.32µM +2Gy	ns	0.0508
X-Irradiation vs Temozolomide + X-irradiation		
1Gy vs 19.7µM +1Gy	ns	>0.9999
1Gy vs 29.5µM + 1Gy	ns	0.4618
1Gy vs 44.32µM +1Gy	Yes**	0.0024
2Gy vs 19.7µM +1Gy	ns	>0.9999
2Gy vs 29.5µM + 1Gy	ns	>0.9999
2Gy vs 44.32µM +1Gy	ns	0.0651

Figure 4.2: The effect of combining External beam X-irradiation with Temozolomide in the UVW cell line. Survival fraction of the UVW cell line after exposure to increasing doses of X-irradiation (A), Temozolomide (B), 1Gy of X-irradiation and increasing concentrations of Temozolomide (C), after exposure to 2Gy of X-irradiation and increasing concentrations of Temozolomide (D) combining both 1Gy and 2Gy combination survivals with Temozolomide given as a single therapy and X-irradiation as a single therapy (E). Combination index values, with the dotted line representing the line of additivity with $CI < 0.9$ showing synergism and $CI > 1$ antagonistic (F) and associated fraction affected for each dose in the Temozolomide- X-irradiation combination shown as a line of best fit from single and combination dose response curves (G). Statistical analysis summary of data for Figure 4.2 (E) data only (H). Data shown is an average of three independent experiments \pm standard deviation. A one-way ANOVA with Bonferroni post testing was performed using GraphPad Prism 10.3.1 software, with p-values of values of $< 0.05 = *$, $< 0.01 = **$, $< 0.001 = ***$ and $P < 0.0001 = ****$ reported as significant against the untreated control for both the single treatments and double combinations (A, B, C and D). A two-way ANOVA with Bonferroni post-test was performed using GraphPad prism 10.3.1 software with P-values of $< 0.05 = *$, $< 0.01 = **$, $< 0.001 = ***$ and $P < 0.0001 = ****$ reported as significant between the relative concentrations of Temozolomide or X-irradiation as single treatments vs the combinations with 1Gy and 2Gy.

Figure 4.2 presents the effects of X-irradiation and TMZ treatments, alone and in combination, on UVW cell clonogenic survival. In Figure 4.2 (A), statistically significant reductions in clonogenic survival were observed following exposure to 0.5Gy, 1Gy, and 2Gy of X-irradiation compared to the untreated control, with reductions of $47\% \pm 4.4\%$, $31\% \pm 6.5\%$, and $53\% \pm 14\%$, respectively (all $P < 0.01$). Figure 4.2 (B) shows statistically significant reductions in clonogenic survival after exposure to 29.5µM and

44.32 μ M TMZ compared to the untreated control, with 40% \pm 7.4% and 48% \pm 5.6% reductions, respectively (both $P < 0.001$).

Figure 4.2 (C) shows statistically significant reductions in clonogenic survival for all combinations of 1Gy X-irradiation with increasing doses of TMZ compared to the untreated control (all $P < 0.0001$), with the greatest reduction observed for 44.32 μ M TMZ + 1Gy (56% \pm 1.4%). Similarly, Figure 4.2 (D) shows further statistically significant reductions for the 2Gy combinations, with the maximum reduction (70% \pm 7.4%) seen for 44.32 μ M TMZ + 2Gy compared to the untreated control ($P < 0.0001$).

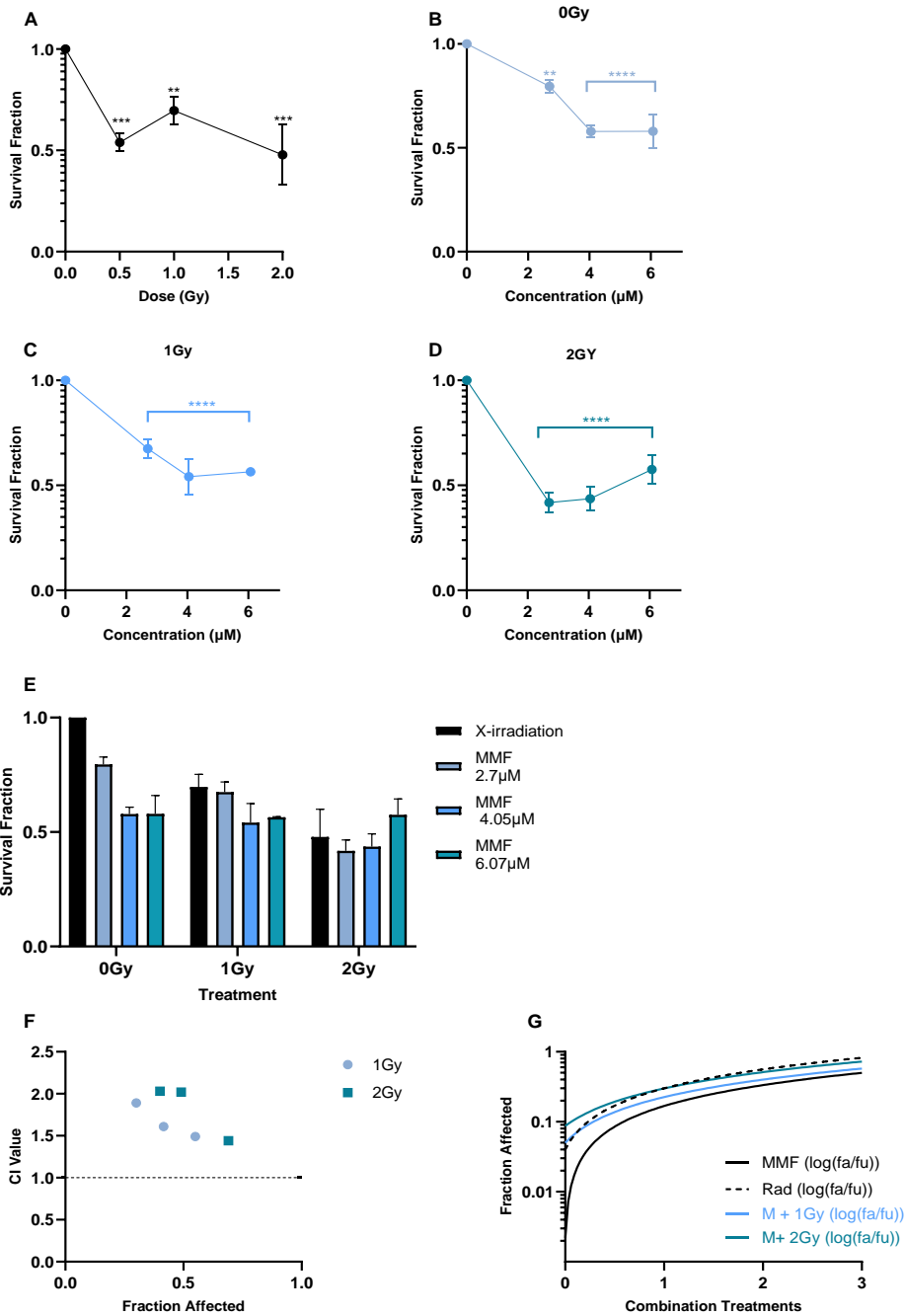
Figure 4.2 (E) compares TMZ alone, X-irradiation alone, and combination treatments. Statistically significant reductions in clonogenic survival were observed for the 19.7 μ M TMZ + 1Gy and 19.7 μ M TMZ + 2Gy combinations compared to 19.7 μ M TMZ alone (both $P < 0.05$). However, neither combination was statistically significantly different from X-irradiation alone. At 19.7 μ M, the 2Gy combination caused a statistically significant greater reduction in survival than the 1Gy combination ($P < 0.05$). Similarly, 44.32 μ M TMZ + 1Gy caused a statistically significant greater reduction in survival compared to 1Gy alone ($P < 0.01$). The combination of 44.32 μ M TMZ + 2Gy provided the greatest reduction in clonogenic survival (70% \pm 6%), which was statistically significantly greater than survival after 44.32 μ M TMZ alone (48% \pm 5.6%) ($P < 0.01$), but not statistically significantly different from 2Gy irradiation alone.

Figure 4.2 (F) presents combination index (CI) analysis results. All TMZ and X-irradiation combinations had CI values > 1.1 , indicating antagonistic interactions with no synergism at the tested concentrations. Figure 4.2 (G) shows the line fits for log (Fa/Fu) values, with R^2 values of 0.96, 0.96, 0.94, and 0.88 for TMZ, RT, TMZ+1Gy, and TMZ+2Gy respectively, confirming good reliability of the CIA data.

Overall, data suggest TMZ combined with 2Gy X-irradiation elicits greater reductions in clonogenic survival compared to 1Gy combinations, with the greatest effect observed with 44.32 μ M TMZ + 2Gy. However, the hypothesis was rejected as combinations of TMZ and X-irradiation were not synergistic.

4.4.2.2 Cytotoxicity of External beam X-irradiation and Monomethyl Fumarate on the UVW cell line.

Following on from double combination of RT with TMZ, UVW glioblastoma cells, were treated with three increasing doses of Monomethyl Fumarate, X-irradiation and the combination of Monomethyl Fumarate combined with either 1Gy or 2Gy of external beam X-irradiation as shown in Figure 4.3. Statistical analysis following a one-way and two-way Anova is shown in 4.3 (H). Combination index analysis and line of fit for the UVW data is shown in (F and G) calculated using Compusyn software.



(H)

Bonferroni's multiple comparisons test	Significance Summary	Adjusted P Value
Two-way ANOVA		
Monomethyl Fumarate vs Monomethyl Fumarate + X-irradiation		
2.7 μ M vs 2.7 μ M +1Gy	Yes*	0.0157
2.7 μ M vs 2.7 μ M +2Gy	Yes****	<0.0001
2.7 μ M + 1Gy vs 2.7 μ M +2Gy	Yes****	<0.0001
4.05 μ M vs 4.05 μ M + 1Gy	ns	0.6182
4.05 μ M vs 4.05 μ M + 2Gy	Yes**	0.0043
4.05 μ M +1Gy vs 4.05 μ M +2Gy	Yes*	0.0379
6.07 μ M vs 6.07 μ M +1Gy	ns	0.9425

6.07µM vs 6.07µM +2Gy	ns	0.9939
6.07µM +1Gy vs 6.07µM +2Gy	ns	0.0379
X-Irradiation vs Monomethyl Fumarate + X-irradiation		
1Gy vs 2.7µM +1Gy	ns	>0.9999
1Gy vs 4.05µM + 1Gy	Yes*	0.0287
1Gy vs 6.07µM +1Gy	ns	0.0868
2Gy vs 2.7µM +1Gy	ns	>0.9999
2Gy vs 4.05µM + 1Gy	ns	>0.9999
2Gy vs 6.07µM +1Gy	ns	0.3872

Figure 4.3: The effect of combining External beam X-irradiation with Monomethyl Fumarate in the UVW cell line. Survival fraction of the UVW cell line after exposure to increasing doses of X-irradiation (A), Monomethyl Fumarate (B), 1Gy of X-irradiation and increasing concentrations of Monomethyl Fumarate (C), after exposure to 2Gy of X-irradiation and increasing concentrations of Monomethyl Fumarate (D), combining both 1Gy and 2Gy combination survivals with Monomethyl Fumarate given as a single therapy and X-irradiation as a single therapy (E). Combination index values, with the dotted line representing the line of additivity with $CI < 0.9$ showing synergism and $CI > 1$ antagonistic (F), associated fraction affected for each dose in the Monomethyl Fumarate- X-irradiation combination shown as a line of best fit from single and combination dose response curves (G). Statistical analysis summary of data from Figure 4.3 (E) only (H). Data shown is an average of three independent experiments \pm standard deviation. A one-way ANOVA with Bonferroni post testing was performed using GraphPad Prism 10.3.1 software, with p-values of values of $< 0.05 = *$, $< 0.01 = **$, $< 0.001 = ***$ and $P < 0.0001 = ****$ reported as significant against the untreated control for both the single treatments and double combinations (A, B, C and D). A two-way ANOVA with Bonferroni post-test was performed using GraphPad prism 10.3.1 software with P-values of $< 0.05 = *$, $< 0.01 = **$, $< 0.001 = ***$ and $P < 0.0001 = ****$ reported as significant between the relative concentrations of Monomethyl Fumarate or X-irradiation as single treatments vs the combinations with 1Gy and 2Gy.

Figure 4.3 presents the effects of X-irradiation and MMF treatments, alone and in combination, on UVW cell clonogenic survival. In Figure 4.3 (A), statistically significant reductions in clonogenic survival were observed following exposure to all doses of X-irradiation compared to the untreated control (all $P < 0.01$). Similarly, Figure 4.3 (B) shows statistically significant reductions in clonogenic survival for all doses of MMF compared to the untreated control (all $P < 0.01$).

In Figure 4.3 (C), combinations of MMF with 1Gy of X-irradiation significantly reduced clonogenic survival compared to the untreated control (all $P < 0.0001$), with the greatest reduction observed after 4.05 μ M MMF + 1Gy (46% \pm 8%). Figure 4.3 (D) shows that combinations with 2Gy of X-irradiation also significantly reduced survival compared to the untreated control (all $P < 0.0001$), with the greatest reduction after 2.7 μ M MMF + 2Gy (59% \pm 4.7%). However, survival increased at higher MMF concentrations in combination with 2Gy, suggesting an antagonistic interaction.

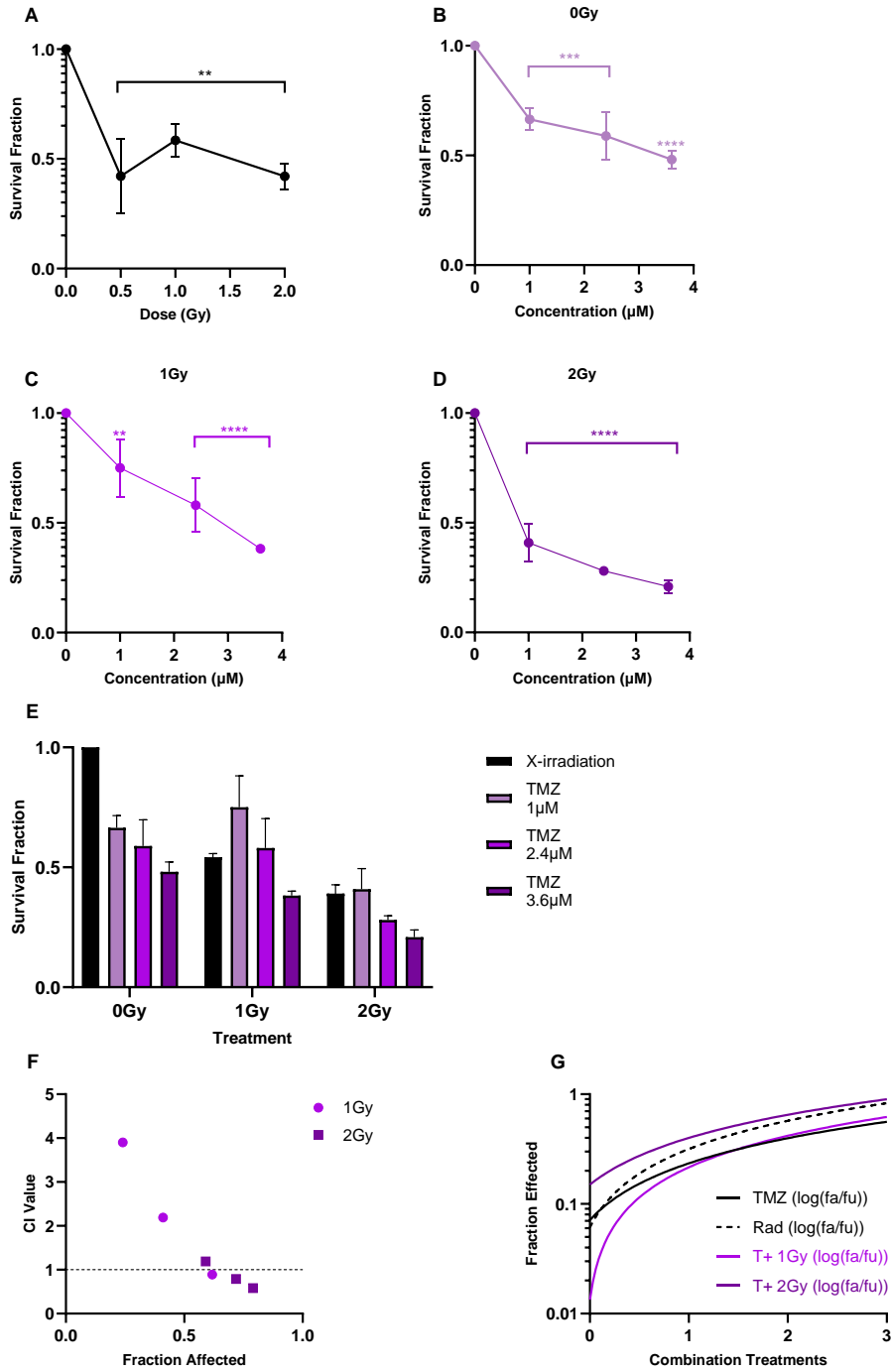
Figure 4.3 (E) compares MMF and X-irradiation as single treatments to their combinations. Statistically significant reductions in clonogenic survival were seen for 2.7 μ M MMF + 1Gy and 2.7 μ M MMF + 2Gy compared to 2.7 μ M MMF alone (both $P < 0.05$) but not compared to X-irradiation alone. A statistically significant reduction was observed between the 2.7 μ M MMF + 2Gy and 2.7 μ M MMF + 1Gy combinations ($P < 0.0001$). Additionally, 4.05 μ M MMF + 2Gy induced a statistically significant reduction in clonogenic survival compared to 4.05 μ M MMF alone ($P < 0.01$) and to 4.05 μ M MMF + 1Gy ($P < 0.05$) but not compared to 2Gy irradiation alone.

Figure 4.3 (F) shows that all MMF and X-irradiation combinations were antagonistic with CI values > 1.1 . Figure 4.3 (G) presents the fa/fu line fits, with R^2 values of 0.96, 0.96, 0.94, and 0.88, indicating good model reliability.

Overall, although combinations of MMF and X-irradiation reduced clonogenic survival compared to the untreated control, no synergistic interactions were observed. The hypothesis was therefore rejected.

4.4.2.3 Cytotoxicity of External beam X-irradiation and Temozolomide on the U87 cell line.

U87 human glioblastoma cells, were treated with three increasing doses of Temozolomide, X-irradiation and the combination of Temozolomide combined with either 1Gy or 2Gy of external beam X-irradiation as shown in Figure 4.4. Statistical analysis following a one-way and two-way Anova is shown in 4.4 (H). Combination index analysis and line of fit for the U87 data is shown in (F and G) calculated using Compusyn software.



(H)

Bonferroni's multiple comparisons test	Significance Summary	Adjusted P Value
Two-way ANOVA		
Temozolomide vs Temozolomide + X-irradiation		
1 μM vs 1 μM +1Gy	ns	0.4336
1 μM vs 1 μM +2Gy	Yes***	0.0004
1 μM + 1Gy vs 1 μM +2Gy	Yes****	<0.0001
2.4 μM vs 2.4 μM + 1Gy	ns	>0.9999
2.4 μM vs 2.4 μM + 2Gy	Yes****	<0.0001

2.4µM +1Gy vs 2.4µM +2Gy	Yes****	<0.0001
3.6µM vs 3.6µM +1Gy	ns	0.2753
3.6µM vs 3.6µM +2Gy	Yes***	0.0002
3.6µM +1Gy vs 3.6µM +2Gy	Yes*	0.0159
X-Irradiation vs Temozolomide + X-irradiation		
1Gy vs 1µM +1Gy	Yes*	0.0286
1Gy vs 2.4µM + 1Gy	ns	>0.9999
1Gy vs 3.6µM +1Gy	ns	0.1485
2Gy vs 1µM +1Gy	ns	>0.9999
2Gy vs 2.4µM + 1Gy	ns	0.6719
2Gy vs 3.6µM +1Gy	ns	0.0762

Figure 4.4: The effect of combining External beam X-irradiation with Temozolomide in the U87 cell line. Survival fraction of the U87 cell line after exposure to increasing doses of X-irradiation (A), Temozolomide (B), 1Gy of X-irradiation and increasing concentrations of Temozolomide (C), after exposure to 2Gy of X-irradiation and increasing concentrations of Temozolomide (D) combining both 1Gy and 2Gy combination survivals with Temozolomide given as a single therapy and X-irradiation as a single therapy (E). Combination index values, with the dotted line representing the line of additivity with $CI < 0.9$ showing synergism and $CI > 1$ antagonistic (F) and associated fraction affected for each dose in the Temozolomide- X-irradiation combination shown as a line of best fit from single and combination dose response curves (G). Statistical analysis summary of data for Figure 4.4 (E) only (H). Data shown is an average of three independent experiments \pm standard deviation. A one-way ANOVA with Bonferroni post testing was performed using GraphPad Prism 10.3.1 software, with p-values of values of $< 0.05 = *$, $< 0.01 = **$, $< 0.001 = ***$ and $P < 0.0001 = ****$ reported as significant against the untreated control for both the single treatments and double combinations (A, B, C and D). A two-way ANOVA with Bonferroni post-test was performed using GraphPad prism 10.3.1 software with P-values of $< 0.05 = *$, $< 0.01 = **$, $< 0.001 = ***$ and $P < 0.0001 = ****$ reported as significant between the relative concentrations of Temozolomide or X-irradiation as single treatments vs the combinations with 1Gy and 2Gy.

Figure 4.4 shows the effects of X-irradiation and TMZ, alone and in combination, on U87 cell clonogenic survival. In Figure 4.4 (A), statistically significant reductions in clonogenic survival were observed after exposure to 0.5Gy, 1Gy, and 2Gy of X-irradiation compared to the untreated control (all $P < 0.01$). Similarly, Figure 4.4 (B) shows statistically significant reductions after exposure to 1µM, 2.4µM, and 3.6µM TMZ compared to the untreated control (all $P < 0.001$).

Figure 4.4 (C) demonstrates statistically significant reductions in survival across all combinations of TMZ with 1Gy X-irradiation compared to the untreated control (all $P < 0.01$), with the greatest reduction ($62\% \pm 1\%$) after exposure to $3.6\mu\text{M}$ TMZ + 1Gy. In Figure 4.4 (D), statistically significant reductions were also observed for all TMZ + 2Gy combinations compared to the untreated control (all $P < 0.0001$), with the maximum reduction ($80\% \pm 3\%$) at $3.6\mu\text{M}$ TMZ + 2Gy.

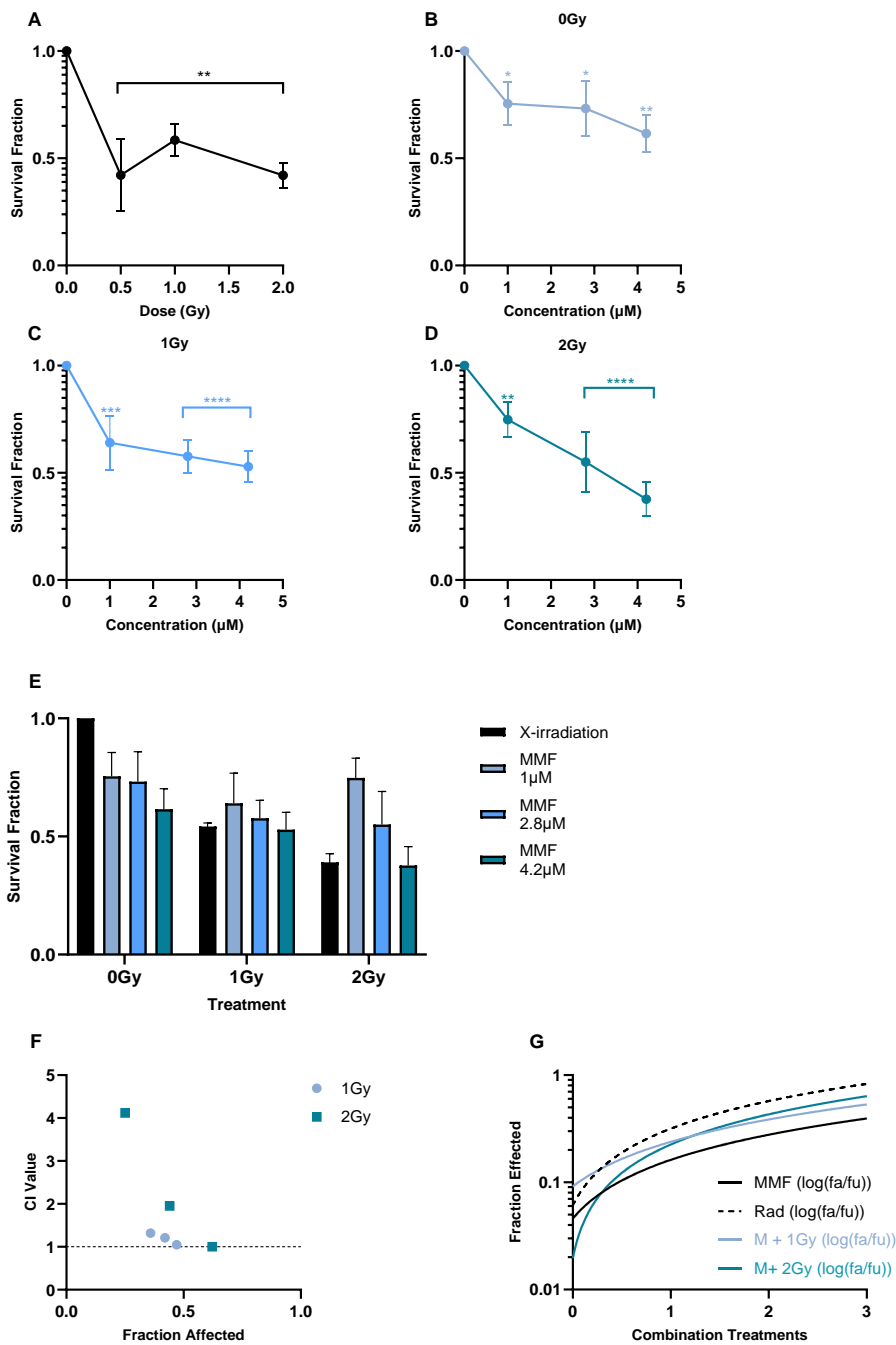
Figure 4.4 (E) compares TMZ alone, X-irradiation alone, and TMZ + X-irradiation combinations. All combinations of TMZ + 2Gy resulted in statistically significant reductions in clonogenic survival compared to TMZ alone and TMZ + 1Gy (all $P < 0.05$). No TMZ + 1Gy combinations significantly reduced survival compared to TMZ alone. Notably, $1\mu\text{M}$ TMZ + 1Gy resulted in a statistically significant increase in survival compared to 1Gy X-irradiation alone ($P < 0.05$). Overall, TMZ + 2Gy combinations were more effective than TMZ alone or TMZ + 1Gy, but not significantly more effective than 2Gy irradiation alone.

Figure 4.4 (F) shows that the combinations $1\mu\text{M}$ TMZ + 1 Gy, $2.4\mu\text{M}$ TMZ + 1Gy, and $1\mu\text{M}$ TMZ + 2Gy were antagonistic ($CI > 1.1$), while $3.6\mu\text{M}$ TMZ + 1Gy, $2.4\mu\text{M}$ TMZ + 2Gy, and $3.6\mu\text{M}$ TMZ + 2Gy were synergistic ($CI < 0.9$). Figure 4.4 (G) shows that TMZ + 2Gy combinations achieved greater fraction affected than TMZ alone, RT alone, or TMZ + 1Gy combinations. R^2 values were 0.86, 0.96, 0.99, and 0.81 for TMZ alone, RT alone, TMZ + 1Gy, and TMZ + 2Gy, respectively, supporting model reliability.

Overall, the data somewhat support the hypothesis, as some combinations of TMZ and X-irradiation were synergistic, particularly with higher concentrations of TMZ combined with 2Gy X-irradiation.

4.4.2.4 Cytotoxicity of External beam X-irradiation and Monomethyl Fumarate on the U87 cell line.

Following on from double combination of RT with TMZ, U87 glioblastoma cells, were treated with three increasing doses of Monomethyl Fumarate, X-irradiation and the combination of Monomethyl Fumarate combined with either 1Gy or 2Gy of external beam X-irradiation as shown in Figure 4.5. Statistical analysis following a one-way and two-way Anova is shown in 4.5 (H). Combination index analysis and line of fit for the U87 data is shown in (F and G) calculated using Compusyn software.



(H)

Bonferroni's multiple comparisons test	Significance Summary	Adjusted P Value
Two-way ANOVA		
Monomethyl Fumarate vs Monomethyl Fumarate + X-irradiation		
1μM vs 1μM +1Gy	ns	0.3786
1μM vs 1μM +2Gy	ns	>0.9999
1μM + 1Gy vs 1μM +2Gy	ns	0.4484
2.8μM vs 2.8μM + 1Gy	ns	0.1259
2.8μM vs 2.8μM + 2Gy	ns	0.0568
2.8μM +1Gy vs 2.8μM +2Gy	ns	>0.9999

4.2µM vs 4.2µM +1Gy	ns	0.7167
4.2µM vs 4.2µM +2Gy	Yes**	0.0090
4.2µM +1Gy vs 4.2µM +2Gy	ns	0.1406
X-Irradiation vs Monomethyl Fumarate + X-irradiation		
1Gy vs 1µM +1Gy	ns	>0.9999
1Gy vs 2.8µM + 1Gy	ns	>0.9999
1Gy vs 4.2µM +1Gy	ns	>0.9999
2Gy vs 1µM +2Gy	Yes**	0.0020
2Gy vs 2.8µM + 2Gy	ns	0.4247
2Gy vs 4.2µM +2Gy	ns	>0.9999

Figure 4.5: The effect of combining External beam X-irradiation with Monomethyl Fumarate in the U87 cell line. Survival fraction of the U87 cell line after exposure to increasing doses of X-irradiation (A), Monomethyl Fumarate (B), 1Gy of X-irradiation and increasing concentrations of Monomethyl Fumarate (C), after exposure to 2Gy of X-irradiation and increasing concentrations of Monomethyl Fumarate (D), combining both 1Gy and 2Gy combination survivals with Monomethyl Fumarate given as a single therapy and X-irradiation as a single therapy (E). Combination index values, with the dotted line representing the line of additivity with $CI < 0.9$ showing synergism and $CI > 1$ antagonistic (F), associated fraction affected for each dose in the Monomethyl Fumarate- X-irradiation combination shown as a line of best fit from single and combination dose response curves (G). Statistical analysis summary of data for Figure 4.5 (E) only (H). Data shown is an average of three independent experiments \pm standard deviation. A one-way ANOVA with Bonferroni post testing was performed using GraphPad Prism 10.3.1 software, with p-values of values of $< 0.05 = *$, $< 0.01 = **$, $< 0.001 = ***$ and $P < 0.0001 = ****$ reported as significant against the untreated control for both the single treatments and double combinations (A, B, C and D). A two-way ANOVA with Bonferroni post-test was performed using GraphPad prism 10.3.1 software with P-values of $< 0.05 = *$, $< 0.01 = **$, $< 0.001 = ***$ and $P < 0.0001 = ****$ reported as significant between the relative concentrations of Monomethyl Fumarate or X-irradiation as single treatments vs the combinations with 1Gy and 2Gy.

Figure 4.5 shows the effects of X-irradiation and MMF, alone and in combination, on U87 cell clonogenic survival. In Figure 4.5 (A), statistically significant reductions in clonogenic survival were observed after exposure to 0.5Gy, 1Gy, and 2Gy of X-irradiation compared to the untreated control (all $P < 0.01$), with the greatest reductions observed for 0.5Gy ($58\% \pm 16\%$) and 2Gy ($58\% \pm 5.8\%$). Figure 4.5 (B) shows that exposure to 1µM, 2.8µM, and 4.2µM MMF also statistically significantly reduced clonogenic survival compared to the untreated control (all $P < 0.05$), with 4.2µM MMF producing the greatest reduction ($39\% \pm 8\%$).

In Figure 4.5 (C), combinations of MMF with 1Gy X-irradiation significantly reduced clonogenic survival compared to the untreated control (all $P < 0.001$), with the maximum reduction observed after 4.2 μ M MMF + 1Gy (48% \pm 7%). Figure 4.5 (D) shows that combinations with 2Gy X-irradiation also significantly reduced clonogenic survival compared to the untreated control (all $P < 0.01$), with the maximum reduction after 4.2 μ M MMF + 2Gy (63% \pm 7%).

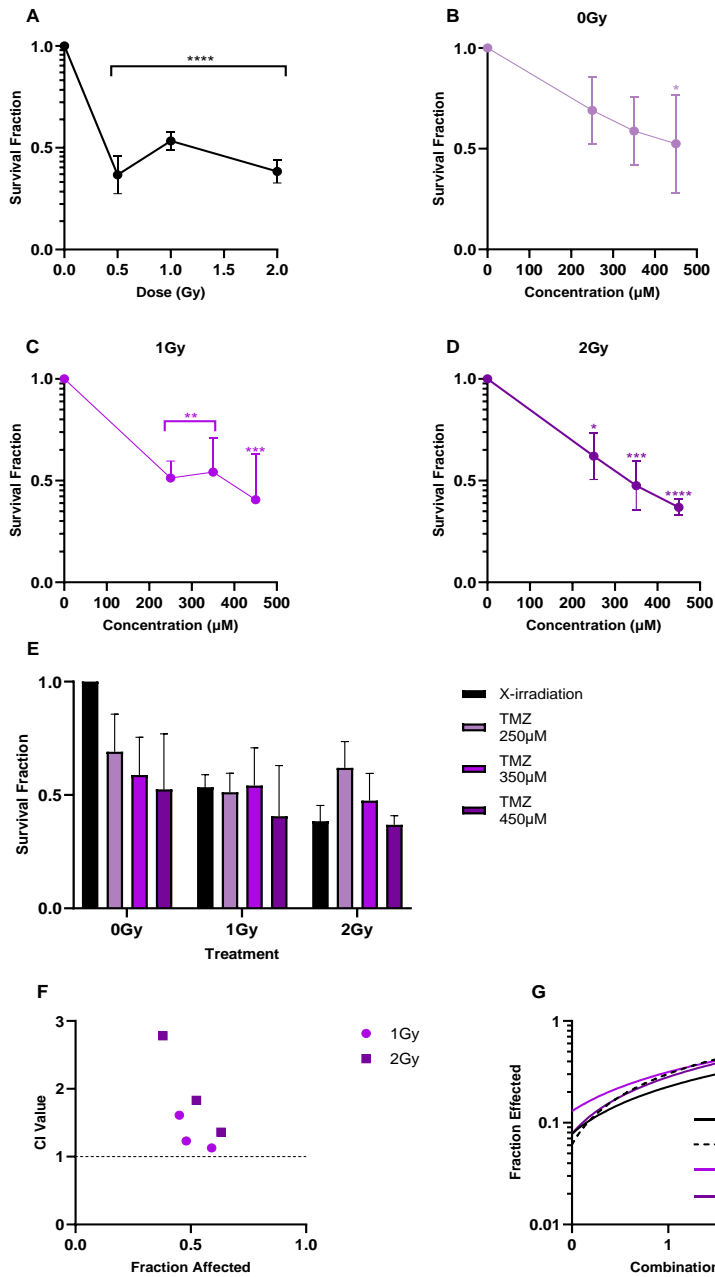
Figure 4.5 (E) compares MMF alone, X-irradiation alone, and their combinations. A statistically significant reduction in clonogenic survival was observed only for 4.2 μ M MMF + 2Gy compared to 4.2 μ M MMF alone ($P < 0.01$). No other combinations significantly differed from MMF alone. No combination significantly reduced survival compared to X-irradiation alone. Furthermore, a statistically significant increase in clonogenic survival was observed for 1 μ M MMF + 2Gy compared to 2Gy alone ($P < 0.01$), suggesting antagonism.

Figure 4.5 (F and G) present the combination index analysis. Additive effects ($CI = 1$) were observed for 4.2 μ M MMF combined with both 1Gy and 2Gy X-irradiation. All other combinations were antagonistic ($CI > 1.1$). Figure 4.5 (G) shows the X-irradiation line achieving a greater fraction affected than MMF alone or the MMF + X-irradiation combinations. R^2 values were 0.88, 0.96, 0.79, and 0.99 for MMF alone, X-irradiation alone, MMF + 1Gy, and MMF + 2Gy, respectively, indicating good reliability of the CIA data.

Overall, the data reject the hypothesis, as no synergistic combinations of MMF and X-irradiation were identified.

4.4.2.5 Cytotoxicity of External beam X-irradiation and Temozolomide on the T98g cell line.

Temozolomide resistant cell line T98g were treated with three increasing doses of Temozolomide, X-irradiation and the combination of Temozolomide combined with either 1Gy or 2Gy of external beam X-irradiation as shown in Figure 4.6. Statistical analysis following a one-way and two-way Anova is shown in 4.6 (H). Combination index analysis and line of fit for the T98g data is shown in (F and G) calculated using Compusyn software.



(H)

Bonferroni's multiple comparisons test	Significance Summary	Adjusted P Value
Two-way ANOVA		
Temozolomide vs Temozolomide + X-irradiation		
250 μM vs 250 μM +1Gy	ns	0.3803
250 μM vs 250 μM +2Gy	ns	>0.9999
250 μM + 2Gy vs 250 μM +2Gy	ns	>0.9999
350 μM vs 350 μM + 1Gy	ns	>0.9999
350 μM vs 350 μM + 2Gy	ns	0.9804
350 μM +1Gy vs 350 μM +2Gy	ns	>0.9999
450 μM vs 450 μM +1Gy	ns	0.9095
450 μM vs 450 μM +2Gy	ns	0.5363
450 μM +1Gy vs 450 μM +2Gy	ns	>0.9999

X-Irradiation vs Temozolomide + X-irradiation		
1Gy vs 250µM +1Gy	ns	>0.9999
1Gy vs 350µM + 1Gy	ns	>0.9999
1Gy vs 450µM +1Gy	ns	>0.9999
2Gy vs 250µM +1Gy	ns	0.3050
2Gy vs 350µM + 1Gy	ns	>0.9999
2Gy vs 450µM +1Gy	ns	>0.9999

Figure 4.6: The effect of combining External beam X-irradiation with Temozolomide in the T98g cell line. Survival fraction of the T98g cell line after exposure to increasing doses of X-irradiation (A), Temozolomide (B), 1Gy of X-irradiation and increasing concentrations of Temozolomide (C), after exposure to 2Gy of X-irradiation and increasing concentrations of Temozolomide (D) combining both 1Gy and 2Gy combination survivals with Temozolomide given as a single therapy and X-irradiation as a single therapy (E Combination index values, with the dotted line representing the line of additivity with $CI < 0.9$ showing synergism and $CI > 1$ antagonistic (F) and associated fraction affected for each dose in the Temozolomide- X-irradiation combination shown as a line of best fit from single and combination dose response curves (G). Statistical analysis summary of data for Figure 4.6 (E) only (H). Data shown is an average of three independent experiments \pm standard deviation. A one-way ANOVA with Bonferroni post testing was performed using GraphPad Prism 10.3.1 software, with p-values of values of $< 0.05 = *$, $< 0.01 = **$, $< 0.001 = ***$ and $P < 0.0001 = ****$ reported as significant against the untreated control for both the single treatments and double combinations (A, B, C and D). A two-way ANOVA with Bonferroni post-test was performed using GraphPad prism 10.3.1 software with P-values of $< 0.05 = *$, $< 0.01 = **$, $< 0.001 = ***$ and $P < 0.0001 = ****$ reported as significant between the relative concentrations of Temozolomide or X-irradiation as single treatments vs the combinations with 1Gy and 2Gy.

Figure 4.6 presents the effects of X-irradiation and TMZ, alone and in combination, on T98G cell clonogenic survival. In Figure 4.6 (A), statistically significant reductions in clonogenic survival were observed after exposure to 0.5Gy, 1Gy, and 2Gy of X-irradiation compared to the untreated control (all $P < 0.0001$), with 0.5Gy inducing the maximum reduction ($64\% \pm 9\%$). Figure 4.6 (B) shows that 450µM TMZ exposure led to a statistically significant reduction in clonogenic survival compared to the untreated control ($48\% \pm 24\%$, $P < 0.05$).

In Figure 4.6 (C), combining increasing concentrations of TMZ with 1Gy X-irradiation resulted in statistically significant reductions in clonogenic survival compared to the

untreated control (all $P < 0.01$), with the maximum reduction ($60\% \pm 1\%$) observed after $450\mu\text{M}$ TMZ + 1Gy. Similarly, Figure 4.6 (D) shows that combining TMZ with 2Gy X-irradiation significantly reduced survival compared to the untreated control (all $P < 0.05$), with the maximum reduction ($62\% \pm 3\%$) seen after $450\mu\text{M}$ TMZ + 2Gy.

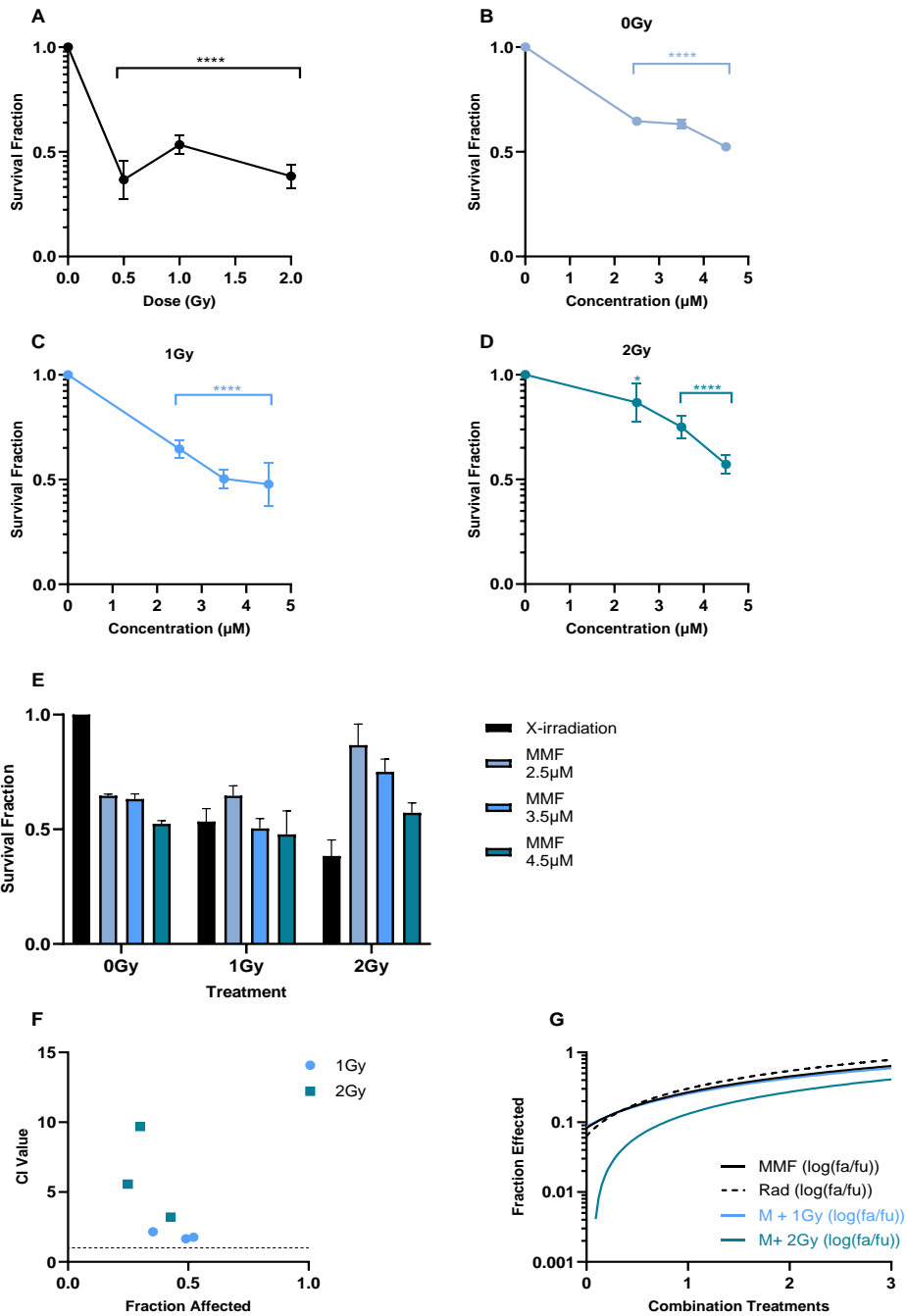
Figure 4.6 (E) compares TMZ alone, X-irradiation alone, and their combinations. No statistically significant differences were observed between TMZ combinations and TMZ alone or X-irradiation alone at any concentration ($P > 0.05$).

Figure 4.6 (F) displays the combination index analysis (CIA), showing that all TMZ and X-irradiation combinations were antagonistic ($CI > 1.1$). Figure 4.6 (G) shows overlapping fa/fu lines for 1Gy and 2Gy combinations with X-irradiation alone, indicating no clear advantage of combinations. R^2 values were 0.84, 0.94, 0.75, and 0.94 for TMZ alone, X-irradiation alone, TMZ + 1Gy, and TMZ + 2Gy respectively, supporting the reliability of the CIA model.

Overall, the data reject the hypothesis, as combinations of TMZ and X-irradiation were not synergistic in the T98G cell line.

4.4.2.6 Cytotoxicity of External beam X-irradiation and Monomethyl Fumarate on the T98g cell line.

T98g human glioblastoma cells, were treated with three increasing doses of Monomethyl Fumarate, X-irradiation and the combination of Monomethyl Fumarate combined with either 1Gy or 2Gy of external beam X-irradiation as shown in Figure 4.7. Statistical analysis following a one-way and two-way Anova is shown in 4.7 (H). Combination index analysis and line of fit for the T98g data is shown in (F and G) calculated using Compusyn software.



(H)

Bonferroni's multiple comparisons test	Significance Summary	Adjusted P Value
Two-way ANOVA		
Monomethyl Fumarate vs Monomethyl Fumarate + X-irradiation		
2.5μM vs 2.5μM +1Gy	ns	>0.9999
2.5μM vs 2.5μM +2Gy	Yes****	<0.0001
2.5μM + 2Gy vs 2.5μM +2Gy	Yes****	<0.0001
3.5μM vs 3.5μM + 1Gy	Yes*	0.0109
3.5μM vs 3.5μM + 2Gy	Yes*	0.0188
3.5μM +1Gy vs 3.5μM +2Gy	Yes****	<0.0001
4.5μM vs 4.5μM +1Gy	ns	0.7691

4.5µM vs 4.5µM +2Gy	ns	0.7034
4.5µM +1Gy vs 4.5µM +2Gy	ns	0.0764
X-Irradiation vs Monomethyl Fumarate + X-irradiation		
1Gy vs 2.5µM +1Gy	ns	0.1164
1Gy vs 3.5µM + 1Gy	ns	>0.9999
1Gy vs 4.5µM +1Gy	ns	>0.9999
2Gy vs 2.5µM +2Gy	Yes****	<0.0001
2Gy vs 3.5µM + 2Gy	Yes****	<0.0001
2Gy vs 4.5µM +2Gy	Yes**	0.0020

Figure 4.7: The effect of combining External beam X-irradiation with Monomethyl Fumarate in the T98g cell line. Survival fraction of the T98g cell line after exposure to increasing doses of X-irradiation (A), Monomethyl Fumarate (B), 1Gy of X-irradiation and increasing concentrations of Monomethyl Fumarate (C), after exposure to 2Gy of X-irradiation and increasing concentrations of Monomethyl Fumarate (D), combining both 1Gy and 2Gy combination survivals with Monomethyl Fumarate given as a single therapy and X-irradiation as a single therapy (E). Combination index values, with the dotted line representing the line of additivity with $CI < 0.9$ showing synergism and $CI > 1$ antagonistic (F), associated fraction affected for each dose in the Monomethyl Fumarate- X-irradiation combination shown as a line of best fit from single and combination dose response curves (G). Statistical analysis summary of data for Figure 4.7 (E) only (H). Data shown is an average of three independent experiments \pm standard deviation. A one-way ANOVA with Bonferroni post testing was performed using GraphPad Prism 10.3.1 software, with p-values of values of $< 0.05 = *$, $< 0.01 = **$, $< 0.001 = ***$ and $P < 0.0001 = ****$ reported as significant against the untreated control for both the single treatments and double combinations (A, B, C and D). A two-way ANOVA with Bonferroni post-test was performed using GraphPad prism 10.3.1 software with P-values of $< 0.05 = *$, $< 0.01 = **$, $< 0.001 = ***$ and $P < 0.0001 = ****$ reported as significant between the relative concentrations of Monomethyl Fumarate or X-irradiation as single treatments vs the combinations with 1Gy and 2Gy.

Figure 4.7 presents the effects of X-irradiation and MMF, alone and in combination, on T98G cell clonogenic survival. In Figure 4.7 (A), statistically significant reductions in clonogenic survival were observed after exposure to 0.5Gy, 1Gy, and 2Gy X-irradiation compared to the untreated control (all $P < 0.0001$), with 0.5Gy inducing the maximum reduction ($64\% \pm 9\%$). A statistically significant reduction was also seen after exposure to 2.5µM, 3.5µM, and 4.5µM MMF (Figure 4.7 (B)), with the maximum reduction ($48\% \pm 1.4\%$) at 4.5µM MMF (all $P < 0.0001$).

In Figure 4.7 (C), combining MMF with 1Gy X-irradiation resulted in statistically significant reductions in clonogenic survival compared to the untreated control (all $P < 0.0001$), with the maximum reduction ($53\% \pm 7\%$) at $4.5\mu\text{M}$ MMF + 1Gy. Similarly, in Figure 4.7 (D), combining MMF with 2Gy X-irradiation significantly reduced survival (all $P < 0.05$), with the maximum reduction ($43\% \pm 3\%$) observed for $4.5\mu\text{M}$ MMF + 2Gy.

Comparative analysis (Figure 4.7 (E)) showed that $2.5\mu\text{M}$ MMF + 2Gy significantly increased clonogenic survival compared to $2.5\mu\text{M}$ MMF alone ($P < 0.0001$), $2.5\mu\text{M}$ MMF + 1Gy ($P < 0.0001$), and 2Gy X-irradiation alone ($P < 0.0001$). Similarly, $3.5\mu\text{M}$ MMF + 2Gy showed statistically significant increases in survival compared to $3.5\mu\text{M}$ MMF + 1Gy and $3.5\mu\text{M}$ MMF alone (both $P < 0.05$). $4.5\mu\text{M}$ MMF + 2Gy showed a statistically significant increase in survival compared to 2Gy alone ($P < 0.0001$). No combination with $4.5\mu\text{M}$ MMF was statistically significantly different compared to MMF alone.

Combination index analysis (Figure 4.7 (F)) confirmed that all MMF + X-irradiation combinations were antagonistic ($CI > 1.1$). Figure 4.7 (G) shows that the 2Gy combinations resulted in the least fraction affected compared to single treatments. R^2 values of 0.86, 0.94, 0.84, and 0.99 indicated good reliability of the CIA data.

Overall, the data reject the hypothesis, as no synergistic combinations between MMF and X-irradiation were identified.

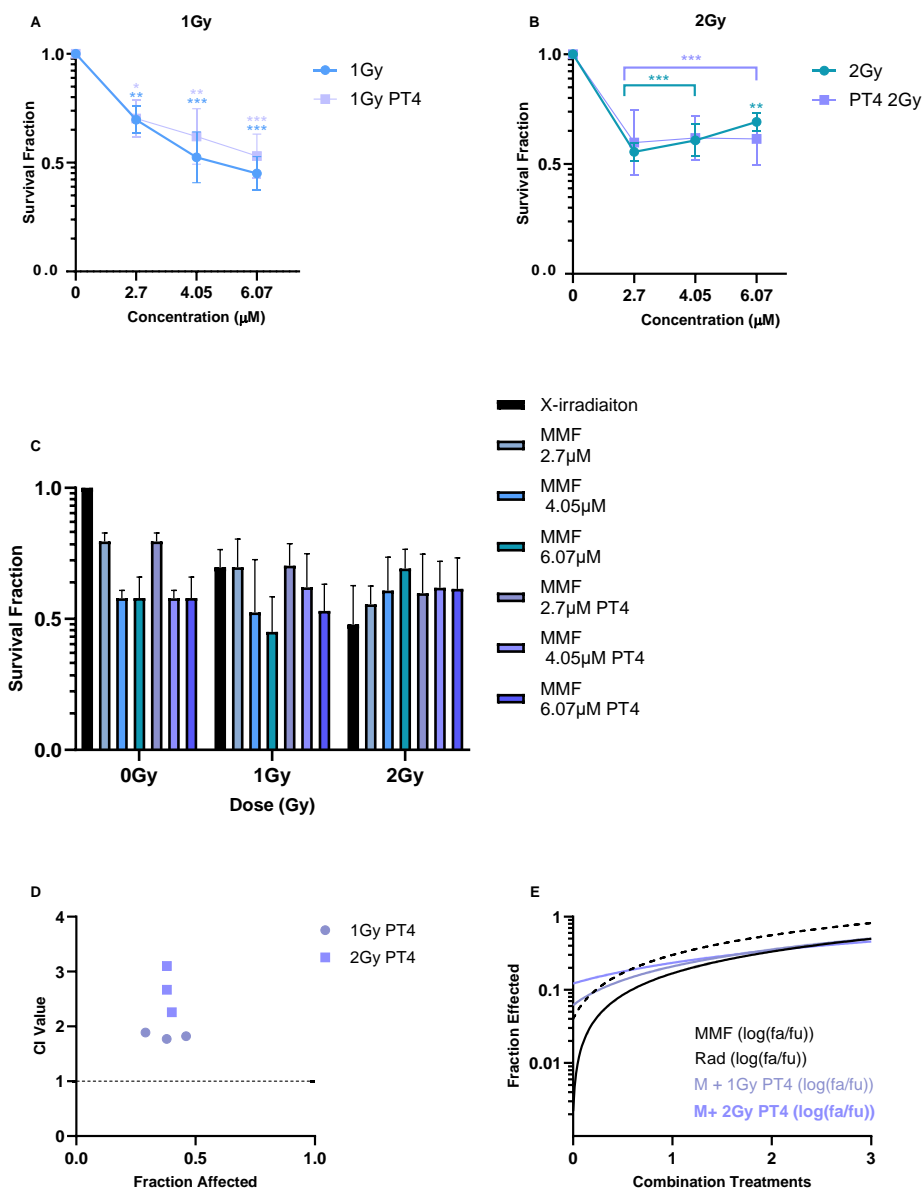
4.4.3 Developing a double combination schedule of Monomethyl Fumarate with External beam X-irradiation on human glioblastoma cell lines.

As seen in Chapter 3, the administration of Monomethyl Fumarate 4- hours prior to Temozolomide resulted in an increased cytotoxic response and increased synergistic response. The data obtained for simultaneous MMF and X-irradiation combinations in Figure 4.3, 4.5 and 4.7 showed no synergistic combinations and in the UVW and T98g cell lines an increase in cell survival was seen after exposure to the 2Gy combinations with MMF when compared to the 1Gy combinations. This could be due to the activation of the cell's antioxidant response preventing cell damage. Scheduling the treatment of MMF for 4h before administration of X-irradiation could deplete the oxidative stress response and allow X-irradiation induced reactive oxygen species to elicit damage to the cells.

Based on previous data we therefore scheduled a pretreatment of 4- hours with MMF followed by X-irradiation for a total exposure time of 24- hours. We hypothesis that the scheduling will cause an increased cytotoxic response than the simultaneous administration.

4.4.3.1 Cytotoxicity of External Beam X-irradiation when combined with Monomethyl Fumarate after a 4- hour pretreatment schedule on the UVW cell line.

The cytotoxic response of the UVW cell line after a 4- hour pretreatment with MMF followed by either 1Gy or 2Gy of X-irradiation and the simultaneous administration of MMF and X-irradiation is shown in Figure 4.8. Statistical analysis following a one-way and two-way Anova is shown in 4.8 (F). Combination index analysis and line of fit for the UVW data is shown in (D and E) calculated using Compusyn software.



(F)

Bonferroni's multiple comparisons test	Significance Summary	Adjusted P Value
Two-way ANOVA		
Monomethyl Fumarate vs Monomethyl Fumarate + X-irradiation - Simultaneous		
2.7 μM vs 2.7 μM +2Gy	Yes*	0.0226
6.07 μM +1Gy vs 6.07 μM +2Gy	Yes*	0.0217

Figure 4.8: The effect of combining external beam X-irradiation with Monomethyl Fumarate as simultaneous administration or as a 4- hour pretreatment of Monomethyl Fumarate (PT4) on the UVW cell line. Survival fraction of the UVW cell line after

exposure to 1Gy of X-irradiation and increasing concentrations of simultaneous and scheduled Monomethyl Fumarate (A), after exposure to 2Gy X-irradiation and increasing concentrations of simultaneous and scheduled Monomethyl Fumarate (B), combining both 1Gy and 2Gy combination survivals with Monomethyl Fumarate given as a single therapy and X-irradiation as a single therapy (C). Combination index values, with the dotted line representing the line of additivity with $CI < 0.9$ showing synergism and $CI > 1$ antagonistic (D), associated fraction affected for each dose in the Monomethyl Fumarate- X-irradiation combination shown as a line of best fit from single and combination dose response curves (E). Statistical analysis summary of data for Figure 4.8 (C) only, data comparisons not shown were not statistically significant (F). Data shown is an average of three independent experiments \pm standard deviation. A one-way ANOVA with Bonferroni post testing was performed using GraphPad Prism 10.3.1 software, with p-values of values of $< 0.05 = *$, $< 0.01 = **$, $< 0.001 = ***$ and $P < 0.0001 = ****$ reported as significant against the untreated control and the double combinations (A, B). A two-way ANOVA with Bonferroni post-test was performed using GraphPad prism 10.3.1 software with P-values of $< 0.05 = *$, $< 0.01 = **$, $< 0.001 = ***$ and $P < 0.0001 = ****$ reported as significant between the relative concentrations of Monomethyl Fumarate or X-irradiation as single treatments vs the combinations with 1Gy and 2Gy

Figure 4.8 presents the effects of simultaneous and scheduled administration of MMF and X-irradiation on UVW cell clonogenic survival. In Figure 4.8 (A), a dose-dependent reduction in clonogenic survival was observed for both administration strategies after 1Gy X-irradiation combined with MMF compared to the untreated control (all $P < 0.05$). The maximum reduction was seen with $6.07 \mu\text{M}$ MMF + 1Gy given simultaneously ($55\% \pm 16\%$), compared to $45\% \pm 8\%$ for the scheduled administration. A two-way ANOVA showed no statistically significant differences between simultaneous and scheduled treatments (Figure 4.8 (G)).

In Figure 4.8 (B), 2Gy X-irradiation combined with MMF resulted in statistically significant reductions in clonogenic survival for both administration types compared to the untreated control (all $P < 0.05$), though no dose-response trend was observed. The maximum reductions were $45\% \pm 5.7\%$ (simultaneous) and $41\% \pm 12\%$ (scheduled) after $2.7 \mu\text{M}$ MMF + 2Gy. No statistically significant differences were detected between simultaneous and scheduled treatments (Figure 4.8 (F)).

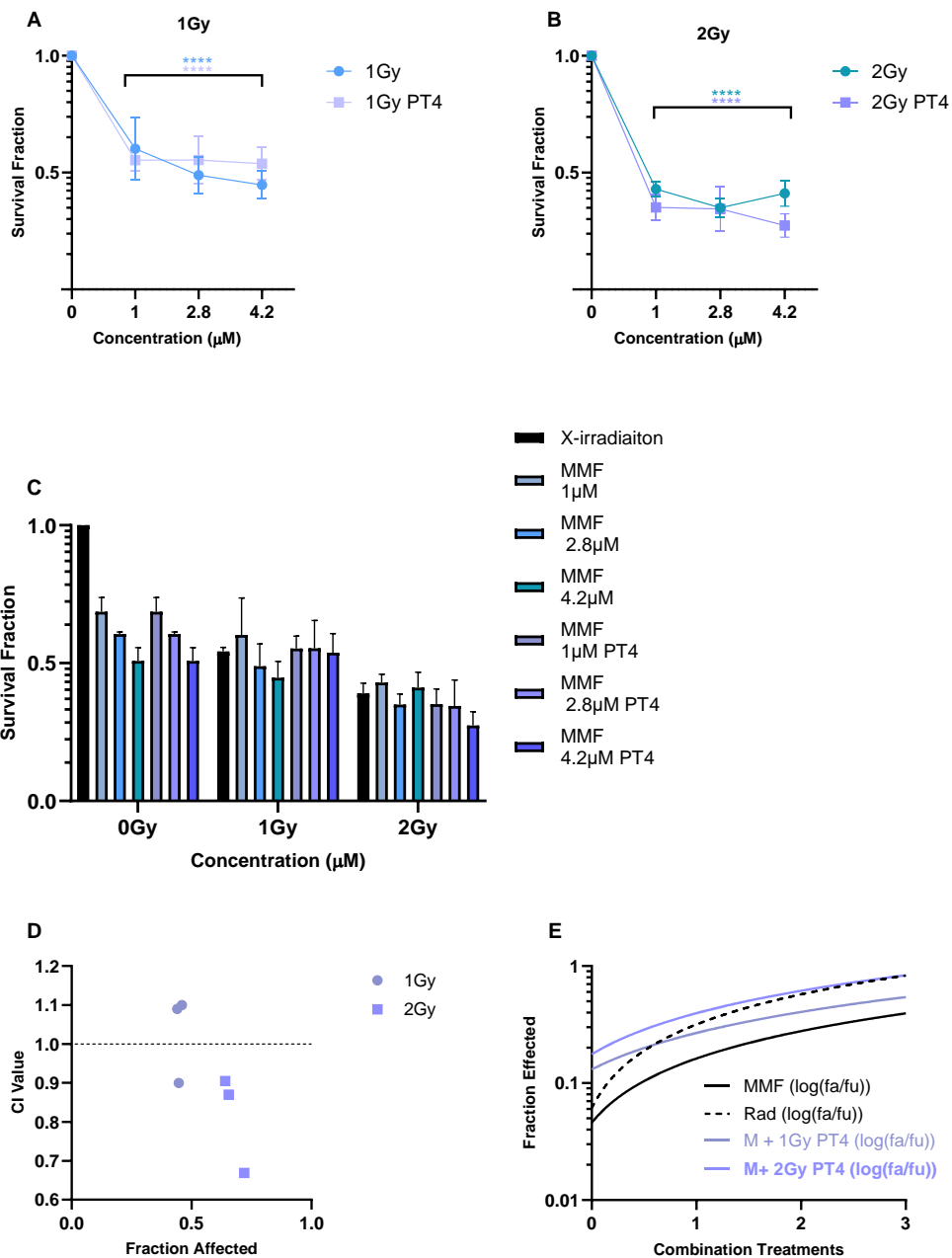
Figure 4.8 (C) compares combinations against single treatments. A statistically significant reduction in clonogenic survival was observed only for 2.7 μ M MMF + 2Gy simultaneous administration compared to 2.7 μ M MMF alone ($P < 0.05$). No other significant differences were found between MMF alone, X-irradiation alone, and the two administration schedules.

Figure 4.8 (D) shows that combination index analysis (CIA) indicated all combinations with X-irradiation PT4 were antagonistic ($CI > 1.1$). Figure 4.8 (E) shows that X-irradiation alone had a greater fraction affected compared to MMF alone and combinations. R^2 values were 0.96, 0.96, 0.86, and 0.55 for MMF alone, X-irradiation alone, MMF + 1Gy, and MMF + 2Gy PT4, respectively. The low R^2 (0.55) for the 2Gy PT4 combinations indicates poor model fit and reduced reliability of the CIA result for this group.

Overall, the data show that scheduled administration of MMF with X-irradiation did not improve cytotoxicity compared to simultaneous administration, and all combinations were antagonistic. Therefore, the hypothesis was rejected.

4.4.3.2 Cytotoxicity of External Beam X-irradiation when combined with Monomethyl Fumarate after a 4- hour pretreatment schedule on the U87 cell line.

The cytotoxic response of the U87 cell line after a 4- hour pretreatment with MMF followed by either 1Gy or 2Gy of X-irradiation and the simultaneous administration of MMF and X-irradiation is shown in Figure 4.9. Statistical analysis following a one way and two-way Anova is shown in 4.9 (F). Combination index analysis and line of fit for the U87 data is shown in (D and E) calculated using Compusyn software.



(F)

Bonferroni's multiple comparisons test	Significance Summary	Adjusted P Value
Two-way ANOVA		
Monomethyl Fumarate vs Monomethyl Fumarate + X-irradiation - Simultaneous		
1μM vs 1μM +1Gy	ns	0.3085
1μM vs 1μM +2Gy	Yes****	<0.0001
1μM + 1Gy vs 1μM +2Gy	Yes**	0.0042
2.8μM vs 2.8μM + 1Gy	ns	>0.9999
2.8μM vs 2.8μM + 2Gy	Yes****	<0.0001
2.8μM +1Gy vs 2.8μM +2Gy	Yes*	0.0246
Monomethyl Fumarate vs Monomethyl Fumarate + X-irradiation - Scheduled (PT4)		
1μM vs 1μM +1Gy	Yes*	0.0335
1μM vs 1μM +2Gy	Yes****	<0.0001

1 μ M + 1Gy vs 1 μ M +2Gy	Yes***	0.0008
2.8 μ M vs 2.8 μ M + 2Gy	Yes****	<0.0001
2.8 μ M +1Gy vs 2.8 μ M +2Gy	Yes***	0.0005
4.2 μ M vs 4.2 μ M +2Gy	Yes***	0.0001
4.2 μ M +1Gy vs 4.2 μ M +2Gy	Yes****	<0.0001
Simultaneous Vs Schedule (2Gy)		
4.2 μ M MMF vs 4.2 μ M MMF PT4	Yes**	0.0039

Figure 4.9: The effect of combining external beam X-irradiation with Monomethyl Fumarate as simultaneous administration or as a 4- hour pretreatment of Monomethyl Fumarate (PT4) on the U87 cell line. Survival fraction of the U87 cell line after exposure to 1Gy of X-irradiation and increasing concentrations of simultaneous and scheduled Monomethyl Fumarate (A) after exposure to 2Gy X-irradiation and increasing concentrations of simultaneous and scheduled Monomethyl Fumarate (B) combining both 1Gy and 2Gy combination survivals with Monomethyl Fumarate given as a single therapy and X-irradiation as a single therapy (C). Combination index values, with the dotted line representing the line of additivity with CI<0.9 showing synergism and CI>1 antagonistic (D), associated fraction affected for each dose in the Monomethyl Fumarate- X-irradiation combination shown as a line of best fit from single and combination dose response curves (E). Statistical analysis summary of data for Figure 4.9 (C) only, data comparisons not shown were not statistically significant (F). Data shown is an average of three independent experiments \pm standard deviation. A one-way ANOVA with Bonferroni post testing was performed using GraphPad Prism 10.3.1 software, with p-values of values of <0.05 = *, <0.01=** <0.001 = *** and P<0.0001=**** reported as significant against the untreated control and the double combinations (A, B). A two-way ANOVA with Bonferroni post-test was performed using GraphPad prism 10.3.1 software with P-values of <0.05 = *, <0.01=**, <0.001 = *** and P<0.0001= **** reported as significant between the relative concentrations of Monomethyl Fumarate or X-irradiation as single treatments vs the combinations with 1Gy and 2Gy

Figure 4.9 presents the effects of simultaneous and scheduled administration of MMF and X-irradiation on U87 cell clonogenic survival. In Figure 4.9 (A), both administrations of MMF with 1Gy X-irradiation resulted in statistically significant reductions in clonogenic survival compared to the untreated control (all P<0.0001). The simultaneous administration of 4.2 μ M MMF + 1Gy achieved a 56% \pm 13% reduction, while scheduled administration achieved a 47% \pm 6% reduction. A two-way

ANOVA showed no statistically significant difference between the two administration methods (Figure 4.9 (F)).

In Figure 4.9 (B), both administrations combined with 2Gy X-irradiation significantly reduced survival compared to the untreated control (all $P < 0.0001$). The scheduled administration of 4.2 μ M MMF + 2Gy resulted in the greatest reduction (73% \pm 5%), compared to 59% \pm 5% for the simultaneous combination. A statistically significant difference between the scheduled and simultaneous administration at 4.2 μ M MMF + 2Gy was detected ($P < 0.01$) (Figure 4.9 (F)).

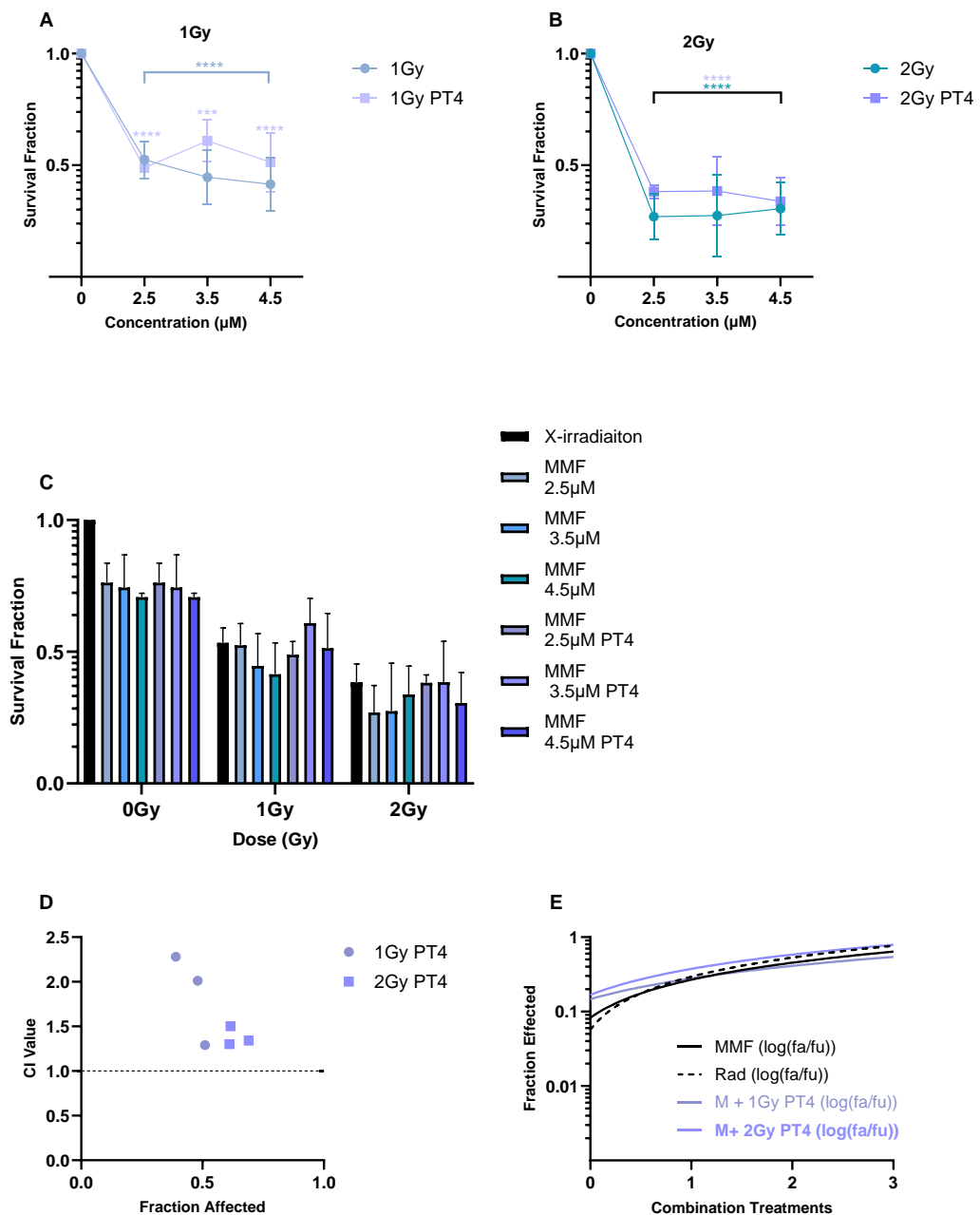
In Figure 4.9 (C), comparison between MMF and combination treatments revealed statistically significant reductions in clonogenic survival between 1 μ M MMF and its combinations with both 1Gy and 2Gy X-irradiation (all $P < 0.0001$). Significant differences were also observed between 2.8 μ M MMF and its combinations with 2Gy (both $P < 0.0001$), and between 4.2 μ M MMF alone and 4.2 μ M MMF + 2Gy scheduled administration (both $P < 0.001$). However, no combination significantly reduced clonogenic survival compared to X-irradiation alone.

Figure 4.9 (D) shows combination index analysis (CIA), where all 2Gy scheduled combinations were synergistic ($CI < 0.9$). The 1 μ M MMF + 1Gy PT4 combination also showed synergy ($CI < 0.9$), while higher doses of MMF combined with 1Gy showed antagonism ($CI > 1.1$). Figure 4.9 (E) displays the line of fit for fa/fu values. R^2 values were 0.88, 0.96, 0.62, and 0.69 for MMF alone, X-irradiation alone, MMF + 1Gy PT4, and MMF + 2Gy PT4, respectively, indicating a poor fit for the combination groups and warranting cautious interpretation of the CIA results.

Overall, the data demonstrate that scheduled administration of MMF with 2Gy X-irradiation, particularly at 4.2 μ M, elicited a statistically significantly greater reduction in clonogenic survival compared to simultaneous administration and MMF alone. Furthermore, synergy was observed in the 2Gy scheduled combinations, supporting the hypothesis that pretreatment enhances cytotoxicity compared to simultaneous administration.

4.4.3.3 Cytotoxicity of External Beam X-irradiation when combined with Monomethyl Fumarate after a 4- hour pretreatment schedule on the T98g cell line.

The cytotoxic response of the T98g cell line after a 4- hour pretreatment with MMF followed by either 1Gy or 2Gy of X-irradiation and the simultaneous administration of MMF and X-irradiation is shown in Figure 4.10. Statistical analysis following a one way and two-way Anova is shown in 4.10 (F). Combination index analysis and line of fit for the T98g data is shown in (D and E) calculated using Compusyn software.



(F)

Bonferroni's multiple comparisons test	Significance Summary	Adjusted P Value
Two-way ANOVA		
Monomethyl Fumarate vs Monomethyl Fumarate + X-irradiation - Simultaneous		
2.5µM vs 2.5µM +1Gy	Yes*	0.0166
2.5µM vs 2.5µM +2Gy	Yes****	<0.0001
2.5µM + 1Gy vs 2.5µM +2Gy	Yes**	0.0094
3.5µM vs 3.5µM + 1Gy	Yes**	0.0021
3.5µM vs 3.5µM + 2Gy	Yes****	<0.0001
4.5µM vs 4.5µM +1Gy	Yes**	0.0025
4.5µM vs 4.5µM +2Gy	Yes***	0.0001
Monomethyl Fumarate vs Monomethyl Fumarate + X-irradiation – Scheduled (PT4)		
2.5µM vs 2.5µM +1Gy	Yes**	0.0050
2.5µM vs 2.5µM +2Gy	Yes****	<0.0001
3.5µM vs 3.5µM + 2Gy	Yes***	0.0002
3.5µM +1Gy vs 3.5µM +2Gy	Yes*	0.0259
4.5µM vs 4.5µM +2Gy	Yes****	<0.0001
4.5µM +1Gy vs 4.5µM +2Gy	Yes*	0.0425

Figure 4.10: The effect of combining external beam X-irradiation with Monomethyl Fumarate as simultaneous administration or as a 4- hour pretreatment of Monomethyl Fumarate (PT4) on the T98g cell line. Survival fraction of the T98g cell line after exposure to 1Gy of X-irradiation and increasing concentrations of simultaneous and scheduled Monomethyl Fumarate (A) after exposure to 2Gy X-irradiation and increasing concentrations of simultaneous and scheduled Monomethyl Fumarate (B) combining both 1Gy and 2Gy combination survivals with Monomethyl Fumarate given as a single therapy and X-irradiation as a single therapy (C). Combination index values, with the dotted line representing the line of additivity with CI<0.9 showing synergism and CI>1 antagonistic (D), associated fraction affected for each dose in the Monomethyl Fumarate- X-irradiation combination shown as a line of best fit from single and combination dose response curves (E). Statistical analysis summary of data for Figure 4.10 (C) only, data comparisons not shown were not statistically significant (F). Data shown is an average of three independent experiments \pm standard deviation. A one-way ANOVA with Bonferroni post testing was performed using GraphPad Prism 10.3.1 software, with p-values of values of <0.05 = *, <0.01=** <0.001 = *** and P<0.0001=**** reported as significant against the untreated control and the double combinations (A, B). A two-way ANOVA with Bonferroni post-test was performed using GraphPad prism 10.3.1 software with P-values of <0.05 = *, <0.01= **, <0.001 = *** and P<0.0001= **** reported as significant between the relative concentrations of Monomethyl Fumarate or X-irradiation as single treatments vs the combinations with 1Gy and 2Gy.

Figure 4.10 presents the effects of simultaneous and scheduled administration of MMF and X-irradiation on T98G cell clonogenic survival. In Figure 4.10 (A), both administration methods with 1Gy X-irradiation resulted in statistically significant reductions in clonogenic survival compared to the untreated control (all $P < 0.001$). The maximum reduction was seen after 4.5 μ M MMF + 1Gy simultaneous administration (59% \pm 9%), while the greatest scheduled administration reduction was 52% \pm 4% after 2.5 μ M MMF + 1Gy. No statistically significant differences were found between the administration methods (Figure 4.10 (F)).

Figure 4.10 (B) shows similar findings for 2Gy X-irradiation, where all combinations statistically significantly reduced clonogenic survival compared to the untreated control (all $P < 0.0001$). Simultaneous administration induced slightly greater reductions in survival than scheduled administration across most concentrations, although differences were not statistically significant (Figure 4.10 (F)).

Figure 4.10 (C) compares combinations with single treatments. Statistically significant reductions were observed for 2.5 μ M MMF + 1Gy (both administration methods) compared to MMF alone ($P < 0.05$). A statistically significant reduction was also observed for 2.5 μ M MMF + 2Gy combinations compared to MMF alone (both $P < 0.0001$). However, no combinations significantly reduced clonogenic survival compared to X-irradiation alone. For 3.5 μ M MMF combinations, reductions compared to MMF alone were significant ($P < 0.01$ for 1 Gy, $P < 0.0001$ for 2Gy simultaneous, $P < 0.001$ for 2Gy scheduled), but again not compared to X-irradiation alone. At 4.5 μ M MMF, only simultaneous combinations significantly reduced survival compared to MMF alone ($P < 0.05$), and a statistically significant reduction was observed between the 1Gy and 2Gy scheduled combinations ($P < 0.05$).

Combination index analysis (Figure 4.10 (D)) indicated all scheduled MMF + X-irradiation combinations were antagonistic ($CI > 1$). Poor model fit was observed, with R^2 values of 0.86, 0.95, 0.52, and 0.69 for MMF alone, X-irradiation alone, MMF + 1Gy PT4, and MMF + 2Gy PT4, respectively (Figure 4.10 (E)), suggesting caution in interpreting the CIA results.

Overall, the data suggest that scheduled administration of MMF with X-irradiation did not significantly improve clonogenic survival reduction over simultaneous combinations. The hypothesis was therefore rejected.

4.4.4 Cytotoxic response of External beam X-irradiation with Temozolomide and Monomethyl Fumarate given as a triple combination either simultaneously or as a schedule in human Glioblastoma cell lines

In glioblastoma the use of Monomethyl Fumarate in combination with both External beam X-irradiation and Temozolomide was required to be interrogated to assess how the addition of Monomethyl Fumarate could contribute to a novel therapy as an addition to the gold standard treatment clinically.

Results from Section 4.4.2 to 4.4.3 show limited efficacy of MMF as a double combination with MMF and X-irradiation. However, lack of synergy and significance in combining MMF with X-irradiation rejected our initial hypothesis that the combination would increase cytotoxicity through radiosensitisation.

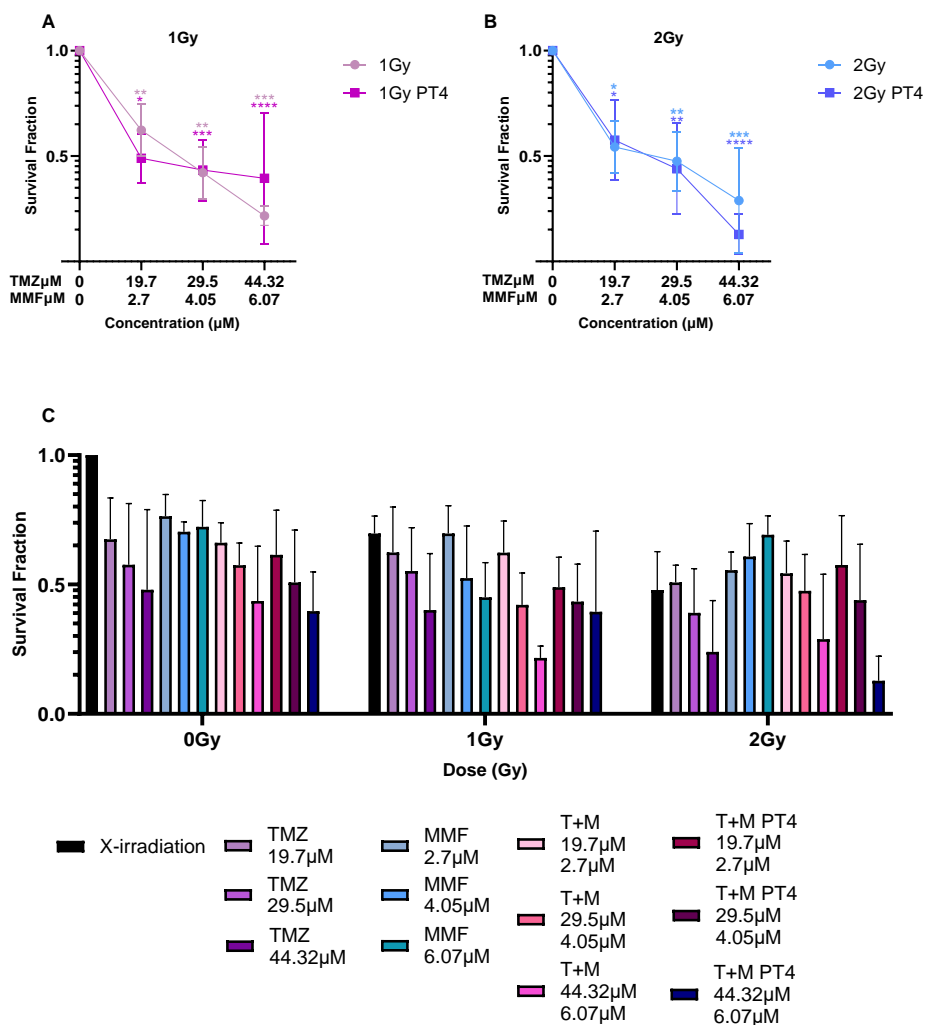
Next, through clonogenic assay and combination index analysis, the triple combination given either simultaneously or as a schedule was investigated. By combining MMF with TMZ and X-irradiation, the reduction in glutathione levels and the oxidative response of the cells, could increase the cytotoxic response of TMZ and X-irradiation.

The same concentrations for MMF, TMZ and X-irradiation used throughout Chapter 4 were also applied for the triple combinations, as these concentrations of MMF and TMZ when combined showed synergy in at least 2 of the concentrations when given as a schedule in Chapter 3 across the cell lines.

We hypothesised the triple combinations would elicit significant reductions in clonogenic survival when compared to the single and double combination treatments and show synergy when combined.

4.4.4.1 Cytotoxic effects of Temozolomide-Monomethyl Fumarate and External beam X-irradiation in the UVW cell line

To compare the cytotoxic effect of the triple combination given either simultaneously or as a scheduled treatment, a clonogenic assay was performed. Figure 4.11 shows the survival fraction of the UVW cell line to combinations of MMF and TMZ with either 1Gy or 2Gy of X-irradiation. Combinations were given either simultaneously or as a 4- hour pretreatment of MMF followed by both TMZ and X-irradiation together. Each treatment response was assessed through clonogenic survival. Statistical analysis following a one-way and two-way Anova is shown in 4.11 (C).



(D)

Bonferroni's multiple comparisons test	Significance Summary	Adjusted P Value
One-way ANOVA – Bonferroni's Post Test		
Control vs Temozolomide + Monomethyl Fumarate + 1Gy X-irradiation		
Control vs T+M +1Gy (19.7µM + 2.7µM)	Yes*	0.0314
Control vs T+M +1Gy (29.5µM + 4.02µM)	Yes***	0.0009
Control vs T+M +1Gy (44.32µM + 6.07µM)	Yes****	<0.0001
Control vs T+M +1Gy PT4 (19.7µM + 2.7µM)	Yes**	0.0029
Control vs T+M +1Gy PT4 (29.5µM + 4.02µM)	Yes**	0.0011
Control vs T+M +1Gy PT4 (44.32µM + 6.07µM)	Yes***	0.0005
Control vs Temozolomide + Monomethyl Fumarate + 2Gy X-irradiation		
Control vs T+M +2Gy (19.7µM + 2.7µM)	Yes*	0.0137
Control vs T+M +2Gy (29.5µM + 4.02µM)	Yes**	0.0044
Control vs T+M +2Gy (44.32µM + 6.07µM)	Yes***	0.0002
Control vs T+M +2Gy PT4 (19.7µM + 2.7µM)	Yes*	0.0236
Control vs T+M +2Gy PT4 (29.5µM + 4.02µM)	Yes**	0.0025
Control vs T+M +2Gy PT4 (44.32µM + 6.07µM)	Yes****	<0.0001
Two-way Anova – Bonferroni's Post Test		
Multiple Comparisons where significant		
0Gy: T+M (44.32µM + 6.07µM) vs 2Gy: T+M PT4 (44.32µM + 6.07µM)	Yes*	0.0274
1Gy: X-irradiation vs 1Gy: T+M (44.32µM + 6.07µM)	Yes*	0.0352
2Gy: MMF 6.07µM vs. 2Gy: T+M 44.32µM 6.07µM	Yes**	0.0069
2Gy: MMF 6.07µM vs. 2Gy: T+M PT4 44.32µM 6.07µM	Yes***	0.0003
1Gy MMF 6.07µM vs 1Gy T+M (44.32µM 6.07µM)	Yes***	0.0004
MMF 6.07µM vs 2Gy T+M (44.32µM 6.07µM)	Yes**	0.0046
MMF 6.07µM vs 2Gy T+M (44.32µM 6.07µM) PT4	Yes****	<0.0001

Figure 4.11: The effect of combining External beam X-irradiation with Monomethyl Fumarate and Temozolomide as simultaneous administration or as a 4- hour pretreatment of Monomethyl Fumarate (PT4) followed by Temozolomide and X-irradiation on the UVW cell line. Survival fraction of the UVW cell line after exposure to 1Gy of X-irradiation, Temozolomide and Monomethyl Fumarate given simultaneously or with a 4-hour Monomethyl Fumarate pretreatment (A). Survival after exposure to 2Gy of X-irradiation and incubation with increasing concentrations of Temozolomide and Monomethyl Fumarate either simultaneously or scheduled (B) combining both 1Gy and 2Gy triple combination survivals with Temozolomide and Monomethyl Fumarate as a double combination and against the single treatments of X-irradiation, Temozolomide and Monomethyl Fumarate given either simultaneously or as a schedule (C). Statistical summary of the significant data following a one-way and two-way ANOVA test with data comparisons not shown, not significant (D). Data shown is an average of three independent experiments \pm standard deviation. A one-way ANOVA with Bonferroni post testing was performed using GraphPad Prism 10.3.1 software, with p-values of values of $<0.05 = *$, $<0.01 = **$ $<0.001 = ***$ and

$P < 0.0001 = ****$ reported as significant against the untreated control and the triple combinations (A, B). A two-way ANOVA with Bonferroni post-test was performed using GraphPad prism 10.3.1 software with P-values of $< 0.05 = *$, $< 0.01 = **$, $< 0.001 = ***$ and $P < 0.0001 = ****$ reported as significant between the relative concentrations of the triple combination.

Figure 4.11 (A) shows the cytotoxic response of the UVW cell line after triple combination exposure with 1Gy of X-irradiation. The scheduled administration of MMF pretreatment for 4- hours followed by both TMZ and X-irradiation displayed a statistically significant reduction in clonogenic survival compared to the control as did simultaneous administration at all combination concentrations (all $P < 0.05$). At the lowest combination of 19.7 μ M TMZ and 2.7 μ M MMF with 1Gy as a schedule (PT4), a 52% reduction in clonogenic survival was achieved $\pm 9\%$ ($P < 0.01$). The concentration combination of 44.32 μ M TMZ and 6.07 μ M MMF with 1Gy, given as a schedule resulted in 56% reduction in clonogenic survival $\pm 11\%$. The same concentration of MMF and TMZ with 1Gy when given simultaneously resulted in a maximum 79% reduction in clonogenic survival $\pm 3\%$. No significant differences were seen between the simultaneous and scheduled administrations at each combination concentration ($P > 0.05$). The data suggests the simultaneous administration of the triple combination to instigate higher levels of cytotoxicity than the MMF pretreatment schedule.

Figure 4.11 (B) displays the cytotoxic response of the triple combination when 2Gy of X-irradiation was administered. Both simultaneous and scheduled administration of MMF in the triple combinations provided a statistically significant dose dependent reduction in clonogenic survival compared to the untreated control for all triple combinations (all, $P < 0.05$). The highest concentration combination of 44.32 μ M TMZ and 6.07 μ M MMF with 2Gy, given as a schedule (PT4) resulted in 88% reduction in clonogenic survival $\pm 12\%$ when compared to the untreated control ($P < 0.0001$). The same concentration of MMF and TMZ with 2Gy when given simultaneously resulted in 72% reduction in clonogenic survival $\pm 20\%$ when compared to the untreated control ($P < 0.001$). No significant difference between the two administrations was determined ($P > 0.05$). Data suggests the schedule with 2Gy of X-irradiation was required to elicit a greater cytotoxic effect at higher concentrations of the combination only.

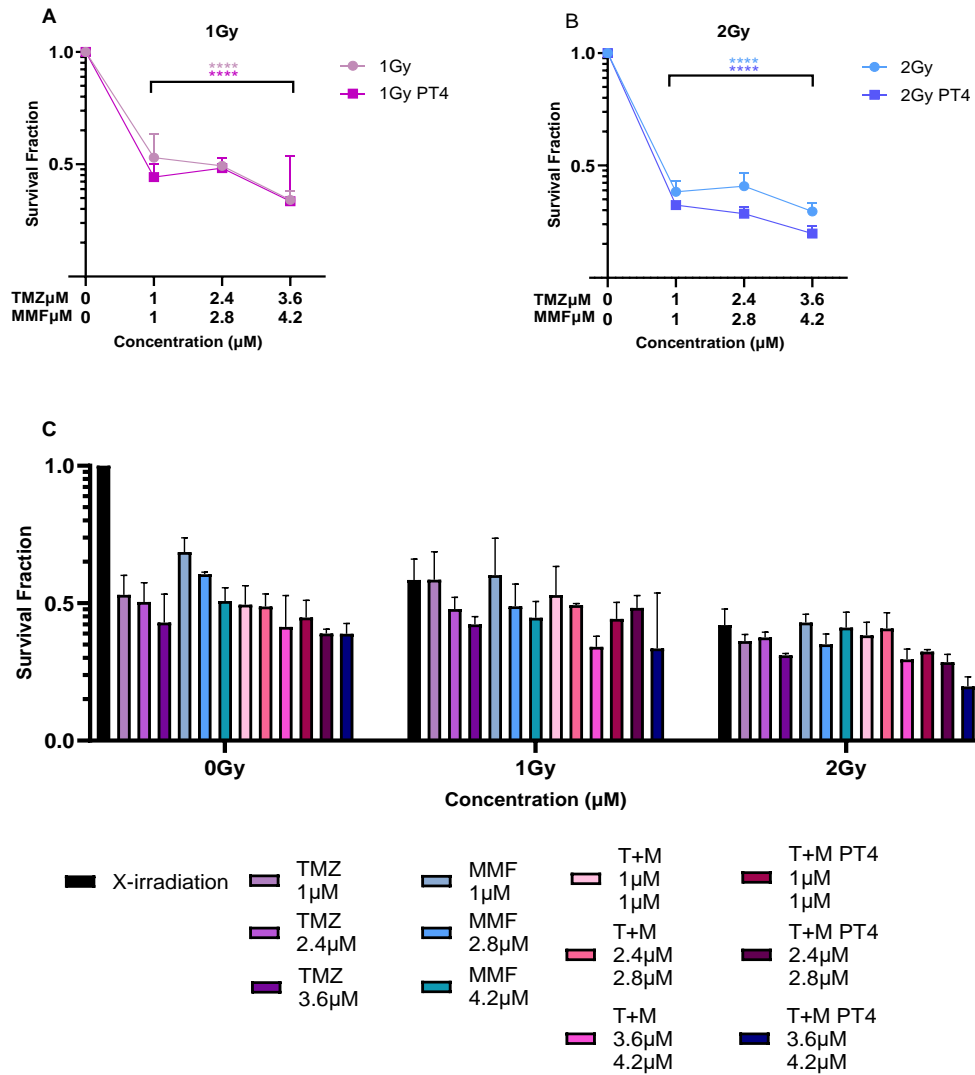
Figure 4.11 (C) displays the cytotoxic response of X-irradiation as a single treatment, TMZ as a single treatment, MMF as a single treatment, the TMZ and MMF double

combination therapies, either simultaneously or scheduled and the triple combinations given either simultaneously or as a schedule, all combination treatments with either 1Gy or 2Gy of X-irradiation. A statistically significant reduction in clonogenic survival was shown after exposure to 2Gy + 44.32 μ M TMZ + 6.07 μ M MMF administered as a scheduled combination compared to 6.07 μ M MMF ($P < 0.05$) but not 44.32 μ M TMZ. The triple combination of 2Gy + 44.32 μ M TMZ + 6.07 μ M given both as a schedule or simultaneously resulted in a statistically significant reduction in clonogenic survival when compared to the double combination of 2Gy X-irradiation combined with 6.07 μ M of MMF (both $P < 0.01$) but not to TMZ double combinations with X-irradiation. The triple combination of 2Gy + 44.32 μ M TMZ + 6.07 μ M MMF was also not significant when compared to 2Gy of X-irradiation alone. The scheduled combination of 2Gy + 44.32 μ M TMZ + 6.07 μ M (PT4) showed a statistically significant reduction in clonogenic survival when compared to the double combination of 44.32 μ M TMZ + 6.07 μ M given simultaneously ($P < 0.05$). A statistically significant reduction in clonogenic survival was shown after exposure to 1Gy + 44.32 μ M TMZ + 6.07 μ M given simultaneously when compared to 1Gy of X-irradiation alone ($P < 0.05$). No other significance was determined from the data, however trends in the data show the 2Gy PT4 with 6.07 μ M of MMF and 44.32 μ M TMZ provide the greatest reduction in clonogenic survival at 88%.

Data is suggestive of a scheduled triple combination producing synergy. However, lack of statistically significant findings comparing single treatments and double treatments consistently to the triple combinations rejects our hypothesis.

4.4.4.2 Cytotoxic effects of Temozolomide-Monomethyl Fumarate and External beam X-irradiation in the U87cell line

To compare the cytotoxic effect of the triple combination given either simultaneously or as a scheduled treatment, a clonogenic assay was performed. Figure 4.12 shows the survival fraction of the U87 cell line to combinations of MMF and TMZ with either 1Gy or 2Gy of X-irradiation. Combinations were given either simultaneously or as a 4- hour pretreatment of MMF followed by both TMZ and X-irradiation together. Each treatment response was assessed through clonogenic survival. Statistical analysis following a one-way and two-way Anova is shown in 4.12 (D).



(D)

Bonferroni's multiple comparisons test	Significance Summary	Adjusted P Value
One-way ANOVA – Bonferroni's Post Test		
Control vs Temozolomide + Monomethyl Fumarate + 1Gy X-irradiation		
Control vs T+M +1Gy (1μM + 1μM)	Yes****	<0.0001
Control vs T+M +1Gy (2.4μM + 2.8μM)	Yes****	<0.0001
Control vs T+M +1Gy (3.6μM + 4.2μM)	Yes****	<0.0001
Control vs T+M +1Gy PT4 (1μM + 1μM)	Yes****	<0.0001
Control vs T+M +1Gy PT4 (2.4μM + 2.8μM)	Yes****	<0.0001
Control vs T+M +1Gy PT4 (3.6μM + 4.2μM)	Yes****	<0.0001
Control vs Temozolomide + Monomethyl Fumarate + 2Gy X-irradiation		
Control vs T+M +2Gy (1μM + 1μM)	Yes****	<0.0001
Control vs T+M +2Gy (2.4μM + 2.8μM)	Yes****	<0.0001
Control vs T+M +2Gy (3.6μM + 4.2μM)	Yes****	<0.0001
Control vs T+M +2Gy PT4 (1μM + 1μM)	Yes****	<0.0001
Control vs T+M +2Gy PT4 (2.4μM + 2.8μM)	Yes****	<0.0001

Control vs T+M +2Gy PT4 (3.6µM + 4.2µM)	Yes****	<0.0001
Two-way Anova – Bonferroni's Post test		
Multiple Comparisons where significant		
TMZ 1µM vs 2Gy + T+M (1µM + 1µM)	Yes****	<0.0001
TMZ 1µM vs 1Gy + T+M (1µM + 1µM) PT4	Yes***	0.0008
TMZ 1µM vs 2Gy + T+M (1µM + 1µM) PT4	Yes****	<0.0001
MMF 1µM vs 1Gy + T+M (1µM + 1µM)	Yes*	0.0454
MMF 1µM vs 2Gy + T+M (1µM + 1µM)	Yes****	<0.0001
MMF 1µM vs 1Gy + T+M (1µM + 1µM) PT4	Yes***	0.0001
MMF 1µM vs 2Gy + T+M (1µM + 1µM) PT4	Yes****	<0.0001
T+M (1µM + 1µM) vs 2Gy + T+M (1µM + 1µM) PT4	Yes*	0.0191
1Gy + T+M (1µM + 1µM) vs 2Gy + T+M (1µM + 1µM) PT4	Yes**	0.0019
1Gy + T+M (1µM + 1µM) vs 2Gy + T+M (1µM + 1µM)	Yes*	0.0442
MMF 2.8µM vs 2Gy + T+M (2.4µM + 2.8µM)	Yes**	0.0033
MMF 2.8µM vs 2Gy + T+M (2.4µM + 2.8µM) PT4	Yes****	<0.0001
1Gy + T+M (2.4µM + 2.8µM) vs 2Gy + T+M (2.4µM + 2.8µM) PT4	Yes**	0.0017
1Gy + T+M (2.4µM + 2.8µM) PT4 vs 2Gy + T+M (2.4µM + 2.8µM) PT4	Yes**	0.0033
4.2µM vs 1Gy + T+M (3.6µM + 4.2µM)	Yes*	0.0245
4.2µM vs 2Gy + T+M (3.6µM + 4.2µM)	Yes**	0.0012
4.2µM vs 1Gy + T+M (3.6µM + 4.2µM)	Yes*	0.0171
4.2µM vs 2Gy + T+M (3.6µM + 4.2µM)	Yes****	<0.0001
T+M (3.6µM + 4.2µM) PT4 vs 2Gy T+M (3.6µM + 4.2µM) PT4	Yes**	0.0060
1Gy vs 1Gy + T+M (3.6µM + 4.2µM)	Yes*	0.0137
1Gy vs 1Gy + T+M (3.6µM + 4.2µM) PT4	Yes*	0.0099

Figure 4.12: The effect of combining External beam X-irradiation with Monomethyl Fumarate and Temozolomide as simultaneous administration or as a 4- hour pretreatment of Monomethyl Fumarate (PT4) followed by Temozolomide and X-irradiation on the U87 cell line. Survival fraction of the U87 cell line after exposure to 1Gy of X-irradiation and Temozolomide and Monomethyl Fumarate given simultaneously or with a 4- hour Monomethyl Fumarate pretreatment (A). Survival after exposure to 2Gy of X-irradiation and incubation with increasing concentrations of Temozolomide and Monomethyl Fumarate either simultaneously or scheduled (B) combining both 1Gy and 2Gy triple combination survivals with Temozolomide and Monomethyl Fumarate as a double combination and against the single treatments of X-irradiation, Temozolomide and Monomethyl Fumarate given either simultaneously or as a schedule (C). Statistical summary of the significant data following a one-way and two-way ANOVA test with data comparisons not shown, not significant (D). Data shown is an average of three independent experiments \pm standard deviation. A one-way ANOVA with Bonferroni post testing was performed using GraphPad Prism 10.3.1 software, with p-values of values of $<0.05 = *$, $<0.01 = **$, $<0.001 = ***$ and $P < 0.0001 = ****$ reported as significant against the untreated control and the triple combinations (A, B). A two-way ANOVA with Bonferroni post-test was performed using

GraphPad prism 10.3.1 software with P-values of $<0.05 = *$, $<0.01 = **$, $<0.001 = ***$ and $P<0.0001 = ****$ reported as significant between the relative concentrations of the triple combination.

Figure 4.12 (A) shows the response of the U87 cell line to 1Gy of X-irradiation with each combination of MMF and TMZ, given either simultaneously or with a 4- hour pretreatment (PT4). All triple combinations show a statistically significant reduction in clonogenic survival compared to the untreated control ($P<0.0001$). Between the administration schedules few differences can be seen across all three treatments and differences in clonogenic survival were insignificant. The scheduled combination (PT4) of $3.6\mu\text{M}$ TMZ with $4.2\mu\text{M}$ MMF with 1Gy of X-irradiation induced a reduction in clonogenic survival of $67\% \pm 20\%$, with the simultaneous administration of the same treatment giving a 66% reduction in clonogenic survival $\pm 3\%$ ($P>0.05$). The data suggests the administration scheduling has no significant effect on the clonogenic survival response of the 1Gy triple combinations.

Figure 4.12 (B) displays the response of the U87 cell line to 2Gy of X-irradiation with each combination. All combination result show a statistically significant reduction in clonogenic survival compared to the untreated control ($P<0.0001$). The scheduled combination (PT4) of $3.6\mu\text{M}$ TMZ with $4.2\mu\text{M}$ MMF with 2Gy of X-irradiation gave a maximum reduction in clonogenic survival of $81\% \pm 3\%$, with the simultaneous administration at the same treatment concentrations showing a 71% reduction in clonogenic survival $\pm 3\%$. Differences in clonogenic survival were not statistically significant at after exposure to the triple combinations at both schedules. At the concentrations of $2.4\mu\text{M}$ TMZ and $2.8\mu\text{M}$ MMF with 2Gy of X-irradiation given as a schedule, 72% reduction in clonogenic survival $\pm 2\%$ was achieved. Although, data suggests the administration scheduling has no significant effect on the clonogenic survival response of the 2Gy triple combinations.

Figure 4.12 (C) compares the clonogenic survival of the triple combinations to TMZ, MMF, X-irradiation, T+M and T+M PT4. The lowest combination showed a statistically significant difference in clonogenic survival between the triple combination 2Gy + T+M ($1\mu\text{M} + 1\mu\text{M}$) compared to $1\mu\text{M}$ of TMZ, $1\mu\text{M}$ of MMF, and the triple combination of 1Gy + T+M ($1\mu\text{M} + 1\mu\text{M}$) (all, $P<0.05$) but not 2Gy of X-irradiation or the double combination ($P>0.05$). Exposure to triple combination 1Gy + T+M ($1\mu\text{M} + 1\mu\text{M}$) showed a statistically significant reduction in clonogenic survival when compared to $1\mu\text{M}$ MMF of alone ($P<0.05$) but not TMZ alone, X-irradiation or the double

combination of T+M. A statistically significant reduction in clonogenic survival was seen between 1Gy + T+M (1 μ M + 1 μ M) PT4 and both 1 μ M of TMZ (P<0.001) 1 μ M of MMF (P<0.001) but not 1Gy of X-irradiation (P>0.05) or the double combination of T+M PT4. Exposure of the U87 cells to 2Gy + T+M (1 μ M + 1 μ M) PT4 showed a statistically significant reduction in clonogenic survival when compared to 1 μ M of TMZ 1 μ M of MMF the double combo T+M (1 μ M + 1 μ M) and the triple combination of 1Gy + T+M (1 μ M + 1 μ M) (all, P<0.05) but not 2Gy of X-irradiation alone.

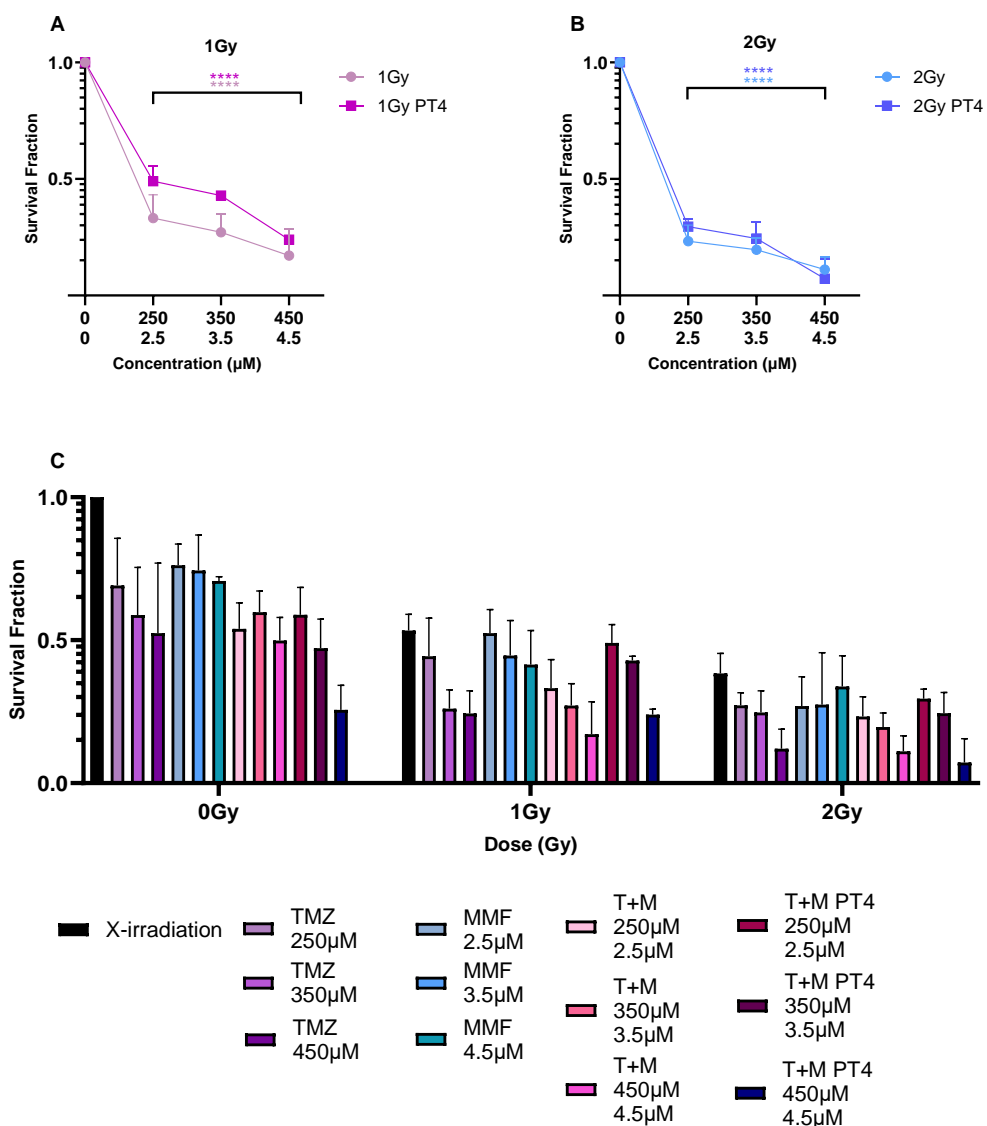
The 2Gy triple combination of T+M (2.4 μ M + 2.8 μ M) showed a statistically significant reduction in clonogenic survival compared to 2.8 μ M of MMF (P<0.01) but not 2.4 μ M of TMZ, 2Gy of X-irradiation or the double combination of T+M. The scheduled administration of 2Gy + T+M (2.4 μ M + 2.8 μ M) PT4 also showed a statistically significant difference in clonogenic survival when compared to 2.8 μ M of MMF, 1Gy + T+M (2.4 μ M + 2.8 μ M) and 1Gy + T+M (2.4 μ M + 2.8 μ M) PT4 (all, P<0.01) but not 2.4 μ M of TMZ or 2Gy of X-irradiation.

The highest combination T+M (3.6 μ M + 4.2 μ M), showed a statistically significant reduction in clonogenic survival when combined with 1Gy or 2Gy of X-irradiation compared to 4.2 μ M of MMF (P<0.05) and 1Gy of X-irradiation (P<0.05) but not TMZ or the double combinations of (T+M). Scheduled combinations of 1Gy or 2Gy T+M (3.6 μ M + 4.2 μ M) showed a statistically significant reduction in clonogenic survival compared to 4.2 μ M of MMF (P<0.05) and for the 1Gy triple combination compared to 1Gy of X-irradiation. The scheduled 2Gy T+M (3.6 μ M + 4.2 μ M), also showed statistically significant reductions in clonogenic survival when compared to the double combination schedule T+M (3.6 μ M + 4.2 μ M) PT4. The highest combination had no other significant findings between the triple combinations and the single and double combination treatments.

Collectively the data suggests the 2Gy PT4 treatment group induced the greatest cytotoxicity overall at each treatment concentration. However, this was not statistically significant over each single treatment and double treatments and the hypothesis was rejected.

4.4.4.3 Cytotoxic effects of Temozolomide-Monomethyl Fumarate and External beam X-irradiation in the T98g cell line

To compare the cytotoxic effect of the triple combination given either simultaneously or as a scheduled treatment, a clonogenic assay was performed. Figure 4.13 shows the survival fraction of the T98g cell line to combinations of MMF and TMZ with either 1Gy or 2Gy of X-irradiation. Combinations were given either simultaneously or as a 4- hour pretreatment of MMF followed by both TMZ and X-irradiation together. Each treatment response was assessed through clonogenic survival. Statistical analysis following a one way and two-way Anova is shown in 4.13 (D).



(D)

Bonferroni's multiple comparisons test	Significance Summary	Adjusted P Value
One-way ANOVA – Bonferroni's Post Test		
Control vs Temozolomide + Monomethyl Fumarate + 1Gy X-irradiation		
Control vs T+M +1Gy (250µM + 2.5µM)	Yes****	<0.0001
Control vs T+M +1Gy (350µM + 3.5µM)	Yes****	<0.0001
Control vs T+M +1Gy (450µM + 4.5µM)	Yes****	<0.0001
Control vs T+M +1Gy PT4 (250µM + 2.5µM)	Yes****	<0.0001
Control vs T+M +1Gy PT4 (350µM + 3.5µM)	Yes****	<0.0001
Control vs T+M +1Gy PT4 (450µM + 4.5µM)	Yes****	<0.0001
Simultaneous vs Schedule		
1Gy T+M (250µM + 2.5µM) vs 1Gy T+M (250µM + 2.5µM) PT4	Yes*	0.0345
1Gy T+M (350µM + 3.5µM) vs 1Gy T+M (350µM + 3.5µM) PT4	Yes*	0.0352
Control vs Temozolomide + Monomethyl Fumarate + 2Gy X-irradiation		
Control vs T+M +2Gy (250µM + 2.5µM)	Yes****	<0.0001
Control vs T+M +2Gy (350µM + 3.5µM)	Yes****	<0.0001
Control vs T+M +2Gy (450µM + 4.5µM)	Yes****	<0.0001
Control vs T+M +2Gy PT4 (250µM + 2.5µM)	Yes****	<0.0001
Control vs T+M +2Gy PT4 (350µM + 3.5µM)	Yes****	<0.0001
Control vs T+M +2Gy PT4 (450µM + 4.5µM)	Yes****	<0.0001
Two-way ANOVA – Bonferroni's Post Test		
Multiple Comparisons where Significant		
1Gy vs 1Gy T+M (250µM + 2.5µM)	Yes*	0.0328
TMZ (250µM) vs 1Gy T+M (250µM + 2.5µM)	Yes****	<0.0001
TMZ (250µM) vs 2Gy T+M (250µM + 2.5µM)	Yes****	<0.0001
TMZ (250µM) vs 1Gy T+M (250µM + 2.5µM)	Yes*	0.0438
TMZ (250µM) vs 2Gy T+M (250µM + 2.5µM)	Yes****	<0.0001
MMF (2.5µM) vs 1Gy T+M (250µM + 2.5µM)	Yes****	<0.0001
MMF (2.5µM) vs 2Gy T+M (250µM + 2.5µM)	Yes****	<0.0001
MMF (2.5µM) vs 1Gy T+M (250µM + 2.5µM) PT4	Yes**	0.0019
MMF (2.5µM) vs 2Gy T+M (250µM + 2.5µM) PT4	Yes****	<0.0001
T+M (250µM + 2.5µM) vs 1Gy T+M (250µM + 2.5µM)	Yes*	0.0363
T+M (250µM + 2.5µM) vs 2Gy T+M (250µM + 2.5µM)	Yes***	0.0009
T+M (250µM + 2.5µM) vs 2Gy T+M (250µM + 2.5µM) PT4	Yes**	0.0014
TMZ (250µM + 2.5µM) vs 2Gy T+M (250µM + 2.5µM)	Yes***	0.0010
TMZ (250µM + 2.5µM) PT4 vs 1Gy + T+M (250µM + 2.5µM)	Yes**	0.0018
TMZ (250µM + 2.5µM) PT4 vs 2Gy T+M (250µM + 2.5µM)	Yes****	<0.0001
TMZ (250µM + 2.5µM) PT4 vs 2Gy T+M (250µM + 2.5µM) PT4	Yes***	0.0002
2Gy T+M (250µM + 2.5µM) vs 1Gy T+M (250µM + 2.5µM) PT4	Yes**	0.0018
1Gy vs 1Gy T+M (350µM + 3.5µM)	Yes**	0.0015
TMZ (350µM) vs 2Gy T+M (350µM + 3.5µM)	Yes**	0.0033
TMZ (350µM) vs 2Gy T+M (350µM + 3.5µM) PT4	Yes*	0.0479
MMF (3.5µM) vs 1Gy T+M (250µM + 2.5µM)	Yes****	<0.0001
MMF (3.5µM) vs 2Gy T+M (250µM + 2.5µM)	Yes****	<0.0001
MMF (3.5µM) vs 1Gy T+M (250µM + 2.5µM) PT4	Yes***	0.0001
MMF (3.5µM) vs 2Gy T+M (250µM + 2.5µM) PT4	Yes****	<0.0001
T+M (350µM + 3.5µM) vs T+M 1Gy (350µM + 3.5µM)	Yes****	<0.0001
T+M (350µM + 3.5µM) vs T+M 2Gy (350µM + 3.5µM)	Yes****	<0.0001
T+M (350µM + 3.5µM) vs T+M 2Gy (350µM + 3.5µM) PT4	Yes****	<0.0001
T+M (350µM + 3.5µM) PT4 vs T+M 1Gy (350µM + 3.5µM)	Yes*	0.0435

T+M (350µM + 3.5µM) PT4 vs T+M 2Gy (350µM + 3.5µM)	Yes***	0.0006
T+M (350µM + 3.5µM) PT4 vs T+M 2Gy (350µM + 3.5µM) PT4	Yes*	0.0102
2Gy T+M (350µM + 3.5µM) vs T+M 1Gy (350µM + 3.5µM) PT4	Yes**	0.0078
1Gy vs 1Gy T+M (450µM + 4.5µM)	Yes****	<0.0001
1Gy vs 1Gy + T+M (450µM + 4.5µM) PT4	Yes***	0.0003
2Gy vs 2Gy T+M (450µM + 4.5µM)	Yes***	0.0009
2Gy vs 2Gy T+M (450µM + 4.5µM) PT4	Yes***	0.0001
TMZ (450µM) vs 2Gy T+M (450µM + 4.5µM) PT4	Yes*	0.0456
MMF (4.5µM) vs 1Gy T+M (450µM + 4.5µM)	Yes****	<0.0001
MMF (4.5µM) vs 2Gy T+M (450µM + 4.5µM)	Yes****	<0.0001
MMF (4.5µM) vs 1Gy T+M (450µM + 4.5µM) PT4	Yes****	<0.0001
MMF (4.5µM) vs 2Gy T+M (450µM + 4.5µM) PT4	Yes****	<0.0001
T+M (450µM + 4.5µM) vs 1Gy T+M (450µM + 4.5µM)	Yes****	<0.0001
T+M (450µM + 4.5µM) vs 2Gy T+M (450µM + 4.5µM)	Yes****	<0.0001
T+M (450µM + 4.5µM) vs 1Gy T+M (450µM + 4.5µM) PT4	Yes**	0.0016
T+M (450µM + 4.5µM) vs 2Gy T+M (450µM + 4.5µM) PT4	Yes****	<0.0001

Figure 4.13: The effect of combining External beam X-irradiation with Monomethyl Fumarate and Temozolomide as simultaneous administration or as a 4- hour pretreatment of Monomethyl Fumarate (PT4) followed by Temozolomide and X-irradiation on the T98g cell line. Survival fraction of the T98g cell line after exposure to 1Gy of X-irradiation and Temozolomide and Monomethyl Fumarate given simultaneously or with a 4- hour Monomethyl Fumarate pretreatment (A). Survival after exposure to 2Gy of X-irradiation and incubation with increasing concentrations of Temozolomide and Monomethyl Fumarate either simultaneously or scheduled (B) combining both 1Gy and 2Gy triple combination survivals with Temozolomide and Monomethyl Fumarate as a double combination and against the single treatments of X-irradiation, Temozolomide and Monomethyl Fumarate given either simultaneously or as a schedule (C). Statistical summary of the significant data following a one-way and two-way ANOVA test, with data comparisons not shown, not significant (D). Data shown is an average of three independent experiments \pm standard deviation. A one-way ANOVA with Bonferroni post testing was performed using GraphPad Prism 10.3.1 software, with p-values of values of $<0.05 = *$, $<0.01 = **$, $<0.001 = ***$ and $P < 0.0001 = ****$ reported as significant against the untreated control and the triple combinations (A, B). A two-way ANOVA with Bonferroni post-test was performed using GraphPad prism 10.3.1 software with P-values of $<0.05 = *$, $<0.01 = **$, $<0.001 = ***$ and $P < 0.0001 = ****$ reported as significant between the relative concentrations of the triple combination.

Figure 4.13 (A) shows the triple combination response when combined with 1Gy of X-irradiation, either simultaneously or with the MMF 4- hour pretreatment. Both combination treatment ranges provided a statistically significant reduction in clonogenic survival compared to the untreated control ($P < 0.0001$). At the lowest concentration of 250 μ M TMZ and 2.5 μ M MMF, with 1Gy of X-irradiation given as a schedule, provided a 51% reduction in clonogenic survival \pm 5%. The same combination when administered simultaneously gave a 67% reduction in clonogenic survival \pm 8%. A statistically significant reduction in clonogenic survival was shown between the simultaneous and scheduled combinations of 250 μ M TMZ and 2.5 μ M MMF ($P < 0.05$). At the second concentration of 350 μ M TMZ and 3.5 μ M MMF with 1Gy of X-irradiation a statistically significant reduction in clonogenic survival was shown between the scheduled triple combination which induced a 58% reduction in clonogenic survival \pm 1% compared to the simultaneously administered triple combination which induced a 73% reduction in clonogenic survival \pm 6% was achieved. The highest concentration of the combination with 450 μ M of TMZ and 4.5 μ M of MMF with 1Gy when given as a schedule gave 77% reduction in clonogenic survival \pm 1% and when administered simultaneously an 83% reduction in clonogenic survival was achieved \pm 9%, the differences in clonogenic survival were not calculated as significant ($P > 0.05$). Data suggests simultaneous administration to instigate a greater cytotoxic effect than the schedule when combined with 1Gy X-irradiation.

Figure 4.13 (B) shows the triple combination response when combined with 2Gy of X-irradiation, either simultaneously or with the MMF 4- hour pretreatment. Both combination treatment ranges provided a statistically significant reduction in clonogenic survival when compared to the untreated control ($P < 0.0001$). The highest concentration of the combination with 450 μ M of TMZ and 4.5 μ M of MMF with 2Gy when given as a schedule showed a 93% reduction in clonogenic survival \pm 6% and when administered simultaneously an 89% reduction in clonogenic survival was achieved \pm 4%. Differences between the scheduled and simultaneous administrations were not significant at all triple combination concentrations ($P > 0.05$).

Figure 4.13 (C) compares the double treatment combinations of TMZ and MMF, and the single treatments of TMZ, MMF and X-irradiation as single treatments to all triple combination administrations. At the lowest combination concentrations of 250 μ M TMZ and 2.5 μ M MMF the 1Gy triple combination showed a statistically significant reduction in clonogenic survival compared to 1Gy of X-irradiation as a single treatment, 250 μ M

TMZ, 2.5 μ M MMF, the double combination of T+M (250 μ M + 2.5 μ M) and compared to the scheduled double combination T+M (250 μ M + 2.5 μ M) PT4 (all, $P < 0.05$). A statistically significant reduction in clonogenic survival was also shown between 2Gy + T+M (250 μ M + 2.5 μ M) and single treatment 250 μ M TMZ, 2.5 μ M MMF, the double combination of T+M (250 μ M + 2.5 μ M) and compared to the scheduled double combination T+M (250 μ M + 2.5 μ M) PT4 (all, $P < 0.001$). The scheduled combination of 1Gy + T+M (250 μ M + 2.5 μ M) PT4 showed a statistically significant difference between cells exposed to 250 μ M TMZ, 2.5 μ M MMF and compared to the 2Gy triple combination of T+M (250 μ M + 2.5 μ M) PT4 (all, $P < 0.05$). The scheduled combination of 2Gy + T+M (250 μ M + 2.5 μ M) PT4 showed a statistically significant decrease in clonogenic survival between cells exposed to 250 μ M TMZ, 2.5 μ M MMF, the double combination of T+M (250 μ M + 2.5 μ M) and the scheduled double combination T+M (250 μ M + 2.5 μ M) (all, $P < 0.001$). Data suggests the simultaneous combination of 1Gy + 250 μ M TMZ and 2.5 μ M MMF to be synergistic over single and double treatments.

At the concentrations of 350 μ M TMZ and 3.5 μ M MMF, the 1Gy simultaneous triple combination induced a statistically significant reduction in clonogenic survival compared to 1Gy of X-irradiation, 3.5 μ M MMF, T+M (350 μ M + 3.5 μ M) and T+M PT4 (350 μ M + 3.5 μ M) (all, $P < 0.01$). The 2Gy triple simultaneously administered combinations provided a statistically significant reduction in clonogenic survival over 350 μ M TMZ, 3.5 μ M MMF, T+M (350 μ M + 3.5 μ M) and T+M PT4 (350 μ M + 3.5 μ M) (all $P < 0.01$). The scheduled triple combination of 1Gy + T+M PT4 (350 μ M + 3.5 μ M), showed a statistically significant reduction in clonogenic survival compared to 3.5 μ M MMF and 2Gy T+M (350 μ M + 3.5 μ M) (both, $P < 0.01$). The scheduled triple combination of 2Gy + T+M PT4 (350 μ M + 3.5 μ M), showed a statistically significant reduction in clonogenic survival compared to 350 μ M TMZ, 3.5 μ M MMF, T+M (350 μ M + 3.5 μ M) and T +M PT4 (350 μ M + 3.5 μ M) (all, $P < 0.05$). Data suggests the 2Gy scheduled triple combination to be synergistic over the double combinations but not X-irradiation.

The highest concentration combination of 450 μ M TMZ and 4.5 μ M MMF, provided a statistically significant reduction in clonogenic survival of 1Gy + T+M (450 μ M and 4.5 μ M) compared to 1Gy of X-irradiation, 4.5 μ M MMF and T+M (450 μ M and 4.5 μ M) (all, $P < 0.0001$). A statistically significant reduction in clonogenic survival was shown between 2Gy + T+M (450 μ M and 4.5 μ M) and single treatments, 2Gy of X-irradiation, 4.5 μ M MMF and double combination T+M (450 μ M and 4.5 μ M) (all $P < 0.001$).

Additionally, the scheduled triple combination of 1Gy + T+M PT4 (450 μ M and 4.5 μ M) showed a statistically significant reduction in clonogenic survival compared to 1Gy of X-irradiation, 4.5 μ M MMF, and double combination T+M PT4 (450 μ M and 4.5 μ M) ($P < 0.01$). The scheduled triple combination of 2Gy + T+M PT4 (450 μ M and 4.5 μ M) showed a statistically significant reduction in clonogenic survival compared to 2Gy of X-irradiation, 450 μ M TMZ, 4.5 μ M MMF, and double combination T+M PT4 (450 μ M and 4.5 μ M) (all, $P < 0.05$).

We hypothesised the triple combinations would elicit significant reductions in clonogenic survival when compared to the single and double combination treatments. However, this was not seen consistently across treatments and the hypothesis was rejected.

4.4.5 Combination Index Analysis of the simultaneous and scheduled administration of Temozolomide-Monomethyl fumarate and External beam X-irradiation in human Glioblastoma cell lines.

Similarly to Chapter 3 and Section 4.4.3, combination index analysis was applied to distinguish whether the combinations would be synergistic, antagonistic or additive. Due to the nature of combination index analysis, experimental data is shown as the line of fit calculated by Compusyn software. The software utilises the equations described in Section 2.9.

Due to the combination of TMZ and MMF showing synergy in Chapter 3, the triple combination was compared to the double combination for determination of the CIA. Triple combination CIA was not evaluated against the single treatments, as the addition of a third treatment must be better than the double treatment for clinical application. It was hypothesised that both scheduled and simultaneous triple combination treatments would be synergistic.

4.4.5.1 Combination Index Analysis of the Temozolomide-Monomethyl Fumarate combinations with External beam X-irradiation in the UVW human glioblastoma cell line.

Figure 4.14 shows the combination index analysis and line of fit for the UVW cell line after treatment with Temozolomide and Monomethyl Fumarate with both 1Gy and 2Gy of external beam X-irradiation given simultaneously or as a MMF 4-hour pretreatment (PT4). The combination index analysis was calculated using Compusyn software with fraction affected calculated from Figure 4.13. The triple combinations were compared to the double combinations of Temozolomide and Monomethyl Fumarate either simultaneously or scheduled. This allows for the detection of a synergistic triple combination, only if it exceeds the combined effect of the double combination.

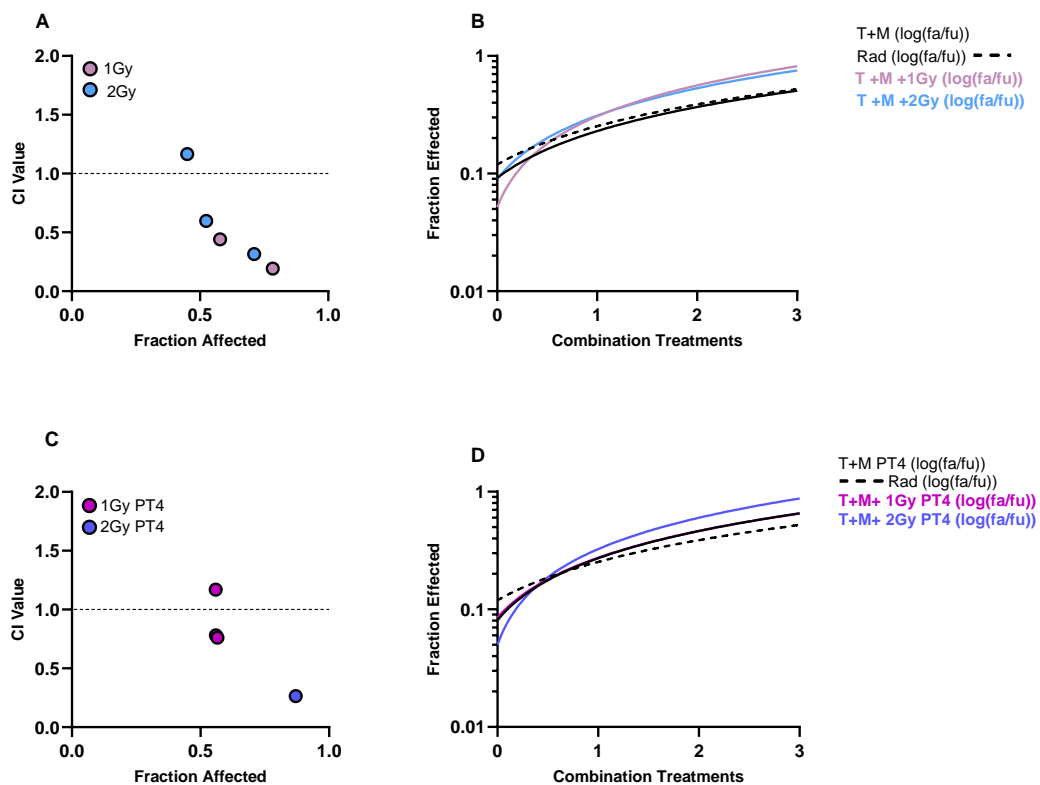


Figure 4.14: Combination index analysis of the Temozolomide-Monomethyl Fumarate combination with either 1Gy or 2Gy of X-irradiation, administered simultaneously or as a 4- hour pretreatment schedule of Monomethyl Fumarate in UVW human glioblastoma cells. Combination index values and associated fraction affected for each dose in the Temozolomide-Monomethyl Fumarate with External beam X-

irradiation combinations given by simultaneous combination (A) or scheduled combination (C). Combination index values, with the dotted line representing the line of additivity with $CI < 0.9$ showing synergism and $CI > 1.1$ antagonistic (A and C). Line of best fit from single and combination dose response curves (B and D).

Figure 4.14 presents the combination index analysis (CIA) results for TMZ and MMF combinations with X-irradiation in UVW cells. In Figure 4.14 (A), simultaneous administration of TMZ and MMF with 1 Gy and 2 Gy X-irradiation showed synergy at the higher combinations (29.5 μ M TMZ + 4.05 μ M MMF and 44.32 μ M TMZ + 6.07 μ M MMF) ($CI < 0.9$). The lowest combination (19.7 μ M TMZ + 2.7 μ M MMF with 1 Gy) was antagonistic ($CI > 1.1$), with a CIA value of 11.77 (not shown in the figure).

Figure 4.14 (C) shows that scheduled administration also resulted in synergistic combinations for 2Gy exposure with 29.5 μ M TMZ + 4.05 μ M MMF and 44.32 μ M TMZ + 6.07 μ M MMF ($CI < 0.9$), and for 1Gy exposure at 29.5 μ M TMZ + 4.05 μ M MMF. However, the lowest and highest scheduled combinations with 1Gy were antagonistic, with the 19.7 μ M TMZ + 2.7 μ M MMF + 1Gy combination yielding a CIA value of 42.8 (not shown).

In the log (F_a/F_u) analysis, simultaneous combinations exhibited a greater fraction affected (F_a) than TMZ+MMF alone and X-irradiation alone (Figure 4.14 (B)). R^2 values were 0.92, 0.98, 0.87, and 0.83 for TMZ+MMF, X-irradiation, and the 1Gy and 2Gy combinations respectively, indicating good model reliability. Scheduled administration (Figure 4.14 (D)) showed a clear separation for the 2Gy combinations but not for the 1Gy combinations, with R^2 values of 0.89, 0.98, 0.84, and 0.96 respectively, also indicating good model reliability.

Overall, the data suggest that in the UVW cell line, the triple combination of TMZ, MMF, and X-irradiation induced synergy following both simultaneous and scheduled administration, supporting the hypothesis.

4.4.5.2 Combination Index Analysis of the Temozolomide-Monomethyl Fumarate combinations with External beam X-irradiation in the U87 human glioblastoma cell line.

Figure 4.15 shows the combination index analysis and line of fit for the U87 cell line with Temozolomide and Monomethyl Fumarate with both 1Gy and 2Gy of external beam X-irradiation given simultaneously or as a MMF 4-hour pretreatment (PT4). The combination index analysis was calculated using Compusyn software with fraction affected calculated from Figure 4.12. The triple combinations were compared to the double combinations of Temozolomide and Monomethyl Fumarate either simultaneously or scheduled. This allows for the detection of a synergistic triple combination, only if it exceeds the combined effect of the double combination.

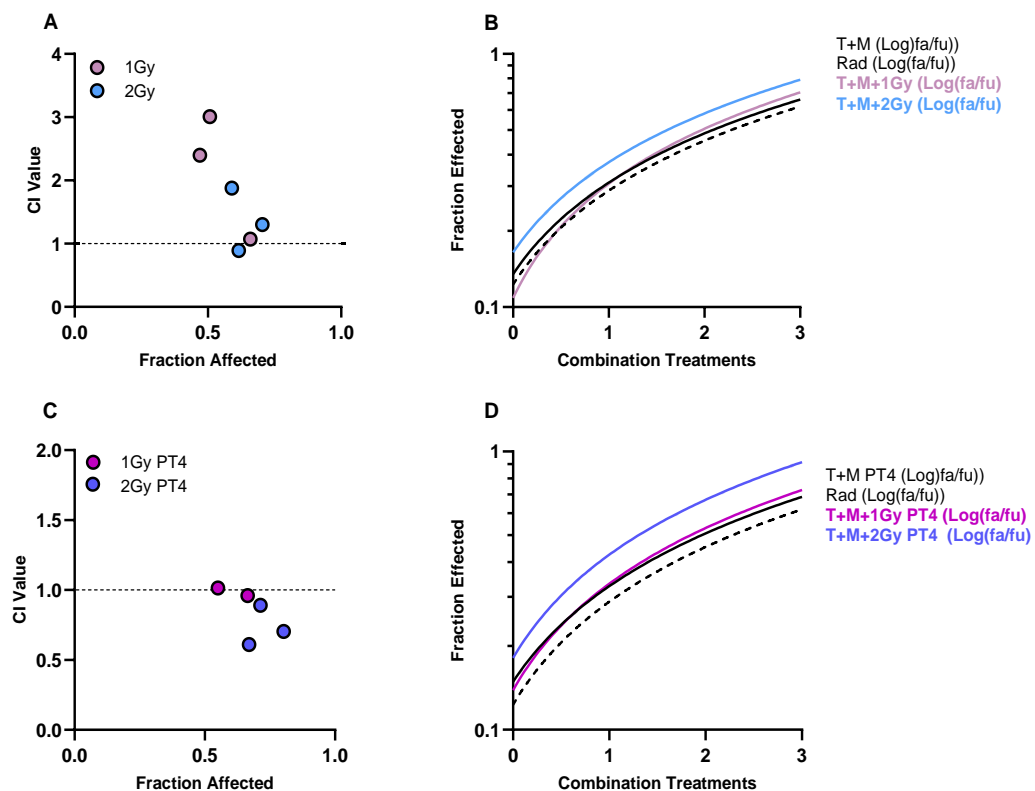


Figure 4.15: Combination index analysis of the Temozolomide-Monomethyl Fumarate combination with either 1Gy or 2Gy of RT, administered simultaneously or as a 4-hour pretreatment schedule of Monomethyl Fumarate in U87 human glioblastoma cells. Combination index values and associated fraction affected for each dose in the Temozolomide-Monomethyl Fumarate with External beam X-irradiation combinations

given by simultaneous combination (A) or scheduled combination (C). Combination index values, with the dotted line representing the line of additivity with $CI < 0.9$ showing synergism and $CI > 1.1$ antagonistic (A and C). Line of best fit from single and scheduled combination dose response curves (B and D).

Figure 4.15 presents the combination index analysis (CIA) results for TMZ and MMF combinations with X-irradiation in T98G cells. In Figure 4.15 (A), simultaneous administration of TMZ and MMF combined with 1 Gy X-irradiation showed no synergistic interactions, with all combinations being antagonistic ($CI > 1.1$). For 2 Gy X-irradiation, only the lowest concentration combination (1 μ M TMZ + 1 μ M MMF) showed synergy ($CI < 0.9$), while higher concentration combinations were antagonistic ($CI > 1.1$).

Scheduled administration (Figure 4.15 (C)) showed synergy for the 3.6 μ M TMZ + 4.2 μ M MMF combination with 1Gy ($CI < 0.9$), while the lower two combinations were antagonistic, with the CIA value for the 2.4 μ M TMZ + 2.8 μ M MMF + 1Gy combination calculated at 5.3 (not shown). With 2Gy X-irradiation, all three scheduled combinations were synergistic ($CI < 0.9$).

Log (Fa/Fu) analysis showed that, under simultaneous administration, the 2Gy combination line exhibited a greater fraction affected (Fa) than TMZ+MMF and X-irradiation alone (Figure 4.15 (B)). However, R^2 values were low (0.71, 0.69, 0.82, and 0.69 for TMZ+MMF, X-irradiation, 1Gy, and 2Gy combinations respectively), indicating low reliability of the CIA for the 2Gy simultaneous data.

For scheduled administration (Figure 4.15 (D)), a distinguishable line was observed for the 2Gy combinations but not for the 1Gy combinations. R^2 values were similarly low (0.67, 0.69, 0.73, and 0.73), again suggesting limited reliability. Nevertheless, the observed synergy aligns with the findings in Section 4.4.6.2, where the 2Gy scheduled triple combination elicited the greatest cytotoxic effect.

Overall, while CIA data reliability was limited, the results suggest that scheduled administration of TMZ and MMF combined with 2Gy X-irradiation enhanced cytotoxicity, supporting the hypothesis.

4.4.5.3 Combination Index Analysis of the Temozolomide-Monomethyl Fumarate combinations with External beam X-irradiation in the T98g human glioblastoma cell line.

Figure 4.16 shows the combination index analysis and line of fit for the T98g cell line with Temozolomide and Monomethyl Fumarate with both 1Gy and 2Gy of external beam X-irradiation given simultaneously or as a MMF 4-hour pretreatment (PT4). The combination index analysis was calculated using Compusyn software with fraction affected calculated from Figure 4.13. The triple combinations were compared to the double combinations of Temozolomide and Monomethyl Fumarate either simultaneously or scheduled. This allows for the detection of a synergistic triple combination, only if it exceeds the combined effect of the double combination.

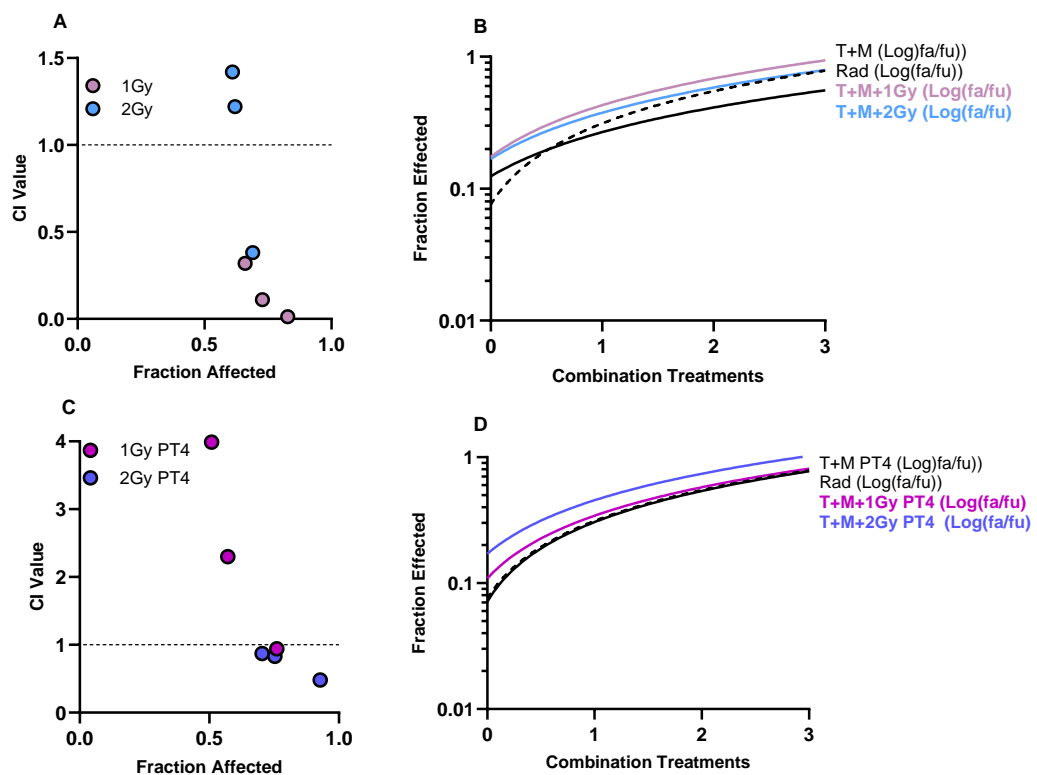


Figure 4.16: Combination index analysis of the Temozolomide-Monomethyl Fumarate combination with either 1Gy or 2Gy of X-irradiation, administered simultaneously or as a 4- hour pretreatment schedule of Monomethyl Fumarate in T98g human glioblastoma cells. Combination index values and associated fraction affected for each dose in the Temozolomide-Monomethyl Fumarate with External beam X-

irradiation combinations given by simultaneous combination (A) or scheduled combination (C). Combination index values, with the dotted line representing the line of additivity with $CI < 0.9$ showing synergism and $CI > 1.1$ antagonistic (A and C). Line of best fit from single and scheduled combination dose response curves (B and D).

Figure 4.16 presents the combination index analysis (CIA) results for triple combinations of TMZ, MMF, and X-irradiation in T98G cells. In Figure 4.16 (A), simultaneous administration of triple combinations with 1Gy resulted in synergy across all concentrations ($CI < 0.9$), whereas for 2Gy, only the highest combination (450 μ M TMZ + 4.5 μ M MMF + 2Gy) was synergistic ($CI < 1.1$).

Figure 4.16 (B) shows the fraction affected over unaffected (F_a/F_u) for the triple combinations compared to the double combination (T+M) and X-irradiation alone. The 1Gy triple combination curve showed a distinguishably greater fraction affected compared to X-irradiation and the T+M double combination. R^2 values were 0.62, 0.93, 0.76, and 0.69 for T+M, X-irradiation, T+M+1Gy, and T+M+2Gy respectively, suggesting moderate reliability of the CIA model but room for improvement, particularly for the combination lines.

In Figure 4.16 (C), scheduled administration of the triple combinations showed that only the highest 1 Gy triple combination (450 μ M TMZ + 4.5 μ M MMF + 1Gy PT4) was synergistic ($CI < 0.9$), with lower doses being antagonistic ($CI > 1.1$). In contrast, all scheduled 2Gy triple combinations were synergistic ($CI < 0.9$).

Figure 4.16 (D) further illustrates this, where the T+M+2Gy PT4 fraction affected curve is clearly distinguishable from the T+M PT4 and X-irradiation curves. R^2 values of 0.93, 0.93, 0.86, and 0.80 were calculated for T+M, X-irradiation, T+M+1Gy PT4, and T+M+2Gy PT4 respectively, indicating good reliability of the CIA model.

Thus, data suggests triple combinations with 2Gy to be synergistic when scheduled but 1Gy triple combinations to be synergistic when simultaneous, both in a dose dependent manner over the double combinations and X-irradiation alone.

Collectively across all three cell lines, the 2Gy scheduled triple combinations were synergistic over X-irradiation and the double combinations of TMZ + MMF at the highest concentrations, suggesting further investigations with these concentrations for future studies.

4.5 Discussion

The purpose of this chapter was to determine whether the combination of External beam X-irradiation with Temozolomide and Monomethyl Fumarate looked promising as a future treatment for Glioblastoma. Due to the increased synergy seen in Chapter 3 when combining MMF and TMZ across the three cell lines, we planned to determine if double combinations of MMF- X-irradiation and TMZ- X-irradiation would be synergistic as double combinations before utilising all three treatments for a triple combination. Due to therapy resistance within patients which is difficult to overcome because of GBM heterogeneity, enhancing the current standards of care with a third treatment option could in the first instance increase the cytotoxicity of the treatments, leaving fewer cancerous cells behind and slow the evolution of therapy resistance. Additionally, utilising a third treatment option may have additional benefits, which for MMF has been seen in Chapter 3. From our data it appears that MMF may have a previously not recorded cytotoxic effect on glioma cancer cells as when administered as a single treatment, MMF caused significant DNA damage (Section 3.4.8). DNA damage caused by MMF was especially shown in the MGMT positive T98g cells, showing some mechanisms independent to our hypothesised mode of action- depletion of glutathione. We aimed in this chapter to assess the cytotoxic response of double combinations of X-irradiation with either TMZ or MMF. We then scheduled the MMF treatments to assess if lower GSH levels - which was demonstrated in Chapter 3 - would increase the cytotoxicity of X-irradiation. Using both scheduled and simultaneous administration we administered the triple combination of treatments and evaluated if any double or triple combinations provided synergy.

4.5.1 Cytotoxic effect of External beam X-irradiation on the human Glioblastoma cell lines

Clonogenic assays were performed by exposing cells to a dose range of X-irradiation from 0.5Gy to 8Gy in all three cell lines. This allowed a single treatment response of the cells to X-irradiation to be evaluated, with each cell line having a different ED_{50} . Unsurprisingly the MGMT positive T98g cell line was most radioresistant with an ED_{50} of 3.2Gy. MGMT positive cells have shown in the literature to contribute to

radioresistance by maintaining genomic stability after radiation induced DNA damage (Brennan *et al.*, 2013; Yun *et al.*, 2024). Both MGMT negative cell lines had varying ED₅₀'s with UVW being 2.4Gy and U87's 1.6Gy. Compared to previous data on these cell lines the T98g cell line responded exactly as expected (Scott, 2020), whereas the UVW cell line was previously shown to have an ED₅₀ of 3.1Gy (Scott, 2020). The U87 cell line is known to be moderately radiosensitive as found in the literature with an ED₅₀ ~ 2Gy (Oancea-Castillo *et al.*, 2017). All three cell lines demonstrated dose hypersensitivity, a common phenomenon in GBM where disproportional levels of cell death occur at lower doses, a useful characteristic when aiming to reduce radioresistance and patient toxicity (Enns *et al.*, 2004).

4.5.2 X-irradiation double combination cytotoxicity and synergy

The data obtained regarding the glioma cells lines response to X-irradiation enabled the design of the double combination. 1Gy was used in combination with TMZ and MMF because we wanted to assess if lower doses of X-irradiation could be successfully combined with TMZ and MMF, reducing the total exposure of patients to chemo-radiotherapy. Additionally, the cell lines showed hypersensitivity and may have an increased cytotoxic response with 1Gy doses. With 2Gy fractions of radiation being utilised clinically, 2Gy was taken as a second X-irradiation dose combination with TMZ and MMF. The concentrations of TMZ and MMF utilised in the combinations were taken from Chapter 3, as these concentrations when administered as a double combination provided synergy in at least 2 of the combinations across all three cell lines.

The double combination of TMZ with X-irradiation at 1Gy and 2Gy in the UVW cell line (Figure 4.2) resulted in a dose dependent reduction in survival fraction when compared to TMZ alone for both the TMZ + 1Gy and TMZ + 2Gy combinations at the lowest concentration of 19.7µM TMZ. The 1Gy double combination at this concentration of TMZ was also significantly different to the 2Gy double combination survival fraction, with the 2Gy combination have a greater reduction in clonogenic viability than the 1Gy combination. However, the combination was not significant when compared to X-irradiation alone at either 1Gy or 2Gy and significant differences in the double combinations to X-irradiation alone was only seen at the highest

concentration combination of 44.32 μ M TMZ + 2Gy when compared to 2Gy alone. Additionally, the CIA determined no TMZ- X-irradiation combination was synergistic, with X-irradiation as a single treatment having a greater cytotoxic effect. As TMZ and X-irradiation would be expected to show synergy, it's possible that compared to the literature we are administering too low a dose of TMZ for the synergistic effect to be clear. Additionally, in MGMT negative cells, the combination of both TMZ and X-irradiation shows greater cytotoxicity when TMZ is given after radiation (Chakravarti *et al.*, 2006). For future work, analysis of an adjuvant TMZ schedule and doses administered may provide more synergy in the double combination.

Relative to the lack of synergy in MGMT negative UVW cells, the U87 cell line (Figure 4.4) showed a significant reduction in clonogenic survival of the U87 TMZ- X-irradiation combinations at 2Gy compared to TMZ alone and the relative 1Gy combinations but not 2Gy of X-irradiation. This translated into the CIA, where the higher concentrations of TMZ when combined with 2Gy of X-irradiation showed synergy, as did the highest 1Gy combination of 3.6 μ M TMZ +1Gy. This suggests the lack of synergy not seen in the UVW cell line may be due to the higher ED₅₀ of the cell line to X-irradiation. The MGMT positive T98g cell line as expected showed no synergy with any of the combinations with either 1Gy or 2Gy of X-irradiation across the TMZ concentration range. A response also shown in the literature, where TMZ and radiation combinations were additive and schedule dependent (Chalmers *et al.*, 2009 (Figure 4.6). As MGMT positive cells have the ability to repair DNA damage induced by TMZ, the cells are suggested to show resistance to the double combination as cellular redox pathways as well as DNA damage response pathways would be activated due to cross talk with other DNA repair pathways (Chalmers *et al.*, 2009; Toulany, 2016).

MMF as a single treatment as discussed in Chapter 3 had a significant cytotoxic response as a single therapy, which was unexpected as there is limited literature on MMF's effect on GBM to determine how MMF is causing the cytotoxicity. Levels of GSH, Nrf2, NF- κ B and Keap1, has been shown to be depleted after DMF exposure and have also been seen to have a role in apoptosis as well as DNA damage through increased oxidative stress, (Morito *et al.*, 2003). Therefore, with MMF being the direct metabolite of DMF, it suggests that MMF may also be causing DNA damage and an increased apoptotic response as a single treatment (Saidu *et al.*, 2019). We were therefore interested to evaluate how the combination of MMF, a reactive oxygen

species reducer via GSH depletion would combine with X-irradiation as we hypothesised that MMF would enhance the cytotoxic effect of X-irradiation when combined.

When applied simultaneously to the UVW cell line (Figure 4.3), as the concentrations of MMF increased the reduction in clonogenic survival decreased with the 1Gy and 2Gy combinations. This suggests as the concentration of MMF increased as did its antioxidant response when combined with X-irradiation. The protective response of MMF on astrocytes has been shown in the literature, where dose dependent protection of the cells to H₂O₂ was seen (Linker *et al.*, 2011). MMF as discussed is able to induce the antioxidant pathway, eliminate ROS and detoxify cells, a response of MMF suggested by our results with the double combination (Saidu *et al.*, 2018). Compared to MMF alone at 6.07µM, the combination of 6.07µM MMF with 2Gy provided similar survival fractions, clearly showing the combined use of the drugs to be antagonistic as also shown from the CIA (CI>1) (Figure 4.3 (F and G)).

In the more radiosensitive U87 cell line, the combination of MMF with 1Gy or 2Gy of X-irradiation reduced clonogenic survival in a dose dependent manner (Figure 4.5). The 4.2µM MMF combination with 2Gy induced a statistically significant reduction in clonogenic survival over MMF alone (P<0.01) but not X-irradiation and from the CIA an adaptive response was shown, implying the double combination does not work better than the single treatments (Figure 4.5 (F and G)). Similarly, the 1Gy combination with 4.2µM of MMF also showed an additive response after the CIA, suggesting the combination does not work better than the single treatments. Possibly increasing the MMF concentrations may provide a synergistic combination if the cytotoxic response is also increased for the double combination and does not rebound survival like the UVW cell line. As literature would suggest, increasing MMF concentrations could lead to a dose-dependent protection of the cell survival to the ROS produced by X-irradiation (Linker *et al.*, 2011). From this future work would suggest increasing the concentrations to see how the cell line responds to MMF and X-irradiation at higher MMF concentrations. Similarly to both the UVW and U87 cell line, the combination of MMF and X-irradiation in the T98g cell line provided no synergistic response, with the 2Gy combinations having higher CI values than the 1Gy combinations (Figure 4.7). This suggests the MMF protective response on the T98g cell line to the ROS was produced by X-irradiation (Linker *et al.*, 2011). Further to this, compared to MMF alone at each relative concentration, the combination with

2Gy had a greater survival fraction, showing again this dose dependent protection of MMF when combined with a treatment that promotes detoxification against ROS.

4.5.3 Scheduled treatments of Monomethyl Fumarate with X-irradiation

As the antagonistic effect of MMF when combined with X-irradiation was clearly shown in all three cell lines, the utilisation of our previous scheduling method used in Chapter 3 was applied. Data from Chapter 3 showed glutathione levels in all three cell lines to decrease after 4- hours of MMF treatment (Section 3.4.5). As the literature has shown (Linker *et al.*, 2011) as well as our data from simultaneous double combinations of MMF with X-irradiation, the protective detoxification mechanisms of MMF are thought to be activated when cells are exposed to oxidative stress in a dose dependent manner (Linker *et al.*, 2011; Saidu *et al.*, 2019). By scheduling a pretreatment of MMF, the decrease in glutathione levels may allow an increased radiation induced cell death, as the antioxidant levels would be lower allowing greater ROS levels to elicit an effect. A study done in 1991, showed DMF at 5 μ M to radiosensitise hamster hypoxic V79 cells to irradiation when DMF was given before irradiation or after irradiation (Held *et al.*, 1991). This would suggest the 4h MMF pretreatment to also sensitise cells to X-irradiation as hypothesised.

The schedule of MMF as a 4- hour pretreatment before exposure to either 1Gy or 2Gy of X-irradiation in the UVW cell line, surprisingly did not enhance the radio-cytotoxic cell death. With no significant reduction in clonogenic survival observed for any scheduled combination compared to MMF alone, or X-irradiation alone, or the simultaneous administrations (Figure 4.16 and Figure 4.19). All scheduled combinations were shown as antagonistic and similarly to the simultaneous administration, cell survival began to increase with the 2Gy combinations as concentrations of MMF increased compared to the initial reduction in clonogenic survival seen after exposure to 2.7 μ M of MMF and 2Gy X-irradiation. The 1Gy combination when given as a schedule, induced a greater reduction in clonogenic survival than the 2Gy combinations, however not over the simultaneous 1Gy combinations. This suggests the insult of ROS at higher doses of radiation to be too high that the antioxidant system was further upregulated to retain homeostasis of the cell. In cancer cells GSH is overproduced and reducing GSH alone, increases ROS

leading to cancer cell death (Yoo *et al.*, 2019). However, combining GSH depletion with an increased production of ROS from X-irradiation, suggests the cancer cells are working harder to maintain their elevated GSH levels. Contrastingly to this however, much literature has shown depletion of GSH or its reduced form Glutathione disulphide (GSSG), to sensitise various cancer cell lines to X-irradiation (Yoo *et al.*, 2019; Zhao *et al.*, 2009). Further to this a study by Oleinick *et al.*, (1988) also showed GSH depletion for 4-hours post-irradiation on A549 cancer cells, prevented DNA-protein cross link and therefore DNA damage is less repaired after X-irradiation and cells undergo cell death. This would therefore suggest that for double combinations of MMF with X-irradiation, further scheduling techniques are required to determine the optimum schedule for the two treatments. Additionally future mechanistic assays on DNA damage and repair would be useful to assess how MMF is interacting with ROS, as MMF at these concentrations as a single treatment in chapter 3, was shown to induce DNA damage. With a lack of literature to demonstrate the effect of MMF and X-irradiation in GBM, further glutathione assays and further methods to assess in more detail what is happening in the GSH pathways would need to be performed to determine how the two treatments are interacting.

Conversely, in the U87 cell line, the scheduled response of 1Gy and 2Gy MMF combinations induced synergy at all 2Gy combinations and at the 1 μ M MMF combination with 1Gy of X-irradiation (Figure 4.17 and 4.20). Both the simultaneous and scheduled combinations of MMF and 1Gy showed similar cytotoxic effects at the 1 μ M MMF combination with the schedule eliciting only 5% greater reduction in clonogenic survival. As the concentrations of MMF increased however, the reduction in clonogenic survival for the scheduled treatments increased by 2%, whereas with the simultaneous administration reduction in clonogenic survival increased by 16%. This suggests a similar response of the U87 cells to the UVW pretreated cells at the lower dose of X-irradiation, where reduction in clonogenic survival reduces as concentrations increase (survival increasing). With the 2Gy scheduled combination we observed a statistically significant reduction in clonogenic survival of the combination to both the simultaneous and scheduled 1Gy combinations at all relative MMF concentrations compared to the untreated control. As the 2Gy schedule was determined to be synergistic and is shown as the most cytotoxic, the dose dependent increase in clonogenic survival did not occur as it did with the 1Gy schedule. As the U87 cell line was more radiosensitive, again it suggests that the level of radiosensitivity of the cell line is important to the effect of the MMF – X-irradiation

combination. This is further confirmed by the T98g cell line, where no synergistic scheduled combinations were found. T98g as the most radioresistant cell line observed a greater decrease in the reduction of clonogenic survival as the 1Gy scheduled combination increased cell survival by 12% between 2.5 μ M MMF and 3.5 μ M MMF. The simultaneously administered 1Gy combinations induced a dose response curve, suggesting again that the increased depletion of GSH results in a greater rebound of cell survival when radiation was administered to maintain cell homeostasis. This is also observed with the 2Gy combinations where the simultaneous combinations elicit a greater reduction in clonogenic survival than the scheduled and at the highest concentration of 4.5 μ M we see a similar reduction in clonogenic survival with a 3% difference (Figure 4.10). As the U87 cell line is the most responsive to the MMF-X-irradiation combination, it supports the literature as the U87 cell line has been suggested in the literature to have lower basal levels of GSH, and lowering GSH by MMF, prevents the U87 cell line from neutralising ROS, unlike the T98g cell line which has higher basal levels of GSH and is less susceptible to ROS (Agnihotri *et al.*, 2016; Jin *et al.*, 2015; Miki *et al.*, 2024). Data from our untreated control GSH levels (Figure 3.8 (B)) also showed in our cell lines, a higher total GSH in the T98g cell line and a lower total GSH in the U87 cell line, supporting literature findings.

The scheduled combination data suggests no benefit of 4-hour pretreatment scheduling of MMF treatment before X-irradiation as synergy was only seen in the U87 cell line. As GBM tumours are highly heterogeneous, further in-depth analysis of MMF's effect on the rebound of the antioxidant pathway would be required to determine how to best utilise the treatments. This could be done by observing the change in GSH levels after administration of both schedules, either via RT-qPCR or western blot. Other antioxidant pathways should also be investigated such as the ARE proteins, after administration to determine how clonogenic reduction is reducing as concentrations increase of the combinations.

4.5.4 Triple combination evaluation and synergy

As the U87 cell line was the only cell line to show synergy with the double combinations, possibly due to its increased radiosensitivity, the triple combination of

Temozolomide, Monomethyl Fumarate and X-irradiation was administered and evaluated through clonogenic assay. To determine if a triple combination would induce greater levels of cytotoxicity, the triple combination was compared to its relative double combination of TMZ and MMF.

The triple combination in the UVW cell line showed synergy of the combinations for both 1Gy and 2Gy combinations and as both simultaneous and scheduled treatments (Figure 4.11). The triple combinations at 1Gy showed a greater reduction in clonogenic survival when administered simultaneously at the highest concentration combination compared to the scheduled treatment. With the 2Gy triple combinations, the scheduled 2Gy combination had an increased reduction in clonogenic survival relative to the simultaneous administration at the highest combination concentration (Figure 4.11). Although at the highest concentration the 2Gy PT4 combination showed the greatest reduction in clonogenic survival, the large error bars prevent this from being deemed statistically significant compared to the other treatment groups aside from T+M ($P < 0.05$). Surprisingly across the treatment groups dissimilar to the double combinations no increases in clonogenic survival were seen as the concentrations or doses of the treatments increased, a response seen previously in the double combinations. This suggests the addition of X-irradiation to the double combination overwhelms the cells with ROS, oxidative stress and DNA damage, enough for cell death to occur. This data is supported by the study by Saidu *et al.*, (2018) which suggested when looking at DMF, increased concentrations of DMF induced oxidative stress and cell death. However, the study also contradicts the findings of the double combinations, where only the U87 cell line showed synergy when MMF was scheduled with X-irradiation. Although the concentrations of MMF are not increasing between the double and triple combinations of X-irradiation, the addition of both TMZ, MMF and X-irradiation could be initiating enough damage that the cells are unable to repair. The lack of literature on the effect of MMF, TMZ and X-irradiation prevents any conclusive theory behind this cell death to be confirmed. However, interrogation of the mechanisms as well as the pathways thought to be involved in the cell death process would aid in elucidating the mechanisms underpinning the effect seen with the triple combination. Additionally, although the 2Gy scheduled combination initiates the greatest reduction in clonogenic survival compared to all treatment groups, the simultaneous treatment groups were found to have more synergistic combinations when compared to the scheduled combinations (Figure 4.14). Thus, this implies for triple combination therapies, the scheduling of treatments is unnecessary. It also

further implies that the scheduling of the treatments may need to be changed for the triple combination, with the literature previously showing, DMF post X-irradiation to be beneficial in causing cell death (Held *et al.*, 1991). Additionally, TMZ has also shown greater cytotoxicity when TMZ is given after radiation (Chakravarti *et al.*, 2006). This therefore suggests that a schedule of X-irradiation, followed by MMF for 4h and then TMZ may induce greater cytotoxicity.

The U87 cell line which was most responsive to the double combinations of MMF with X-irradiation, showed no difference in the 1Gy triple combinations between the scheduled and simultaneous administration. With the 2Gy schedule we seen an increased cytotoxicity significant over T+M and T+M PT4 at the highest concentration of 3.6 μ m TMZ and 4.2 μ m MMF. Additionally, all three scheduled 2Gy triple combinations were synergistic with only 1 combination of the 2Gy triple combination when simultaneous shown as synergistic. This supports our hypothesis that a scheduled triple combination would have an increased cytotoxic effect compared to the simultaneous administration (Figure 4.12 and 4.15). The 1Gy triple combinations when given either as a schedule or simultaneously provide limited synergy with only 1 schedule combination with 1Gy providing synergy, compared to the double combinations. Again, this suggest with the triple insult, the cells are less likely to be able to survive, with the lowered GSH levels after 4 hour making the cells more susceptible to the damage of TMZ and X-irradiation.

The T98g cell line, which has shown no synergy in the double combinations, surprisingly was susceptible to the triple combination with increased cytotoxic response and synergy (Figure 4.13 and 4.16). At the lower concentration 1Gy triple combinations the simultaneous administration was shown to be better than the schedule with an increased reduction in clonogenic survival at all concentrations and all points being synergistic. The scheduled 1Gy triple combination only provided synergy at the highest combination and were shown as increasingly antagonistic as the concentration range lowered. Between the 2Gy administrations of the triple combination, little difference in cytotoxicity was observed however compared to the relative double combination, the 2Gy scheduled treatment was shown to be synergistic at all concentrations, whereas when simultaneous only 1 combination was synergistic compared to the double combination. The data in Figure 4.13 and 4.16 shows all three components of TMZ, MMF and X-irradiation to be required for an increased cytotoxic response. The T98g cell line was most responsive to the MMF-

TMZ double combination and by addition of X-irradiation, this suggests the cellular redox pathways as well as DNA damage response pathways which would be activated due to cross talk were overwhelmed by the insult of X-irradiation (Chalmers *et al.*, 2009; Toulany, 2016; Gouws and Pretorius, 2011). With the 1Gy triple combination showing more synergy when simultaneously administered, it does support previous discussion of the schedule at lower doses of X-irradiation, activating the cells cellular defence mechanisms at a quicker rate. A possible mechanism not seen with the 2Gy schedule as the insult initiated after GSH depletion is too much for the cell.

Overall, the data has supported our hypothesis of a triple combination being synergistic irrespective of MGMT status as this has been proven in all three cell lines. However, for the triple combination to be progressed to murine models or clinical trial, the mechanism behind the increasing cell survival with the double combinations, must be investigated as at lower doses of X-irradiation the simultaneous administration has shown to be more synergistic in the UVW and T98g cell line. Conversely at the higher dose of X-irradiation the schedule has shown to be more synergistic than the simultaneous administration in all three cell lines. Additionally, for the progression of the triple combinations, it would be beneficial in future work to establish a radioresistant colonised population of the U87 cell line and to apply the triple combination to this cell line to assess the response on cell survival, as this would represent the population of patients who have built up radioresistance and are the least susceptible to treatment options. Different scheduling time points such as TMZ+MMF 24 hours after X-irradiation could also be useful as TMZ in patients clinically is often given after radiotherapy.

4.6 Conclusions

Data collected in Chapter 4, has proven the potential of combining Monomethyl fumarate with the standard of care, Temozolomide and external beam radiotherapy, although this requires further work and interrogation. By addition of this triple treatment, the cytotoxic response was increased compared to the double combinations, as well as safe use of combining a lower dose of X-irradiation. Synergy was observed across all three cell lines in the triple combinations, despite varying

levels of synergy and cytotoxicity when the double combinations with X-irradiation were evaluated.

The increased reduction in clonogenic survival from the triple combination is thought to be through an influx of DNA damage too severe for the cell to repair. With MMF as a single treatment inducing toxicity in the cell lines, when combining with these other treatments in specific schedules the drug is also able to sensitise cells to TMZ damage more so than radiation. As with the radiation double combinations with MMF, we found that both MMF and X-irradiation worked antagonistically in the UVW and T98g cell line. The variability between scheduling the triple treatments and the X-irradiation dose in the three cell lines, prevents any definite conclusive remarks on the triple combination and although the data supports our hypothesis, further experimentation is required to dissect the cause behind the variation.

To fully evaluate the triple combinations, alternative scheduling techniques should be trialled to find a schedule that is consistently more synergistic. This is important, as although we are seeing synergy at some triple combinations, we are also seeing antagonistic responses. This suggests the combination could improve and ultimately is important to pin down as patient response to the triple combination will vary from 2D culture and it would be important to ensure a clearer synergistic drug interaction trend. Weaknesses of this chapter were the lack of mechanistic interrogation as well as ROS assays, as both are important to understand how the triple combinations are working. Once the X-irradiator becomes available these assays will be completed before publication.

Data is suggestive of repurposed Monomethyl Fumarate being an important and promising treatment option for combined use with the standard of care in GBM patients.

Chapter 5

Assessing the effects of combination therapies using Temozolomide and Monomethyl Fumarate on three-dimensional spheroid models of Human Glioblastoma

5.1 Introduction

Due to the vast heterogeneity within GBM, progression of treatment options has been limited, as much preclinical testing relies on 2D cell culture, a model which does not directly represent the GBM environment. *In Vitro* 2D cell culture models are a useful tool for initial preliminary testing, however 2D models poorly translate into *in vivo* models due to the differences in cell growth rate, lack of extracellular matrix interactions, lack of hypoxic environments and oncogenic signalling (Barbosa *et al.*, 2021; Paolillo *et al.*, 2021). 2D cell culture utilises an oxygen tension of 20% whereas *in vivo* GBM oxygen tension ranges from 0.1-10%, creating a more resistant environment for the treatments to overcome. The poor translation from 2D to *in vivo* models results in ~90% of treatment trials failing to reach clinical use (Musah-Eroje and Watson, 2019).

An intermediate 3D model for GBM is now extensively used as a research tool to trial candidate drugs before moving to *in vivo* models. These models which grow in 3D *in vitro* cell culture systems, have cell-cell interactions and have shown to achieve hypoxic cores which allows for some replication of a tumour microenvironment (Musah-Eroje and Watson, 2019). These 3D models include spheroids, neurospheres, organoids, tumoroids, scaffolds and explant culture (Pape *et al.*, 2021)

Spheroid models can mimic aspects of the tumour microenvironment such as an oxygen gradient, the presence of a hypoxic core, nutrient gradient and pH gradient as shown in Figure 5.1 (Pape *et al.*, 2021). Although the spheroid models create a hurdle for candidate treatments to overcome before being moved to *in vivo*, they still don't account for the extracellular matrix, immune reaction and varied cell populations. Therefore, treatments which do exhibit a good response in 3D models would still need

to be trialled *in vivo* before moving to clinic. 3D spheroid models are, however, incredibly useful as they act as a tumour mimic meaning that there are less animals sacrificed in *in vivo* studies since the factors mentioned above can be assessed more thoroughly, in comparison to the 2D model (Pape *et al.*, 2021; Barbosa *et al.*, 2021).

To further investigate the combinations of Temozolomide (TMZ) and Monomethyl Fumarate (MMF), the treatments were applied in 3D spheroid models along with external beam X-irradiation. Glioblastoma multicellular spheroids were grown in spinner flasks, where the free-floating single cell suspensions were cultured with a magnetic rotating rod to allow the clustering of cells into a spheroid (Paolillo *et al.*, 2021). Spheroid structures are composed of layers with a hypoxic core formation once the spheroid reaches around 300-400nm in diameter, a layer of quiescent cells and an outer proliferating layer, as shown in Figure 5.1 (Bredel-Geissler *et al.*, 1992; Mehta *et al.*, 2012; Paolillo *et al.*, 2021). These spheroid models mimic the proliferating cells found on the outer areas of tumours where nutrient and oxygen supplies are prevalent and the hypoxic inner areas where necrotic cells accumulate (Hirschhaeuser *et al.*, 2010).

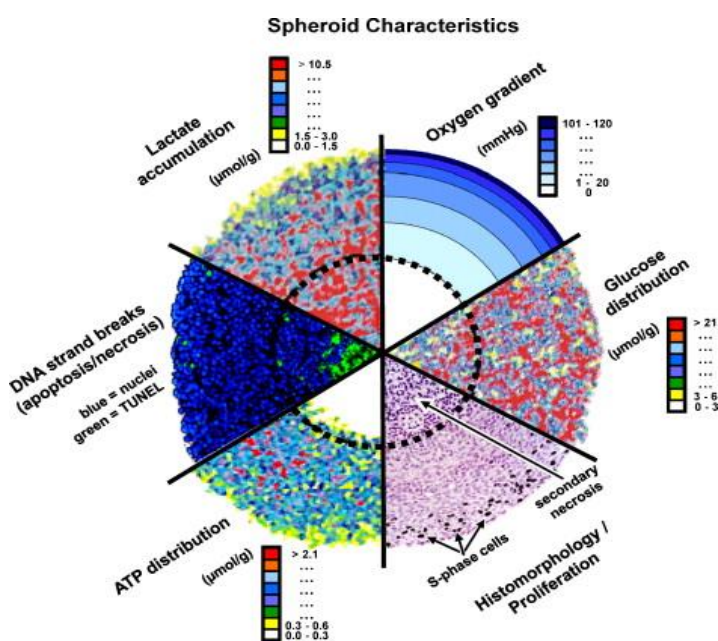


Figure 5.1: Combined representation of the different gradients in a spheroid section from the inner hypoxic core to the proliferating outer layer, showing levels of O₂, glucose, ATP, lactate, as well as the proliferating and necrotic/apoptotic cells. Taken from (Hirschhaeuser *et al.*, 2010).

An additional benefit of the spheroid model is that it allows for the effects of treatments to be monitored over longer time periods for high throughput parameters, which is beneficial in observing long term effects of treatments. Therefore, by monitoring the spheroids growth over time, the full effects of the treatment modalities can be investigated beyond the traditional 2D models such as a clonogenic assay (Akay *et al.*, 2018).

By applying our treatments to multicellular spheroids (MTS), we hypothesise each single treatment – TMZ, MMF and X-irradiation – will have a significant reduction in spheroid volume over time. We also hypothesise that based on the results of Chapter 3 and 4, the synergistic combinations will translate across into our 3D models, with the combinations reducing spheroid volume (V/V_0) over time compared to the untreated control, TMZ and MMF alone. T98g cell line multicellular spheroids were unable to thrive in the methods used and could not be carried forward for 3D studies. Due to the institutes external beam X-irradiation being broken, triple combinations were not applied to the spheroid model and will be carried out once a new machine becomes available to use. This will be performed before any future *in vivo* work.

5.2 Aims

The aims of this chapter were:

- To assess the effects of single treatments Temozolomide, Monomethyl Fumarate and External beam X-irradiation on the growth of 3D spheroids derived from the UVW and U87 cell lines.
- To assess the effects of the double combination of Temozolomide and Monomethyl Fumarate on 3D spheroid derived from UVW and U87 cell lines.
- To assess the effects of the scheduled administration of the double combination of Temozolomide and Monomethyl Fumarate on 3D spheroids derived from the UVW and U87 cell lines.

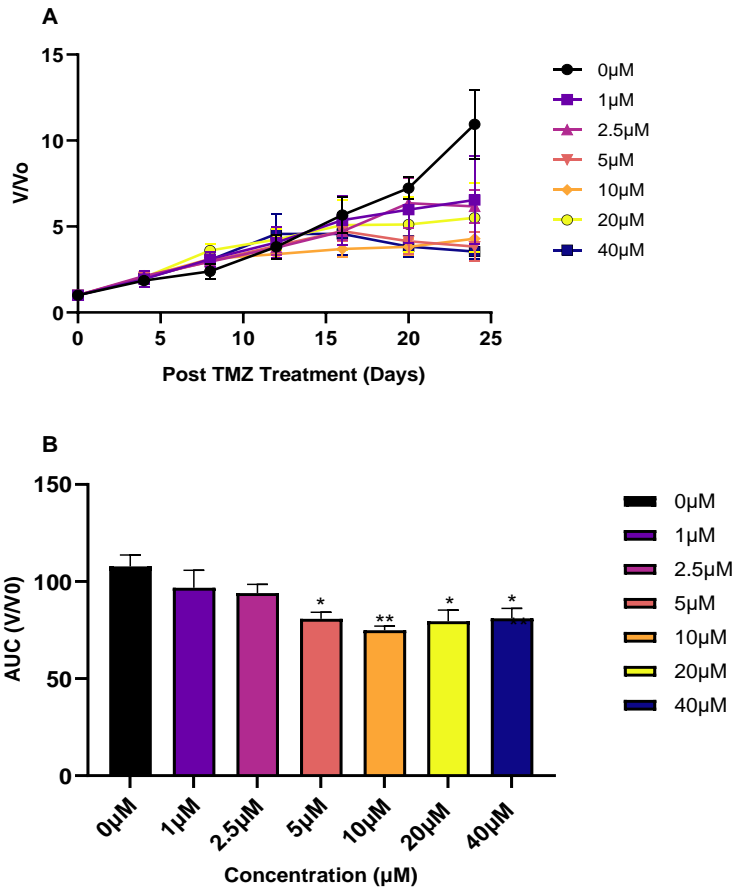
5.3 Results

5.3.1 Effects of Temozolomide on UVW and U87 3D Multicellular spheroid growth

To assess the effect of Temozolomide (TMZ) as a single treatment on the UVW and U87 multicellular spheroids, spheroids were treated with an increasing range of Temozolomide and the change in volume measured over 24 days. The concentration range utilised was kept consistent for both cell lines as to encapsulate the change from 2D to 3D (1uM to 40uM). Statistical analysis included a Shapiro-Wilks test to confirm normal distribution, followed by a one-way ANOVA with Bonferroni's post-test to compare area under the curve (AUC) across treatment groups against the untreated control. Additionally, a two-way ANOVA was performed to assess the effect of TMZ concentration on spheroid growth across the time points (days) compared to the untreated control. The volume of the control at each time point (day) was compared to the volume of the treated spheroids at each concentration of TMZ at the same day (V/V_0). Representative spheroid imaged are shown in Appendix 4 (A and B).

5.3.1.1 The Effect of Temozolomide on UVW Multicellular Spheroid Growth over time

The effect of Temozolomide (TMZ) on the growth of UVW multicellular spheroids was evaluated following incubation with a range of TMZ concentrations, as shown in Figure 5.2. Spheroid growth was monitored over 24 days, with images captured every 3-4 days.



(C)

One-way ANOVA – Shapiro Wilks Normal Distribution		
Bonferroni's Multiple comparisons test	AUC Significance Summary	Adjusted P Value
0 μM vs 5 μM	Yes *	0.0234
0 μM vs 10 μM	Yes **	0.0048
0 μM vs 20 μM	Yes *	0.0165
0 μM vs 40 μM	Yes *	0.0250
Two-way ANOVA – Comparison of V/V ₀		
Bonferroni's Multiple comparisons test	V/V ₀ Significance Summary	Adjusted P value
Day 20		
0 μM vs 10 μM	Yes*	0.0468
0 μM vs 40 μM	Yes*	0.0474
Day 24		
0 μM vs 1 μM	Yes**	0.0038
0 μM vs 2.5 μM	Yes**	0.0013
0 μM vs 5 μM	Yes****	<0.0001
0 μM vs 10 μM	Yes****	<0.0001
0 μM vs 20 μM	Yes***	0.0002
0 μM vs 40 μM	Yes****	<0.0001

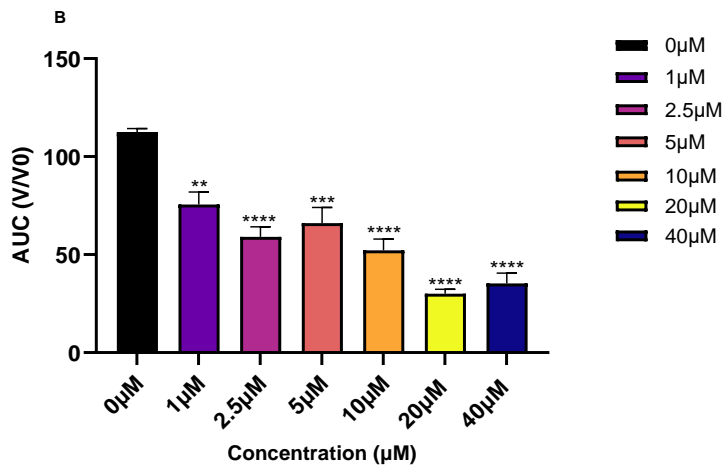
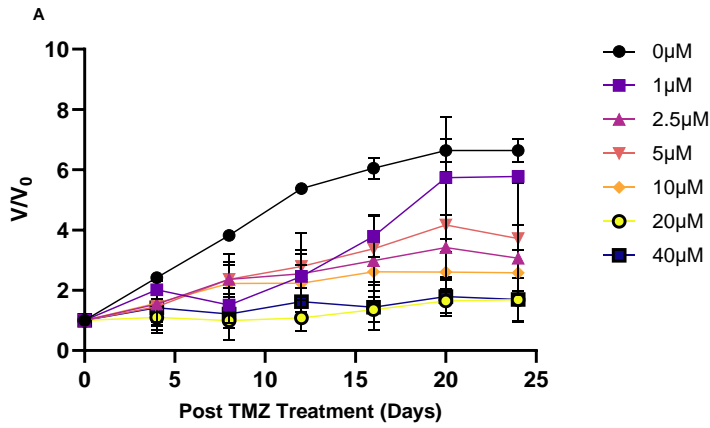
Figure 5.2: The UVW human glioblastoma multicellular spheroid growth curves (V/V_0) after treatment with increasing doses of Temozolomide over 24 days, with images captured every 3-4 days (A). Comparison of the area under the curve of the change in volume (V/V_0) of the Temozolomide treated UVW spheroids to the untreated control (B). Data shown is an average of three independent experiments \pm SEM, with 12 individual spheroids per concentration group. Statistical analysis was performed using a Shapiro-Wilks distribution to check normal distribution and followed by a one-way ANOVA with Bonferroni's post-test to compare AUC against the untreated control with significant data comparisons only shown (C). A two-way ANOVA was used to compare V/V_0 changes every 4 days (C). Statistical analysis was performed using GraphPad Prism 10.3.1 software, with P-values of values of $<0.05 = *$, $<0.01 = **$, $<0.001 = ***$ and $P < 0.0001 = ****$ reported as significant.

In UVW derived MTS treated with increasing concentrations of TMZ, AUC analysis revealed significant reductions in the AUC after incubation of the spheroids with concentrations of TMZ $\geq 5 \mu\text{M}$ compared to the untreated control AUC following a one-way ANOVA test (all. $P < 0.05$). A two-way ANOVA test showed a significant reduction in spheroid growth (V/V_0) at day 20 after exposure to TMZ concentrations of $10 \mu\text{M}$, and $40 \mu\text{M}$, compared to the untreated control (all $P < 0.05$). At day 24, following a two-way ANOVA, a statistically significant reduction in spheroid growth (V/V_0) after exposure to TMZ concentrations was seen after exposure to $5 \mu\text{M}$, $10 \mu\text{M}$, $20 \mu\text{M}$, and $40 \mu\text{M}$ TMZ, compared to the untreated control (all $P < 0.05$). No statistical significance was determined between treatment concentrations and the untreated control for day 4, 8, 12 or 16, following a two-way ANOVA.

UVW derived MTS data for TMZ treated spheroids suggested that TMZ induced statistically significant reduction in spheroid volume compared to the untreated control and AUC, supporting the hypothesis.

5.3.1.2 The Effect of Temozolomide on U87 Multicellular Spheroid Growth over time

The effect of Temozolomide (TMZ) on the growth of U87 multicellular spheroids (MTS) was evaluated following incubation with a range of TMZ concentrations, as shown in Figure 5.3. Spheroid growth was monitored over 24 days, with images captured every 3-4 days.



(C)

One-way ANOVA – Shapiro Wilks Normal Distribution		
Bonferroni's Multiple comparisons test	AUC Significance Summary	Adjusted P Value
0µM vs 1µM	Yes**	0.0015
0µM vs 2.5µM	Yes****	<0.0001
0µM vs 5µM	Yes ***	0.0002
0µM vs 10µM	Yes ****	<0.0001
0µM vs 20µM	Yes ****	<0.0001
0µM vs 40µM	Yes ****	<0.0001
Two-way ANOVA – Comparison of V/V_0		
Bonferroni's Multiple comparisons test	V/V_0 Significance Summary	Adjusted P value
Day 12		
0µM vs 20µM	Yes **	0.0034
0µM vs 40µM	Yes *	0.0187
Day 16		
0µM vs 10µM	Yes *	0.0462
0µM vs 20µM	Yes ***	0.0009

0 μ M vs 40 μ M	Yes **	0.0012
Day 20		
0 μ M vs 10 μ M	Yes **	0.0077
0 μ M vs 20 μ M	Yes ***	0.0003
0 μ M vs 40 μ M	Yes ***	0.0005
Day 24		
0 μ M vs 2.5 μ M	Yes *	0.0316
0 μ M vs 10 μ M	Yes **	0.0071
0 μ M vs 20 μ M	Yes ***	0.0004
0 μ M vs 40 μ M	Yes ***	0.0004

Figure 5.3: The U87 human glioblastoma multicellular spheroid growth curves (V/V_0) after treatment with increasing doses of Temozolomide over 24 days, with images captured every 3-4 days (A). Comparison of the area under the curve of the change in volume (V/V_0) of the Temozolomide treated U87 spheroids to the untreated control (B). Data shown is an average of three independent experiments \pm SEM, with 12 individual spheroids per concentration group. Statistical analysis was performed using a Shapiro-Wilks distribution to check normal distribution and followed by a one-way ANOVA with Bonferroni's post-test to compare AUC against the untreated control with significant data comparisons only shown (C). A two-way ANOVA was used to compare V/V_0 changes every 4 days (C). Statistical analysis was performed using GraphPad Prism 10.3.1 software, with P-values of values of $<0.05 = *$, $<0.01 = **$, $<0.001 = ***$ and $P < 0.0001 = ****$ reported as significant.

In U87 derived MTS treated with increasing concentrations of TMZ, a statistically significant reduction in spheroid growth (V/V_0) was observed across treatment groups following a two-way ANOVA test (Figure 5.3 (B and C)). A concentration of 20 μ M and 40 μ M TMZ, showed a statistically significant reduction in spheroid volume (V/V_0) compared to the untreated control at day 12, 16, 20 and 24 (all $P < 0.05$). Exposure of the spheroids to 10 μ M TMZ, resulted in a statistically significant reduction in spheroid volume compared to the untreated control at day 16, 20 and 24 (all, $P < 0.05$). At day 24, the two-way ANOVA analysis calculated a statistically significant reduction in spheroid volume after 2.5 μ M TMZ exposure vs the untreated control ($P < 0.05$). AUC analysis revealed significant reductions in the AUC after exposure to concentrations $\geq 1\mu$ M TMZ compared to the untreated control AUC (all, $P < 0.05$). No other statistically significant differences were observed for any other days or treatment groups.

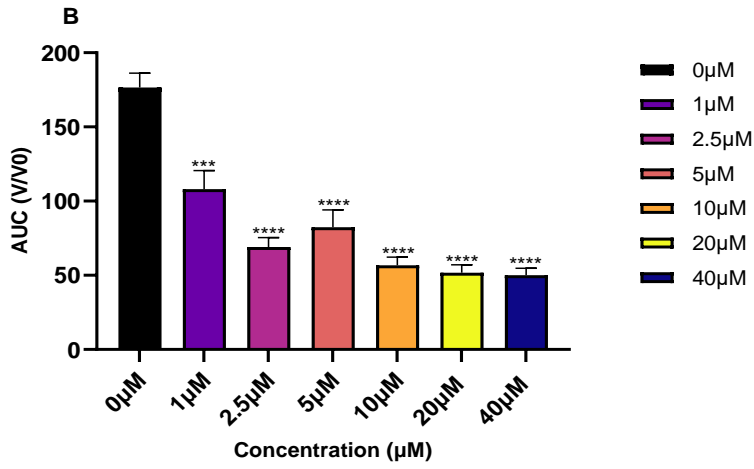
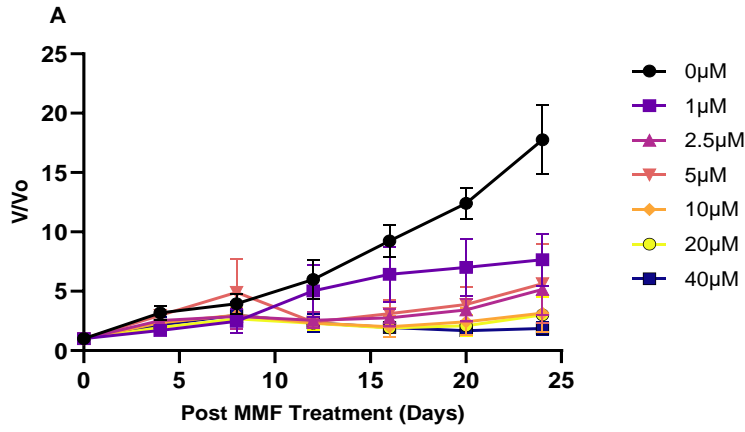
U87 derived MTS data for TMZ treated spheroids observed TMZ to induce a statistically significant reduction in spheroid volume compared to the untreated control and AUC, further supporting the hypothesis.

5.3.2 Effects of Monomethyl Fumarate on UVW and U87 3D Multicellular Spheroid growth

To assess the effect of Monomethyl Fumarate (MMF) as a single treatment on the UVW and U87 derived multicellular spheroids, spheroids were treated with an increasing range of Monomethyl Fumarate and the change in volume measured over 24 days. The concentration range was kept consistent for both cell lines as to encapsulate the change from 2D to 3D (1 μ M to 40 μ M). Statistical analysis included a Shapiro-Wilks test to confirm normal distribution, followed by a one-way ANOVA with Bonferroni's post-test to compare area under the curve (AUC) across treatment groups against the untreated control. Additionally, a two-way ANOVA was performed to assess the effect of MMF concentration on spheroid growth across the time points (days) compared to the untreated control (V/V_0). Representative spheroid imaged are shown in Appendix 4 (C and D).

5.3.2.1 Effects of Monomethyl Fumarate on UVW spheroid growth

To assess the effect of Monomethyl Fumarate as a single treatment on the UVW multicellular spheroids, spheroids were treated with an increasing range of Monomethyl Fumarate and the change in volume measured over 24 days as shown in Figure 5.4.



(C)

One-way ANOVA – Shapiro Wilks Normal Distribution		
Bonferroni's Multiple comparisons test	AUC Significance Summary	Adjusted P Value
0µM vs 1µM	Yes ***	0.0007
0µM vs 2.5µM	Yes ****	<0.0001
0µM vs 5µM	Yes ****	<0.0001
0µM vs 10µM	Yes ****	<0.0001
0µM vs 20µM	Yes ****	<0.0001
0µM vs 40µM	Yes ****	<0.0001
Two-way ANOVA – Comparison of V/Vo		
Bonferroni's Multiple comparisons test	V/Vo Significance Summary	Adjusted P value
Day 16		
0µM vs 2.5µM	Yes **	0.0090
0µM vs 5µM	Yes *	0.0178
0µM vs 10µM	Yes **	0.0019

0 μ M vs 20 μ M	Yes **	0.0015
0 μ M vs 40 μ M	Yes **	0.0016
Day 20		
0 μ M vs 2.5 μ M	Yes ****	<0.0001
0 μ M vs 5 μ M	Yes ****	<0.0001
0 μ M vs 10 μ M	Yes ****	<0.0001
0 μ M vs 20 μ M	Yes ****	<0.0001
0 μ M vs 40 μ M	Yes ****	<0.0001
Day 24		
0 μ M vs 1 μ M	Yes ****	<0.0001
0 μ M vs 2.5 μ M	Yes ****	<0.0001
0 μ M vs 5 μ M	Yes ****	<0.0001
0 μ M vs 10 μ M	Yes ****	<0.0001
0 μ M vs 20 μ M	Yes ****	<0.0001
0 μ M vs 40 μ M	Yes ****	<0.0001

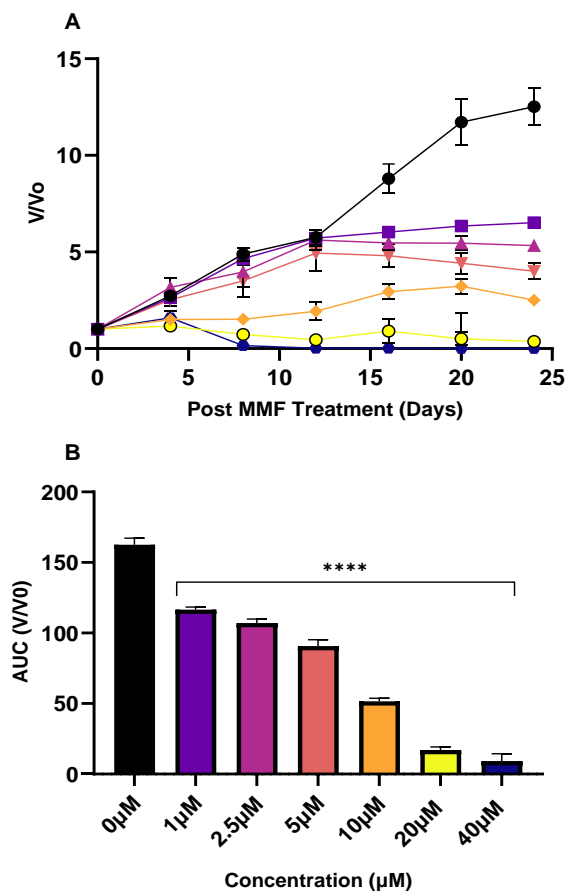
Figure 5.4: The UVW human glioblastoma multicellular spheroid growth curves (V/V_0) after treatment with increasing doses of Monomethyl Fumarate over 24 days, with images captured every 3-4 days (A Comparison of the area under the curve of the change in volume (V/V_0) of the Monomethyl Fumarate treated UVW spheroids to the untreated control (B). Data shown is an average of three independent experiments \pm SEM, with 12 individual spheroids per concentration group. Statistical analysis was performed using a Shapiro-Wilks distribution to check normal distribution and followed by a one-way ANOVA with Bonferroni's post-test to compare spheroid V/V_0 and AUC against the untreated control with significant data comparisons only shown (C). A two-way ANOVA was used to compare V/V_0 changes every 4 days (C). Statistical analysis was performed using GraphPad Prism 10.3.1 software, with P-values of values of $<0.05 = *$, $<0.01 = **$, $<0.001 = ***$ and $P < 0.0001 = ****$ reported as significant.

From Figure 5.4, the effect of increasing concentrations of MMF on UVW MTS growth can be seen. A statistically significant reduction in AUC was observed for all UVW derived MTS treated with MMF, following a one-way ANOVA, compared to the AUC for the untreated control over 24 days (all $P < 0.001$). The change in spheroid volume (V/V_0) also showed statistically significant reductions in spheroid volume after exposure to MMF at concentrations $\geq 2.5\mu\text{M}$ compared to the untreated control when analysed at day 16, 20 and 24 (Figure 5.4 (C)). Exposure of the spheroids to a concentration of $1\mu\text{M}$ MMF, resulted in a statistically significant change in spheroid volume at day 24 compared to the untreated control ($P < 0.0001$). On days 4, 8 and 12 there was no statistically significant changes against the untreated control for any treatment exposure (all $P > 0.05$).

The data therefore shows that MMF significantly reduces UVW spheroid volume over time, supporting the hypothesis.

5.3.2.2 Effects of Monomethyl Fumarate on U87 spheroid growth

To assess the effect of Monomethyl Fumarate as a single treatment on the U87 multicellular spheroids (MTS), spheroids were treated with an increasing range of Monomethyl Fumarate and the change in volume measured over 24 days as shown in Figure 5.5.



(C)

One-way ANOVA – Shapiro Wilks Normal Distribution		
Bonferroni's Multiple comparisons test	AUC Significance Summary	Adjusted P Value
0 μM vs 1 μM	Yes ****	<0.0001

0μM vs 2.5μM	Yes ****	<0.0001
0μM vs 5μM	Yes ****	<0.0001
0μM vs 10μM	Yes ****	<0.0001
0μM vs 20μM	Yes ****	<0.0001
0μM vs 40μM	Yes ****	<0.0001
Two-way ANOVA – Comparison of V/V₀		
Bonferroni's Multiple comparisons test	V/V ₀ Significance Summary	Adjusted P value
Day 8		
0μM vs 10μM	Yes ***	0.0001
0μM vs 20μM	Yes ****	<0.0001
0μM vs 40μM	Yes ****	<0.0001
Day 12		
0μM vs 10μM	Yes ****	<0.0001
0μM vs 20μM	Yes ****	<0.0001
0μM vs 40μM	Yes ****	<0.0001
Day 16		
0μM vs 1μM	Yes **	0.0039
0μM vs 2.5μM	Yes ***	0.0002
0μM vs 5μM	Yes ****	<0.0001
0μM vs 10μM	Yes ****	<0.0001
0μM vs 20μM	Yes ****	<0.0001
0μM vs 40μM	Yes ****	<0.0001
Day 20		
0μM vs 1μM	Yes ****	<0.0001
0μM vs 2.5μM	Yes ****	<0.0001
0μM vs 5μM	Yes ****	<0.0001
0μM vs 10μM	Yes ****	<0.0001
0μM vs 20μM	Yes ****	<0.0001
0μM vs 40μM	Yes ****	<0.0001
Day 24		
0μM vs 1μM	Yes ****	<0.0001
0μM vs 2.5μM	Yes ****	<0.0001
0μM vs 5μM	Yes ****	<0.0001
0μM vs 10μM	Yes ****	<0.0001
0μM vs 20μM	Yes ****	<0.0001
0μM vs 40μM	Yes ****	<0.0001

Figure 5.5: The U87 human glioblastoma multicellular spheroid growth curves (V/V₀) after treatment with increasing doses of Monomethyl Fumarate over 24 days, with images captured every 3-4 days (A). Comparison of the area under the curve of the change in volume (V/V₀) of the Monomethyl Fumarate treated U87 spheroids to the untreated control (B). Data shown is an average of three independent experiments ± SEM, with 12 individual spheroids per concentration group. Statistical analysis was performed using a Shapiro-Wilks distribution to check normal distribution and followed by a one-way ANOVA with Bonferroni's post-test to compare spheroid V/V₀ and AUC against the untreated control with significant data comparisons only shown (C). A two-way ANOVA was used to compare V/V₀ changes every 4 days (C). Statistical analysis

was performed using GraphPad Prism 10.3.1 software, with P-values of values of $<0.05 = *$, $<0.01 = **$, $<0.001 = ***$ and $P < 0.0001 = ****$ reported as significant.

The effect of increasing concentrations of MMF on U87 derived MTS is demonstrated in Figure 5.5 (B). There was a statistically significant reduction in AUC after exposure to all concentrations of MMF - $1\mu\text{M}$ to $40\mu\text{M}$ – compared to the untreated control (all, $P < 0.0001$). Application of a two-way ANOVA showed statistically significant reductions in spheroid volume (V/V_0) for all concentrations of MMF - $1\mu\text{M}$ to $40\mu\text{M}$ – at days 16, 20 and 24, compared to the untreated control (all, $P < 0.01$) (Figure 5.5(C)). Analysis at day 8 and 12 also showed statistically significant reductions in spheroid volume (V/V_0) compared to the untreated control after exposure to $10\mu\text{M}$, $20\mu\text{M}$ and $40\mu\text{M}$ MMF (all, $P < 0.001$) (Figure 5.5(C)). No significant changes in spheroid volume between any treatment groups were observed at day 4.

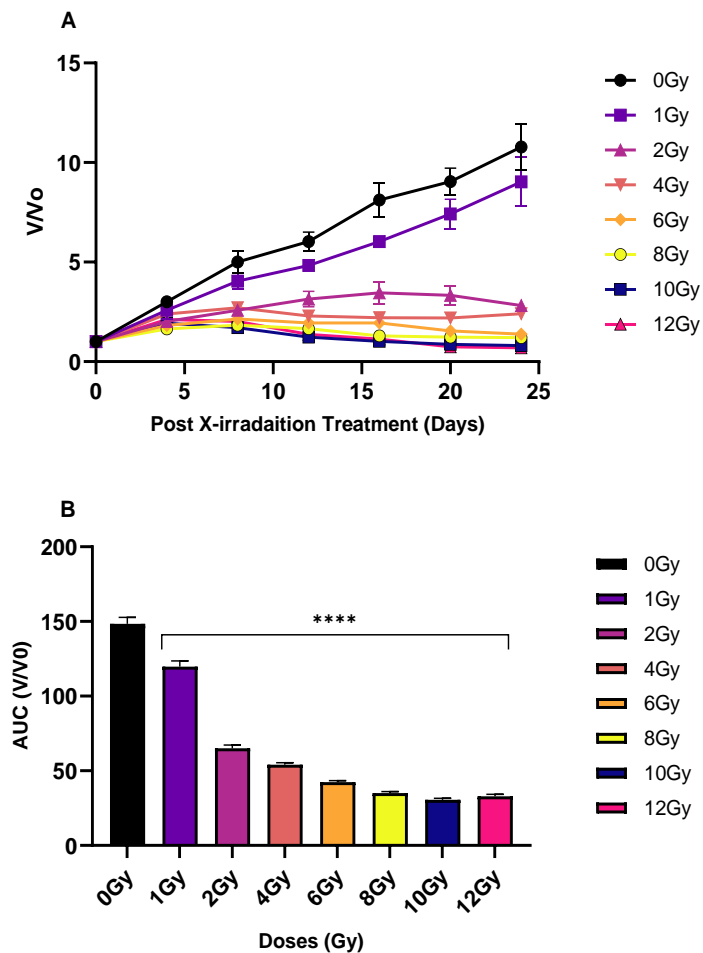
These data suggest that MMF has a statistically significant impact on MTS growth over time following incubation with concentrations as low as $1\mu\text{M}$ MMF, supporting the hypothesis.

5.3.3 Effects of External X- Beam Irradiation on UVW and U87 3D Multicellular Spheroid growth

To assess the effect of External X-Beam irradiation (X-irradiation) as a single treatment on the UVW and U87 multicellular spheroids, spheroids were treated with an increasing range of X-irradiation and the change in volume measured over 24 days. The concentration range was kept consistent for both cell lines as to encapsulate the change from 2D to 3D (1Gy to 12Gy). Statistical analysis included a Shapiro-Wilks test to confirm normal distribution, followed by a one-way ANOVA with Bonferroni's post-test to compare area under the curve (AUC) across treatment groups against the untreated control. Additionally, a two-way ANOVA was performed to assess the effect of X-irradiation concentration on spheroid growth across the time points (days) compared to the untreated control (V/V_0). Representative spheroid imaged are shown in Appendix 4 (E and F).

5.3.3.1 Effects of External X- Beam Irradiation UVW spheroid growth

To assess the effect of X-irradiation as a single treatment on the UVW multicellular spheroids (MTS), spheroids were treated with increasing doses of X-irradiation and the change in volume measured over 24 days as shown in Figure 5.6.



0Gy vs 10Gy	Yes ****	<0.0001
0Gy vs 12Gy	Yes ****	<0.0001
Two-way ANOVA – Comparison of V/V ₀		
Bonferroni's Multiple comparisons test	V/V ₀ Significance Summary	Adjusted P value
Day 8		
0Gy vs 2Gy	Yes ***	0.0002
0Gy vs 4Gy	Yes ***	0.0005
0Gy vs 6Gy	Yes ****	<0.0001
0Gy vs 8Gy	Yes ****	<0.0001
0Gy vs 10Gy	Yes ****	<0.0001
0Gy vs 12Gy	Yes ****	<0.0001
Day 12		
0Gy vs 2Gy	Yes ****	<0.0001
0Gy vs 4Gy	Yes ****	<0.0001
0Gy vs 6Gy	Yes ****	<0.0001
0Gy vs 8Gy	Yes ****	<0.0001
0Gy vs 10Gy	Yes ****	<0.0001
0Gy vs 12Gy	Yes ****	<0.0001
Day 16		
0Gy vs 1Gy	Yes**	0.0025
0Gy vs 2Gy	Yes ****	<0.0001
0Gy vs 4Gy	Yes ****	<0.0001
0Gy vs 6Gy	Yes ****	<0.0001
0Gy vs 8Gy	Yes ****	<0.0001
0Gy vs 10Gy	Yes ****	<0.0001
0Gy vs 12Gy	Yes ****	<0.0001
Day 20		
0Gy vs 2Gy	Yes ****	<0.0001
0Gy vs 4Gy	Yes ****	<0.0001
0Gy vs 6Gy	Yes ****	<0.0001
0Gy vs 8Gy	Yes ****	<0.0001
0Gy vs 10Gy	Yes ****	<0.0001
0Gy vs 12Gy	Yes ****	<0.0001
Day 24		
0Gy vs 1Gy	Yes*	0.0234
0Gy vs 2Gy	Yes ****	<0.0001
0Gy vs 4Gy	Yes ****	<0.0001
0Gy vs 6Gy	Yes ****	<0.0001
0Gy vs 8Gy	Yes ****	<0.0001
0Gy vs 10Gy	Yes ****	<0.0001
0Gy vs 12Gy	Yes ****	<0.0001

Figure 5.6: The UVW human glioblastoma multicellular spheroid growth curves (V/V₀) after treatment with increasing doses of X-irradiation over 24 days, with images captured every 3-4 days (A). Comparison of the area under the curve of the change in volume (V/V₀) of the X-irradiation treated UVW spheroids to the untreated control (B). Data shown is an average of three independent experiments ± SEM, with 12 individual spheroids per concentration group. Statistical analysis was performed using a Shapiro-Wilks distribution to check normal distribution and followed by a one-way ANOVA with Bonferroni's post-test to compare spheroid V/V₀ and AUC against the

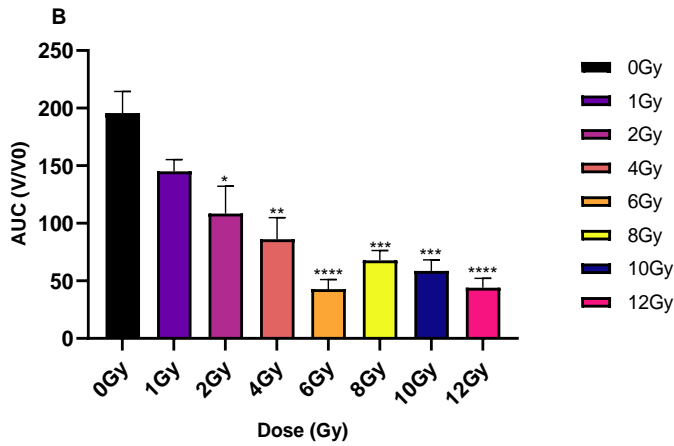
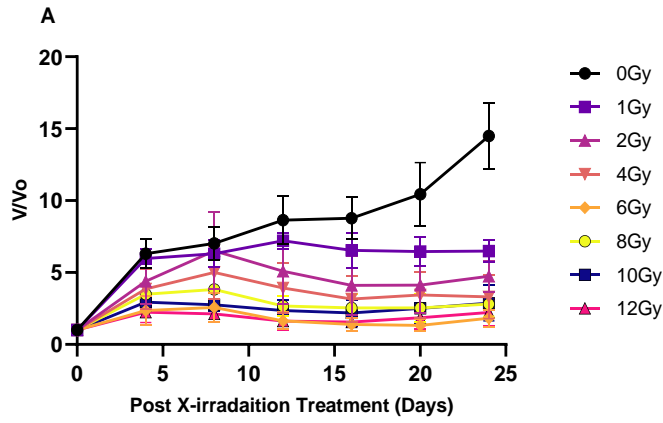
untreated control (C). A two-way ANOVA was used to compare V/V_0 changes every 4 days (C). Statistical analysis was performed using GraphPad Prism 10.3.1 software, with P-values of values of $<0.05 = *$, $<0.01 = **$, $<0.001 = ***$ and $P < 0.0001 = ****$ reported as significant.

The effect of increasing doses of X-irradiation on the UVW cell line shown in Figure 5.6, demonstrated a statistically significant reduction in AUC following a one-way ANOVA analysis, for all doses of X-irradiation – 1Gy to 12Gy – compared to the untreated control (all $P < 0.0001$) (Figure 5.6(B)). Two-way ANOVA analysis on the change in spheroid volume (V/V_0) over time, showed that doses ≥ 2 Gy caused a statistically significant reduction in spheroid volume compared to the untreated control at days 8, 12, 16, 20 and 24 (all $P < 0.001$) (Figure 5.6(C)). Exposure of the UVW spheroids to 1Gy of X-irradiation induced a statistically significant reduction in spheroid volume compared to the untreated control at day 16 and 24 (all $P < 0.05$). No significant changes in spheroid volume were observed for day 4 after exposure to any X-irradiation dose compared to the untreated control.

Data in Figure 5.6 collectively shows UVW spheroid volume to be significantly reduced after exposure to doses ≥ 1 Gy of X-irradiation supporting the hypothesis of single treatments reducing spheroid volume over time.

5.3.3.2 Effects of External X- Beam Irradiation U87 spheroid growth

To assess the effect of X-irradiation as a single treatment on the U87 multicellular spheroids, spheroids were treated with increasing doses of X-irradiation and the change in volume measured over 24 days as shown in Figure 5.7.



(C)

One-way ANOVA – Shapiro Wilks Normal Distribution		
Bonferroni's Multiple comparisons test	AUC Significance Summary	Adjusted P Value
0Gy vs 1Gy	ns	0.7001
0Gy vs 2Gy	Yes *	0.0168
0Gy vs 4Gy	Yes **	0.0019
0Gy vs 6Gy	Yes ****	<0.0001
0Gy vs 8Gy	Yes ***	0.0003
0Gy vs 10Gy	Yes ***	0.0001
0Gy vs 12Gy	Yes ****	<0.0001
Two-way ANOVA – Comparison of V/Vo		
Bonferroni's Multiple comparisons test	V/Vo Significance Summary	Adjusted P value
Day 12		
0Gy vs 1Gy	ns	0.5894
0Gy vs 2Gy	ns	<0.0001
0Gy vs 4Gy	ns	<0.0001
0Gy vs 6Gy	Yes **	0.0014
0Gy vs 8Gy	Yes *	0.0129

0Gy vs 10Gy	Yes **	0.0066
0Gy vs 12Gy	Yes **	0.0013
Day 16		
0Gy vs 1Gy	ns	>0.9999
0Gy vs 2Gy	ns	0.1556
0Gy vs 4Gy	Yes *	0.0261
0Gy vs 6Gy	Yes ***	0.0005
0Gy vs 8Gy	Yes **	0.0072
0Gy vs 10Gy	Yes **	0.0034
0Gy vs 12Gy	Yes ***	0.0008
Day 20		
0Gy vs 1Gy	ns	0.4988
0Gy vs 2Gy	Yes**	0.0062
0Gy vs 4Gy	Yes **	0.0014
0Gy vs 6Gy	Yes ****	<0.0001
0Gy vs 8Gy	Yes ***	0.0001
0Gy vs 10Gy	Yes ***	0.0001
0Gy vs 12Gy	Yes ****	<0.0001
Day 24		
0Gy vs 1Gy	Yes***	0.0001
0Gy vs 2Gy	Yes ****	<0.0001
0Gy vs 4Gy	Yes ****	<0.0001
0Gy vs 6Gy	Yes ****	<0.0001
0Gy vs 8Gy	Yes ****	<0.0001
0Gy vs 10Gy	Yes ****	<0.0001
0Gy vs 12Gy	Yes ****	<0.0001

Figure 5.7: The U87 human glioblastoma multicellular spheroid growth curves (V/V_0) after treatment with increasing doses of X-irradiation over 24 days, with images captured every 3-4 days (A). Comparison of the area under the curve of the change in volume (V/V_0) of the X-irradiation treated U87 spheroids to the untreated control (B). Data shown is an average of three independent experiments \pm SEM, with 12 individual spheroids per concentration group. Statistical analysis was performed using a Shapiro-Wilks distribution to check normal distribution and followed by a one-way ANOVA with Bonferroni's post-test to compare AUC against the untreated control (C). A two-way ANOVA was used to compare V/V_0 changes every 4 days (C). Statistical analysis was performed using GraphPad Prism 10.3.1 software, with P-values of values of $<0.05 = *$, $<0.01 = **$, $<0.001 = ***$ and $P < 0.0001 = ****$ reported as significant.

Figure 5.7 shows the change in spheroid volume (V/V_0) in U87 derived MTS after exposure to increasing doses of X-irradiation. One-way ANOVA analysis on AUC displayed a statistically significant reduction in AUC after exposure to all doses of X-irradiation 1Gy – 12Gy compared to the untreated control AUC (all, $P < 0.05$) (Figure 5.7 (B and C)). A statistically significant reduction in spheroid volume compared to the untreated control at day 12, 16, 20 and 24 was seen after exposure to doses ≥ 6 Gy (all, $P < 0.01$) (Figure 5.7 (A and C)). Two-way ANOVA analysis at day 16, 20 and 24

showed that 4Gy exposure resulted in a statistically significant reduction in spheroid volume compared to the untreated control (all, $P < 0.05$) (Figure 5.7 (A and C)). Two-way ANOVA analysis at day 20 and 24 displayed a 2Gy exposure of X-irradiation to result in a statistically significant reduction in spheroid volume compared to the untreated control (all, $P < 0.01$) (Figure 5.7 (A and C)). Two-way ANOVA analysis at day 24 showed a statistically significant reduction in spheroid volume compared to the untreated control after exposure to 1Gy of X-irradiation ($P < 0.001$). No significant changes in spheroid volume were seen in any of the treatment groups at days 4 and 12.

Figure 5.7 collectively shows a significant dose responsive decrease in U87 spheroid volume to increasing doses of X-irradiation supporting the hypothesis of single treatments reducing spheroid volume over time.

5.3.4 Effects of combining Temozolomide and Monomethyl Fumarate on UVW and U87 3D Multicellular spheroid growth

Following on from single treatments of Temozolomide (TMZ) and Monomethyl Fumarate (MMF), the concentrations of Temozolomide and Monomethyl Fumarate used throughout the project were applied to the 3D multicellular spheroid (MTS) models. The combinations used in chapter 3, which were shown to result in synergistic treatment interactions and thus were used for both simultaneous and scheduled administration (PT4) in the spheroid models. The table below, highlights these concentrations (Table 5.1). It was hypothesised that the combination of TMZ and MMF would result in a significant decrease in spheroid volume compared to each single treatment. Representative spheroid imaged are shown in Appendix 4 (G and H).

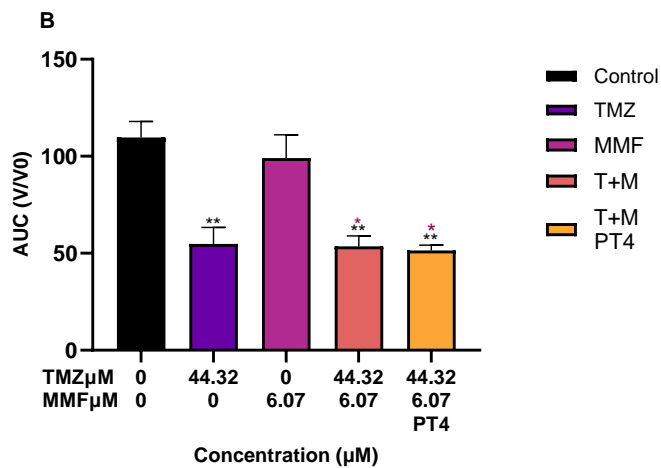
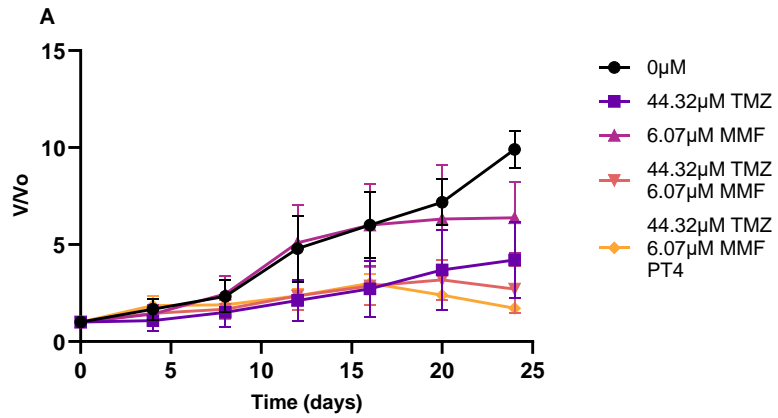
UVW cell line	
Treatment	Concentration
TMZ (T)	44.32 μ M
MMF (M)	6.07 μ M
TMZ+ MMF (T+M)	44.32 μ M + 6.07 μ M
TMZ + MMF PT4 (T+M PT4)	6.07 μ M 4h + 44.32 μ M

U87 Cell line	
TMZ (T)	2.4 μ M
MMF (M)	2.8 μ M
TMZ+ MMF (T+M)	2.4 μ M + 2.8 μ M
TMZ + MMF PT4 (T+M PT4)	2.4 μ M 4h + 2.8 μ M

Table 5.1: The concentrations of Temozolomide and Monomethyl Fumarate applied on the UVW and U87 cell line for combination studies on spheroid volume changes.

5.3.4.1 The effect of combining Temozolomide and Monomethyl Fumarate on UVW spheroid growth.

Single concentrations of Temozolomide and Monomethyl Fumarate as well as the relative simultaneous combination and scheduled combination effect of both on UVW MTS are shown in Figure 5.8. Change in volume (V/V_0) was observed over 24 days, as shown in Figure 5.8 following the concentrations shown in Table 5.1.



(C)

One-way ANOVA – Shapiro Wilks Normal Distribution		
Bonferroni's Multiple comparisons test	AUC Significance Summary	Adjusted P Value
Control vs TMZ	Yes **	0.0077
Control vs MMF	ns	>0.9999
Control vs (T+M)	Yes**	0.0064
Control vs (T+M PT4)	Yes**	0.0049
MMF vs (T+M)	Yes *	0.0277
MMF vs (T+M PT4)	Yes *	0.0207

Two-way ANOVA – Comparison of V/Vo		
Bonferroni's Multiple comparisons test	V/Vo Significance Summary	Adjusted P value
Day 20		
Control vs TMZ	ns	0.3380
Control vs MMF	ns	>0.9999
Control vs (T+M)	ns	0.1561
Control vs (T+M PT4)	Yes *	0.0411
TMZ vs MMF	ns	>0.9999

TMZ vs (T+M)	ns	>0.9999
TMZ vs (T+M PT4)	ns	>0.9999
MMF vs (T+M)	ns	0.5619
MMF vs (T+M PT4)	ns	0.1764
(T+M) vs (T+M PT4)	ns	>0.9999
Day 24		
Control vs TMZ	Yes**	0.0073
Control vs MMF	ns	0.3231
Control vs (T+M)	Yes***	0.0003
Control vs (T+M PT4)	Yes****	<0.0001
TMZ vs MMF	ns	>0.9999
TMZ vs (T+M)	ns	>0.9999
TMZ vs (T+M PT4)	ns	>0.9999
MMF vs (T+M)	ns	0.2580
MMF vs (T+M PT4)	ns	0.0514
(T+M) vs (T+M PT4)	ns	>0.9999

Figure 5.8: The UVW human glioblastoma multicellular spheroid growth curves (V/V_0) after treatment with 44.32 μ M Temozolomide, 6.07 μ M Monomethyl Fumarate and the combination of both given either simultaneously (T+M) or as a 4- hour MMF pretreatment (T+M PT4), over 24 days, with images captured every 3-4 days (A). Comparison of the area under the curve of the change in volume (V/V_0) of the combination treated UVW spheroids to the untreated control and single drug treated spheroids (B). Data shown is an average of three independent experiments \pm SEM, with 12 individual spheroids per concentration group. Statistical analysis was performed using a Shapiro-Wilks distribution to check normal distribution and followed by a one-way ANOVA with Bonferroni's post-test to compare spheroid AUC against the untreated control (C). A two-way ANOVA was used to compare V/V_0 changes every 4 days between treatment groups (C). Statistical analysis was performed using GraphPad Prism 10.3.1 software, with P-values of values of $<0.05 = *$, $<0.01 = **$, $<0.001 = ***$ and $P < 0.0001 = ****$ reported as significant.

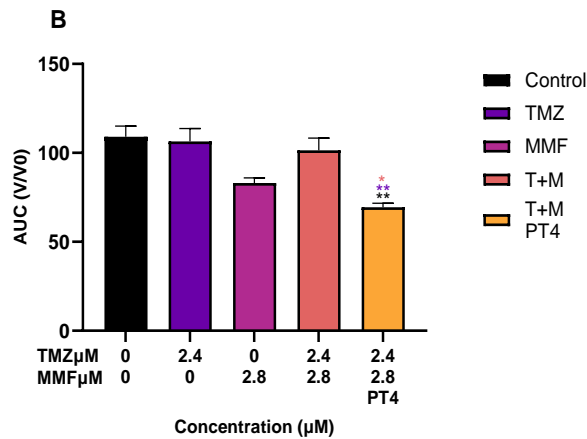
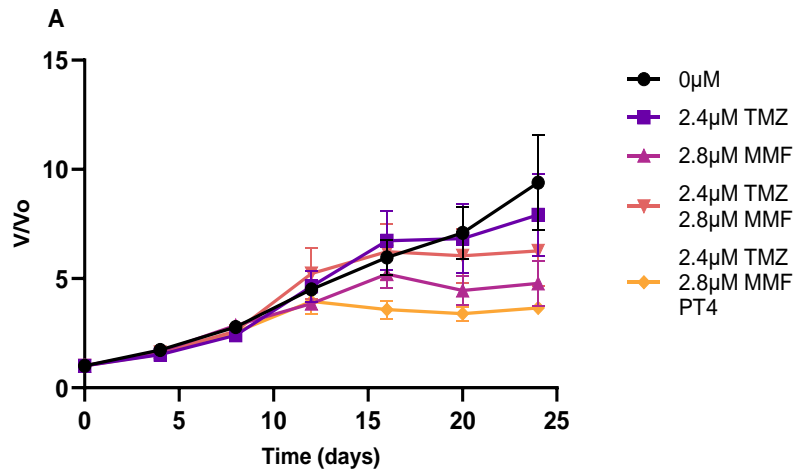
Figure 5.8 demonstrates the effect of TMZ, MMF and the combination of both given either simultaneously or as a schedule on spheroid volume (V/V_0) over 24 days in UVW derived MTS. Figure 5.8 (B) showed a statistically significant reduction in AUC after exposure to 44.32 μ M TMZ given alone and 44.32 μ M TMZ + 6.07 μ M MMF given both as a schedule (T+M PT4) and simultaneously (T+M) compared to the AUC for the untreated control (all, $P < 0.01$). Both the simultaneous and scheduled combinations showed a statistically significant reduction in AUC when compared to 6.07 μ M MMF as a single drug (both, $P < 0.05$). No statistically significant differences in AUC were observed for the combinations compared to TMZ or each other.

Two-way ANOVA analysis on the change in spheroid volume (Figure 5.8 (A)) suggested that the scheduled combination (T+M PT4) induced a statistically significant reduction in spheroid volume compared to the untreated control at day 20 ($P < 0.05$). At day 24, a statistically significant reduction in spheroid volume was observed for TMZ, T+M and T+M PT4, compared to the untreated control (Figure 5.8 (C)) but not against the individual treatments as monotherapies. No other significant changes were calculated at day 4, 8, 12 and 16 between treatment groups.

These data collectively do not fully support our hypothesis of the combined treatment of MMF and TMZ reducing spheroid volume, as both the simultaneous and scheduled combinations only significantly reduced spheroid volume when compared to MMF alone and the untreated control when comparing AUC, and against the untreated control when comparing V/V_0 .

5.3.4.2 The effect of combining Temozolomide and Monomethyl Fumarate on U87 spheroid growth.

Single concentrations of Temozolomide and Monomethyl Fumarate as well as the relative simultaneous combination and scheduled combination effect of both on U87 MTS are shown in Figure 5.9. Change in volume (V/V_0) was observed over 24 days, as shown in Figure 5.11 following the concentrations shown in Table 5.1.



(C)

One-way ANOVA – Shapiro Wilks Normal Distribution		
Bonferroni's Multiple comparisons test	AUC Significance Summary	Adjusted P Value
Control vs (TMZ + MMF PT4)	Yes **	0.0044
TMZ vs (TMZ + MMF PT4)	Yes **	0.0074
(TMZ + MMF) vs (TMZ + MMF PT4)	Yes *	0.0202
Two-way ANOVA – Comparison of V/Vo		
Bonferroni's Multiple comparisons test	V/Vo Significance Summary	Adjusted P value
Day 20		
Control vs TMZ	ns	>0.9999
Control vs MMF	ns	>0.3062
Control vs (T+M)	ns	>0.9999
Control vs (T+M PT4)	Yes *	0.0282
TMZ vs MMF	ns	0.5108
TMZ vs (T+M)	ns	>0.9999
TMZ vs (T+M PT4)	ns	0.0535
MMF vs (T+M)	ns	>0.9999
MMF vs (T+M PT4)	ns	>0.9999
(T+M) vs (T+M PT4)	ns	0.3012

Day 24		
Control vs TMZ	ns	0.0073
Control vs MMF	Yes **	0.0025
Control vs (T+M)	ns	0.1109
Control vs (T+M PT4)	Yes****	<0.0001
TMZ vs MMF	ns	0.1070
TMZ vs (T+M)	ns	>0.9999
TMZ vs (T+M PT4)	Yes **	0.0066
MMF vs (T+M)	ns	>0.9999
MMF vs (T+M PT4)	ns	>0.9999
(T+M) vs (T+M PT4)	ns	0.3194

Figure 5.9: The U87 human glioblastoma multicellular spheroid growth curves (V/V_0) after treatment with increasing doses of 2.4 μ M Temozolomide, 2.8 μ M Monomethyl Fumarate and the combination of both given either simultaneously (T+M) or as a 4-hour MMF pretreatment (T+M PT4), over 24 days, with images captured every 3-4 days (A). Comparison of the area under the curve of the change in volume (V/V_0) of the combination treated U87 spheroids to the untreated control and single drug treated spheroids (B). Data shown is an average of three independent experiments \pm SEM, with 12 individual spheroids per concentration group. Statistical analysis was performed using a Shapiro-Wilks distribution to check normal distribution and followed by a one-way ANOVA with Bonferroni's post-test to compare AUC against the untreated control (C). A two-way ANOVA was used to compare V/V_0 changes every 4 days between treatment groups (C). Statistical analysis was performed using GraphPad Prism 10.3.1 software, with P-values of values of $<0.05 = *$, $<0.01 = **$, $<0.001 = ***$ and $P < 0.0001 = ****$ reported as significant.

Figure 5.9 illustrates the effect of TMZ, MMF, and their combination—administered either simultaneously or as a schedule—on spheroid volume (V/V_0) over 24 days. Figure 5.9(B) showed a statistically significant reduction in AUC following treatment with 44.32 μ M TMZ + 6.07 μ M MMF, administered as a schedule (T+M PT4) compared to the untreated control, TMZ alone and the simultaneously administered combination (T+M) (all, $P < 0.05$). However, no significant differences were observed when the combination treatments were compared to MMF alone.

A two-way ANOVA analysing changes in spheroid volume (Figure 5.9 (A)) displayed exposure of the U87 derived MTS to the scheduled combination of (T+M PT4) to significantly reduce spheroid volume at day 20 compared to the untreated control (P

< 0.05). By day 24, significant reductions in spheroid volume were observed for MMF and T+M PT4 treatments compared to the untreated control (both, $P < 0.01$) (Figure 5.9 (C)). The scheduled combination (T+M PT4) also induced a statistically significant reduction in spheroid volume compared to TMZ alone at day 24 ($P < 0.01$) but not MMF alone. No significant changes in spheroid volume were observed at day 4, 8, 12 and 16.

Overall, Figure 5.9 again does not fully support our hypothesis that the combined treatment of MMF and TMZ would result in greater spheroid volume reduction. While the scheduled combination T+M PT4, showed significant reductions in AUC compared to TMZ alone, simultaneously combined T+M alone and the untreated control, they did not demonstrate additional efficacy compared to MMF alone. Furthermore, the scheduled combination treatment was only significantly reduced compared to the untreated control and TMZ when comparing V/V_0 .

5.5 Discussion

The aims of this chapter were to assess the effects of single treatments Temozolomide (TMZ), Monomethyl Fumarate and External beam X-irradiation on UVW and U87 multicellular tumour spheroids (MTS). Once single treatments were evaluated and the dose range required to elicit a significant reduction in spheroid volume observed, the combination of TMZ and MMF, was applied to the MTS for UVW and U87 cell lines to assess if the combination resulted in a significant decrease in spheroid volume compared to the single treatments. Further to this, as previously shown, scheduling MMF 4- hours prior to the administration of TMZ, resulted in a synergistic response and a significant reduction in clonogenic survival compared to simultaneous administration. The scheduled double combination was applied to MTS in the UVW and U87 cell line and its reduction in spheroid volume compared to both the single treatments and the simultaneous combination. Due to access to the External beam X-irradiation being limited throughout this study, and then becoming non-functional, the triple combination effects seen in 2D could not be applied to the 3D model. The institute of Strathclyde is in the process of replacing the X-irradiator and once available the triple combinations applied in Chapter 4 will be carried out in MTS for the UVW and U87 cell line.

As the T98g cell line is an MGMT positive cell line, the evaluation of the combination model in T98g MTS would have been useful. Future studies will include different methods of culturing T98g MTS to assess how the combinations translate into the TMZ resistant cell line. Combining the T98g cell line with UVW and U87 cell lines to create a mosaic spheroid model which is heterogeneous and further represents a patient tumour could be a model to overcome the cell lines inability to form spheroids. A mosaic spheroid model would not only create a heterogenous population but could have potential to incorporate the T98g MGMT positive cell line as to test the combinations and hypoxic core formation further (Boyd *et al.*, 2002).

5.5.1 Effects of Temozolomide on 3D Multicellular tumour spheroid models.

Both UVW and U87 spheroids showed dose responsive reductions in spheroid volume to increasing concentrations of TMZ. UVW spheroids were less responsive to TMZ than U87 spheroids, with the U87 spheroids displaying a significant reduction in area under the curve (AUC) at a concentration of 1 μ M compared to the untreated control. The UVW spheroids did not show a statistically significant reduction in the AUC until 5 μ M of TMZ was administered. Contrastingly when observing spheroid volume changes over time, after 24 days the UVW cell line showed all concentrations of TMZ to have a significant reduction in spheroids volume compared to the untreated control (all, $P < 0.01$). The U87 cell line however, at day 24, showed significant reductions in spheroid volume compared to the untreated control after spheroids were exposed to 2.5 μ M, 10 μ M, 20 μ M and 40 μ M (all, $P < 0.05$). Although both cell lines had varied significant responses, the data correlates well with the 2D monolayer clonogenic assay results from Section 3.4.2, where the UVW cell line had an IC_{50} of 19.7 μ M and the U87 cell an IC_{50} of 1.6 μ M with TMZ. TMZ studies on spheroid volume changes supports previous data from this study and previous reports from the literature (Günther *et al.*, 2003). Data also supports the use of TMZ at the concentrations of 44.32 μ M on UVW spheroids and 2.4 μ M on U87 spheroids for the combinations with MMF, as a significant reduction in spheroid volume and AUC was observed for these concentrations. Overall, our data supports the hypothesis of single treatment TMZ significantly reducing spheroid volume over time.

5.5.2 Effects of Monomethyl Fumarate on 3D Multicellular tumour spheroid models.

Monomethyl Fumarates response on GBM spheroids has never been researched previously. However, from previous studies Dimethyl Fumarate (DMF) when applied to GBM spheroids did not cause a dose-dependent reduction in spheroid volume (Scott, 2020). MMF is the direct metabolite of DMF and would therefore expect MMF to have an increased cancer cell death response than DMF. This increased potency with MMF over DMF was seen in 2D clonogenic assays in this study (Chapter 3) and was also seen in pancreatic cancer and breast cancer studies using MMF on MTS (Gardiner, 2023; Mullen, 2024). The mechanisms behind this increased cancer cell death is not fully known and literature suggests it is through depletion of glutathione which upregulates oxidative stress. The effect of MMF on pancreatic spheroids (Mullen, 2024) and breast cancer cell line spheroids (Gardiner, 2023), both showed significant dose response reductions in spheroid volume. It was therefore hypothesised that MMF would have a significant dose dependent reduction on UVW and U87 spheroids. From both UVW and U87 data (Figure 4 and 5), clear dose response reductions in spheroid volume can be observed compared to the untreated control. AUC analysis on both cell lines revealed a statistically significant reduction in AUC after exposure to all concentrations of MMF (all, $P < 0.001$) compared to the untreated control AUC. In the U87 cell line, there was a direct dose response reduction in AUC as the concentrations of MMF increased whereas in the UVW cell line (Figure 5.4(B)) there were smaller reductions in AUC as the concentrations increased compared to the untreated control. MMF concentrations on the UVW cell line of 10 μ M, 20 μ M and 40 μ M resulted in an AUC value of 56.54, 51.79 and 50.14 respectively, compared to the U87 cell line where MMF concentrations of 10 μ M, 20 μ M and 40 μ M provided an AUC value of 51.56, 17.86 and 9.22 respectively. This suggests that the U87 cell line spheroids were more sensitive to MMF than the UVW MTS. This again correlated well with the 2D response of MMF on the UVW and U87 cell line, where MMF had an IC_{50} of 2.7 μ M in UVW cells, and 1.9 μ M in U87 cells (Figure 3.2 and 3.3 respectively). Reductions in spheroid volume (V/V_0) were observed after exposure to all concentrations of MMF to significantly reduce spheroid volume compared to the untreated control at day 24 in the UVW derived MTS (all $P < 0.0001$) (Figure 5.4(A)). In the U87 cell line, all concentrations of MMF significantly reduced spheroid volume compared to the untreated control at day 16 (all, $P < 0.01$) (Figure 5.5(A)). Again, this

shows the increased sensitivity of the U87 cell line to MMF. The increased sensitivity of the U87 cell line to MMF we hypothesise, possibly prevented synergistic combinations when simultaneously combined with TMZ in 2D studies, which may translate into 3D studies (Figure 3.6 and 3.9). This would be due to MMF alone eliciting a high cytotoxic response and reduction in U87 cell survival after treatment which was not significantly increased after combining MMF with TMZ. Our data supports the hypothesis of single treatment MMF significantly reducing spheroid volume over time compared to the untreated control. As this is the first study on the use of MMF on GBM spheroids, the data supports MMF having an as yet unknown cell death inducing mechanism of action on GBM cells. From the extensive mechanistic assay interrogation applied in Chapter 3, data for our MTS is hypothesising DNA damage from MMF on the proliferating outer layers of the spheroid as well as good penetration of the drug. Further investigative studies on drug penetration of MMF on 3D models would be useful to elucidate the mechanisms. This could be achieved in future studies using fluorescent DNA damage markers such as H2AX and confocal imaging (Riffle *et al.*, 2017). Additionally, spheroids could be dissociated and a comet assay performed similar to Section 3.4.10. Furthermore, MMF, as shown in section 3.4.5, depletes glutathione in a time dependent manner, with both U87 and UVW cell lines returning to basal GSH levels over time. In a study by Ogunrinu and Sontheimer, (2010), findings suggested glioma cells have an increased need for GSH to maintain growth under hypoxic conditions. As MMF depletes GSH by binding to intracellular GSH and inhibition of Nrf2 and therefore GSH transcription (Saidu *et al.*, 2017), this mechanism could be contributing to the dose dependent reduction in spheroid volume seen over time as less GSH is available after MMF exposure preventing initial inhibition of spheroid growth. An assay to compare GSH levels in spheroids treated with increasing concentrations of MMF over time, would be beneficial in future studies to further elucidate MMF's effect in GBM. GSH could be detected in spheroids by lysing the spheroids with either monochlorobimane which detects reduced GSH, and fluorescence measured (Marrazzo *et al.*, 2019). Additionally, trichloroacetic acid can be used to determine ATP and GSH levels in spheroids (Walker *et al.*, 2000).

5.5.3 Effects of External beam X-irradiation on 3D Multicellular tumour spheroid models.

Radiotherapy is given to almost all GBM patients and is central to patient treatment regardless of surgical intervention and patient IDH/MGMT status (Li *et al.*, 2022). Radiation is given to GBM patients in fractions of 2Gy for a total of 60Gy (Li *et al.*, 2022). Radiotherapy as previously mentioned causes DNA damage through direct and indirect mechanisms which rely on the presence of oxygen. Oxygen oxidises radical DNA lesions in DNA, therefore resistance seen with radiotherapy is due to hypoxic areas in the GBM tumour microenvironment (Wang *et al.*, 2018). With 2Gy being given in fractions clinically, we hypothesised a dose responsive inhibition of GBM spheroid growth over time. Both cell lines, UVW (Figure 5.6) and U87 (Figure 5.7) after exposure to increasing doses of X-irradiation (1-12Gy) had reductions in AUC with all doses having a statistically significant reduction in AUC than the untreated control (all $P < 0.05$). Analysing the reduction in spheroid volume over time suggested that the UVW spheroids after exposure to all doses of X-irradiation, exhibited significantly reduced spheroid volume compared to the untreated control after and including day 16 (all $P < 0.01$) (Figure 5.6(A)). Additionally, in the UVW cell line derived MTS there was a clear dose dependent reduction in AUC, after all X-irradiation doses compared to the untreated control, showing X-irradiation at any dose to significantly reduce spheroid volume over time. In the U87 cell line spheroids, a significant reduction in spheroid volume compared to the untreated control was observed after day 24 for all doses of X-irradiation (all $P < 0.001$). Further to this, with the U87 spheroids there was the greatest reduction in AUC after 6Gy exposure with an AUC of 42.8, after which the doses of 8Gy, 10Gy and 12Gy showed an increased AUC with a value of 67.84, 58.73 and 44.07 respectively. Exposure to 1Gy of X-irradiation unlike the UVW MTS, did not significantly reduce AUC over time compared to the untreated control. Data is surprising for the U87 cell line as the U87 cell line when exposed to X-irradiation in 2D monolayer cultures was the most sensitive and provided an ED_{50} of 1.6Gy, compared to UVW's ED_{50} in 2D monolayer of 2.4Gy. Comparison of these findings to the literature, shows U87 spheroids having a clear and distinguishable dose dependent reduction in spheroid volume compared to the untreated control when exposed to 5, 10 and 20Gy of X-irradiation (Fedrigo *et al.*, 2011). However, in the study by Fedrigo *et al.*, (2011), the maximum dose of radiotherapy given was 20Gy which showed no change in spheroid volume over time,

whereas after 10y doses in the study showed some growth of the spheroids, which correlates well with the 10Gy exposure data present here. Previous data from the Boyd lab on the response of U87 spheroids to increasing doses of X-irradiation also showed that exposure of spheroids to 6Gy of X-irradiation resulted in a lower AUC than 8Gy (McCabe *et al.*, 2023). Thus, the data seen in our study of X-irradiation on U87 derived MTS correlates well with the literature, and suggests the MTS to have an increased resistance to X-irradiation compared to the UVW MTS. Further experimentation into the possible mechanism behind this could be higher doses of X-irradiation causing significant oxygen depletion in spheroids promoting further hypoxia and therefore resistance (Beckers *et al.*, 2024). This has been seen in the literature, where flash irradiation causes the hypoxic core to expand temporarily and engulf oxygenated cells (Khan *et al.*, 2021). By use of immunohistochemistry, spheroids treated with 6Gy and 12Gy could be subjected to the pimonidazole hypoxia assay to assess if the higher doses of X-irradiation are leading to increased hypoxia within the spheroids (Riffle *et al.*, 2017). Collectively, our data supports our hypothesis of X-irradiation as a single treatment significantly reducing spheroid volume over time.

5.5.4 Effects of combining Temozolomide and Monomethyl Fumarate on 3D Multicellular tumour spheroid models.

Previous data collected in Chapter 3, showed synergy when combining TMZ and MMF in 2D monolayered cell culture of the UVW cell line. When the combination of both TMZ and MMF was scheduled as a 4- hour pretreatment of MMF followed by TMZ for a total of 24 hours in the U87 cell line in 2D cell culture, the combinations were also shown to be synergistic. To assess how these combinations translate into 3D spheroid models, the concentrations of TMZ and MMF used for each cell line throughout mechanistic studies in Chapter 3, were applied to spheroids grown to ~300nm with hypoxic core formation. Both simultaneous and scheduled administration of the combinations were applied to the spheroids as well as the corresponding single treatments. Our hypothesis that the combination of TMZ and MMF would translate across into 3D models by causing enhanced spheroid growth inhibition was surprisingly rejected as both the simultaneous and scheduled combinations for UVW and U87 spheroids did not significantly reduce AUC or spheroid volume compared to TMZ alone and MMF alone, respectively. Both AUC and spheroid volume were

reduced for the scheduled combinations compared to the untreated control in both cell line derived MTS. Both combinations (T+M) and (T+M PT4) AUC were significantly reduced over MMF and the untreated control in the UVW spheroids but not TMZ alone. Whereas in the U87 cell line, only the scheduled combination (T+M PT4) significantly reduced AUC compared to the untreated control, TMZ alone and T+M but not MMF. Although the data was not as expected, it does correlate well with the 2D combination data, where only scheduled combinations were synergistic in the U87 cell line, and in the UVW cell line the combination of 44.32 μ M TMZ and 6.07 μ M MMF was synergistic at either administration, simultaneous or scheduled. Further to this, in the U87 cell line, the response of MMF is more potent than the UVW cell line in 2D, with this translating into the 3D models, and preventing the combination for having a combined greater effect at reducing AUC or spheroid volume when compared to MMF. As this is the first report of combining TMZ and MMF on GBM spheroid models, the lack of significance over both the single agents is incomparable to any previous data. However, although insignificant, we can clearly see the schedule in both cell lines, to have the smallest change in tumour volume over time. Also, both MMF and TMZ as single treatments showed potent dose response curves and inhibition of spheroid volume at the concentrations used in the combinations, it would suggest synergy when combined. Data suggests the need for optimisation of the schedule in 3D models and the combinations. By investigating the changes on GSH levels after MMF treatment, as previously discussed, the treatment schedule may also need adjusted in 3D models. Further to this, in the T98g cell line the combinations at all concentrations were synergistic at either a scheduled or simultaneous administration in 2D monolayer, which the UVW and U87 cell line did not show. As the T98g cell line, in this study is representative of the MGMT positive patients, resistant to TMZ due to the DNA damage repair mechanism being unsilenced, it could be hypothesised in T98g spheroid models, the combination would translate better into 3D models. Data shown prompts further investigation into the combination of TMZ and MMF in 3D spheroid models, as the scheduled combination did have the smallest change in spheroid volume. This will be performed once a method to grow the T98g spheroids to a size of ~300nm is achieved or as previously mentioned by creating mosaic spheroids, combining all cell lines to create a heterogenous MTS.

5.6 Conclusions

Data shown throughout Chapter 5, supported our hypothesis of the single treatments Temozolomide, Monomethyl Fumarate and External beam X-irradiation to induce statistically significant reductions in spheroid volume and AUC over time compared to the untreated controls. However, the hypothesis for our combinations of TMZ and MMF to significantly reduce AUC and spheroid volume when compared to the single treatments and untreated control, given either as a schedule or simultaneously were only partially supported. For each cell line – UVW and U87 – there was no significant reduction in spheroid volume/AUC over spheroids exposed to the corresponding doses of each single drug, TMZ or MMF. As the UVW cell line did induce significant reductions in AUC and V/V0 when combined (both T+M and T+M PT4) over MMF, and the U87 cell line did induce significant reductions in AUC and V/V0 when scheduled (T+M PT4) over TMZ, the hypothesis was partially validated.

To better understand the reasoning behind this, further IHC, imaging and development of mosaic spheroids as mentioned should be used to check levels of hypoxia over time, levels of GSH over time and DNA damage over time (Boyd *et al.*, 2002; Marrazzo *et al.*, 2019; Riffle *et al.*, 2017). These are areas of interest, as hypoxic tumour environments require higher levels of GSH to grow, therefore investigating GSH levels in MMF, TMZ, (T+M) and (T+M PT4) treated spheroids, may help decipher how GSH is affecting the 3D models (Ogunrinu and Sontheimer, 2010). DNA damage response in the spheroids would also be useful as during mechanistic studies in Chapter 3, the combinations as well as TMZ and MMF showed an increase in Tail movement (AU) representative of increased DNA damage (Figure 3.18 and 3.19). How this response is translating with the treatments into 3D would help uncover the reason behind the lack of significance over both single treated spheroids. Additionally, mosaic spheroids would be an interesting model to apply our combination as all three cell lines individually have a variable response to MMF, TMZ and the combinations. By combining the cell lines, the heterogeneity of GBM tumours as well as cell-cell interactions would be interesting before progression of the combinations. Finally, as mentioned, the triple combination studies of TMZ, MMF and X-irradiation in the 3D MTS model has yet to be carried out. It is hypothesised that the addition of X-irradiation at 1Gy and 2Gy to our double combinations will significantly reduce spheroid volume over all single treatments.

Chapter 6

Preliminary Study - Interrogating the varied response of Dimethyl Fumarate and Monomethyl Fumarate on 2D human Glioblastoma cell lines.

6.1 Introduction

To further promote the use of DMF in glioblastoma (GBM) treatment, previous studies in colon and breast cancers have demonstrated that DMF modulates the NrF2/HO-1/NQO1/DJ1 antioxidant pathway, resulting in cancer cell death (Chen *et al.*, 2021). Parkinsonism-associated deglycase 1 (DJ1) is a key regulator of the oxidative stress response, facilitating NrF2 dissociation from Keap1 and promoting antioxidant defence's (Zhang *et al.*, 2020). High concentrations of DMF have been reported to inhibit DJ1 and subsequently suppress NrF2 activity (Saidu *et al.*, 2019). Inhibition of DJ1, and thus NrF2, in GBM cells may decrease GSH levels, disrupting redox homeostasis and promoting cell death. This mechanism has also been implicated in colon cancer, where DJ1 inhibition led to increased oxidative stress and cell death (Saidu *et al.*, 2019). DMF has been shown to deplete intracellular glutathione (GSH) levels, elevate reactive oxygen species (ROS), and drive cancer cell death in a concentration- and time-dependent manner (Brennan *et al.*, 2015; Saidu *et al.*, 2019). Given its promising preclinical effects, DMF has been evaluated in a Phase I clinical trial in GBM patients in combination with temozolomide (TMZ) and radiotherapy, showing positive outcomes in a limited cohort (Shafer *et al.*, 2020).

GSH, a major antioxidant, is activated via NrF2 nuclear translocation and binding to antioxidant response elements (AREs) with musculoaponeurotic fibrosarcoma oncogene homolog (MAF) proteins (Jaganjac *et al.*, 2020; Saidu *et al.*, 2019). Activation of this pathway upregulates antioxidant enzymes including HO-1, NQO1, and glutathione peroxidases, as well as promotes GSH synthesis and recycling (Jaganjac *et al.*, 2020; Saidu *et al.*, 2019).

In cancer, particularly GBM, upregulation of NrF2 and GSH enhances tumorigenesis and therapy resistance (Kennedy *et al.*, 2020). NrF2 has been associated with IDH mutations in GBM and contributes to malignant proliferation. Downregulation of NrF2 has been shown to promote apoptosis (Awuah *et al.*, 2022). Targeting NrF2 could

therefore enhance chemotherapy effectiveness by reducing GSH-mediated detoxification and ROS scavenging, as well as downregulating GPX4 an essential enzyme protecting against ferroptosis (Niu *et al.*, 2021).

DMF and MMF are also known to deplete GSH through direct conjugation (succination), further increasing oxidative stress and promoting cell death (Zheng *et al.*, 2015). Ferroptosis a distinct, iron and ROS-dependent form of cell death results from uncontrolled lipid peroxidation and can be triggered by GPX4 inactivation (Ursini and Maiorino, 2020; Galaris *et al.*, 2019). As GPX4 function depends on GSH, fumarate mediated GSH depletion may promote ferroptosis, although this mechanism remains incompletely characterised in GBM (Niu *et al.*, 2021).

Emerging evidence suggests that targeting ferroptosis could offer a novel therapeutic avenue for GBM, with GPX4 inhibitors under investigation (Zhuo *et al.*, 2022). Notably, DMF has been shown to induce ferroptosis in large B-cell lymphoma in a concentration and time-dependent manner, further supporting its potential in GBM (Schmitt *et al.*, 2021).

However, studies have shown heterogeneity in the effects of fumarate esters. MMF, for example, does not modulate Nrf2 in primary GBM cells (Dent *et al.*, 2020), while DMF at high concentrations activated the Nrf2-HO-1 axis (Gillard *et al.*, 2015). Comparative analyses have indicated that DMF and Monoethyl fumarate deplete GSH and modulate the Nrf2/Keap1 pathway differently (Brennan *et al.*, 2015). Moreover, transcriptomic profiling revealed distinct gene expression responses to DMF, MMF, diroximel fumarate (DRF), and isosorbide dimethyl fumarate (IDMF) in astrocytes, with DRF and IDMF, but not MMF significantly upregulating Nrf2 and HO-1 expression (Swindell *et al.*, 2022).

While these studies were conducted in non-cancerous cells, they highlight the differential activity of fumarates across cell types. Other targets, such as DJ1 and GPX4, may also contribute to the therapeutic effects of DMF and MMF in GBM. Figure 6.1 provides a schematic overview of the proposed mechanisms of DMF and MMF action on Nrf2, NF- κ B, GPX4, and DJ1 pathways.

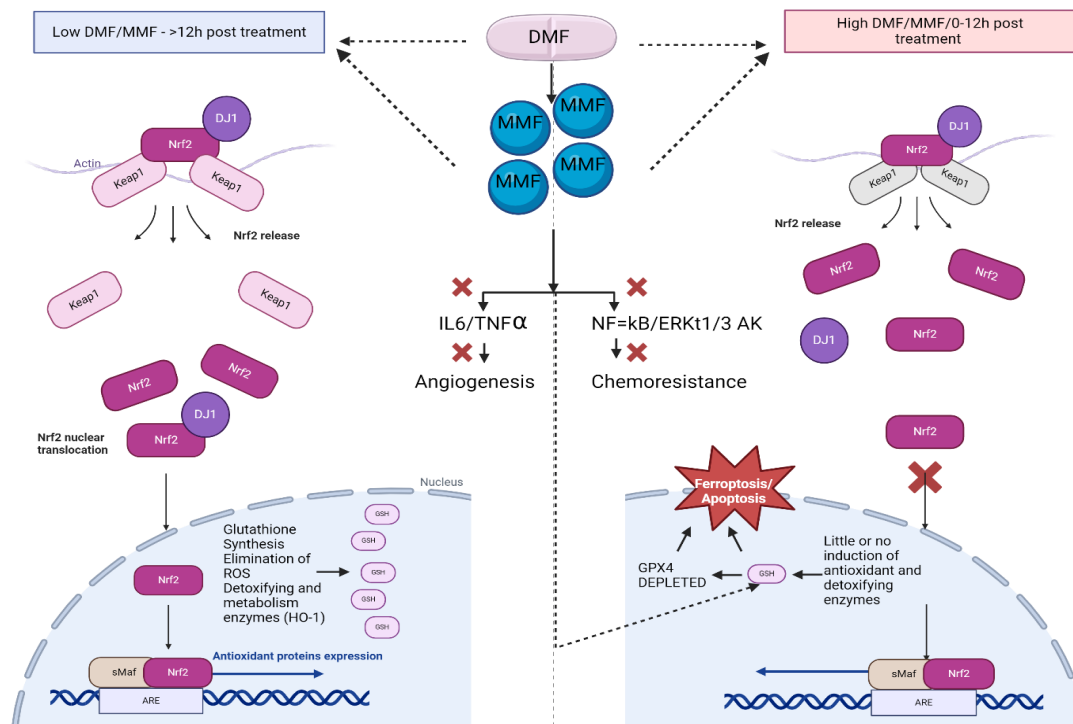


Figure 6.1: Proposed collective potential target pathways of DMF or MMF. DMF hydrolysis to MMF and modulation of the Nrf2, DJ1, GSH, GPX4, NF- κ B, IL-6 and TNF- α pathways. The effect of time and concentration highlight the dose dependent and time dependent importance of fumarate administration for GBM treatment. Adapted from (Avci *et al.*, 2020; Brennen *et al.*, 2015, Saidu *et al.*, 2019; Shafer *et al.*, 2020). Created using Biorender.

Therefore, whether MMF would function similarly or differently to DMF in GBM is not fully understood. Previous studies in the Boyd group (Gardiner, 2023, Mullen, 2024), have shown DMF and MMF to work differently in breast and pancreatic studies, and the study by Scott, (2020) reported the synergistic combination of DMF, TMZ and RT in GBM. To compare the DMF and MMF response in GBM cells, we utilised the IC_{50} values calculated in Chapter 3 and chose a concentration higher and a concentration lower for both drugs and applied these to RT-qPCR assays, ferroptosis assays and glutathione assays to assess if DMF and MMF affect GSH levels differently, if DMF and MMF alter gene expression of the key pathways discussed and if DMF and MMF are able to induce ferroptosis. We hypothesised that both DMF and MMF have different mechanisms of action with MMF expected to have more of an effect on GSH depletion, ferroptosis instigation and on the gene expression analysed by RT-QPCR. We also hypothesis a time and concentration dependant response.

6.2 Aims

The aims of this chapter were:

- To assess if Dimethyl Fumarate and Monomethyl Fumarate have different effects on glutathione levels over time which is concentration dependent.
- To determine if Dimethyl Fumarate and Monomethyl Fumarate function differently on the expression of genes NrF2, P65, DJ1 and GPX4
- To decipher if Dimethyl Fumarate or Monomethyl Fumarate instigate ferroptosis.

6.3 Materials and Methods

6.3.2 Cell treatment

Cells were treated following the same protocol as section 2.4 and 2.5. Treatment concentrations used throughout the chapter are shown in Table 6.1

Treatment	Concentration μM
U87 Cell Line	
Dimethyl Fumarate	9.60 μM
	38.4 μM
Monomethyl Fumarate	0.95 μM
	3.80 μM
T98g Cell line	
Dimethyl Fumarate	0.95 μM
	3.80 μM
Monomethyl Fumarate	0.80 μM
	3.12 μM

Table 6.1: The concentrations of DMF and MMF used throughout chapter 6 studies

6.4 Results

6.4.1 Comparison of the effect of Dimethyl Fumarate and Monomethyl Fumarate on Glutathione depletion in the UVW, U87 and T98g human glioblastoma cell lines

To determine the effects of DMF and MMF on glutathione levels in GBM cells, glutathione assay was performed as described in Section 3.4.4. From our previous data in Chapter 3 – 3.4.4, we reported that generally in the 3 cell lines, GSH levels were higher in the post exposure time points compared to the total exposure time points, where the drug was left on for 4h, 24h and 48h. Additionally when looking at GSH levels after MMF exposure time in Section 3.4.4, 4h and 24h exposure times GSH levels were significantly decreased by MMF. Therefore, utilising these time points allowed for MMF and DMF exposure on GSH levels to be monitored directly over time. As the literature has shown GSH levels return to control levels by 24h with DMF, therefore again the use of time points after the exposure times was not relevant when only looking at comparing the fumarates. Due to previous data results on the fumarates (Brennan *et al.*, 2015; Gardiner, 2023; Mullen, 2024; Swindell *et al.*, 2022) we hypothesised MMF and DMF would elicit different reductions on the relative GSH levels at each time point and concentration. We also hypothesised that the higher concentrations of both DMF and MMF would induce significant reduction in GSH levels overall (Saidu *et al.*, 2019). We also hypothesise between 4h and 24h treatment exposure times, 4h exposure will induce reduced GSH level when compared to the 24h GSH levels. UVW cell line data was not included for this preliminary data and will be completed for publication

6.4.1.1 Comparison of the effect of Dimethyl Fumarate and Monomethyl Fumarate on Glutathione levels in the U87 and T98g cell line.

Figure 6.2 shows the data when U87 and T98g cells were treated with two concentrations of MMF and DMF, both lower and higher than the IC_{50} for either 4-hours or 24- hours (Table 6.1). The data presented for each time point was normalised

to the control levels of total glutathione, calculated from the standard curve for comparison. A two-way ANOVA was applied to determine significant changes in GSH levels between time points, between concentrations and changes between both time and concentration to the untreated control.

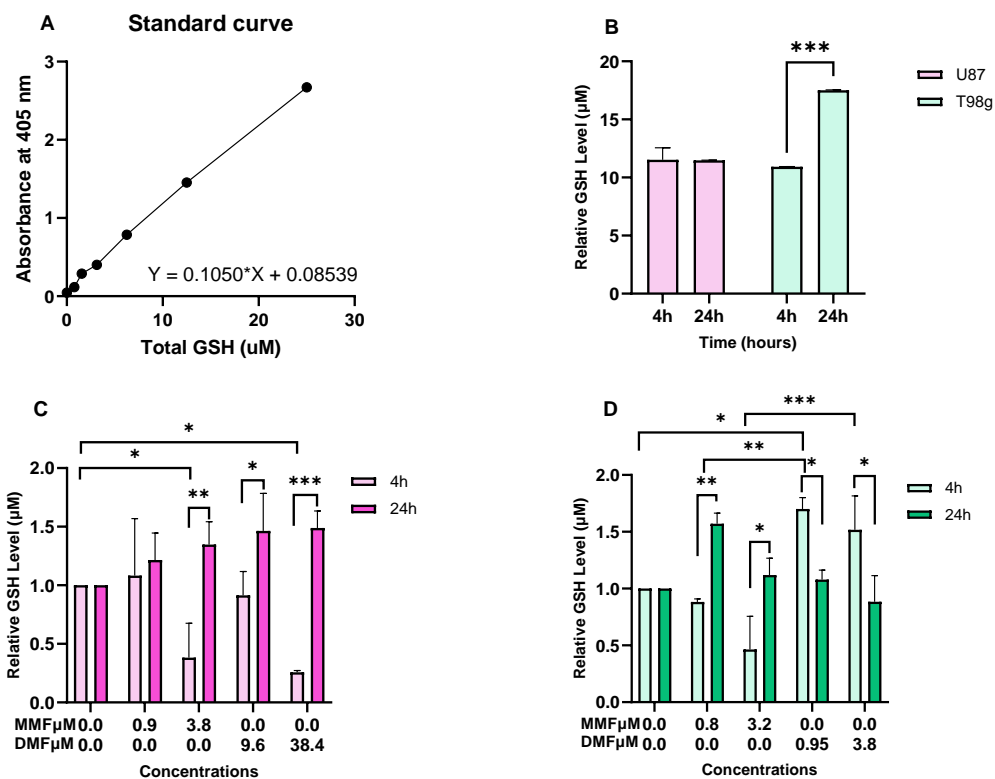


Figure 6.2: Relative glutathione levels in the cell lines after timed exposures of 4h and 24h to Monomethyl Fumarate and Dimethyl Fumarate after exposure to two different concentrations. Standard curve used to determine total GSH levels (A). Untreated control cells for both cell lines at each time point (B). Relative GSH levels in the U87 cell line normalised to the untreated control (C). Relative GSH levels in the T98g cell line normalised to the untreated control (D). Data reported is an average of two independent experiments \pm standard deviation. A two-way ANOVA with Bonferroni post testing was performed using GraphPad prism 10.3.1 comparing each treated and untreated group to each other, showing only the statistically significant differences with P-values of $<0.05 = *$, $<0.01 = **$, $<0.001 = ***$ and $P < 0.0001 = ****$ reported as significant.

Figure 6.2 presents the analysis of total and relative GSH levels after MMF and DMF exposure across the U87, and T98G cell lines. Figure 6.2 (A) shows the standard

curve used to calculate total GSH levels. In Figure 6.2 (B), comparison of untreated controls revealed a statistically significant difference in GSH levels between 4h and 24h only in the T98G cell line ($P<0.0001$), suggesting potential error in the 4h measurement as previously higher GSH levels ($\sim 20\mu\text{M}$) were reported in Figure 6.8 (B).

In U87 cells (Figure 6.2 (C)), significant GSH depletion compared to the untreated control was observed after 4h exposure to $3.8\mu\text{M}$ MMF and $38.4\mu\text{M}$ DMF (both $P<0.05$). Significant differences between 4h and 24h exposures were found for $3.8\mu\text{M}$ MMF, $9.6\mu\text{M}$ DMF, and $38.4\mu\text{M}$ DMF ($P<0.05$), further supporting a time-dependent response. No differences between MMF and DMF treatments were observed.

In T98G cells (Figure 6.2 (D)), exposure to $0.95\mu\text{M}$ DMF led to a statistically significant increase in GSH levels compared to the untreated control ($P<0.05$). Significant time-dependent differences were observed for all MMF and DMF concentrations, with MMF showing an initial decrease and DMF showing an initial increase at 4h followed by opposite changes at 24h ($P<0.05$). Statistically significant differences were also found between MMF and DMF treatments at 4h ($P<0.001$ and $P<0.01$), partially supporting differential activity between the fumarates in T98G cells.

Overall, the data partially support the hypothesis that MMF and DMF induce a time- and concentration-dependent reduction in GSH levels. However, as significant differences between MMF and DMF were only consistently found in T98G cells and not across all lines, the hypothesis that the two fumarates act differently on GSH depletion was rejected.

6.4.2 Modulation of NrF2, P65, GPX4 and DJ1 after exposure to Monomethyl Fumarate and Dimethyl Fumarate on human glioblastoma cell lines via RT-qPCR.

By use of RT-qPCR we aimed to distinguish whether MMF and DMF worked similarly in altering the expression of these genes in GBM cell lines and if by depletion of GPX4 the cells may be undergoing ferroptosis. Data will also show if DMF and MMF effects on GSH shown in 6.4.1 correspond to the fold change in gene expression.

A concentration half of the IC_{50} and double the IC_{50} were used to also distinguish if the changes in gene expression after DMF and MMF exposure were concentration dependent (Table 6.1). The same time points as the glutathione assay were applied to corroborate the data and to see if changes in NrF2, P65, DJ1 and GPX4 could be further explained by correlation with the GSH levels after 4h and 24h exposure to DMF and MMF.

Based on the changes in relative GSH found after DMF and MMF exposure on the U87 and T98g cell lines in 6.4.1, we hypothesised that the higher concentrations of MMF and DMF after 4h exposure would lower the expression of GPX4 which is dependent on its co-factor GSH. We also hypothesised a similar response for NrF2, P65 and DJ1 gene expression, based on literature reports of higher concentrations of DMF inhibiting NrF2, DJ1 and P65 more so than the lower concentrations of DMF which was shown to activate the genes (Saidu *et al.*, 2019). We also hypothesises both MMF and DMF alter the 4 genes expressions differently between 4h and 24h based on previous data and literature reports of a time dependent inhibition of GSH which may translate into the NrF2/DJ1/P65 genes (Brennan *et al.*, 2015). By comparing DMF and MMF changes on the gene expression we hypothesise the two drugs to work differently with respect to modulating gene expression, as literature reports have suggested (Swindell *et al.*, 2022).

6.4.2.1 The effect of Dimethyl Fumarate and Monomethyl Fumarate on NrF2, P65, GPX4 and DJ1 expression in the U87 and T98g cell line.

Figure 6.3 shows the fold change in NrF2 (A) P65 (B) GPX4 (C) and Dj1 (D) gene expression after incubation of the U87 and T98g cells with two concentrations of MMF

and DMF (Table 6.1). Fold change was calculated using the $\Delta\Delta C_t$ method to reference gene GAPDH. A two-way ANOVA was applied to determine significant changes in fold change between time points, between concentrations and between both time and concentration to the untreated control. Statistical analysis is shown in Table 6.2 for all significant changes only. Appendix 5 shows supplementary amplification plots and the untreated control cells variation in fold change.

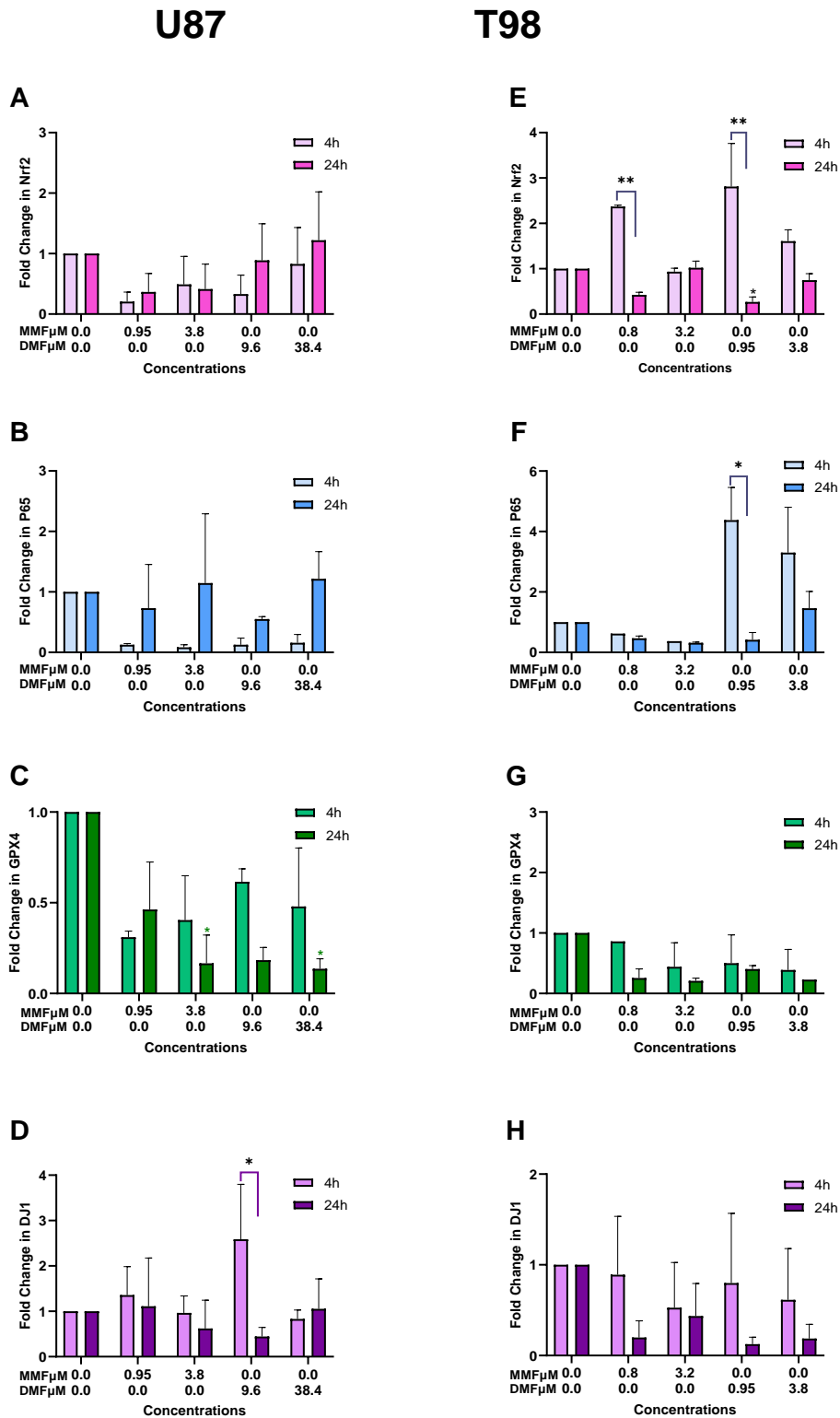


Figure 6.3: Modulation in U87 (left) and T98g (right) cells on Nrf2 (A, E) P65 (B, F) GPX4 (C, G) and DJ1 (D, H) gene expression after timed exposures of 4h and 24h to Monomethyl Fumarate and Dimethyl Fumarate quantified by RT-qPCR. Data reported

is an average of two independent experiments \pm standard deviation. A two-way ANOVA with Bonferroni post testing was performed using GraphPad prism 10.3.1 comparing each treated and untreated group to each other, with P-values of $<0.05 = *$, $<0.01 = **$, $<0.001 = ***$ and $P < 0.0001 = ****$ reported as significant.

Two-way Anova with Bonferroni's post test		
Treatment	Significant Summary	Adjusted P value
U87		
<u>GPX4 Fold Change</u>		
Control vs 24h MMF 3.8 μ M	Yes*	0.0498
Control vs 24h DMF 38.4 μ M	Yes*	0.0403
<u>DJ1 Fold Change</u>		
MMF 9.6 μ M vs DMF 38.4 μ M 4h	Yes*	0.0381
T98g		
<u>NrF2 Fold Change</u>		
Control vs 4h DMF 0.95 μ M	Yes*	0.0257
MMF 0.8 μ M 4h vs 24h	Yes**	0.0079
DMF 0.95 μ M 4h vs 24h	Yes**	0.0011
<u>P65 Fold Change</u>		
DMF 0.95 μ M 4h vs 24h	Yes*	0.0181

Table 6.2: Statistically significant changes following a two-way ANOVA with Bonferroni post testing for Figures represented in Figure 6.3, with P-values of $<0.05 = *$, $<0.01 = **$, $<0.001 = ***$ and $P < 0.0001 = ****$ reported as significant. Non-significant data was not shown in the table.

In the U87 cell line (Figure 6.3 (A)), no statistically significant changes in NrF2 gene expression were observed after 4h or 24h exposure to either DMF or MMF at both concentrations tested compared to the untreated control. Although trends suggested a time-dependent reduction with lower fold changes at 4h, inconsistencies between treatments and time points led to the rejection of the time- and concentration-dependent hypotheses, as well as the hypothesis that DMF and MMF would differentially modulate NrF2.

Similarly, no statistically significant changes in P65 expression were found (Figure 6.3 (B)). Trends indicated greater reductions in P65 gene expression at 4h compared to 24h for both DMF and MMF treatments; for example, 0.95 μ M MMF induced an 88% decrease after 4h, but only a 27% decrease after 24h. However, due to the lack of

statistical significance, the hypotheses of time-dependent and differential modulation were rejected.

In contrast, GPX4 gene expression showed some statistically significant reductions. Exposure to 3.8 μ M MMF and 38.4 μ M DMF for 24h caused 84% and 87% reductions in GPX4 expression respectively (both $P < 0.05$). However, as no consistent trends across concentrations and time points were identified, the concentration- and time-dependent hypotheses were rejected.

Finally, a statistically significant relative fold change in DJ1 gene expression (Figure 6.3 (D)) was seen between 4h and 24h exposure of 9.6 μ M of DMF ($P < 0.05$). 9.6 μ M of DMF exposure after 4h resulted in a 2.58 ± 1.71 fold change, indicative of a 158% increase in DJ1 expression, whereas 24h exposure of 9.6 μ M of DMF on the U87 cells resulted in a 0.44 ± 0.28 fold change, indicative of a 56% decrease in DJ1 gene expression, with both significantly different. No other significance was determined following a two-way ANOVA test, and again the hypothesis was rejected.

Overall, across all genes studied (NrF2, P65, GPX4, DJ1), the lack of consistent or significant findings led to the rejection of the proposed hypotheses regarding time-dependent, concentration-dependent, and differential effects between DMF and MMF in the U87 cell line., as no trends in time, concentration, or between MMF and DMF exposure allows for conclusions to be drawn.

In the T98g cell line, Figure 6.3 (E) showed a statistically significant reduction in NrF2 gene expression after exposure to 0.95 μ M DMF for 24h compared to the untreated control ($P < 0.05$), with a 74% decrease (fold change 0.26 ± 0.15). A statistically significant time-dependent reduction was also observed between 4h and 24h for both 0.8 μ M MMF and 0.95 μ M DMF exposures (both $P < 0.01$), where 4h treatment initially increased NrF2 expression before significantly decreasing by 24h. However, no significant differences were found between DMF and MMF treatments, and since gene expression levels were lower after 24h rather than 4h, the hypothesis of a time-dependent or drug-specific effect was rejected.

For GPX4 expression (Figure 6.3 (G)), no statistically significant changes were found after exposure to DMF or MMF at either concentration or time point compared to the untreated control. Although the greatest reduction was seen after 24h exposure to 3.2 μ M MMF (79% decrease) and the greatest increase after 24h exposure to 3.8 μ M DMF (59% increase), these changes were not significant. As no consistent trends

were evident, the hypothesis of time- and concentration-dependent GPX4 modulation was rejected.

Similarly, DJ1 gene expression (Figure 6.3 (H)) showed no statistically significant changes after exposure to DMF or MMF at any time point or concentration compared to the untreated control. Although trends suggested DJ1 expression was lower after 24h exposure to both fumarates—with the greatest reduction seen after 24h exposure to 0.95 μ M DMF (88% decrease)—the lack of statistical significance meant no conclusions could be drawn, and the hypothesis was again rejected.

Overall, consistent with findings in the U87 cell line, the T98g cell line data largely lacked significant results. Although a significant time-dependent response was observed for NrF2 following lower concentration treatments, the direction of the effect (greater reductions at 24h rather than 4h) contradicted the hypothesis. No drug-specific differences between MMF and DMF were evident, leading to the overall rejection of the proposed hypotheses. Collectively the data for all genes tested rejected our hypothesis. The lack of significant results prevented conclusions to be drawn from time and concentration dependent reductions in gene expression as well as differences between MMF and DMF on the targeted genes in these cell line.

6.4.3 Ferroptosis induction in human glioblastoma cells after treatment with Monomethyl Fumarate and Dimethyl Fumarate.

As DMF and MMF have shown both in this study and by (Scott, 2020) to deplete GSH levels in the U87 and T98g cell lines, the cytotoxic response of both DMF and MMF could be explained further by the induction of ferroptosis through a knock on depletion of GPX4 after GSH depletion. Further to this however, DMF has been shown to inhibit Nf-kb and P65 phosphorylation in glioma cells (Shafer *et al.*, 2020), therefore possibly preventing the RSL3 mediated activation of the ferroptosis pathway. In non-cancer cells MMF has been shown to have no effect on the Nf-kb pathway, therefore in GMB cells MMF could be upregulating the P65 pathway and inducing ferroptosis of the cells (Gillard *et al.*, 2015).

With ferroptosis so closely connected to the pathways DMF and MMF are thought to impact, it suggested the possibility of DMF and MMF possibly inducing ferroptosis in the GBM cell lines. By use of inducers erastin and RSL3, as well as ferrostatin an inhibitor of lipid peroxidation, an MTT assay was performed to see if ferroptosis could be the mechanism behind DMF and MMF induced cell death seen throughout Chapter 3. Table 6.2 below, shows the concentrations used throughout the assay.

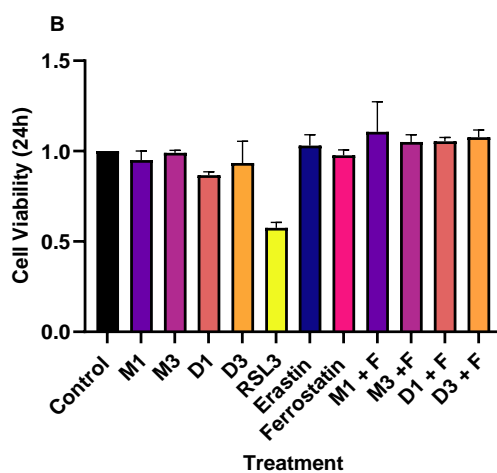
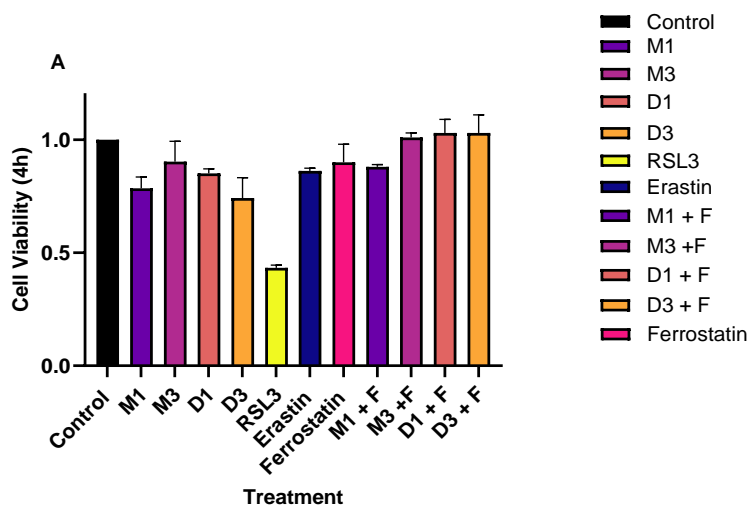
Treatment	Concentration μM
U87 Cell Line	
Dimethyl Fumarate	D1 = 9.60 μM
	D3 = 38.4 μM
Monomethyl Fumarate	M1 = 0.95 μM
	M3 = 3.80 μM
T98g Cell line	
Dimethyl Fumarate	D1 = 0.95 μM
	D3 = 3.80 μM
Monomethyl Fumarate	M1 = 0.80 μM
	D3 = 3.12 μM
All Cell Lines	
Ferrostatin (F)	F = 10nM
Erastin	10nM
RSL3	10nm

Table 6.3: The concentrations of each treatment used in the ferroptosis assay throughout section 6.4.3

As both DMF and MMF have shown to deplete GSH levels, and we have observed reduction in the expression of GPX4 gene expression in all cell lines, we hypothesised that DMF and MMF would induce ferroptosis at the higher concentrations of each drug. By comparison of DMF and MMF reductions in viability being significantly lower than the DMF and MMF + ferrostatin cell viability, it would support the hypothesis. Furthermore, reductions in cell viability caused by exposure of the cells to DMF and MMF if insignificantly different to RSL3 and Erastin induced reduction in cell viability would further support the hypothesis

6.4.3.1 Induction of Ferroptosis after exposure to Dimethyl Fumarate and Monomethyl Fumarate in the U87 cell line.

Figure 6.4 displays the effects on U87 cell viability after exposure to RSL3, erastin, ferrostatin, Dimethyl Fumarate and Monomethyl Fumarate after 4h (A) or 24h (B) exposure to the treatments. A one-way ANOVA with Bonferroni post-test was applied to detect significant changes and are shown in (C) for 4h and (D) 24h.



(C)

One-way ANOVA with Bonferroni's Post test (4h)		
Comparisons	Summary	Adjusted P Value
Control vs. M1	Yes*	0.0104
Control vs. D3	Yes**	0.0026
Control vs. RSL3	Yes****	<0.0001
M1 vs. RSL3	Yes**	0.0022
M3 vs. RSL3	Yes***	0.0001
D1 vs. RSL3	Yes***	0.0004
D1 vs. D1 + F	Yes*	0.0276
D3 vs. RSL3	Yes**	0.0073
D3 vs. D3 + F	Yes***	0.0008
Ferrostatin vs. RSL3	Yes***	0.0001
RSL3 vs. Erastin	Yes***	0.0003
RSL3 vs. M1 + F	Yes***	0.0002
RSL3 vs. M3 + F	Yes****	<0.0001
RSL3 vs. D1 + F	Yes****	<0.0001
RSL3 vs. D3 + F	Yes****	<0.0001

(D)

One- Way ANOVA with Bonferroni's Post test (24h)		
Comparisons	Summary	Adjusted P Value
Control vs. RSL3	Yes****	<0.0001
M1 vs. RSL3	Yes**	0.0080
M3 vs. RSL3	Yes**	0.0032
D1 vs. D1 + F	Yes*	0.0320
D3 vs. RSL3	Yes*	0.0116
Ferrostatin vs. RSL3	Yes**	0.0043
RSL3 vs. Erastin	Yes**	0.0013
RSL3 vs. M1 + F	Yes***	0.0003
RSL3 vs. M3 +F	Yes***	0.0009
RSL3 vs. D1 + F	Yes***	0.0008
RSL3 vs. D3 + F	Yes***	0.0005

Figure 6.4: The effect on cell viability of the U87 cell line after exposure to Dimethyl Fumarate, Monomethyl Fumarate, the ferroptosis inducers RSL3 (10nm) and erastin (10nm), the ferroptosis inhibitor ferrostatin (10nm) and the combination of Dimethyl Fumarate (D1 = 9.6 μ M, D3 = 38.4 μ M) and Monomethyl Fumarate (M1 = 0.95 μ M, M3 3.8 μ M) with ferrostatin (10nm) for either 4h (A) or 24h (B) time points. Data reported is an average of two independent experiments \pm standard deviation. A one-way ANOVA with Bonferroni post testing was performed using GraphPad prism 10.3.1 comparing treatments to each other at the 4h (C) and 24h (D) time points, with P-values of <0.05 = *, <0.01= **, <0.001 = *** and P<0.0001= **** reported as significant, with non-significant differences not shown.

Figure 6.4 (A and C) shows U87 cell viability following 4h exposure to DMF, MMF, and ferroptosis modulators. A statistically significant reduction in viability was observed after exposure to M1 (0.95 μ M MMF), reducing viability by 10% \pm 5 compared to the untreated control (P<0.05), and after exposure to D3 (38.4 μ M DMF), which reduced viability by 26% \pm 9 (P<0.01). Exposure to RSL3 (10nM) resulted in a 57% \pm 1.2 reduction in cell viability compared to the untreated control (P<0.0001).

RSL3 significantly reduced viability compared to all other treatments, including ferrostatin, erastin, MMF, DMF, and their combinations with ferrostatin (all, P<0.001). A statistically significant difference in viability was observed between D1 (9.6 μ M DMF) and D1+F (P<0.05), and between D3 (38.4 μ M DMF) and D3+F (P<0.05), suggesting that DMF may induce ferroptosis at these concentrations. However, as

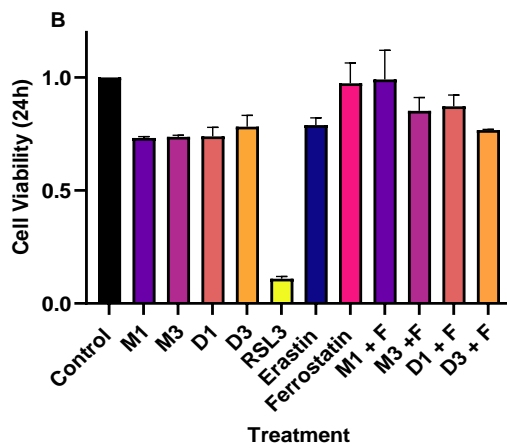
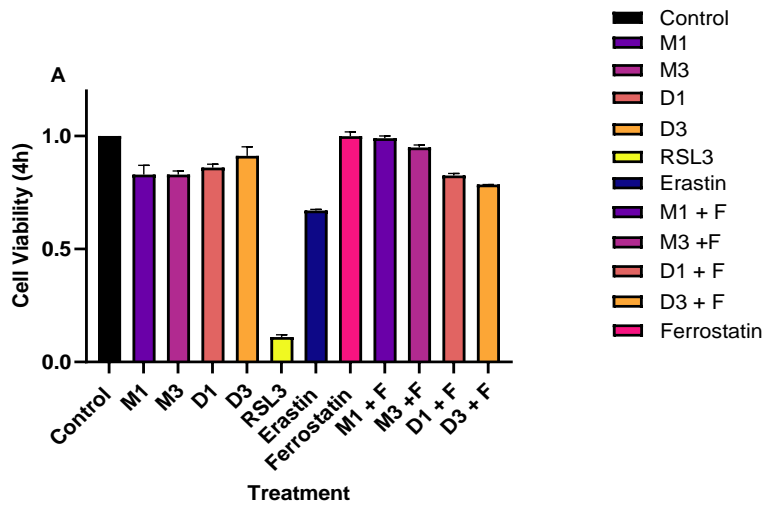
viability reductions with DMF remained significantly different from RSL3, complete confirmation of ferroptosis induction could not be made.

Figure 6.4 (B and D) shows the cell viability after 24h exposure. RSL3 significantly reduced cell viability by $43\% \pm 3$ compared to the untreated control ($P < 0.0001$) and when compared to all other treatments (all, $P < 0.001$). U87 cells exposed to D1 ($9.6\mu\text{M DMF}$) for 24h resulted in a $14\% \pm 1.9$ reduction in viability, which was statistically significant compared to D1+F ($P < 0.05$) and not statistically different from RSL3-induced viability loss.

Overall, the data partially support the hypothesis that DMF induces ferroptosis in U87 cells. The significant protection by ferrostatin at $9.6\mu\text{M DMF}$ after 4h and 24h exposures, and the lack of significant difference from RSL3 at 24h, suggest that DMF may induce ferroptosis at specific concentrations and time points.

6.4.3.2 Induction of Ferroptosis after exposure to Dimethyl Fumarate and Monomethyl Fumarate in the T98g cell line.

Figure 6.5 displays the effects on T98g cell viability after exposure to RSL3, erastin, ferrostatin, Dimethyl Fumarate and Monomethyl Fumarate after 4h (A) or 24h (B) exposure to the treatments. A one-way ANOVA with Bonferroni post-test was applied to detect significant changes and are shown in (C) for 4h and (D) 24h.



(C)

One-way ANOVA with Bonferroni's Post test (4h)		
Comparisons	Summary	Adjusted P Value
Control vs. M1	Yes****	<0.0001
Control vs. M3	Yes****	<0.0001
Control vs. D1	Yes***	0.0006
Control vs. D3	Yes*	0.0421
Control vs. RSL3	Yes****	<0.0001
Control vs. Erastin	Yes****	<0.0001
Control vs. D1 + F	Yes****	<0.0001
Control vs. D3 + F	Yes****	<0.0001
M1 vs. Ferrostatin	Yes****	<0.0001
M1 vs. RSL3	Yes****	<0.0001
M1 vs. Erastin	Yes***	0.0002
M1 vs. M1 + F	Yes***	0.0002
M3 vs. Ferrostatin	Yes****	<0.0001
M3 vs. RSL3	Yes****	<0.0001
M3 vs. Erastin	Yes***	0.0002
M3 vs. M3 + F	Yes**	0.0029

D1 vs. Ferrostatin	Yes***	0.0007
D1 vs. RSL3	Yes****	<0.0001
D1 vs. Erastin	Yes****	<0.0001
D3 vs. Ferrostatin	Yes*	0.0461
D3 vs. RSL3	Yes****	<0.0001
D3 vs. Erastin	Yes****	<0.0001
D3 vs. D3 + F	Yes**	0.0017
Ferrostatin vs. RSL3	Yes****	<0.0001
Ferrostatin vs. Erastin	Yes****	<0.0001
Ferrostatin vs. D1 + F	Yes****	<0.0001
Ferrostatin vs. D3 + F	Yes****	<0.0001
RSL3 vs. Erastin	Yes****	<0.0001
RSL3 vs. M1 + F	Yes****	<0.0001
RSL3 vs. M3 +F	Yes****	<0.0001
RSL3 vs. D1 + F	Yes****	<0.0001
RSL3 vs. D3 + F	Yes****	<0.0001
Erastin vs. M1 + F	Yes****	<0.0001
Erastin vs. M3 +F	Yes****	<0.0001
Erastin vs. D1 + F	Yes***	0.0002
Erastin vs. D3 + F	Yes**	0.0042

(D)

One-way ANOVA with Bonferroni's Post test (4h)		
Comparisons	Summary	Adjusted P Value
Control vs. M1	Yes*	0.0249
Control vs. M3	Yes*	0.0291
Control vs. D1	Yes*	0.0310
Control vs. RSL3	Yes****	<0.0001
M1 vs. RSL3	Yes****	<0.0001
M1 vs. M1 + F	Yes*	0.0329
M3 vs. RSL3	Yes****	<0.0001
D1 vs. RSL3	Yes****	<0.0001
D3 vs. RSL3	Yes****	<0.0001
Ferrostatin vs. RSL3	Yes****	<0.0001
RSL3 vs. Erastin	Yes****	<0.0001
RSL3 vs. M1 + F	Yes****	<0.0001
RSL3 vs. M3 +F	Yes****	<0.0001
RSL3 vs. D1 + F	Yes****	<0.0001
RSL3 vs. D3 + F	Yes****	<0.0001

Figure 6.5: The effect on cell viability of the T98g cell line after exposure to Dimethyl Fumarate, Monomethyl Fumarate, the ferroptosis inducers RSL3 (10nm) and erastin (10nm), the ferroptosis inhibitor ferrostatin (10nm) and the combination of Dimethyl Fumarate (D1 = 0.95µM, D3 = 3.8µM) and Monomethyl Fumarate (M1 = 0.8µM, M3 3.2µM) with ferrostatin (10nm) for either 4h (A) or 24h (B) time points. Data reported is an average of two independent experiments ± standard deviation. A one-way ANOVA with Bonferroni post testing was performed using GraphPad prism 10.3.1

comparing treatments to each other at the 4h (C) and 24h (D) time points, with P-values of $<0.05 = *$, $<0.01 = **$, $<0.001 = ***$ and $P<0.0001 = ****$ reported as significant, with non-significant differences not shown.

Figure 6.5 (A and C) shows the effect of 4h exposure to MMF, DMF, and ferroptosis modulators on T98g cell viability. A statistically significant reduction in cell viability was observed after treatment with M1 ($0.8\mu\text{M}$), M3 ($3.2\mu\text{M}$), D1 ($0.95\mu\text{M}$), and D3 ($3.8\mu\text{M}$), resulting in reductions of $17\% \pm 4$, $17\% \pm 1.5$, $14\% \pm 1.5$, and $9\% \pm 4$, respectively, compared to the untreated control (all, $P<0.05$).

Exposure to D1+F and D3+F also significantly reduced viability by $18\% \pm 0.8$ and $22\% \pm 0.09$, respectively, compared to the untreated control ($P<0.0001$). RSL3 (10nM) induced an $89\% \pm 1$ reduction in viability, which was significantly greater than all other treatments (all, $P<0.0001$). Erastin exposure caused a $33\% \pm 5$ reduction in viability compared to the untreated control ($P<0.0001$).

Compared to ferrostatin-treated cells, exposure to D1+F and D3+F significantly reduced cell viability (both, $P<0.0001$). A significant rescue effect by ferrostatin was observed when comparing M1, M3, and D3 to their respective ferrostatin co-treatments, suggesting MMF induced ferroptosis at both concentrations, and DMF induced ferroptosis at the higher concentration. However, significant differences between DMF/MMF treatments and classical ferroptosis inducers (RSL3 and erastin) partially reject the hypothesis that fumarates alone induce strong ferroptosis.

Figure 6.5 (B and D) shows the effects after 24h exposure. Statistically significant reductions in viability were observed for M1 ($0.8\mu\text{M}$) and M3 ($3.2\mu\text{M}$) ($27\% \pm 0.06$ and $26\% \pm 0.7$, respectively; both, $P<0.05$) and for D3 ($3.8\mu\text{M}$ DMF) with a $27\% \pm 4$ reduction compared to the untreated control ($P<0.05$).

RSL3 exposure for 24h induced a $90\% \pm 9$ reduction in viability ($P<0.0001$), significantly greater than MMF, DMF, ferrostatin, erastin, and their combinations (all, $P<0.001$). A significant difference was observed between M1 and M1+F treatment ($P<0.05$), suggesting MMF-induced ferroptosis at lower concentrations after 24 h.

Overall, after 24h, MMF appeared to induce ferroptosis at lower concentrations, evidenced by rescue with ferrostatin. However, the significant difference between MMF/DMF treatments and RSL3-induced cell death, and the lack of a dose-dependent effect, led to partial rejection of the hypothesis that fumarates robustly induce ferroptosis.

6.5 Discussion

The aim of this chapter was to determine whether Dimethyl Fumarate (DMF) and Monomethyl Fumarate (MMF) functioned similarly or differently on the key pathways they have been identified to modulate in the literature. These pathways as discussed, were downregulation of glutathione (GSH), modulation on the expression of Nrf2, NF- κ B /P65 and DJ1 and induction of ferroptosis through GPX4 depletion. The use of the fumarates in GBM is to increase oxidative stress in the cancerous cells by depletion of antioxidant glutathione to make cancer cells more likely to succumb to cell death by synergising with Temozolomide and Radiotherapy (which induce ROS as part of their mode of action). Within the literature, the fumarate family of esters, have shown to function differently on these pathways (Swindell *et al.*, 2022). Additionally, studies on the fumarates have shown them to work in a time dependent (Brennan *et al.*, 2015) and concentration dependent manner (Saidu *et al.*, 2019).

As we assume MMF had a different mode of action to DMF as shown by research in our group (Gardiner, 2023; Mullen, 2024), by performing a glutathione assay, RT-qPCR and a ferroptosis assay, we aimed to decipher how the two fumarates are working differently and if their effect on GBM cells was also concentration and time dependent. Due to time limitations, all assays in Chapter 6 were only repeated in two biological replicates, however a minimum of 3 technological replicates was applied for each concentration of DMF and MMF used, and for each time point.

6.3.1 Glutathione Assay

In our studies we demonstrated GSH levels in the U87 cell line to be reduced when compared to the control at higher administered concentrations of DMF and MMF, and in a time dependent manner with cells incubated with DMF or MMF for 4hrs having GSH levels significantly lower than 24h GSH levels. Data for these cell lines correlates well with the literature where this time and concentration dependent response has previously been reported for DMF (Brennan *et al.*, 2015; Saidu *et al.*, 2019). However, comparison between DMF and MMF's effect on GSH levels showed no significant differences between the two drugs on GSH downregulation. This suggests that in the MGMT negative cell line DMF and MMF work in a similar manner to deplete GSH.

Although not directly comparable this contradicts the cytotoxicity seen between MMF and DMF on the U87 cell line (Figure 3.3). It does however suggest that the variability in cytotoxicity could be due to each individual drugs mode of action, with data suggesting MMF induces DNA damage. To compare if DMF induced DNA damage and to confirm MMF's induction of DNA damage, a H₂AX assay should be performed, which will show double stranded breaks. This result is also contrasting to the literature where direct comparison of DMF and MMF showed DMF to form spontaneous GSH conjugates at a quicker rate than MMF, with MMF's effect on GSH not thought to be through spontaneous GSH conjugation (Schmidt *et al.*, 2007). This suggests then that MMF's effect on GSH when comparing it to DMF may be different at earlier time points, and that MMF's depletion of GSH is through downregulation of the antioxidant pathway and not by GSH conjugation. These experimentations by Schmidt *et al.*, (2007) were performed via spectroscopy and computational chemistry. The study by Brennan *et al.*, (2015) reported that DMF reduced GSH levels in astrocytes between 30mins and 12 hours with GSH levels increasing above the control after 24h. An increase in GSH levels after 24h exposure to DMF was seen in our study in the U87 cell line, correlating well with the literature (Figure 6.2(C)). Overall, the data supports our hypothesis of a time and concentration dependent effect of DMF and MMF on GSH levels, however lack of significant differences between DMF and MMF reject our hypothesis and suggest use of an earlier time points to see potential differences.

Within the T98g cell line, GSH levels were significantly reduced after exposure to higher concentrations of MMF for 4h but were also significantly increased after exposure to DMF for 4h and 24h. Data also showed significant changes between MMF and DMF at the higher and lower concentrations after 4h exposure ($P < 0.05$). Suggesting in the T98g cell line the hypothesis of MMF and DMF working differently was supported. However, our data didn't correlate well with the literature again, where a time and concentration dependent deletion of GSH was seen on cells after exposure to the fumarate DMF, as we observed increased GSH levels after 4h exposure. (Brennan *et al.*, 2015; Saidu *et al.*, 2019). Additionally, in our study only MMF depleted GSH levels after 4h exposure, with all other treatments either increasing or being close to control levels of GSH. This data also doesn't coincide well with Figure 3.8, where MMF was seen to keep GSH levels depleted until post 48h. The variability of these two T98g cells line assays on GSH, could be explained by the significant increase in Total GSH levels of the untreated control to the 4h total GSH. Previous untreated control data in Figure 3.8 (B) showed the T98g cell line to have basal levels

over time of $\sim 20\mu\text{M}$. The lower total GSH level seen in Figure 6.2 (B) could suggest error in the experiment or absorbance reading. This would also cause a knock on effect where the 4h experimental data would show higher GSH levels than if compared to total GSH levels of $\sim 20\mu\text{M}$. DMF also lowered GSH levels insignificantly against the 4h exposure to, contradicting literature and previous studies in this cell line by Scott, (2020), where a time dependent GSH depletion was seen with DMF (Brennan *et al.*, 2015). DMF's response in the T98g cell line therefore rejected our hypothesis of a time dependent mechanism behind GSH depletion and suggests further experimentation is required to determine why our data is different to the literature. An explanation for the difference is that in the T98g cell line, studies have reported after 6 hour exposure to DMF, NrF2 was activated and NrF2 subcellular localisation occurred at a concentration of $35\mu\text{M}$ DMF (Wang *et al.*, 2024). Therefore, at our time points of 4h and 24h, the rapid formation of GSH conjugates may have already occurred and activation of NrF2 will activate the downstream antioxidant pathways and upregulate GSH. The concentrations of DMF used on the T98g cell line in our study were lower than the literature, and therefore again the DMF depletion of GSH may be seen at higher concentrations of DMF. Data for the T98g cell line did however support our hypothesis of MMF and DMF working differently to deplete GSH levels as there was a significant difference between the low concentrations of DMF and MMF, and at the high concentrations of DMF and MMF when comparing GSH levels, again this is due to the high levels of GSH after DMF exposure. Although we aren't seeing the time dependent response of DMF we did see a concentration dependent response, as higher concentrations of DMF had lower GSH levels when compared to the lower concentration of DMF's effect on GSH.

Overall MMF data for both cell lines somewhat correlated well with Chapter 3 – Section 3.4.4 where 4h exposure of MMF significantly depleted GSH levels. Overall, a time dependent and concentration dependent trend in GSH depletion was seen after MMF and DMF exposure on the GBM cell lines. However, the two fumarates were only significantly different in the T98g cell line, suggesting at these time points and concentrations DMF and MMF do not work differently on altering GSH levels in the MGMT negative cell lines, but do in the MGMT positive cell line. This is good clinically, as treatments for MGMT+ patients are restricted and clinically, if MMF works better in MGMT+ patients it has potential to target a clinical cohort of patients.

6.3.2 RT-qPCR

6.3.2.1 NrF2

Relative fold change of NrF2 gene expression in the U87 cell line demonstrated MMF to lower NrF2 gene expression more than DMF, although the differences were not statistically significant. DMF also marginally increased NrF2 gene expression after 24h exposure which contradicts the literature (Saidu *et al.*, 2019). Lower concentrations of both DMF and MMF induced a larger reduction in NrF2 gene expression than the higher concentrations when compared to the control, again contradicting the research by Saidu *et al.*, (2019) but supporting the findings of Brennan *et al.*, (2015), where DMF increases NrF2 expression in the nucleus as concentrations increase. Data correlated well with the relative GSH levels of DMF and MMF on the U87 cell line in Figure 6.2 (A). Further investigation into the effect of DMF and MMF on NrF2 modulation, the difference between nuclear and cellular NrF2 levels should be performed using immunofluorescence to visualise NrF2 localisation within the cells or by targeting the genes downstream of NrF2 such as hemeoxygenase-1 would also support the trends in downregulation seen after exposure to high concentrations of DMF and MMF. Furthermore, only two biological replicates were performed for this assay and a further repeat before publication would benefit distinguishing trends.

NrF2 gene expression in the T98g cell line showed significant changes in NrF2 gene expression between 4h and 24h exposure to both DMF and MMF at the lower concentrations. After 4h exposure of the lower concentrations NrF2 gene expression was increased which correlates well to the literature studies where after 6h exposure to DMF, NrF2 expression was activated in the T98g cell line (Wang *et al.*, 2024). Our data also showed increases in NrF2 expression after high concentration of DMF and MMF exposure compared to low concentrations of DMF and MMF exposure, again similar to the findings by Brennan *et al.*, (2015). After 24h both DMF and MMF at the lower concentrations reduced NrF2 expression compared to the 24h fold change in NrF2 after exposure to higher concentrations of DMF and MMF, contradicting the literature where higher concentrations of DMF are thought to downregulate NrF2 gene expression and low concentrations enhance NrF2 gene expression (Saidu *et al.*, 2019). MMF did not significantly alter the NrF2 gene expression at any concentration or time point compared to the untreated control, which has been found in literature

studies on GBM primary cells and transcriptomic analysis (Dent *et al.*, 2020; Swindell *et al.*, 2022). Overall, for MMFs effect on NrF2 gene expression, the higher concentrations did downregulate NrF2 gene expression, correlating well with the Glutathione assay data (Figure 6.2) where MMF is suggested to downregulate GSH via a different target than forming GSH conjugates and this may be through NrF2 downregulation (Schmidt *et al.*, 2007). Collectively before conclusions can be made on the response of DMF and MMF on NrF2 gene expression modulation, further experimentation such as western blot on NrF2 should be performed, TransAM DNA binding assay to separate nuclear and cytoplasmic NrF2 fractions could also be performed as well as RT-qPCR of the downstream targets of NrF2. The data would suggest DMF and MMF do work differently on NrF2 gene expression.

6.3.2.2 P65

P65 is crucial for the transcriptional activity of NF- κ B as it contains the transactivation domain that drives gene expression and is the most studied component of the NF- κ B homo and heterodimeric complexes (Liu *et al.*, 2008). DMF is a known inhibitor of NF- κ B, by inhibiting the signals from the Rel proteins, such as P65 and NF- κ B translocation to the nucleus in GBM cells (Ghods *et al.*, 2013). NF- κ B is highly expressed in GBM tumours and promotes chemoresistance, with inhibition of this pathway enhancing apoptosis of the cells (Avci *et al.*, 2020). Comparison of DMF, MMF and Monoethyl Fumarate in the literature have reported differing effects on NF- κ B inhibition, with MMF and MEF not seen to affect NF- κ B signalling in Ramos blue B lymphocytes (Gillard *et al.*, 2015). MMF alone in GBM primary isolates was also not seen to significantly inactivate the NF- κ B signalling pathway in the literature (Dent *et al.*, 2020). Our data demonstrated in the U87 reduction of P65 gene expression after 4h exposure to DMF and MMF (Figure 6.3 (B)). The reduction in P65 gene expression in the U87 cell line was not concentration dependent as no significant differences were seen between the concentrations. However, after 24h exposure to both DMF and MMF the P65 gene expression was greater than the corresponding 4h changes in relative fold change. The higher concentrations of DMF and MMF, also induced a slight increase in P65 gene expression which was unexpected as studies in breast cancer cells have shown inhibition of the pathway in a dose dependent manner (Kastrati *et al.*, 2016). In Ramos blue B lymphocytes, DMF was seen to reduce P65

expression in a time and concentration dependent manner, however these findings did not translate into the U87 cell line suggesting that the fumarates may have different effect on different cancer cells with differing molecular pathologies and genetic backgrounds.

It is also possible that the data achieved in this study was not reliable as the reliability of the P65 data was further questioned by the T98g data for P65 gene expression after exposure to DMF and MMF (Figure 6.5), as DMF upregulated the P65 gene expression and after 4h exposure, which is contradictive of the literature where DMF is a known inhibitor of the NF- κ B pathway (Ghods *et al.*, 2013). Additionally, MMF was seen to reduce the expression of P65 at both concentrations, and as MMF has shown limited modulation of the P65 pathway in GBM cells, it questions the results of both DMF and MMF on P65 gene expression seen in our data. By completing the third biological replicate or use of a different assay such as western blotting to detect total phosphorylation levels of P65 in cytoplasmic and nuclear fractions, the results seen in the U87 and T98g cell lines can be further interrogated before conclusions can be made. An ELISA could also be performed to quantify P65 DNA binding activity in nuclear extracts, which would determine DMF and MMF's effects on P65 DNA binding activity. Overall, the hypothesis was rejected as no trends in concentration or time dependent reduction in P65 gene expression was seen. The data also doesn't show significant differences between DMF and MMF, suggesting both work similarly on P65 expression.

6.3.2.3 GPX4

Depletion of GPX4 is a known inducer of ferroptosis, the iron dependent cell death pathway. As GPX4 levels are maintained by glutathione (GSH), and DMF and MMF have shown to have inhibitory effects on GSH levels, it can be hypothesised that fumarates further inhibit the downstream target of GSH, GPX4 (Li *et al.*, 2020). Depletion of GPX4 could induce a ferroptosis cell death pathway in the GBM cells, which could explain the cytotoxicity observed with the drugs on the GBM cell lines in Section 3.4.2. NF- κ B has been proposed to protect cells from ferroptosis by activating ferroptosis inhibitors such as SLC7A11 (Wang *et al.*, 2023). As DMF and MMF showed some downregulation of P65 from our RT-qPCR analysis, it also suggests this could be the mechanism behind cell death after administration of the fumarates. All cell lines

showed a depletion of GPX4 gene expression after the administration of DMF and MMF (Figure 6.4, 6.3, 6.4). The U87 cell line was the only cell line to show significant reduction in GPX4 gene expression compared to the control at the higher concentrations of DMF and MMF. No consistent trends between time points or concentrations or between DMF and MMF rejected our hypothesis that the fumarates would significantly reduce GPX4 in a time and concentration dependent manner. This was hypothesised as glutathione assays in Section 6.4.1 did show some trends in time and concentration consistent with the literature. DMF has been shown to instigate ferroptosis through GSH depletion in cancerous cells (Schmitt *et al.*, 2021), and with the reduction in GPX4 data is suggestive of this, however no conclusions can be formed due to the lack of significant findings. However, activation of NrF2 via DMF has also been shown to prevent ferroptosis, due to upregulation of GSH-GPX4 (Sun *et al.*, 2016; Yang *et al.*, 2021). As discussed previously, DMF is known to form rapid GSH-conjugates and MMF is thought to work on the antioxidant pathway, therefore in theory, the activation of NrF2 by DMF would not necessarily upregulate GSH as the antioxidant would be directly depleted by DMF. MMF on the other hand, has shown in our RT-QPCR data to lower NrF2 gene expression at the higher concentrations suggesting the reduction in GPX4 expression is linked to the antioxidant pathway (Schmidt *et al.*, 2007). Overall, our data suggests that GPX4 gene expression is reduced by DMF and MMF, however further investigation using ferroptosis assays would be needed to confirm this.

6.3.2.4 DJ1

DJ1 is a multifunctional protein with different mechanisms of action in chronic diseases such as cancer (Mencke *et al.*, 2021). The small protein is known to have a role in apoptosis, autophagy and the antioxidant system (Mencke *et al.*, 2021). DJ1 is a regulator of NrF2-dependent antioxidant signalling and regulates NrF2s interaction with Keap1 (Saidu *et al.*, 2017). DMF has been shown in OVCAR3 ovarian cancer cells, to deplete DJ1 in a dose dependent manner (Saidu *et al.*, 2017). The U87 cell line demonstrated no significant depletions of DJ1 gene expression between DMF and MMF concentrations and the time points compared to the control (Figure 6.3 D). DMF increased the DJ1 gene expression as expected (Saidu *et al.*, 2017) at the lower concentration for 4h exposure. Higher concentrations of DMF did not show any trends

in DJ1 gene expression with the gene expression slightly increased after 24h and lowered at 4h. This increase somewhat correlates to the results of the NrF2 gene expression changes seen in the U87 cell line, as DMF at the higher concentration after 24h exposure also increased NrF2 gene expression. The T98g cell line showed reductions in DJ1 at all concentrations and time points although these were not significant changes when compared to the control (Figure 6.3 H). DJ1 gene expression was seen to be lower after 24h exposure over the expression changes seen after 4h. Patterns in the data also closely match what was seen for the NrF2 changes in gene expression for each concentration and time point for DMF and MMF in the T98g cell line (Figure 6.3 I). Contradictory to the literature, the lower concentrations of both DMF and MMF were seen to instigate a greater reduction in DJ1 gene expression when compared to the higher concentrations (Saidu *et al.*, 2017). Similarly to NrF2, DJ1 expression in GBM is upregulated and has been found to correlate to poor prognosis and aggressiveness of the disease (Wang *et al.*, 2013). Additionally, this study showed GSH depletion and NrF2 depletion by DMF to be interrelated in the cytotoxic effect of DMF in the cancer cells (Saidu *et al.*, 2017). As DJ1 regulates NrF2 activation it could be suggested that earlier reductions in DJ1 by 4h exposure led to lowered expression of NrF2 over time. Overall, changes in DJ1 gene expression are not correlating well with the NrF2 changes in gene expression after DMF and MMF exposure, suggesting DMF and MMF to both have an effect on DJ1 gene expression. NrF2 is known to be upregulated in GBM, and also contradictory literature suggests DMF activates NrF2 expression in GBM (Kourakis *et al.*, 2020). Further interrogation is therefore required to decipher clearer trends, by use of a larger range of concentrations and times, the changes in gene expression may show more distinct patterns. Additionally, results are the product of two biological replicates and completion of a third replicate may reduce the large error bars, allowing for more significant changes to be interpreted. No significant differences between the DMF and MMF imposed changes on DJ1 gene expression suggest the two fumarates to work similarly, rejecting our hypothesis and as no significant differences between concentration and time dependent effects of DMF and MMF were seen it also rejected our hypothesis. As previously suggested, by broadening our range of concentrations used and time points, clearer distinctions in trends may be seen.

6.3.2.5 RT-qPCR summary

Collectively the RT-qPCR data lacked significant findings which would elucidate the mechanisms behind DMF and MMF cytotoxicity and why they differ on the GBM cells. The variability and lack of consistent findings supports that further analysis is needed and use of different techniques. Western blots using NrF2, P65, Hemeoxygenase-1, DJ1, GPX4 and glutathione S-transferase were all planned to be executed. However, in our hands and the hands of other lab groups, the western blots were unable to be completed, and it was concluded that the antibodies were not effective. These western blot assays will be completed as part of post-doctoral studies as will further RT-qPCR to complete the three biological replicates. Application of a reaction oxygen species assay with Dichlorodihydrofluorescein Diacetate (DCFH-DA), will also determine if DMF and MMF are upregulating intracellular ROS via the depletion of GSH, and will also show if the two are working differently. Overall, the data does imply reduction of NrF2, DJ1, GPX4 and P65, however the concentrations and time points these reductions occur are not consistent across the cell lines.

6.3.3 Ferroptosis

As we have proven, MMF in the GBM cell lines depletes glutathione in a time and concentration dependent manner (Section 6.4.1). DMF's effect on GSH has been shown in the literature to deplete GSH by rapid formation of GSH conjugates (Brennan *et al.*, 2015). Studies by Scott, (2020) on the UVW and T98g cell lines also showed DMF to deplete GSH levels in a time dependent manner but not concentration dependent manner. DMF in our hands only significantly depleted GSH levels in the T98g cell line. RT-qPCR data also showed all cell lines to have a reduced expression of GPX4 when compared to the control. This was suggestive of MMF and possibly DMF instigated ferroptosis in the cells, and being the mode of cell death observed when MMF was applied as a single treatment to the cells (Section 3.4.2). Both cell lines when exposed to DMF, MMF and RSL3 showed significant differences between the RSL3 reduction in viability and the DMF and MMF induced reduction in viability. The reduction in cell viability after exposure to erastin was less pronounced and no significant differences between erastin and the single treatments of DMF and MMF were seen in the U87 cell line, this suggests the MGMT negative cell lines are more sensitive to an RSL3 induced ferroptosis than erastin. RSL3 requires activation of the NF- κ B pathway, which is upregulated in GBM, supporting the increased reduction in

RSL3 induced cell viability (Avci *et al.*, 2020). Erastin inhibits system x_c , an amino acid transporter system which reduces cystine to cysteine which is needed for GSH syntheses (Sato *et al.*, 2018). As the antioxidant system is upregulated in GBM, higher concentrations of Erastin may be needed to induce greater levels of decreased cell viability. Within the T98g cell line, erastin induced significantly greater levels of cell viability reduction than the single treatments of DMF and MMF after 4h exposure but not after 24h, suggesting erastin also works in a time dependent manner. By comparison of the single treatment reduction in cell viability to cell viability after DMF and MMF were combined with ferrostatin, the instigation of ferroptosis could be implied. Within the U87 cell line, DMF as a single treatment at both concentrations significantly reduced cell viability when compared to the corresponding combination of DMF + ferrostatin after 4h. This suggests within the U87 cell line, DMF but not MMF causes ferroptosis of the cells. Data is surprising as MMF as a single treatment at the higher concentration induced significant reductions in GSH levels and was also shown to significantly reduce the expression of GPX4. The data is also suggestive of DMF and MMF having different effects on the cell lines, a hypothesis which has so far mainly been rejected. The effect of DMF and MMF on the various pathways surrounding ferroptosis should be performed to assess if the induction of ferroptosis by DMF is through a pathway independent to GSH/GPX4 depletion. Contrastingly, in the T98g cell line, MMF at both concentrations after 4h exposure induced significantly lower levels of cell viability when compared to MMF + ferrostatin treated cells. By 24h only the lower concentration of MMF induced significantly lower levels of cell viability compared to MMF + ferrostatin. DMF also induced significant reductions in cell viability after 4h exposure to the higher concentration of DMF vs DMF + ferrostatin. Again, this suggests DMF and MMF to have different modes of action in the T98g cell line, a hypothesis which was supported by the glutathione assay. Additionally, the data suggest ferroptosis may occur in a time dependent manner, similar to the reductions of GSH, which correlates well as lower GSH levels would deplete GPX4 and instigate ferroptosis. Additionally, in the T98g cell line, GPX4 gene expression was reduced more by MMF than DMF, again correlating well with the result. Overall, the data does suggest DMF and MMF to induce ferroptosis, however again trends in the data suggest this is time and concentration dependent. The hypothesis was partially rejected as not all cell lines were suggestive of ferroptosis, however time and concentration dependent activity of DMF and MMF was seen, supporting the hypothesis. Again, by using a larger range of concentrations and time points, the

trends in the data may become clearer. Similarly to the previous data, only two biological replicates were performed and by completing the third data would become more reliable and decipherable. Supplementary experimentation should be performed, such as a lipid peroxidation assay, detection of lipid ROS after exposure to DMF and MMF would further confirm if the significant findings are in fact due to ferroptosis.

6.6 Conclusions

Dimethyl Fumarate and Monomethyl Fumarate throughout the literature have shown a surprising variation on their mechanistic functions. The literature has shown contradictory results, which creates a gap in knowledge. Further to this as DMF/MMF have a neuroprotective role in non-cancerous cells, the cytotoxic effect of the fumarates in cancerous cells becomes further elusive. A theme in the literature is that DMF depletes GSH in a time dependent manner (Brennan *et al.*, 2015), this has been proven by Scott, (2020) and somewhat proven in this study, as the time dependent theme was seen in the MGMT negative cell lines but not the MGMT positive cell line. No literature reports have investigated why an MGMT positive cell line would respond differently to DMF than an MGMT negative cell line, and again comparison of the different mutations within each cell line may help uncover a possible explanation. The time dependent response was also proven to apply to MMF, as in two independent GSH studies, MMF has shown to deplete GSH levels up to 4h after exposure, after while GSH levels increase. This is thought to be due to the highly regulated redox system within the cells, which in response to depletion of an antioxidant would compensate by upregulating levels over time to reach homeostasis and prevent cell death. This homeostatic balance, in cancerous cells would be more profound as the cell signalling pathways are irregular and would be promoting cancer cell survival. A second theme in the literature when trying to decipher the role of DMF and MMF, was DMF's switch from neuroprotective to cytotoxic being concentration dependent (Saidu *et al.*, 2019). This was supported by this study as we observed GSH levels to be depleted in a concentration dependent manner, and differences were seen on gene expression modulation between the two concentrations of DMF and MMF used, although these were small differences and insignificant. Ferroptosis assay analysis

also suggested MMF to induce ferroptosis in a concentration and time dependent manner, further supporting literature findings. The variability within each assay however rejected our hypothesis of DMF and MMF working differently, a common theme in the literature and in other studies by our lab (Brennan *et al.*, 2015; Gardiner, 2023; Mullen, 2024; Swindell *et al.*, 2022). Conclusively, although not definite, the data supports that DMF and MMF work in a time and concentration dependent manner. DMF and MMF have both shown to elicit effects on GSH, NrF2, P65, Dj1 and GPX4, all of which further implicates the fumarates' primary role to be on the antioxidant system within GBM. This further promotes the benefit of repurposing the fumarates for GBM treatment as downregulation of the antioxidant system will allow current treatments to elicit more of an effect on damaging cancerous cells.

Chapter 7

Conclusions and Future work

Glioblastoma is the most aggressive form of brain cancer. Survival of patients diagnosed is devastatingly low, with median survival in adult patients being approximately 14.6 months. Few patients survive to 5-years post diagnosis, with a 5-year survival of only 27.2% after combination treatments, (Grech *et al.*, 2020; Schaff and Mellinghoff, 2023). Progression in the treatment of GBM has been limited in part to the blood brain barrier, which prevents many drugs penetrating into the brain and thus being useful in treating the disease. Additionally due to the aggressive nature of the disease, patients develop resistance to treatments or already possess factors such as MGMT positive status, which limit the effectiveness of the current gold standard chemotherapy TMZ.

To our knowledge this is the first study combining TMZ and radiotherapy with MMF in these cell lines. MMF has been shown throughout literature studies to have a different effect on cells than DMF as discussed previously. We therefore aimed to investigate whether MMF would synergise well with the current gold standard treatments, with application of a third treatment aiming to lower the doses of the current GBM treatments, in order to alleviate some of the resistance build up in patients as well as the impact of high dose chemo and radiation therapy on patient quality of life. With little alternative options for GBM treatment, MMF could provide patients with better prognostic outcomes.

Data collated showed MMF to synergise well with TMZ when scheduled due to a time dependant depletion of GSH levels. This scheduling technique with MMF and TMZ has to our knowledge never been performed in a GBM model before and strongly suggests MMF's ability to deplete GSH levels and enhance the effects of chemotherapy TMZ. We also surprisingly found a DNA damage mode of action for MMF in all cell lines, suggesting its use as a single treatment option for patients with fewer treatment options. MMF alone has shown to have an effect in both 2D and 3D models, reducing GBM cell survival and spheroid growth. Further work looking into MMF's potential role as a single treatment option could be beneficial and contribute to further research and knowledge in the field by highlighting alternative targeting pathways for novel drug repurposing. Data also was suggestive of the possibility of

ferroptosis induced death in GBM cells which could be further explored in the field by utilising the fumarates. It also suggests a potential treatment option for MGMT positive patients, as the T98g cell line showed synergy at both scheduled and simultaneous treatments, as well as an increased sensitivity to MMF. Omics profiling of the T98g, UVW and U87 cell lines could highlight pathways in GBM which MMF in the T98g cell line may be targeting to cause this increased sensitivity.

By comparing DMF and MMF we were unable to conclude on whether the fumarates work differently in GBM and future work should focus on refining and deciphering the differences between DMF and MMF. This could be achieved through reactive oxygen species assays, utilising the GSH kit to determine total and oxidised GSH levels and by a lipid peroxidation assay to decipher ferroptosis in a more robust way. Additionally, as MMF showed a significant DNA damage response, direct comparison of DMF and MMF on these cell lines as well as additional MGMT positive cell lines using an H2Ax assay would be beneficial for not only confirmation of MMF's mode of action but also to assess if DMF is also behaving in this manner in the cell lines. Further to focusing on MMF's mode of action, western blot assays are crucial to understand the effect of the fumarates in these GBM cell lines on the antioxidant pathway and its downstream targets. Completion of these assays as well as the remainder of chapter 6 should contribute significantly to the knowledge in the literature surrounding repurposing the fumarates.

Our data supported a potentially synergistic triple combination, however, to further the combination data for MMF TMZ and Radiation, once access to the X-irradiator is available, mechanistic interrogation of the triple combination will be completed. Alternative scheduling models should also be investigated alongside reactive oxygen species assays and GSH assays, as the trends in data from the double combinations suggest a rebound in GSH protecting cells and promoting survival. This data would be vital as clinically patients would need to adhere to tight scheduling regimes if the combination of treatments, when not combined appropriately can cause antagonism, resulting in poorer patient health.

Data from this work also showed the combination of TMZ and MMF to translate into 3D models, however, once mechanistic and scheduling interrogation has provided a result, the response of the triple combination in 3D multicellular spheroids should be completed. A known mechanism can then be investigated in the 3D spheroid models by immunofluorescence on spheroid sections post treatment. Determining whether

the same mechanisms of action can penetrate through into a spheroid model would benefit not only possible future use of the combinations but also MMF as a single treatment. We also aim to incorporate the Temozolomide resistant MGMT positive T98g cells into mosaic spheroids with U87 and UVW cell lines to investigate how the triple combination would affect a heterogenous 3D model. Once complete, we would aim to move studies into animal models, using xenograft models to complete the full potential of the combination of MMF in GBM.

The mode of action of not only MMF but the combinations could also be further interrogated by developing resistant cell lines to TMZ and radiation. These resistant cell lines which have been developed for other cancer cell lines in our lab, could be used in both 2D and 3D models, and would in practise partially represent how MMF would function in patients who have developed resistance.

Overall, data from this study supported our hypothesis of MMF synergising well with the current standards of care and also highlighted differences between MMF and DMF such as cytotoxicity. It also showed MMF's use in tackling GBM as a single treatment and a DNA damage response not previously known. From the data collected in this study, it suggests Monomethyl Fumarate could be an appropriate additional treatment for GBM patients, not only in combination with the current standard of care but also as a single treatment option.

Chapter 8

References

- Abbas, T. and Dutta, A. (2009) 'p21 in cancer: intricate networks and multiple activities', *Nature Reviews. Cancer*, 9(6), pp. 400–414. Available at: <https://doi.org/10.1038/nrc2657>.
- Adamiec-Organisciok, M. *et al.* (2023) 'Compensative Resistance to Erastin-Induced Ferroptosis in GPX4 Knock-Out Mutants in HCT116 Cell Lines', *Pharmaceuticals*, 16(12), p. 1710. Available at: <https://doi.org/10.3390/ph16121710>.
- Agnihotri, S. *et al.* (2013) 'Glioblastoma, a Brief Review of History, Molecular Genetics, Animal Models and Novel Therapeutic Strategies', *Archivum Immunologiae et Therapiae Experimentalis*, 61(1), pp. 25–41. Available at: <https://doi.org/10.1007/s00005-012-0203-0>.
- Agnihotri, S. *et al.* (2016) 'PINK1 Is a Negative Regulator of Growth and the Warburg Effect in Glioblastoma', *Cancer Research*, 76(16), pp. 4708–4719. Available at: <https://doi.org/10.1158/0008-5472.CAN-15-3079>.
- Agnihotri, S., Aldape, K.D. and Zadeh, G. (2014) 'Isocitrate dehydrogenase status and molecular subclasses of glioma and glioblastoma', *Neurosurgical Focus*, 37(6), p. E13. Available at: <https://doi.org/10.3171/2014.9.FOCUS14505>.
- Ahmadi-Beni, R. *et al.* (2019) 'Role of dimethyl fumarate in the treatment of Glioblastoma: A review article', *Iranian Journal of Neurology*, 18(3), pp. 127–133.
- Akay, M. *et al.* (2018) 'Drug Screening of Human GBM Spheroids in Brain Cancer Chip', *Scientific Reports*, 8(1), p. 15423. Available at: <https://doi.org/10.1038/s41598-018-33641-2>.
- Aldape, K. *et al.* (2015) 'Glioblastoma: pathology, molecular mechanisms and markers', *Acta Neuropathologica*, 129(6), pp. 829–848. Available at: <https://doi.org/10.1007/s00401-015-1432-1>.
- Ali, M.Y. *et al.* (2020) 'Radioresistance in Glioblastoma and the Development of Radiosensitizers', *Cancers*, 12(9), p. 2511. Available at: <https://doi.org/10.3390/cancers12092511>.
- Al-Jaderi, Z. and Maghazachi, A.A. (2016) 'Utilization of Dimethyl Fumarate and Related Molecules for Treatment of Multiple Sclerosis, Cancer, and Other Diseases', *Frontiers in Immunology*, 7. Available at: <https://doi.org/10.3389/fimmu.2016.00278>.
- Allen, M. *et al.* (2016) 'Origin of the U87MG glioma cell line: Good news and bad news', *Science Translational Medicine*, 8(354). Available at: <https://doi.org/10.1126/scitranslmed.aaf6853>.
- Almeida Lima, K. *et al.* (2023) 'Temozolomide Resistance in Glioblastoma by NRF2: Protecting the Evil', *Biomedicines*, 11(4), p. 1081. Available at: <https://doi.org/10.3390/biomedicines11041081>.

- de Almeida Sassi, F. *et al.* (2012) 'Glioma revisited: from neurogenesis and cancer stem cells to the epigenetic regulation of the niche', *Journal of Oncology*, 2012, p. 537861. Available at: <https://doi.org/10.1155/2012/537861>.
- Alomari, S. *et al.* (2021) 'Drug Repurposing for Glioblastoma and Current Advances in Drug Delivery—A Comprehensive Review of the Literature', *Biomolecules*, 11(12), p. 1870. Available at: <https://doi.org/10.3390/biom11121870>.
- Alves, S.R. *et al.* (2023) 'Characterization of glioblastoma spheroid models for drug screening and phototherapy assays', *OpenNano*, 9, p. 100116. Available at: <https://doi.org/10.1016/j.onano.2022.100116>.
- Alwithenani, A. *et al.* (2023) 'Unlocking the potential of dimethyl fumarate: enhancing oncolytic HSV-1 efficacy for wider cancer applications', *Frontiers in Immunology*, 14, p. 1332929. Available at: <https://doi.org/10.3389/fimmu.2023.1132929>.
- Alzial, G. *et al.* (2022) 'Wild-type isocitrate dehydrogenase under the spotlight in glioblastoma', *Oncogene*, 41(5), pp. 613–621. Available at: <https://doi.org/10.1038/s41388-021-02056-1>.
- Angom, R.S., Nakka, N.M.R. and Bhattacharya, S. (2023) 'Advances in Glioblastoma Therapy: An Update on Current Approaches', *Brain Sciences*, 13(11), p. 1536. Available at: <https://doi.org/10.3390/brainsci13111536>.
- Annovazzi, L., Mellai, M. and Schiffer, D. (2017) 'Chemotherapeutic Drugs: DNA Damage and Repair in Glioblastoma', *Cancers*, 9(6), p. 57. Available at: <https://doi.org/10.3390/cancers9060057>.
- Antonelli, M. and Poliani, P.L. (2022) 'Adult type diffuse gliomas in the new 2021 WHO Classification', *Pathologica*, 114(6), pp. 397–409. Available at: <https://doi.org/10.32074/1591-951X-823>.
- Arabzadeh, A. *et al.* (2021) 'Therapeutic potentials of resveratrol in combination with radiotherapy and chemotherapy during glioblastoma treatment: a mechanistic review', *Cancer Cell International*, 21(1), p. 391. Available at: <https://doi.org/10.1186/s12935-021-02099-0>.
- Arnold, M. *et al.* (2019) 'Progress in cancer survival, mortality, and incidence in seven high-income countries 1995–2014 (ICBP SURVMARK-2): a population-based study', *The Lancet Oncology*, 20(11), pp. 1493–1505. Available at: [https://doi.org/10.1016/S1470-2045\(19\)30456-5](https://doi.org/10.1016/S1470-2045(19)30456-5).
- Ashburn, T.T. and Thor, K.B. (2004) 'Drug repositioning: identifying and developing new uses for existing drugs', *Nature Reviews Drug Discovery*, 3(8), pp. 673–683. Available at: <https://doi.org/10.1038/nrd1468>.
- Avci, N.G. *et al.* (2020) 'NF-κB inhibitor with Temozolomide results in significant apoptosis in glioblastoma via the NF-κB(p65) and actin cytoskeleton regulatory pathways', *Scientific Reports*, 10(1), p. 13352. Available at: <https://doi.org/10.1038/s41598-020-70392-5>.
- Averill-Bates, D.A. (2023) 'The antioxidant glutathione', in *Vitamins and Hormones*. Elsevier, pp. 109–141. Available at: <https://doi.org/10.1016/bs.vh.2022.09.002>.

- Awuah, W.A. *et al.* (2022) 'Exploring the role of Nrf2 signaling in glioblastoma multiforme', *Discover Oncology*, 13(1), p. 94. Available at: <https://doi.org/10.1007/s12672-022-00556-4>.
- Babaloui, S. (2022) 'Radiosensitization of Glioma Cells by Temozolomide (TMZ): A Colony Formation Assay', *Journal of Biomedical Physics and Engineering*, 12(1). Available at: <https://doi.org/10.31661/jbpe.v0i0.1223>.
- Backes, C. *et al.* (2015a) 'New insights into the genetics of glioblastoma multiforme by familial exome sequencing', *Oncotarget*, 6(8), pp. 5918–5931. Available at: <https://doi.org/10.18632/oncotarget.2950>.
- Backes, C. *et al.* (2015b) 'New insights into the genetics of glioblastoma multiforme by familial exome sequencing', *Oncotarget*, 6(8), pp. 5918–5931. Available at: <https://doi.org/10.18632/oncotarget.2950>.
- Backos, D.S., Franklin, C.C. and Reigan, P. (2012) 'The role of glutathione in brain tumor drug resistance', *Biochemical Pharmacology*, 83(8), pp. 1005–1012. Available at: <https://doi.org/10.1016/j.bcp.2011.11.016>.
- Bae, T., Hallis, S.P. and Kwak, M.-K. (2024) 'Hypoxia, oxidative stress, and the interplay of HIFs and NRF2 signaling in cancer', *Experimental & Molecular Medicine*, 56(3), pp. 501–514. Available at: <https://doi.org/10.1038/s12276-024-01180-8>.
- Bai, J., Varghese, J. and Jain, R. (2020) 'Adult Glioma WHO Classification Update, Genomics, and Imaging: What the Radiologists Need to Know', *Topics in Magnetic Resonance Imaging*, 29(2), pp. 71–82. Available at: <https://doi.org/10.1097/RMR.0000000000000234>.
- Bai, Z. *et al.* (2023) 'Perspectives and mechanisms for targeting mitotic catastrophe in cancer treatment', *Biochimica et Biophysica Acta (BBA) - Reviews on Cancer*, 1878(5), p. 188965. Available at: <https://doi.org/10.1016/j.bbcan.2023.138965>.
- Banerjee, V. *et al.* (2021) 'Synergistic potential of dual andrographolide and melatonin targeting of metastatic colon cancer cells: Using the Chou-Talalay combination index method', *European Journal of Pharmacology*, 897, p. 173919. Available at: <https://doi.org/10.1016/j.ejphar.2021.173919>.
- Barbarite, E. *et al.* (2017) 'The role of brachytherapy in the treatment of glioblastoma multiforme', *Neurosurgical Review*, 40(2), pp. 195–211. Available at: <https://doi.org/10.1007/s10143-016-0727-6>.
- Barbosa, M.A.G. *et al.* (2021) '3D Cell Culture Models as Recapitulators of the Tumor Microenvironment for the Screening of Anti-Cancer Drugs', *Cancers*, 14(1), p. 190. Available at: <https://doi.org/10.3390/cancers14010190>.
- Basso, J. *et al.* (2018) 'Repurposing drugs for glioblastoma: From bench to bedside', *Cancer Letters*, 428, pp. 173–183. Available at: <https://doi.org/10.1016/j.canlet.2018.04.039>.
- Batash, R. *et al.* (2017) 'Glioblastoma Multiforme, Diagnosis and Treatment; Recent Literature Review', *Current Medicinal Chemistry*, 24(27). Available at: <https://doi.org/10.2174/0929867324666170516123206>.

- Beckers, C., Pruschy, M. and Vetrugno, I. (2024) 'Tumor hypoxia and radiotherapy: A major driver of resistance even for novel radiotherapy modalities', *Seminars in Cancer Biology*, 98, pp. 19–30. Available at: <https://doi.org/10.1016/j.semcan.2023.9.006>.
- Begagić, E. et al. (2024) 'Understanding the Significance of Hypoxia-Inducible Factors (HIFs) in Glioblastoma: A Systematic Review', *Cancers*, 16(11), p. 2089. Available at: <https://doi.org/10.3390/cancers16112089>.
- Begg, K. and Tavassoli, M. (2020) 'Inside the hypoxic tumour: reprogramming of the DDR and radioresistance', *Cell Death Discovery*, 6(1), p. 77. Available at: <https://doi.org/10.1038/s41420-020-00311-0>.
- Berger, A.A. et al. (2021) 'Monomethyl Fumarate (MMF, Bafiertam) for the Treatment of Relapsing Forms of Multiple Sclerosis (MS)', *Neurology International*, 13(2), pp. 207–223. Available at: <https://doi.org/10.3390/neurolint13020022>.
- Berkmen, Y.M. and Lande, A. (1975a) 'Chest roentgenography as a window to the diagnosis of Takayasu's arteritis', *The American Journal of Roentgenology, Radium Therapy, and Nuclear Medicine*, 125(4), pp. 842–846. Available at: <https://doi.org/10.2214/ajr.125.4.842>.
- Berkmen, Y.M. and Lande, A. (1975b) 'Chest roentgenography as a window to the diagnosis of Takayasu's arteritis', *The American Journal of Roentgenology, Radium Therapy, and Nuclear Medicine*, 125(4), pp. 842–846. Available at: <https://doi.org/10.2214/ajr.125.4.842>.
- Biserova, K. et al. (2021) 'Cancer Stem Cells: Significance in Origin, Pathogenesis and Treatment of Glioblastoma', *Cells*, 10(3), p. 621. Available at: <https://doi.org/10.3390/cells10030621>.
- Blumenthal, D.T. and Cannon-Albright, L.A. (2008) 'Familiality in brain tumors', *Neurology*, 71(13), pp. 1015–1020. Available at: <https://doi.org/10.1212/01.wnl.0000326597.60605.27>.
- Booth, L. et al. (2014) 'Regulation of dimethyl-fumarate toxicity by proteasome inhibitors', *Cancer biology & therapy*, 15, pp. 1647–1657. Available at: <https://doi.org/10.4161/15384047.2014.967992>.
- Boyd, M. et al. (1999) 'Noradrenaline transporter gene transfer for radiation cell kill by 131I meta-iodobenzylguanidine', *Gene Therapy*, 6(6), pp. 1147–1152. Available at: <https://doi.org/10.1038/sj.gt.3300905>.
- Boyd, M. et al. (2002) 'Transfectant mosaic spheroids: a new model for evaluation of tumour cell killing in targeted radiotherapy and experimental gene therapy', *The Journal of Gene Medicine*, 4(5), pp. 567–576. Available at: <https://doi.org/10.1002/jgm.293>.
- Bredel-Geissler, A. et al. (1992) 'Proliferation-associated oxygen consumption and morphology of tumor cells in monolayer and spheroid culture', *Journal of Cellular Physiology*, 153(1), pp. 44–52. Available at: <https://doi.org/10.1002/jcp.1041530108>.
- Brennan, C.W. et al. (2013) 'The Somatic Genomic Landscape of Glioblastoma', *Cell*, 155(2), pp. 462–477. Available at: <https://doi.org/10.1016/j.cell.2013.09.034>.

Brennan, M.S. *et al.* (2015) 'Dimethyl Fumarate and Monoethyl Fumarate Exhibit Differential Effects on KEAP1, NRF2 Activation, and Glutathione Depletion In Vitro', *PLOS ONE*. Edited by Y. Tsuji, 10(3), p. e0120254. Available at: <https://doi.org/10.1371/journal.pone.0120254>.

Bresciani, G. *et al.* (2023) 'Novel potential pharmacological applications of dimethyl fumarate—an overview and update', *Frontiers in Pharmacology*, 14, p. 1264842. Available at: <https://doi.org/10.3389/fphar.2023.1064842>.

Brown, K.F. *et al.* (2018) 'The fraction of cancer attributable to modifiable risk factors in England, Wales, Scotland, Northern Ireland, and the United Kingdom in 2015', *British Journal of Cancer*, 118(8), pp. 1130–1141. Available at: <https://doi.org/10.1038/s41416-018-0029-6>.

Brown, N.F. *et al.* (2022) 'Survival Outcomes and Prognostic Factors in Glioblastoma', *Cancers*, 14(13), p. 3161. Available at: <https://doi.org/10.3390/cancers14133161>.

Butler, M. *et al.* (2020) 'MGMT Status as a Clinical Biomarker in Glioblastoma', *Trends in Cancer*, 6(5), pp. 380–391. Available at: <https://doi.org/10.1016/j.trecan.2020.02.010>.

Bv, H. and Jolly, M.K. (2024) 'Proneural-mesenchymal antagonism dominates the patterns of phenotypic heterogeneity in glioblastoma', *iScience*, 27(3), p. 109184. Available at: <https://doi.org/10.1016/j.isci.2024.109184>.

C. Short, S. A. Mitchell, P. Boultou, S. (1999) 'The response of human glioma cell lines to low-dose radiation exposure', *International Journal of Radiation Biology*, 75(11), pp. 1341–1348. Available at: <https://doi.org/10.1080/095530099139214>.

Campione, E. *et al.* (2022) 'The Role of Glutathione-S Transferase in Psoriasis and Associated Comorbidities and the Effect of Dimethyl Fumarate in This Pathway', *Frontiers in Medicine*, 9, p. 760852. Available at: <https://doi.org/10.3389/fmed.2022.760852>.

Canon, J. *et al.* (2015) 'The MDM2 Inhibitor AMG 232 Demonstrates Robust Antitumor Efficacy and Potentiates the Activity of p53-Inducing Cytotoxic Agents', *Molecular Cancer Therapeutics*, 14(3), pp. 649–658. Available at: <https://doi.org/10.1158/1535-7163.MCT-14-0710>.

Cantidio, F.S. *et al.* (2022) 'Glioblastoma — treatment and obstacles', *Reports of Practical Oncology and Radiotherapy*, p. VM/OJS/J/90766. Available at: <https://doi.org/10.5603/RPOR.a2022.0076>.

Chakravarti, A. *et al.* (2006) 'Temozolomide-Mediated Radiation Enhancement in Glioblastoma: A Report on Underlying Mechanisms', *Clinical Cancer Research*, 12(15), pp. 4738–4746. Available at: <https://doi.org/10.1158/1078-0432.CCR-06-0596>.

Chalmers, A.J. *et al.* (2009) 'Cytotoxic Effects of Temozolomide and Radiation are Additive- and Schedule-Dependent', *International Journal of Radiation Oncology*Biophysics*Physics*, 75(5), pp. 1511–1519. Available at: <https://doi.org/10.1016/j.ijrobp.2009.07.1703>.

- Chambless, L.B. *et al.* (2015) 'The relative value of postoperative versus preoperative Karnofsky Performance Scale scores as a predictor of survival after surgical resection of glioblastoma multiforme', *Journal of Neuro-Oncology*, 121(2), pp. 359–364. Available at: <https://doi.org/10.1007/s11060-014-1640-x>.
- Chen, K. *et al.* (2021) 'Dimethyl Fumarate Induces Metabolic Crisis to Suppress Pancreatic Carcinoma', *Frontiers in Pharmacology*, 12, p. 617714. Available at: <https://doi.org/10.3389/fphar.2021.617714>.
- Chen, P.-H., Tseng, W.H.-S. and Chi, J.-T. (2020) 'The Intersection of DNA Damage Response and Ferroptosis—A Rationale for Combination Therapeutics', *Biology*, 9(8), p. 187. Available at: <https://doi.org/10.3390/biology9080187>.
- Chen, R. *et al.* (2017) 'Glioma Subclassifications and Their Clinical Significance', *Neurotherapeutics*, 14(2), pp. 284–297. Available at: <https://doi.org/10.1007/s13311-017-0519-x>.
- Chen, W. *et al.* (2014) 'High-throughput Image Analysis of Tumor Spheroids: A User-friendly Software Application to Measure the Size of Spheroids Automatically and Accurately', *Journal of Visualized Experiments*, (89), p. 51639. Available at: <https://doi.org/10.3791/51639-v>.
- Chen, Z. *et al.* (2023) 'Proton versus photon radiation therapy: A clinical review', *Frontiers in Oncology*, 13, p. 1133909. Available at: <https://doi.org/10.3389/fonc.2023.933909>.
- Cho, N.S. *et al.* (2023) 'The Future Glioblastoma Clinical Trials Landscape: Early Phase 0, Window of Opportunity, and Adaptive Phase I–III Studies', *Current Oncology Reports*, 25(9), pp. 1047–1055. Available at: <https://doi.org/10.1007/s11912-023-01433-1>.
- Chong, C.R. and Sullivan, D.J. (2007) 'New uses for old drugs', *Nature*, 448(7154), pp. 645–646. Available at: <https://doi.org/10.1038/448645a>.
- Chou, T.-C. (2006) 'Theoretical Basis, Experimental Design, and Computerized Simulation of Synergism and Antagonism in Drug Combination Studies', *Pharmacological Reviews*, 58(3), pp. 621–681. Available at: <https://doi.org/10.1124/pr.58.3.10>.
- Chou, T.-C. (2010) 'Drug Combination Studies and Their Synergy Quantification Using the Chou-Talalay Method', *Cancer Research*, 70(2), pp. 440–446. Available at: <https://doi.org/10.1158/0008-5472.CAN-09-1947>.
- Chou, T.-C. and Talalay, P. (1984) 'Quantitative analysis of dose-effect relationships: the combined effects of multiple drugs or enzyme inhibitors', *Advances in Enzyme Regulation*, 22, pp. 27–55. Available at: [https://doi.org/10.1016/0065-2571\(84\)90007-4](https://doi.org/10.1016/0065-2571(84)90007-4).
- Colwell, N. *et al.* (2017) 'Hypoxia in the glioblastoma microenvironment: shaping the phenotype of cancer stem-like cells', *Neuro-Oncology*, 19(7), pp. 887–896. Available at: <https://doi.org/10.1093/neuonc/now258>.
- Daisy Precilla, S. *et al.* (2022) 'Crosstalk between PI3K/AKT/mTOR and WNT/ β -Catenin signaling in GBM - Could combination therapy checkmate the collusion?',

Cellular Signalling, 95, p. 110350. Available at: <https://doi.org/10.1016/j.cellsig.2022.110350>.

D'Alessio, A. *et al.* (2019) 'Pathological and Molecular Features of Glioblastoma and Its Peritumoral Tissue', *Cancers*, 11(4), p. 469. Available at: <https://doi.org/10.3390/cancers11040469>.

De Souza, I. *et al.* (2022) 'High levels of NRF2 sensitize temozolomide-resistant glioblastoma cells to ferroptosis via ABCC1/MRP1 upregulation', *Cell Death & Disease*, 13(7), p. 591. Available at: <https://doi.org/10.1038/s41419-022-05044-9>.

Delgado-López, P.D. *et al.* (2020) 'A comprehensive overview on the molecular biology of human glioma: what the clinician needs to know', *Clinical and Translational Oncology*, 22(11), pp. 1909–1922. Available at: <https://doi.org/10.1007/s12094-020-02340-8>.

Delgado-Martín, B. and Medina, M.Á. (2020) 'Advances in the Knowledge of the Molecular Biology of Glioblastoma and Its Impact in Patient Diagnosis, Stratification, and Treatment', *Advanced Science*, 7(9), p. 1902971. Available at: <https://doi.org/10.1002/advs.201902971>.

Denny, B.J. *et al.* (1994) 'NMR and Molecular Modeling Investigation of the Mechanism of Activation of the Antitumor Drug Temozolomide and Its Interaction with DNA', *Biochemistry*, 33(31), pp. 9045–9051. Available at: <https://doi.org/10.1021/bi00197a003>.

Dent, P. *et al.* (2020) 'Fingolimod Augments Monomethylfumarate Killing of GBM Cells', *Frontiers in Oncology*, 10, p. 22. Available at: <https://doi.org/10.3389/fonc.2020.00022>.

Department of Medical Oncology, Centro Hospitalar de São João, Porto, Portugal *et al.* (2017) 'Current Standards of Care in Glioblastoma Therapy', in Department of Neurosurgery, University Hospitals Leuven, Leuven, Belgium and S. De Vleeschouwer (eds) *Glioblastoma*. Codon Publications, pp. 197–241. Available at: <https://doi.org/10.15586/codon.glioblastoma.2017.ch11>.

Department of Neurosurgery, Jordan University Hospital and Medical School, University of Jordan, Amman, Jordan *et al.* (2017) 'Epidemiology and Outcome of Glioblastoma', in Department of Neurosurgery, University Hospitals Leuven, Leuven, Belgium and S. De Vleeschouwer (eds) *Glioblastoma*. Codon Publications, pp. 143–153. Available at: <https://doi.org/10.15586/codon.glioblastoma.2017.ch8>.

Detchou, D. and Barrie, U. (2024) 'Interleukin 6 and cancer resistance in glioblastoma multiforme', *Neurosurgical Review*, 47(1), p. 541. Available at: <https://doi.org/10.1007/s10143-024-02783-5>.

Dietlein, F., Thelen, L. and Reinhardt, H.C. (2014) 'Cancer-specific defects in DNA repair pathways as targets for personalized therapeutic approaches', *Trends in Genetics*, 30(8), pp. 326–339. Available at: <https://doi.org/10.1016/j.tig.2014.06.003>.

Dixon, S.J. and Olzmann, J.A. (2024) 'The cell biology of ferroptosis', *Nature Reviews Molecular Cell Biology*, 25(6), pp. 424–442. Available at: <https://doi.org/10.1038/s41580-024-00703-5>.

- Dong, P. *et al.* (2018) 'Cyclin D/CDK4/6 activity controls G1 length in mammalian cells', *PLOS ONE*. Edited by X. Liu, 13(1), p. e0185637. Available at: <https://doi.org/10.1371/journal.pone.0185637>.
- Dührsen, L. *et al.* (2019) 'Seizures as presenting symptom in patients with glioblastoma', *Epilepsia*, 60(1), pp. 149–154. Available at: <https://doi.org/10.1111/epi.14615>.
- Eguchi, Y., Shimizu, S. and Tsujimoto, Y. (1997) 'Intracellular ATP levels determine cell death fate by apoptosis or necrosis', *Cancer Research*, 57(10), pp. 1835–1840.
- Eisenbarth, D. and Wang, Y.A. (2023) 'Glioblastoma heterogeneity at single cell resolution', *Oncogene*, 42(27), pp. 2155–2165. Available at: <https://doi.org/10.1038/s41388-023-02738-y>.
- El Khayari, A. *et al.* (2022) 'Metabolic Rewiring in Glioblastoma Cancer: EGFR, IDH and Beyond', *Frontiers in Oncology*, 12, p. 901951. Available at: <https://doi.org/10.3389/fonc.2022.901951>.
- Elder, J.B. and Chiocca, E.A. (2011) 'Editorial: Low Karnofsky Performance Scale score and glioblastoma multiforme', *Journal of Neurosurgery*, 115(2), pp. 217–219. Available at: <https://doi.org/10.3171/2010.9.JNS101438>.
- Elwakeel, A. *et al.* (2019) 'Implementation of the Chou-Talalay method for studying the in vitro pharmacodynamic interactions of binary and ternary drug combinations on MDA-MB-231 triple negative breast cancer cells', *Synergy*, 8, p. 100047. Available at: <https://doi.org/10.1016/j.synres.2019.100047>.
- England, B., Huang, T. and Karsy, M. (2013) 'Current understanding of the role and targeting of tumor suppressor p53 in glioblastoma multiforme', *Tumor Biology*, 34(4), pp. 2063–2074. Available at: <https://doi.org/10.1007/s13277-013-0871-3>.
- Enns, L. *et al.* (2004) 'Low-Dose Radiation Hypersensitivity Is Associated With p53-Dependent Apoptosis', *Molecular Cancer Research*, 2(10), pp. 557–566. Available at: <https://doi.org/10.1158/1541-7786.357.2.10>.
- Erasimus, H. *et al.* (2016) 'DNA repair mechanisms and their clinical impact in glioblastoma', *Mutation Research/Reviews in Mutation Research*, 769, pp. 19–35. Available at: <https://doi.org/10.1016/j.mrrev.2016.05.005>.
- Ercelik, M. *et al.* (2023) 'Olea europaea Leaf Phenolics Oleuropein, Hydroxytyrosol, Tyrosol, and Rutin Induce Apoptosis and Additionally Affect Temozolomide against Glioblastoma: In Particular, Oleuropein Inhibits Spheroid Growth by Attenuating Stem-like Cell Phenotype', *Life*, 13(2), p. 470. Available at: <https://doi.org/10.3390/life13020470>.
- Esemen, Y. *et al.* (2022) 'Molecular Pathogenesis of Glioblastoma in Adults and Future Perspectives: A Systematic Review', *International Journal of Molecular Sciences*, 23(5), p. 2607. Available at: <https://doi.org/10.3390/ijms23052607>.
- Evans, E. and Staffurth, J. (2018) 'Principles of cancer treatment by radiotherapy', *Surgery (Oxford)*, 36(3), pp. 111–116. Available at: <https://doi.org/10.1016/j.mpsur.2017.12.006>.

- Fan, Y. *et al.* (2022a) 'Burden and trends of brain and central nervous system cancer from 1990 to 2019 at the global, regional, and country levels', *Archives of Public Health*, 80(1), p. 209. Available at: <https://doi.org/10.1186/s13690-022-00965-5>.
- Fan, Y. *et al.* (2022b) 'Burden and trends of brain and central nervous system cancer from 1990 to 2019 at the global, regional, and country levels', *Archives of Public Health*, 80(1), p. 209. Available at: <https://doi.org/10.1186/s13690-022-00965-5>.
- Fang, Q. (2024) 'The Versatile Attributes of MGMT: Its Repair Mechanism, Crosstalk with Other DNA Repair Pathways, and Its Role in Cancer', *Cancers*, 16(2), p. 331. Available at: <https://doi.org/10.3390/cancers16020331>.
- Fedrigo, C.A. *et al.* (2011) 'Radioresistance of human glioma spheroids and expression of HSP70, p53 and EGFr', *Radiation Oncology*, 6(1), p. 156. Available at: <https://doi.org/10.1186/1748-717X-6-156>.
- Filomeni, G., Rotilio, G. and Ciriolo, M.R. (2002) 'Cell signalling and the glutathione redox system', *Biochemical Pharmacology*, 64(5–6), pp. 1057–1064. Available at: [https://doi.org/10.1016/S0006-2952\(02\)01176-0](https://doi.org/10.1016/S0006-2952(02)01176-0).
- Fisher, J.L. *et al.* (2007) 'Epidemiology of Brain Tumors', *Neurologic Clinics*, 25(4), pp. 867–890. Available at: <https://doi.org/10.1016/j.ncl.2007.07.002>.
- Floor, S.L. *et al.* (2012) 'Hallmarks of cancer: of all cancer cells, all the time?', *Trends in Molecular Medicine*, 18(9), pp. 509–515. Available at: <https://doi.org/10.1016/j.molmed.2012.06.005>.
- Fouad, Y.A. and Aanei, C. (2017) 'Revisiting the hallmarks of cancer', *American Journal of Cancer Research*, 7(5), pp. 1016–1036.
- Frantzi, M. *et al.* (2020) 'Drug repurposing in oncology', *The Lancet Oncology*, 21(12), p. e543. Available at: [https://doi.org/10.1016/S1470-2045\(20\)30610-0](https://doi.org/10.1016/S1470-2045(20)30610-0).
- Fuentes-Fayos, A.C. *et al.* (2023) 'Metformin and simvastatin exert additive antitumour effects in glioblastoma via senescence-state: clinical and translational evidence', *eBioMedicine*, 90, p. 104484. Available at: <https://doi.org/10.1016/j.ebiom.2023.104484>.
- Fusco, N. *et al.* (2020) 'PTEN Alterations and Their Role in Cancer Management: Are We Making Headway on Precision Medicine?', *Genes*, 11(7), p. 719. Available at: <https://doi.org/10.3390/genes11070719>.
- Galaris, D., Barbouti, A. and Pantopoulos, K. (2019) 'Iron homeostasis and oxidative stress: An intimate relationship', *Biochimica et Biophysica Acta (BBA) - Molecular Cell Research*, 1866(12), p. 118535. Available at: <https://doi.org/10.1016/j.bbamcr.2019.118535>.
- Gareton, A. *et al.* (2020) 'The histomolecular criteria established for adult anaplastic pilocytic astrocytoma are not applicable to the pediatric population', *Acta Neuropathologica*, 139(2), pp. 287–303. Available at: <https://doi.org/10.1007/s00401-019-02088-8>.

Gardiner, H. (2024) *The development of novel combinations therapies for the treatment of triple negative breast cancer*. University of Strathclyde. Available at: <https://doi.org/10.48730/32V4-WY52>.

Garnier, D. *et al.* (2018) 'Divergent evolution of temozolomide resistance in glioblastoma stem cells is reflected in extracellular vesicles and coupled with radiosensitization', *Neuro-Oncology*, 20(2), pp. 236–248. Available at: <https://doi.org/10.1093/neuonc/nox142>.

Ghods, A. *et al.* (2013) 'Beneficial actions of the anti-inflammatory dimethyl fumarate in glioblastomas', *Surgical Neurology International*, 4(1), p. 160. Available at: <https://doi.org/10.4103/2152-7806.123656>.

Gilbert, H.F. (1995) '[2] Thiol/disulfide exchange equilibria and disulfidebond stability', in *Methods in Enzymology*. Elsevier, pp. 8–28. Available at: [https://doi.org/10.1016/0076-6879\(95\)51107-5](https://doi.org/10.1016/0076-6879(95)51107-5).

Gillard, G.O. *et al.* (2015) 'DMF, but not other fumarates, inhibits NF- κ B activity in vitro in an Nrf2-independent manner', *Journal of Neuroimmunology*, 283, pp. 74–85. Available at: <https://doi.org/10.1016/j.jneuroim.2015.04.006>.

Goff, K.M., Zheng, C. and Alonso-Basanta, M. (2022) 'Proton radiotherapy for glioma and glioblastoma', *Chinese Clinical Oncology*, 11(6), pp. 46–46. Available at: <https://doi.org/10.21037/cco-22-92>.

Gola, L. *et al.* (2023) 'MMF induces antioxidative and anaplerotic pathways and is neuroprotective in hyperexcitability in vitro', *Free Radical Biology and Medicine*, 194, pp. 337–346. Available at: <https://doi.org/10.1016/j.freeradbiomed.2022.12.010>.

Gold, R., Linker, R.A. and Stangel, M. (2012) 'Fumaric acid and its esters: An emerging treatment for multiple sclerosis with antioxidative mechanism of action', *Clinical Immunology*, 142(1), pp. 44–48. Available at: <https://doi.org/10.1016/j.clim.2011.02.017>.

Gong, J.P., Traganos, F. and Darzynkiewicz, Z. (1994) 'A Selective Procedure for DNA Extraction from Apoptotic Cells Applicable for Gel Electrophoresis and Flow Cytometry', *Analytical biochemistry*, 218, pp. 314–9. Available at: <https://doi.org/10.1006/abio.1994.1184>.

Gousias, K., Theocharous, T. and Simon, M. (2022) 'Mechanisms of Cell Cycle Arrest and Apoptosis in Glioblastoma', *Biomedicines*, 10(3), p. 564. Available at: <https://doi.org/10.3390/biomedicines10030564>.

Gouws, C. and Pretorius, P.J. (2011) 'O6-methylguanine-DNA methyltransferase (MGMT): Can function explain a suicidal mechanism?', *Medical Hypotheses*, 77(5), pp. 857–860. Available at: <https://doi.org/10.1016/j.mehy.2011.07.055>.

Gramatzki, D. *et al.* (2018) 'Bevacizumab may improve quality of life, but not overall survival in glioblastoma: an epidemiological study', *Annals of Oncology*, 29(6), pp. 1431–1436. Available at: <https://doi.org/10.1093/annonc/mdy106>.

Grech, N. *et al.* (2020) 'Rising Incidence of Glioblastoma Multiforme in a Well-Defined Population', *Cureus*, 12(5), p. e8195. Available at: <https://doi.org/10.7759/cureus.8195>.

Grochans, S. *et al.* (2022) 'Epidemiology of Glioblastoma Multiforme-Literature Review', *Cancers*, 14(10), p. 2412. Available at: <https://doi.org/10.3390/cancers14102412>.

Günther, W. *et al.* (2003) 'Temozolomide induces apoptosis and senescence in glioma cells cultured as multicellular spheroids', *British Journal of Cancer*, 88(3), pp. 463–469. Available at: <https://doi.org/10.1038/sj.bjc.6600711>.

Guo, B., Liao, W. and Wang, S. (2021) 'The clinical significance of glutathione peroxidase 2 in glioblastoma multiforme', *Translational Neuroscience*, 12(1), pp. 032–039. Available at: <https://doi.org/10.1515/tnsci-2021-0005>.

Guo, G. *et al.* (2020) 'IKBKE enhances TMZ-chemoresistance through upregulation of MGMT expression in glioblastoma', *Clinical and Translational Oncology*, 22(8), pp. 1252–1262. Available at: <https://doi.org/10.1007/s12094-019-02251-3>.

Hamisch, C. *et al.* (2017) 'Impact of treatment on survival of patients with secondary glioblastoma', *Journal of Neuro-Oncology*, 133(2), pp. 309–313. Available at: <https://doi.org/10.1007/s11060-017-2415-y>.

Han, G. and Zhou, Q. (2016) 'Dimethylfumarate induces cell cycle arrest and apoptosis via regulating intracellular redox systems in HeLa cells', *In Vitro Cellular & Developmental Biology - Animal*, 52(10), pp. 1034–1041. Available at: <https://doi.org/10.1007/s11626-016-0069-2>.

Han, S. *et al.* (2020) 'IDH mutation in glioma: molecular mechanisms and potential therapeutic targets', *British Journal of Cancer*, 122(11), pp. 1580–1589. Available at: <https://doi.org/10.1038/s41416-020-0814-x>.

Hanahan, D. (2022) 'Hallmarks of Cancer: New Dimensions', *Cancer Discovery*, 12(1), pp. 31–46. Available at: <https://doi.org/10.1158/2159-8290.CD-21-1059>.

Hanahan, D. and Weinberg, R.A. (2000) 'The Hallmarks of Cancer', *Cell*, 100(1), pp. 57–70. Available at: [https://doi.org/10.1016/S0092-8674\(00\)81683-9](https://doi.org/10.1016/S0092-8674(00)81683-9).

Hanahan, D. and Weinberg, R.A. (2011) 'Hallmarks of cancer: the next generation', *Cell*, 144(5), pp. 646–674. Available at: <https://doi.org/10.1016/j.cell.2011.02.013>.

Hanif, F. *et al.* (2017) 'Glioblastoma Multiforme: A Review of its Epidemiology and Pathogenesis through Clinical Presentation and Treatment', *Asian Pacific Journal of Cancer Prevention*, 18(1). Available at: <https://doi.org/10.22034/APJCP.2017.18.1.3>.

Harder, B.G. *et al.* (2019) 'Inhibition of phosphatidylinositol 3-kinase by PX-866 suppresses temozolomide-induced autophagy and promotes apoptosis in glioblastoma cells', *Molecular Medicine*, 25(1), p. 49. Available at: <https://doi.org/10.1186/s10020-019-0116-z>.

Harvey, C.J. *et al.* (2009) 'Nrf2-regulated glutathione recycling independent of biosynthesis is critical for cell survival during oxidative stress', *Free Radical Biology and Medicine*, 46(4), pp. 443–453. Available at: <https://doi.org/10.1016/j.freeradbiomed.2008.10.040>.

- Hashemi, M. *et al.* (2023) 'Progress in targeting PTEN/PI3K/Akt axis in glioblastoma therapy: Revisiting molecular interactions', *Biomedicine & Pharmacotherapy*, 158, p. 114204. Available at: <https://doi.org/10.1016/j.biopha.2022.114204>.
- Hau, P., Stupp, R. and Hegi, M.E. (2007) 'MGMT Methylation Status: The Advent of Stratified Therapy in Glioblastoma?', *Disease Markers*, 23(1–2), p. 159242. Available at: <https://doi.org/10.1155/2007/159242>.
- He, W. *et al.* (2021) 'HIF-1 α Hydroxyprolines Modulate Oxygen-Dependent Protein Stability Via Single VHL Interface With Comparable Effect on Ubiquitination Rate', *Journal of Molecular Biology*, 433(22), p. 167244. Available at: <https://doi.org/10.1016/j.jmb.2021.167244>.
- Hegi, M.E. and Stupp, R. (2015) 'Withholding temozolomide in glioblastoma patients with unmethylated MGMT promoter—still a dilemma?: Table 1.', *Neuro-Oncology*, 17(11), pp. 1425–1427. Available at: <https://doi.org/10.1093/neuonc/nov198>.
- Held, K.D. *et al.* (1991) 'Postirradiation Sensitization of Mammalian Cells by the Thiol-Depleting Agent Dimethyl Fumarate', *Radiation Research*, 127(1), p. 75. Available at: <https://doi.org/10.2307/3578091>.
- Hernandez, J.J. *et al.* (2017) 'Giving Drugs a Second Chance: Overcoming Regulatory and Financial Hurdles in Repurposing Approved Drugs As Cancer Therapeutics', *Frontiers in Oncology*, 7, p. 273. Available at: <https://doi.org/10.3389/fonc.2017.00273>.
- Hirschhaeuser, F. *et al.* (2010) 'Multicellular tumor spheroids: An underestimated tool is catching up again', *Journal of Biotechnology*, 148(1), pp. 3–15. Available at: <https://doi.org/10.1016/j.jbiotec.2010.01.012>.
- Ho, I.A.W. and Shim, W.S.N. (2017) 'Contribution of the Microenvironmental Niche to Glioblastoma Heterogeneity', *BioMed Research International*, 2017, pp. 1–13. Available at: <https://doi.org/10.1155/2017/9634172>.
- Hoogendoorn, A. *et al.* (2021) 'Emerging Therapeutic Applications for Fumarates', *Trends in Pharmacological Sciences*, 42(4), pp. 239–254. Available at: <https://doi.org/10.1016/j.tips.2021.01.004>.
- Hou, X. *et al.* (2024) 'Global, Regional, and National Burden of Brain and Other Cns Cancer, 1990–2021: A Systematic Analysis for the Global Burden of Disease Study 2021 and the Forecast between 2021 and 2035'. SSRN. Available at: <https://doi.org/10.2139/ssrn.5025897>.
- Huang, J. *et al.* (2022) 'The comparative burden of brain and central nervous system cancers from 1990 to 2019 between China and the United States and predicting the future burden', *Frontiers in Public Health*, 10, p. 1018836. Available at: <https://doi.org/10.3389/fpubh.2022.1018836>.
- Hubrecht, R.C. and Carter, E. (2019) 'The 3Rs and Humane Experimental Technique: Implementing Change', *Animals: an open access journal from MDPI*, 9(10), p. 754. Available at: <https://doi.org/10.3390/ani9100754>.

- Ironside, S. *et al.* (2017) 'Optimal Therapies for Newly Diagnosed Elderly Patients with Glioblastoma', *Current Treatment Options in Oncology*, 18(11), p. 66. Available at: <https://doi.org/10.1007/s11864-017-0508-7>.
- Isaac, O. and Thiemer, K. (1975) '[Biochemical studies on camomile components/III. In vitro studies about the antipeptic activity of (–)-alpha-bisabolol (author's transl)]', *Arzneimittel-Forschung*, 25(9), pp. 1352–1354.
- Jackson, C.B. *et al.* (2019) 'Temozolomide Sensitizes MGMT-Deficient Tumor Cells to ATR Inhibitors', *Cancer Research*, 79(17), pp. 4331–4338. Available at: <https://doi.org/10.1158/0008-5472.CAN-18-3394>.
- Jaganjac, M. *et al.* (2020) 'The NRF2, Thioredoxin, and Glutathione System in Tumorigenesis and Anticancer Therapies', *Antioxidants*, 9(11), p. 1151. Available at: <https://doi.org/10.3390/antiox9111151>.
- Jakubowicz-Gil, J. *et al.* (2013) 'Apoptosis induction in human glioblastoma multiforme T98G cells upon temozolomide and quercetin treatment', *Tumor Biology*, 34(4), pp. 2367–2378. Available at: <https://doi.org/10.1007/s13277-013-0785-0>.
- Janjua, T.I. *et al.* (2021) 'Frontiers in the treatment of glioblastoma: Past, present and emerging', *Advanced Drug Delivery Reviews*, 171, pp. 108–138. Available at: <https://doi.org/10.1016/j.addr.2021.01.012>.
- Jezierzański, M. *et al.* (2024) 'Temozolomide (TMZ) in the Treatment of Glioblastoma Multiforme—A Literature Review and Clinical Outcomes', *Current Oncology*, 31(7), pp. 3994–4002. Available at: <https://doi.org/10.3390/curroncol31070296>.
- Jin, L. *et al.* (2015) 'Glutamate Dehydrogenase 1 Signals through Antioxidant Glutathione Peroxidase 1 to Regulate Redox Homeostasis and Tumor Growth', *Cancer Cell*, 27(2), pp. 257–270. Available at: <https://doi.org/10.1016/j.ccell.2014.12.006>.
- Kaina, B. (2019) 'Temozolomide in Glioblastoma Therapy: Role of Apoptosis, Senescence and Autophagy. Comment on Strobel *et al.*, Temozolomide and Other Alkylating Agents in Glioblastoma Therapy. *Biomedicines* 2019, 7, 69', *Biomedicines*, 7(4), p. 90. Available at: <https://doi.org/10.3390/biomedicines7040090>.
- Kaina, B., Margison, G.P. and Christmann, M. (2010) 'Targeting O 6-methylguanine-DNA methyltransferase with specific inhibitors as a strategy in cancer therapy', *Cellular and Molecular Life Sciences*, 67(21), pp. 3663–3681. Available at: <https://doi.org/10.1007/s00018-010-0491-7>.
- Kaluzki, I. *et al.* (2019) 'Dimethylfumarate Inhibits Colorectal Carcinoma Cell Proliferation: Evidence for Cell Cycle Arrest, Apoptosis and Autophagy', *Cells*, 8(11), p. 1329. Available at: <https://doi.org/10.3390/cells8111329>.
- Kanderi, T., Munakomi, S. and Gupta, V. (2024) 'Glioblastoma Multiforme', in *StatPearls*. Treasure Island (FL): StatPearls Publishing. Available at: <http://www.ncbi.nlm.nih.gov/books/NBK558954/> (Accessed: 20 July 2024).
- Kapałczyńska, M. *et al.* (2018) '2D and 3D cell cultures - a comparison of different types of cancer cell cultures', *Archives of medical science: AMS*, 14(4), pp. 910–919. Available at: <https://doi.org/10.5114/aoms.2016.43743>.

- Karsy, M. (2015) 'Erratum: A practical review of prognostic correlations of molecular biomarkers in glioblastoma', *Neurosurgical Focus*, 38(6), p. E13. Available at: <https://doi.org/10.3171/2015.4.FOCUS14755a>.
- Kaspar, J.W., Niture, S.K. and Jaiswal, A.K. (2009) 'Nrf2:INrf2 (Keap1) signaling in oxidative stress', *Free Radical Biology and Medicine*, 47(9), pp. 1304–1309. Available at: <https://doi.org/10.1016/j.freeradbiomed.2009.07.035>.
- Kastenhuber, E.R. and Lowe, S.W. (2017) 'Putting p53 in Context', *Cell*, 170(6), pp. 1062–1078. Available at: <https://doi.org/10.1016/j.cell.2017.08.028>.
- Kastrati, I. *et al.* (2016) 'Dimethyl Fumarate Inhibits the Nuclear Factor κB Pathway in Breast Cancer Cells by Covalent Modification of p65 Protein', *Journal of Biological Chemistry*, 291(7), pp. 3639–3647. Available at: <https://doi.org/10.1074/jbc.M115.679704>.
- Kasznicki, J., Sliwinska, A. and Drzewoski, J. (2014) 'Metformin in cancer prevention and therapy', *Annals of Translational Medicine*, 2(6), p. 57. Available at: <https://doi.org/10.3978/j.issn.2305-5839.2014.06.01>.
- Kennedy, L. *et al.* (2020) 'Role of Glutathione in Cancer: From Mechanisms to Therapies', *Biomolecules*, 10(10), p. 1429. Available at: <https://doi.org/10.3390/biom10101429>.
- Kesari, S. *et al.* (2017) 'ACTR-55. TUMOR TREATING FIELDS WITH SECOND LINE TREATMENT COMPARED TO SECOND LINE TREATMENT ALONE IN PATIENTS AT FIRST RECURRENCE OF GLIOBLASTOMA – A POST HOC ANALYSIS OF THE EF-14 PHASE 3 CLINICAL TRIAL', *Neuro-Oncology*, 19(suppl_6), pp. vi13–vi13. Available at: <https://doi.org/10.1093/neuonc/nox168.046>.
- Khabibov, M. *et al.* (2022) 'Signaling pathways and therapeutic approaches in glioblastoma multiforme (Review)', *International Journal of Oncology*, 60(6), p. 69. Available at: <https://doi.org/10.3892/ijo.2022.5359>.
- Khan, S. *et al.* (2021) 'Multicellular Spheroids as In Vitro Models of Oxygen Depletion During FLASH Irradiation', *International Journal of Radiation Oncology*Biophysics*Physics*, 110(3), pp. 833–844. Available at: <https://doi.org/10.1016/j.ijrobp.2021.01.050>.
- Khazaei, M. and Pazhouhi, M. (2017) 'Temozolomide-Mediated Apoptotic Death Is Improved by Thymoquinone in U87MG Cell Line', *Cancer Investigation*, 35(4), pp. 225–236. Available at: <https://doi.org/10.1080/07357907.2017.1289383>.
- Khodamoradi, F. *et al.* (2017) 'The Incidence and Mortality of Brain and central nervous system cancer and their relationship within human development index in the world', *World Cancer Research Journal*, 4(4), pp. 1–5.
- King, J.L. and Benhabbour, S.R. (2021) 'Glioblastoma Multiforme—A Look at the Past and a Glance at the Future', *Pharmaceutics*, 13(7), p. 1053. Available at: <https://doi.org/10.3390/pharmaceutics13071053>.
- Kirby, S. and Purdy, R.A. (2014) 'Headaches and Brain Tumors', *Neurologic Clinics*, 32(2), pp. 423–432. Available at: <https://doi.org/10.1016/j.ncl.2013.9.006>.

- Kirstein, A., Schmid, T.E. and Combs, S.E. (2020) 'The Role of miRNA for the Treatment of MGMT Unmethylated Glioblastoma Multiforme', *Cancers*, 12(5), p. 1099. Available at: <https://doi.org/10.3390/cancers12051099>.
- Koo, N., Sharma, A.K. and Narayan, S. (2022) 'Therapeutics Targeting p53-MDM2 Interaction to Induce Cancer Cell Death', *International Journal of Molecular Sciences*, 23(9), p. 5005. Available at: <https://doi.org/10.3390/ijms23095005>.
- Korkmaz, I.N. (2024) 'Investigation of the effects of thiazole compounds on thioredoxin reductase 1 (TrxR1), glutathione S-transferase (GST), and glutathione reductase (GR) targeted human brain glioblastoma cancer (U-87 MG)', *Biotechnology and Applied Biochemistry*, p. bab.2589. Available at: <https://doi.org/10.1002/bab.2589>.
- Kourakis, S. *et al.* (2020) 'Dimethyl Fumarate and Its Esters: A Drug with Broad Clinical Utility?', *Pharmaceuticals*, 13(10), p. 306. Available at: <https://doi.org/10.3390/ph13100306>.
- LaRiviere, M.J. *et al.* (2019) 'Proton Therapy', *Hematology/Oncology Clinics of North America*, 33(6), pp. 989–1009. Available at: <https://doi.org/10.1016/j.hoc.2019.08.006>.
- Larjavaara, S. *et al.* (2007) 'Incidence of gliomas by anatomic location', *Neuro-Oncology*, 9(3), pp. 319–325. Available at: <https://doi.org/10.1215/15228517-2007-016>.
- Lategan, T.W. *et al.* (2021) 'Pharmacokinetics and Bioavailability of Monomethyl Fumarate Following a Single Oral Dose of Bafiertam™ (Monomethyl Fumarate) or Tecfidera® (Dimethyl Fumarate)', *CNS Drugs*, 35(5), pp. 567–574. Available at: <https://doi.org/10.1007/s40263-021-00799-9>.
- Lee, E. *et al.* (2018a) 'Comparison of glioblastoma (GBM) molecular classification methods', *Seminars in Cancer Biology*, 53, pp. 201–211. Available at: <https://doi.org/10.1016/j.semcan.2018.07.006>.
- Lee, E. *et al.* (2018b) 'Comparison of glioblastoma (GBM) molecular classification methods', *Seminars in Cancer Biology*, 53, pp. 201–211. Available at: <https://doi.org/10.1016/j.semcan.2018.07.006>.
- Lee, S.Y. (2016) 'Temozolomide resistance in glioblastoma multiforme', *Genes & Diseases*, 3(3), pp. 198–210. Available at: <https://doi.org/10.1016/j.gendis.2016.04.007>.
- Leung, S.Y. *et al.* (2000) 'Chromosomal instability and p53 inactivation are required for genesis of glioblastoma but not for colorectal cancer in patients with germline mismatch repair gene mutation', *Oncogene*, 19(35), pp. 4079–4083. Available at: <https://doi.org/10.1038/sj.onc.1203740>.
- Li, C. *et al.* (2021) 'Mitochondrial DNA stress triggers autophagy-dependent ferroptotic death', *Autophagy*, 17(4), pp. 948–960. Available at: <https://doi.org/10.1080/15548627.2020.1739447>.
- Li, J. *et al.* (2020) 'Ferroptosis: past, present and future', *Cell Death & Disease*, 11(2), p. 88. Available at: <https://doi.org/10.1038/s41419-020-2298-2>.

- Li, J., Feng, L. and Lu, Y. (2022) 'Glioblastoma multiforme: Diagnosis, treatment, and invasion', *Journal of Biomedical Research*, 37(1), pp. 47–58. Available at: <https://doi.org/10.7555/JBR.36.20220156>.
- Li, R. *et al.* (2022) 'Radiotherapy for glioblastoma: clinical issues and nanotechnology strategies', *Biomaterials Science*, 10(4), pp. 892–908. Available at: <https://doi.org/10.1039/D1BM01401C>.
- Li, S. *et al.* (2021) 'RSL3 Drives Ferroptosis through NF- κ B Pathway Activation and GPX4 Depletion in Glioblastoma', *Oxidative Medicine and Cellular Longevity*. Edited by Y.-R. Sun, 2021(1), p. 2915019. Available at: <https://doi.org/10.1155/2021/2915019>.
- Liebelt, B.D. *et al.* (2016) 'Glioma Stem Cells: Signaling, Microenvironment, and Therapy', *Stem Cells International*, 2016, pp. 1–10. Available at: <https://doi.org/10.1155/2016/7849890>.
- Lin, L. *et al.* (2023) 'Nrf2 signaling pathway: current status and potential therapeutic targetable role in human cancers', *Frontiers in Oncology*, 13, p. 1184079. Available at: <https://doi.org/10.3389/fonc.2023.984079>.
- Linker, R.A. *et al.* (2011) 'Fumaric acid esters exert neuroprotective effects in neuroinflammation via activation of the Nrf2 antioxidant pathway', *Brain*, 134(3), pp. 678–692. Available at: <https://doi.org/10.1093/brain/awq386>.
- Litjens, N.H.R. *et al.* (2004) 'Pharmacokinetics of oral fumarates in healthy subjects', *British Journal of Clinical Pharmacology*, 58(4), pp. 429–432. Available at: <https://doi.org/10.1111/j.1365-2125.2004.02145.x>.
- Liu, A. *et al.* (2016) 'Genetics and Epigenetics of Glioblastoma: Applications and Overall Incidence of IDH1 Mutation', *Frontiers in Oncology*, 6. Available at: <https://doi.org/10.3389/fonc.2016.00016>.
- Liu, G.-H., Qu, J. and Shen, X. (2008) 'NF- κ B/p65 antagonizes Nrf2-ARE pathway by depriving CBP from Nrf2 and facilitating recruitment of HDAC3 to MafK', *Biochimica et Biophysica Acta (BBA) - Molecular Cell Research*, 1783(5), pp. 713–727. Available at: <https://doi.org/10.1016/j.bbamcr.2008.01.002>.
- Liu, H. *et al.* (2022) 'Therapeutic strategies of glioblastoma (GBM): The current advances in the molecular targets and bioactive small molecule compounds', *Acta Pharmaceutica Sinica B*, 12(4), pp. 1781–1804. Available at: <https://doi.org/10.1016/j.apsb.2021.12.019>.
- Liu, S., Pi, J. and Zhang, Q. (2022) 'Signal amplification in the KEAP1-NRF2-ARE antioxidant response pathway', *Redox Biology*, 54, p. 102389. Available at: <https://doi.org/10.1016/j.redox.2022.102389>.
- Liu, Y. *et al.* (2021) 'The Role of Biomimetic Hypoxia on Cancer Cell Behaviour in 3D Models: A Systematic Review', *Cancers*, 13(6), p. 1334. Available at: <https://doi.org/10.3390/cancers13061334>.
- Livak, K.J. and Schmittgen, T.D. (2001) 'Analysis of Relative Gene Expression Data Using Real-Time Quantitative PCR and the 2- $\Delta\Delta$ CT Method', *Methods*, 25(4), pp. 402–408. Available at: <https://doi.org/10.1006/meth.2001.1262>.

Lu, Y., Liu, Y. and Yang, C. (2017) 'Evaluating In Vitro DNA Damage Using Comet Assay', *Journal of Visualized Experiments*, (128), p. 56450. Available at: <https://doi.org/10.3791/56450>.

Mair, M.J. *et al.* (2021) 'A basic review on systemic treatment options in WHO grade II-III gliomas', *Cancer Treatment Reviews*, 92, p. 102124. Available at: <https://doi.org/10.1016/j.ctrv.2020.102124>.

Mairs, R.J. *et al.* (2007) 'Microsatellite analysis for determination of the mutagenicity of extremely low-frequency electromagnetic fields and ionising radiation in vitro', *Mutation Research/Genetic Toxicology and Environmental Mutagenesis*, 626(1–2), pp. 34–41. Available at: <https://doi.org/10.1016/j.mrgentox.2006.08.005>.

Majd, N.K. *et al.* (2021) 'The promise of DNA damage response inhibitors for the treatment of glioblastoma', *Neuro-Oncology Advances*, 3(1), p. vdab015. Available at: <https://doi.org/10.1093/naajnl/vdab015>.

Malakhov, N. *et al.* (2018) 'Patterns of care and outcomes for glioblastoma in patients with poor performance status', *Journal of Clinical Neuroscience*, 52, pp. 66–70. Available at: <https://doi.org/10.1016/j.jocn.2018.03.006>.

Mansouri, A. *et al.* (2019) 'MGMT promoter methylation status testing to guide therapy for glioblastoma: refining the approach based on emerging evidence and current challenges', *Neuro-Oncology*, 21(2), pp. 167–178. Available at: <https://doi.org/10.1093/neuonc/nyy132>.

Mantione, M.E. *et al.* (2024) 'Disrupting pro-survival and inflammatory pathways with dimethyl fumarate sensitizes chronic lymphocytic leukemia to cell death', *Cell Death & Disease*, 15(3), p. 224. Available at: <https://doi.org/10.1038/s41419-024-06602-z>.

Marrazzo, P., Angeloni, C. and Hrelia, S. (2019) 'Combined Treatment with Three Natural Antioxidants Enhances Neuroprotection in a SH-SY5Y 3D Culture Model', *Antioxidants*, 8(10), p. 420. Available at: <https://doi.org/10.3390/antiox8100420>.

Matteo, P. *et al.* (2022) 'New and Old Horizons for an Ancient Drug: Pharmacokinetics, Pharmacodynamics, and Clinical Perspectives of Dimethyl Fumarate', *Pharmaceutics*, 14(12), p. 2732. Available at: <https://doi.org/10.3390/pharmaceutics14122732>.

Maugeri, R. *et al.* (2016) 'Aquaporins and Brain Tumors', *International Journal of Molecular Sciences*, 17(7), p. 1029. Available at: <https://doi.org/10.3390/ijms17071029>.

Mazzoleni, A. *et al.* (2024) 'Chromosomal instability: a key driver in glioma pathogenesis and progression', *European Journal of Medical Research*, 29(1), p. 451. Available at: <https://doi.org/10.1186/s40001-024-02043-8>.

McCabe, S.M. (2023) *Raman spectroscopy for the investigation of gold nanoparticles in Glioblastoma*. University of Strathclyde. Available at: <https://doi.org/10.48730/A57M-AG78>.

McAleavey, P.G., Walls, G.M. and Chalmers, A.J. (2022) 'Radiotherapy-drug combinations in the treatment of glioblastoma: a brief review', *CNS Oncology*, 11(2), p. CNS86. Available at: <https://doi.org/10.2217/cns-2021-0015>.

- McKinnon, C. *et al.* (2021) 'Glioblastoma: clinical presentation, diagnosis, and management', *BMJ*, p. n1560. Available at: <https://doi.org/10.1136/bmj.n1560>.
- Mehta, G. *et al.* (2012) 'Opportunities and challenges for use of tumor spheroids as models to test drug delivery and efficacy', *Journal of Controlled Release*, 164(2), pp. 192–204. Available at: <https://doi.org/10.1016/j.jconrel.2012.04.045>.
- Mencke, P. *et al.* (2021) 'The Role of DJ-1 in Cellular Metabolism and Pathophysiological Implications for Parkinson's Disease', *Cells*, 10(2), p. 347. Available at: <https://doi.org/10.3390/cells10020347>.
- Mesfin, F.B., Karsonovich, T. and Al-Dhahir, M.A. (2024) 'Gliomas', in *StatPearls*. Treasure Island (FL): StatPearls Publishing. Available at: <http://www.ncbi.nlm.nih.gov/books/NBK441874/> (Accessed: 24 November 2024).
- Miki, K. *et al.* (2024) 'Glutaminolysis is associated with mitochondrial pathway activation and can be therapeutically targeted in glioblastoma', *Cancer & Metabolism*, 12(1), p. 35. Available at: <https://doi.org/10.1186/s40170-024-00364-0>.
- Miller, K.D. *et al.* (2021) 'Brain and other central nervous system tumor statistics, 2021', *CA: A Cancer Journal for Clinicians*, 71(5), pp. 381–406. Available at: <https://doi.org/10.3322/caac.21693>.
- Miranda-Filho, A. *et al.* (2016) 'Cancers of the brain and CNS: global patterns and trends in incidence', *Neuro-Oncology*, p. now166. Available at: <https://doi.org/10.1093/neuonc/now166>.
- Moen, E.L. *et al.* (2014) 'The Role of Gene Body Cytosine Modifications in *MGMT* Expression and Sensitivity to Temozolomide', *Molecular Cancer Therapeutics*, 13(5), pp. 1334–1344. Available at: <https://doi.org/10.1158/1535-7163.MCT-13-0924>.
- Molenaar, R.J. *et al.* (2014) 'The driver and passenger effects of isocitrate dehydrogenase 1 and 2 mutations in oncogenesis and survival prolongation', *Biochimica Et Biophysica Acta*, 1846(2), pp. 326–341. Available at: <https://doi.org/10.1016/j.bbcan.2014.05.004>.
- Monteiro, A. *et al.* (2017) 'The Role of Hypoxia in Glioblastoma Invasion', *Cells*, 6(4), p. 45. Available at: <https://doi.org/10.3390/cells6040045>.
- Morgan, M.P., Finnegan, E. and Das, S. (2022) 'The role of transcription factors in the acquisition of the four latest proposed hallmarks of cancer and corresponding enabling characteristics', *Seminars in Cancer Biology*, 86, pp. 1203–1215. Available at: <https://doi.org/10.1016/j.semcancer.2022.10.002>.
- Morito, N. *et al.* (2003) 'Nrf2 regulates the sensitivity of death receptor signals by affecting intracellular glutathione levels', *Oncogene*, 22(58), pp. 9275–9281. Available at: <https://doi.org/10.1038/sj.onc.1207024>.
- Mukherjee, S. *et al.* (2020) '*SMARCB1* Gene Mutation Predisposes to Earlier Development of Glioblastoma: A Case Report of Familial GBM', *Journal of Neuropathology & Experimental Neurology*, 79(5), pp. 562–565. Available at: <https://doi.org/10.1093/jnen/nlaa022>.

- Mullen, C. (2024) *Development of novel combination therapies for the treatment of pancreatic cancer*. University of Strathclyde. Available at: <https://doi.org/10.48730/6VT3-H583>.
- Murphrey, M.B. *et al.* (2024) 'Biochemistry, Epidermal Growth Factor Receptor', in *StatPearls*. Treasure Island (FL): StatPearls Publishing. Available at: <http://www.ncbi.nlm.nih.gov/books/NBK482459/> (Accessed: 25 April 2024).
- Musah-Eroje, A. and Watson, S. (2019) 'A novel 3D in vitro model of glioblastoma reveals resistance to temozolomide which was potentiated by hypoxia', *Journal of Neuro-Oncology*, 142(2), pp. 231–240. Available at: <https://doi.org/10.1007/s11060-019-03107-0>.
- Nakamura, M. (2001) 'Promoter methylation of the DNA repair gene MGMT in astrocytomas is frequently associated with G:C -> A:T mutations of the TP53 tumor suppressor gene', *Carcinogenesis*, 22(10), pp. 1715–1719. Available at: <https://doi.org/10.1093/carcin/22.10.1715>.
- Nam, J.Y. and De Groot, J.F. (2017) 'Treatment of Glioblastoma', *Journal of Oncology Practice*, 13(10), pp. 629–638. Available at: <https://doi.org/10.1200/JOP.2017.025536>.
- Nasrallah, M.L.P. *et al.* (2020) 'A dual-genotype oligoastrocytoma with histologic, molecular, radiological and time-course features', *Acta Neuropathologica Communications*, 8(1), p. 115. Available at: <https://doi.org/10.1186/s40478-020-00998-3>.
- Nelson, J.S. *et al.* (2012) 'Potential risk factors for incident glioblastoma multiforme: the Honolulu Heart Program and Honolulu-Asia Aging Study', *Journal of Neuro-Oncology*, 109(2), pp. 315–321. Available at: <https://doi.org/10.1007/s11060-012-0895-3>.
- Nguyen, N. *et al.* (2021) 'Identifying the optimal cutoff point for MGMT promoter methylation status in glioblastoma', *CNS Oncology*, 10(3), p. CNS74. Available at: <https://doi.org/10.2217/cns-2021-0002>.
- Niu, B. *et al.* (2021) 'Application of glutathione depletion in cancer therapy: Enhanced ROS-based therapy, ferroptosis, and chemotherapy', *Biomaterials*, 277, p. 121110. Available at: <https://doi.org/10.1016/j.biomaterials.2021.121110>.
- Norris, J.N. *et al.* (2023) 'Glioblastoma in pregnant patient with pathologic and exogenous sex hormone exposure and family history of high-grade glioma: A case report and review of the literature', *Surgical Neurology International*, 14, p. 169. Available at: https://doi.org/10.25259/SNI_58_2023.
- Oancea-Castillo, L.R. *et al.* (2017) 'Comparative analysis of the effects of a sphingosine kinase inhibitor to temozolomide and radiation treatment on glioblastoma cell lines', *Cancer Biology & Therapy*, 18(6), pp. 400–406. Available at: <https://doi.org/10.1080/15384047.2017.1323583>.
- Obrador, E. *et al.* (2024) 'Glioblastoma Therapy: Past, Present and Future', *International Journal of Molecular Sciences*, 25(5), p. 2529. Available at: <https://doi.org/10.3390/ijms25052529>.

- Ogunrinu, T.A. and Sontheimer, H. (2010) 'Hypoxia Increases the Dependence of Glioma Cells on Glutathione *', *Journal of Biological Chemistry*, 285(48), pp. 37716–37724. Available at: <https://doi.org/10.1074/jbc.M110.161190>.
- Ohgaki, H. and Kleihues, P. (2005) 'Population-Based Studies on Incidence, Survival Rates, and Genetic Alterations in Astrocytic and Oligodendroglial Gliomas', *Journal of Neuropathology & Experimental Neurology*, 64(6), pp. 479–489. Available at: <https://doi.org/10.1093/jnen/64.6.479>.
- Ohgaki, H. and Kleihues, P. (2007) 'Genetic Pathways to Primary and Secondary Glioblastoma', *The American Journal of Pathology*, 170(5), pp. 1445–1453. Available at: <https://doi.org/10.2353/ajpath.2007.070011>.
- Ohgaki, H. and Kleihues, P. (2011) 'Genetic profile of astrocytic and oligodendroglial gliomas', *Brain Tumor Pathology*, 28(3), pp. 177–183. Available at: <https://doi.org/10.1007/s10014-011-0029-1>.
- Ohgaki, H. and Kleihues, P. (2013a) 'The Definition of Primary and Secondary Glioblastoma', *Clinical Cancer Research*, 19(4), pp. 764–772. Available at: <https://doi.org/10.1158/1078-0432.CCR-12-3002>.
- Ohgaki, H. and Kleihues, P. (2013b) 'The Definition of Primary and Secondary Glioblastoma', *Clinical Cancer Research*, 19(4), pp. 764–772. Available at: <https://doi.org/10.1158/1078-0432.CCR-12-3002>.
- Okamoto, Y. *et al.* (2004) 'Population-based study on incidence, survival rates, and genetic alterations of low-grade diffuse astrocytomas and oligodendrogliomas', *Acta Neuropathologica*, 108(1), pp. 49–56. Available at: <https://doi.org/10.1007/s00401-004-0861-z>.
- Olar, A. and Aldape, K.D. (2014) 'Using the molecular classification of glioblastoma to inform personalized treatment', *The Journal of Pathology*, 232(2), pp. 165–177. Available at: <https://doi.org/10.1002/path.4282>.
- Oleinick, N.L. *et al.* (1988) 'Inhibition of radiation-induced DNA-protein cross-link repair by glutathione depletion with L-buthionine sulfoximine', *NCI monographs: a publication of the National Cancer Institute*, (6), pp. 225–229.
- Oprita, A. *et al.* (2021) 'Updated Insights on EGFR Signaling Pathways in Glioma', *International Journal of Molecular Sciences*, 22(2), p. 587. Available at: <https://doi.org/10.3390/ijms22020587>.
- Ostrom, Q.T. *et al.* (2014) 'The epidemiology of glioma in adults: a “state of the science” review', *Neuro-Oncology*, 16(7), pp. 896–913. Available at: <https://doi.org/10.1093/neuonc/nou087>.
- Ostrom, Q.T., Francis, S.S. and Barnholtz-Sloan, J.S. (2021) 'Epidemiology of Brain and Other CNS Tumors', *Current Neurology and Neuroscience Reports*, 21(12), p. 68. Available at: <https://doi.org/10.1007/s11910-021-01152-9>.
- Pan, H. *et al.* (2013) 'The involvement of Nrf2–ARE pathway in regulation of apoptosis in human glioblastoma cell U251', *Neurological Research*, 35(1), pp. 71–78. Available at: <https://doi.org/10.1179/1743132812Y.0000000094>.

- Pan, P.C. and Magge, R.S. (2020) 'Mechanisms of EGFR Resistance in Glioblastoma', *International Journal of Molecular Sciences*, 21(22), p. 8471. Available at: <https://doi.org/10.3390/ijms21228471>.
- Paolillo, M., Comincini, S. and Schinelli, S. (2021) 'In Vitro Glioblastoma Models: A Journey into the Third Dimension', *Cancers*, 13(10), p. 2449. Available at: <https://doi.org/10.3390/cancers13102449>.
- Pape, J., Emberton, M. and Cheema, U. (2021) '3D Cancer Models: The Need for a Complex Stroma, Compartmentalization and Stiffness', *Frontiers in Bioengineering and Biotechnology*, 9, p. 660502. Available at: <https://doi.org/10.3389/fbioe.2021.660502>.
- Park, C.-K. *et al.* (2012) 'The Changes in MGMT Promoter Methylation Status in Initial and Recurrent Glioblastomas', *Translational Oncology*, 5(5), pp. 393-401. Available at: <https://doi.org/10.1593/tlo.12253>.
- Park, J.H. and Lee, H.K. (2022) 'Current Understanding of Hypoxia in Glioblastoma Multiforme and Its Response to Immunotherapy', *Cancers*, 14(5), p. 1176. Available at: <https://doi.org/10.3390/cancers14051176>.
- Pasquini, L. *et al.* (2021) 'Deep Learning Can Differentiate IDH-Mutant from IDH-Wild GBM', *Journal of Personalized Medicine*, 11(4), p. 290. Available at: <https://doi.org/10.3390/jpm11040290>.
- Patro, B.S. *et al.* (2011) 'WRN helicase regulates the ATR–CHK1-induced S-phase checkpoint pathway in response to topoisomerase-I–DNA covalent complexes', *Journal of Cell Science*, 124(23), pp. 3967–3979. Available at: <https://doi.org/10.1242/jcs.081372>.
- Pawlowska, E. *et al.* (2018) 'An Interplay between Senescence, Apoptosis and Autophagy in Glioblastoma Multiforme—Role in Pathogenesis and Therapeutic Perspective', *International Journal of Molecular Sciences*, 19(3), p. 889. Available at: <https://doi.org/10.3390/ijms19030889>.
- Peeters, M.C.M. *et al.* (2020) 'Prediagnostic symptoms and signs of adult glioma: the patients' view', *Journal of Neuro-Oncology*, 146(2), pp. 293–301. Available at: <https://doi.org/10.1007/s11060-019-03373-y>.
- Pellot Ortiz, K.I. *et al.* (2023) 'MDM2 Inhibition in the Treatment of Glioblastoma: From Concept to Clinical Investigation', *Biomedicines*, 11(7), p. 1879. Available at: <https://doi.org/10.3390/biomedicines11071879>.
- Perrin, S.L. *et al.* (2019) 'Glioblastoma heterogeneity and the tumour microenvironment: implications for preclinical research and development of new treatments', *Biochemical Society Transactions*, 47(2), pp. 625–638. Available at: <https://doi.org/10.1042/BST20180444>.
- Phillips, H.S. *et al.* (2006) 'Molecular subclasses of high-grade glioma predict prognosis, delineate a pattern of disease progression, and resemble stages in neurogenesis', *Cancer Cell*, 9(3), pp. 157–173. Available at: <https://doi.org/10.1016/j.ccr.2006.02.019>.

- 'Posters' (2023) *FEBS Open Bio*, 13(S2), pp. 61–258. Available at: <https://doi.org/10.1002/2211-5463.11646>.
- 'Posters' (2024) *FEBS Open Bio*, 14(S2), pp. 92–516. Available at: <https://doi.org/10.1002/2211-5463.11837>.
- Pouchieu, C. *et al.* (2016) 'Descriptive epidemiology and risk factors of primary central nervous system tumors: Current knowledge', *Revue Neurologique*, 172(1), pp. 46–55. Available at: <https://doi.org/10.1016/j.neurol.2015.10.007>.
- Pucci, B., Kasten, M. and Giordano, A. (2000) 'Cell Cycle and Apoptosis', *Neoplasia*, 2(4), pp. 291–299. Available at: <https://doi.org/10.1038/sj.neo.7900101>.
- Qi, Z. *et al.* (2015) 'The role of Gliadel wafers in the treatment of newly diagnosed GBM: a meta-analysis', *Drug Design, Development and Therapy*, p. 3341. Available at: <https://doi.org/10.2147/DDDT.S85943>.
- Ravi, S. *et al.* (2022) 'An Update to Hallmarks of Cancer', *Cureus* [Preprint]. Available at: <https://doi.org/10.7759/cureus.24803>.
- Reuss, David.E. (2023) 'Updates on the WHO diagnosis of IDH-mutant glioma', *Journal of Neuro-Oncology*, 162(3), pp. 461–469. Available at: <https://doi.org/10.1007/s11060-023-04250-5>.
- Ricciardi, L. *et al.* (2022) 'Carmustine Wafers Implantation in Patients With Newly Diagnosed High Grade Glioma: Is It Still an Option?', *Frontiers in Neurology*, 13, p. 884158. Available at: <https://doi.org/10.3389/fneur.2022.884158>.
- Riffle, S. *et al.* (2017) 'Linking hypoxia, DNA damage and proliferation in multicellular tumor spheroids', *BMC Cancer*, 17(1), p. 338. Available at: <https://doi.org/10.1186/s12885-017-3319-0>.
- Rominiyi, O. and Collis, S.J. (2022) 'DDRugging glioblastoma: understanding and targeting the DNA damage response to improve future therapies', *Molecular Oncology*, 16(1), pp. 11–41. Available at: <https://doi.org/10.1002/1878-0261.13020>.
- Rosito, M. *et al.* (2020) 'Exploring the Use of Dimethyl Fumarate as Microglia Modulator for Neurodegenerative Diseases Treatment', *Antioxidants*, 9(8), p. 700. Available at: <https://doi.org/10.3390/antiox9080700>.
- Saadeh, F.S., Mahfouz, R. and Assi, H.I. (2018) 'EGFR as a clinical marker in glioblastomas and other gliomas', *The International Journal of Biological Markers*, 33(1), pp. 22–32. Available at: <https://doi.org/10.5301/ijbm.5000301>.
- Sacks, P. and Rahman, M. (2020) 'Epidemiology of Brain Metastases', *Neurosurgery Clinics of North America*, 31(4), pp. 481–488. Available at: <https://doi.org/10.1016/j.nec.2020.06.001>.
- Saha, L., Singh, N. and Rawat, K. (2024) 'Neuroprotection induced by dimethyl fumarate', in *Natural Molecules in Neuroprotection and Neurotoxicity*. Elsevier, pp. 1465–1486. Available at: <https://doi.org/10.1016/B978-0-443-23763-8.00036-1>.
- Said, M.M. *et al.* (2023) 'Myelotoxicity of Temozolomide Treatment in Patients with Glioblastoma Is It Time for a More Mechanistic Approach?', *Cancers*, 15(5), p. 1561. Available at: <https://doi.org/10.3390/cancers15051561>.

Saidu, N.E.B. *et al.* (2017) 'Dimethyl Fumarate Controls the NRF2/DJ-1 Axis in Cancer Cells: Therapeutic Applications', *Molecular Cancer Therapeutics*, 16(3), pp. 529–539. Available at: <https://doi.org/10.1158/1535-7163.MCT-16-0405>.

Saidu, N.E.B. *et al.* (2019) 'Dimethyl fumarate, a two-edged drug: Current status and future directions', *Medicinal Research Reviews*, 39(5), pp. 1923–1952. Available at: <https://doi.org/10.1002/med.21567>.

Sales, A. *et al.* (2022) 'Surgical Treatment of Glioblastoma: State-of-the-Art and Future Trends', *Journal of Clinical Medicine*, 11(18), p. 5354. Available at: <https://doi.org/10.3390/jcm11185354>.

Salles, D. *et al.* (2020) 'Pilocytic Astrocytoma: A Review of General, Clinical, and Molecular Characteristics', *Journal of Child Neurology*, 35(12), pp. 852–858. Available at: <https://doi.org/10.1177/0883073820937225>.

Sánchez-Sanz, A. *et al.* (2024) 'Neuroprotective and Anti-Inflammatory Effects of Dimethyl Fumarate, Monomethyl Fumarate, and Cannabidiol in Neurons and Microglia', *International Journal of Molecular Sciences*, 25(23), p. 13082. Available at: <https://doi.org/10.3390/ijms252313082>.

Santucci, C. *et al.* (2020) 'Progress in cancer mortality, incidence, and survival: a global overview', *European Journal of Cancer Prevention*, 29(5), pp. 367–381. Available at: <https://doi.org/10.1097/CEJ.0000000000000594>.

Sato, M. *et al.* (2018) 'The ferroptosis inducer erastin irreversibly inhibits system xc- and synergizes with cisplatin to increase cisplatin's cytotoxicity in cancer cells', *Scientific Reports*, 8(1), p. 968. Available at: <https://doi.org/10.1038/s41598-018-19213-4>.

Sattiraju, A., Sai, K.K.S. and Mintz, A. (2017) 'Glioblastoma Stem Cells and Their Microenvironment', in A. Birbrair (ed.) *Stem Cell Microenvironments and Beyond*. Cham: Springer International Publishing (Advances in Experimental Medicine and Biology), pp. 119–140. Available at: https://doi.org/10.1007/978-3-319-69194-7_7.

Schaff, L.R. and Mellinghoff, I.K. (2023) 'Glioblastoma and Other Primary Brain Malignancies in Adults: A Review', *JAMA*, 329(7), p. 574. Available at: <https://doi.org/10.1001/jama.2023.0023>.

Schmidt, T.J., Ak, M. and Mrowietz, U. (2007) 'Reactivity of dimethyl fumarate and methylhydrogen fumarate towards glutathione and N-acetyl-L-cysteine—Preparation of S-substituted thiosuccinic acid esters', *Bioorganic & Medicinal Chemistry*, 15(1), pp. 333–342. Available at: <https://doi.org/10.1016/j.bmc.2006.09.053>.

Schmitt, A. *et al.* (2021) 'Dimethyl fumarate induces ferroptosis and impairs NF- κ B/STAT3 signaling in DLBCL', *Blood*, 138(10), pp. 871–884. Available at: <https://doi.org/10.1182/blood.2020009404>.

Scott, D. (2020) *Development of a novel combination radio- chemotherapy for glioblastoma multiforme*. University of Strathclyde. Available at: <https://doi.org/10.48730/GBMCH-NV61>.

Shafer, D. *et al.* (2020) 'Phase I trial of dimethyl fumarate, temozolomide, and radiation therapy in glioblastoma', *Neuro-Oncology Advances*, 2(1), p. vdz052. Available at: <https://doi.org/10.1093/noajnl/vdz052>.

Shafizadeh, M. *et al.* (2022) 'Effects of Dimethyl Fumarate on the Karnofsky Performance Status and Serum S100 β Level in Newly Glioblastoma Patients: A Randomized, Phase-II, Placebo, Triple Blinded, Controlled Trial', *Galen Medical Journal*, 11. Available at: <https://doi.org/10.31661/gmj.v11i.1897>.

Shah, N. *et al.* (2011) 'Comprehensive Analysis of MGMT Promoter Methylation: Correlation with MGMT Expression and Clinical Response in GBM', *PLoS ONE*. Edited by C. Jones, 6(1), p. e16146. Available at: <https://doi.org/10.1371/journal.pone.0016146>.

Shahcheraghi, S.H. *et al.* (2022) 'The Role of NRF2/KEAP1 Pathway in Glioblastoma: Pharmacological Implications', *Medical Oncology*, 39(7), p. 91. Available at: <https://doi.org/10.1007/s12032-022-01693-0>.

Sharma, P. *et al.* (2023) 'Tumor microenvironment in glioblastoma: Current and emerging concepts', *Neuro-Oncology Advances*, 5(1), p. vdad009. Available at: <https://doi.org/10.1093/noajnl/vdad009>.

Sharma, S. *et al.* (2009) 'Role of MGMT in tumor development, progression, diagnosis, treatment and prognosis', *Anticancer Research*, 29(10), pp. 3759–3768.

Shen, J. *et al.* (2023) 'Targeting the p53 signaling pathway in cancers: Molecular mechanisms and clinical studies', *MedComm*, 4(3), p. e288. Available at: <https://doi.org/10.1002/mco2.288>.

Shikalov, A., Koman, I. and Kogan, N.M. (2024) 'Targeted Glioma Therapy—Clinical Trials and Future Directions', *Pharmaceutics*, 16(1), p. 100. Available at: <https://doi.org/10.3390/pharmaceutics16010100>.

Silantyev, A. *et al.* (2019) 'Current and Future Trends on Diagnosis and Prognosis of Glioblastoma: From Molecular Biology to Proteomics', *Cells*, 8(8), p. 863. Available at: <https://doi.org/10.3390/cells8080863>.

Simon, T., Jackson, E. and Giamas, G. (2020) 'Breaking through the glioblastoma micro-environment via extracellular vesicles', *Oncogene*, 39(23), pp. 4477–4490. Available at: <https://doi.org/10.1038/s41388-020-1308-2>.

Singh, N. *et al.* (2020) 'Mechanisms of temozolomide resistance in glioblastoma - a comprehensive review', *Cancer Drug Resistance* [Preprint]. Available at: <https://doi.org/10.20517/cdr.2020.79>.

Śledzińska, P. *et al.* (2021) 'Prognostic and Predictive Biomarkers in Gliomas', *International Journal of Molecular Sciences*, 22(19), p. 10373. Available at: <https://doi.org/10.3390/ijms221910373>.

Smittenaar, C.R. *et al.* (2016) 'Cancer incidence and mortality projections in the UK until 2035', *British Journal of Cancer*, 115(9), pp. 1147–1155. Available at: <https://doi.org/10.1038/bjc.2016.304>.

Socha, J. *et al.* (2016) 'Outcome of treatment of recurrent glioblastoma multiforme in elderly and/or frail patients', *Journal of Neuro-Oncology*, 126(3), pp. 493–498. Available at: <https://doi.org/10.1007/s11060-015-1987-7>.

Soni, V. *et al.* (2021) 'In Vitro and In Vivo Enhancement of Temozolomide Effect in Human Glioblastoma by Non-Invasive Application of Cold Atmospheric Plasma', *Cancers*, 13(17), p. 4485. Available at: <https://doi.org/10.3390/cancers13174485>.

Stark, A.M. *et al.* (2012) 'Glioblastoma: Clinical characteristics, prognostic factors and survival in 492 patients', *Clinical Neurology and Neurosurgery*, 114(7), pp. 840–845. Available at: <https://doi.org/10.1016/j.clineuro.2012.01.026>.

Stein, J.M. (1975) 'The effect of adrenaline and of alpha- and beta-adrenergic blocking agents on ATP concentration and on incorporation of ³²Pi into ATP in rat fat cells', *Biochemical Pharmacology*, 24(18), pp. 1659–1662. Available at: [https://doi.org/10.1016/0006-2952\(75\)90002-7](https://doi.org/10.1016/0006-2952(75)90002-7).

Strobel, H. *et al.* (2019) 'Temozolomide and Other Alkylating Agents in Glioblastoma Therapy', *Biomedicines*, 7(3), p. 69. Available at: <https://doi.org/10.3390/biomedicines7030069>.

Stupp, R. *et al.* (2005) 'Radiotherapy plus Concomitant and Adjuvant Temozolomide for Glioblastoma', *New England Journal of Medicine*, 352(10), pp. 987–996. Available at: <https://doi.org/10.1056/NEJMoa043330>.

Sun, X. *et al.* (2016) 'Activation of the p62-Keap1-NRF2 pathway protects against ferroptosis in hepatocellular carcinoma cells', *Hepatology*, 63(1), pp. 173–184. Available at: <https://doi.org/10.1002/hep.28251>.

Sung, H. *et al.* (2021) 'Global Cancer Statistics 2020: GLOBOCAN Estimates of Incidence and Mortality Worldwide for 36 Cancers in 185 Countries', *CA: A Cancer Journal for Clinicians*, 71(3), pp. 209–249. Available at: <https://doi.org/10.3322/caac.21660>.

Suvà, M.L. and Tirosh, I. (2020) 'The Glioma Stem Cell Model in the Era of Single-Cell Genomics', *Cancer Cell*, 37(5), pp. 630–636. Available at: <https://doi.org/10.1016/j.ccell.2020.04.001>.

Swindell, W.R., Bojanowski, K. and Chaudhuri, R.K. (2022) 'Transcriptomic Analysis of Fumarate Compounds Identifies Unique Effects of Isosorbide Di-(Methyl Fumarate) on NRF2, NF-kappaB and IRF1 Pathway Genes', *Pharmaceuticals*, 15(4), p. 461. Available at: <https://doi.org/10.3390/ph15040461>.

Szylberg, M. *et al.* (2022) 'MGMT Promoter Methylation as a Prognostic Factor in Primary Glioblastoma: A Single-Institution Observational Study', *Biomedicines*, 10(8), p. 2030. Available at: <https://doi.org/10.3390/biomedicines10082030>.

Tai, S.-H. *et al.* (2021) 'Cinnamophilin enhances temozolomide-induced cytotoxicity against malignant glioma: the roles of ROS and cell cycle arrest', *Translational Cancer Research*, 10(9), pp. 3906–3920. Available at: <https://doi.org/10.21037/tcr-20-3426>.

Tan, A.C. *et al.* (2020) 'Management of glioblastoma: State of the art and future directions', *CA: A Cancer Journal for Clinicians*, 70(4), pp. 299–312. Available at: <https://doi.org/10.3322/caac.21613>.

Tang, J.-H. *et al.* (2016) 'Downregulation of HIF-1a sensitizes U251 glioma cells to the temozolomide (TMZ) treatment', *Experimental Cell Research*, 343(2), pp. 148–158. Available at: <https://doi.org/10.1016/j.yexcr.2016.04.011>.

Tang, Q. *et al.* (2022) 'Tubeimoside-I sensitizes temozolomide-resistant glioblastoma cells to chemotherapy by reducing MGMT expression and suppressing EGFR induced PI3K/Akt/mTOR/NF- κ B-mediated signaling pathway', *Phytomedicine*, 99, p. 154016. Available at: <https://doi.org/10.1016/j.phymed.2022.154016>.

Tang, T. *et al.* (2022) 'Knockdown of Nrf2 radiosensitizes glioma cells by inducing redox stress and apoptosis in hypoxia', *Translational Cancer Research*, 11(11), pp. 4105–4116. Available at: <https://doi.org/10.21037/tcr-22-1420>.

Tang, Y., Yu, P. and Cheng, L. (2017) 'Current progress in the derivation and therapeutic application of neural stem cells', *Cell Death & Disease*, 8(10), pp. e3108–e3108. Available at: <https://doi.org/10.1038/cddis.2017.504>.

Tesileanu, C.M.S. *et al.* (2022) 'Temozolomide and Radiotherapy versus Radiotherapy Alone in Patients with Glioblastoma, IDH -wildtype: Post Hoc Analysis of the EORTC Randomized Phase III CATNON Trial', *Clinical Cancer Research*, 28(12), pp. 2527–2535. Available at: <https://doi.org/10.1158/1078-0432.CCR-21-4283>.

The EVOLVE-MS-2 Study Group *et al.* (2020) 'Diroximel Fumarate Demonstrates an Improved Gastrointestinal Tolerability Profile Compared with Dimethyl Fumarate in Patients with Relapsing–Remitting Multiple Sclerosis: Results from the Randomized, Double-Blind, Phase III EVOLVE-MS-2 Study', *CNS Drugs*, 34(2), pp. 185–196. Available at: <https://doi.org/10.1007/s40263-020-00700-0>.

Tomicic, M.T. *et al.* (2015) 'Apoptosis induced by temozolomide and nimustine in glioblastoma cells is supported by JNK/c-Jun-mediated induction of the BH3-only protein BIM', *Oncotarget*, 6(32), pp. 33755–33768. Available at: <https://doi.org/10.18632/oncotarget.5274>.

Toulany, M. (2016) 'DNA Repair Pathways as a Potential Target for Radiosensitization', in M.S. Anscher and K. Valerie (eds) *Strategies to Enhance the Therapeutic Ratio of Radiation as a Cancer Treatment*. Cham: Springer International Publishing, pp. 253–287. Available at: https://doi.org/10.1007/978-3-319-45594-5_11.

Tso, C.-L. *et al.* (2006) 'Distinct Transcription Profiles of Primary and Secondary Glioblastoma Subgroups', *Cancer Research*, 66(1), pp. 159–167. Available at: <https://doi.org/10.1158/0008-5472.CAN-05-0077>.

Ursini, F. and Maiorino, M. (2020) 'Lipid peroxidation and ferroptosis: The role of GSH and GPx4', *Free Radical Biology and Medicine*, 152, pp. 175–185. Available at: <https://doi.org/10.1016/j.freeradbiomed.2020.02.027>.

Valiyaveetti, D. *et al.* (2018) 'Effect of valproic acid on survival in glioblastoma: A prospective single-arm study', *South Asian Journal of Cancer*, 07(03), pp. 159–162. Available at: <https://doi.org/10.4103/sajc.sajc.188.17>.

- Varricchio, A. and Yool, A.J. (2023) 'Aquaporins and Ion Channels as Dual Targets in the Design of Novel Glioblastoma Therapeutics to Limit Invasiveness', *Cancers*, 15(3), p. 849. Available at: <https://doi.org/10.3390/cancers15030849>.
- Vašková, J. *et al.* (2023) 'Glutathione-Related Enzymes and Proteins: A Review', *Molecules*, 28(3), p. 1447. Available at: <https://doi.org/10.3390/molecules28031447>.
- Verhaak, R.G.W. *et al.* (2010) 'Integrated Genomic Analysis Identifies Clinically Relevant Subtypes of Glioblastoma Characterized by Abnormalities in PDGFRA, IDH1, EGFR, and NF1', *Cancer Cell*, 17(1), pp. 98–110. Available at: <https://doi.org/10.1016/j.ccr.2009.12.020>.
- Vollmann-Zwerenz, A. *et al.* (2020) 'Tumor Cell Invasion in Glioblastoma', *International Journal of Molecular Sciences*, 21(6), p. 1932. Available at: <https://doi.org/10.3390/ijms21061932>.
- Wahl, D.R. *et al.* (2017) 'Glioblastoma Therapy Can Be Augmented by Targeting IDH1-Mediated NADPH Biosynthesis', *Cancer Research*, 77(4), pp. 960–970. Available at: <https://doi.org/10.1158/0008-5472.CAN-16-2008>.
- Walker, T.M., Rhodes, P.C. and Westmoreland, C. (2000) 'The differential cytotoxicity of methotrexate in rat hepatocyte monolayer and spheroid cultures', *Toxicology in Vitro*, 14(5), pp. 475–485. Available at: [https://doi.org/10.1016/S0887-2333\(00\)00036-9](https://doi.org/10.1016/S0887-2333(00)00036-9).
- Wang, C. *et al.* (2013) 'The positive correlation between DJ -1 and β -catenin expression shows prognostic value for patients with glioma', *Neuropathology*, 33(6), pp. 628–636. Available at: <https://doi.org/10.1111/neup.12041>.
- Wang, G. *et al.* (2017) 'Advances in the targeting of HIF-1 α and future therapeutic strategies for glioblastoma multiforme', *Oncology Reports*, 37(2), pp. 657–670. Available at: <https://doi.org/10.3892/or.2016.3309>.
- Wang, H. *et al.* (2018) 'Cancer Radiosensitizers', *Trends in Pharmacological Sciences*, 39(1), pp. 24–48. Available at: <https://doi.org/10.1016/j.tips.2017.11.003>.
- Wang, H.-H. *et al.* (2017) 'GADD45A plays a protective role against temozolomide treatment in glioblastoma cells', *Scientific Reports*, 7. Available at: <https://doi.org/10.1038/s41598-017-06851-3>.
- Wang, Q. *et al.* (2017) 'Tumor Evolution of Glioma-Intrinsic Gene Expression Subtypes Associates with Immunological Changes in the Microenvironment', *Cancer Cell*, 32(1), pp. 42-56.e6. Available at: <https://doi.org/10.1016/j.ccell.2017.06.003>.
- Wang, R. *et al.* (2022) 'Regulatory pattern of abnormal promoter CpG island methylation in the glioblastoma multiforme classification', *Frontiers in Genetics*, 13, p. 989985. Available at: <https://doi.org/10.3389/fgene.2022.989985>.
- Wang, T. *et al.* (2024) 'Dimethyl fumarate improves cognitive impairment and neuroinflammation in mice with Alzheimer's disease', *Journal of Neuroinflammation*, 21(1), p. 55. Available at: <https://doi.org/10.1186/s12974-024-03046-2>.

- Wang, X. *et al.* (2015) 'NF- κ B inhibitor reverses temozolomide resistance in human glioma TR/U251 cells', *Oncology Letters*, 9(6), pp. 2586–2590. Available at: <https://doi.org/10.3892/ol.2015.3130>.
- Wang, Z. *et al.* (2021) 'The adaptive transition of glioblastoma stem cells and its implications on treatments', *Signal Transduction and Targeted Therapy*, 6(1), p. 124. Available at: <https://doi.org/10.1038/s41392-021-00491-w>.
- Weller, M. *et al.* (2015) 'Glioma', *Nature Reviews Disease Primers*, 1(1), p. 15017. Available at: <https://doi.org/10.1038/nrdp.2015.17>.
- Wen, P.Y. *et al.* (2020) 'Glioblastoma in adults: a Society for Neuro-Oncology (SNO) and European Society of Neuro-Oncology (EANO) consensus review on current management and future directions', *Neuro-Oncology*, 22(8), pp. 1073–1113. Available at: <https://doi.org/10.1093/neuonc/noaa106>.
- Wesolowski, J.R., Rajdev, P. and Mukherji, S.K. (2010) 'Temozolomide (Temodar)', *American Journal of Neuroradiology*, 31(8), pp. 1383–1384. Available at: <https://doi.org/10.3174/ajnr.A2170>.
- Wesseling, P. and Capper, D. (2018) 'WHO 2016 Classification of gliomas', *Neuropathology and Applied Neurobiology*, 44(2), pp. 139–150. Available at: <https://doi.org/10.1111/nan.12432>.
- Westphal, M., Maire, C.L. and Lamszus, K. (2017) 'EGFR as a Target for Glioblastoma Treatment: An Unfulfilled Promise', *CNS Drugs*, 31(9), pp. 723–735. Available at: <https://doi.org/10.1007/s40263-017-0456-6>.
- Wick, W. *et al.* (2017) 'Lomustine and Bevacizumab in Progressive Glioblastoma', *New England Journal of Medicine*, 377(20), pp. 1954–1963. Available at: <https://doi.org/10.1056/NEJMoa1707358>.
- Wirsching, H.-G. and Weller, M. (2017) 'Glioblastoma', in J. Moliterno Gunel, J.M. Piepmeyer, and J.M. Baehring (eds) *Malignant Brain Tumors*. Cham: Springer International Publishing, pp. 265–288. Available at: https://doi.org/10.1007/978-3-319-49864-5_18.
- Womeldorff, M., Gillespie, D. and Jensen, R.L. (2014) 'Hypoxia-inducible factor–1 and associated upstream and downstream proteins in the pathophysiology and management of glioblastoma', *Neurosurgical Focus*, 37(6), p. E8. Available at: <https://doi.org/10.3171/2014.9.FOCUS14496>.
- Wrensch, M. *et al.* (1997) 'Familial and Personal Medical History of Cancer and Nervous System Conditions among Adults with Glioma and Controls', *American Journal of Epidemiology*, 145(7), pp. 581–593. Available at: <https://doi.org/10.1093/oxfordjournals.aje.a009154>.
- Wrensch, M. *et al.* (2005) 'The molecular epidemiology of gliomas in adults', *Neurosurgical Focus*, 19(5), pp. 1–11. Available at: <https://doi.org/10.3171/foc.2005.19.5.6>.
- Wu, J.L. *et al.* (2004) 'I κ B α M suppresses angiogenesis and tumorigenesis promoted by a constitutively active mutant EGFR in human glioma cells', *Neurological*

Research, 26(7), pp. 785–791. Available at: <https://doi.org/10.1179/016164104225014139>.

Wu, N. *et al.* (2016) 'Alpha-Ketoglutarate: Physiological Functions and Applications', *Biomolecules & Therapeutics*, 24(1), pp. 1–8. Available at: <https://doi.org/10.4062/biomolther.2015.078>.

Wu, W. *et al.* (2021) 'Glioblastoma multiforme (GBM): An overview of current therapies and mechanisms of resistance', *Pharmacological Research*, 171, p. 105780. Available at: <https://doi.org/10.1016/j.phrs.2021.105780>.

Wynn, D. *et al.* (2020) 'Monomethyl fumarate has better gastrointestinal tolerability profile compared with dimethyl fumarate', *Multiple Sclerosis and Related Disorders*, 45, p. 102335. Available at: <https://doi.org/10.1016/j.msard.2020.102335>.

Xiao, Z. *et al.* (2003) 'Chk1 Mediates S and G2 Arrests through Cdc25A Degradation in Response to DNA-damaging Agents', *Journal of Biological Chemistry*, 278(24), pp. 21767–21773. Available at: <https://doi.org/10.1074/jbc.M300229200>.

Xiao, Z.-Z. *et al.* (2020) 'Carmustine as a Supplementary Therapeutic Option for Glioblastoma: A Systematic Review and Meta-Analysis', *Frontiers in Neurology*, 11, p. 1036. Available at: <https://doi.org/10.3389/fneur.2020.01036>.

Xie, Y. *et al.* (2016) 'Ferroptosis: process and function', *Cell Death & Differentiation*, 23(3), pp. 369–379. Available at: <https://doi.org/10.1038/cdd.2015.158>.

Yalamarty, S.S.K. *et al.* (2023) 'Mechanisms of Resistance and Current Treatment Options for Glioblastoma Multiforme (GBM)', *Cancers*, 15(7), p. 2116. Available at: <https://doi.org/10.3390/cancers15072116>.

Yang, K. *et al.* (2022) 'Glioma targeted therapy: insight into future of molecular approaches', *Molecular Cancer*, 21(1), p. 39. Available at: <https://doi.org/10.1186/s12943-022-01513-z>.

Yang, L. *et al.* (2012) 'Hypoxia and hypoxia-inducible factors in glioblastoma multiforme progression and therapeutic implications', *Experimental Cell Research*, 318(19), pp. 2417–2426. Available at: <https://doi.org/10.1016/j.yexcr.2012.07.017>.

Yang, Y. *et al.* (2021) 'Dimethyl fumarate prevents ferroptosis to attenuate acute kidney injury by acting on NRF2', *Clinical and Translational Medicine*, 11(4), p. e382. Available at: <https://doi.org/10.1002/ctm2.382>.

Yao, Y. *et al.* (2016) 'Dimethyl Fumarate and Monomethyl Fumarate Promote Post-Ischemic Recovery in Mice', *Translational Stroke Research*, 7(6), pp. 535–547. Available at: <https://doi.org/10.1007/s12975-016-0496-0>.

Yapici, F.I., Bebbler, C.M. and Von Karstedt, S. (2024) 'A guide to ferroptosis in cancer', *Molecular Oncology*, 18(6), pp. 1378–1396. Available at: <https://doi.org/10.1002/1878-0261.13649>.

Yates, J.W., Chalmer, B. and McKegney, F.P. (1980) 'Evaluation of patients with advanced cancer using the karnofsky performance status', *Cancer*, 45(8), pp. 2220–2224. Available at: [https://doi.org/10.1002/1097-0142\(19800415\)45:8<2220::AID-CNCR2820450835>3.0.CO;2-Q](https://doi.org/10.1002/1097-0142(19800415)45:8<2220::AID-CNCR2820450835>3.0.CO;2-Q).

- Yazdi, M.R. and Mrowietz, U. (2008) 'Fumaric acid esters', *Clinics in Dermatology*, 26(5), pp. 522–526. Available at: <https://doi.org/10.1016/j.clindermatol.2008.07.001>.
- Yi, G. *et al.* (2019) 'Acquired temozolomide resistance in MGMT-deficient glioblastoma cells is associated with regulation of DNA repair by DHC2', *Brain*, 142(8), pp. 2352–2366. Available at: <https://doi.org/10.1093/brain/awz202>.
- Yi, L. *et al.* (2019) 'Notch1 signaling pathway promotes invasion, self-renewal and growth of glioma initiating cells via modulating chemokine system CXCL12/CXCR4', *Journal of Experimental & Clinical Cancer Research*, 38(1), p. 339. Available at: <https://doi.org/10.1186/s13046-019-1319-4>.
- Yoo, D. *et al.* (2019) 'Glutathione-Depleting Pro-Oxidant as a Selective Anticancer Therapeutic Agent', *ACS Omega*, 4(6), pp. 10070–10077. Available at: <https://doi.org/10.1021/acsomega.9b00140>.
- Yoshikawa, M.H. *et al.* (2023) 'Modifiable risk factors for glioblastoma: a systematic review and meta-analysis', *Neurosurgical Review*, 46(1), p. 143. Available at: <https://doi.org/10.1007/s10143-023-02051-y>.
- Young, R.M. *et al.* (2015) 'Current trends in the surgical management and treatment of adult glioblastoma', *Annals of Translational Medicine*, 3(9), p. 121. Available at: <https://doi.org/10.3978/j.issn.2305-5839.2015.05.10>.
- Youssef, G. and Miller, J.J. (2020) 'Lower Grade Gliomas', *Current Neurology and Neuroscience Reports*, 20(7), p. 21. Available at: <https://doi.org/10.1007/s11910-020-01040-8>.
- Yu, W. *et al.* (2020) 'O6-Methylguanine-DNA Methyltransferase (MGMT): Challenges and New Opportunities in Glioma Chemotherapy', *Frontiers in Oncology*, 9, p. 1547. Available at: <https://doi.org/10.3389/fonc.2019.01547>.
- Yuan, F. *et al.* (2022) 'HSP27 protects against ferroptosis of glioblastoma cells', *Human Cell*, 35(1), pp. 238–249. Available at: <https://doi.org/10.1007/s13577-021-00645-6>.
- Yun, H.S. *et al.* (2024) 'MGMT inhibition regulates radioresponse in GBM, GSC, and melanoma', *Scientific Reports*, 14(1), p. 12363. Available at: <https://doi.org/10.1038/s41598-024-61240-x>.
- Zarneshan, S.N. *et al.* (2023) 'Exploiting pivotal mechanisms behind the senescence-like cell cycle arrest in cancer', in *Advances in Protein Chemistry and Structural Biology*. Elsevier, pp. 1–19. Available at: <https://doi.org/10.1016/bs.apcsb.2022.11.007>.
- Zhang, L. *et al.* (2020) 'Role of DJ-1 in Immune and Inflammatory Diseases', *Frontiers in Immunology*, 11, p. 994. Available at: <https://doi.org/10.3389/fimmu.2020.00994>.
- Zhang, W. *et al.* (2024) 'GPX4, ferroptosis, and diseases', *Biomedicine & Pharmacotherapy*, 174, p. 116512. Available at: <https://doi.org/10.1016/j.biopha.2024.116512>.

Zhang, X. (2012) 'Resveratrol reverses temozolomide resistance by downregulation of MGMT in T98G glioblastoma cells by the NF- κ B-dependent pathway', *Oncology Reports* [Preprint]. Available at: <https://doi.org/10.3892/or.2012.1715>.

Zhang, Y. *et al.* (2018) 'The p53 Pathway in Glioblastoma', *Cancers*, 10(9), p. 297. Available at: <https://doi.org/10.3390/cancers10090297>.

Zhang, Y. *et al.* (2022) 'Short-term exposure to dimethyl fumarate (DMF) inhibits LPS-induced I κ B ζ expression in macrophages: implications for the pharmacological activity of DMF'. Available at: <https://doi.org/10.21203/rs.3.rs-2308926/v1>.

Zhang, Z. *et al.* (2020) 'Overcoming cancer therapeutic bottleneck by drug repurposing', *Signal Transduction and Targeted Therapy*, 5(1), p. 113. Available at: <https://doi.org/10.1038/s41392-020-00213-8>.

Zhao, Y. *et al.* (2009) 'Increase in thiol oxidative stress via glutathione reductase inhibition as a novel approach to enhance cancer sensitivity to X-ray irradiation', *Free Radical Biology and Medicine*, 47(2), pp. 176–183. Available at: <https://doi.org/10.1016/j.freeradbiomed.2009.04.022>.

Zheng, L. *et al.* (2015) 'Fumarate induces redox-dependent senescence by modifying glutathione metabolism', *Nature Communications*, 6(1), p. 6001. Available at: <https://doi.org/10.1038/ncomms7001>.

Zhu, J. *et al.* (2014) 'Differential Nrf2 expression between glioma stem cells and non-stem-like cells in glioblastoma', *Oncology Letters*, 7(3), pp. 693–698. Available at: <https://doi.org/10.3892/ol.2013.1260>.

Zhu, Y. *et al.* (2022) 'Characterization of Temozolomide Resistance Using a Novel Acquired Resistance Model in Glioblastoma Cell Lines', *Cancers*, 14(9), p. 2211. Available at: <https://doi.org/10.3390/cancers14092211>.

Zhu, Z. *et al.* (2018) 'Glutathione reductase mediates drug resistance in glioblastoma cells by regulating redox homeostasis', *Journal of Neurochemistry*, 144(1), pp. 93–104. Available at: <https://doi.org/10.1111/jnc.14250>.

Zhuo, S. *et al.* (2022) 'Emerging role of ferroptosis in glioblastoma: Therapeutic opportunities and challenges', *Frontiers in Molecular Biosciences*, 9, p. 974156. Available at: <https://doi.org/10.3389/fmolb.2022.974156>.

Zotero | Settings > Storage (2024). Available at: <https://www.zotero.org/settings/storage> (Accessed: 2 February 2024).

Zou, Y. *et al.* (2021) 'TRPC5 mediates TMZ resistance in TMZ-resistant glioblastoma cells via NFATc3-P-gp pathway', *Translational Oncology*, 14(12), p. 101214. Available at: <https://doi.org/10.1016/j.tranon.2021.101214>.

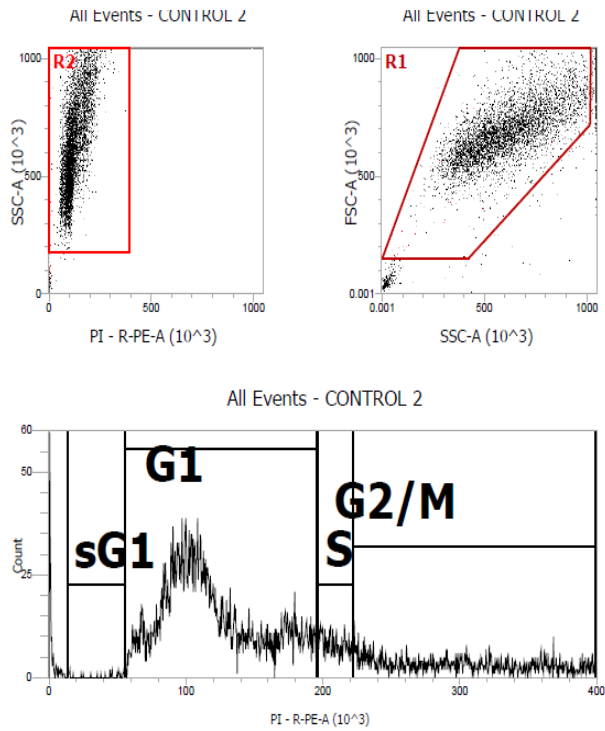
Zugazagoitia, J. *et al.* (2016) 'Current Challenges in Cancer Treatment', *Clinical Therapeutics*, 38(7), pp. 1551–1566. Available at: <https://doi.org/10.1016/j.clinthera.2016.03.026>.

(2024). Available at: <https://erp7-web3.ds.strath.ac.uk/BusinessWorld/Custom/ReqPunchOut.aspx> (Accessed: 2 April 2024).

Appendix

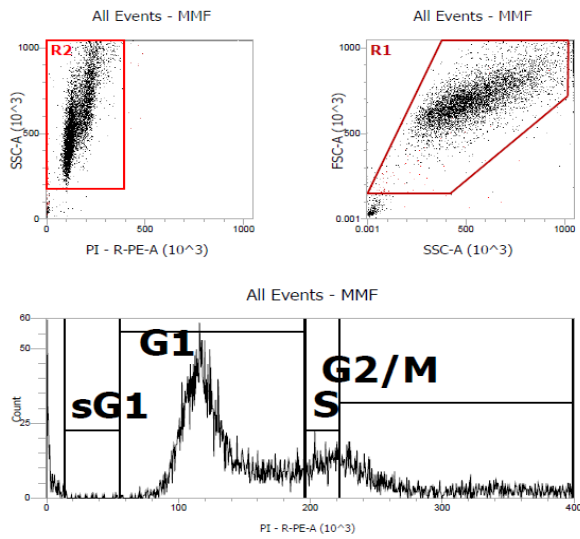
Appendix 1 – Cell Cycle Flow Cytometry Plots

(A)



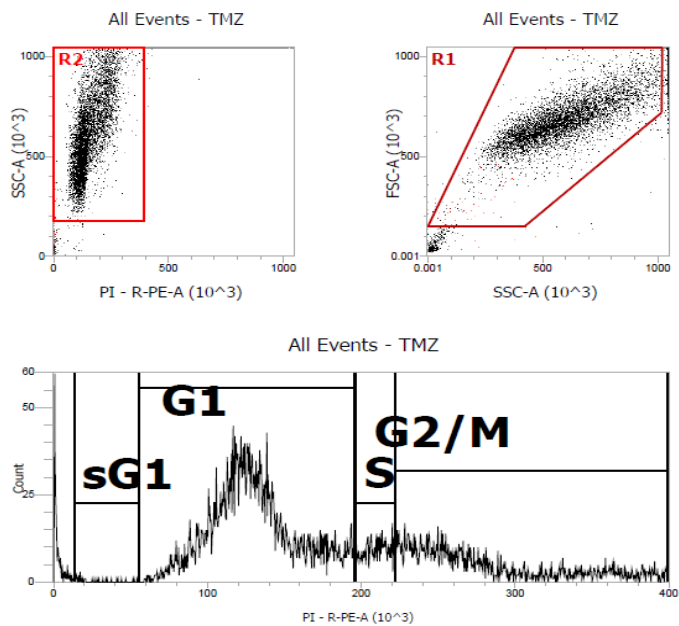
Appendix 1 (A): Representative flow cytometry plots for UVW control. FSC/SSC and gating strategy.

(B)



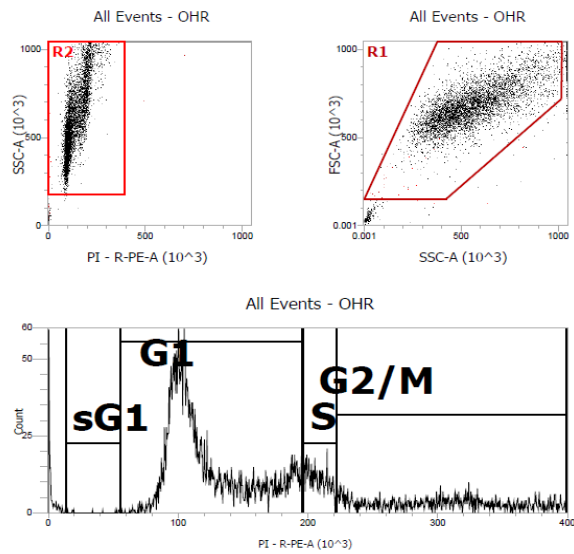
Appendix 1 (B): Representative flow cytometry plots for UVW MMF treated cells. FSC/SSC and gating strategy

(C)



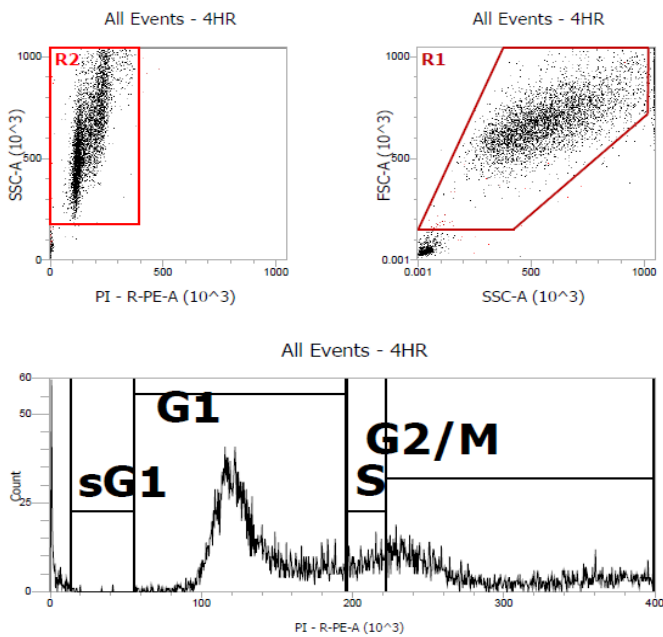
Appendix 1 (C): Representative flow cytometry plots for UVW TMZ treated cells. FSC/SSC and gating strategy

(D)



Appendix 1 (D): Representative flow cytometry plots for UVW TMZ + MMF treated cells. FSC/SSC and gating strategy

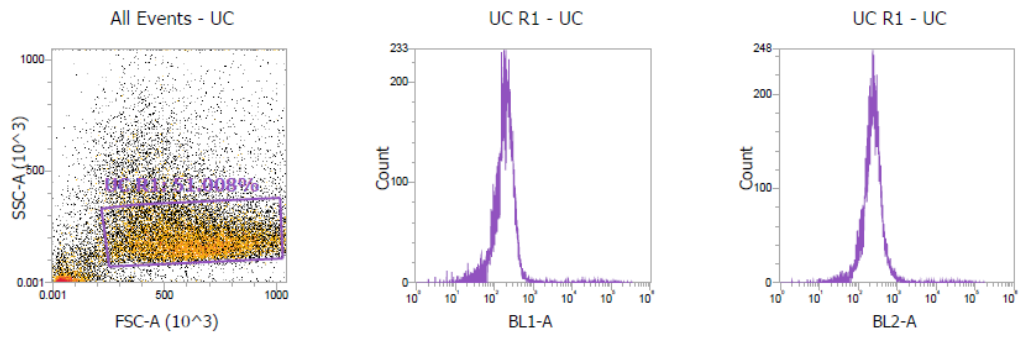
(E)



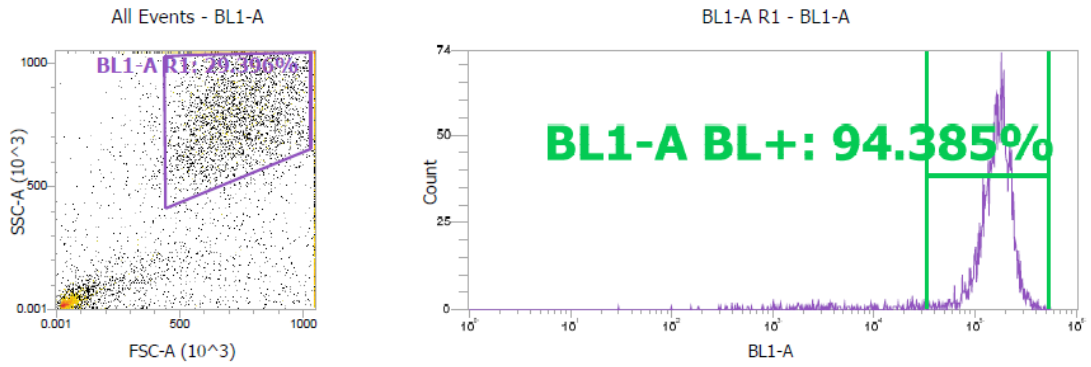
Appendix 1 (E): Representative flow cytometry plots for UVW TMZ + MMF PT4 treated cells. FSC/SSC and gating strategy

Appendix 2 – Annexin V Flow Cytometry Plots

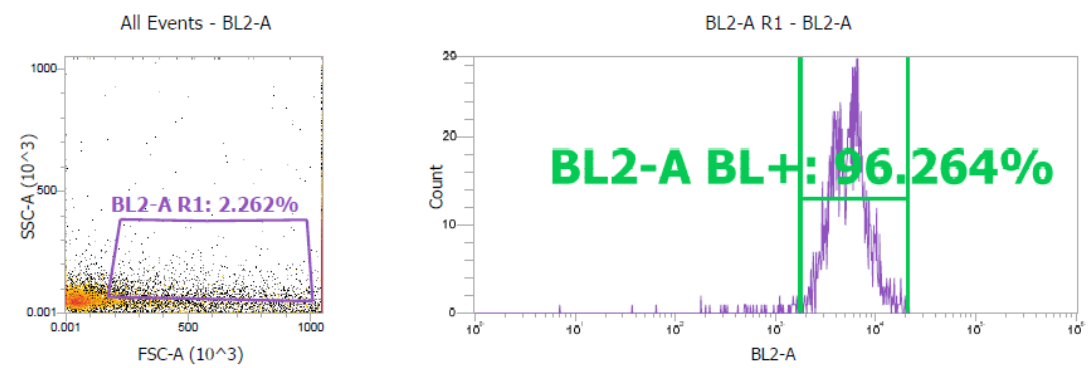
Appendix 2 (A)



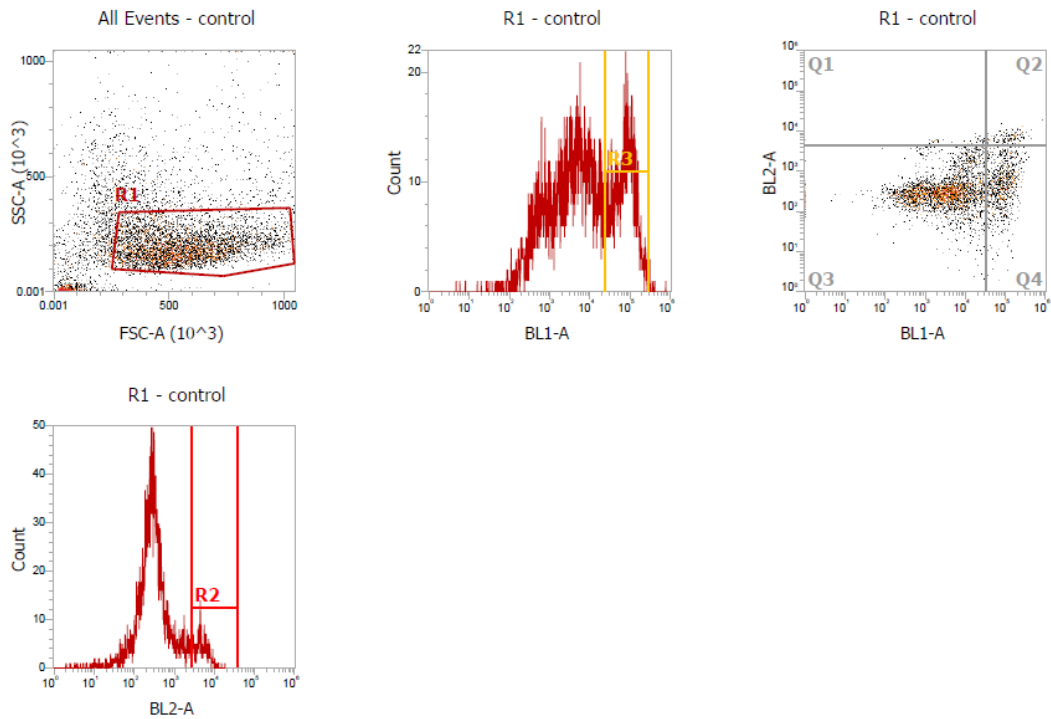
(B)



(C)



(D)



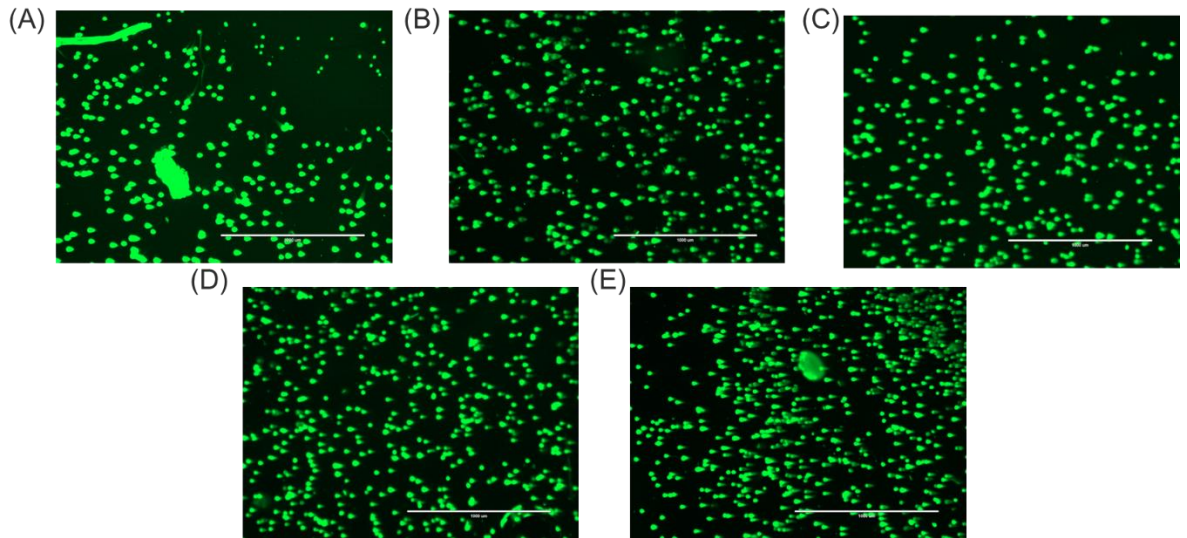
(E)

Name	X Parameter	Y Parameter	Count	%Total	%Gated
All Events	N/A	N/A	10,000	100.000	100.000
R1	FSC-A	SSC-A	4,928	49.280	49.280
R3	BL1-A		1,632	16.320	33.117
Q1	BL1-A	BL2-A	77	0.770	1.563
Q2	BL1-A	BL2-A	165	1.650	3.350
Q3	BL1-A	BL2-A	3,457	34.570	70.179
Q4	BL1-A	BL2-A	1,227	12.270	24.909
R2	BL2-A		415	4.150	8.421

Appendix 2 : Representative flow cytometry plot for Annexin V FSC/SSC and gating strategy. Untreated control cells with no PI or FITC (A). FITC only stained cells treated with Triton X (B). PI only treated cells treated with H₂O₂ (C). BL1 = FITC, BL2 = PI, Q1 = necrosis, Q2 = Late apoptosis, Q3 = non apoptotic (viable) and Q4 = Early apoptosis. Data shown is UVW control cells (D). Attune X output showing number of cells, percent gated and the percentage of cells in each quadrant (E).

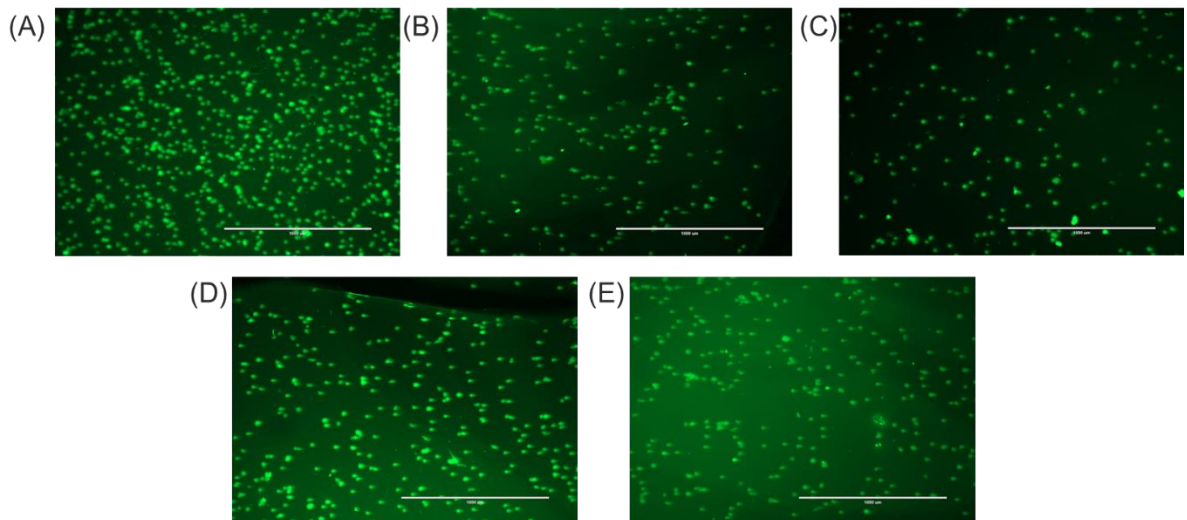
Appendix 3 – Comet Assay Images

(A)



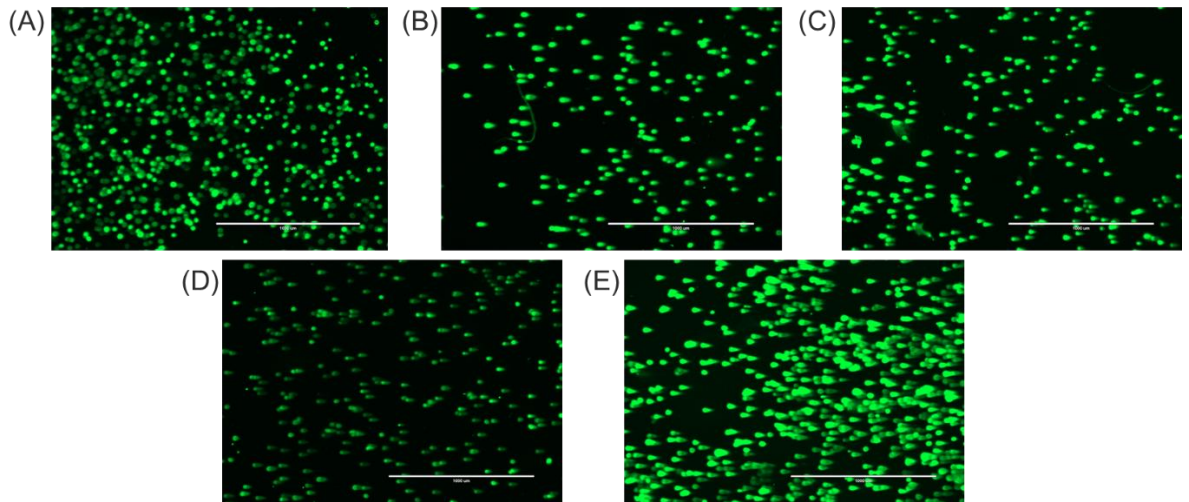
Appendix 3 (A): Representative Images of the UVW cell line comet assay after post 24h exposure to treatment. Control (A), TMZ (B), MMF (C), TMZ + MMF(D) and TMZ + MMF PT4 (E). Data shown is 1 image from ~5 taken per comet slide. Images represents 1 technical replicate. (Figure 3.19 (B)).

(B)



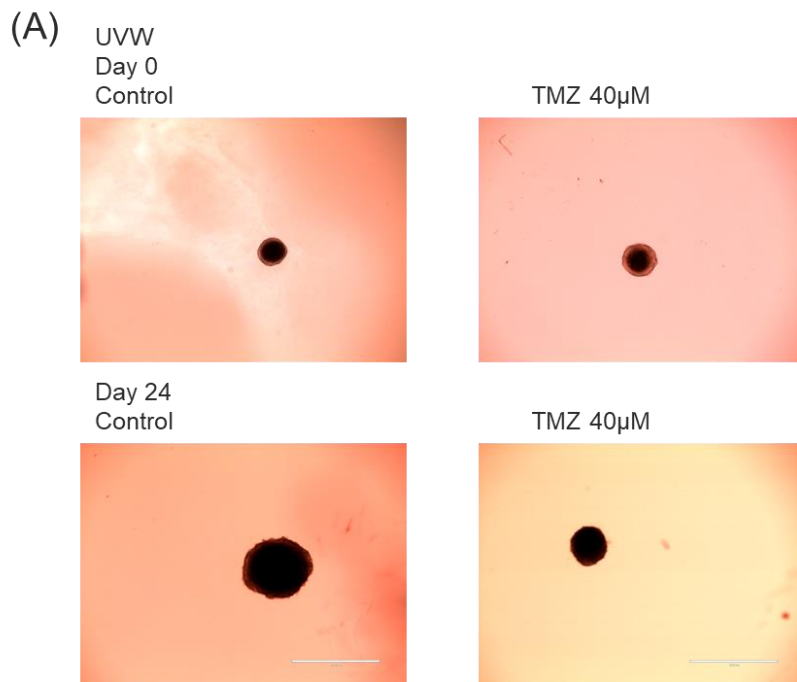
Appendix 3 (B): Representative Images of the U87 cell line comet assay after post 24h exposure to treatment. Control (A), TMZ (B), MMF (C), TMZ + MMF(D) and TMZ + MMF PT4 (E). Data shown is 1 image from ~5 taken per comet slide. Images represents 1 technical replicate. (Figure 3.20 (B)).

(C)

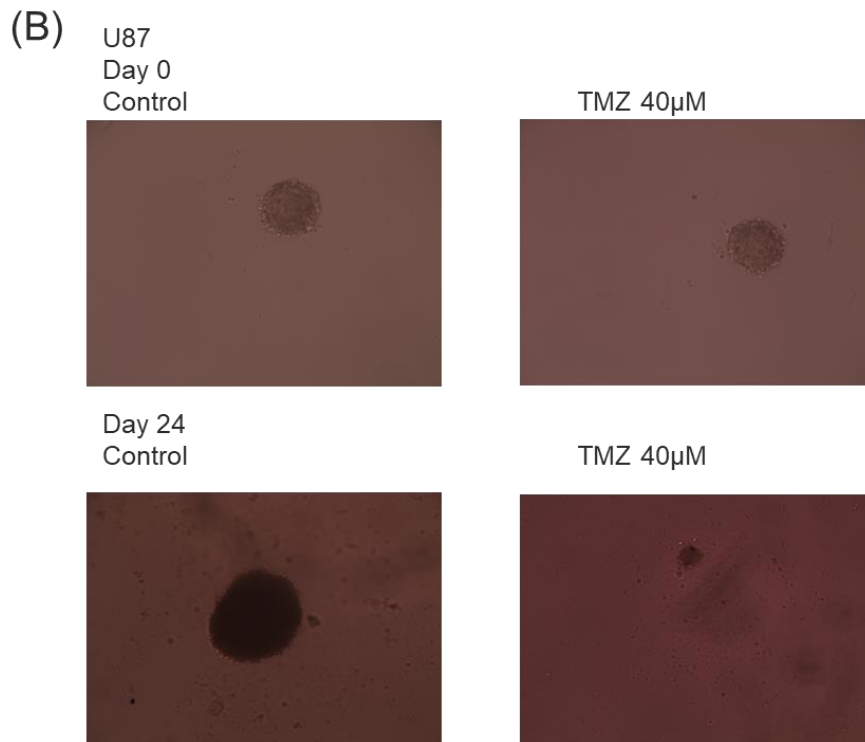


Appendix 3 (C): Representative Images of the T98g cell line comet assay after post 24h exposure to treatment. Control (A), TMZ (B), MMF (C), TMZ + MMF(D) and TMZ + MMF PT4 (E). Data shown is 1 image from ~5 taken per comet slide. Images represents 1 technical replicate. (Figure 3.21 (B)).

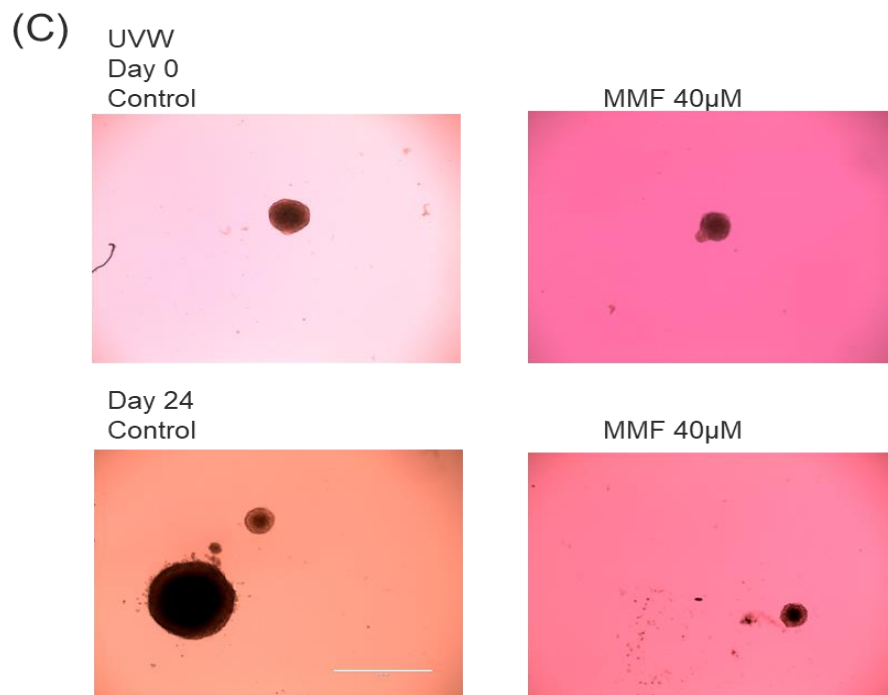
Appendix 4 – Spheroid Images



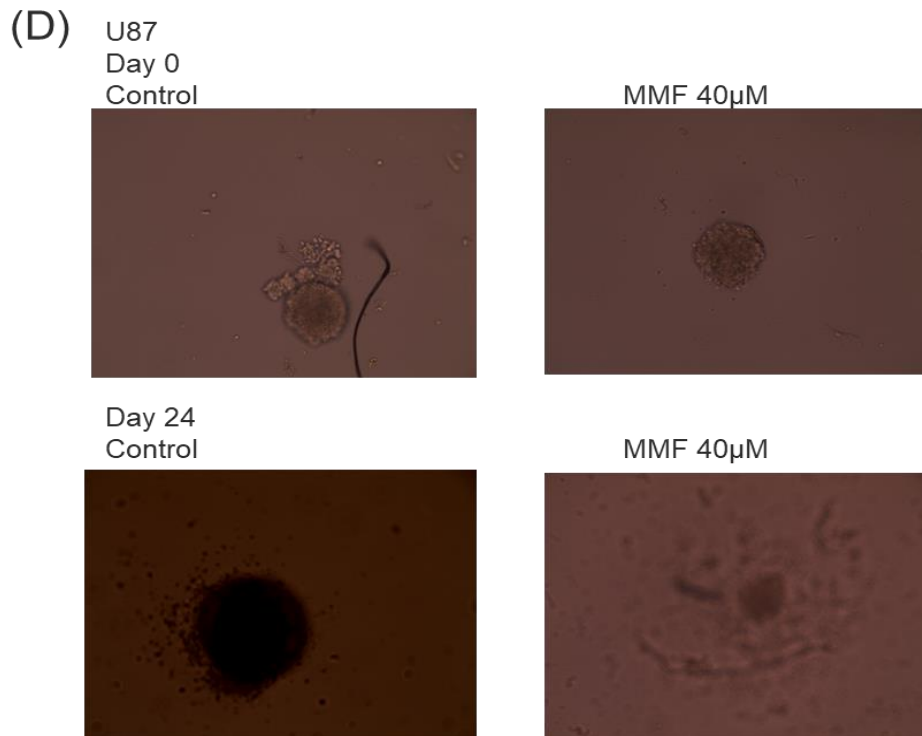
Appendix 4 (A): UVW spheroids shown at day 0 and day 24. Left hand images show the untreated control spheroids and right hand side images show TMZ treated spheroids.



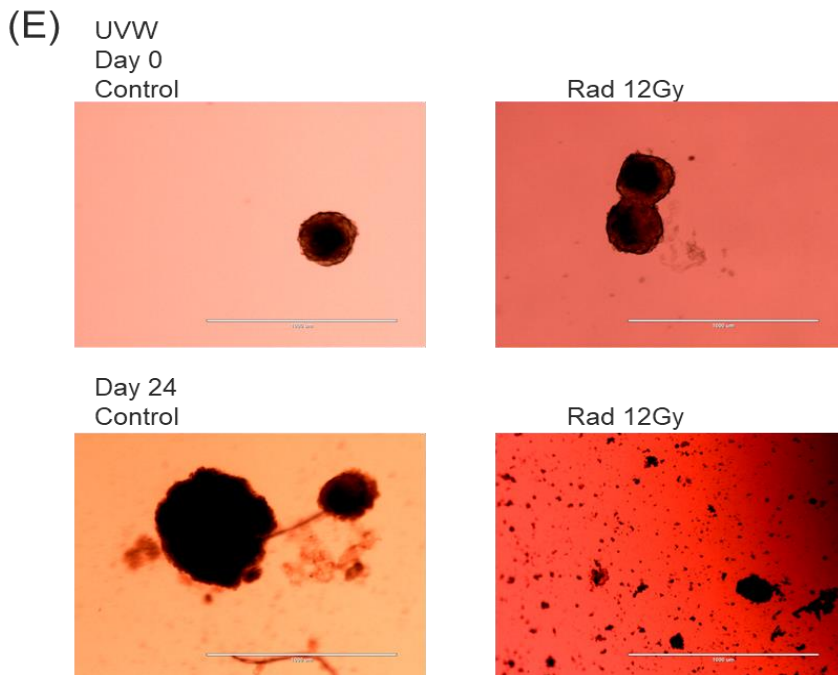
Appendix 4 (B): U87 spheroids shown at day 0 and day 24. Left hand images show the untreated control spheroids and right hand side images show TMZ treated spheroids.



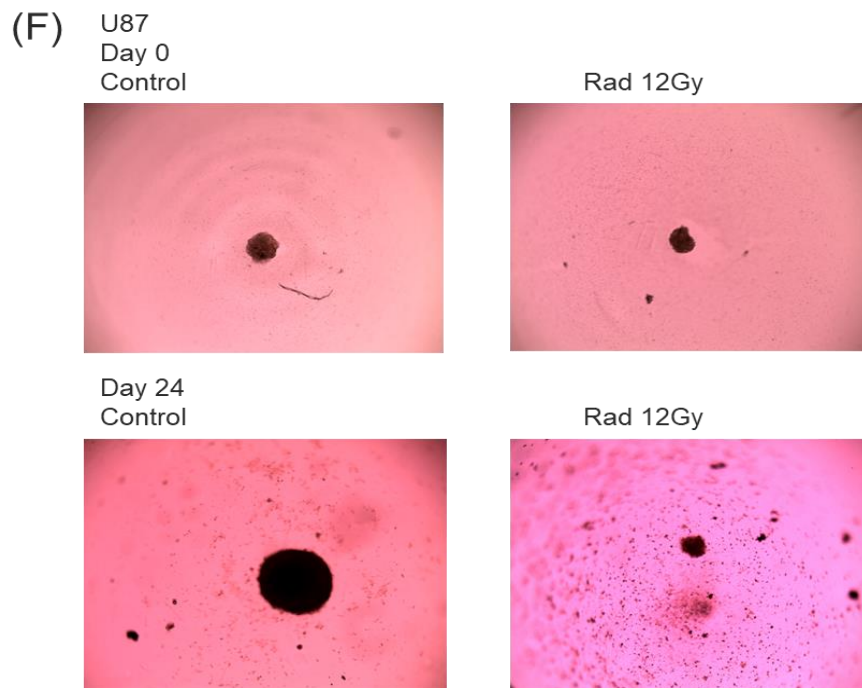
Appendix 4 (C): UVW spheroids shown at day 0 and day 24. Left hand images show the untreated control spheroids and right hand side images show MMF treated spheroids.



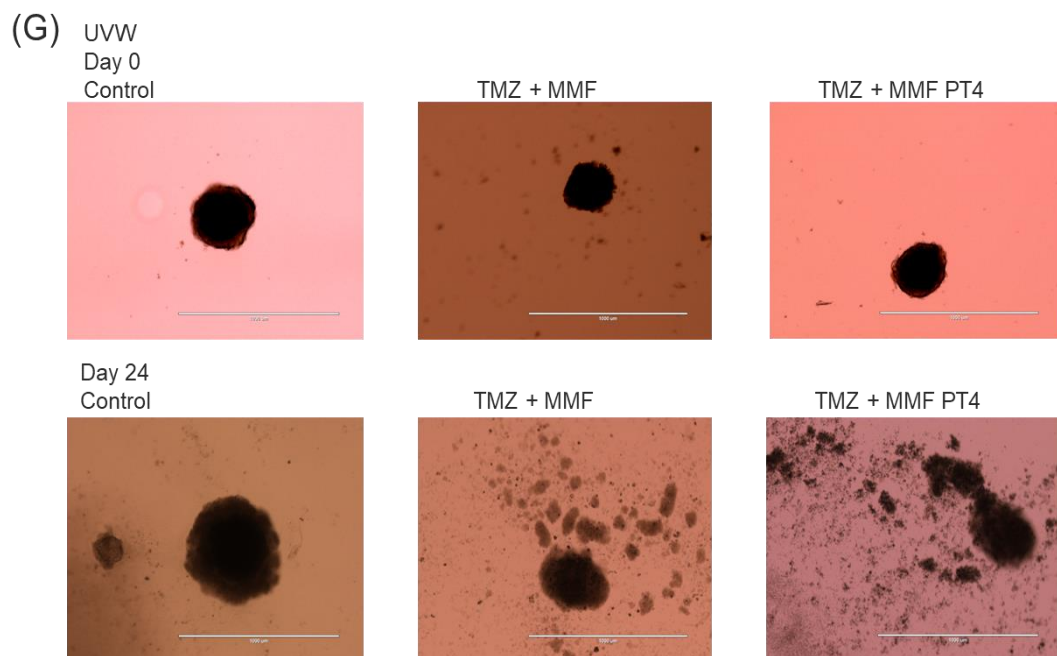
Appendix 4 (D): U87 spheroids shown at day 0 and day 24. Left hand images show the untreated control spheroids and right hand side images show MMF treated spheroids.



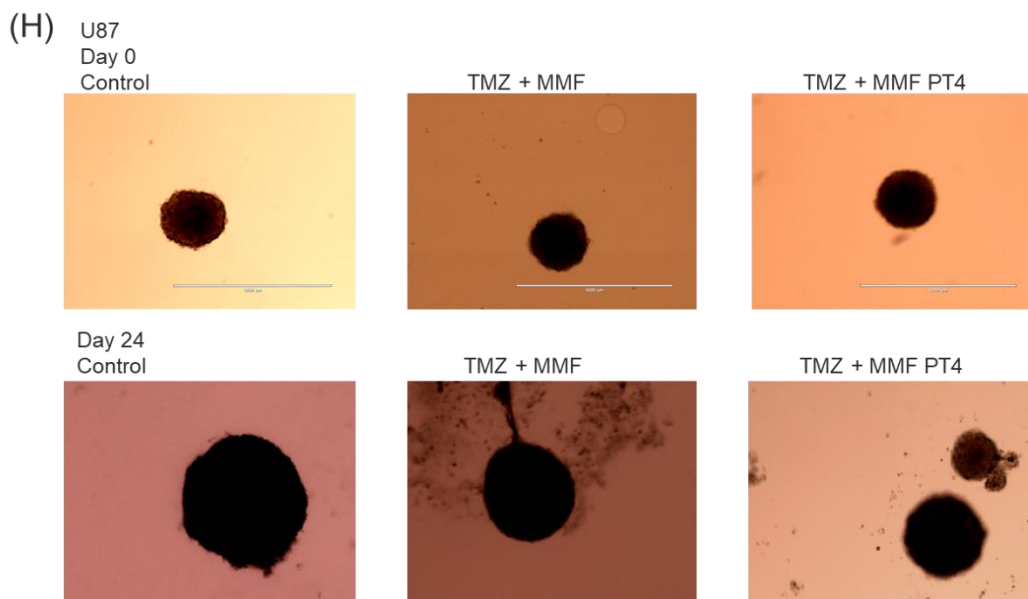
Appendix 4 (E): UVW spheroids shown at day 0 and day 24. Left hand images show the untreated control spheroids and right hand side images show Radiation treated spheroids.



Appendix 4 (F): U87 spheroids shown at day 0 and day 24. Left hand images show the untreated control spheroids and right hand side images show Radiation treated spheroids.



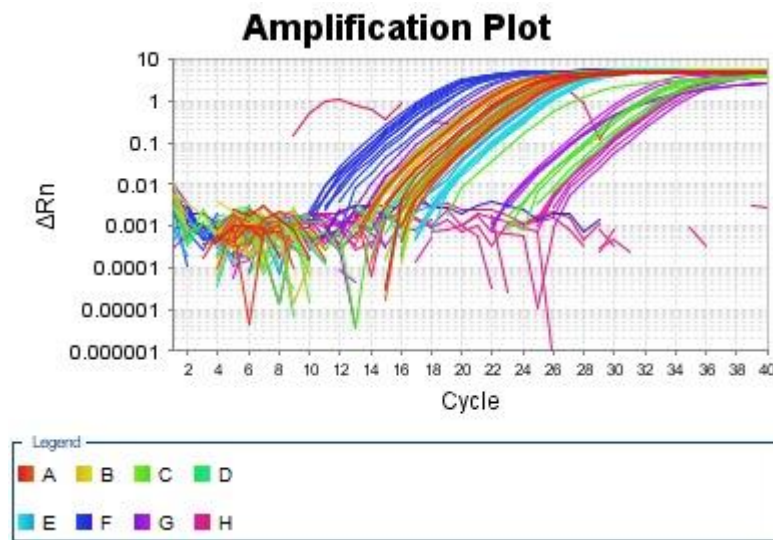
Appendix 4 (F): UVW spheroids shown at day 0 and day 24. Left hand images show the untreated control spheroids, middle images show the combination of TMZ + MMF and right hand side images show TMZ + MMF PT4 schedule treated spheroids.



Appendix 4 (G): U87 spheroids shown at day 0 and day 24. Left hand images show the untreated control spheroids, middle images show the combination of TMZ + MMF and right hand side images show TMZ + MMF PT4 schedule treated spheroids.

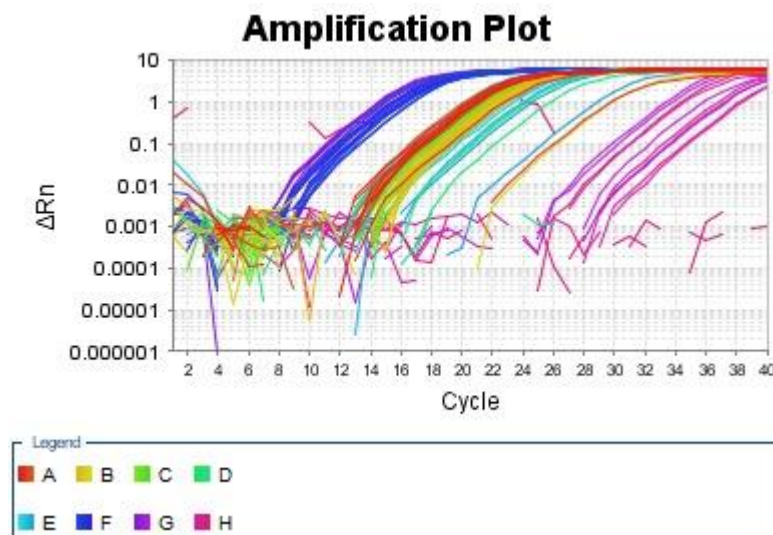
Appendix 5 – RT-qPCR

(A)



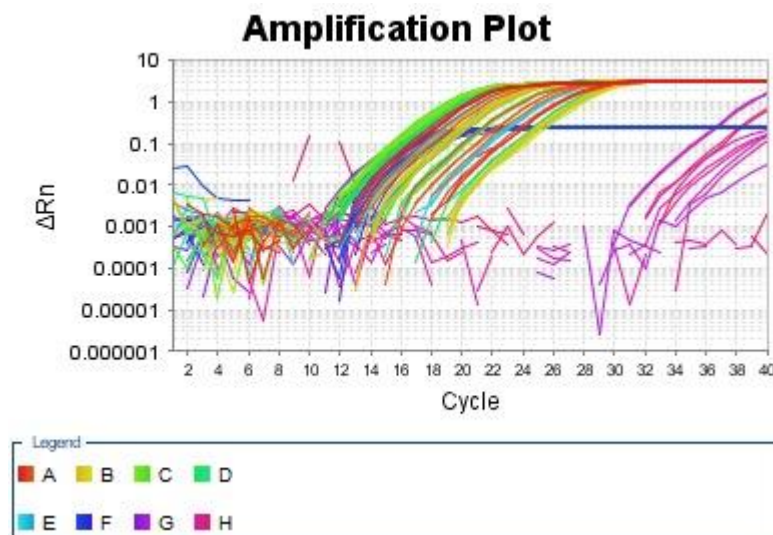
Appendix 5(A): UVW Nrf2 and P65 amplification plot for one replicate of the RT-qPCR. Data shown is a mix of Nrf2, P65, GAPDH reference gene, RT controls, primer controls and water controls.

(B)



Appendix 5(B): U87 Nrf2 and P65 amplification plot for one replicate of the RT-qPCR. Data shown is a mix of Nrf2, P65, GAPDH reference gene, RT controls, primer controls and water controls.

(C)



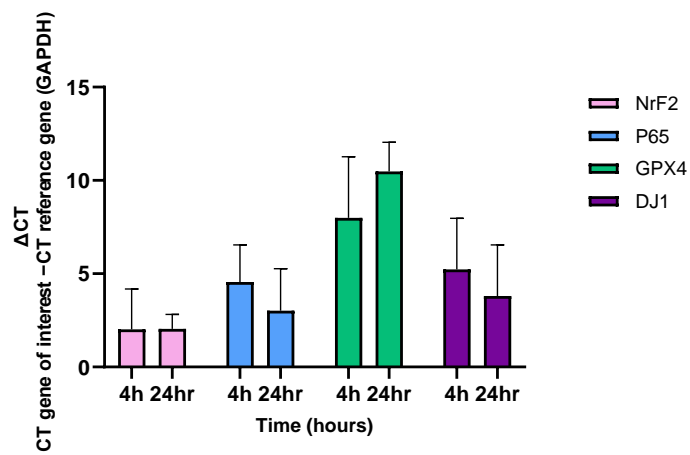
Appendix 5(C): T98g Nrf2 and P65 amplification plot for one replicate of the RT-qPCR. Data shown is a mix of Nrf2, P65, GAPDH reference gene, RT controls, primer controls and water controls.

(D)

Well	Omit	Flag	Sample Name	Target Name	Ct	Ct Mean
A1	FALSE	No Flag	Control 0h	NrF2	18.866	18.90385
A8	FALSE	No Flag	Control 4h	NrF2	15.735	16.09832
D3	FALSE	No Flag	MMF 75 0h	NrF2	15.739	15.7719
D9	FALSE	No Flag	DMF 75 0h	NrF2	21.159	21.33416
E1	FALSE	No Flag	MMF 75 4h	NrF2	15.767	15.77598
E8	FALSE	No Flag	DMF 75 4h	NrF2	18.697	18.82997
F1	FALSE	No Flag	Control 0h	GAPDH	17.393	17.41983
F3	FALSE	No Flag	Control 4h	GAPDH	15.593	15.61944

Appendix 5(D): Output from StepOne Software Version 2.3. Ct mean values were taken for the $\Delta\Delta CT$ method using GAPDH as a reference gene. Samples were plated in triplicate for each time point and concentration.

(E)



Appendix 5 (E): Δ CT method output for the untreated control genes of interest minus the CT reference gene (GAPDH). The Figure shows the variable Δ CT values between time points.